9th EUROPEAN CONFERENCE ON

CONTROLLED FUSION AND PLASMA PHYSICS

OXFORD 17 - 21 SEPTEMBER 1979

Invited Papers

9th EUROPEAN CONFERENCE ON

CONTROLLED FUSION AND PLASMA PHYSICS

OXFORD 17-21 SEPTEMBER 1979

INVITED PAPERS

ADDITIONAL CONTRIBUTED PAPERS
SUPPLEMENTARY PAPERS
POST DEADLINE PAPERS

31120

ORGANISED BY UKAEA CULHAM LABORATORY
UNDER THE AUSPICES OF THE EUROPEAN PHYSICAL SOCIETY

Max-Planck-Institut für Plasmaphysik
25. FEB. 1980
Bibliothek

Additonal copies of this volume (Price £12.50) are available from:

Public Relations Office
Culham Laboratory
Abingdon
Oxfordshire OX14 3DB
England

PREFACE

This volume contains the texts of **Invited Papers** presented at the 9th European Conference on Controlled Fusion and Plasma Physics. The speakers were chosen by the Papers Selection Committee and their papers appear in the order of presentation at the Conference.

Following the invited papers are the four-page texts of those contributed papers which arrived too late to be included in the first volume, of the post-deadline papers presented at the Conference, together with supplementary pages to some contributed papers.

A final List of Participants appears at the end of this volume. For easy referencing, the page numbering of the two volumes is consecutive.

Direct reproduction by photographic processes means that the authors must bear responsibility for their texts; only the minimum of editorial work has been done. We wish to thank the authors for providing copy suitable for this type of publication.

LOCAL ORGANISING COMMITTEE

LOCAL ORGANISING COMMITTEE

R J Bickerton (Chairman)
A Gibson
P A Davenport (Scientific Secretary)
J H C Maple (Administrative Secretary)

PAPERS SELECTION COMMITTEE

D Pfirsch	– Max Planck Institut, Garching, FRG
D D Ryutov	– Nuclear Physics Institution, Novosibirsk, USSR
M H Key	– Rutherford Laboratory, Chilton, Oxon, UK
J Tachon	– Centre d'Etudes Nucleaires, Fontenay, France
A Gibson	– JET Joint Undertaking, Abingdon, Oxon, UK
P A Davenport	– Culham Laboratory, Abingdon, Oxon, UK (Scientific Secretary)

CONTENTS

Additional Contributed Papers

Post-deadline Papers

Supplementary Papers

INTRODUCTORY ADDRESS BY R S PEASE

Ladies and Gentlemen, it is my honour and pleasure to welcome you to Britain and to Oxford for this meeting of the Plasma Physics Division of the European Physical Society, the ninth in the series "European Conference on Controlled Fusion and Plasma Physics". This meeting is now held every two years. The first such meeting was held in Munich in 1966, indeed somewhat before the formal establishment of the European Physical Society itself; and in line with this vigorous beginning, plasma has become one of the most active and expanding of the Society's Divisions. With this expansion there has been a growing world-wide interest in the European research work, so that this year we are pleased to welcome colleagues from many countries of the world - Australia and New Zealand, from Japan and America, and India, for example, who come of course not only to listen but also to present accounts of their work, which is on a very substantial scale and is a major contribution to the progress of our subject. Particularly noteworthy are the numerous and interesting papers from the United States of America.

This year a new group of scientists is contributing to the meeting. We are especially grateful that Prof Li Zhengwu, Mr Ye Youzhang and Mr Gu Yongnian have come to the conference from research laboratories in the People's Republic of China. A number of workers from Europe have been privileged to visit

laboratories in the People's Republic of China, so we are beginning to learn something of their substantial and growing activity. But we must be very pleased that Prof Li, Director of the South-western Institute of Physics, has accepted the invitation to give us a paper describing the research work on controlled fusion in China. The search for the route to the practical realization of controlled nuclear fusion as a major new source of energy is a task of very great significance to mankind. We must all warmly welcome this new research and look forward to a great contribution from the People's Republic of China.

If we look a little closer to home, at the European scene, this conference is marked by the appearance of some of our colleagues in a new affiliation, for, since the last Plasma Physics Division meeting, the governments of the European Community countries have established the JET Project - the Joint European Torus - a Joint Undertaking under the Treaty of Rome, and many of our colleagues - though not yet enough - are now members of this Joint Undertaking. The physical construction now started is a concrete realization of the determination of the countries of Western Europe to work together to solve the very difficult problems which still lie ahead in controlled nuclear fusion. The Director of JET, Dr Hans-Otto Wüster, and myself are naturally very glad that conference delegates will be able to come out to see the work in progress at Culham, both in the laboratories and on the buildings for JET. We should recall that it was our European colleagues from the Soviet Union who carried out so much of the critically important pioneering work upon which JET is based.

Your Programme Committee, for whose work we must be deeply grateful, has attracted a broad range of contributions in which are described researches on the many different systems which might achieve thermonuclear fusion.

To the large range of magnetic field systems studied are added a gratifying number of most interesting papers on the so-called inertial confinement - both by lasers and relativistic beams. This is a rapidly progressing subject where we can now look forward to comparing the local products with those from California. The programme - rightly in my view - starts and ends with papers dealing directly with the hoped-for end-product of our work - energy-producing thermonuclear systems.

If we look a little outside our laboratories or outside this hall today, we must be aware that the problem we study, the physics of the release of controlled thermonuclear energy, is beginning to impinge more directly on the needs of ordinary people; for new large-scale sources of energy are now perceived to be essential to provide a good standard of living for all in the world and if the world is to avoid the dangers of stresses arising from real energy shortage. It is our urgent task to show how or if fusion may be developed to be a realistic option to be compared with the other possible sources of energy, both nuclear and non-nuclear, for the 21st century. Therefore it is of more than academic interest to society to know how our work is progressing.

To many of the delegates this broad situation is familiar. Both by using magnetic field systems, and by using so-called inertial confinement methods, it is now routine for experimental apparatus to generate, control and sustain matter at temperatures exceeding those in the centre of the sun - say $20M^{o}K$ - for times of about a second in the case of the magnetic systems. The maximum temperatures achieved so far - about $70M^{o}$ - exceed the minimum for a net production of energy and are only a short way from the $100\text{-}200M^{o}$ needed for energy production in reactors outlined by engineering studies. Likewise the

magnetic thermal insulation achieved is such that those needed for a reactor also seem to be within the possible range of experiments now under construction.

I am very grateful to Prof Husimi for the opportunity to show you his new form of presentation of our progress. You will recall that the target thermonuclear conditions can be described roughly by the triple product of plasma number density n , confinement time τ_e and temperature T. When the experimental achievement is plotted as a function of the cumulative number of scientific papers (on a log-log plot), a straight line is obtained, as shown in Fig. 1. In this conference there are 210 papers, and on this basis the $n\tau_e T$ should be advanced by only a rather modest amount - I leave the detailed comparison between observation and theory to Dr Engelmann's expertise in his closing address, but hope indeed that we can do better than prediction.

We must conduct our studies with a real sense of urgency if we are to be able to place before society a convincing account of the fusion option before the 21st century. And, for this reason I believe, there has been a very generous response from all countries involved to the needs of the study group set up by the International Atomic Energy Agency - the so-called INTOR Study Group - set up to make suggestions of the magnitude and objectives of the next big step in magnetic confinement which might be taken following the present generation of large tokamaks under construction (TFTR in the USA, JET in Europe, JT-60 in Japan and T-15 in the Soviet Union), in an international effort to speed the progress. So far the work of this study group is by no means complete. But it is evident that in trying to forecast the performance of large systems, we are still seriously hampered by the inadequacy of our understanding of the physics

of high temperature plasmas in magnetic fields. Even in the most widely studied magnetic confinement system - the Tokamak - the experimental observation of that key quantity describing the magnetic thermal insulation - the energy confinement time - still eludes a soundly based simple explanation. We are, anyhow before the start of this conference, unable to give a convincing physics account of the observed confinement time in existing experiments and how it will extrapolate to large systems and in the presence of thermonuclear reactions. Indeed the empirical formula used so far by the INTOR Study Group cannot, it appears, be explained in terms of simple basic plasma physics. Of course we are not wholly ignorant, but I at least am in that well-known grey area of "I should understand this better than I do, but I don't"; a state in which countless men have entered this Examination Hall.

It is my conviction that a major function of this conference is to improve our knowledge and understanding of plasma physics, so that this kind of serious lacuna in our ability to describe and forecast the behaviour of high temperature plasma is eliminated, so that we can forecast more generally and reliably for serious engineering work the conditions in which high temperature plasma can be produced, controlled and contained for adequate times and with sufficient amounts to enable practical energy production to be achieved. The hopes of many ordinary people who help pay for this work must therefore be linked with the success of this task.

For this week, Culham Laboratory's particular role - that of the host organization - is to ensure that at the conference you have both a useful and enjoyable time. This task has been delegated almost entirely to the Local

Organizing Committee chaired by Dr R J Bickerton. They and their associates on the Ladies Committee must take the credit for any success we may achieve. And I hope that in the course of this week you (and your families when present) will find time to see and enjoy something of the interesting and beautiful city of Oxford, its colleges and the surrounding country.

May I now close by wishing you every success, and pass the proceedings to your chairman, Dr F Engelmann.

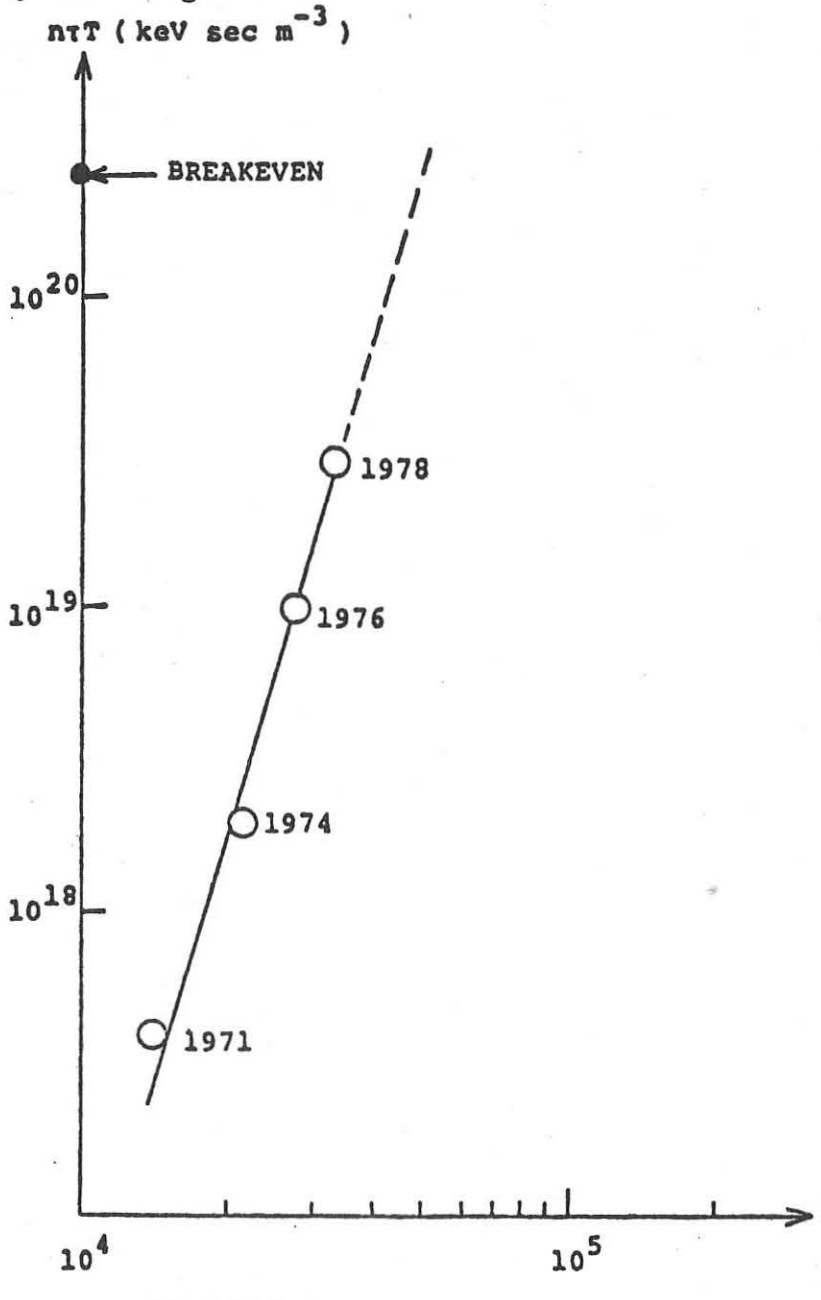

図1 プラズマ核融合関係論文累積数と点火条件指数（nτT）

THE THEORY OF A FUSION REACTOR

K. V. Roberts
Culham Laboratory,Abingdon,Oxfordshire OX14 3DB,
England.
(EURATOM/UKAEA Fusion Association)

1. Introduction

The intention of the Organizing Committee cannot have been that this opening paper should present an account of progress in an already well established area of fusion research, but rather that plasma theoreticians and computational physicists might be provoked into helping to fill an evident gap in our knowledge. Indeed there are very few contributions that deal explicitly with reactors at this Conference, with the notable exception of the final invited paper [1] which is a Review of Fusion Reactor Problems by Dr.Grieger. Nevertheless even that paper concentrates on DEMO or even pre-DEMO devices rather than on a working commercial reactor.

During the last few months there has however been much activity in at least a closely-related area, namely the theoretical and computational basis for the INTOR project, a joint international design study involving teams from the USA,USSR,Europe and Japan. INTOR is not intended to be a commercial thermonuclear reactor nor even a demonstration reactor or 'DEMO', but it represents the furthest along this path that theoretical analysis has reached so far and many detailed computer calculations have by now been carried out. The INTOR study throws a good deal of light on how a tokamak reactor is expected to operate and on what further experimental, theoretical, computational and technological research is required. Although it would not be appropriate to quote the INTOR results in detail in advance of publication [2], many people at this Conference will have taken part in the study and had access to the July 1979 Draft Report.

This paper recalls briefly and in broad outline some of the reactor plasma problems that we still face and indicates the directions in which future theoretical and computational research may be expressed to go. It is concerned almost entirely with the tokamak reactor in its ignition form, since although the beam-driven tokamak reactor has been worked on actively during recent years in several variants it has been well reviewed in an article by Jassby [3]. Concentration on the ignition tokamak does not imply that the author necessarily believes this to be the most likely candidate. The engineering complexity of toroidal devices together with the long breeding time and high power density in fast fission reactors suggests that a mirror hybrid reactor might soon become increasingly recognized as an attractive option. However although all thermonuclear reactors have many features in common, the mirror is sufficiently different to the ignition tokamak, being an open-field-line, steady-state system driven by continuous neutral-beam injection, to make a parallel discussion only confusing, and of course there are the variants such as the tandem and reversed-field mirrors which have their own particular features. Alternative closed-line systems such as the reversed-field pinch and the stellarator are less well understood than the tokamak

and once again sufficiently different to merit a separate discussion.

Since ignition may well be achieved in tokamak devices such as JET, TFTR and JT60 which are now under construction it is pertinent to consider the direction which plasma theory ought to take once this goal has been reached. Some people may believe that the task of the plasma physicists will by then have been fulfilled and that it will then become the job of the engineers to enclose the burning plasma by an appropriate blanket. This would be a serious over-simplification. All indications are that an ignited plasma is a highly-structured dynamical system requiring a great deal of detailed diagnostic experimentation and theoretical analysis, followed by careful design and optimization. Since a thermonuclear reactor will certainly be an expensive installation costing more than £1000M at present prices it is important to get it right. Therefore the theoretical and experimental understanding obtained from existing devices must be built into sophisticated computer codes which are validated by the available information and then used as extrapolation tools in the design of future, larger devices. This has of course been the situation for many years in fission reactor engineering.

Nevertheless, it appears that plasma theory may undergo a change of life once ignition has been achieved since above the ignition point many of the usual concepts are reversed. The energy and particle confinement times in a stable plasma may be too long leading to thermal instability, ash and impurity concentration and fuel depletion. In order to attain the Nirvana of a quasi-steady state with high β and optimum profiles, thermal energy produced by α-particle heating must be extracted from each element of the plasma as fast as it is generated, and in fact the electral power of the reactor is directly proportional to the rate at which thermal energy can be removed from the plasma. In addition new fuel must be continuously fed in and ash and impurities removed. An interesting question is whether instabilities can provide a steady state, and if so, will it automatically turn out to be the optimum steady state that we require or will some detailed feedback control be required? Instabilities and transport processes whose deleterious consequences below the ignition point have previously been studied will therefore need to be re-investigated as possible mechanisms for the technological control of the burning plasma. One example is temperature control by ripple diffusion [1,2]. Indications are therefore that plasma theory will be at least as vigorous after the change of life as before.

2. Heat Transfer Problem

Plasma physicists have been concerned with the particle and energy confinement problem for so long that it is perhaps necessary to remind ourselves of the dual problem of heat transfer, namely that 1/5 of the thermonuclear energy output is deposited in the plasma by α-particle heating and must be

continuously extracted if a quasi-steady state is to be maintained. We therefore need an effective mechanism for energy extraction, i.e. for losing heat from the plasma. (At least in tokamaks - in mirror devices heat conduction along the field lines is too high and must be reduced in some way).

This leads to a paradox: at the operating temperature during the burn phase we must achieve an energy loss rate of about $\frac{1}{2}$ the net electrical output from the station, (assuming 40% overall efficiency), but while the plasma temperature is being increased during the start-up phase the energy loss rate has to be much lower, otherwise the cost of auxiliary heating such as neutral beam injection or radio-frequency will be too high. To take a numerical example, a 5 GW thermal, 2 GW electrical station must achieve a 1 GW rate of extraction of heat from the plasma during the burn phase. During the start-up phase the energy loss rate of this magnitude (at 50% efficiency) an electrical supply of more than 2 GW into the auxiliary heating system, so that for this phase of each pulse the network would see a negative power station even taking into account the fact that the thermal capacity of the blanket would keep the main generators running.

Empirical indications are that the energy loss rate during the start-up phase will be sufficiently low for auxiliary heating to work economically. We do not of course know yet what the natural loss rate will be during the burn phase but there is no reason to believe that it will be sufficiently high, indeed the Alcator scaling shows that the energy containment time increases with density and there is some indication that it also increases with temperature, both opposite to what would be needed for control.

An analogous situation occurs in fission reactors, where the growth of the neutron population must be stopped as soon as the operating flux level is reached, and the problem is solved quite simply by the insertion of absorbing control rods. In a thermonuclear reactor we need some mechanism for enhancing the energy loss in a controlled way. In the absence of such a mechanism what happens is well known: due to the fall of ohmic heating power with temperature and the strong temperature dependence of the thermonuclear reaction rate there is a temperature range $T_1 < T < T_u$ in which the net input power $P(T)$ is negative, followed by a range $T_u < T < T_2$ in which it is positive. This leads to two stable operating points S_1, S_2 and one unstable point U (the ignition point). The range (S_1, U) can be crossed by auxiliary heating, but then in the absence of additional heat losses or of a β-limit the temperature will stabilize itself at the upper point S_2. This occurs at some 50 Kev which is well above the temperature of about 15 Kev at which the available β is used most efficiently. To avoid loss of containment by exceeding β_{max} it will then be necessary

to lower the density, leading to a substantial reduction in thermonuclear power output.

In an experimental apparatus such as INTOR it may be possible to control the burn phase by adjusting the thermonuclear reaction rate, e.g., by raising and lowering the density or by adiabatic change of temperature by major radius compression and decompression [4]. But in the commercial reactor our problem must be to get the energy out while keeping the reaction rate at the maximum allowed by β_{max} and the cross-section curve, partly to achieve full efficiency and partly to avoid thermal cycling of the blanket structure. Such schemes therefore do not seem to help : instead of adjusting the thermonuclear energy production rate to the available heat loss, one must instead adjust the heat loss to be the maximum obtainable energy production rate determined by $\beta^2_{max} B^4_{max}$ since both β_{max} and the maximum magnetic field strength B_{max} are already rather low. Therefore it seems to be necessary to have some method for adjusting the energy containment time in a controlled way, analogous to the insertion and removal of control rods in a fission reactor. The timescale required is of order seconds,and some excess containment must be kept in hand to allow for fuel depletion and impurity influx.

Controlled energy extraction is a major problem and insufficient is known about it. Methods that have been proposed include enhancing the ripple diffusion by reducing the uniformity of the magnetic field, and the possibility that turbulence due to nonlinear instabilities when β_{max} is exceeded might adjust the energy loss rate automatically (β-limiter or thermostat effect). Radiative cooling by controlled impurity injection has also been proposed but such radiation would fall on the first wall: for a given maximum permissable wall loading the output of the reactor will be increased if as much as possible of the energy is removed via a divertor rather than being allowed to reach the wall itslf. Therefore only particle or collective plasma transport processes rather than radiative processes should preferably be employed.

3. Profile Control

In addition to heat extraction, another whole area of interest for any combustion system is fuel injection and heat removal. In the case of a toroidal thermonuclear reactor we must include the control of the density and temperature profiles as a function of ψ (the poloidal flux), and of the profiles of fuel mix or D-T ratio, of the helium ash and of the several impurity species and ionization levels. Subject to the various constraints there will be an optimum set of profiles, and methods are required for controlling the profiles and for stabilizing as close as possible to this optimum.

Control of the temperature profiles is of course part of the energy extraction problem, but may also be required in order to control the radial transport of fuel, ash and impurity species. Temperature control near the wall is also important to minimize wall damage and impurity influx.

A third area of interest is magnetic control. If the problems of continuous fuel injection and of ash and impurity removal can be solved, then we may wish to extend the burn phase for as long as the available volt-seconds will allow. This means that the pressure profile $p(\psi)$ and the q-profile $q(\psi)$ which maximize β should be maintained quasi-constant in time. So far such profiles have been investigated analytically and computationally and some consideration given as to how they might be set up; it is clear that the requirement that they should be maintained for an extended period is compatible with the various evolutionary transport, diffusion and heating processes that take place within the plasma and some additional control may be required.

Magnetic control of the overall position and shape of the plasma should however be more straightforward. In addition to such control of the equilibrium, some feedback stabilization may be needed for low-n free-boundary modes due to the absence of a perfectly conducting wall.

4. Evolution Codes

So far we have considered only problems that arise during the burn phase, which is the main operating phase of the reactor. In fact three phases have been identified by the INTOR Workshop [2] namely start-up, burn and shutdown, together with a number of sub-phases (Table 1), and the sequence should be much the same

Table 1, Reactor Phases[2]

Phase	Sub-phase
1. START-UP	Ionization and current initiation
	Current rise, $T_e \leq$ 100ev
	Current rise, 100 ev $\leq T_e \leq$ 1 Kev ($I \rightarrow I_{max}$, main ohmic heating)
	Additional heating to ignition
2. BURN	
3. SHUT-DOWN	Initiation of shut-down
	Shut-down paper
	Cool
	Decrease current

in a reactor. These have been simulated on the computer and discussed by the INTOR Workshop but will not be discussed further here.

One of the principal aims of plasma theory and of computational plasma physics must indeed be to simulate by computer the time evolution of all these phases and subphases, sufficiently accurately so that appropriate engineering decisions can be made about the optimum design and operation of fusion reactors. This is the stage which

fission-reactor theory reached many years ago, where one has a number of empirically-validated, internationally-available codes embodying past reactor experience.

At the heart of fusion reactor theory we should therefore put the evolution codes (Table 2). These are usually referred to as tokamak transport codes but it should be emphasized that processes other than transport are becoming increasingly important,

Table 2. Evolution Codes

(Describe stable, intended mode of operation, + limited classes of instabilities)

Type	Geometry	Independent Variables	Instabilities
0D	Global (point)	t	temporal
1D	Cylindrical	(r,t)	temporal radial m=n=o
1½D	Toroidal	(R,z,t) or (ψ,t)	temporal n=o

Data Base

Theoretical equations
Theoretical rate and transport coefficients
Empirical data and scaling laws
Intuition (e.g. for turbulence not yet observed)

for example ohmic, auxiliary and α-particle heating, re-adjustment of equilibrium, fuel depletion by burnup and so on.

These evolution codes are first of all used to describe the stable intended mode of operation of the reactor, but depending on their geometry they can also describe limited classes of instabilities. All of them can describe temporal instabilities in which parameters such as the ion and electron temperatures, the β and q(a) values and the species ratios depart from their intended norms. The 1D can describe radial, m=n=o instabilities in which the profiles become incorrect, for example if the plasma becomes too hot or too cold at the centre or the outside. The 1½D codes can describe shape and position instabilities, the class of deformations which is included depending on whether or not symmetry is imposed about the horizontal midplane. But none of them describe helical instabilities in which azimutual symmetry (i.e. rotational symmetry in the ϕ-direction about the vertical axis) becomes broken.

The data base for the codes is partly theoretical, partly empirical and partly intuitive. At present our knowledge of transport coefficient is quit limited, as can be seen from the empirical Alcator Scaling law [1,2,5] ,

$$\tau_e = 5\ 10^{-21}\ \bar{n}\ a^2 \qquad (s)$$

which appears to be much too simple and whose significance is not well understood, and from the wide scatter in the plots of measured energy containment times. The data base will become more reliable as more calculations are carried out and compared with each other and with better experimental measurements, and must indeed do so if reactor performance estimates are to have quantitative significance.

There is much more work going on than is reported at this Conference, the 0D and 1D codes being used for INTOR as well as for JET, and the other large tokamaks now under construction and for existing devices, while there are several 1½D codes already in operation but still under active development.

The 0D codes average across the whole plasma and lead to coupled ordinary differential equations. Their advantage is that they are easy to program, fast to run and produce only a limited amount of output. But radial profiles and radial transport processes are not yet well understood and it is difficult to know how to do the averaging. It seems however that these global codes are useful at the present time for overall surveys and will remain useful even when computers become larger and faster, because the profiles will themselves become better understood by then both from experiment and from 1D and 1½D simulations so that the 0D codes can be better normalized. The 1D codes are of course the work-horses oftokamak simulation theory and an immense number of runs have been carried out.

5. 1½D Evolution Codes

1½D codes require much more computer storage and computer time, and although several successful codes now exist they are so far less well developed and include fewer physical processes than the established 1D codes. Physically we imagine the plasma as confined by a set of nested topologically-toroidal shells which are in fact the magnetic surfaces whose projections in the (R,Z)-plane are the poloidal field lines ψ = constant. The timestep calculation takes place in two stages. In Stage I we think of the shells as fixed in space and allow a number of entropy-generating processes to take place, for example heat production and diffusion, particle diffusion, thermonuclear burning, relative motion of the B_T flux through the B_p surfaces

and so on. Then in Stage II we temporarily freeze all the entropy-generating processes and re-adjust the positions of the surfaces to restore pressure equilibrium $\nabla p = \underline{j} \times \underline{B}$.

This algorithm was put forward by Grad and Hogan [6] and has also been used in the ATHENE1 code by Christiansen,Roberts and Long [7,8,9] for high-β 1D reversed field pinch (RFP) calculations. There are a few complexities in the $1\frac{1}{2}$D model and the final version may not yet have been achieved but physically the picture is rather clear. The model is called $1\frac{1}{2}$D because the entropy-generating processes of Stage I are averaged over the surfaces calculated in Stage II using ψ as an effective radial co-ordinate. For much of the complicated physics one can use an ordinary 1D evolution code and there is no need to go to 2DMHD; in fact it would be inappropriate because the time-scales for processes across and along the magnetic field lines are quite different.

There are several reasons why a $1\frac{1}{2}$D evolution code will be essential for quantitatively-accurate reactor simulation. A D-shaped or other non-circular cross-section is likely to be used, the aspect ratio R/a will be relatively small, and we shall be working as close to the maximum β as possible. Distortions from cylindrical symmetry will therefore be substantial and equilibrium calculations show that the magnetic surfaces are likely to be much closer together at the outside of the torus than at the inside. The effect of finite wall conductivity and of the lumped poloidal field coils must also be allowed for. A $1\frac{1}{2}$D code will be the basis for realistic calculations of the evolution of FCT equilibria, ideal and resistive MHD instability, trapped-particle effects, neutral-beam injection, RF propagation and absorption, the evolution of fast-ion and α-particle populations, impurity behaviour, and the transport of neutral atoms (e.g. by Monte Carlo). An interesting question is whether the compression of the magnetic surfaces at the outside of the torus might provide an automatic β-limit, e.g. by increased neoclassical ion thermal conductivity or α-particle loss. It will also be necessary in future tokamak evolution codes to adopt a high-β approach as the RFP codes already do and to treat B_T as a variable rather than as a geometrically-given construct proportional to 1/R.

6. Other Plasma Codes

Several other types of plasma code will be required by the fusion reactor engineer (Table 3 : the list is meant to be illustrative rather than exhaustive).

Table 3. Some other types of plasma code

Equilibrium (included in $1\frac{1}{2}$D evolution)
2D ideal MHD stability (ERATO,PEST)
2D resistive MHD stability
2D ballooning
3D non-linear consequence of instability
Neutral beam injection
RF heating
Penetration of neutrals (Monte Carlo)
Divertor operation
Wall interaction
Ripple effects
Likelihood of disruption

One of the best-developed areas is ideal linear MHD stability theory, where we have 2D codes such as ERATO and PEST for the low-n modes and more recently ballooning theory and codes for high-n. Since MHD stability presumably controls the safe β-limit at each instant of time in a working reactor, and since it is desirable to keep as near to the limit as can safely be done in order to maximize the thermonuclear output, we need to be able to make a 2D stability analysis at each stage of an evolution calculation, and perhaps also to provide such a facility as a routine diagnostic tool for the reactor operator for monitoring the stability of the plasma during a long pulse. In a similar way the possibility of a major disruption may also need to be continuously monitored by computer in view of the damage that it might cause.

There is a good deal still to be achieved in stability theory. Resistive and other non-ideal effects must be incorporated into the 2D codes, including the influence of a resistive wall, plasma rotation and feedback stabilization, and we also need to understand the non-linear consequences of high-n and internal low-n modes. Do they actually matter or could they be beneficial or even essential in keeping the centre of the plasma well stirred, so controlling the temperature and density profiles, fuel mix, ash and impurity concentration etc? How low could the ion-temperature fluctuations be in a reacting plasma undergoing relaxation oscillations or small-scale turbulence, and would the corresponding fluctuations in the neutron output be acceptable from the standpoint of thermal shock?

7. International Collaboration

Clearly a rather large suite of fusion reactor codes will be needed. It will take a long time and effort to write these and to verify that they are indeed correct; and I hope that before long we shall be able to establish more fully, just as in fission reactor work, the three main principles of:

1. An international library of fusion reactor codes
2. Adequate code documentation
3. Code validation

The codes need to be portable between different types of computer, but they also need to be compatible with each other so that the output from one code is in the right format to be used as the input for another. In the fission reactor field the AEA reactor physicists and engineers have developed the COSMOS system for this purpose, and COSMOS is now widely used throughout the UK nuclear industry, particularly for data and codes associated with the fast reactor project. The OLYMPUS Programming System [10]which has been developed at Culham for the design construction,documentation,operation and exchange of codes might also be extended to meet this requirement. Both systems are analogous to the CAMAC system used in electronics.

The Magnetic Fusion Energy Computer Centre (MFECC)network operated in the USA provides a powerful tool for collaboration between all the various US fusion groups, who are access their codes from any site, to exchange codes readily and to build up a common on-line library. A similar network would be advantageous in Europe, particularly in association with the JET Project and with the CRAY-1 computer now installed at Garching.

Another development which can be foreseen is the establishment of direct data links between the US, European and Japanese fusion computer networks.

Theoretical and experimental physics rely on the publication of refereed papers in the open journal literature. For physics computer codes the journal 'Computer Physics Communications' (CPC)[11] provides a similar facility and several hundred well-documented,tested,refereed codes have by now been published in this journal and are available from the CPC International Physics Program Library, including the laser and magnetic fusion codes MEDUSA [12], ATHENE 1 [9], CASTOR 2 [13] which are in widespread use. It is intended to publish ERATO and other important fusion codes in a similar way and to make the CPC library available on-line on the main fusion computer systems.

8. Concluding Remarks

I hope to have made it clear that theoretical plasma physics will not come to an end once ignition has been achieved; an ignited tokamak plasma is a complex engineering mechanism and a whole new set of interesting problems is beginning to emerge concerning the control of such a mechanism and its maintenance in an optimum state throughout the pulse. Table 4 indicates some of the items in a future theoretical reactor programme; it is of course a shopping-list which is quite incomplete, and a similar list

Table 4. Future Theoretical Reactor Programmes

1. Develop a scheme for exchanging codes and for collaborating in their use.
2. Build up an international Library of fusion codes.
3. Validate them by comparison with empirical data and with each other.
4. Study methods for:
   - Extracting thermal energy from the plasma
   - Keeping the plasma well stirred
   - Keeping the plasma clean
   - Optimising the n,T profiles
   - Maintaining a quasi-steady FCT State
   - Operation of the divertor
5. Examine the non-linear consequences of instabilities
6. Search for useful applications for the wide range of instabilities that is now available.
7. Look for a β-limiter.
8. Is it possible for instabilities automatically to maintain an optimum steady state (as in the Taylor RFP mechanism) or will continuous feedback control be needed?
9. How close to the rocks of low-n MHD modes and major disruptions can one in practice sail?

could be given for other reactor lines such as the mirror, stellarator and reversed-field pinch.

References

[1] G.Grieger, 'Review of Fusion Reactor Problems' Paper E3.2 of this conference.

[2] INTOR Report to be published by IAEA Vienna

[3] D.L.Jassby, Nuclear Fusion 17 309 (1977)

[4] K.Borrass, K.Lackner, E.Minardi, Paper DP16 of this conference

[5] M.Murakami, H.P.Eubank, Physics Today, May 1979 pp25-32

[6] H.Grad & J.Hogan, Phys. Rev. Let. 24 1337 (1970)

[7] K.V.Roberts and J.P.Christiansen, Comput.Phys.Commun. 10 264 (1975)

[8] J.P.Christiansen,K.V.Roberts and J.W.Long, Comput.Phys. Commun. 14 423 (1978)

[9] J.P.Christiansen and K.V.Roberts, Nuclear Fusion 18 181 (1978)

[10] K.V.Roberts,Comput.Phys.Commun. 7 237 (1974), J.P.Christiansen and K.V.Roberts Comput.Phys.Commun. 7 245 (1974)

[11]'Computer Physics Communications' published by North-Holland, Vol 1 (1969) to Vol 18 (1979)

[12] J.P.Christiansen, D.E.T.F.Ashby and K.V.Roberts, Comput.Phys.Commun. 7 271 (1974)

[13] J.P.Christiansen and N.K.Winsor, Comput.Phys.Commun. 17 413 (1979)

U.S. PLANNING FOR FUSION ENERGY DEVELOPMENT
A REPORT ON WORK IN PROGRESS

Dr. Michael Roberts, Director
Division of Planning and Projects
Office of Fusion Energy
U.S. Department of Energy

I. INTRODUCTION

In the past year, there have been significant scientific and technological advances in fusion. Not only is there a set of achievements in individual areas, but there is importantly a growing understanding of the synthesis of various pieces in the fusion program. These technical achievements coupled with a growing appreciation of the energy situation have led the U.S. program into a serious replanning effort. The work presented in this paper represents a current "snapshot" of the thinking that is resulting from discussions within the Office of Fusion Energy and with a broad consensus of the U.S. fusion community.

The policy of the Department of Energy for fusion energy is to develop its highest potential. This policy represents a significant evolution of thinking about the fusion program that has been intensified with the establishment of the United States Department of Energy. Two elements of the policy represent a continuation of earlier views, the first is the maintenance of the breadth and strength of the scientific base and the second is the belief in a strong and fruitful participation in a growing international cooperation program. The evolution is toward four elements, the first is a clear and strong focus on the Engineering Test Facility; the second, supporting the ETF, is an emphasis on reactor oriented concepts aimed at developing an economically competitive energy option; the third is defining a goal of fusion's highest potential which results in our program developing not simply the first way to produce fusion but a sufficiently broad set of options so that the fusion technology that is developed represents an economically competitive option with the other energy options at the time; lastly, the policy represents an evolution toward a program that is consistent with the nation's overall energy policy as it develops. The planning described in this paper supports that policy and presents a number of different paces covering the range from current support of the program to a significant acceleration of that program.

II. THE TECHNICAL BASIS FOR THE REPLANNING

Since the contributions to this conference cover the full range of technical progress in considerable depth and expertise, this paper will only present a sampling of these technical advances as support for the thesis that the technical status today is well advanced beyond that of 1976 and is sufficient to replan the program with some confidence. Figure 1 illustrates perhaps the most striking measure of overall progress toward the fusion goal--namely the steady and considerable increase in the energy gain, Q, with time. The neutral beam power used for supplemental heating is shown in parentheses next to the name of the device used in these experiments (TFM stands for Tokamak Flexibility Modification and represents a set of improvements to the basic TFTR facility).

In the years before the 1976 plan (ERDA 76/110-0, 1, 2, 3, 4), reactor studies projected plasma betas on the order of one or two percent with consequently large sizes and low power densities. In the past two years, the ISX device was used to investigate the experimental limits of high beta tokamak plasmas. Figure 2 illustrates the fact that the betas already achieved in ISX are at or above the earlier projections used in the reactor studies, hold promise of higher betas that would lead to economic operation of reactors and already represent achievements that will allow a fusion reaction to be ignited in a tokamak.

Over the past year, five new significant U.S. devices have been put into operation. The experimental programs of PDX, Doublet-III, ISX-B and Alcator C are expected to continue the steady growth and understanding and achievement exemplified by the high temperature results from PLT in 1978. The fifth device, the Tandem Mirror Experiment, TMX, has recently been commissioned and the first TMX results are encouraging for the tandem mirror concept. A steady state has been maintained for 25 ms, long compared both to the longest previous times $\sim$ 10 ms and very long compared to characteristic stability times. In terms of the actual characteristics of the tandem mirror operation, there appears to be evidence that the system is working as expected. Beta in the end plugs is five to fifteen percent with a five percent beta in the solenoid; the objective of 50% is within a factor of five. There appears to be good electron heat confinement as measured by an electron temperature $\sim$ 166 eV in the end plug, close to the objective of 200 eV and these also is evidence of end-plugging.

These three samples represent a picture of experimental achievements in both the tokamak and mirror field. Based upon these recent advances in the tokamak area and with increased expectations as well, we now believe that the TFTR should provide more information and more achievements than simply breakeven which was the objective at the initiation of the project. Figure 3 illustrates this change in expectation and projections for the TFTR based upon the higher β and longer pulse lengths now believed appropriate.

As bright as the present situation looks and bright as the expectations are, it is clear that not all the problems have been solved. In particular, there is a crucial physics issue remaining and that is the control of particles (e.g., impurities) on a long time. With this recognition, there is associated a broad attack on the problem. There are four different techniques being employed in this attack: materials choice for the limiter and liner; magnetic diversion; start up methods; and flow control. Facilities of significant size and importance around the world are being used to study this particular problem. In the United States, the ISX-B and PLT devices are already being used for this purpose and the PDX and Doublet-III devices now coming into operation will be addressing similar issues. Addressing these problems will also be the ASDEX and TEXTOR facilities in Germany and the JT-60 in Japan. Even with the uncertainties in the full solution of the long time particle control problem, we do have sufficient understanding today from the PLT and ISX data to know that the impurity status today will allow us to do reactor experiments, i.e., generate plasmas in the reactor regime even though we cannot know today that full reactor operation is possible.

A principal difference between the status today and that three or five years ago is that in the technological area. Figure 4 is a schematic diagram of the large coil project being built in the United States with participation from Euratom, Switzerland, and the Government of Japan. In this project, which is now in the design and fabrication stage, superconducting coils of the type to be used in subsequent large reactor experiments will be tested at half (ETF) scale in a six coil array. The experiences developed from the LCP operation will feed directly into the coil design for the next large step in the fusion program.

An important problem recognized early in the fusion program is that of materials development for reactor operation. Figure 5 illustrates the two phases, near and long term, into which the materials development can be divided and indicates schematically the role played by FMIT. In addition to magnet and materials development as well as neutral beam, vacuum systems and other hardware areas, issues of concern in the field of environment and safety have been identified (tritium, activation, biological effects of magnetic fields, lithium safety and accident analysis) and programs initiated to deal with these issues.

The preceding paragraphs have discussed highlights of both the scientific and technological advances over the past few years. In addition to the separate physics and technology viewpoints, we must also look at the growing synthesis across the program. This synthesis is both among the scientific concepts, that is, among the tokamak, the mirror, and the pinch devices and is also among the various components of the fusion program, i.e., science, technology, and engineering. A direct outcome of the understanding of the tokamak and mirror results is in the area

of the evolution of new synergistic concepts. A number of examples can be given. The energy transport theory of EBT is based on the tokamak developments. As a result of the knowledge developed in the tokamak area and the resurgence of interest in the stellarator, the modern stellarator characteristics now approach the basic tokamak parameters. In a third area, the calculations of spheromak stability are based upon the tokamak analysis and in a fourth area, the tandem mirror which represents an important evolution in the mirror development is based itself on simple mirror concepts.

In addition to the straightforward applications of the tokamak and mirror theory as mentioned above, one of the most exciting ideas, that of the compact toroid concepts, has come from and is supported by all of the base programs, the tokamak, the mirror and the theta pinch programs. Figure 6, illustrates this concept in two embodiments, the spheromak coming from the tokamak and the field reversed mirror from the mirror.

Although each of these advances and elements of synthesis can be understood individually, it is in the reactor systems studies that all the elements are put together into a coherent whole. Based on this technical progress, the current reactor systems studies do reveal an increased flexibility for the fusion power generation. There are a number of reasons for this view. Firstly, looking over the period of the 1970's, our projections of tokamak reactors have been scaled down in size and scaled toward more simple devices. In the early part of the 1970's, we were dealing with experiments whose minor radius was on the order of a few tens of centimeters. At the same time we were projecting reactors whose minor radius was in terms of meters. Over the period of the '70's, the experiments that we are now dealing with and have under construction approach 1 meter in radius and the projected sizes for reactors have come down to where minor radiuses on the order of one and a quarter to one and a half meters are being used for the designs of the ETF and Intor. Secondly, in the complementary area of mirror reactors, the expectation for energy gain $Q > 1$ has increased significantly with the development of the tandem mirror concept. Thirdly, as we strive for steady state or long pulse operation in a tokamak, the EBT concept offers steady state operation as an inherent part of its characteristics. With progress in each of these areas, now the convergence into the idea of the compact torus promises small and simple reactors. Underlying each of these approaches is the fact that they all utilize common scientific principles and, by and large, common technologies.

III. THE ELEMENTS OF THE PLAN AND DESCRIPTIONS OF THE PLANS THEMSELVES

Engineering Test Facility

A direct result of the technical advances, thoughtful discussion and policy evolution of the past year or two is the identification of the

Engineering Test Facility (ETF) as a central element of the U.S. fusion policy. The ETF has two principal technical objectives. The first is to test, develop and demonstrate technological feasibility of fusion; the second affiliated objective is to provide the bulk of the engineering data base for fusion. From a programmatic standpoint, the Engineering Test Facility provides a clear, strong and timely focus for effectively all the activities in the program. The ETF emphasizes system integration which makes clear the evolution in thinking from earlier views of the next step which emphasized physics scaling as much as engineering.

To illustrate this changing orientation, one can enumerate the basic characteristics as shown in Table I. The ETF must be first and foremost a fusion source. This fusion source then is used in a device with characteristics that do emphasize the engineering orientation. These can be enumerated as shown in the table.

A question central to the ETF decision-making process is the importance associated with choosing one particular confinement concept for the ETF driver and the applicability of the information gained. Figure 7 illustrates the thesis that the knowledge gained from the ETF is applicable to advancement of any confinement concept. In this chart we have enumerated some of the outstanding technology areas in the ETF and compared the requirements and the kind of knowledge gained from the operation of an ETF based on a tokamak with the requirements of the other leading concepts. The notation "similar" means that the requirements and the information gained from a tokamak based ETF would either be directly applicable to the others or would be results of tests even more severe than those required by any of the other four. In the fueling area, the solid dot indicates that the RFP requires a batch burn rather than the continuous flow in the other devices. In the next group of areas, the solid dots indicate no pulsed requirements. The notation ACPTF refers to an alternate concepts physics test facility described in a subsequent paragraph. Those items in a box have substantially different requirements and those items marked with a circle have no requirements in that area. On the basis of information such as that presented in Figure 7, we have made the judgment that a tokamak-based ETF would provide the overwhelming majority of the engineering data base for all fusion concepts and that using a mirror-based ETF would provide a significant fraction of the information for the other concepts with correspondingly lower percentages for the other concepts.

Major Fusion Assessment

The question of how and when and in which direction to proceed with the ETF is clearly the most important near-term decision for the U.S. fusion program. As we prepare for this decision, we are also looking at the overall program and have identified the next major program decision

following the operation of the ETF as an overall assessment of the status of the fusion program. As indicated in Figure 8, at the point of operation of the ETF or some time shortly thereafter, we intend to make a major fusion assessment leading to a decision, which would be made some time in the decade beginning around 1990 to select one of three paths as shown.

The plans discussed in this paper are all based upon taking a confident path and advancing directly to a demonstration plant. This change in viewpoint is a significant one and represents a key advance since the 1976 plan, namely that there is a strong likelihood of satisfying the EPR function in the engineering oriented ETF and demonstration plants. This view is based on both the recent scientific advances and technological advances and that our expectations for TFTR and JET operation are certainly much higher today than they were in 1976.

Role of Alternate Concepts

Alternate concepts are being pursued in the U.S. program for two programmatic objectives. The first is to develop reactor designs that are more economically attractive than the present tokamak design--in particular, that means looking for designs that are smaller in size, that are simpler in mechanical design and preferably are long pulse or steady state. This has clearly been fruitful in the compact torus reactor design area. The second objective is to stimulate new insights that are helpful to the overall fusion program. In particular, work originated for alternate concepts has had significant impact on the mainline program. For example, theoretical work on stellarators is now being applied to tokamaks to study ripple and bundle divertors. The work in the area of 3D equilibrium calculations represents a particular example of sophisticated techniques for computing stellarator equilibria with finite beta which were developed at New York University and Los Alamos Scientific Laboratory. These techniques are now being applied to tokamaks with ripple to determine finite beta equilibria and will be used to compute the resulting particle orbits in transport. These are the only 3-D codes available for these problems.

The role of alternate concepts in the fusion program is a strong one and is centrally represented in the plans as illustrated in Figure 9. The ACPTF would be used to bring the level of physics knowledge for the most attractive alternate concept up to the point of being able to make a choice between the ETF driver and the alternate concept for the EPR or Demo. The solid and dashed lines represent likely and less likely probabilities for each of the choices. The notation "alternate applications" indicates how non-electric applications development could move through an ACPTF into a demonstration plant activity.

International Cooperation

To speed fusion development, the U.S. participates in many productive international cooperative activities. In particular, our joint activities with the European Community center informally about Zephyr, the ignition test reactor experiment being studied at Garching and the Reversed Field Pinch experiment being considered in Culham and with the Italian laboratories. At the same time, there are agreements in place and in progress with the USSR and with the Government of Japan on bilateral bases for personnel exchanges and in the Japanese agreement for large project involvements, in particular with Doublet III. On an international organization level, the United States participates in IAEA activities, in particular, the exciting and productive INTOR workshop and the predecessor and parallel large tokamak workshops. In addition, the United States participates through the IEA with other member countries in the Large Coil Project and in a number of materials development projects.

In addition, we work with a number of other countries, whose fusion interests are on a somewhat smaller scale, through personnel exchange to the benefit of both sides and to the overall fusion program. Many of these vigorous international cooperative activities have come into being since the time of the previous plan. They represent a strong new element in the overall fusion program.

Included in our planning is a range of cooperative activities providing significant benefits to fusion. These activities begin with the longest standing and traditional element--personnel exchanges--in which individuals contribute their knowledge and experience to joint discussions with colleagues in other countries. These exchanges range from short visits and tours to meeting participation and workshops. Beyond personnel exchanges comes the area of hardware support in which particular elements and designs are exchanged or provided to support one another's experiments. As we move toward larger experiments in which the individual magnets, beams and other systems become of significant complexity and cost, this element becomes an ever more important part of the cooperative activities. A step beyond these first two activities is one of joint experimental testing in which participants from one country are involved with experimental activities in the facilities of another. As examples, the United States has been privileged to have participants in the TEXTOR program and numerous countries have had scientists participating in experiments in the various U.S. laboratories. A new area coming from the various bilateral exchanges is that of joint planning in which two or more countries work together in developing a most effective way of dealing with a multitude of ideas and avenues on relatively restricted resources. Perhaps the highest order of cooperative activities is a participation in the conception, development, construction and operation of major facilities. A principal example of a start in this area is the enthusiastic involvement of the four major fusion blocs in the INTOR workshop.

Schedular Planning

The two elements of the planning implementation that can be quantified directly are the times required for major facilities and the overlaps between succeeding major facilities. In Figure 10 is shown the nominal succession of events for a large facility using the ETF as a specific example in this case. Project time is considered to start when a commitment is made to conceptual design which itself is actually based on earlier work of definition and scoping.

In Figure 11 are shown three different paces or overlaps between two succeeding major facilities which are distinguished by patterns of information flow. In particular, the ETF and EPR/Demo facilities are shown.

The Planning Cases

In developing specific cases for the fusion program planning, there has been an evolution in methodology from the 1976 plan through to the planning cases shown in this paper. The 1976 plan developed five logics covering a range from constant budget to a maximum acceleration case. As the program has evolved, those five cases appear to transform naturally into three, examples of which are shown here. In the first case, defined in Base Case A, shown in Figure 12, the outcome is developed on the basis of funding constraints which are a constant budget plus increments for the construction costs of the ETF and EPR/Demo device. The Department of Energy's fusion program plan is consistent with Case A for the near term through the ETF decision but would be reassessed as the situation warrants at that time. Planning Case B, also shown in Figure 12, is defined principally by technical considerations. Case B requires a serious start on the ETF Conceptual Design in the next year and also requires a start on the preliminary design before the output of the TFTR which would then serve to confirm the design choices. The MFTF program is assumed to continue through to a situation that would allow the tandem mirror to be a candidate for the EPR/Demo and another alternate confinement scheme could be carried through to the Demo stage as well. Case C, illustrated in the lower part of Figure 12, is an even more rapid case which aims at a demonstration plant on the line in the year 1995. Case C results in completion dates even earlier than Case B but requires additional funds to cover the costs associated with speed-up, early starts, and increased risk.

In each of the planning cases, what is shown is the schedule and arrangement of the principal facilities with the clear understanding that this program includes a wealth of information associated with smaller facilities, international activities, theoretical and technological support. The principal near term decision is that associated with

beginning the ETF but in each case there are also three other major events listed, the major fusion assessment described earlier, the operation on line of the demonstration plant, and the initial operational capability (IOC) which defines the availability of a fraction of a quad of electrical energy on the grid.

The near term yearly costs associated with these three cases are basically the current rate of expenditure in Case A, an approximately 50% increase in Case B and for Case C an approximate doubling. It must be pointed out that the choice of paces is not a simple one derived from the dates and costs associated with this planning exercise. There are certainly at least two other types of considerations--differences in cases within the fusion option, and comparison of the fusion option with other competing options. In the former case, one must evaluate the difficult issues of financial and programmatic risk and applicable methods of discounting or assessing cost/benefit. In the latter case, difficult choices must be made based on a perception of urgency for the eventual pay-off of fusion, for market needs in different forms of energy and the status of competing energy options.

IV. SUMMARY

The U.S. fusion program planning process can be characterized in a few statements. One, it is appropriate now to replan the U.S. fusion program. Two, there is a constantly improving technical situation which results in an improved basis for planning projections. Three, the program logic has two principal points, 1) an ETF providing generic engineering information paralleled by an ACPTF for the development of an alternate concept(s) with the two facilities leading to a choice of pace and direction at the EPR/Demo stage; 2) the overall plan is expected to be strongly supported by a range of international cooperation activities. Four, three cases can be used to characterize the range of projections as shown in Figure 12.

FIGURE 1

CONTINUING INCREASE IN Q IS MOST STRIKING MEASURE OF OVERALL PROGRESS TOWARD FUSION GOAL

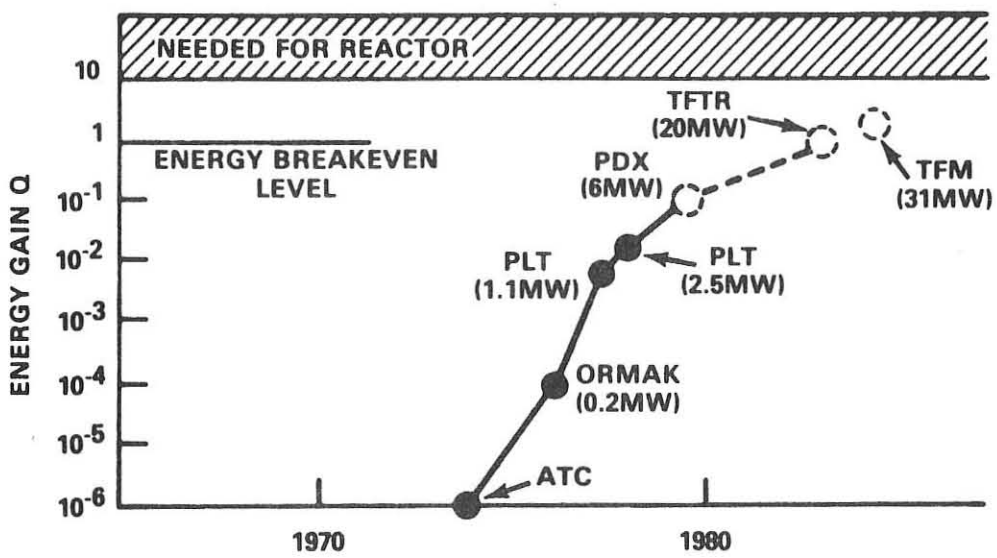

FIGURE 2

ISX DATA INDICATES SUFFICIENT PRESSURE CAN BE HELD IN A TOKAMAK TO IGNITE A FUSION REACTION

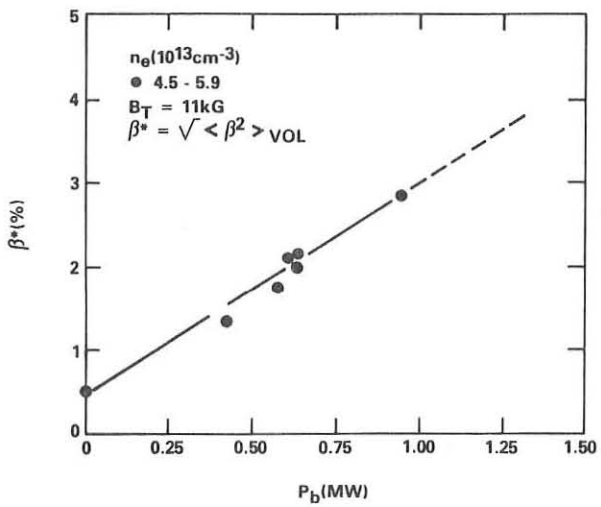

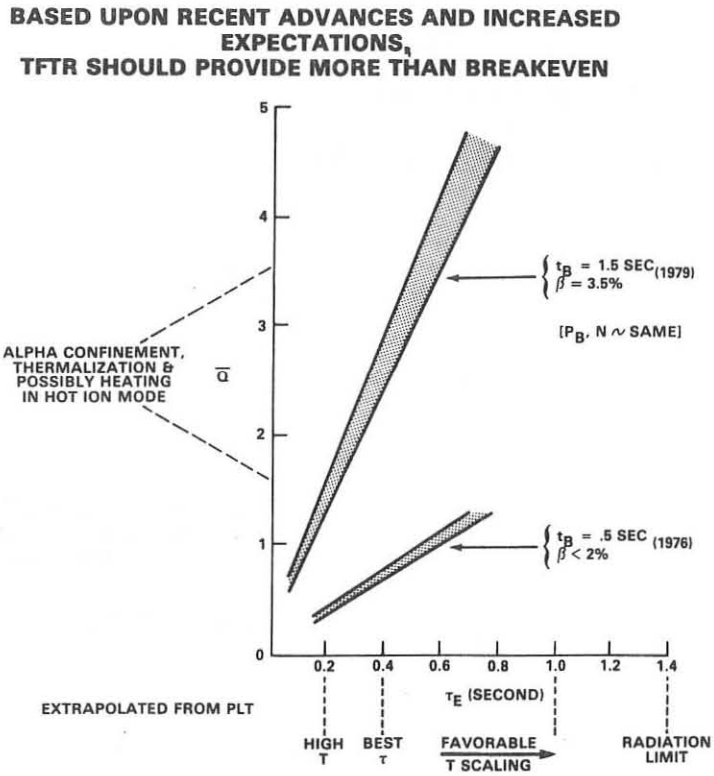

Figure 3

FIGURE 4

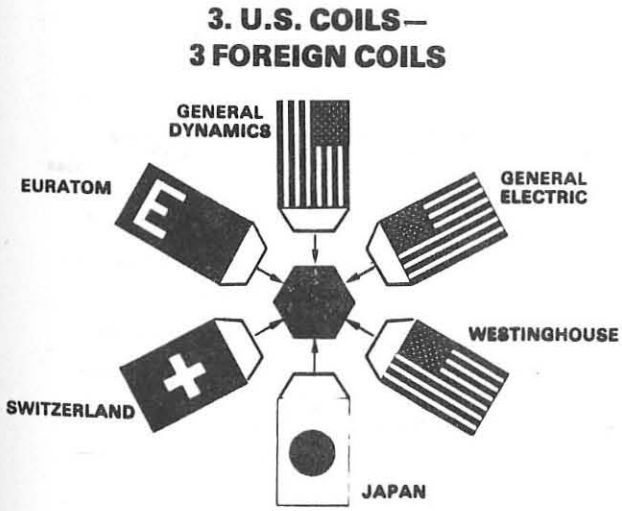

FIGURE 5

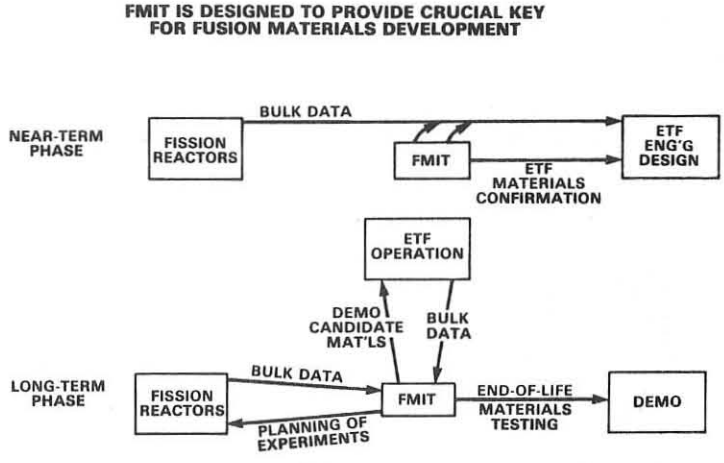

TABLE I

INITIAL TOKAMAK ETF CHARACTERISTICS EMPHASIZE ENGINEERING ORIENTATION

- FUSION SOURCE (IGNITED D-T, R ~ 5m, a ~ 1.2/1.9m, β ~ 7%)
- LONG BURN PULSE ($t_{burn} \gtrsim$ 100 sec)
- HIGH DUTY CYCLE ($\gtrsim$ 50%)
- MODULAR BLANKET CAPABILITY WITH MODULE INTERCHANGEABILITY
- TEST BED FOR COMPONENTS, MATERIALS AND OPERATION
- POWER TEST LOOP (P ~ 1MW$_e$)

FIGURE 6

COMPACT TOROID CONCEPTS EVOLVED FROM AND ARE SUPPORTED BY THE TOKAMAK, MIRROR AND THETA PINCH PROGRAMS

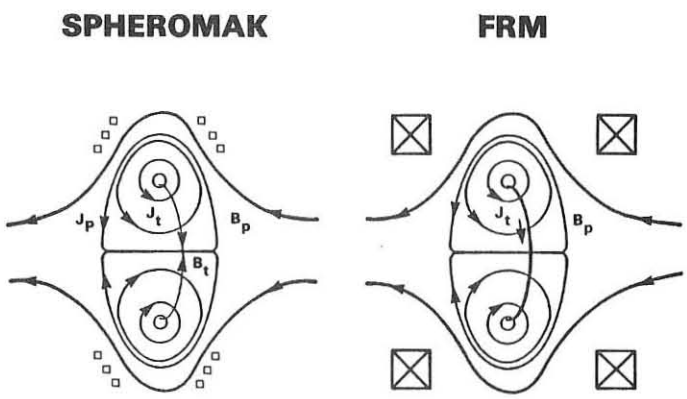

FIGURE 7

KNOWLEDGE GAINED FROM ETF IS APPLICABLE TO ADVANCEMENT OF ANY CONFINEMENT CONCEPT

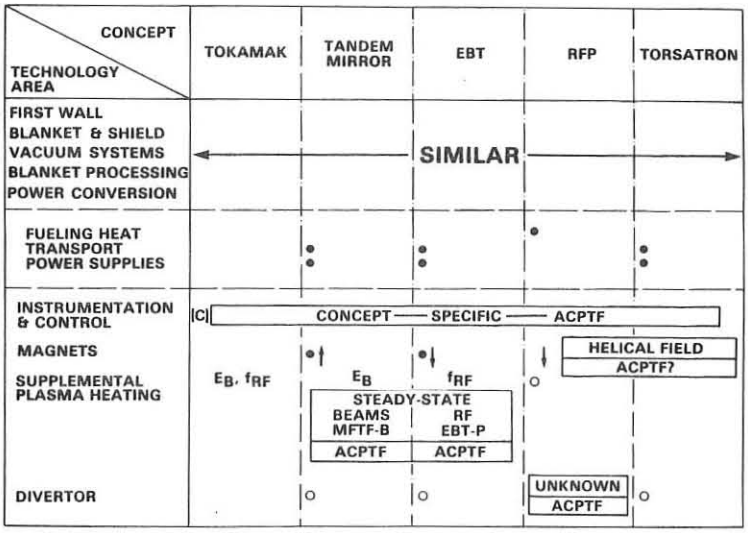

FIGURE 8

AFTER ETF, NEXT MAJOR FUSION PROGRAM DECISION IS OVERALL ASSESSMENT

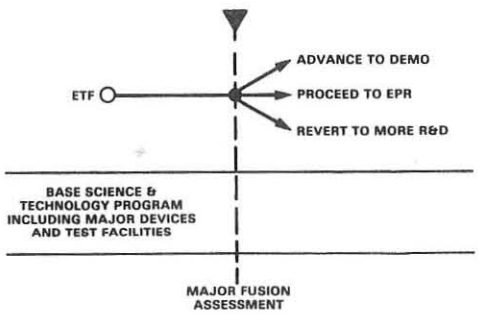

FIGURE 9

ALTERNATE CONCEPT DEVELOPMENT PARALLELS ETF LEADING TO EPR/DEMO DECISION

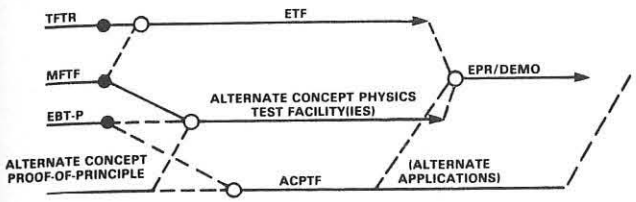

PHYSICS TEST FACILITY IS CONCEPT SPECIFIC

FIGURE 10

EACH MAJOR FACILITY STEP IS CHARACTERIZED BY FIVE PHASES OF VARYING TIME DURATION

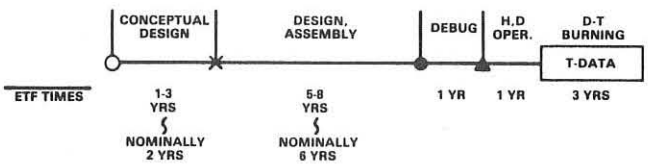

ASSUMING PROGRAM WORKS TOWARD SOLUTION OF NON-TECHNICAL PROBLEMS IN PARALLEL(SITE, CONTRACTOR SELECTIONS & FISCAL, ADMINISTRATIVE REQUIREMENTS)

FIGURE 11

THREE DIFFERENT PACES ARE DISTINGUISHED BY INFORMATION FLOW

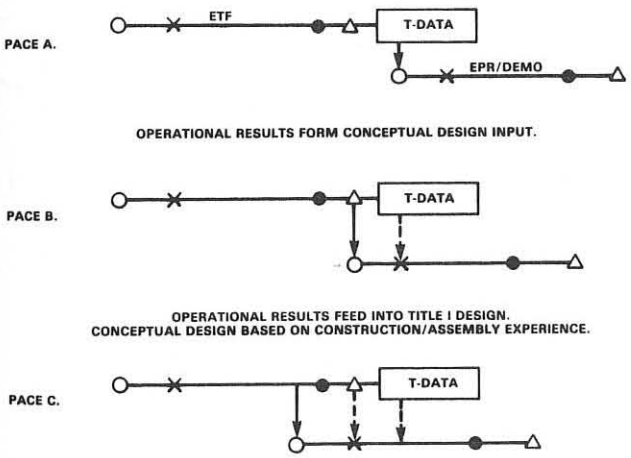

OPERATIONAL RESULTS FORM CONCEPTUAL DESIGN INPUT.

OPERATIONAL RESULTS FEED INTO TITLE I DESIGN.
CONCEPTUAL DESIGN BASED ON CONSTRUCTION/ASSEMBLY EXPERIENCE.

OPERATIONAL RESULTS CONFIRM DESIGN CHOICES AND TRIGGER DETAILED DESIGN AND FABRICATION.
CONCEPTUAL DESIGN BASED ON CONSTRUCTION EXPERIENCE.

FIGURE 12

THE THREE PLANNING CASES COVER A WIDE RANGE OF POSSIBLE PATHS

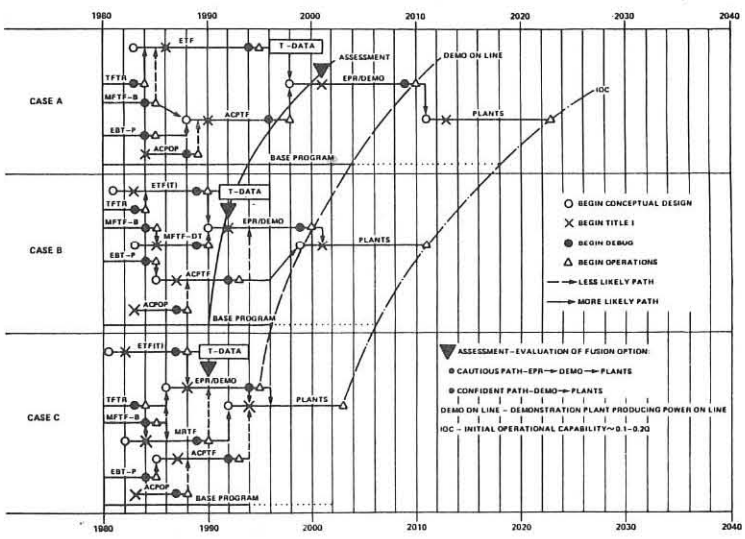

in 9th Europ.Conf.on Controlled Fusion and Plasma Physics, Invited Papers; UKAEA Culham Lab., Abingdon, Oxon, 1979, p. 211

Disruption Investigations at the Institute of Plasmaphysics Garching

Gerhart v. Gierke
Max-Planck-Institut für Plasmaphysik
D-8046 Garching, IPP-EURATOM Association

Introduction: The investigation of the current disruption played an important role from the beginning of the tokamak research. The main features of the external disruption have already been reported by our Russian collegues in the early tokamak publications. At this time the disruption was observed and investigated mainly by electric and magnetic measurements like $\dot{I}$, I, the loop voltage and the signals of distributed B_Θ coils for mode analysis. In the following years many sophisticated diagnostic tools have been developed and nowadays the full spectra of diagnostics contribute to our knowledge. The development of surface barrier diodes for measuring the soft X-rays, turned out to be especially informative as they gave insight into the behaviour of the plasma interior. A lot of work - all over the world - has been put into the measuring of the current distribution. Unfortunately all these methods have not been developed to a state that guarantees the accuracy we need for the understanding of the current disruption. The use of resonant helical fields at the Pulsator gave the first experimental hints of the important role of island formation and profile shape for the development of the disruption 1).

Whereas the Pulsator has already a long tradition in the field of current disruption it turned out during the last year that the Wendelstein WVII A is an extremely useful experiment for such investigation - paradoxly enough just because the disruption can be avoided by the Stellarator field.
Discharge conditions, usually not accessible in a pure tokamak, are accessible by this means. Both experiments gave new insights into current disruption during the past year.

The different types of disruptions and the new findings at Garching shall be discussed in the order of importance for the tokamak discharge.

Internal disruptions: Garching did not contribute to the knowledge of the hollow current disruption. Such a disruption seems to be no danger for the tokamak discharge. It rather helps to establish a sound current profile. Some authors report that such a discharge is later on stronger endangered for following disruptions than others. But this may also be caused by impurities present from the very beginning and not as a consequence of the disruption.

To the understanding of the internal disruption Pulsator contributed the knowledge during the last years that the hard X-rays are modulated by the sawteeth. The investigation, how the runaways responsible for the hard X-ray burst, manage to leave the confinement region lead via the calculation of the drift orbits to a possible explanation of the high density limit of Pulsator which is characterized by a hard disruption 2). This will be discussed later on.

At Innsbruck 3) Pulsator reported on the observation of accumulation of impurities in later stages of the discharge. These results can now be affirmed by a refined diagnostic 4) 5). This prove of inward diffusion of high Z impurities as it is predicted by the neoclassical theory has directly nothing to do with the subject of this talk. The observation and explanation connected with this experiment justifies however, the mentioning of it here.

The observation is that the accumulation of impurities starts slowly but that with increasing density and disappearing of the sawteeth the increase of the accumulation becomes steeper and steeper till the discharge is terminated by an external disruption (Fig.1). A possible explanation is that in a normal tokamak discharge the neoclassical inward diffusion is much smaller than the anomalous outward diffusion which is independant from Z. In the inner part of the discharge the sawteeth are also responsible for a very effective convection and therefore mixing of species. With increasing density the ratio of the diffusion coefficients alters till the neoclassical contribution starts to win. But now the sawtooth oscillation is stopped as a result of the increase of high Z material and the increase of resistance in the interior of the discharge, the current profile broadened and q_o prevented from dropping below 1.

There remains no driving mechanism for internal disruptions. And now the high Z material can diffuse inward unhindered. Thus we have here not only the proof of neoclassical inward diffusion but also the proof that by altering the resistance we can influence the current profile and prevent the internal disruption. Naturally by broadening the profile the edges are steepened and an external disruption is caused in due course.
The critical density above which the accumulation occurs is dependant on the density increase. The density increase is achieved by neutral gas inflow which alters also the current profile. A peaked current profile responds by an increased sawtooth activity so that a higher density is necessary to overcome the anomalous diffusion.

In the light of these findings we have to consider the non-neoclassical behaviour of the transport and the sawteeth oscillations as a windfall which - by preventing the accumulation of high Z impurities - enables the development and the sustaining of the normal tokamak discharge.

Main disruption: The most dangerous disruption is the main disruption. It is now the more or less general opinion that the m=2, n=1 tearing mode is mainly responsible for the development of this instability but that another helicity is needed in addition to trigger the instability (usually 3/2). This mode is numerically always observed when the gradient of the current distribution is steep enough. As an example some results of the numerical three dimensional calculation by D.Biskamp 6) are shown. Fig.2 demonstrates the dependence of the calculated fictive island width as it is growing with time (measured in poloidal Alfén times, S = magnetic Reynolds number). One observes that the 2/1 island is growing linearly with time but that the growth of the 3/2 island, after an initial linear increase, is accellerated considerably. This happens when the two islands are touching each other as it can be seen in Fig.3 of the magnetic surfaces where in a short time a strong ergodization takes place which eventually fills the whole confinement region.

Such calculations with similar results have also been done at Oak Ridge. The calculations including viscosity, finite resistance etc. are extended now to finite β_{pol} to see whether the later on mentioned β_{pol} effect can be observed.

Though in Wendelstein VII A not much experimental time has been devoted to investigations connected with disruptions,a rather informative picture of the tearing mode activity and its dependence on different parameters can already be drawn 7) 8) 9)
For low external rotational transform, t_o, the ohmically heated Stellarator behaves like a tokamak. Differences come up at higher t_o. To first order the q value of such a discharge is given by

$$q = \frac{1}{t} = \frac{1}{t_o + t_{pl}}$$

. As t_o in WVII A is approximately independent on r the q profiles are qualitatively similar to tokamak profiles.
The dependence of the observed modes on the q value at the effective limiter radius q (a) is shown in Fig.4 at higher rotational transform t_o = 0.11. Fig.5 shows the dependence at fixed value q (a), t_o = 0.14 on the plasma density. The behaviour of the main mode 2/1 can be understood qualitatively by looking on Fig.6 which shows the different current density profiles (profile 5 which was measured with He + O 2% Ne, is equivalent to a profile in pure He with $n_{eo} = 8.5\ 10^{13}\ cm^{-3}$). The radius of the q=2 surface stays almost constant, but the gradient of the current density near to this surface changes considerably. Fig. 7 shows now a comparison of the experiments with numerical calculations of the 2/1 tearing mode saturation amplitude. The current profile is calculated from temperature profile assuming proportionality to $T_e^{3/2}$. The measured temperature profile is fitted by

$$T_e(r) = T_e(0)\ \frac{1}{1 + \left(\frac{r}{r_o}\right)^{2\alpha}}$$

r_o defines the width and depends mainly on I_p, α is a measure for the steepness and depends mainly on n_e. The saturation width of the tearing mode island is calculated in the usual way 10) 11) termining thereby also the amplitude of the perturbation field.

Though this procedure is only approximative and one-dimensional, the calculations are in good agreement with the experimental results. It has been reported earlier that an increasing external rotational transform t_o decreases the relative amplitude of the 2/1 mode. But as the numerical comparison and Fig.8 show, this can be explained without assuming a direct stabilizing effect of the Stellarator fields. The observed influence is mainly due to the changed current density profile in the neighbourhood of the q=2 surface on the 2/1 mode.

In W VII A the density limit due to disruption is a strong function of t_o as shown in FIG.9. At low t_o it is fixed by the Murakami-limit well established for ohmically heated tokamaks. The mode behaviour is described by the already mentioned Fig.4. Though the numerous observations can not easily be brought into one picture, the 2/1 mode and its dependence on t_o and n_e as described earlier could be made responsible for the disruptions. In the higher regime only the 3/2 mode with small amplitude is observed. Whether this mode, stationary 2/1 islands or some other not well identified and rapidly growing modes are responsible for the disruption is still unclear.

It can be shown that the Stellarator field has a stabilizing effect on the equilibrium position of the current column. Due to the large aspect ratio already a very small rotational transform ($t_o \sim$ 0.003 ... 0.004) has in W VII A the same positioning effect as the usual inhomogeneous vertical field in a tokamak. At normal operating values the discharge is therefore much better stabilized against perturbations of the temperature profile or loss of internal inductance or β_{pol} than a tokamak. Therefore it is quite plausible that changes in these parameters in a tokamak may cause a complete loss of the equilibrium and consequently of the current, whereas in the Stellarator only a soft disruption occurs after which the discharge recovers and the original values may be obtained if sufficient energy resources are made available. Such minor disruptions are frequently observed. It therefore seems possible that also in a tokamak the difference between soft and hard disruptions is only quantitatively and depends on whether the equilibrium is completely lost or can be reestablished.

In Pulsator various conditions have been identified which lead to a current disruption 12). Here practically in all cases a growing 2/1 mode is preceeding the disruption. But a detailed analysis shows that the different cases have quite different reproducible features which can be classified according to growth rate, frequency, change in frequency, poloidal symmetry and radial extent. The final evolution of the gross instability is very similar in all cases observed, it will however, be quite difficult to identify and classify the upcoming instability in time in order to find the proper remedy.
The question arises whether one single feedback system would be sufficient to stabilize the different disruptions. An attempt was made to change the current density profile with superimposed a.c. currents (with 1oo to 2ooo Hz) 13) 14). Though the calculations show an effective heating of the edges and drastically changed profiles no such effects could be observed. It is surprising that the medium-sized current oszillation ($\leq$ 2o %) have no effect on discharges as long as they are far from the critical values (q, n_e). Large amplitudes up to 8o % show growing m=2 modes and lead to disruptions. The already mentioned tearing mode calculations show that with small amplitudes the Δ' varies sinusoidally around the d.c.value but that with large amplitudes the average over an a.c.period is increased strongly above the d.c.value. The calculation shows also that the large a.c. modulation alters the distance between the 2/1 and 3/2 islands. It was therefore tried to influence the stability behaviour by sawtooth modulation with different sign. Though qualitatively the observed 2/1 mode showed the expected differences in the two different cases, the expected improvement of the gross stability could not be obtained.

The disruptions mentioned so far can all be at least qualitatively understood by the tearing mode theory with usually 2/1 mode as the initiating effect. But the surprising sharp high density limit ($\overline{n_e} = 1.15 \cdot 1o^{2o}\ m^{-3}$) in Pulsator is difficult to explain. The β_{pol} values at the density limit varied for different discharge parameters in such a way that $\beta_{pol/qa}$=const.=0.36 was found with an accuracy better than 1o %.
Many of the observed features as the increasing and saturating 2/1 mode, the starting of the disruption after the sawtooth has

broadened the profile, corresponds with the tearing mode picture. However, the sharp limit is asking for an explanation 15). It has been reported already at Innsbruck that with increasing β_{pol} the compression of the magnetic surfaces at the outside of the torus produces a deformation of the magnetic islands which supports the ergodization of the field lines. This effect can be simulated with the help of the m = 2/n = 1 helical windings on the Pulsator. Fig. 10 shows the calculated magnetic surfaces at different β_{pol}, which shows the sudden ergodization between $1.5 < \beta_{pol} < 1.6$. Preliminary experiments 16) confirm these findings with the helical fields disruptions are triggered at various densities. The critical helical current decreases with increasing density. The absolute values coincide fairly well with the calculated ones. It therefore seems plausible that also for the high density limit a sudden ergodization due to the increasing β_{pol} is responsible. Also the observed increasing runaway losses before the disruption can easily be explained by an increased ergodization.

Finally I would like to show a new diagnostic tool which is extremely useful for the investigation of fast events like disruptions 17). The University of Stuttgart developed a Ruby-Laser Amplifier System which delivers about 25 equidistant pulses of MW peak power during one flash lamp discharge. Fig.11 and 12 show the first application on Pulsator during a disruption where the normally used ruby laser was replaced by such a spiking laser.

Conclusion: Though there was much progress made in the understanding of the disruption phenomena during the last years we are far from the goal. Nearly every parameter which we would like to improve (q, energy content, ß, confinement) seems to bear danger for the stability of the discharge. Only little experience is available on non-circular cross-section which allow larger plasma currents to be used at given q_α but where the tendency towards the mode coupling should increase and thus the ergodization may become worse. No reliable method for accurate profile shaping has been proven yet experimentally. No reliable stabilization or feedback scheme has been demonstrated. One hope, though very little, is that stability will improve in the collisionless regime we are approaching now. However, the larger machines which will confine

such plasmas will have difficulties to investigate disruptions thoroughly, because due to the large energy content only occasional disruptions can be tolerated. Therefore we have to make use of the present-day machines as much as possible to perform experiments for the investigation and the control of the disruption.

References:

1) Karger, F., Proc. of 5th Int.Conference on Plasma Physics and Contr. Nuclear Fus. Res., Tokyo (1974) I, 179

2) Fußmann, G., Proc. of 7th Conf. on Plasma Physics and Contr. Nuclear Fusion Research, Innsbruck (1978) IAEA-CN-37/T-4

3) Engelhardt W., et al., 7th Conf. on Plasma Physics and Contr. Nucl. Fusion Research, Innsbruck (1978), IAEA-CN-37/A-5

4) W.Engelhardt, O.Klüber et al., Proc. of Symposium on Disruptive Instabilities in Toroidal Devices, Garching (1979), A6

5) W.Engelhardt, S.Sesnic et al., 9th Europ.Conf. on Contr. Fus. and Plasma Physics, Oxford (1979) Contributed Papers D2.1

6) D.Biskamp, Proc. of Symposium on Disruptive Instabilities in Toroidal Devices, Garching (1979) A2

7) W VII A Team, Proc. of Symposium on Disruptive Instabilities in Toroidal Devices, Garching (1979) D6

8) W VII A Team. Proc. of Symposium on Disruptive Instabilities in Toroidal Devices, Garching (1979) D7

9) W VII A Team, 9th Europ. Conf. on Contr.Fus. and Plasma Physics, Oxford (1979) Contributed Papers BP23

1o) Rutherford, P.H., Phys.Fluids 16 (1973) 19o3

11) Callen, J.D., et al., Proc.7th Int.Conf. Innsbruck (1978) 1, IAEA, Vienna (1979) 415

12) Pulsator Team, Meeting of the Americ.Physic.Society, Boston (1979)

13) S.v.Goeler, J.Gernhardt, W.Engelhardt,et al., Proc. of Symposium on Disruptive Instabilities in Toroidal Devices, Garching (1979) A5

14) S.v.Goeler, J.Gernhardt, W.Engelhardt, et al., 9th Europ.Conf. on Contr.Fus. and Plasma Physics, Oxford (1979)Contributed Papers EP6

15) G.Fußmann and H.Zehrfeld, Proc. of Symposium on Disruptive Instabilities in Toroidal Devices, Garching(1979) B4

16) G.Fußmann, et al., 9th Europ.Conf. on Contr.Fus. and Plasma Physics, Oxford (1979) Contributed Papers EP5

17) R.Behn, H.Röhr, K.H.Steuer and D.Meisel, "Thomson Scattering from a Tokamak Plasma with a Repetitively Q-Switched Ruby-Laser" to be published

Figure Captions

FIG. 1 Two nearly identical shots of Pulsator showing the sharp increase of the X-ray signal after the saw-teeth oszillation has stopped (a)

FIG. 2 Numerically calculated "fictive" islands with vs time. Note the sharp non-linear increase of W32

FIG. 3 Calculated magnetic surfaces at different times. The fast ergodization takes place if the 2/1 and 3/2 islands are overlapping

FIG. 4 Mode behaviour (amplitude, frequency) in W VII A vs plasma current resp. q_a. In the upper picture the density and confinement time dependence is shown.

FIG. 5 The same as FIG. 4 vs density

FIG. 6 Current profile in W VII A at different densities. The radius of the q=2 surface is nearly independent of density

FIG. 7 Comparison of a rough tearing mode calculation with experiment (W VII A)

FIG. 8 W VII A discharges with similar $n_e(r)$ and $j(r)$ but different t_o

FIG. 9 Disruption limit in W VII A

FIG. 1o Calculated magnetic surfaces for Pulsator with superimposed helical 2/1 field with different β_{pol}

FIG. 11 Measured signals of the spiking Ruby-Laser system during a disruption in Pulsator

FIG. 12 Evaluation of the spiking Ruby-Laser signals during a disruption

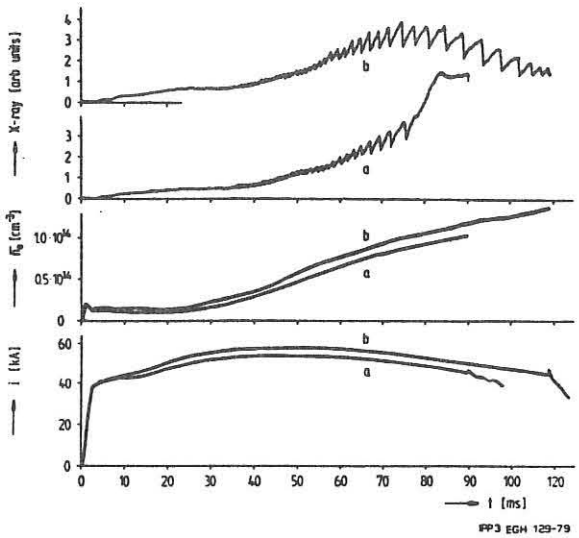

FIG. 1

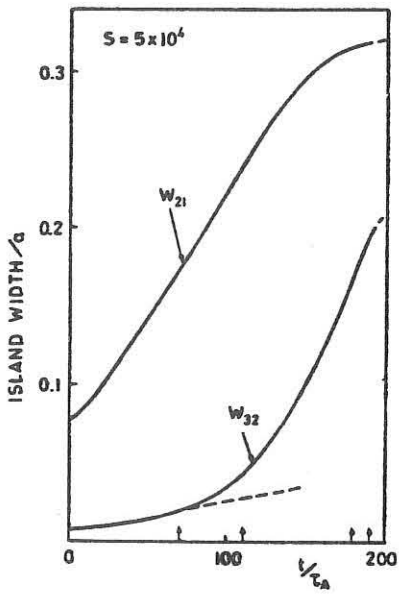

FIG. 2

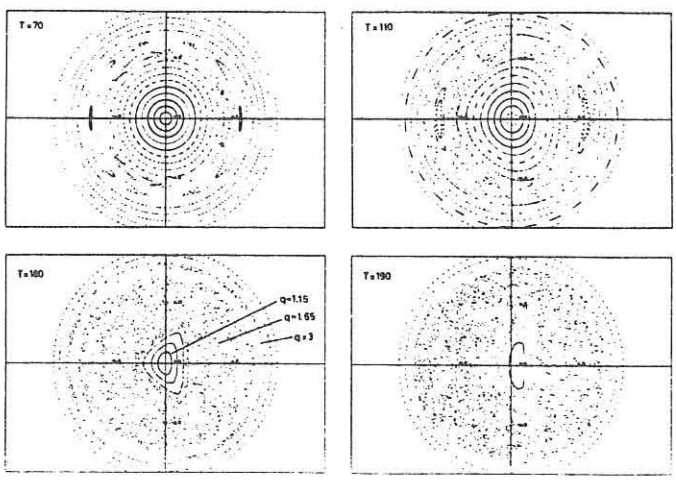

FIG. 3

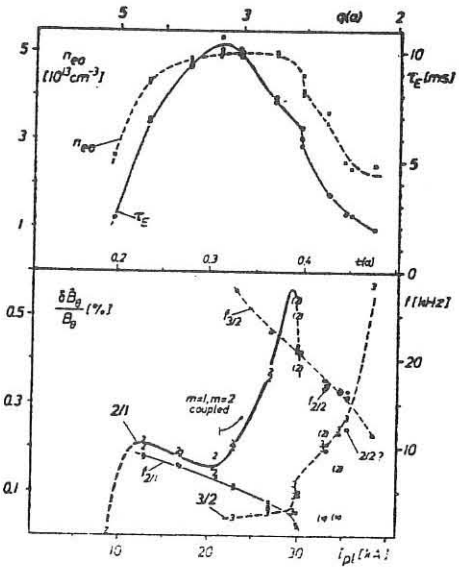

12.4.78: B_o = 3.5 T, ϵ_o = 0.11, HELIUM

FIG.4

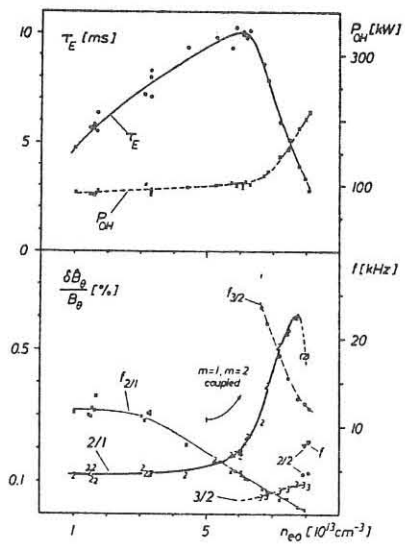

14.6.78: B_o = 3.5 T, ϵ_o = 0.14, I_{pl} = 20 kA, q(a) = 2.9, He

FIG. 5

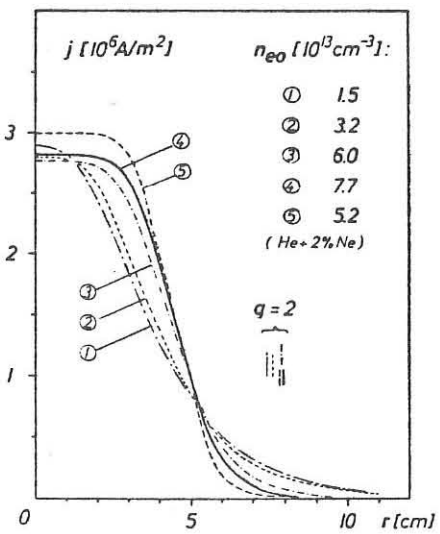

B_o = 3.5T, ϵ_o = 0.14, I_{pl} = 20 kA, q(a) = 2.9, He

FIG.6

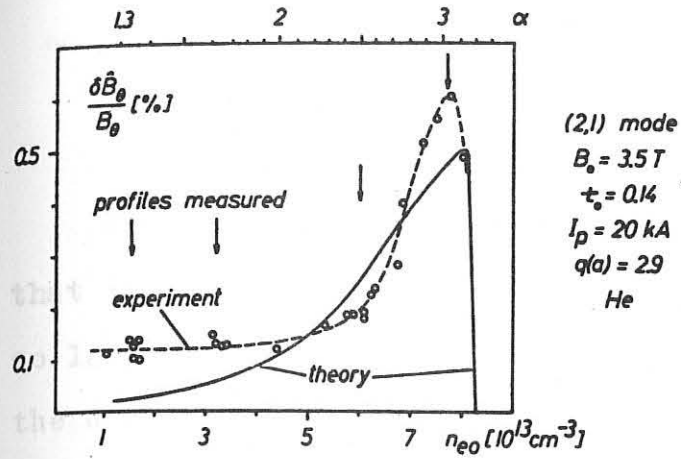

FIG. 7

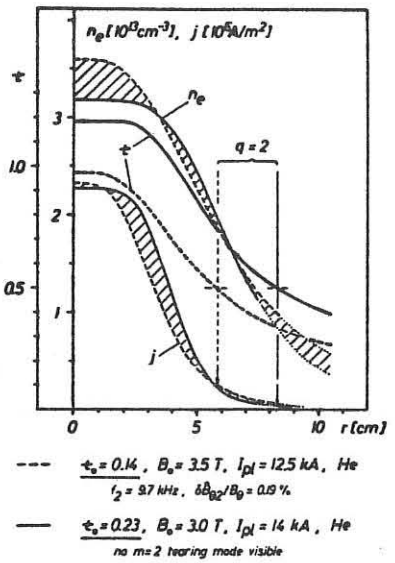

discharges with similar $n_e(r)$ and $j(r)$, but different ε_o

FIG. 8

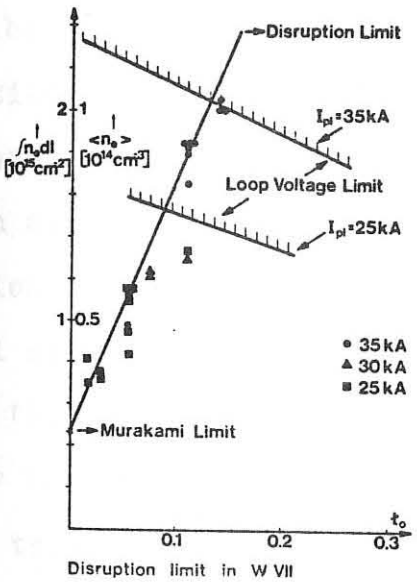

FIG. 9

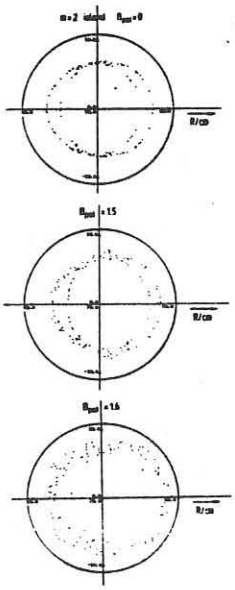

FIG. 10

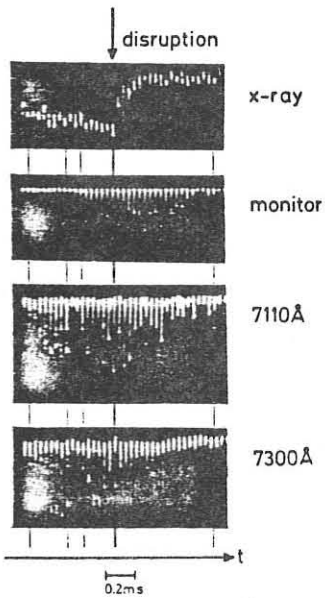

FIG. 11

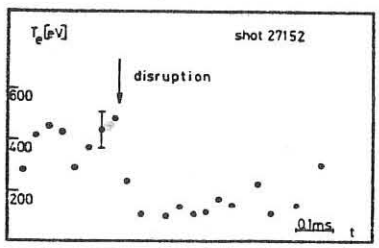

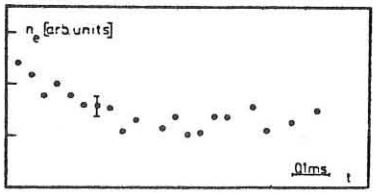

FIG. 12

PRESENT STATE OF STELLARATOR RESEARCH

By
G.S. Voronov and M.S. Rabinovich
P.N. Lebedev Physical Institute Moscow USSR.

The scale and rate of the stellarator research is not so high now, that is why the volume of information, obtained for the last year, is not so large. However, during this year there was continued working out of the data obtained, finding out the role of the stellarator programme in creating a future reactor, and picking out the most important problems requiring urgent solution. We must note that the stellarator programme cannot be treated in isolation from tokamak research. We must direct our attention not on comparing which of the systems is the best one but on an understanding of the deep similarity of plasma containment physics in both systems. But the difference between these systems yields much information about the physics of plasma containment in toroidal systems as well as about the development of various types of tokamaks, stellarators and their hybrids. It is not reasonable to neglect the large and valuable information obtained on tokamaks in stellarator research, and in the tokamak programme some important results obtained on stellarators must be taken into account. First of all, we must note the possibility to overcome the disruption instability, the problems of the initial stage of a discharge, a magnetic limiter, and divertors. We are going to discuss these questions below.

In the introduction we would like to treat some general questions. The stellarator programme may have different purposes. The most ambitious one is the creation of a thermonuclear reactor on the basis of a stellarator. But due to the similarity of the physics of tokamaks and stellarators, which we have mentioned above, there are possible some other programmes, which are less ambitious. On the one hand, we may study how to improve tokamaks and divertors by using helical windings and on the other hand, we may use stellarators to understand deeply the physics of toroidal containment. Our opinion is that all these three

directions should exist. But we must carefully define our problems in projecting and research on the devices in order not to draw groundless conclusions. When we are concerned with tokamaks, the system is well defined in practice. Some improvements of tokamaks don't change the system itself; when you construct a tokamak you may be sure of satisfactory results.

The term "stellarator" covers numerous very different devices. Sometimes they have new names: heliotron, torsatron etc. It is important to realise that among them there are bad as well as good systems. If you are going to construct stellarators with regard only to the main parameters: major and minor plasma radius, rotational transform angle, magnetic field, then there is a high probability of obtaining a "bad" system. It is necessary to calculate in advance such characteristics as banana and superbanana orbits, the mean minimum value for magnetic field, the the limiting current.

As for the reactor based on a stellarator, there are two problems: achievement of high β and superbanana diffusion and ion thermal conductivity. Our opinion is that it is possible to achieve sufficient values of β and thermal conductivity. For this purpose it is necessary to have systems with a mean minimum magnetic field and, possibly, a three dimensional magnetic axis. Thus the stellarator may be used for a future reactor, its merits and demerits will mainly lie in the solution of technical and engineering problems.

In the meanwhile, the stellarator programme is not directed toward the construction of a reactor, the stellarator-reactor programme is only just beginning to develop. The main emphasis of the operating devices are directed on the studying of the physics of toroidal plasma containment. A large volume of information has been obtained on the physics of current carrying plasma containment in a modern stellarator. Of course, a large amount of important data was obtained from the

stellarators of the previous generation. We must mention the work on the currentless plasma production by ion cyclotron heating on the Uragan I in 1973 [15]. The main conclusion of this work is that the ion loss channel in a currentless stellarator is classical. But now we are going to discuss the transition to the modern plasma parameters in the temperature range of 1 keV and densities up to 10^{14} cm^{-3}. Unfortunately, only the first steps have been done in this direction on the Cleo and the w-vii A. In the near future we expect new results from the L-2, Urugan 2, and later from the Urugan -III devices. But in the meantime we are forced to turn our attention to the ohmically heated plasma. We may study the nature of the energy losses ouer electron and ion channels, the problem of the disruptive instability, magnetic limiter, and the nature of plasma losses in a stellarator. The main data are obtained for the plato regime but there are also some data on the bananan regime and stabilisation of the banana diffusion in "Vint-20".

The present report has been based principally on the material presented at Innsbruck [5,6,7], Zvenigorod [10,11,16], on papers presented at this conference [17-26], on working meetings at Zdikov [13] and Inssbruck [14] and on several earlier publications [1-4, 8, 9, 12, 15, 27, 28]. In the preparation of this report very useful discussions were held with practically everyone working in the stellarator programme,and with their associates and rivals. Especially valuable were the discussions with H.G. Wobig, G. Grieger, G. Runner, S. Shohet, D. Lees, I.S. Spigel, I.M. Kovrizhnykh, I.S. Danilkin, S.E. Grebenshzhikov,

- 4 -

O.I.Fedyanin, V.D.Shafranov, V.T.Tolok, V.A.Suprunenko.

There are 13 stellarators operating in the work: five in the USSR, two in West Germany, one in France, one in England, two in Japan, and one in the USA. We know of another four large projected stellarators.

Table one gives the parameters of three largest stellarators

Table of stellarators

		Cleo	L-2	W-VIIA
1. Major radius	Rcm	90	100	200
2. Minor radius of vessel	r cm	14	17.5	17
3. Mean plasma radius	a cm	10	11.5	9
4. Rotational transform on the axis	t(o)	0	0.28	0.23
5. Rotational transform at the edge	t(a)	0.6	0.78	0.23
6. Shear	θ	0.42	0.42	0
7. Toroidal field	B	20	20	35
8. Poloidal (vacuum) field	B_p	1.3	1.6	0.35
9. Equivalent current	I_{eq}	46-66	55-92	8-16
10. Discharge current	I	8-25	12-20	13-35
11. Ohmic-heating power	P_{oh}	60	25-30	350
12. Flux	Φ vsec	0.8	0.2	2.2
13. Mean plasma density	n_e $10^{13}cm^{-3}$	0.3-6	0.5-3.5	1-10
14. Energy lifetime	τ_E msec	10	12	12
15. Limiter radius	r_i	13	absent	13.5
16. Electron temperature	T_e ev	100-1000	200-600	200-700
17. Ion temperature	T_i ev	80-300	90-150	100-300

§ 1. Magnetic field structure

One of the most important characteristics of the stellarator in comparison with the tokamak is the possibility to vary widely the magnetic field structure. Figure I shows the rotational transform of magnetic lines of force in vacuum versus radius for the four largest stellarators, operating now: Wendelstein VIIA (West Germany), Cleo (England), L-2 (USSR) and Heliotron-D (Japan). The field structure of the Wendelstein VIIA is practically without shear, and cleo, L-2 and Heliotron-D have rather large shear.

In Cleo, the rotational transform at the centre is zero, in W-IIIA and L-2 $t(0) \sim 0.2$, in Heliotron-D $t(0) = 0.5$. The difference between the values of $t(a)$ at the edge is especially strong: $t(a) = 0.23$ for w-vii A, 0.6-0.8 for Cleo and L-2, and $t(a) = 1.5$ for Heliotron-D.

All these differences in the vacuum magnetic field structure will play an important role in the experiments with currentless plasmas. But at present, these experiments have only just begun. In the meantime, the main data on plasma containment in stellarators was obtained in the ohmic heating regime.

In this case, a poloidal current field being added to a poloidal stellarator field change substantially the field structure. In order, to characterize a field in the current regime it is convenient to introduce the rotational transform angle $t_\Sigma = t_{st} + t_p$ and the reciprocal to it value of the effective safety factor:

$$q = 1/t_\Sigma$$

As in the W-VIIA stellarator $t_{st} = \text{Const}$, the $t_\Sigma(r)$ profile and, respectively, $q(r)$ remain qualitatively the same ones as in tokamaks 28.

The region with $q = 1$ is at the centre and the point $q = 2$ ($\iota_2 = 0.5$) is at the edge or is absent. (Fig.2).

The stellarators with a large shear, where ι_{st} vary strongly with r, may have very different magnetic field structure. It depends strongly on the radial current distribution and on the value of relative contribution of the current rotational angle ι_p, which is proportional to γ/β. Fig. 3 show a set of strongly differing current distributions. Figs 4,5 show the dependence for these current distributions in the Cleo and L-2 stellarators for different values of the parameter γ/β. One may see that the field structure differs qualitatively from that one in tokamak. At low currents $q = 2$ is reached within the plasma column, but q decreases closer to the edge of the plasma. With increasing the current, the dependence becomes complicated and nonmonotonic. Depending on the current distribution $q = 1$ may be reached close to the centre of the plasma column, at the edge of the plasma or in both these points simultaneously.

§ 2. Electron thermal conductivity

In stellarators electron thermal conductivity remains anomalous as in tokamaks i.e. it exceeds neoclassical value.

A study of the dependence of τ_E on the current [5,6,7] showed that it depends strongly on the drift parameter

$$\xi = \frac{u_e}{v_{Te}} \sim \frac{J}{n_e\sqrt{T_e}} \qquad (I)$$

where J is the curent density (Fig.6).

Fig.6 show that with increasing the current, thermal isolation in a plasma of the stellarator becomes worse after some critical value. However, the dependence on the drift parameter is

not important for tokamaks as the value:

$$\xi = 5.3\,10^{-4}\,\frac{B_{KG}}{n_e/10^{14}\sqrt{T_{e\,kev}}\,q} \qquad (2)$$

is low enough for the plasma of a reactor.

If we assume the linear dependence

$$\chi_e = Const\cdot\xi = Const\cdot\frac{J(r)}{r^2 n_e\sqrt{T_e}} \qquad (3)$$

from an electron energy balance and neglect radiational losses and ion heating then we obtain the following formula for the maximum electron temperature:

$$T_{e\,max} = Const\cdot J\sqrt{Z_{ef}\,q_a(q_a-1)} \qquad (4)$$

This formula has been derived by G.E.Guest et al [27] for tokamaks assuming $q_a \leq 4$. It is supposed that current density at the centre is limited by the condition: $q = 1$

$$J_{max} = \frac{5B}{\pi R} \qquad (5)$$

In the case of a stellarator with the rotational transform at the centre not equal to zero $t(0) = t_o$

$$J_{max} = \frac{5B}{\pi R}(1-t_o) \qquad (6)$$

and for $T_{e\,max}$ we obtain

$$T_{e\,max} = Const\cdot\sqrt{a^2 Z_{ef}\frac{B}{R}(1-t_o)} \qquad (7)$$

This dependence was verified according to the data of the Wendelstein VII A stellarator [28] (Fig.7). There is also shown the point which is tipical for the L-2 stellarator regime.

However, from satisfying this scaling law as well as any other scaling law for χ_e it does not follows that radial dependence is: $\chi_e(r) = Const\cdot\frac{J(r)}{r^2 n_e(r)\sqrt{T_e(r)}}$

As in the case when ohmic heating makes the main contribution to plasma confinement and heating (this case takes place in the Wendelstein VII A experiments), the scaling law may be determined with an accuracy up to the arbitrary function of the combination of the following parameters: plasma current, density, temperature etc. That was studied in details in report of Dr.Mukhovatov at the Zvenigorod Conference [16].

In order to "separate the variables" in the scaling law it would be very valuable to make corresponding measurements for the Cleo and the L-2 stellarators where the current makes contribution only in the plasma heating and the confinement is mainly due to a poloidal field of a stellarator.

The dependence, $\chi_e(r)$ calculated from the experimentally measured electron temperature profiles, has a complicated nonmonotonous nature. Figures 8 and 9 show Te profiles for the Wendelstein VII A and L-2 stellarators. In the case W-VIIA the data are obtained by means of laser scattering, for the L-2 there also used the data of Te measurements over soft X-ray radiation and spectroscopy.

The particularity of the Te profiles is that they are flat at the centre. The calculation of $\tau_E(r)$ assuming Z_{eff} = Const and allowing for the trapped particle contribution in the decrease of conductivity, show that this flat part corresponds to the region, limited by $q = 1$. This conclusion is also verified by measurements of the sawtooth oscillation profile.

At the edge of the plasma, the electron temperature is rather low in the relatively large region. It is, apparently, due to the radiational cooling by the radiation of light oxygen and carbon impurities.

§ 3. Ion thermal conductivity

The measured values of the ion temperature for stellarators [2,3,4] are lower than those predicted by the Artsimovich formula according to neoclassical theory if $\mathcal{J}_p$ is the sum of the plasma current and the "effective" current producing a poloidal field identical to a stellarator one.

$$T_i = \frac{5.9\cdot 10^{-7}}{\sqrt{A}} \left(\mathcal{J}_p B R \overline{n}_e\right)^{1/3}; \quad \mathcal{J}_p = \mathcal{J} + \mathcal{J}_{eq} \qquad \text{(Fig.10)}$$

With increasing ion temperature the relative deviation of T_i from the Artsimovich formula decreases (see Fig.11).

So far we refer to the ion temperature of a hydrogen plasma. The data W-VIIA show that in the case of helium the T_i values lie above the Artsimovich temperature curve. However, it is well known that the Artsimovich formula does not give the correct dependence of T_i on A also in the case of tokamaks.

Excess heat losses of ions at the low ion temperature in stellarators may be associated with the flat temperature and density profiles which are natural for stellarators. It is possible that the excess heat transport is due to the large temperature gradients and is not associated with the large thermal conductivity. An attempt to recalculate the ion heat transport, taking into account the actual temperature distributions, was made by Dr Wobig for the Wendelstein VIIA (see Fig.12). We may see that with increasing T_i the ratio χ_i/χ_{Ncl} really goes to 1.

In 1973 it was shown on the "Uragan" stellarator [15] that in a currentless plasma with hot ions (T_i = 500 ev, $T_e \sim 50$ ev,) when ion losses dominate, the ion thermal conductivity is close to the neoclassical one.

§ 4. Sawtooth oscillations

Sawtooth oscillations of the soft X-ray radiation intensity were observed in the W-VII A and L-2 [18] stellarators. Fig. 13 show typical oscillations in L-2. The points, where the phase change its sign lie 4.5 cm upper and 3 cm lower the axis. The cause of this asymmetry is unclear. In the W-VII A stellarator the oscillation distributions were taken off along the horisontal axis. The phase-change point lie in the distance of 6.5 cm from the axis. With the increasing current the phase - change point moves closer to the edge of the plasma (see Figs 14 and 15).

The phase-change point in W-VII A corresponds to the $q = 1$, calculated on the assumption that $Z_{ef} = \text{Const}$ from the experimentally measured current distributions (Fig. 15).

In the case of the L-2 stellarator the situation is more complicate. The experimentally measured electron temperature profile's rather flat (see Fig.9). But the displacement of the phase-change point towards the plasma edge with the current increasing (see Fig.14) show that the current distribution is peaked. But if we take into account the decrease in thermal conductivity due to the trapped electrons, than the current profil will be really peaked. In this case, the $t_z(r)$ dependence is not monotoneous (See Fig.16). The $q=1$ point is almost in the required place and moves toward the edge with the increase in current.

But we must take into account that this calculation was made on the assumption of $Z_{ef} = \text{Const}$ and we don't know the real distribution of $Z_{ef}(r)$.

§ 5. Increase in plasma density

In the Cleo, W-VIIA and L-2 stellarators the study of the increase in density by gas puffing during the discharge, was carried out (5, 6, 17) Figure 20 shows plasma density versus time at the pulse gas puffing during the discharge. We may see that the density increases almost linearly with time. The maximum density which may be achieved is limited by the discharge duration. The rate of the density growth is $\sim 10^{15}$ sec^{-1}.

An almost identical rate is usual for the other stellarators. It exceeds the rate of the density growth for tokamaks at the same conditions (i.e. heating power and wall cleaning).

In tokamaks the maximum rate of the density growth is limited by the disruptive instability. The stability region is limited by the current density at $q = 1$ and by the q value at the edge of the plasma.

Fig. 17 shows the discharge stability region during the pulse gas puffing in the W-VIIA, Cleo and L-2 stellarators. In stellarators, the current density at the centre at $q = 1$ is proportional to

$$\frac{B}{R}(1-t_0)$$

At the small rotational transform angles $t_{st} \leq 0.14$ the stability region corresponds to this one in tokamaks. And at the edge of this region the disruption instabilities are observed.

When the rotation transform angle increases, $t_{st} > 0.14$, the disruption instabilities are not observed. In addition to that the stable regime, far over the stable region of tokamaks, may be obtained.

Max-Planck-Institut für Plasmaphysik
8046 Garching bei München

In this case, the maximum rate of the density growth, is limited by the available heating power. In the L-2 and Cleo the systematic study of the stability region was not conducted. In Fig. 17 there are shown the points which corresponds to the stable regimes with the maximum density.

With the density growth, the electron temperature decreases and the ion temperature practically does not change (Figs 18, 19). At the same time the energy containment of plasma increases and ohmic heating power almost does not increase (Fig. 20,21). The radiational losses notably increase especially at the periphery. Careful investigations of the energy lifetime dependence on the density were carried out on the W-VIIA stellarator (See Fig.22). At first τ_E increases with n_e .But when the rate of gas puffing is high, in order to obtain high density, a series of phenomena arise, which lead to the decrease in τ_E .

The power of impurity radiation from the edge of the plasma increases sharply. As a result, the current channel becomes narrow due to the cooling at the edge. The region with high thermal conductivity limited by the surface with $q = 1$ increases, and the region between $q = 1$ and the edge of the plasma where there are sharp gradients T_e becomes more narrow. As a result, the heating losses grow and τ_E decreases. In the case of ohmic heating, the maximum available density increases with current (see Fig. 22).

At present with the available power heating it might be obtained with the plasma density up to 10^{14} cm^{-3} in the W-VIIA,

$3.10^{13}cm^{-3}$, Cleo and $2.5.10^{13}cm^{-3}$ in the L-2.

The problem of increasing the plasma density is one of the most important problems in the stellarator programme. We expect that the progress in this direction may be achieved by using auxiliary heating methods.

§ 6. Collisionless region

As a thermonuclear reactor will operate at low collision frequencies then it is very important to study plasma behaviour in this condition. Unfortunately the present plasma parameters are not high enough to reach this region. For the majority of devices, the collision parameter corresponds to the plateau of the neoclassical curve.

Under these conditions, the experimental data may be obtained only from the model experiments with low temperature plasma, when the required collision frequency is achieved due to the low density.

Though it is not so easy to apply the results of such model experiments to the plasma with high density and temperature, but some results obtained in such experiments are very interesting.

In the "Vint-20" torsatron it became possible to go for into the banana region with collision parameter up to 3.0-50, by decreasing the plasma density up to $n_e \sim 10^9 cm^{-3}$.

At the same time the measurements of plasma lifetime showed that the transport coefficient exceeds neoclassical values and grows while going for into the banana region.

When the high frequency field is applied it becomes possible to decrease the transport rate in some times. Apparently,

this phenomenon is due to the transform of a large number of the trapped particles into the free ones by using high frequency field.

If it will be possible to apply this method of decreasing the trapped particles contribution into the transport coefficient, on the devices with high plasma parameters, than it would be of great importance for the construction of the reactor on the base of a stellarator and for the stellarator programme in general.

% 7. Nonohmic heating methods

The main contribution in information on plasma containment in stellarators is made by ohmic heating method. But this method (in contrast to that one in tokamaks) cannot be treated as the "natural" one. An use of this method in stellarators is forced and it may be treated as an artifitial one. The question of using a stellarator as the basis for a thermonuclear reactor depends on the results of a study of the currentless regime. In the last few years some progress for applying non ohmic heating methods in stellarators has been achieved: the experiments on plasma heating by neutral beam were started on the Cleo and W-VIIA stellarators, the research on HF-plasma heating are conducted in the Saturn and Vega stellarators.

In Cleo, in the first experiment on plasma heating by neutral beam with the energy of 24 keV, the power of 8 kW was contributed to a plasma. Its value was rather low in comparison with the ohmic heating power (60 kw) though the power contributed to ions (4 kw) was an essential part of the power coming from electrons to ions (15 kw). There was observed the increase in the ion

temperature $\Delta T_i \sim 30$ ev that is just 25% of T_i .This result is very important as it shows that there is no increase in the heat losses due to ions during plasma heating by neutral beam. Certainly, in the near future the most important problem for these experiments will be the increase in neutral beam power, than the beam would make the main contribution in the heating power.

In the Cleo there were also conducted first experiments on laser injection into plasma.[19] Solid deuterium pellet 0.3 mm in diameter and 0.5 mm in length falled freely in the gravitational field and at the moment when the pellet crossed the centre, the vacuum chamber was shooted by a powerful impuls of the CO_2 laser. The laser produced an energy of 1500 j at pulse duration of 200 nsec .

In these first experiments there were obtained the plasma density of $5.10^{12} cm^{-3}$ the ion temperature of 500 eV (during the filling) the electron temperature of 1 eV. Plasma density and temperature decreased fast ($\tau_p \sim$ 2 msec) .A large amount of neutrals was observed ($n_0 \sim 10^{11} cm^{-3}$).

The results of the first experiments are to a large extent unclear and contradictory. The experiments must be continued.

At present our emphasis are directed on studying the new heating methods in stellarators but there is another problem i.e. to investigate currentless plasma or plasma which is heated in a large extent not by current. In stellarators, such a plasma was produced in small size devices up to 1973 and now we expect the new stage in this problem.

§ 8. Magnetic limiter

The magnetic field structure of stellarators out of the last closed magnetic surface is similar to the field structure of a divertor. The field lines near the angles of a separatrix goes far from the magnetic surface around the conductors of a helical winding. Therefore in the absence of a material limiter which is less than the dimentions of the last magnetic surface, stellarator may operate with the magnetic limiter. That made it possible to operate without the material limiter in the L-2. In the Vint 20 stellarators, there were made the measurements of the plasma which flows to the wall in different points around the magnetic surface. The results of these measurements show that in the points which are located opposite to the angles of a separatrix, the value of plasma flow exceeds essentially the mean over the cross section value (see Fig.23). A similar pattern was observed in the L-2, Uragan-2 and Sirius. On a wall of a vacuum chamber it might be seen the helical line which was formed by plasma wall interaction in the L-2 Stellaratur (Fig.24).

The surface of the helical line with the trace of plasma wall interaction in the vacuum chamber of L-2 is 2700 cm^2.

If we suppose that all the energy losses occur only into the surface of this helical line the load on the wall is about 10 wt/cm^2. In this case the value of Z_{ef} and the impurity flux appears to be almost as those ones on the other devices (i.e. Cleo, W-VII A) which use the usual material limiters [4].

In designing the new stellarators, it would be desirable to use the magnetic field structure which is out of the last closed magnetic surface in order to construct the divertor.

For this purpose it is sufficient to remove for a litle distance a wall of a vacuum chamber. The Uragan-3 would be such type of a stellarator with the divertor.

§ 9. Improoving of Tokamak by the helical winding

Now it is already well known that the adding of a helical field improves essentially plasma containment in a toroidal trap. Fig.25 show that the energy lifetime values in stellarators lies above the curve which corresponds to the Mirnov sealing law for tokamaks.

If we take into account the contribution of a poloidal field of helical winding by the most simple way i.e. by replacing the poloidal current field for the total poloidal field than the points displace correspondingly towards the tokamak curve.

Thus we may obtain an approximate estimate of the effect of plasma containment improvement due to the addition of a helical winding if we take the ratio of the poloidal fields:

$$\tau_E^{St} / \tau_E^{T} = 1 + \frac{B_p^{St}}{B_p^{T}}$$

The manifestation of the stabilizing effect of a helical field may be seen from the fact that no copper shell or vertical field is required to maintain the plasma equilibrium.

In the W-VIIA, there is no necessity in a transverse field when $t_{St} > 0.14$. In the L-2 where the minimum value of $t_{St}(0) = 0.18$ there is allways equilibrium in the absence of a transverse field. When the external transverse field is added the displacement of the current centre of gravity is observed. The value of this displacement has the dependence on the transverse field strength (see Fig.26).

The suppression of the disruption instability is the most important result of the introduction of a helical winding. The experiments in the W-VIIA stellarator showed that the suppression of the disruption instability occurs when the value of an additional poloidal field which provides the obtaining of the rotational transform angle is $\iota > 0.14$. No disruption instability is observed in the L-2 and Cleo. The absence of the disruption instability provides more fast density growth and makes it possible to work with higher densities when the discharge duration is sufficiently long.

§ 10. Conclusion

Last year at the Innsbruck conference the stellarator session was concerned with the problems which require solution in the framework of the stellarator programme:

1) further research on χ_e and χ_i
2) working in the currentless regime
3) obtaining high density
4) finding an adequate method of plasma heating
5) a study of the operation of the magnetic limiter
6) study of limiting β
7) study of state regime, fuelling, injecting pellets
8) to make large the available region of γ/β working with $q < 1$
9) continuing the search for better stellarator configurations force-free configurations, non round cross-section, various methods of helical field formation
10 improving tokamaks parameters by adding a helical field
11 collisionless regime, superbanana problems

12) physical problems of stellarator operation as a reactor (behaviour of α-particles, steady-state burning

13) developing a conceptual project of a reactor based on the stellarator

As we may see from the information presented here, in some points of this programme an essential progress has been achieved and new data were obtained.

But there are some problems which progress very slowly especially in experiments. First of all it is the question of the finite β in stellarators. Plasma parameters in modern devices may provide only $\beta \sim 0.1\%$ due to the absence of the heating methods which are powerful enough.

$\beta \sim 2\%$ - remains the most important success which has been achieved in Helitron D ^{32} at a very low plasma temperature ~20 ev. In the near future we expect the progress in the experimental study of finite β, if the powerful nonohmic heating methods which are preparing now in some devices, will be used.

At present, we may expect to obtain in stellarators $\beta \sim 10\%$ which is necessary for the reactor. It is possible that for this purpose it would be necessary to use the devices with three-dimensional magnetic axis and the mean field minimum. In connection with designing stellarators of the next generation, the problem of finding better configurations plays more important role.

In solving the engineering and technological problems (such as: formation of strong magnetic fields in large volume, applying superconductivity, production of devices operating stationary or for a longtime) the stellarators are more far from tokamaks than in research of the physics of plasma containment.

At the same time the work which has been done show that the stellarator programme became an essential part of the whole controlled thermonuclear programme. And its role in the CTF programme grows with developing new heating methods in the present devices and constructing stellarators of the next generation.

Figure captions

1. Dependence of the rotational transform in vacuum on the radius for the four stellarators
2. Dependence of the rotational transform on the radius for the different values of plasma current in "Wendelstein VIIA" stellarator
3. Current density distributions, normalized to unity, used to calculate Figs 4 and 5
4. Total rotational transform for the current distributions shown in Fig.3 for values γ/β = 0.5 and 1.3 in Cleo (solid lines) and L-2 (dotted lines) respectively
5. The same as Fig. 4 but for $\gamma/\beta = 2$
6. Dependence of the energy lifetime on the drift parameter $\xi = \frac{u_e}{v_{Te}}$
7. Maximum electron temperature corresponding to the Guest scaling law
8. Electron temperature and plasma density profile in the Wendelstein-VII A stellarator
9. Electron temperature profile in the L-2 stellarator
10. Comparison between the experimentally measured ion temperature values and those calculated from the Artsimovich formula
11. The same as Fig.10; data from W VIIA
12. Dependence of the ion thermal conductivity on the ion temperature
13. Sawtooth oscillations in L-2
14. Dependence of the phase-change point on γ/β for L-2
15. The same as Fig.14; data from W-VII A
16. Total rotational transform versus radius in the regime given in Fig.11 for L-2

17. Limitations on the plasma density for different currents and rotational transform angles of the stellarator. The density is normalized to the value $\frac{B_0}{R}(1-t_0)$ which is proportional to the current density at the centre of the column

18. Electron temperature as a function of the plasma density in L-2 with pulsed gas puffing

19. Electron and ion temperature as a function of plasma density in WVIIA

20. Current, plasma density and radiation power versus time in L-2 with pulsed gas puffing

21. Ohmic-heating power and radiation in W VIIA

22. Energy lifetime in W VIIA versus plasma density

23. Plasma flux to the wall as a function of the azimuthal angle in Vint.-20

24. Photo of the track on the wall of the vacuum chamber after 20000 shots in the L-2 stellarator

25. Comparison of the experimental lifetimes for tokamaks and stellarators . The straight line represents the Mirnow scaling law.

26. Dependence of the displacement of the current centre of gravity on the transvers magnetic field components $B_{\perp j}$ and $B_{\perp}$

REFERENCES

1. M.S.Rabinovich "Current state of the stellarator research" Preprint Lebedev Physical Institute N 29 Moscow 1979.
2. J.S.Shpiegel "Ohmic heating experiments in the L-2 stellarator" VIII European Conference on controlled fusion and Plasma Physics. Praga 1977 VII p.109.
3. D.W.Atkinson et al. "Heating and confinement in the Cleo stellarator" VIII Fusion Praga 1977 v II p.93.
4. H.Wobig "Ohmic heating experiments in the W-VII A stellarator". VIII Fusion. Praga 1977 v II p.73.
5. D.W.Atkinson et al. "Heating, confinment and fluctuation in the Cleo stellarator" VII IAEA Insbruk 1978 report CN-37-H-1.
6. The W-VIIA team "Energy and partical confinement in the ohmically heated W-VII A Stellarator" VII JAEA Insbruck 1978 report CN-37-H-2.
7. The W-VII A team "Investigation of the m=2 mode at q valyes around 2 in the W-VII A Stellarator" VII IAEA Insbruck 1978 report CN-37-H-3.
8. D.K.Akulina et al. "Plasma current equilibrium and effective charge of plasma in the L-2 stellarator" VII IAEA Insbruck 1978 report CN-37-H-4.
9. D.K.Akulina et al. "Energy balance for ohmically heated plasma in the L-2 stellarator". Physica plasmi v 4 p.1022 1978.
10. D.K.Akulina et al. "Ohmic heating of the plasma in the L-2 stellarator with pulse gas putting" report on the Zvenigorod Conference Moscow 1979.
11. M.S.Berejetskiy et al. "Some special features of ohmic discharge in the L-2 stellarator" report on the Zvenigorod Conference Moscow 1979.

12. R.J.Bickerton "Survey of Tokamak experiments" Preprint Culhem England CLM-R-176 1977.

13. M.S.Rabinovich, J.S.Shpigel, V.T.Tolok, H.Wobig, V.D.Shafranov, S.M.Hamberger, B.Streibl, K.Miamoto, Working group on stellarators Zdikov Chechoslovakia 1977.

14. Proceedings of unofficial meeting on stellarator research Insbruck Austria 1978.

15. A.G.Dikjy et al. "Energy confinement of Hf heating plasma in the stellarator Uragan". VI European Conference on Plasma Physics and Controlled Fusion Moscow 1973 v 1 p.105.

16. V.S.Muchovatov "The Tokamak research" report on the Zvenigorod Conference Moscow 1979.

17. D.K.Akulina et al. "Ohmic heating of plasma in the L-2 stellarator with pulsed injection of gas" report BP29(a) on this Conference.

18. M.S.Berezhetskii et al. "Some features of ohmically heated discharges in the L-2 stellarator". report BP29(b) on this Conference.

19. D.W.Atkinson et al. "Confinement of low and zero current plasmas in the Cleo stellarator" report A2.6 on this Conference.

20. V.K.Bocharov "The effect of stochastic electric fields on plasma transport in the range of low collision frequencies in a torsatron with high helical inhomogeneity". This Conference. report BP 30.

21. V.S.Vostsenya et al "Studies of plasms -surface interaction at the KFTI stellarators" This Conference report BP 32.

22. N.F.Perepelkin et al. "Current turbulent ion heating in modulation instability regime and caviton transport in a stellarator in a high magnetic field". This Conference report BP 31.

23. S.S.Kalinichenko et al., "Some specific features of generation and heating of currentless plasma". This Conference report AP9.

24. V.A.Suprunenko, U.V.Gubarev "Ohmic heating of the plasma in the closed toroidal magnetic traps." KFTI Preprint 79-7 Kahrkov 1979.

25. V.S.Voitsenya et al "Effect of fluctuating electric fields on superbanana diffusion of plasma in a stellarator".VIII Fusion Praga 1977 v.1 p.124.

26. V.K.Bocharov et al. "Experimental investigation of current discharge plasma confinement in L==1 Torsatron in the region of Low frequency collisions". VIII Fusion Praga 1977 v 1 p.125.

27. G.E.Guest, R.C.Miller, W.W.Pfeiffer, E.Waltz GA-A 1483. General Atomic San Diego 1978

28. W-VII A Team, "The Maximum electron temperature in the W-VII A stellarator and comparison with tokamak discharges". IPP 2/241 1978.

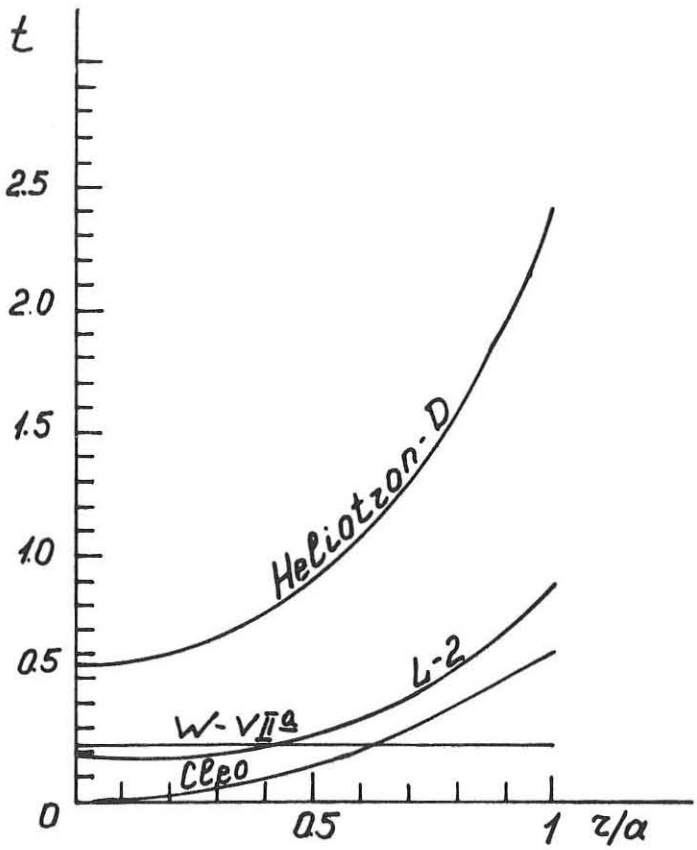

Fig. 1. Dependence of the rotational transform in vacuum on the radius for the four stellarators

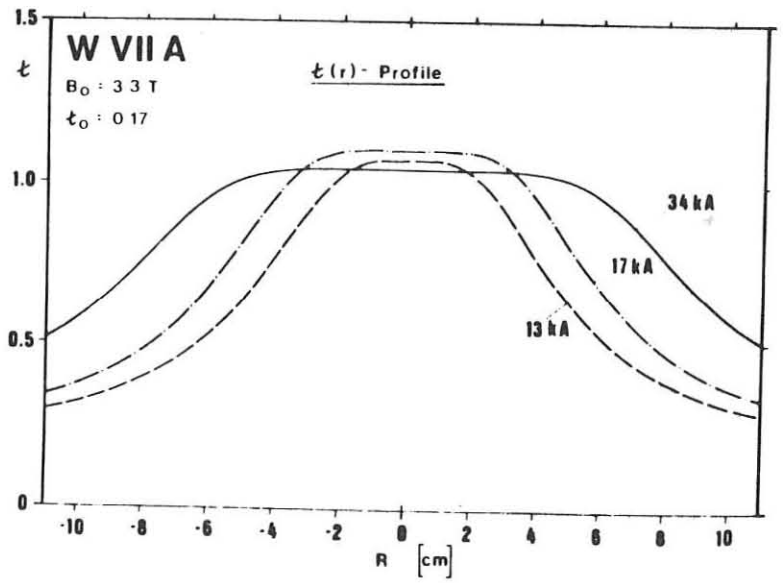

Fig. 2. Dependence of the rotational transform on the radius for the different values of plasma current in "Wendelstein VIIA stellarator

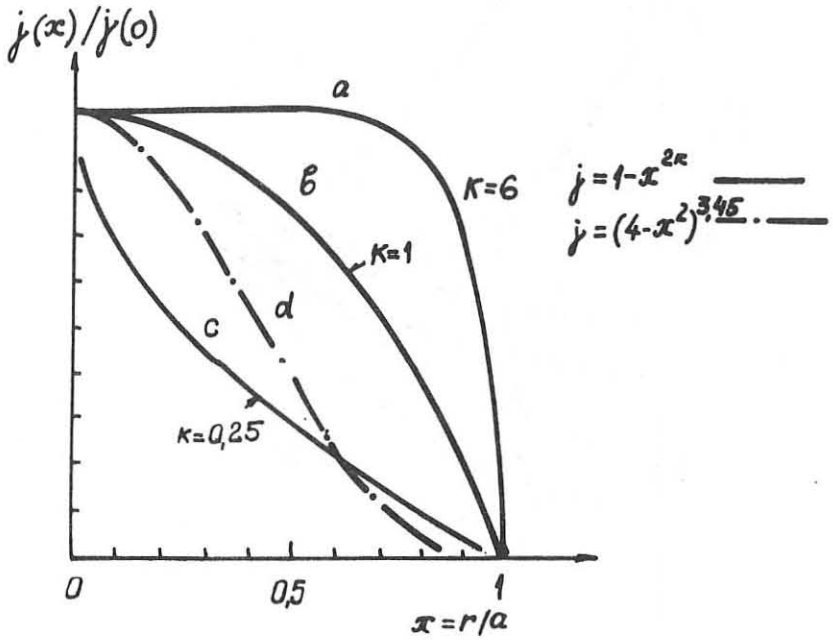

Fig. 3. Current density distributions, normalized to unity used to calculate Figs 4 and 5

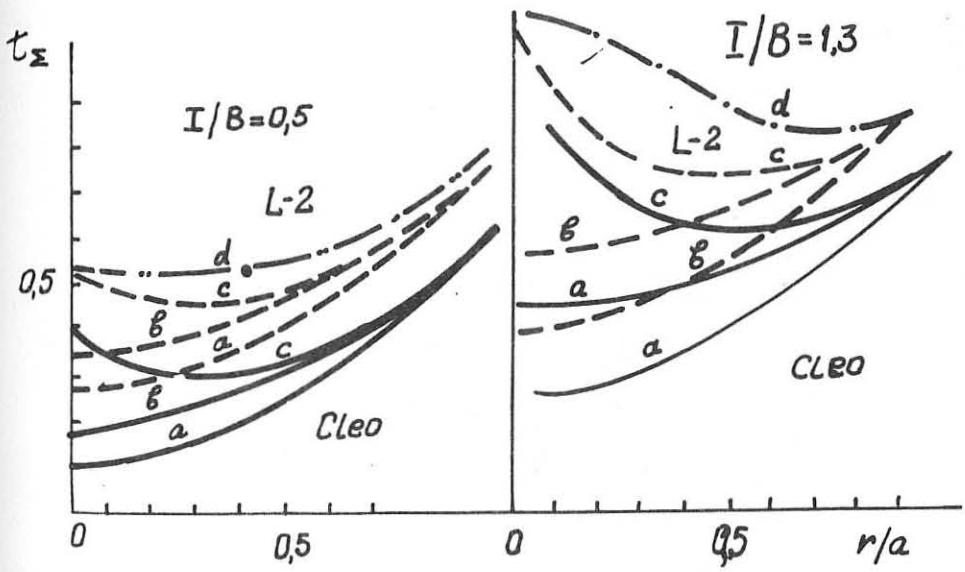

Fig. 4. Total rotational transform for the current distributions shown in Fig.3 for values I/B = 0.5 and 1.3 in Cleo (solid lines) and L-2 (dotted lines) respectively

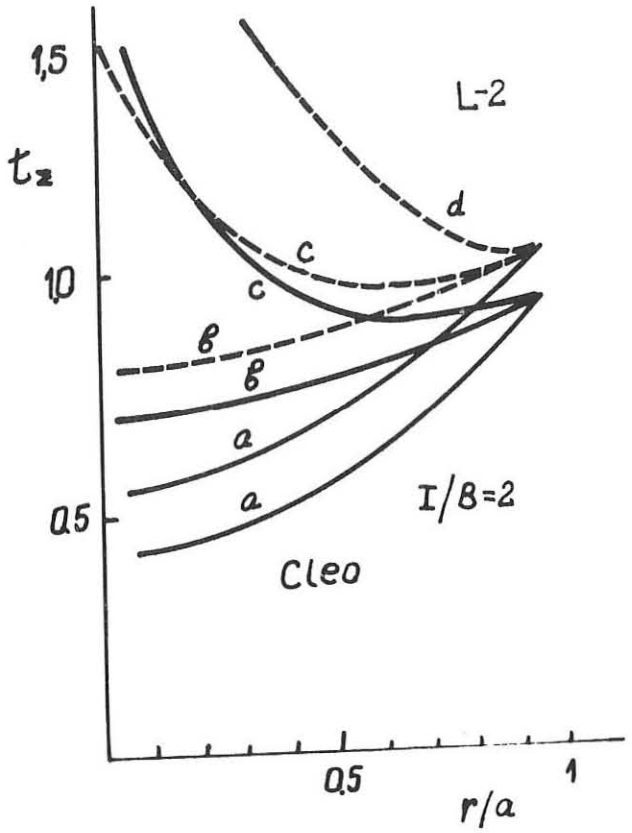

Fig.5. The same as Fig. 4 but for $\gamma/\beta = 2$

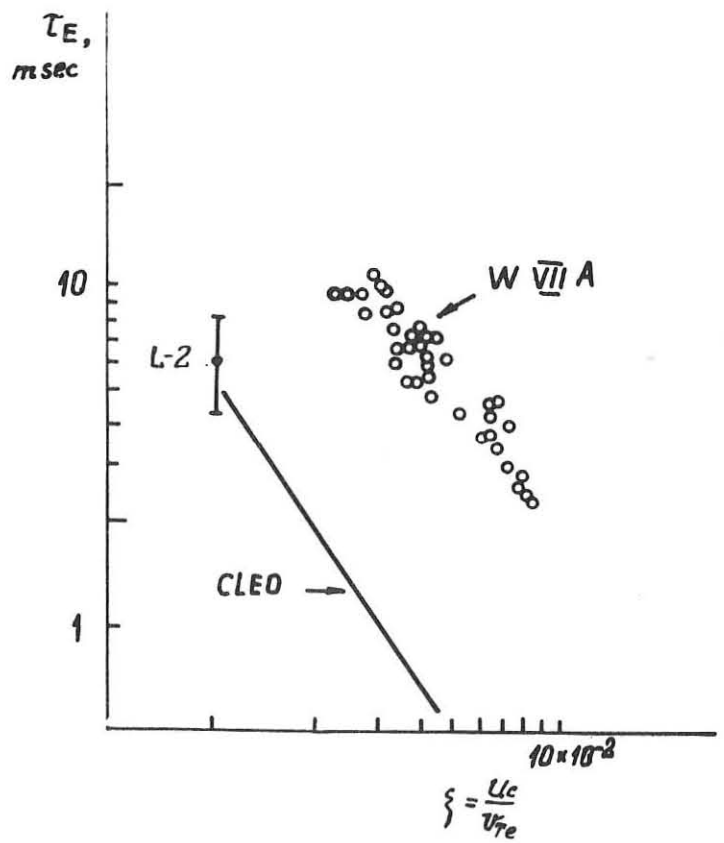

Fig.6. Dependence of the energy lifetime on the drift parameter

$$\xi = \frac{u_e}{}$$

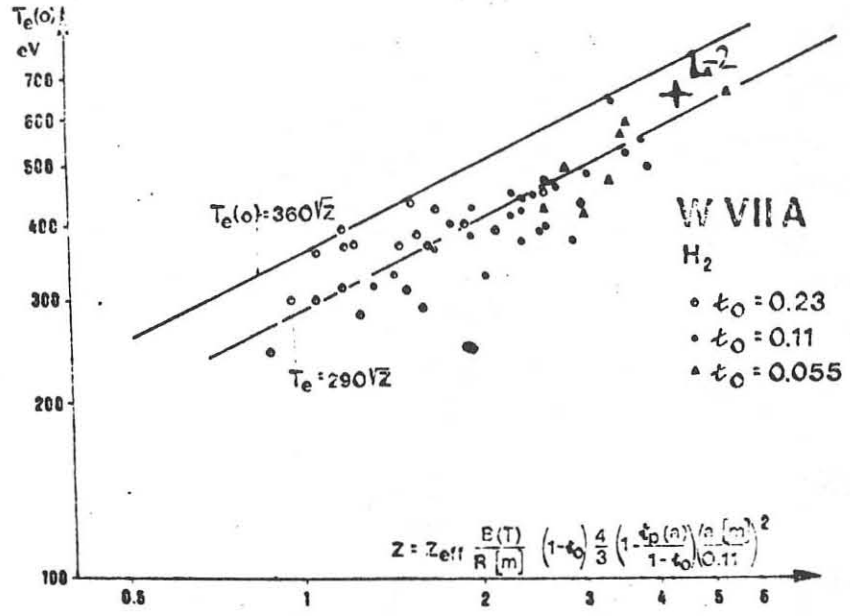

Fig.7. Maximum electron temperature corresponding to the Guest scaling law

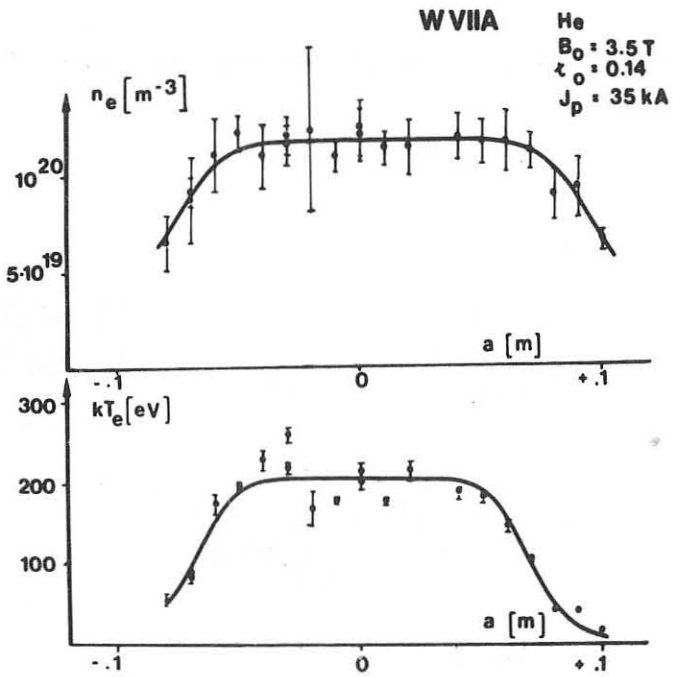

Fig.8. Electron temperature and plasma density profile in the Wendelstein-VII A stellarator

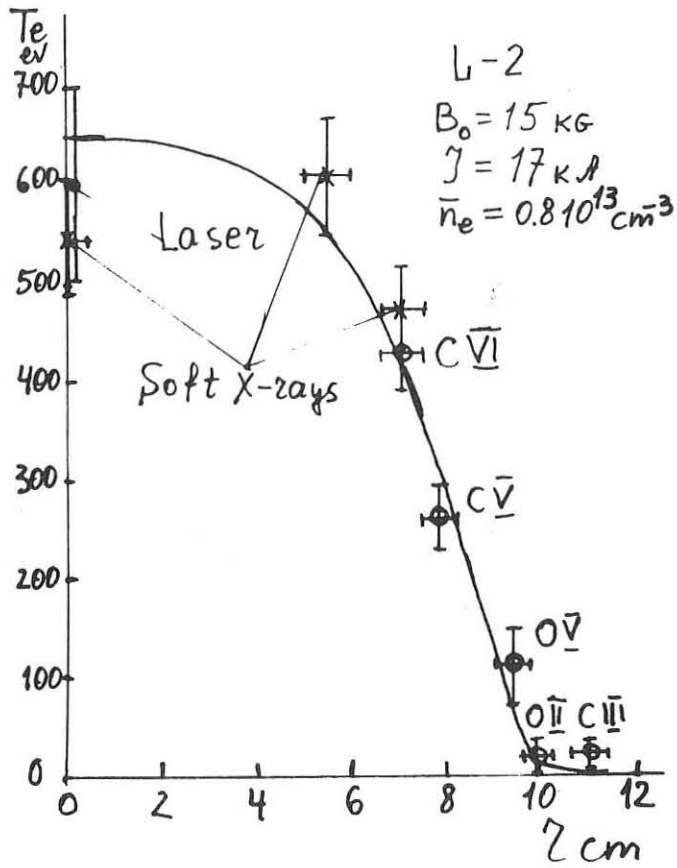

Fig.9. Electron temperature profile in the L-2 stellarator

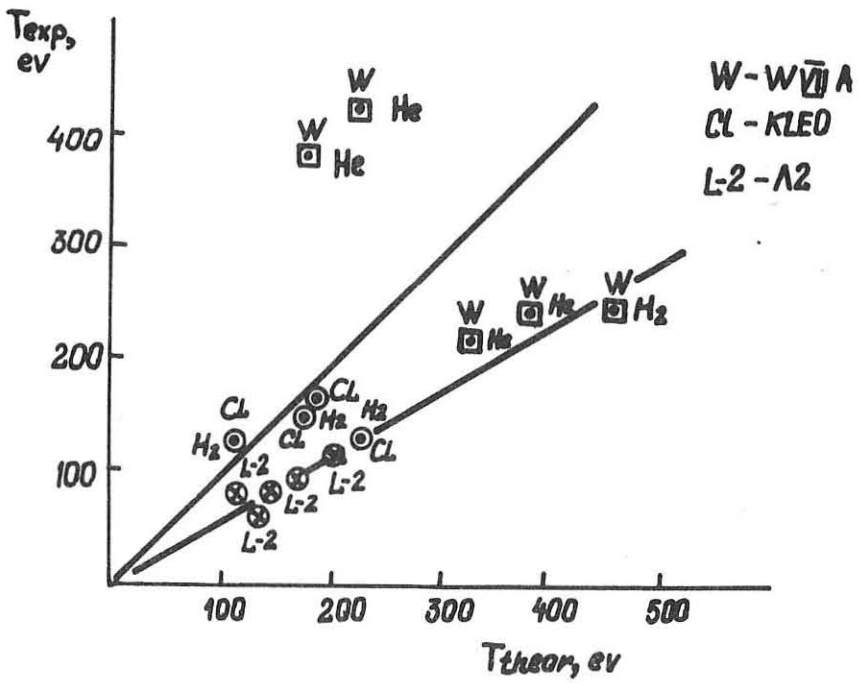

Fig.10. Comparison between the experimentally measured ion temperature values and those calculated from the Artsimovich formula

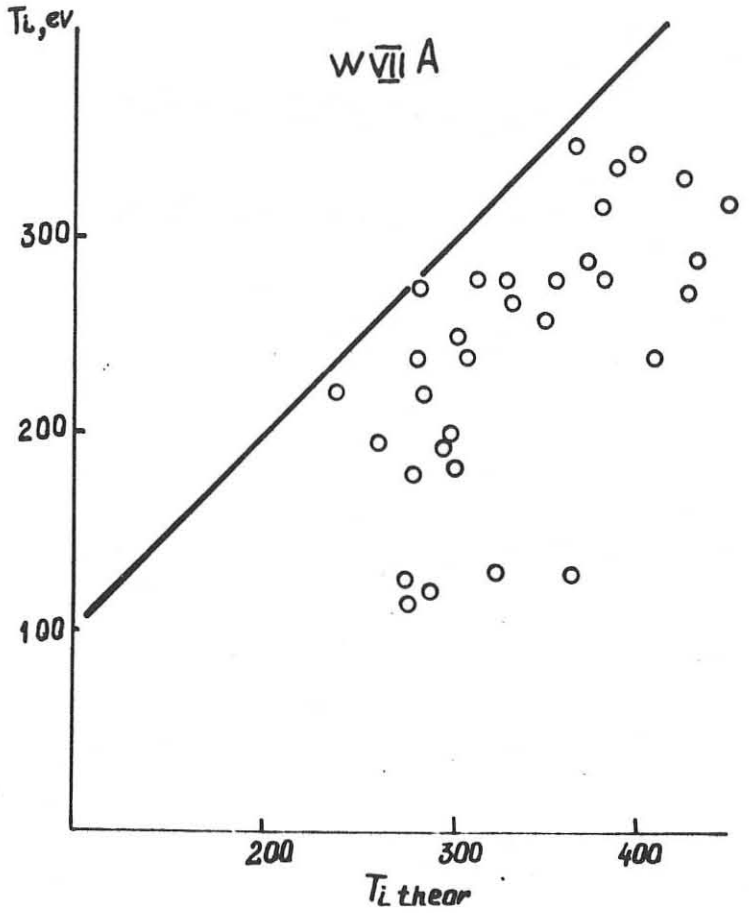

Fig.11. The same as Fig.10; data from W VIIA

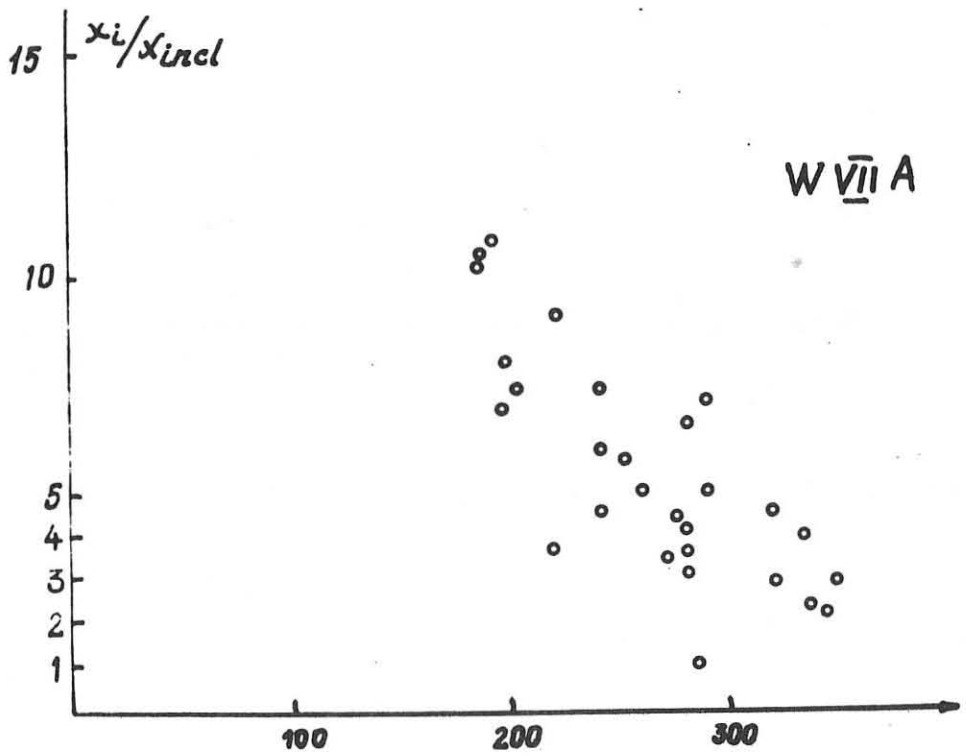

Fig.12. Dependence of the ion thermal conductivity on the ion temperature

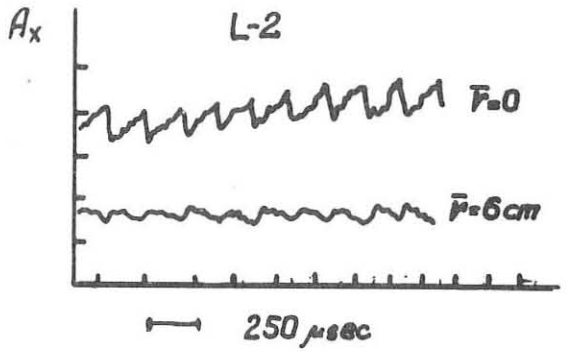

Fig.13. Sawtooth oscillations in L-2

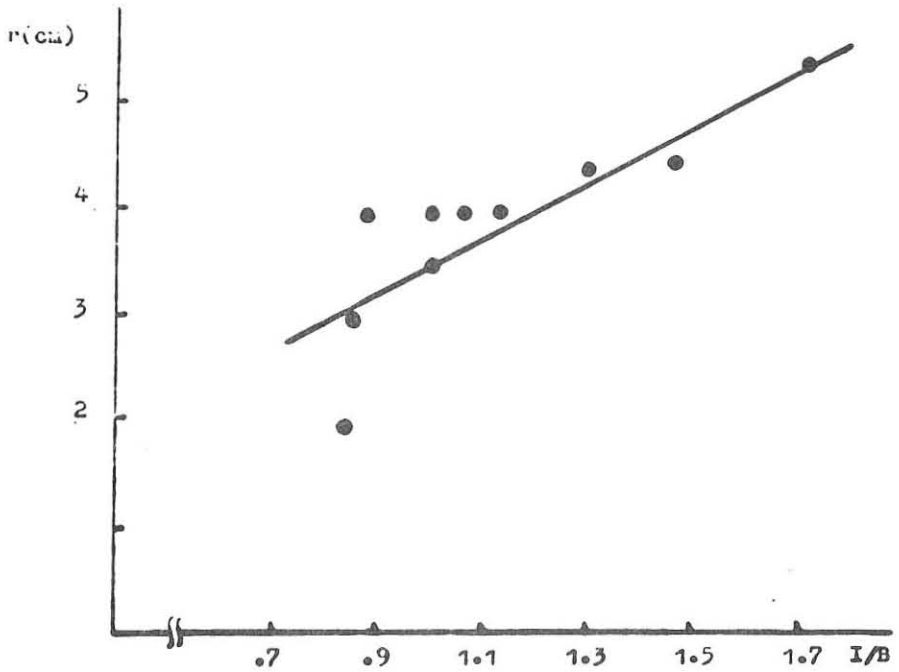

Fig.14. Dependence of the phase-change point on $\tilde{J}/\beta$ for L-2

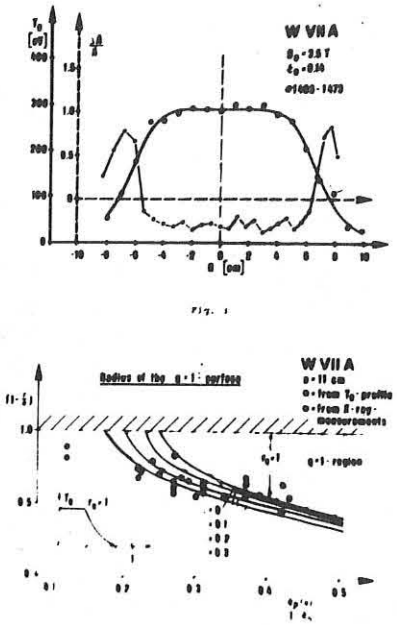

Fig.15. The same as Fig.14; data from W-VII A

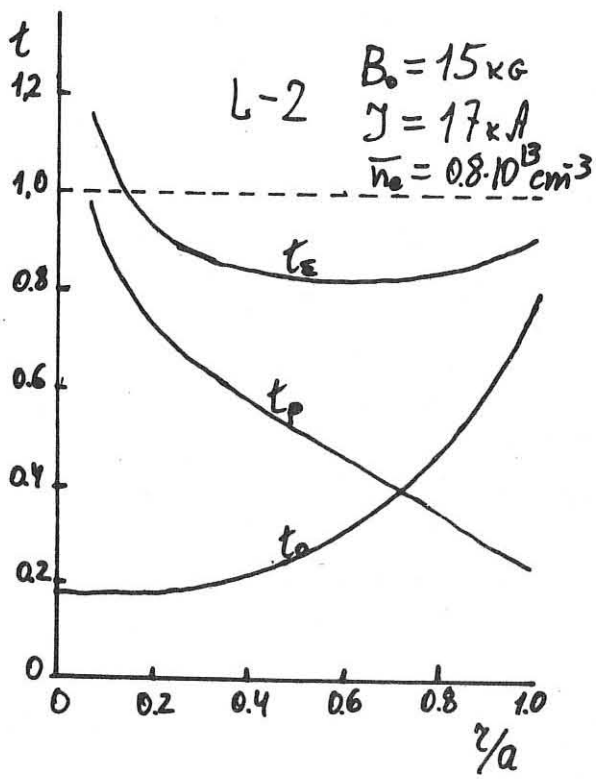

Fig.16. Total rotational transform versus radius in the regime given in Fig.11 for L-2

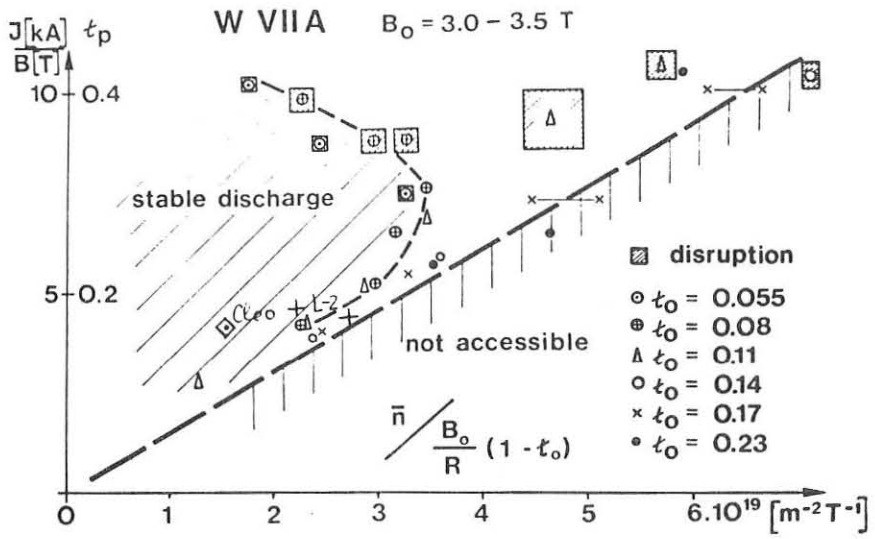

Fig.17. Limitations on the plasma density for different currents and rotational transform angles of the stellarator. The density is normalized to the value $\frac{B_0}{R}(1-t_0)$ which is proportional to the current density at the centre of the column

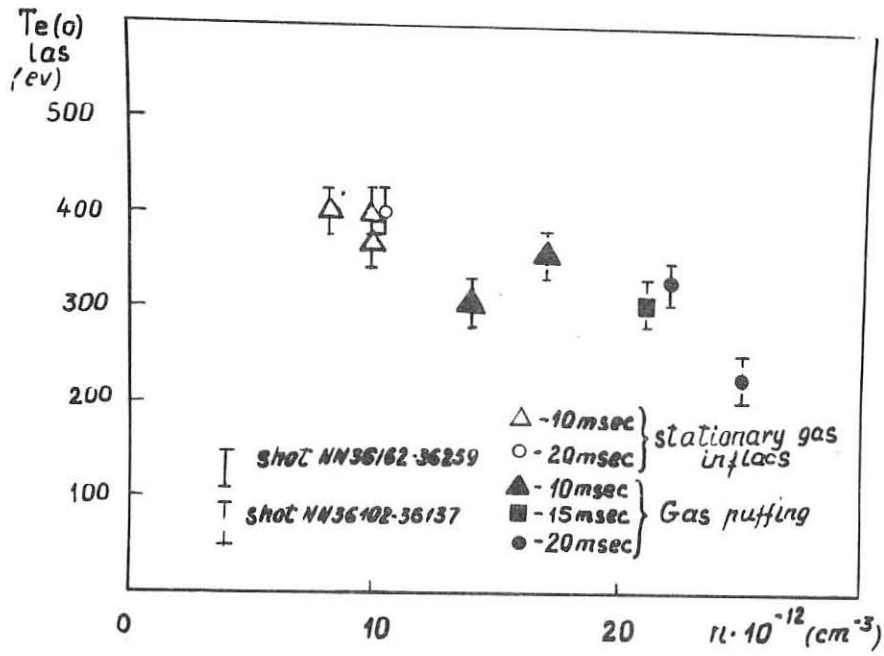

Fig.18. Electron temperature as a function of the plasma density in L-2 with pulsed gas puffing

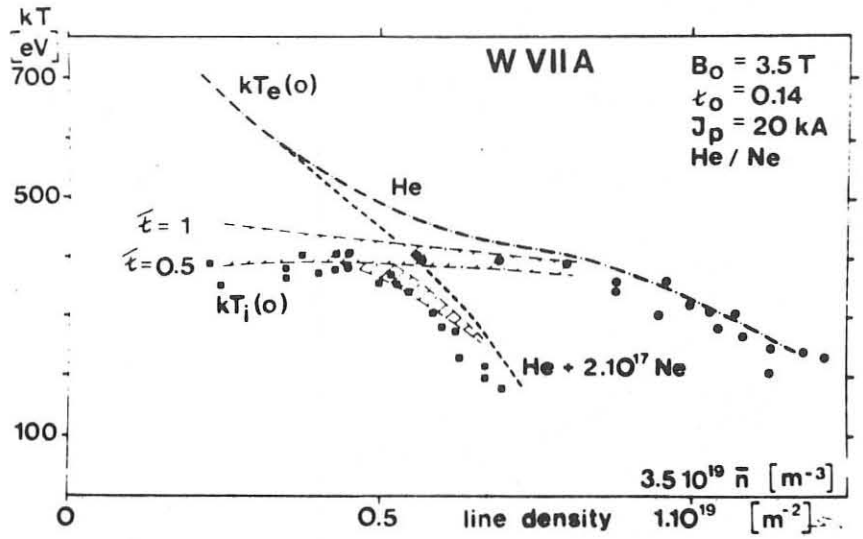

Fig. 19. Electron and ion temperature as a function of plasma density in WVIIA

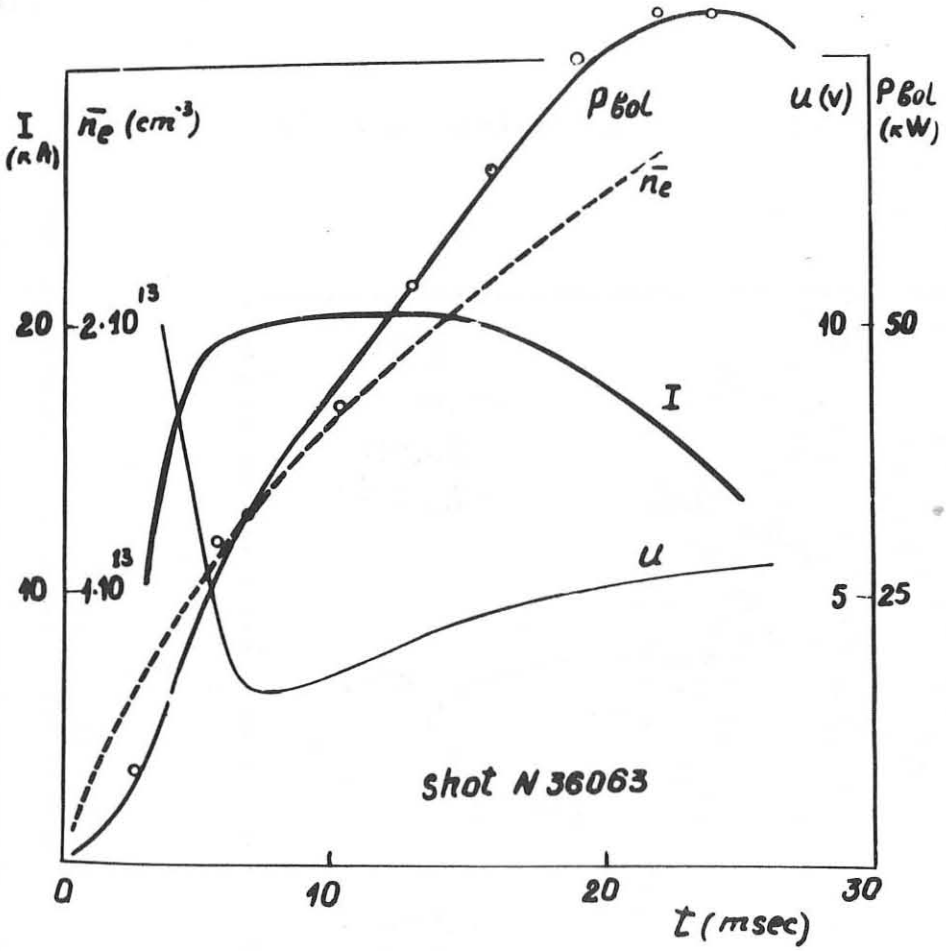

Fig. 20. Current, plasma density and radiation power versus time in L-2 with pulsed gas puffing

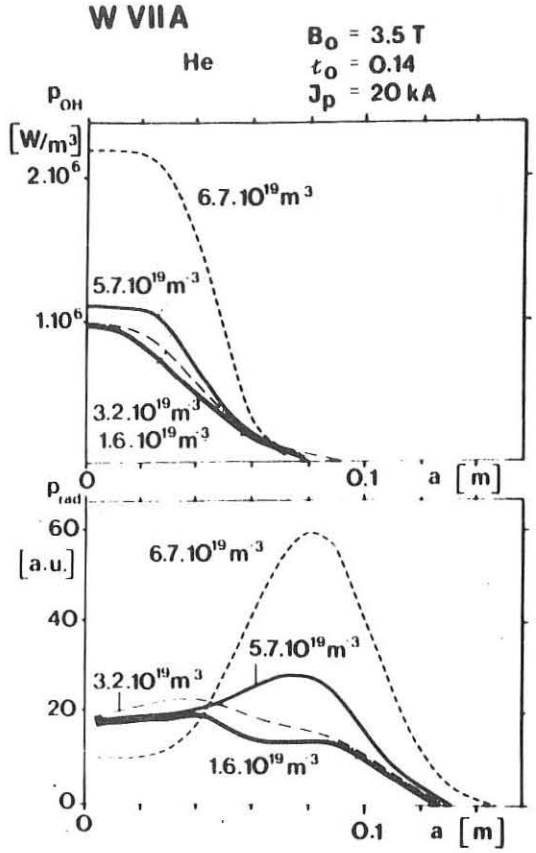

Fig. 21. Ohmic-heating power and radiation in W VIIA

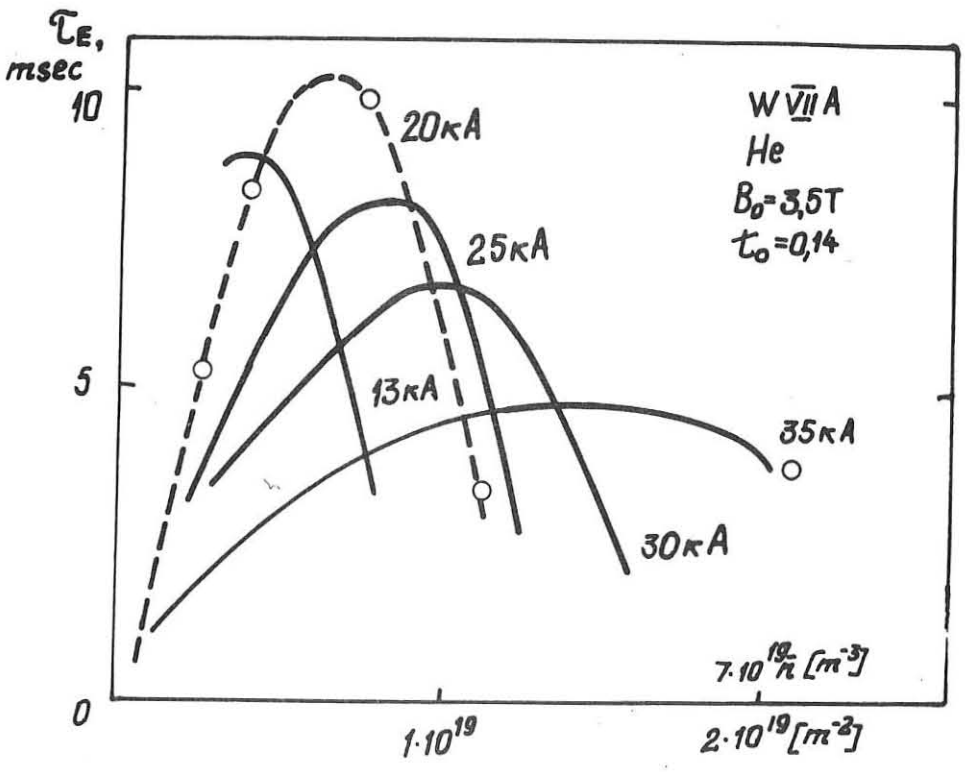

Fig. 22. Energy lifetime in W VIIA versus plasma density

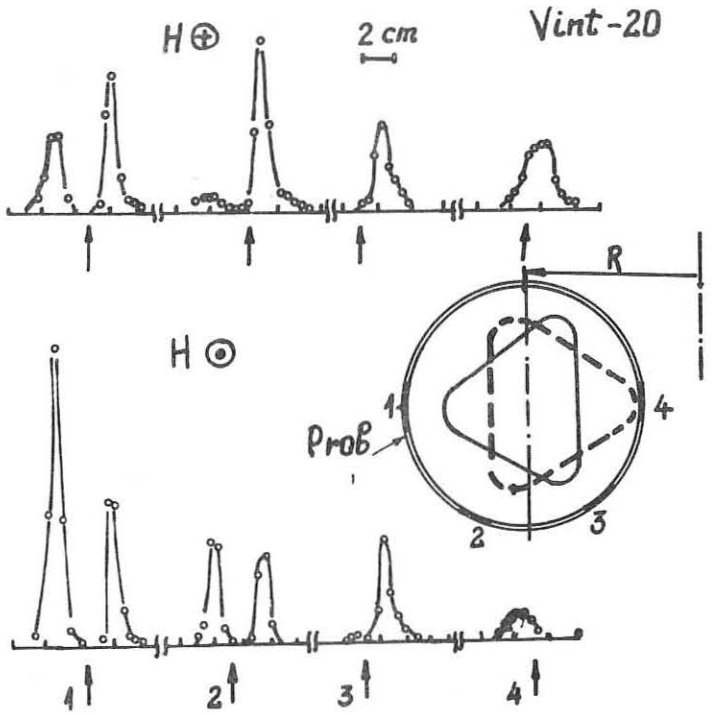

Fig. 23. Plasma flux to the wall as a function of the azimuthal angle in Vint-20

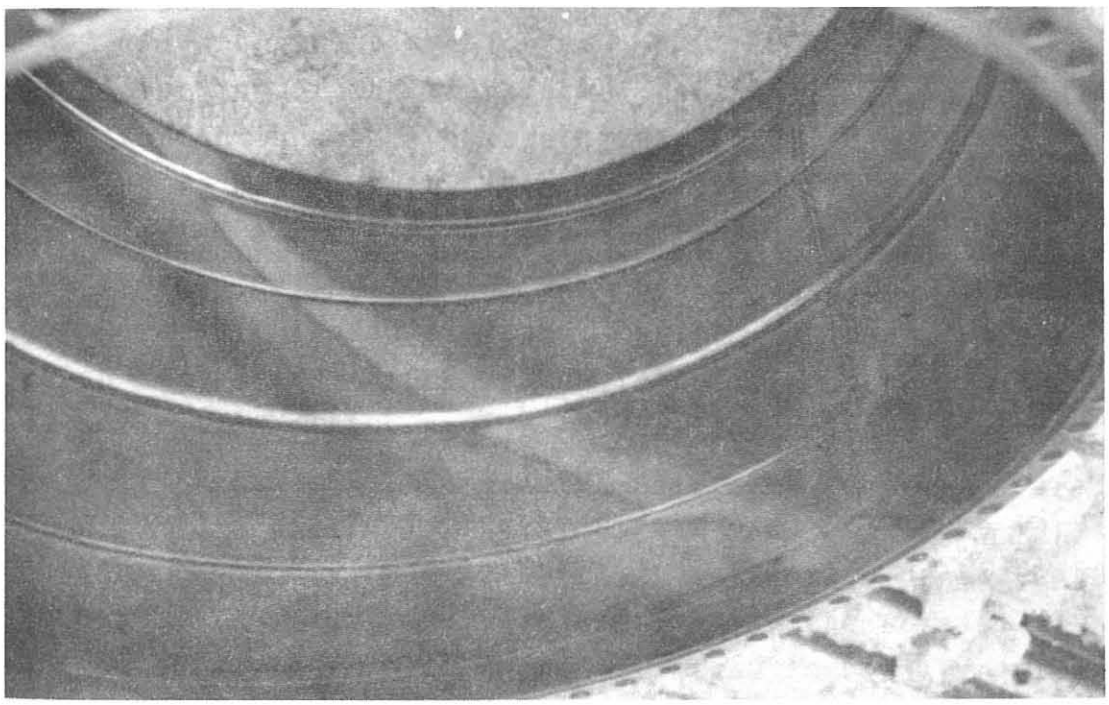

Fig. 24. Photo of the track on the wall of the vacuum chamber after 20000 shots in the L-2 stellarator

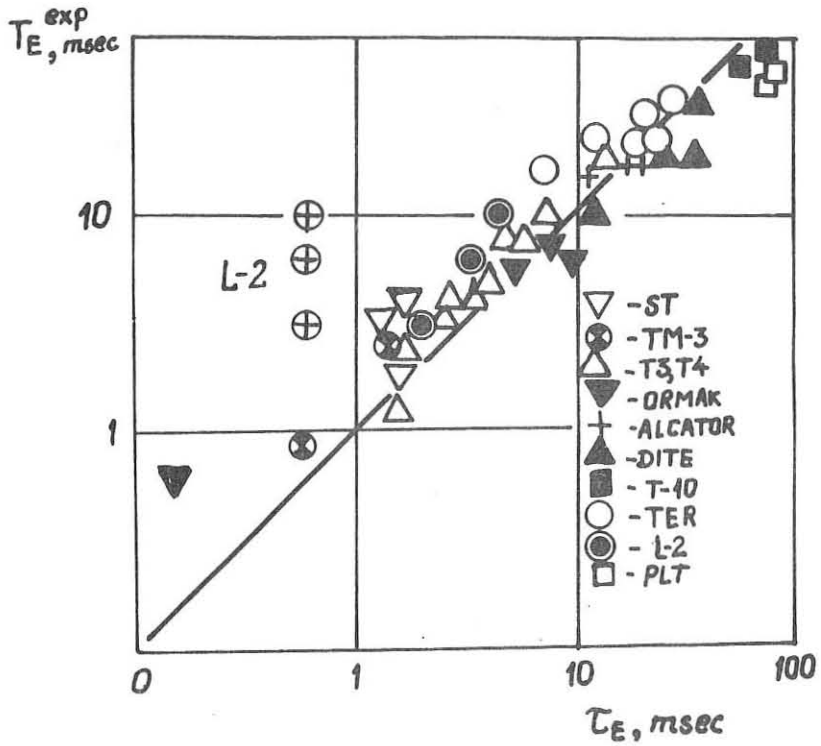

Fig. 25. Comparison of the experimental lifetimes for tokamaks and stellarators . The straight line represents the Mirnow scaling law.

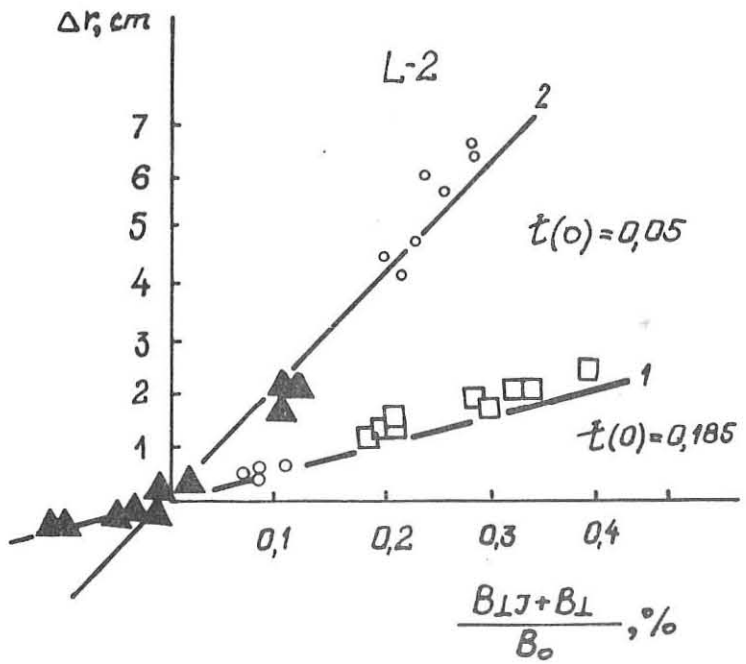

Fig. 26. Dependence of the displacement of the current centre of gravity on the transvers magnetic field components $B_{\perp J}$ and $B_{\perp}$

EXPERIMENTAL RESULTS FROM THE FT TOKAMAK

U.Ascoli-Bartoli, G.Bardotti, R.Bartiromo, M.Brusati, P.Buratti,[★]
A.De Angelis, F.De Marco, M.Gasparotto, R.Giannella, M.Grolli,
M.Martone, L.Pieroni, G.B.Righetti, M.Samuelli, A.Tanga, V.Zanza

Associazione EURATOM-CNEN sulla Fusione, Centro di Frascati,
C.P. 65 - 00044 Frascati, Rome, Italy

INTRODUCTION

The Frascati Tokamak (FT) is a high field machine with main parameters resulting from a compromise between large current densities and relatively large size. They are major radius R = 83 cm, liner minor radius b = 23 cm, maximum toroidal field B_T = 100 kG, B_T flat top duration 1 sec. All the windings and the copper shell are cooled at liquid nitrogen temperature.

The machine has been operating at cryogenic temperature since April 1978 with toroidal field up to 80 kG and plasma currents up to 600 kA. The working gas was hydrogen and the limiter (molybdenum) had a radius of 18.5 cm. The first results have been reported elsewhere (Ref.1).

Two major modifications have since been made on FT:

a) the molybdenum limiter has been replaced with a stainless steel limiter of the same radius in order to reduce to a minimum the radiation losses although radiation was not an important loss for the plasma core.
b) The inversion of the transformer generator. In FT an air core transformer is used; voltage is applied by discharging the primary magnetic energy into a resistor. Other resistors can be inserted at several programmed times. In this way only a voltage decreasing in time is produced and the plasma does not have an extended plateau. A system has been implemented which reconnects the generator to the transformer with inverted polarity and thus applies a constant voltage of about 1.5 V to the plasma for about 1 sec.

Using this system it has been possible to produce very long discharges routinely (Fig.1) operating at fields up to 80 kG. The presently available voltage has limited the possibility of producing such a very flat current plateau to relatively low currents ($I \lesssim 300$ kA) and density ($\bar{n} \sim 1\times10^{14}$ cm^{-3}). At higher densities very long duration discharges are again produced but the

★ *On leave from Scuola Normale Superiore, Pisa, Italy*

current has a slow decay.

When the applied voltage terminates, the current decays with its L/R period. We have never tried to control the end of the current; therefore two different cases occur: either the plasma current reaches the zero value without any disruption, or after a long decay it can terminate abruptly with a small disruption (Fig.2).

The maximum value of the peak density attained up to now is $\hat{n} = 4.5 \times 10^{14}$ cm^{-3} with a confinement time of 33 ms (see the T_e and n_e profiles in Fig.3) giving a value of $\hat{n}\tau_E$ of 1.5×10^{13} cm^{-3} sec.

In section I we report the working procedures to obtain a *good* discharge in FT and the general plasma characteristics; in section II we describe a typical high density discharge in detail; in section III we discuss plasma confinement. Most of the work here referred has been done in D_2.

1. GAS INFLUX, VERTICAL FIELD PROGRAMMING AND GENERAL PLASMA CHARACTERISTICS

Gas is injected through a piezoelectric fast valve. The gas pulse consists of a sequence of elementary pulses, whose frequency can be varied at different presettable times. In this way a highly flexible gas puffing is obtained.

In order to produce the current shapes shown in Figs 1,2 and a discharge without disruptions and with good plasma characteristics, it is necessary to have an accurate adjustement of 1) the centering of the plasma column; 2) the initial current and density rise.

1) We have verified that the centering of the plasma column is beneficial to the energy confinement. Previously the discharge was slightly displaced outward, since the vertical field was mainly generated by the copper shell. By controlling the position with a careful programming of gas puffing and of the vertical field, for given current and average density the energy confinement time has increased by about 50%.

   In Figure 4 the electron energy confinement time versus $\langle n_e T_e \rangle / I$ is shown. The dots refer to discharges before the improved positioning of the column and the circles the present discharges.

In Figure 4 all the discharges with the better confinement are in D_2, while the ones with the worst confinement are in H_2; but we have checked that the improvement does not depend on the nature of the gas. The maximum energy confinement time obtained so far is 40 ms.

The diffusion time of the copper shell is about 1.5 sec at LN temperature; due to the four gaps in the shell the vertical field required for equilibrium is to a large extent produced by external coils whose current must be empirically adjusted in relation to the gas puffing.

2) Linear rise of the current to levels of 80-140 kA in 10-12 ms followed by a slower rise is essential (Fig.5). The filling pressure must not be too small in order to avoid run-away electrons and not too high otherwise it can influence either the risetime of the current or the level it reaches after 10-12 ms inducing strong MHD activity that prevents the discharge to develop in a smooth way. If these conditions are met the discharge attains its peak current without any disruptive instabilities nor any detectable MHD activity.

Z_{eff} as measured by resistivity and by soft x-rays radiation is close to unity at all densities. To obtain this result a Taylor type discharge cleaning is performed for some hours every day after heating the vacuum vessel to room temperature; the cleaning discharges are made with a repetition rate of 1 Hz, a current of 3 kA and a duration of 10 ms.

The H_α behaviour at the gas inlet port follows the gas influx and during the first 150 ms the measured ionization rate corresponds closely to the rate of increase of the total number of electrons. At given machine parameters after a maximum value of density is reached, if we try to force more neutral gas in we have no disruptions. The only observed effect is that the density does not increase (Fig.6). In order to reach higher densities it is necessary to increase the plasma current.

The intensity of the vacuum UV lines of oxygen presents three distinct phases: a) the ionization peak; b) a low intensity plateau; c) a sharp increase of the emission when the mean electron density attains a value of about 10^{14} cm^{-3}. Even the H_α (at a port different from the gas inlet port) presents a similar phenomenon with strong gas puffing.

The ionization peak gives an oxygen concentration of

1-3 × 10^{11} cm^{-3}, while at the low intensity plateau the total power radiated by oxygen is about 80 kW which is small compared with ohmic input power (about 700 kW).

The subsequent emission enhancement is not associated with an increase of Z_{eff} nor with an increase of the soft X rays emission from the plasma core. The total radiated power becomes an important fraction of the ohmic power.

On the soft X ray spectra, lines of heavy impurities (Fe, Mn, Cr) are observed (Fig.7). The corresponding concentration is estimated to be relatively low. For example, the iron concentration is found to be about 10^{10} cm^{-3}. The radiation losses from the plasma centre appear relatively weak (~ .2 W/cm^3 compared with an average ohmic power density of 1.5 W/cm^3). It turns out that the FT discharge is transport dominated except at the outer layers after the emission enhancement.

At high density the ion temperature is close to the electron temperature. We have verified this by analysing fast neutrals and neutrons measurements.

II. TIME EVOLUTION OF A TYPICAL HIGH DENSITY DISCHARGE

In this section we discuss the results obtained in a typical high density FT discharge (B_T = 60 kG, I_p ~ 300 kA, $\bar{n}$ ~ 2 × 10^{14} cm^{-3}).

In Figure 8 the time behaviour of some plasma parameters are reported.

The electron temperature shows a marked skin effect which disappears at 80 ms; Figure 9 shows the T_e profiles during the first 100 ms.

There seems to be evidence of a major readjustement of the discharge occurring between 250 ms and 500 ms; actually several phenomena take place in this time interval: a) a dip in the envelope of the radial profiles of electron temperature (Fig.8d); b) the ratio $\tau_{Ee} I^{1/3}/\langle n \rangle$ which is generally constant in FT (see sect.III), decreases slightly; c) there is the maximum of the emission of the O lines; d) the end of overthermal features in the soft X-ray and electron cyclotron emission (see below).

Up to 400 ms the emission in the soft X-rays and in the electron cyclotron harmonics is strongly non thermal. The X-ray spectrum is highly distorted and a strong emission of the K_α

lines of Cr, Mn, and Fe is present (Fig.10). These lines, whose excitation energy (~ 6 keV) is much above the thermal energy, are effectively excited by overthermal electrons. The level of the emission at 2 ω_{ce} is quite enhanced respect to the thermal values. These effects are discussed in detail in another paper in this Conference. (Bartiromo et al. Paper B2.5).

In Figure 8c the time evolution of peak ion temperature as measured by neutrons is shown. In Figure 11 the ionic temperature in the central region is reported at 300 ms as measured by passive fast neutrals. As expected electron and ion temperatures are very close. Actually in the first phase of the discharge neutrons give a higher temperature probably due to non thermal effects.

The emission of the 1032 Å line of OVI and the 630 Å line of OV along different plasma chords has been measured shot by shot with a scanning UV monochromator. The results have been Abel inverted. Our apparatus does not allow to check the presence of up and down asymmetry but we have computed that the ion toroidal vertical drift is negligible in our case (Ref.2). During the low intensity plateau the density of the above mentioned two ions peaks in the extreme periphery. During the emission enhancement and up to 400 ms, at present there are not enough data for interpretation. Later on the OV and OVI densities peak quite internally (r = 12 - 14 cm); assuming for the ions an inward radial motion, the drift velocity turns out to be quite high (~10^5 cm/sec). The OVI peak density varies less than a factor 2 (~ 3×10^{10} cm^{-3}) confirming that the enhancement is due to a displacement of the ion position and a modification of their drift.

III. SCALING LAWS AND DENSITY LIMITS

Measurements of the radial profiles of electron density n and electron temperature T_e, of plasma current I and resistive voltage V allow us to calculate the electron energy replacement time $\tau^{\star}_{Ee}$ defined as

$$\tau^{\star}_{Ee} = \frac{3}{2} \langle nT_e \rangle \, 2\pi^2 Ra^2/VI \qquad (1)$$

where a, R are respectively the minor and major radii and < > is the volume average. Most of the work on FT has been at high density ($n \gtrsim 1 \times 10^{14}$ cm^{-3}) where the ion temperature is close to

the electron temperature, and the therefore $\tau^{\star}_{Ee}$ is about one half of the total energy confinement time τ_E.

When the dominant energy losses are the electron energy losses (and ion losses are negligible) $\tau^{\star}_{Ee}$ can be identified with the electron energy confinement time τ_{Ee} defined as the ratio of electron thermal energy to the total electron power lost.

The FT results show clearly a linear dependence of $\tau^{\star}_{Ee}$ on $< n >$ and, by comparing with other tokamaks, on a^2. Furthermore on tokamaks (such as Alcator A and ISX-A) where the ion losses have become non negligible, the dependence of $\tau^{\star}_{Ee}$ with n has shown signs of saturation at relatively high densities. (Ref.3,4) Such a saturation has not been observed up to now on FT therefore we will continue to identify $\tau^{\star}_{Ee}$ with τ_{Ee}.

The analysis of the FT data indicates a further dependence of τ_{Ee} on $< T_e >$ (with $<T_e> = <nT_e>/< n >$) and I which is of the form $\tau_{Ee} \sim n\, a^2 <T_e>/I$ as indicated in Fig.4. It should be noted that all the FT results correspond to values of effective Z very close to unity and therefore no Z dependence will appear in the following considerations. By comparing the FT data with results of other tokamaks the complete τ_{Ee} dependence is found to be (Refs 1,5):

$$\tau_{Ee} \sim <n>\, a^2\, \frac{<T_e>}{I} \left(\frac{a}{R}\right)^2 R \qquad (2)$$

and hence

$$V \sim \left(\frac{R}{a}\right)^2 \qquad (3)$$

However up to now FT is ohmically heated and therefore $<T_e>$ and I are connected. From Eq.3 and Ohm's law we have

$$<T_e> \sim \left(\frac{I}{R}\right)^{2/3} \qquad (4)$$

Therefore from a purely experimental point of view we cannot exclude a dependence of the form

$$\tau_{Ee} \sim <n>\, a^2 \left(\frac{<T_e>}{(I/R)^{2/3}}\right)^{\alpha} \left(\frac{R}{I}\right)^{1/3} \left(\frac{a}{R}\right)^2 \qquad (5)$$

where α is an unknown quantity (Ref. 6).

In Figure 12 τ_{Ee} is shown as a function of $<n> I_p^{-1/3}$.

It has been found also on FT that the peak density which can be reached (with ohmic heating) has a limit of the Murakami type with $\hat{n}$ (cm^{-3}) $\leqslant 5 \times 10^{14}$ B_T (kG)/R(cm).

REFERENCES

(1) U. Ascoli-Bartoli et al. "Proc. VII Int. Conference on Plasma Physics and Controlled Nuclear Fusion Research", Innsbruck, 1978 - IAEA-Vienna, Paper CN-37/C-1

(2) J.L. Terry et al., Phys. Rev. Letts 39, 1615 (1977)

(3) A. Gondhalekar et al. "Proc. VII Int. Conference on Plasma Physics and Controlled Nuclear Fusion Research", Innsbruck, 1978 - IAEA-Vienna, Paper CN-37/C-4

(4) M. Murakami et al. "Proc.VII Int.Conference on Plasma Physics and Controlled Nuclear Fusion Research", Innsbruck,1978 - IAEA-VIENNA, Paper CN-37/N-4

(5) B. Coppi, E. Mazzucato, Phys. Letts 71A, 337 (1979)

(6) L. Pieroni, F. Santini, S.E. Segre, Report 79.26 Associazione EURATOM-CNEN sulla Fusione, Centro di Frascati, Frascati, Rome, Italy

FIGURE CAPTIONS

Fig. 1 - Plasma current evolution for a low density discharge ($\bar{n} \leq 1 \times 10^{14}$ cm^{-3}).

Fig. 2 - Plasma current, magnet current and loop voltage evolution and their end.

Fig. 3 - Electron density and temperature profiles for a very high density discharge.

Fig. 4 - Electron energy confinement time: the dots and circles refer to the discharges before and after the better centering of the discharge.

Fig. 5 - Shape of the plasma current at the beginning of the discharge.

Fig. 6 - Behaviour of the maximum average density vs. the gas influx for fixed machine parameters.

Fig. 7 - Soft X-ray thermal spectrum.

Fig. 8 - Evolution of a typical high density discharge; a) Plasma current and loop voltage; b) line average density and D_α radiation at the fast valve port; c) peak ion temperature as measured by neutrons; d) $T_e(r,t)$; e) $n_e(r,t)$; f) time evolution of the electron energy confinement time; g) diametral brightness of the 1032 Å and 630 Å lines of OVI and OV (arbitrary units not in scale); h) flux of the soft X-rays; i) emission of the electron cyclotron second harmonic.

Fig. 9 - Initial evolution of the electron temperature.

Fig.10 - Non thermal X-ray spectrum.

Fig.11 - Ion temperature in the central region by passive fast neutrals measurements.

Fig.12 - Electron energy confinement time vs $\langle n \rangle I^{-1/3}$.

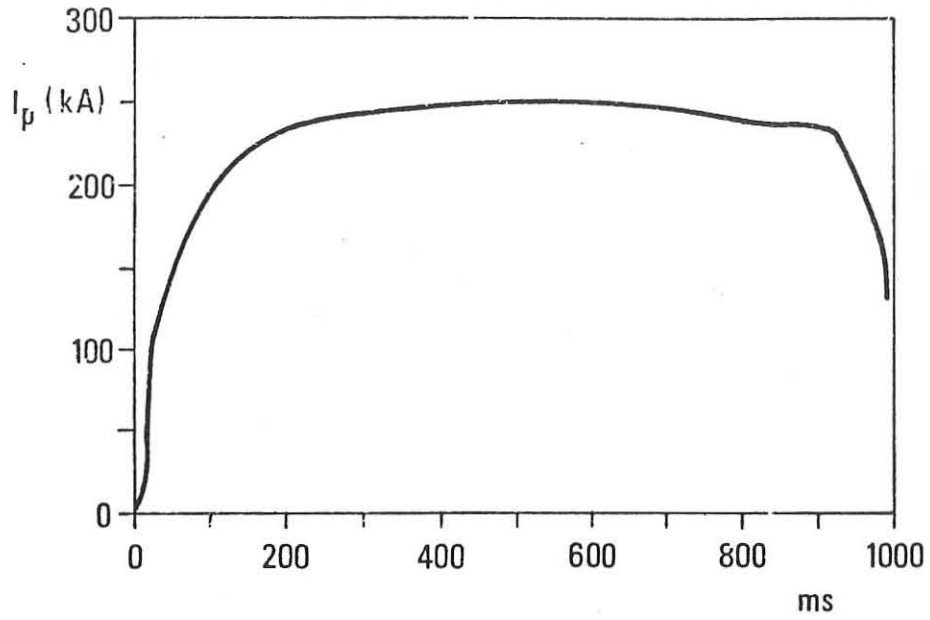
300
I_p (kA)
200
100
0
0
200
400
600
800
1000
ms

Fig. 1

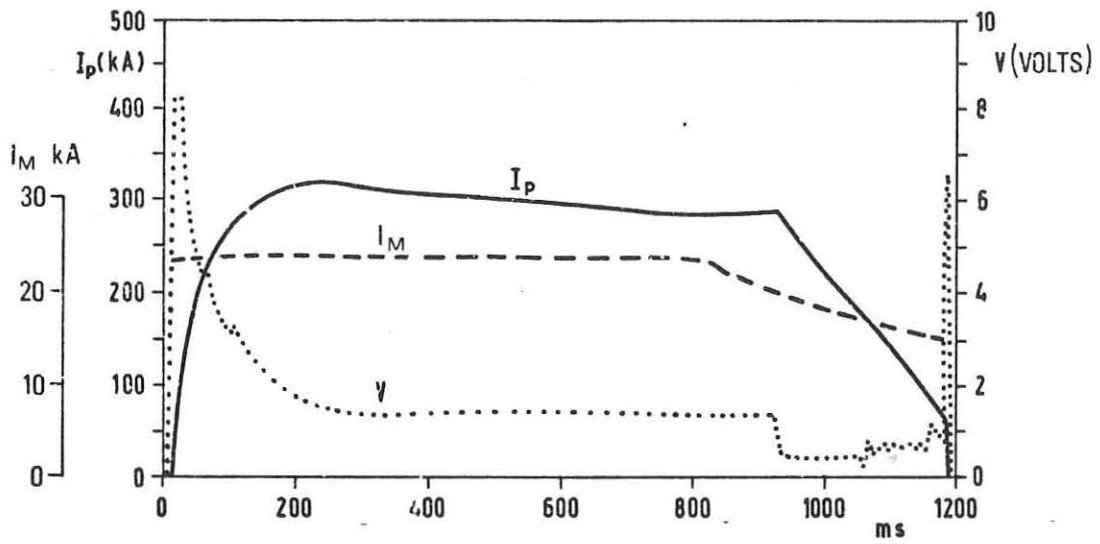
500
I_p(kA)
400
i_M kA
30
300
20
200
10
100
0
0
I_p
I_M
V
200
400
600
800
1000
1200
ms
10
V(VOLTS)
8
6
4
2
0

Fig. 2

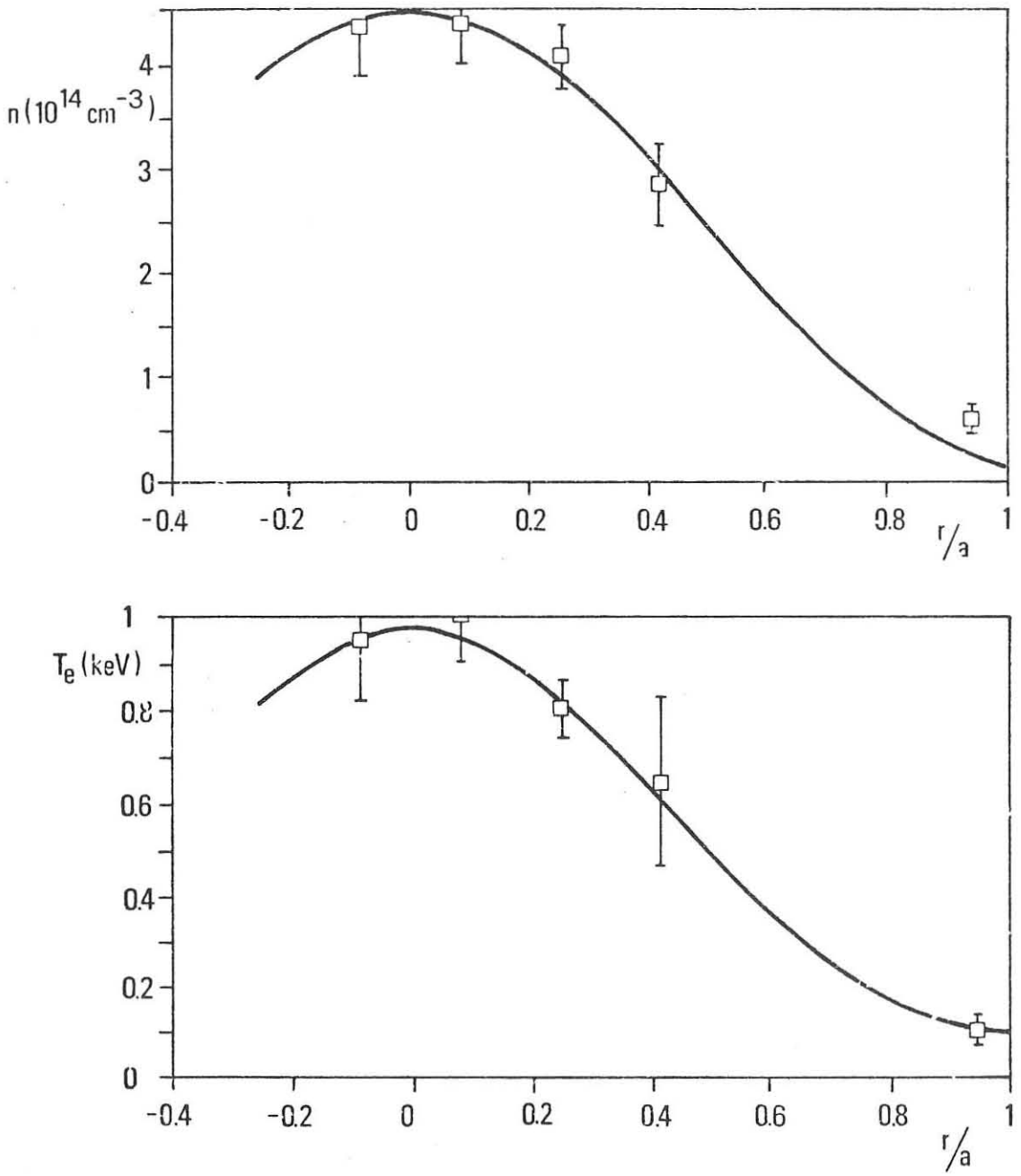
n (10^14 cm^-3)
4
3
2
1
0
-0.4
-0.2
0
0.2
0.4
0.6
0.8
1
r/a
T_e (keV)
1
0.8
0.6
0.4
0.2
0
-0.4
-0.2
0
0.2
0.4
0.6
0.8
1
r/a

Fig. 3

11

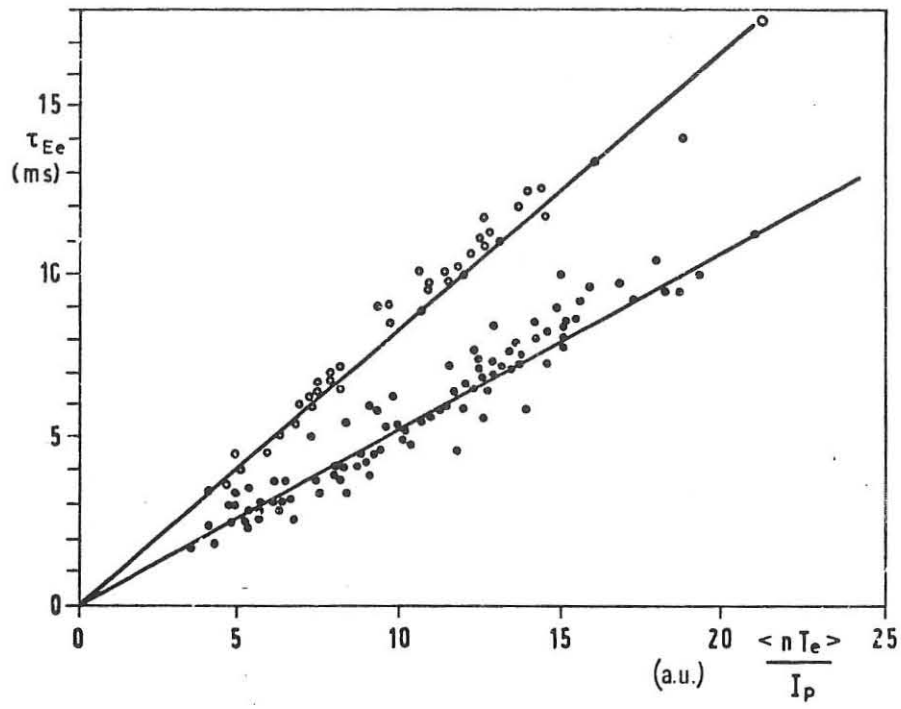

Fig. 4

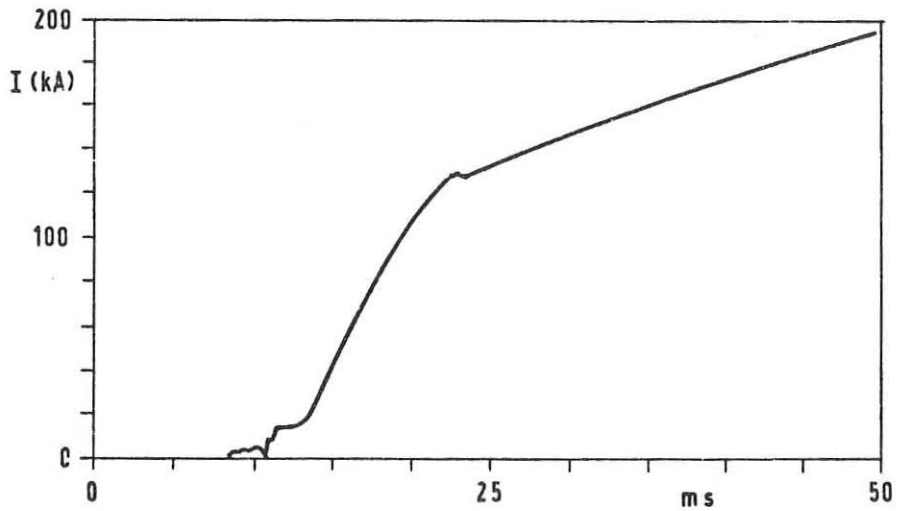

Fig. 5

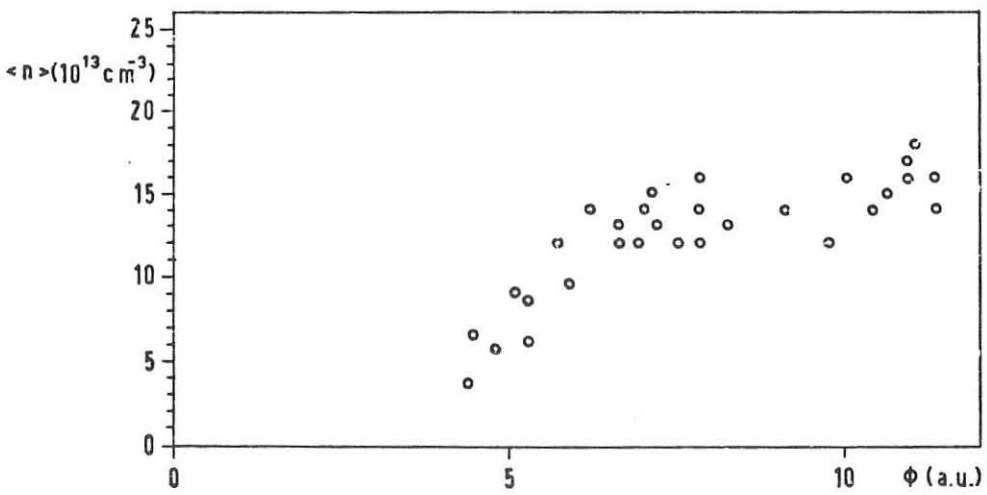

Fig. 6

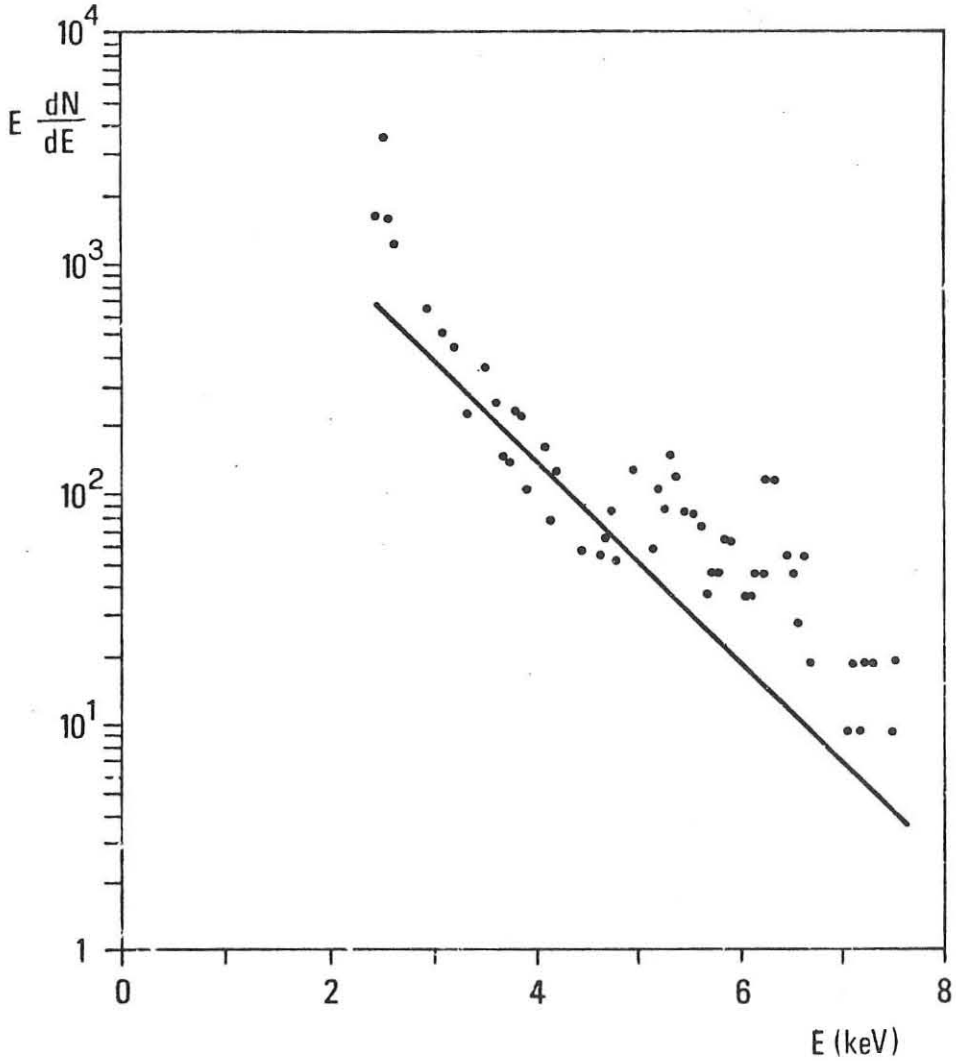

Fig. 7

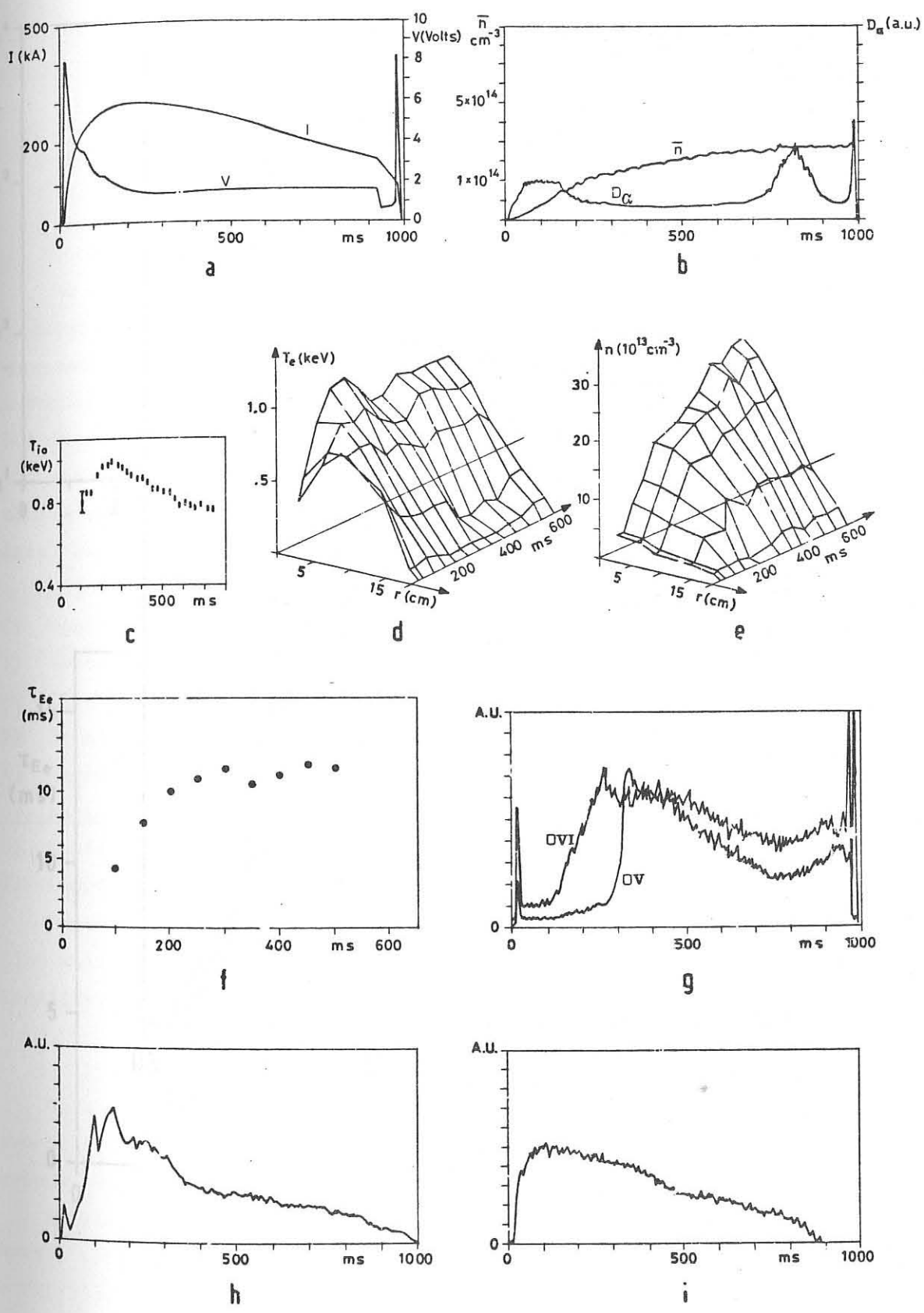
I (kA)
V(Volts)
I
V
ms
a
$\bar{n}$ cm^{-3}
D_α (a.u.)
5×10^{14}
1×10^{14}
$\bar{n}$
D_α
ms
b
T_{io} (keV)
0.8
0.4
500 ms
c
T_e (keV)
1.0
.5
5
15 r (cm)
200
400 ms 600
d
n (10^{13}cm^{-3})
30
20
10
5
15 r (cm)
200
400 ms 600
e
τ_{Ee} (ms)
10
5
200
400 ms 600
f
A.U.
OVI
OV
ms
g
A.U.
500 ms 1000
h
A.U.
500 ms 1000
i

Fig. 8

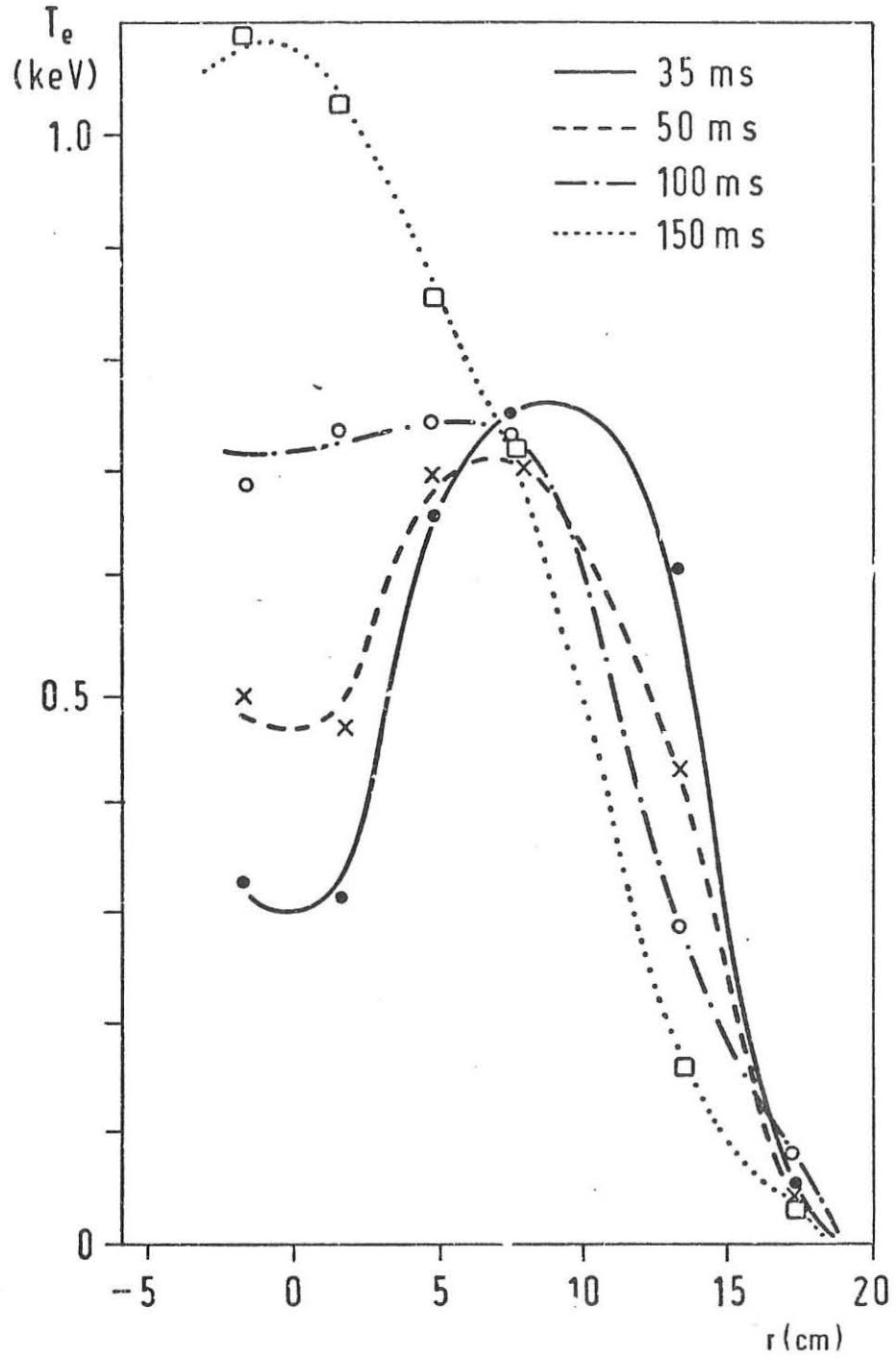

Fig. 9

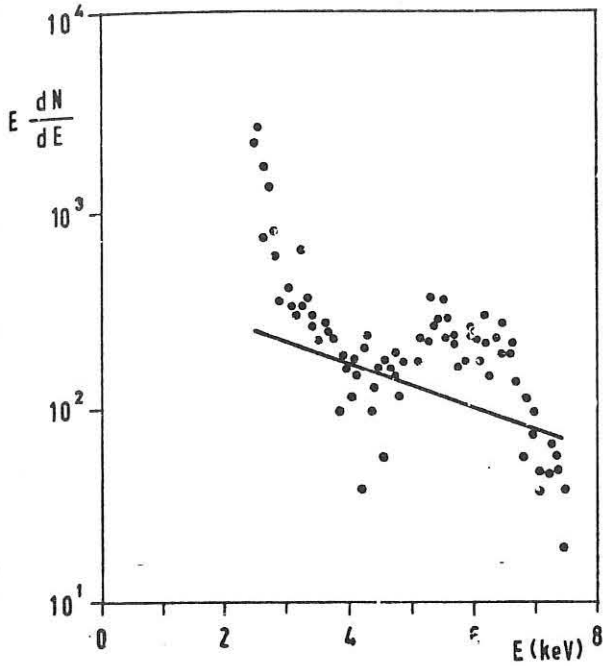

Fig. 10

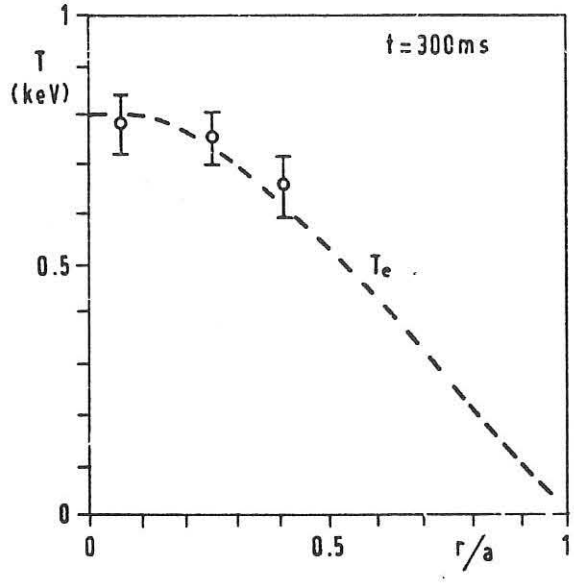

Fig. 11

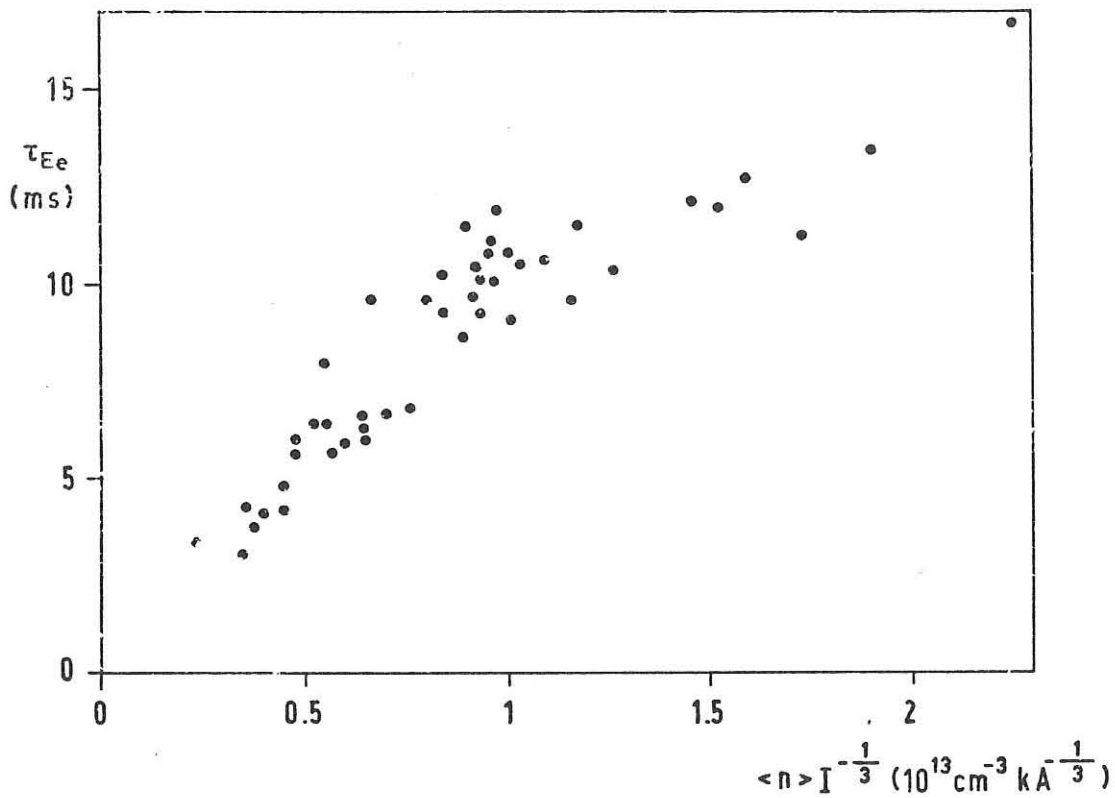

Fig. 12

PROGRESS IN JAPANESE TOKAMAK RESEARCH

FUJISAWA, Noboru and MORI, Sigeru
Japan Atomic Energy Research Institute,
Tokai-mura, Naka-gun, Ibaraki-ken, Japan

1. Introduction

We shall describe in this report recent progress in tokamak experiments in Japan. Great progress in the understanding of tokamak confinement has been made in the past few years. In particular, notable developments in impurity control, low-q discharge, scaling law, scrape-off plasma and radiofrequency heating have been achieved.

Several tokamak-type devices are now operating in Japan. Their machine parameters are summarized in Fig. 1.1. Details of their experimental results are given in individual reports [1∿59]

Major significant progress in the Japanese tokamak experiments includes

(1) Precise control of the plasma position,
(2) Successful operation of non-circular tokamaks with and without a divertor,
(3) Stable very low-q and high density discharges,
(4) Understanding of the origin of impurities and their control,
(5) Better understanding of scaling laws,
(6) Scaling laws for plasma parameters in the scrape-off layer,
(7) Successful radiofrequency heating at 200 kW.

In the following sections, we are going to discuss tokamak experiments, which will be described by conventionally classifying into equilibrium, stability, confinement, impurity, scrape-off plasma and heating.

2. Equilibrium

We shall begin with the equilibrium of tokamak configuration. Japan has several tokamak devices of medium-to-small size, in which plasmas with various cross-sections have been successfully obtained.

Stable D-shaped plasmas have been made in TNT and HYBTOK. Figure 2.1 shows a contour map of the electron temperature by the Thomson scattering in TNT[55], which is equipped with active and passive field shaping coils. The elongation ratio expected to be 1.5 with an average decay index of -0.2. The elongation is consistent with the outer magnetic surface obtained by magnetic probes. Moreover, the elongation was confirmed directly by the plasma current distribution determined from the probe measurements in low current discharges[54]. In HYBTOK, which has shaping coils and no

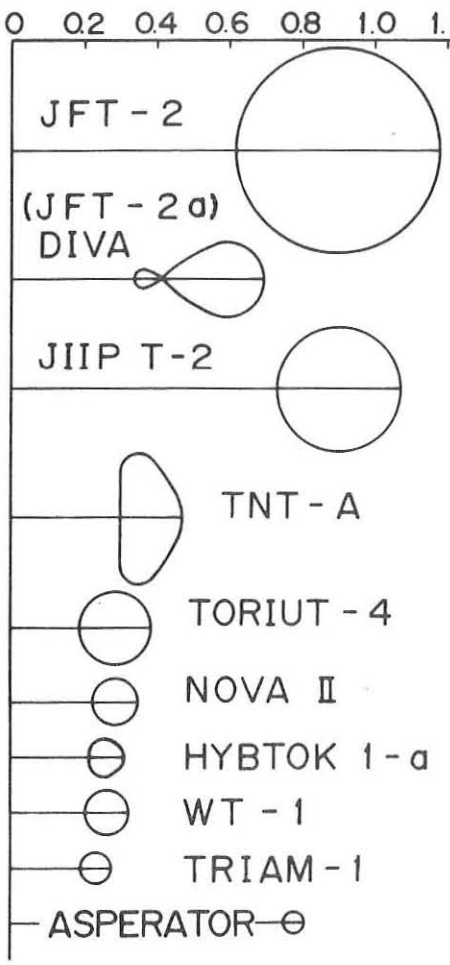

	R (cm)	a (cm)	B_t (kG)	I_p (kA)	Remarks
JFT-2	90	28	16	150	
(JFT-2a) DIVA	60	10	20	80	Divertor
JIIP T-2	91	17	30	160	Feedback Control
TNT-A	40	9/14	4.4	50	D-Shape
TORIUT-4	30	10	4	10	B_t-Compression
NOVA II	30	6	15	15	
HYBTOK 1-a	30	7.5	7	25	D-Shape
WT-1	28	6	19	20	Wave Heating
TRIAM-1	25	4	40	18	High Field
ASPERATOR	80	3	5	10	Helical Axis

Fig. 1.1 Tokamak-type devices in Japan.

conducting shell, D-shaped configurations were confirmed with the obsevation of the mode changes of mhd instabilities, which was also consistent with the outer magnetic field distributions[56, 57].

The stable teardrop-like configurations with a separatrix magnetic surface have been successfully obtained in DIVA by using a divertor coil and a copper shell[21∿23]. The configurations were investigated in detail by a several kind of measurements; (1) comparing the measured poloidal field distributions along the inner surface of the shell with the numerically calculated results, (2) electron density profiles of the main and the scrape-off plasmas, (3) tracing the runaway electrons during the discharge, (4) sawtooth oscillation profiles. These results confirm the teardrop-like configurations with separatrix magnetic surfaces. The discharges with the divertor are realized with I_D/I_p=0.7∿2.0 as shown in Fig. 2.2, where I_D and I_p are the divertor and discharge currents, respectively. When I_D/I_p <0.7, plasmas have no separatrix surface and change into conventional teardrop-like plasmas. Figure 2.3 shows that the surface with a safety factor of q=1 is elongated in very low q discharges[45]. Furthermore, the dynamic magnetic limiter operations, which will be able to control the

plasma diameter and current profile, have been demonstrated[23]. The configurations stably changed with a time constant of the energy confinement time as shown in Fig. 2.2.

A precise control of the plasma position has been successfully done over a period much longer than the confinement time in JIPP T-2[49] as shown in Fig. 2.4, and in TRIAM-1, both of which have resistive shells. The feedback and feedforward control system have been used in JIPP T-2 and the preprogramed one in TRIAM-1.

In DIVA, superthermal electrons (100 eV∿100 keV) are well guided along the diverted magnetic field lines to the divertor. Figure 2.5 shows the path of the high energy electrons[29]. The spread of the path may be explained by the fact that a non-axisymmetric perturbation deforms the old separatrix magnetic surface and makes an ergodic region around the separatrix. The $\delta B/B=0.1\%$ is expected, where δB and B are the perturbation ideal separatrix magnetic surface and makes an ergodic region around the appears to give no adverse effect on the confinement, and contrarily it could reduce the heat flux density on the material surface.

In summary, the following results have been obtained concerning the equilibrium.

(1) Stable non-circular configurations have been successfully obtained.
(2) The configuration stably changes with a time constant of the energy confinement time.
(3) Precise plasma position control has been done.
(4) It was indicated that a non-axisymmetric perturbations deform the separatrix magnetic surface.

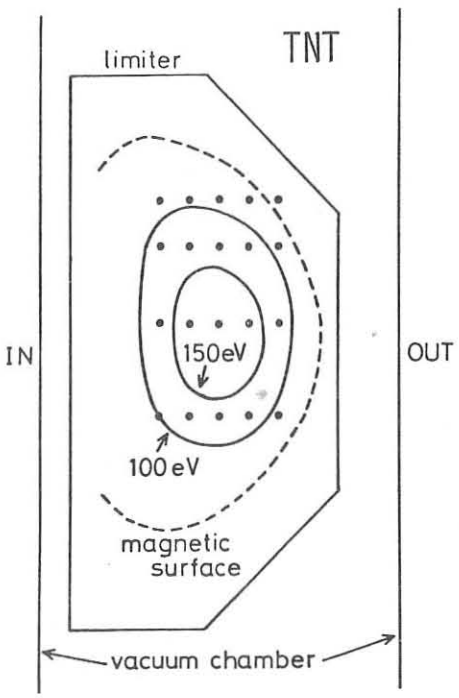

Fig.2.1 Contour map of electron temperature of discharges with I_p=20kA, V_L=4V, $\bar{N}$=-0.2. Contours are estimated from vertical and radial temperature profiles by Thomson scattering measurements. Measuring points are shown by closed circles. Dashed line gives magnetic surface obtained probe measurements.

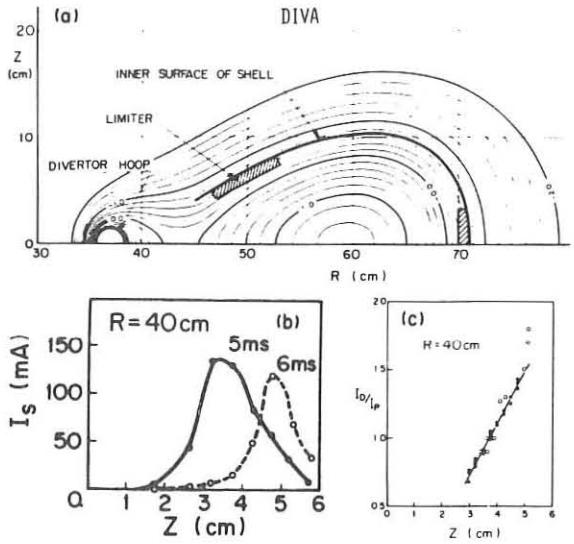

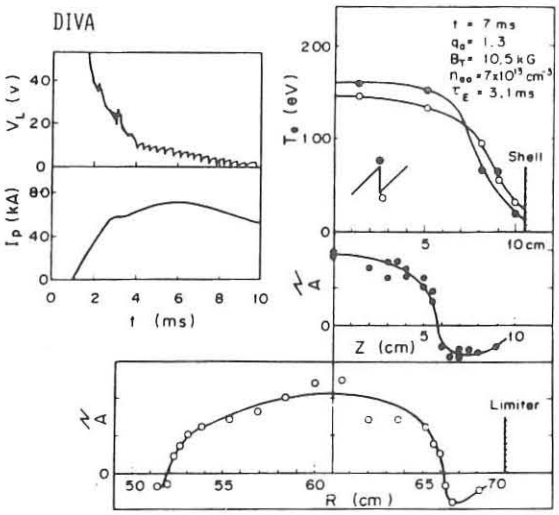

Fig. 2.3 Radial and vertical profiles of sawtooth oscillation with q_a=1.3 very low-q discharges.

Fig. 2.2 (a) An example of equilibrium configuration with uniform current, β_p=0.1, and I_D/I_p=0.9 from numerical calculation. (b) Profiles of ion saturation current I_S in the divertor region. The solid line correspond to I_D/I_p=0.9 and the dotted to the case where I_D/I_p is increased from 0.9 at 5ms to 1.8 at 5.4ms. (c) Positions of the peaks of ion saturation current profiles (O) and X-ray intensity(●) from a movable target at R=40cm for various I_D/I_p.

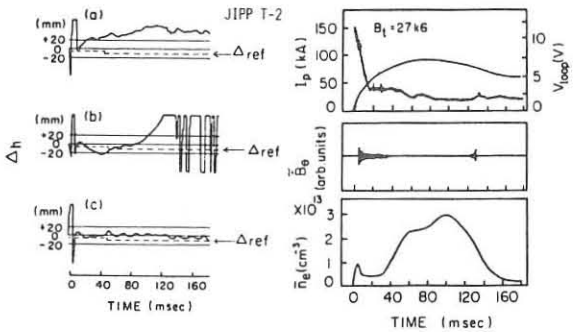

Fig. 2.4 (a) Feedback only. (b) Feedforward only. (c) Combined system. Δ_h is the horizontal displacement of plasma position. Right figures are evolution of plasma parameters in the case (c).

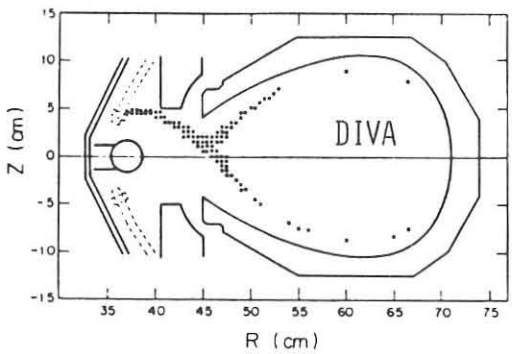

Fig. 2.5 Path of high energy electrons (10keV - 100keV).

3. Stability

Stable low-q discharges free from current disruptions offer a possibility for realizing a low-cost reactor. It also reduces serious electrical and mechanical problems of a large tokamak device. Major progress has been made in understanding the current disruptions and obtaining the stable low-q discharges. Here, we describe the disruptive instabilities

and the very low-q discharges.

The discharges with $q_a=3\sim4$ disrupt in some cases. In particular, most of the dirty discharges often terminate in the current disruptions. The most suspicious candidate for them is the resistive tearing mode and in most of the cases the m/n=2/1 tearing mode induces large negative spikes. These current disruptions can be easily suppressed by the choice of suitable current profiles.

In JIPP T-2, low-q discharges have been obtained with additional gas puffing and the rise of the discharge current as shown in Fig. 3.1[51]. The rising current(or the gas puffing) alone heats(or cools) the peripheral plasma, and the plasmas become unstable. Both the current rise and gas puffing lead to a favorable current profile. The experimental results on the stabilization of the disruptions agree well with the estimate from the tearing mode analysis.

The more effective method to control the current profile is the titanium gettering. Figure 3.2 shows that the attainable q_a in JFT-2 decreases with the reduction of radiation losses by the titanium gettering. These less impurity discharges with $q_a>2$ can be easily disrupted by injecting a small amount of impurities. This behavior can be well understood as a sudden growth of the m/n=2/1 mode and large island formation predicted by the linear tearing mode calculations. In the calculation, the impurity cooling and internal m/n=1/1 disruption play an important role in the growth of the m/n=2/1 mode[44].

The stable discharges with $q_a<2$ can be successfully obtained in DIVA by the titanium gettering. The discharges with and without the divertor are both stable. The typical discharge characteristics with $q_a<2$ are shown in Fig. 3.3[45]. When the discharge current crosses through the $q_a=2$, the magnetic field perturbations grow, but they do not lead to the disruption. The minimum q_a value obtained in DIVA in $q_a=0.85$ as shown in Fig. 3.4. The discharges with $q_a<1.3$ have poor confinement. For example, the confinement time of the discharge with $q_a=1.05$ is only 50 μs, and the loop voltage is high. However, the discharges with $q_a>1.3$ have quite similar characteristics as the normal ones.

In other devices except DIVA, the $q_a=2$ cannot be crossed stably. In JFT-2, just before the disruption, the radiation loss does not increase and remains around 10% of the Joule input as shown in Fig. 3.2. The observed fluctuation with the m/n=2/1 mode is supposed to be a surface kink mode. Possible candidates which enable us to attain q less than 2 in DIVA are;

(a) separatrix magnetic surface,

(b) shell stabilization,

(c) non-circular cross-section,

(d) current profile.

The presence of the separatrix reduces the magnetic fluctuation as shown in Fig. 3.5. It is quite probable that the separatrix stabilizes the surface kink mode and that the stable very low-q discharges can be realized more easily in DIVA with the separatrix. The shell plays an important role in stabilizing the surface kink mode. In DIVA, which is usually operated with the ratio of radius of the shell to the limiter b/a=1.2, discharges with b/a=1.35 can also stably cross the q_a=2 and can reach q_a=1.65. Hence the shell is not a definitive factor in stabilizing the surface kink mode. The noncircular cross-section and the current profile are both possible stabilizing factors. Up to now, however, there is no answer on which is the most determining factor in stabilizing the surface kink mode.

It should be noted that no major disruption takes place in discharges with $q_a<2$. Figure 3.6 shows the number of occurrence of the disruptions at differenct q_a, when neon is injected into stable q_a=1.6 discharges. The major disruptions never occur during the period with $q_a<2$. This fact indicates that the surface with q_a=2 inside the plasma is required in inducing the current disruption.

In conclusion, the following results have been obtained in the low-q discharges.

(1) Stable discharges with $q_a<2$ can be successfully obtained with and without the divertor, and no major disruption is observed in both cases.

(2) The obtained minimum q_a is 0.85. When $q_a>1.3$, the discharges have good confinement characteristics, but discharges with $q_a<1.3$ have poor confinement.

(3) The separatrix magnetic surface stabilizes the surface kink mode.

(4) The disruption-free discharges with $q_a>2$ can be easily obtained by a suitable current profile control.

(5) The current disruption in discharges with $q_a>2$ seems to be induced by the resistive tearing mode.

4. Confinement

The understanding of tokamak confinement has advanced in the past few years. Simple scaling laws can cover most of the data in many devices.

Titanium gettering reduces the radiation loss at the plasma periphery by preventing the release of light impurities, and yield a broad hot plasma core, improving in consequence the confinement time. Figure 4.1 shows the

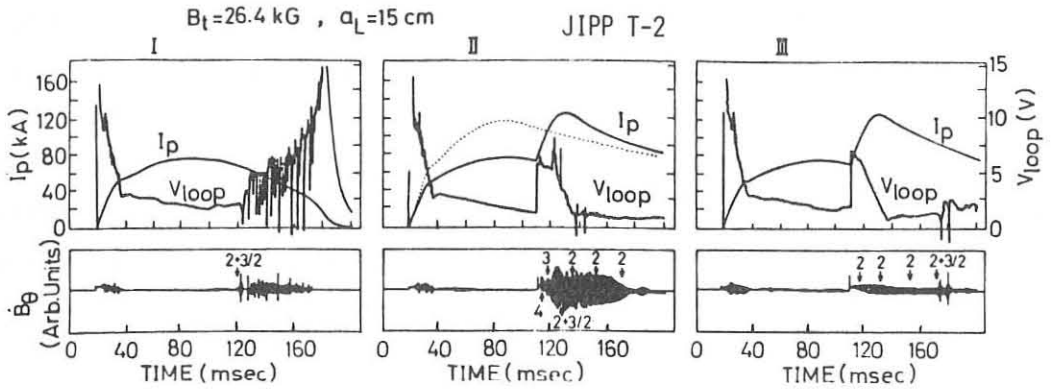

Fig.3.1 Comparison of three types of discharges. caseI: with only the strong gas puffing, caseII: with only the second current rise, caseIII: the optimum combination between the gas puffing and the second current rise.

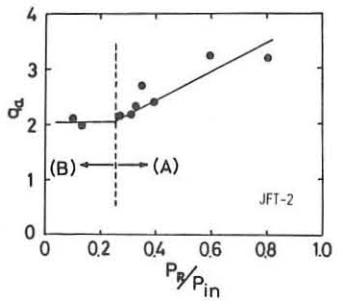

Fig.3.2 The attainable q_a. P_R and P_{in} are radiation loss and Joule input power just before disruption.

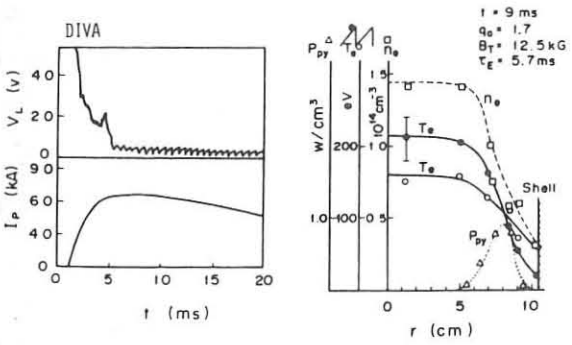

Fig.3.3 Typical plasma characteristics in a q_a<2 discharge.

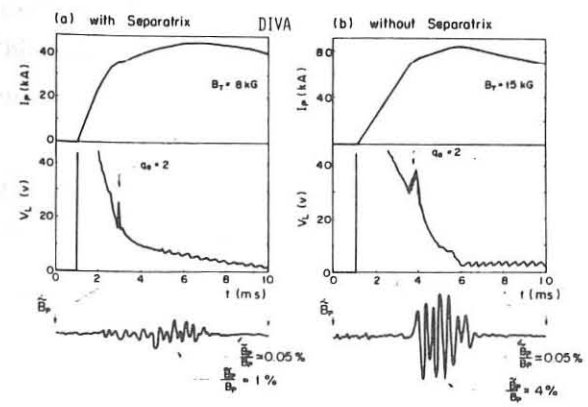

Fig.3.5 Discharges with and without separatrix.

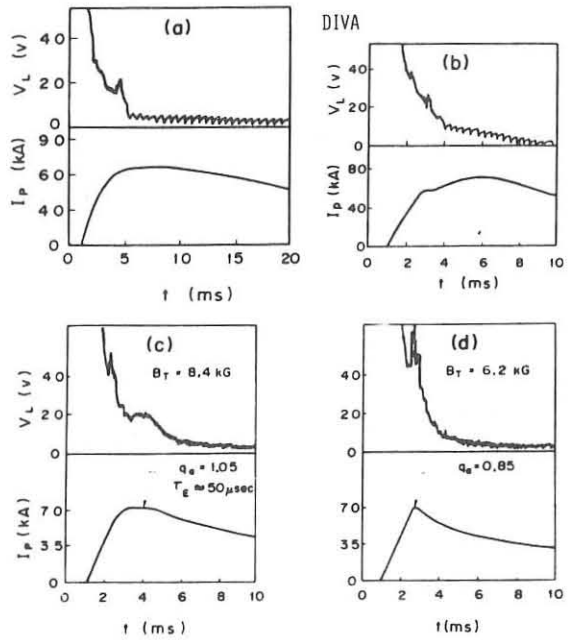

Fig.3.4 Discharges with q_a<2. (a) q_a=1.7, (b) q_a=1.3, (c) q_a=1.05, (d) q_a=0.85.

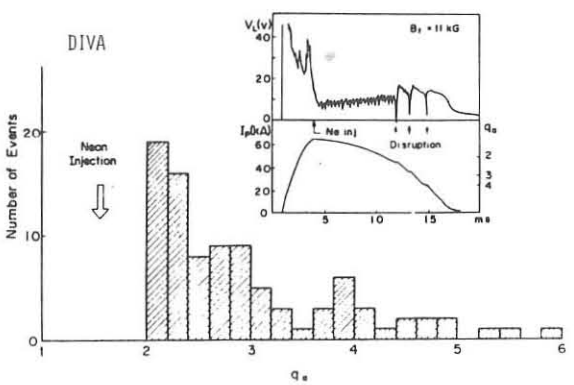

Fig.3.6 Number of occurrence of observed disruption at different q_a when neon is injected into stable q_a=1.6 discharges. Disruption never occurs in q_a<2.

effect of the titanium gettering in JFT-2[11]. The reduction of the radiation loss due to oxygen impurity broadens the hot plasma core. This results in the increase of the energy confinement time by a factor 1.6. It can be be seen that even the confinement time without the titanium gettering is longer than estimated from the ALCATOR scaling. This fact shows that larger machines are in a better position than small ones on the radiation loss due to light impurity. The titanium gettering further increases the energy confinement time.

In DIVA, the energy confinement time and the average particle confinement time with and without the divertor have been investigated over a wide range of the plasma parameters. The energy confinement time with the divertor is in good agreement with the ALCATOR scaling law, except that the divertor increases the energy confinement time by a factor of 2.5. The divertor reduces the radiation loss due to the impurities and broadens the hot core as in the titanium gettering as shown in Fig. 4.2[43]. In contrast with the energy confinement time, no significant improvement is observed in the average particle confinement time.

The increase in the energy confinement time is due to the broadening of the electron temperature profile as mentioned above. In discharges with large radiation loss, the heat escaping from the hot core is radiated at the plasma periphery. It is viewed as if an imaginary limiter exists at the plasma periphery and hence the energy confinement time decreases. On the other hand, the particle does not escape abruptly at the radiation-rich region. Therefore, the particle confinement time does not strongly depend on the radius of the hot core.

The heat-diffusion coefficient in the hot core is derived from the profiles with and without the divertor. They are $(3\sim4)\times10^{3}\,cm^{2}\cdot s^{-1}$ in both cases[34]. This small difference is consistent with the fact the divertor increases the energy confinement time by increasing the effective radius.

The radius of the plasma hot core is a more important factor determining the energy confinement than the normal limiter radius. So in Fig.4.3, the half radius of the electron temperature profile is used instead. This modified ALCATOR scaling describes well the observed energy confinement time in various conditions of many devices.

Figure 4.3 includes the low-q discharges in DIVA. In the low-q discharges the internal sawtooth oscillation governs the confinement. The period during the temperature rising phase has a good confinement time, and most of the energy is lost during the internal disruption. It is well

understandable that the confinement except for the internal disruption follows the modified ALCATOR scaling law.

From a view point of the high β plasma confinement, it is very interesting to know the density limit in very low-q discharges with $q_a<2$. Since they show no current disruption, it is very easy to increase the density. Figure 4.4 shows the normalized density, i.e. $\bar{n}_e R/B_t$ Up to now, $\bar{n}_e R/B_t=4\sim5$ can be easily obtained in the very low-q discharges[45].

The results on the confinement study are summarized as follows.

(1) The reduction of the radiation loss by decreasing impurities increases the energy confinement time by a factor of 2∿3. The improvement in the confinement time is due to broadening of the plasma hot core.

(2) The diffusion and thermal conduction coefficients hardly change by reducing radiation loss.

(3) The particle confinement time is roughly equal to the energy confinement time, and its scaling is in agreement with the ALCATOR scaling.

(4) The modified ALCATOR scaling can well describe the observed energy confinement time obtained up to now.

(5) The very low-q discharges have desirable aspects for the high β tokamak with the high density.

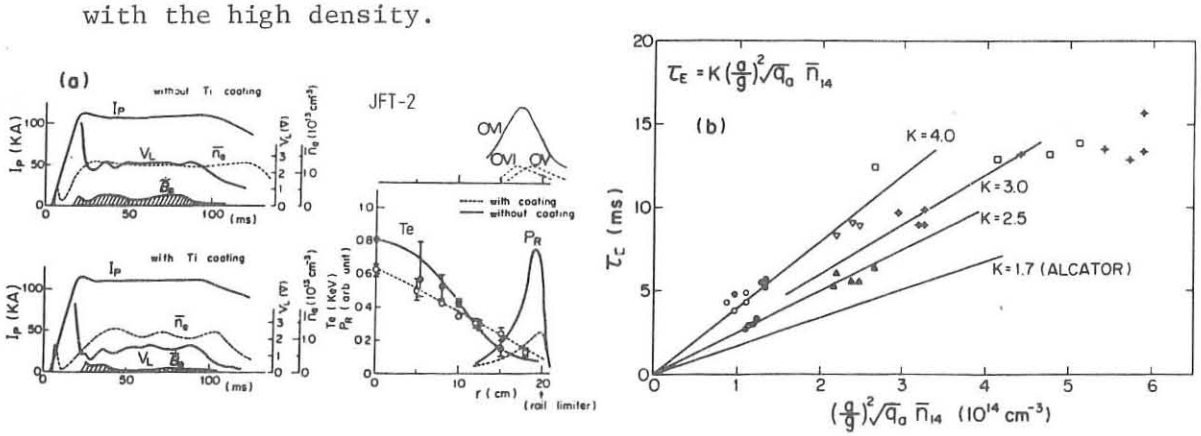

Fig. 4.1 Effect of Ti-gettering. (a)Radial profiles of electron temperature and radiation loss with and without Ti-gettering, and OVI and OV line emission. (b)Energy confinement time. Discharge conditions are following: □, ▽, ⊗, o; limiter radius a=20cm, q_a=4 with Ti-gettering, ▲, ●; a=20cm, q_a=4 without Ti-getting, ✱, ✱; a=25cm, q_a=4 without Ti-gettering.

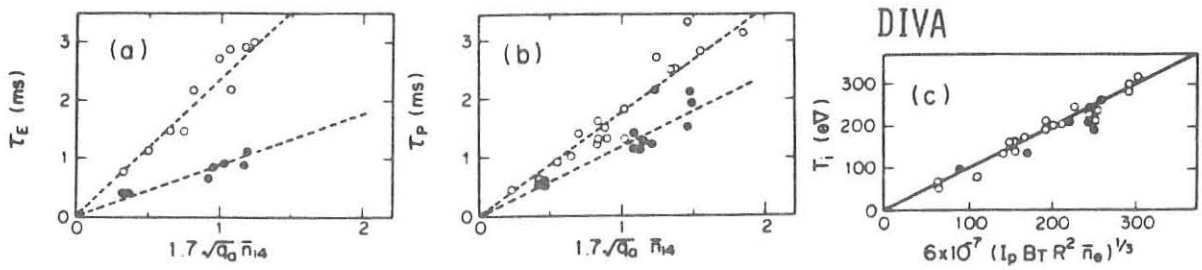

Fig. 4.2 Energy confinement time τ_E, average particle confinement time τ_p and central ion temperature Ti with (o) and without divertor (●). I_p: plasma current, q_a: safety factor, $\bar{n}_{14}=\bar{n}_e/(10^{14}\mathrm{cm}^{-3})$ and $(I_p B_T R^2 \bar{n}_e)$ in $(\mathrm{A\cdot G\cdot cm^2\cdot cm^{-3}})$.

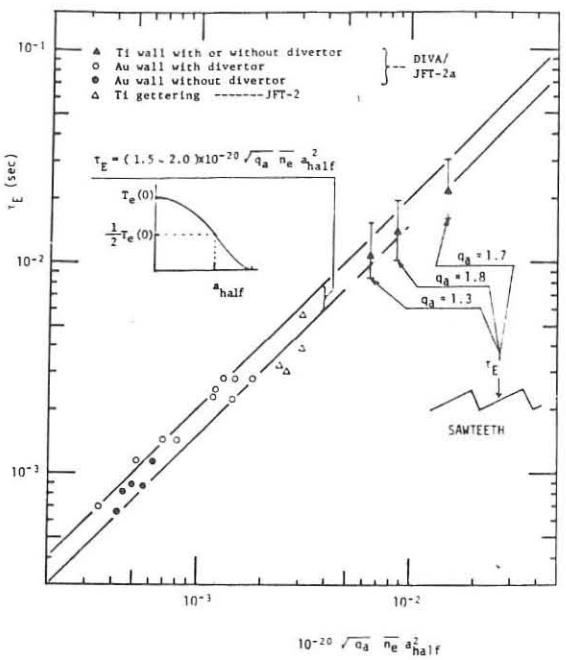

Fig.4.3 Modified empirical scaling law of energy confinement time where a_{half} is a half radius of an electron temperature profile.

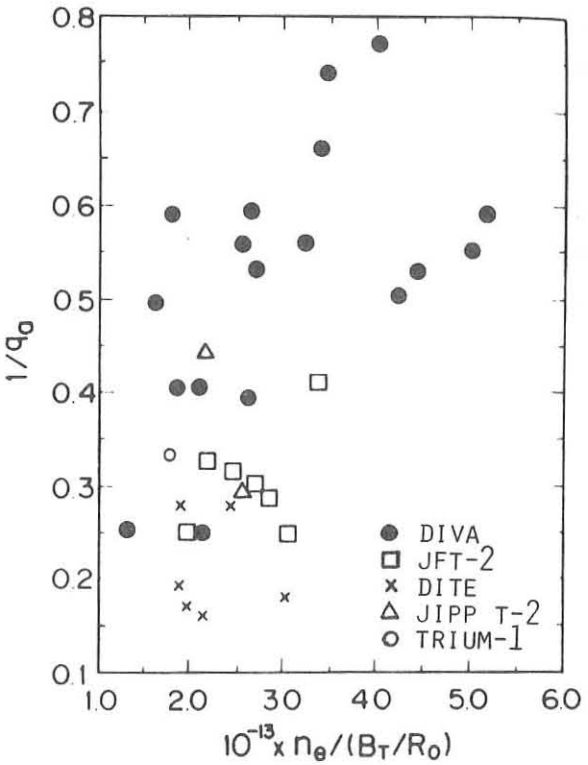

Fig.4.4 Normalized mean electron density where $n_e(cm^{-3})$, $B_T(T)$, $R_o(m)$.

5. Impurity

It is well known that impurities pose one of the most important problems to be solved to realize tokamak reactors. Since the completely impurity-free discharges cannot be expected, it is extremely important to control the impurities. Great progress in the impurity control has been made in the tokamak experiment in Japan.

Metal impurities have serious influences on future large tokamaks. The possible mechanisms of the metal impurity influx are sputtering, arcing and evaporation. In JFT-2, the limiter surface temperature has been measured with an infrared camera as shown in Fig.5.1[16]. The limiter surface temperature in discharges without runaway electrons can be interpreted by taking account of the heat flux of a Maxwellian plasma onto it [7]. In discharges with energetic electrons, the limiter temperature becomes high. es. However, the surface temperature is 400∿600°C at most, and the thermal evaporation can be ruled out.

In DIVA, aluminum samples are inserted into the diverted plasma to clarify the metal impurity origin. The arcing phenomena were observed only in cases with the dirty sample surface[30]. The arcing does not take place on the clean sample surface in normal discharges.

These results suggest that the major mechanism for the metal impurity production is the sputtering. The sputtering yield depends on the species

of incident particles and their energy. The incident particles are accelerated by the sheath potential in front of the surface, and hence the electron temperature in the scrape-off layer plasma is an important quantity. Figure 5.2 shows that the impurity(Mo) in JFT-2 reduce with decrease of the electron temperature in the scrape-off plasma[18]. If metal is used as wall material, the electron temperature of the plasma which touches a wall must be enough low, for example, a few tens of eV. A carbon limiter was tested in JFT-2 and it was found that the macroscopic discharge characteristics were almost equivalent to those with Mo limiters[15].

The species of the incident particles is an another important factor. In Fig.5.3, the intensity of the Au-I line radiation in DIVA that correlates to the quantity of the metal impurity efflux is plotted as a function of applied voltage to the wall. The left region below 400 V can be understood with the self-sputtering of the gold[30]. The right region above 400 V can be interpreted with the sputtering by the hydrogen in addition to the self-sputtering. The comparison between a hydrogen discharge and a helium one shows that the increase in the metal efflux is due to the difference between the sputtering yields of the helium and the hydrogen ions[18]. In discharges with the scrape-off plasma temperature of 20∿40 eV and the large quantity of light impurities, the sputtering due to the light impurities becomes dominant, and the metal impurities decrease with reducing the light impurities[18].

When the impurities are released from the wall, it is important to know what percentage of the impurity goes into the plasma hot core. The impurity injection experiment has been done in DIVA[35∿39]. The impurity influx going to the hot column are presented as shown in Fig.5.4. The injected impurities are screened out by shielding effect of the scrape-off plasma and by the anomalous transport in the peripheral plasma. In the discharges without the divertor, 80 % of the released impurities are screened out. In the discharges with the divertor, 94 % of the impurities are shielded in the injection into the main plasma, and only less than 0.3 % of the impurities injected into the divertor region flows back into the main plasma. Except for the above-mentioned shielding effect, the divertor reduces the plasma-wall interaction by guiding the loss plasma from the main chamber into the burial chamber. Figure 5.5 shows that the divertor reduces the impurity radiation loss by a factor of 2∿4. The effective reduction is observed in the high current discharges.

In conclusion, the following results have been obtained concerning the impurity.

(1) The major mechanism of the metallic impurity production is the sputtering by the ions accelerated in the sheath potential in front of the surface.

(2) The evaporation of the limiter surface takes place by the local deposition of high energy electrons in the low density discharges, and by arcing in an unstable discharge or in a dirty limiter surface.

(3) The divertor reduces the impurity radiation loss by reducing the plasma-wall interaction and shielding the impurity influx.

(4) The impurities released from the vacuum chamber are screened out by shielding effect of the scrape-off plasma and by the anomalous transport in the peripheral plasma.

(5) The discharge characteristics with the carbon limiters are the same as with the Mo limiters.

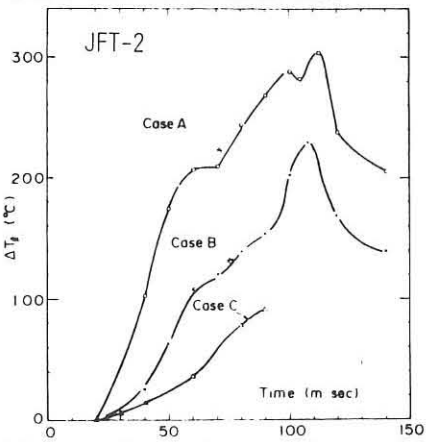

Fig.5.1 Surface temperature rise of Mo limiter with discharge current of 110kA, line density of A)1.3×10^{13}, B)2.5×10^{13}, C)$6\times10^{13}cm^{-3}$. Surface temperature before discharge is around 300°C.

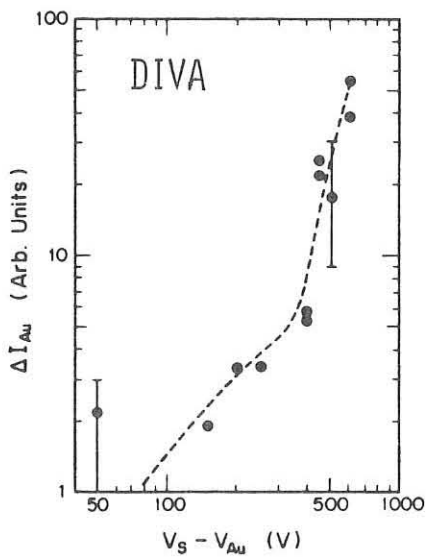

Fig.5.3 Dependence of Au line radiation intensities on the voltage applied to the gold-plated shell. V_S-V_{Au} is the potential gap between the plasma space potential and the gold-plated shell.

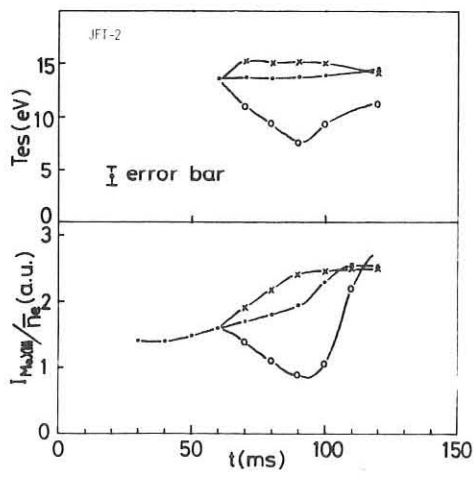

Fig.5.2 Metal impurity(Mo limiter) when electron temperature in scrape-off layer is varied in discharge current of 100kA.

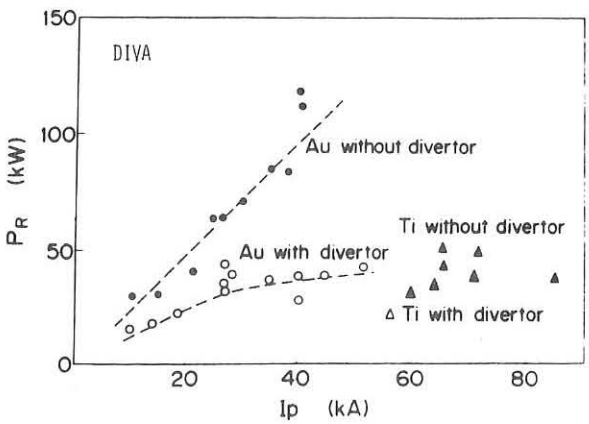

Fig.5.5 Radiation loss power v.s. plasma current.

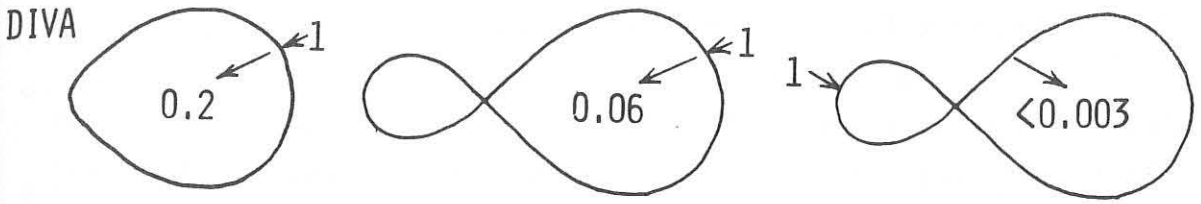

Fig.5.4 Impurity influx into the plasma hot core when impurities are injected to the main and the diverted plasmas with and without the divertor.

6. Scrape-off plasma

The plasma parameters in the scrape-off layer are important not only for studying the confinement characteristics, but also for the control of the impurity production. The energy and particle balances in the main plasma influence the plasma parameters in the scrape-off layer. The measurement of the scrape-off plasma is equivalent to the determination of the gross confinement. Inversely, when the scrape-off plasma is limited from the impurity contamination, the heat transfered to the scrape-off plasma is restricted within a limit, and therefore the main plasma energy must be radiated by some methods except the convection and the conduction.

The heat flux into the scrape-off layer is $(P_{in}-P_R)$, where P_{in} and P_R are the input power and the radiation loss power including the charge-exchanged particle loss, respectively. On the other hand, the heat loss from the layer is $\gamma T_{es} F_p$, where the radiation loss in the scrape-off is negligible and γ, T_{es} and F_p are the heat transmission rate, the average electron temperature in the scrape-off layer and the total particle loss flux from the main plasma, respectively. The energy conservation gives

$$T_{es} = \frac{3}{2} \frac{\tau_p}{\tau_E} \frac{\bar{T}_e + \bar{T}_i}{\gamma} \left(1 - \frac{P_R}{P_{in}}\right) \quad \text{eV} \qquad (1)$$

where τ_p, τ_E, $\bar{T}_e$, $\bar{T}_i$ are the particle confinement time, the energy confinement time, the average electron and ion temperature of the main plasma, respectively[34]. Figure 6.1 shows the relation between the measured electron temperature T_{es}^M in the scrape-off layer and the γT_{es} calculated from the parameters in the main plasma in DIVA[43]. The obtained γ are well understood by the sheath model including the effect of secondary electrons and epithermal electrons. The profile of the electron temperature is nearly constant over the scrape-off layer[14].

When the modified ALCATOR scaling law is applied to the particle confinement time ($\tau_p = 0.5\tau_E \propto \sqrt{q} n_e a_{half}^2$), as mentioned previously, the following relation is derived.

$$P_{in} - P_R = \frac{\gamma L T_{es}}{2\sqrt{q}} \left(\frac{a}{a_{half}}\right)^2 \quad \text{W} \qquad (2)$$

where L(cm) is the length of the torus. When $a/a_{half}=\sqrt{2}$, q=3, γ=8,

$$P_{in} - P_R = 4.6\ LT_{es} \quad W \tag{3}$$

In the medium-sized tokamak (L=5m), $P_{in}-P_R$=100∿200kW, therefore T_{es}=45∿90eV is reasonable values. This equation indicates that in the future large tokamak (L=20m, P_{in}=40MW), the electron temperature in the scrape-off layer increases up to 4.3keV with the impurity-free plasma(P_R=0). The large machines have to be equipped with the divertor or the magnetic limiter which are able to receive the plasma of a few keV. When the normal limiter is used, the electron temperature in the scrape-off layer must be less than 100eV in order to avoid the impurity contamination due to the ion sputtering. So, $P_{in}-P_R$ is limited within 0.9MW, and most of the input power must be radiated as a radiation loss. It is necessary to cool the peripheral plasma by the light impurity.

The electron density in the scrape-off layer is determined by the particle balance between the influx into the scrape-off layer from the main plasma and the out flux consisting of the parallel flow to the magnetic field and the cross-field diffusion. Figure 6.2 is the electron density profiles in JFT-2, the density decays like an exponential, which is in good agreement with the simple model giving[14]

$$n = n_a \exp\left(\frac{a - r}{\lambda}\right) , \quad \lambda = \left(\frac{L^* D}{2v_f}\right)^{1/2} \tag{4}$$

where λ is the characteristic width of the scrape-off layer and L^*, D, v_f are the length of the magnetic field line between the material surfaces in the scrape-off layer, the cross-field diffusion coefficient, the parallel particle flow velocity to the field, respectively. In DIVA, $v_f=(\frac{1}{2}\sim\frac{1}{3})c_s$ (c_s: sound velocity) is experimentally identified[43]. The region I and II in Fig.6.2 correspond to the scrape-off layer behind the rail and the aperture limiters, respectively. The λ in the II region gives the diffusion coefficient D =(1∿4) m^2/s. This value is of the order of the Bohm diffusion coefficient. In DIVA, the divertor efficiency η_p(=particle into the divertor/total particle loss flux) for the particle flux was investigated as shown in Fig.6.3. The observed results coincide in the parametrical dependence with the simple model using the Bohm diffusion[43].

The total particle outflux from the main plasma is N/τ_p, and when the modified ALCATOR scaling law is applied to the particle confinement time $\tau_p=0.5\tau_E$, the outflux is given as follows

$$\frac{N}{\tau_p} = \pi L\ 10^{18} . \quad 1/s$$

The average density in the scrape-off layer is

$$n = \frac{N/\tau_p}{2\pi a \lambda v_f} . \tag{5}$$

The average electron density of the future large tokamak is almost same as one of the present tokamak, because $N/\tau_p \propto L$, $2\pi a\lambda v_f \propto a$.

The heat flow in the scrape-off layer has been intensively investigated in DIVA and JFT-2[37,7]. The heat flux into the material surface is given as

$$q = \gamma T_{es} n v_f \ . \qquad (6)$$

As shown in Fig.6.4, the observed heat transmission coefficient γ is 8∿16, which includes the effect of the higher electron component and the secondary electron emission.

The following results have been obtained concerning the scrape-off plasma.

(1) The energy and particle conservation laws give the simple formula for the plasma parameters in the scrape-off layer.

(2) The average electron temperature of the scrape-off plasma is presented in Eqs. (1) or (2). The radial profile of the temperature is almost constant.

(3) The average electron density in the scrape-off layer presented in Eq.(5). The density decays like an exponential in Eq.(4).

(4) The particle flux parallel to the magnetic field is $(1/2\sim1/3)nc_s$, and the cross-field diffusion is Bohm-like.

(5) The heat flux density to the material surface is presented in Eq.(6).

(6) The plasma parameters in the scrape-off layer are very important not only in the confinement study, but also in the impurity control.

(7) The scrape-off plasma has an ability to shield the impurity influx.

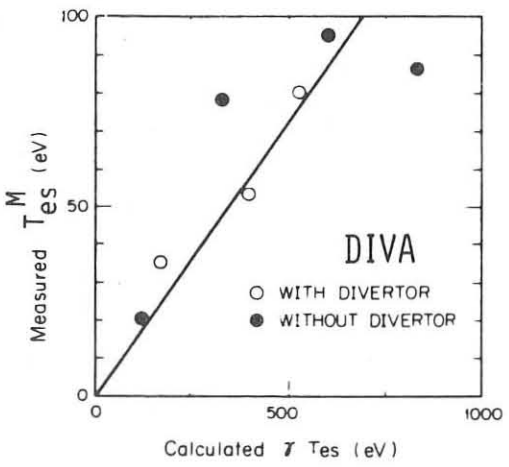

Fig.6.1 Measured electron temperature T_{es}^{M} and calculated γT_{es} in a scrape-off layer plasma.

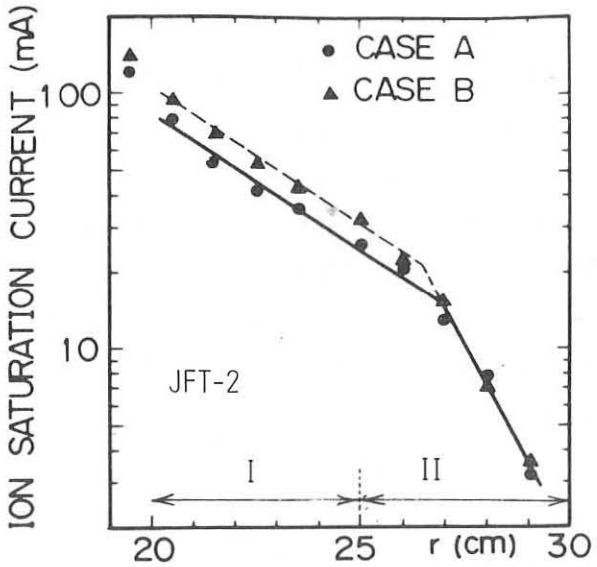

Fig.6.2 Radial profile of ion saturation current in cases A(n_e=1.3x10^{13} cm^{-3}) and B(n_e=2.7x10^{13}cm^{-3}). Regions I and II are behind rail and aperture limiters, respectively.

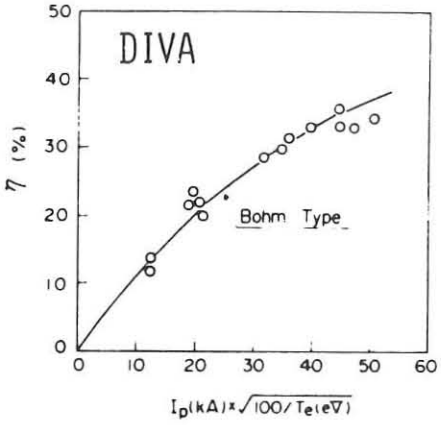

Fig.6.3 Particle divertor efficiency.

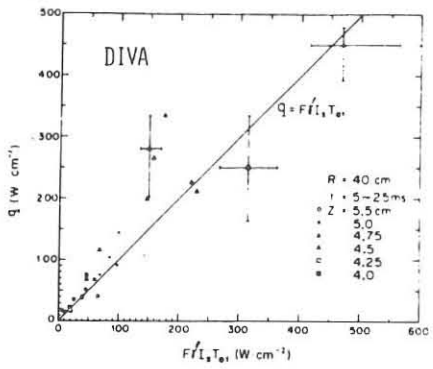

Fig.6.4 Relation between q and $F\gamma I_s T_e$ for two component models. F=1∿2 is a correction factor for two component model.

7. Heating.

Neutral beam heating, radiofrequency heating, turbulent heating, and compression heating have been studied in Japan. In particular, the radio-frequency waves of about 200kW near lower hybrid and ion cyclotron frequency have been successfully demonstrated to be effective in the ion heating.

In JFT-2 and JIPP T-2, the ion heating has been obtained by the lower hybrid heating with a power level of 200kW[9,49]. The ion temperature rise is directly proportional to the radiofrequency power at a rate of about 1eV/kW as shown in Fig.7.1. The heating efficiency of ions is 15∿30%. It is important to notice that the ion temperature rise shows no saturation up to a power level of 200kW, and no adverse effect on the plasma confinement.

In comparison to the neutral beam heating, the physics of the lower hybrid heating is not clear. Some progress in that point has been made[20]. The parametric decay into the cold lower hybrid waves and the ion cyclotron waves has been observed in the heating experiments. The observed decay takes place at the plasma surface and some fraction of the radiofrequency energy was absorbed nearby. The maximum ion heating takes place when the parametric decay remarkably reduces, as shown in Fig.7.2. More efficient ion heating will be expected if the parametric instability is well controlled.

Recently, remarkable progress in the ion cyclotron heating with a power level of 200kW has been made in DIVA, as shown in Fig.7.3. The heating experiment using the second harmonic cyclotron frequency of a deutron plasma with a minority proton component was carried out under the extremely pure wall condition ($Z_{eff}\simeq 1$). The good results is due to the improvement in the

antenna electrostatistically shielded by the full Farady shield, which increases the ion heating efficiency up to above 100%. The improvement of the heating efficiency increases the ratio of the ion temperature increment to the radiofrequency power to ∿2eV/kW, which is 2 times as large as the lower hybrid heating (Fig.7.4). The ion temperature exceeds the electron temperature over the whole plasma cross-section. The ion energy balance can be explained by the neoclassical theory.

The most favorable ion heating has been observed in the following conditions.

(1) The two-ion hybrid resonance layer is located closely at the plasma center, so the cyclotron resonance layer is on the outer side of the plasma cross-section.

(2) The proton-to-deutron ratio satisfies ε_p=5∿10%.

The results indicate that the heating mechanism is due to the mode conversion of the magnetosonic wave at the two-ion hybrid resonance layer. The ion cyclotron heating can be applied to a D-T reactor by adding small amount of hydrogen in a D-T plasma. The power density of the radiofrequency wave in the experiment reaches 1.4Wcm^{-3} without any deleterious effect, and this value is higher enough for the future large tokamak.

The results obtained in the heating are as follows.

(1) The radiofrequency ion heating with a power level of 200kW near the lower hybrid and the ion cyclotron frequencies have been successfully carried out.

(2) The ion temperatures rise in direct proportion to the radiofrequency power at a rate of 1∿2 eV/kW.

(3) The understanding on the radiofrequency heating mechanism has been advanced.

(4) The high power density of the radiofrequency wave never gives an adverse effect on the plasma confinement.

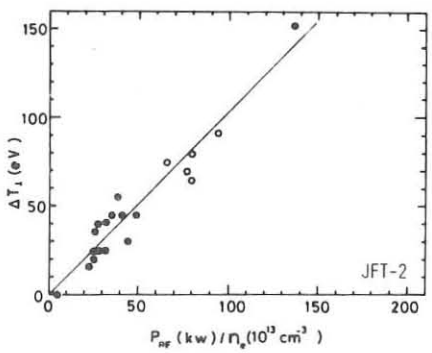

Fig.7.1 Power dependence of ion temperature rise. ● and o are ion temperatures from perpendicular charge-exchange measurement for 650 and 750 MHz.

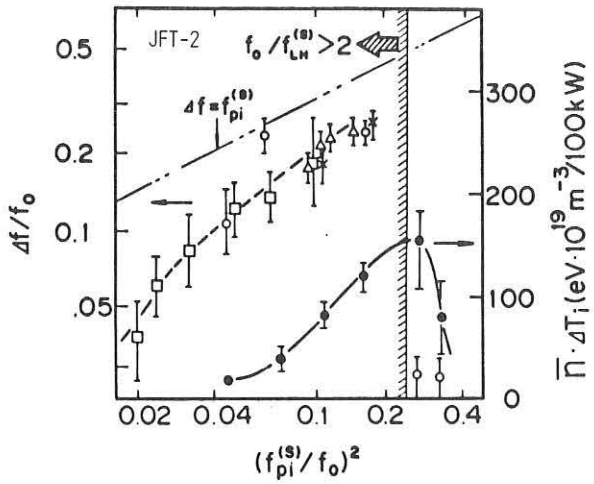

Fig.7.2 Frequency spread Δf and gross ion heating efficiency $n\Delta T_i$ v.s.$(f_{pi}^{(s)}/f_o)^2$. Toroidal fields are as follows; o(Bt=1.8T),□ (Bt=1.4T), Δ and x(Bt=1.3T) and ● (Bt=1.8T). The dotted line indicates $\Delta f=f_{pi}^{(s)}$.

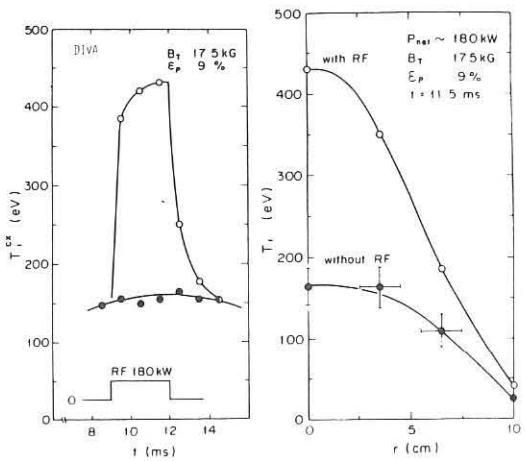

Fig.7.3 Time evolution and radial profiles of ion temperatures from charge exchange, Doppler broadning of OVII, CV and CIV lines and Katsumata probe measurements.

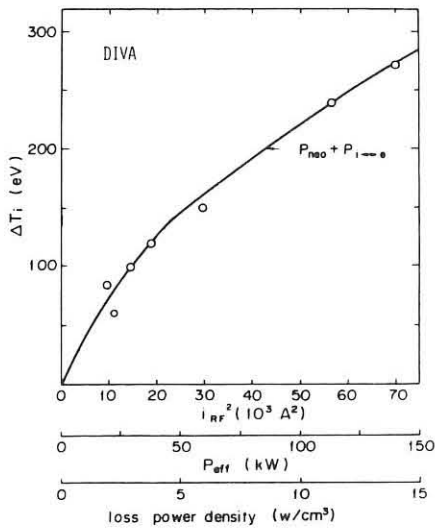

Fig.7.4 Ion temperature rise versus square of antenna current or effective radiofrequency power irradiation to plasma. The solid line shows calculation of sum of loss power density due to neoclassical thermal conduction and electron-ion coupling.

8. Summary

Recent Japanese tokamak experiments have been surveyed in this report. The major results are summarized as follows;

(1) Successful operation of non-circular tokamaks with and without a divertor, and precise control of the plasma position.

(2) Stable very low-q and very high density discharges.

(3) Understanding of impurity production and its control.

(4) Increased understanding of scaling laws.

(5) Scaling laws for plasma parameters in a scrape-off layer.

(6) Successful radiofrequency heating with a power of 200 kW.

Acknowledgements

We wish to thank all the tokamak experimental groups in Japan for placing their results at our disposal. We would also like to express our gratitude to our colleagues at JAERI.

References

[JFT-2]

[1] Y.GOMAY, T.TAZIMA, N.FUJISAWA, N.SUZUKI and S.KONOSHIMA: Japan Atomic Energy Research Institute Report JAERI-M 6647(1976).

[2] T.SOMETANI and N.FUJISAWA: Japan Atomic Energy Research Institute Report JAERI-M 6689(1976).

[3] H.MAEDA, N.FUJISAWA, Y.SHIMOMURA, A.FUNAHASHI, H.OHTSUKA, et al.: in Plasma Physics and Controlled Nuclear Fusion Research(Proc. 6th Int. Conf. Berchtesgaden, 1976) Vol.2, IAEA, Vienna(1977) 289.

[4] T.SOMETANI, N.FUJISAWA and K.HASEBE: Japanese J. Applied Phys. 16(1977) 1343.

[5] Y.GOMAY, T.TAZIMA and N.FUJISAWA: J. Vac. Sci. Technol., 15(1978)103.

[6] K.ODAJIMA, M.WAKATANI, M.MAENO and N.FUJISAWA: Physics Fluids 21 (1978)846.

[7] Y.GOMAY, N.FUJISAWA, M.MAENO, N.SUZUKI, K.UEHARA, et al.: Nuclear Fusion 18(1978)849.

[8] T.NAGASHIMA and N.FUJISAWA: Proc. of Joint Varenna-Grenoble Int. Symp. on Heating in Toroidal Plasma(1978)281.

[9] T.FUJII, N.FUJISAWA, A.FUNAHASHI, T.HIRAYAMA, T.IMAI, et al.: in Plasma Physics and Controlled Nuclear Fusion Research (Proc. 7th Int. Conf. Innsbruck, 1978) IAEA-CN-A-4-2.

[10] T.HIRAYAMA, N.FUJISAWA, Y.GOMAY, M.MAENO, K.UEHARA, et al.: J.Nuclear Materials 76&77(1978)452.

[11] S.KONOSHIMA, N.FUJISAWA, M.MAENO, N.SUZUKI, T.YAMAMOTO, et al.: J. Nuclear Materials 76&77(1978)581.

[12] T.SOMETANI and N.FUJISAWA: Plasma Physics 20(1978)1101.

[13] M.SHIHO, S.KONOSHIMA, A.FUNAHASHI, S.KASAI, T.SUGIE, et al.: Nuclear Fusion 18(1978)1705.

[14] K.UEHARA, Y.GOMAY, T.YAMAMOTO, N.SUZUKI, M.MAENO, et al.: Plasma Physics 21(1979)89.

[15] Y.GOMAY, S.KONOSHIMA, N.FUJISAWA, M.MAENO, et al.: Japanese J. Applied Physics 18(1979)1317.

[16] M.MAENO, H.KAWAKAMI, Y.GOMAY, N.FUJISAWA, N.SUZUKI, et al.: Japanese J. Applied Physics 18(1979)

[17] M.MAENO, N.SUZUKI, S.KONOSHIMA, T.YAMAMOTO, M.SHIMADA. et al.: Symp. on Current Disruption in Toroidal Devices, Garching(1979).

[18] N.SUZUKI, N.FUJISAWA, S.KONOSHIMA, M.MAENO, M.SHIMADA. et al.: in Controlled Fusion and Plasma Physics (Proc. 9th Europ. Conf. Oxford, 1979).

[19] Y.GOMAY, N.FUJISAWA and M.MAENO: to be published in J. Nuclear Materials.

[20] T.IMAI, T.NAGASHIMA, T.YAMAMOTO, K.UEHARA, S.KONOSHIMA, et al.: to be published in Phys. Rev. Lett..

[DIVA]

[21] H.MAEDA, Y.SHIMOMURA, A.KITSUNEZAKI, H.OHTSUKA, M.NAGAMI, et al.: Nuclear Fusion 16(1976)148.

[22] Y.SHIMOMURA, H.MAEDA, H.OHTSUKA, A.KITSUNEZAKI, T.NAGASHIMA, et al.: Physics Fluids 19(1976)1635.

[23] Y.SHIMOMURA, H.OHTSUKA, H.MAEDA, S.YAMAMOTO, H.KIMURA, et al: Nuclear Fusion 16(1976)4.

[24] H.MAEDA, N.FUJISAWA, Y.SHIMOMURA, A.FUNAHASHI, H.OHTSUKA, et al.: in Plasma Physics and Controlled Nuclear Fusion Research (Proc. 6th Int. Conf. Berchtesgaden, 1976) Vol.2, IAEA, Vienna(1977)289.

[25] H.MAEDA, H.OHTSUKA, Y.SHIMOMURA, H.KIMURA, N.UEDA, et al.: Int. Symp. on Plasma-Wall Interaction, Julich.(1976).

[26] Y.SHIMOMURA: Nuclear Fusion 17(1977)626.

[27] S.YAMAMOTO, H.MAEDA, Y.SHIMOMURA, K.ODAJIMA, N.NAGAMI, et al.: In Controlled Fusion and Plasma Physics (Proc. 8th Europ. Conf. Prague, 1977) Vol.1(1977)33.

[28] Y.SHIMOMURA: Nuclear Fusion 17(1977)6.

[29] S.YAMAMOTO, S.SENGOKU, H.KIMURA, Y.SHIMOMURA, H.MAEDA, et al.: Nuclear Fusion 18(1978)205.

[30] K.OHASA, H.MAEDA, S.YAMAMOTO, N.NAGAMI, H.OHTSUKA, et al.: Nuclear Fusion 18(1978)872, and J. Phys. Soc. Japan 46(1979)1635.

[31] K.ODAJIMA, H.KIMURA, H.MAEDA and K.OHASA: Japanese J. Applied Physics 17(1978)1281.

[32] DIVA Group: Proc. of Joint Varenna-Grenoble Int. Symp. on Heating in Toroidal Plasma(1978).

[33] H.MAEDA, S.SENGOKU, H.KIMURA, H.OHTSUKA, K.OHASA, et al.: In Plasma Physics and Controlled Nuclear Fusion Research(Proc. 7th Int. Conf. Innsbruck, 1978) IAEA-CN-3-1.

[34] Y.SHIMOMURA and H.MAEDA: J. Nuclear Materials 76&77(1978)45.

[35] M.NAGAMI, H.MAEDA, S.KASAI, S.SENGOKU, T.SUGIE, et al.: J. Nuclear Materials 76&77(1978)521.

[36] M.NAGAMI, H.MAEDA, M.SHIHO, T.SUGIE, Y.SHIMOMURA, et al.: Nuclear Fusion 18(1978)1217.

[37] H.KIMURA, H.MAEDA, N.UEDA, M.SEKI, H.KAWAMURA, et al.: Nuclear Fusion 18(1978)1195.

[38] S.SENGOKU, M.NAGAMI, H.MAEDA, S.KASAI, T.YAMAUCHI, et al.: J. Phys. Society of Japan 45(1978)1385.

[39] M.NAGAMI, Y.SHIMOMURA, H.MAEDA, S.KASAI, T.YAMAUCHI, et al.: Nuclear Fusion 18(1978)1347.

[40] K.ODAJIMA, H.MAEDA, M.SHIHO, H.KIMURA, S.YAMAMOTO, et al.: Nuclear Fusion 18(1978)1337.

[41] H.OHTSUKA, H.KIMURA, Y.SHIMOMURA, H.MAEDA, S.YAMAMOTO, et al.: Plasma Physics 20(1978)749.

[42] S.KASAI, A.FUNAHASHI, M.NAGAMI, T.SUGIE and T.YAMAUCHI: J. Physical Society of Japan 46(1979)241.

[43] DIVA Group: Nuclear Fusion 18(1978)1619.

[44] K.ODAJIMA, M.NAGAMI, S.YAMAMOTO, H.OHTSUKA, S.SENGOKU, et al.: Symp. on Current Disruption in Toroidal Devices, Garching(1979).

[45] DIVA Group: Japan Atomic Energy Research Institute Report JAERI-M 8205(1979).

[JIPP T-2]

[46] J.FUJITA, M.FUJIWARA, Y.HAMADA, S.ITOH, K.KADOTA, et al.: in Plasma Physics and Controlled Nuclear Fusion Research (Proc. 6th Int. Conf. Berchtesgaden, 1976) Vol.2, IAEA, Vienna(1977)95.

[47] J.FUJITA, Y.HAMADA, S.ITOH, K.KADOTA, K.KAWAHATA, et al.: in Controlled Fusion and Plasma Physics(8th Europ. Conf. Prague, 1977) Vol.1, 6.

[48] K.TOI, S.ITOH, J.FUJITA, K.KADOTA, K.KAWAHATA, et al.: IPPJ-322(1978).

[49] J.FUJITA, S.ITOH, K.KADOTA, K.KAWAHATA, K.KAWASUMI, et al.: in Plasma Physics and Controlled Nuclear Fusion Research(Proc. 7th Int. Conf. Innsbruck, 1978) N-2.

[50] K.TOI, S.ITOH, K.KADOTA, K.KAWAHATA, N.NODA, et al.: in Symp. on Current Disruptions in Toroidal Device(Garching, 1979).

[51] K.TOI, S.ITOH, K.KADOTA, K.KAWAHATA, N.NODA, et al.: IPPJ-372(1979).

[TNT]

[52] H.TOYAMA, K.MAKISHIMA, H.KANEKO, M.NOGUCHI and S.YOSHIKAWA: Phys. Rev. Lett. 37(1976)18.

[53] H.TOYAMA, S.INOUE, K.ITOH, A.IWAHASHI, H.KANEKO, et al.: in Plasma Physics and Controlled Nuclear Fusion Research(Proc. 6th Conf. Berchtesgaden, 1976) Vol.1, IAEA, Vienna(1977)323.

[54] H.TOYAMA, T.DODO, A.IWAHASHI, H.KANEKO, K.MAKISHIMA, et al.: in Controlled Fusion and Plasma Physics(8th Europ. Conf., Prague, 1977) Vol.1, 10.

[55] H.TOYAMA, A.IWAHASHI, H.KANEKO, Y.KAWADA, K.MAKISHIMA, et al.: in Plasma Physics and Controlled Nuclear Fusion Research(Proc. 7th Inter. Conf., Insbruck, 1978) IAEA-CN-37/T-2.

[HYBTOK]

[56] K.SAKURAI, T.KUZUSHIMA, Y.TANAKA and T.OKUDA: J. Phys. Soc. Japan 44 (1978)1051.

[57] T.OKUDA, Y.TANAKA, K.SAKURAI, K.NAKAMURA, M.HATA, et al.: in Controlled Fusion and Plasma Physics(8th Europ. Conf., Prague, 1977) Vol.1, 121.

[58] T.OKUDA, Y.TANAKA, S.TAKAMURA, K.SAKURAI, K.NAKAMURA, et al.: in Plasma Physics and Controlled Nuclear Fusion Research(Proc. 7th Intern. Conf., Innsbruck, 1978) IAEA-CN-37/T-2.

[59] S.TAKAMURA and T.OKUDA: Proc. of Joint Varenna-Grenoble Int. Symp. on Heating in Toroidal Plasma(1978)155.

PROGRESS IN MIRROR MACHINE RESEARCH*

T. K. Fowler and F. H. Coensgen
Lawrence Livermore Laboratory, University of California
Livermore, California 94550

ABSTRACT

The Mirror Fusion Program in the U.S. is now focussed on two concepts that can obtain high values of the power gain factor Q. These are the tandem mirror and field reversed mirror concepts. A new facility called TMX has been constructed to test the principles of the tandem mirror. A further attempt to create field reversal is being carried out in the 2XIIB facility (renamed Beta II) with neutral beam injection into a reversed-field target plasma to be created by a magnetized coaxial gun. During the next 5 years, the main mirror facilities in the U.S. will be the TMX, Beta II, and a large mirror device called MFTF scheduled to operate by 1982. The program based on these facilities will be outlined and initial experimental results from TMX will be discussed.

INTRODUCTION

The present mirror program grew out of the 2XIIB experiment at Lawrence Livermore Laboratory. The main results, as reported at Berchtesgaden,[1] were: (1) ion energies >10 keV at densities up to 10^{14} cm^{-3}, (2) beta values of order unity, and (3) the successful control of microinstabilities. Armed with this new information, we then set out to find ways to design mirror reactors of higher Q (the ratio of fusion power to input power). This led, by 1976, to the tandem mirror concept[2] and the field reversed mirror (Fig. 1). The tandem mirror uses the ambipolar potential of two mirror machines to plug up the ends of a solenoid electrostatically. The field reversed mirror depends upon the closure of magnetic lines within a high beta plasma ring. Here we will describe the present status of the experimental program to explore these ideas and some new developments in the tandem mirror reactor concept.

*Work performed under the auspices of the U.S. Department of Energy by the Lawrence Livermore Laboratory under contract number W-7405-ENG-48.

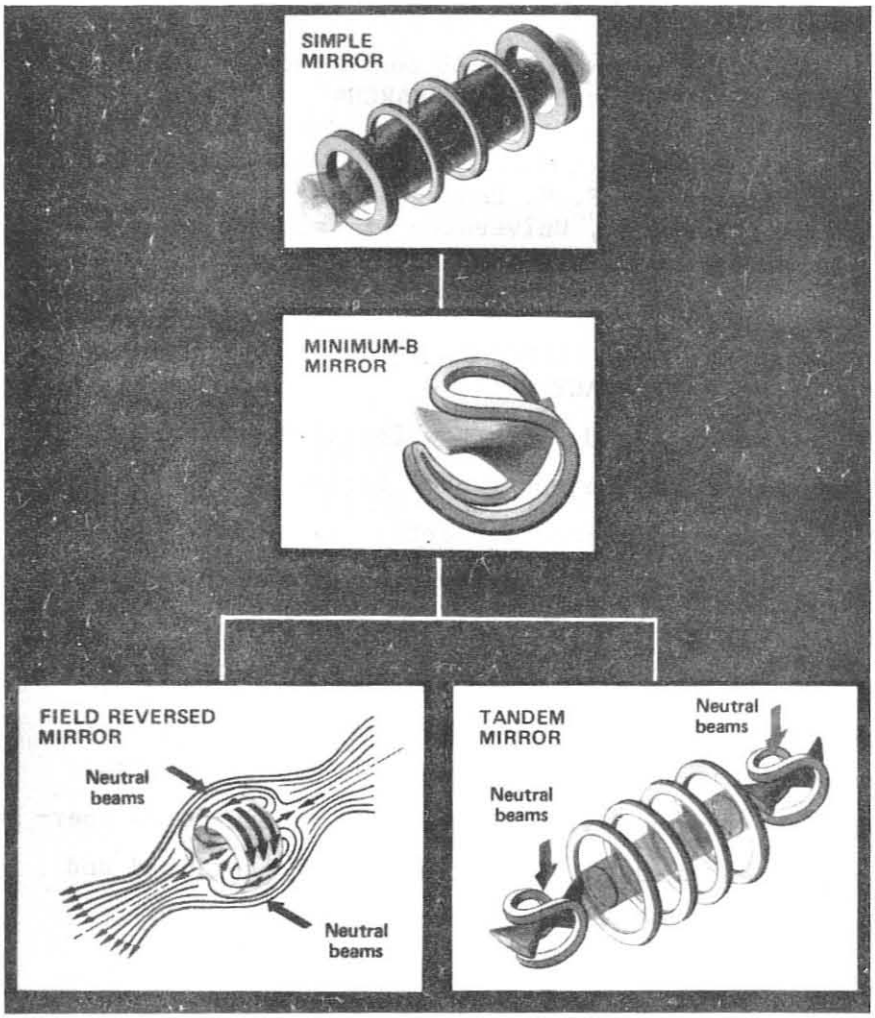

Fig. 1. Evolution of the high-Q tandem mirror and field reversed mirror from earlier concepts.

FIELD REVERSED MIRROR

The field reversed mirror offers the possibility of a small reactor (Fig. 2), if the system is MHD stable. Encouraged by the remarkable stability of field-reversed theta pinches[3] and electron rings,[4] a couple of years ago we set out to create a similar field reversed configuration by neutral beam injection in 2XIIB. Though we did not quite reach field reversal, we believe the limiting factor was end losses rather than anything having to do with field reversal itself. We did achieve a 90% depression of the field on axis at $\beta \sim 2$ and beta was still increasing with beam current at the maximum current available (500 A).[5]

We are now embarking on a different course in which we first create a field reversed plasma ring and then inject neutral beams to heat it. The reversed field is to be created by a magnetized coaxial gun (Fig. 3) of a type developed by Alfvén and co-workers.[6] This is a coaxial gun

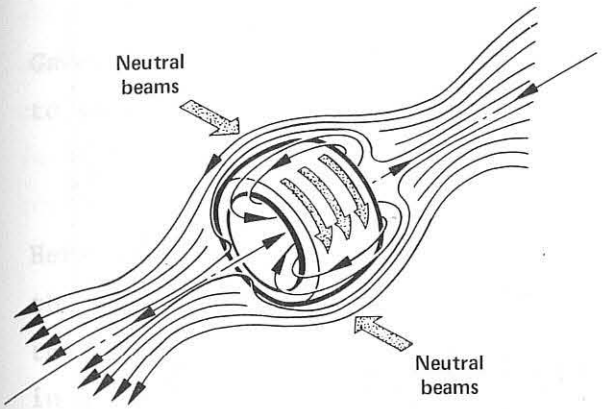

Fig. 2. Example parameters for a field reversed mirror cell; a small reactor would consist of a few cells in series.

Parameter	Value
Vacuum field	50 kG
Plasma length	20 cm
Plasma radius	6 cm
Beam energy	⩽200 keV
Fusion energy gain (Q)	5 to 9
Fusion power	19 MW/cell

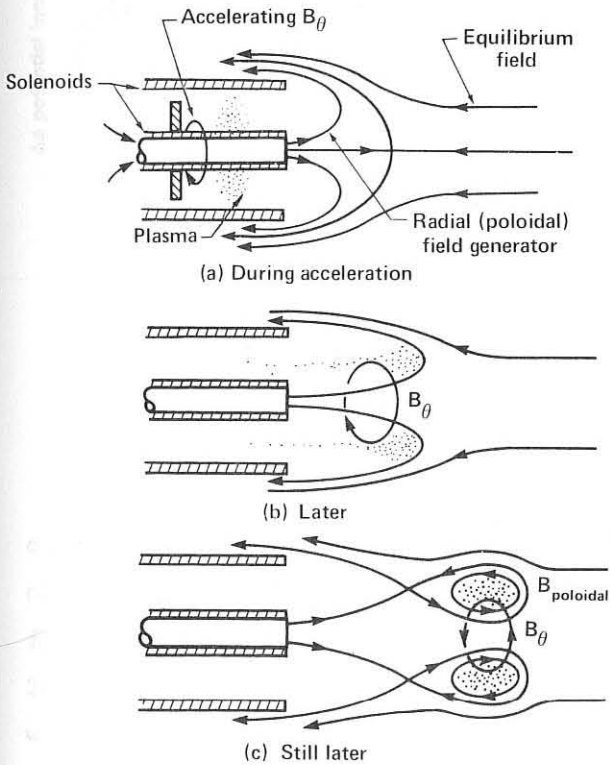

Fig. 3. The magnetized coaxial gun produces field-reversed plasma rings.

with a superposed magnetic field created by a solenoid along the center electrode. When the gun fires, the ejected plasma ring picks up the superposed poloidal flux. In our experiment the field-reversed ring created by the gun is to be injected along a guide field into the 2XIIB facility, renamed Beta II (Fig. 4). A fast gate coil serves to capture the injected ring between two magnetic mirrors. If the ring is confined about

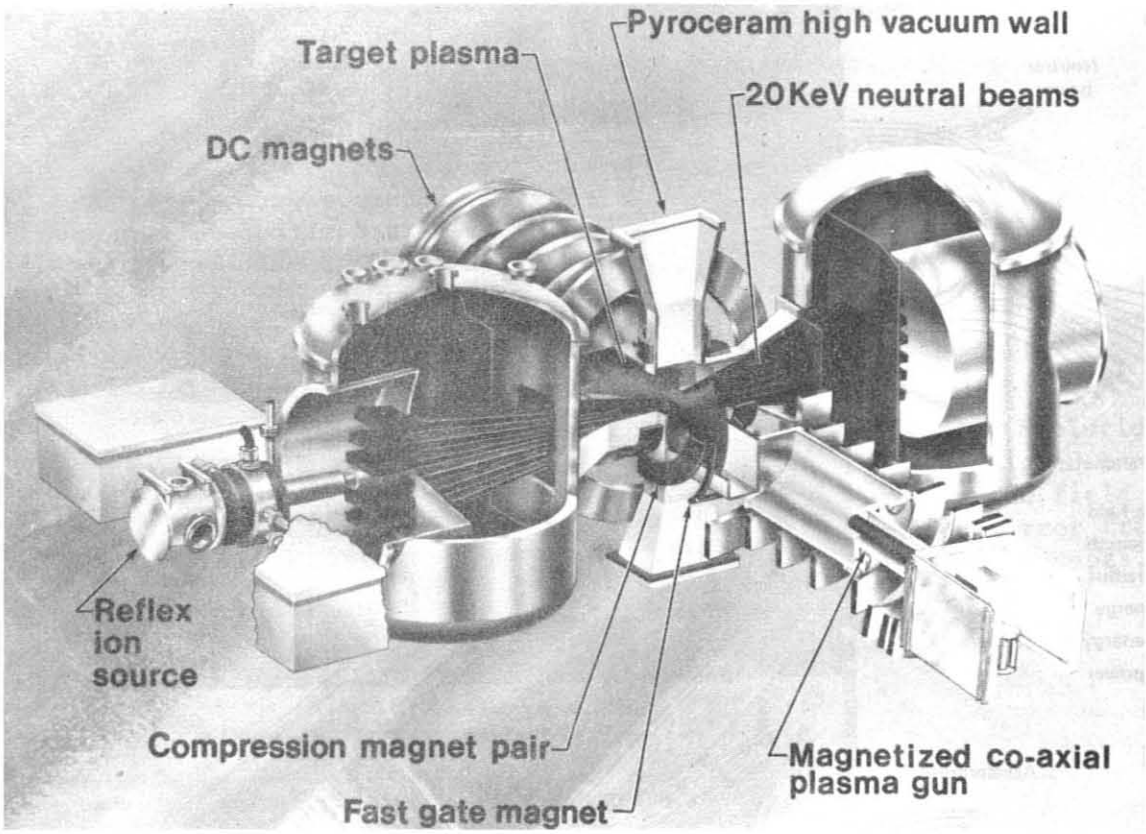

Fig. 4. Sketch of the Beta II facility at Livermore.

1 ms, the 5 MW neutral beam system on Beta II should be able to heat the ring to temperatures of several keV. The gun has been installed on Beta II and experiments are now beginning. In addition, an improved version of the gun is under development at Los Alamos Scientific Laboratory.

TANDEM MIRROR RESULTS

Since the tandem mirror concept was first presented at Berchtesgaden,[7] construction of several tandem mirror experiments has been undertaken including the Gamma 6 at Tsukuba University, Japan; Ambal 1 at Novosibirsk; the Phaedrus at the University of Wisconsin; and the TMX at Livermore. The Tsukuba group is also proposing the construction of a larger tandem facility, Gamma 10, and at Livermore we are considering the possibility of modifying the Mirror Fusion Test Facility (MFTF) to a tandem geometry (MFTF-B). The MFTF is presently planned as a large superconducting single mirror device scheduled for completion by 1982. In MFTF-B this would serve as one end plug of a tandem and a duplicate would be constructed to serve as the second end plug with a 25 m-long solenoid between them. A decision to proceed with MFTF-B depends on TMX results.

The first experimental data on tandem mirrors was obtained in Gamma 6 in which it was shown that a potential well is created according to the expected relationship

$$\Delta\phi \propto T_e \ln n_p/n_c \quad .$$

Here T_e is the electron temperature and n_p/n_c is the ratio of density in the end mirror cells (or "end plugs") and the center cell. Figure 5 shows the increase in $\Delta\phi$ as T_e is increased by increasing neutral beam injection in the end plugs.[8]

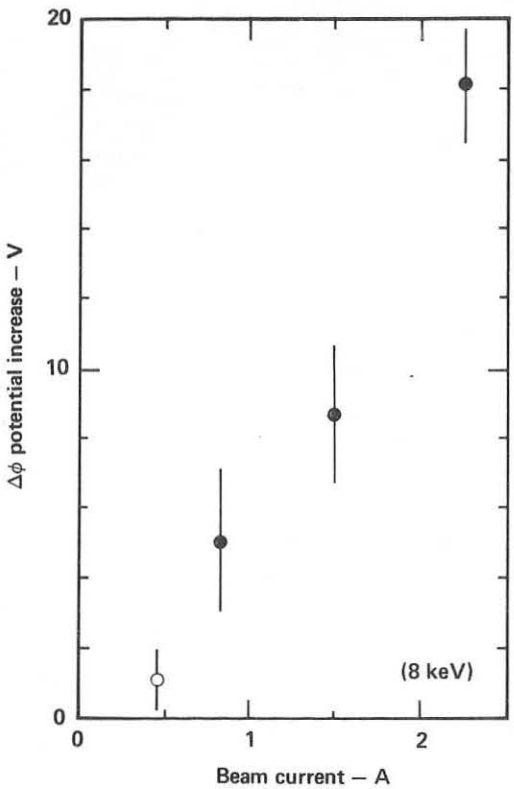

Fig. 5. Increase of the tandem mirror potential as the electron temperature is increased by neutral beam heating (Gamma 6 data).

The largest tandem mirror experiment is TMX (Fig. 6). In this facility the end plugs are minimum-B mirror machines with a midplane field of 10 kG and the central cell is a solenoid about 5 m in length with a field that can be varied up to 2 kG. There are 24 neutral beams, 16 at 20 kV and 8 at 40 kV. At full design level the total injected current will be about 500 A at each end, for a pulse length of 25 ms.

Construction of TMX began in March 1977. The first plasma experiments began in July of 1979, with the neutral beams operating in the range of 100-200 A per plug, roughly one-third of the ultimate capability. At the time this paper is being prepared, experiments have been carried out for about one month.

While the TMX results are very preliminary, we can already express cautious optimism concerning several features of the new tandem mirror

concept.[9] During the first month of operation it has been possible routinely to maintain a steady state tandem mirror plasma configuration that is grossly stable for the full 25 ms duration of the neutral beams. At present beam currents, beta in the end plugs is in the range 5-15% and

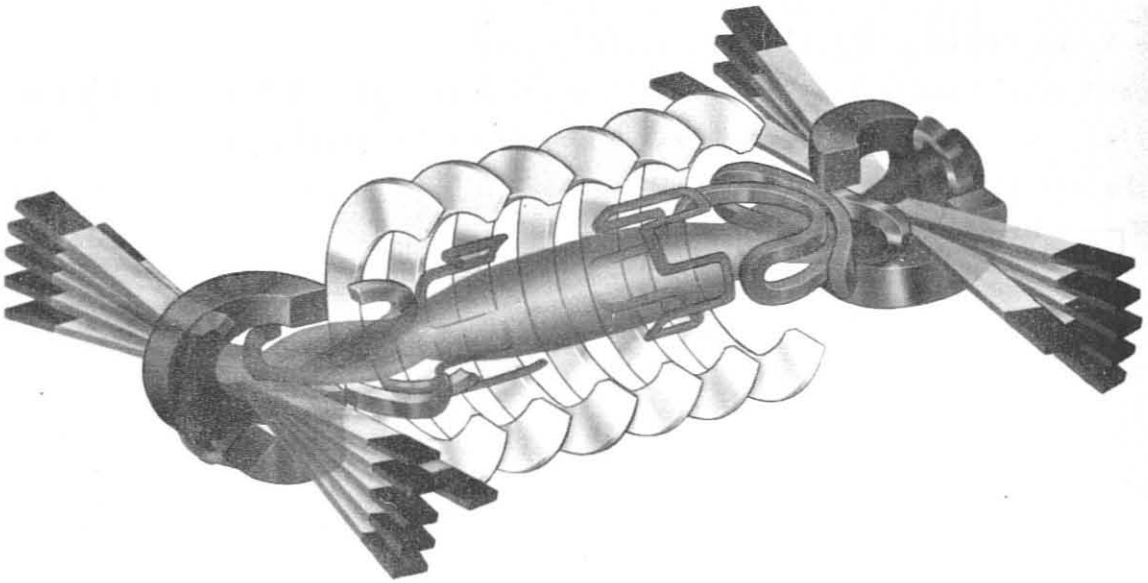

Fig. 6. Sketch of the TMX showing the end plugs with neutral beams and 5 m solenoid.

beta in the center cell is 5%. After an initial starting period, microstability of the end plugs is maintained solely by the outflow of plasma from the central cell (without assistance from external cold plasma sources as was necessary in 2XIIB). We cannot yet say much about the confinement of ions in the central cell except that confinement times of several milliseconds have been obtained thus far at a center cell density around 10^{13} cm^{-3}. There does appear to be some electrostatic plugging, as evidenced by an increase in the end loss current through one plug when the neutral beams are turned off in that plug (Fig. 7). Ion energies in the end plugs are 10 keV or more, consistent with beam injection. Ion temperatures in the center cell are low as expected, probably <100 eV; these temperatures are maintained as the center cell density is increased by gas injection into the center region, as indicated by the steady rise in diamagnetic signal as the line density increases (Fig. 8).

One of the most encouraging TMX results thus far is the electron temperature. Figure 9 shows T_e in one end plug as determined by Thomson scattering. These values are higher than those obtained in 2XIIB at comparable injection power and indicate effective electron heat confinement in TMX. In TMX, electrons are isolated from the walls by an ambipolar

sheath created by the 150:1 decrease in magnetic field between the plugs and the end walls and the corresponding decrease in density as the escaping plasma expands in the decreasing field. This is an essential feature of tandem mirror design that may also find applications in other confinement geometries, such as bundle divertors in tokamaks.

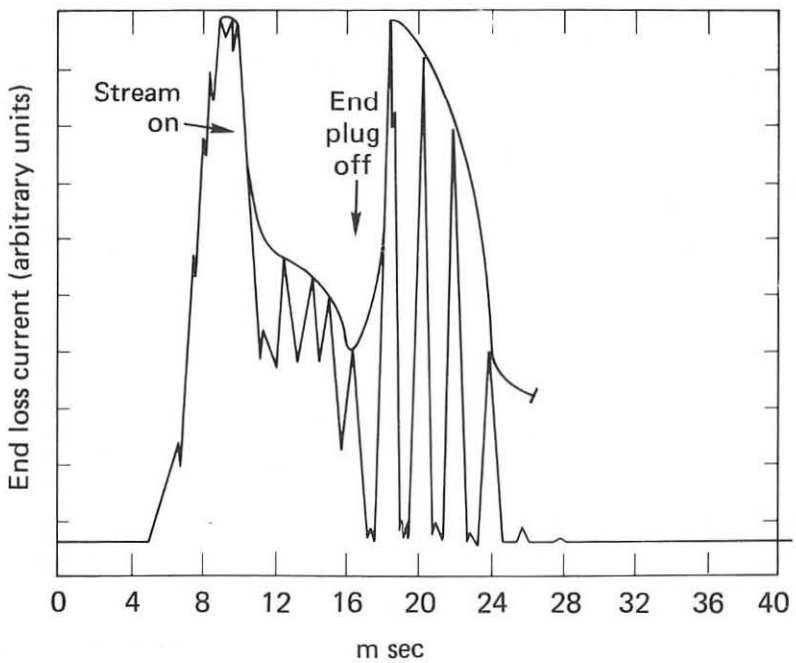

Fig. 7. Evidence that the end loss current increases in TMX when the end plug is turned off.

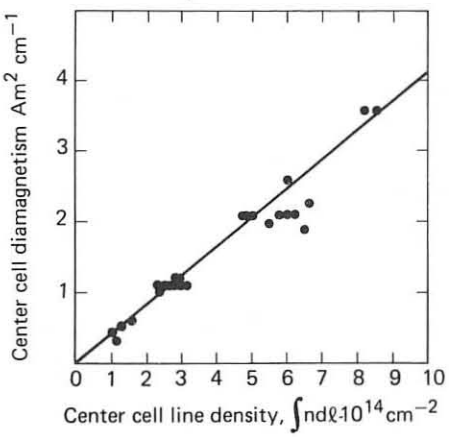

Fig. 8. The diamagnetic signal in the center cell of TMX increases with density.

IMPROVED TANDEM MIRROR REACTOR

Earlier this year, Baldwin and Logan introduced an improved version of the tandem mirror reactor that promises higher Q values with simpler technology in the end plugs.[10] An artist's sketch is shown in Fig. 10. The new feature, called a "thermal barrier," is produced by adding a simple mirror (the barrier coil) at the end of the solenoid and by separating

the end plugs from the solenoid to create a deep field depression, as shown in Fig. 11. In the absence of collisions, as plasma flows out of

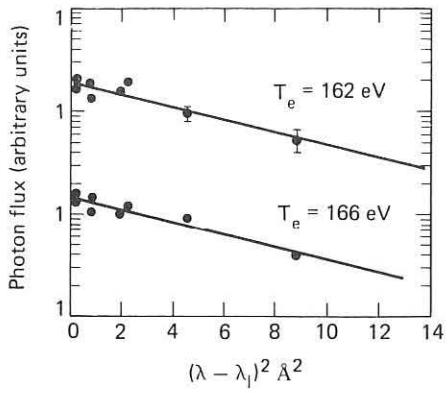

Fig. 9. Thomson scattering data from one end plug of TMX indicating good electron heat confinement.

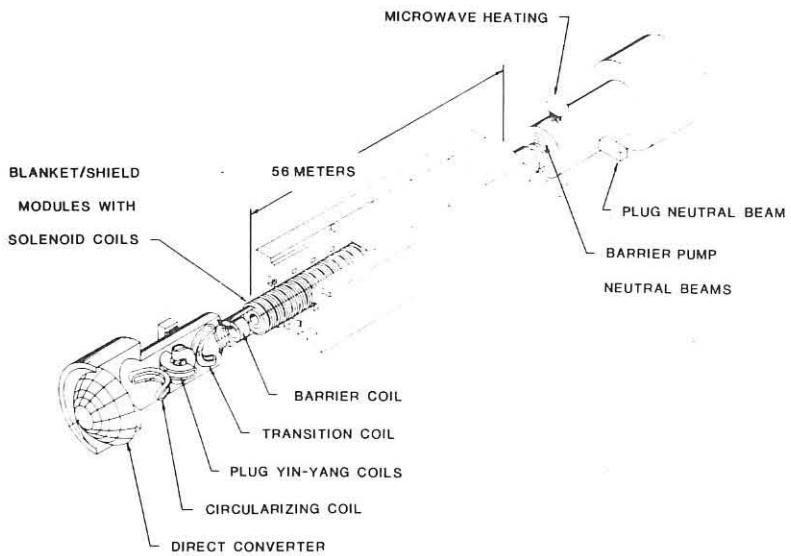

Fig. 10. Artist's sketch of the improved tandem mirror reactor with thermal barriers.

the solenoid toward the plugs, its density would decrease in crossing the region of depressed field. This decrease in density would create a depression in the positive potential that acts as a "thermal barrier" isolating the electrons in the end plug from those in the solenoid. If we now apply ECRH or other auxiliary heating to the end plug, the electrons there can be heated to a high temperature--much higher than that in the solenoid. With a high electron temperature in the plug, the potential peak in the plug necessary to confine the ions escaping from the solenoid can be generated with a much lower density n_p in the end plug. In fact, as is shown in Fig. 11, n_p can be less than n_c, the density in the solenoid, whereas in the original tandem mirror concept $n_p >> n_c$. It is this

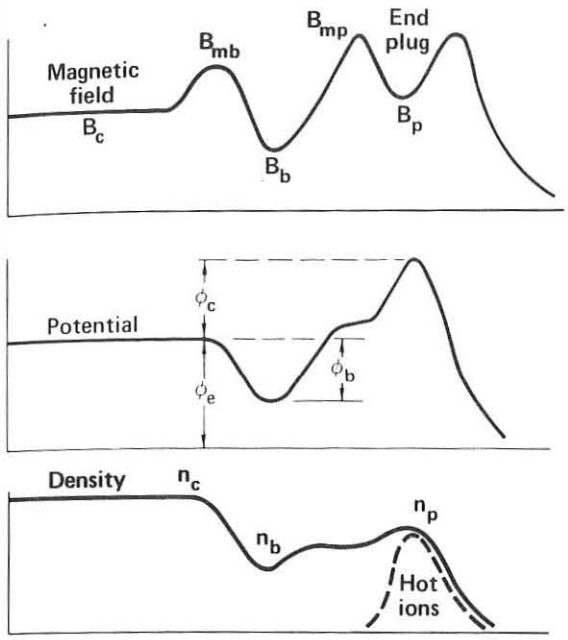

Fig. 11. Curves showing the magnetic field, potential and density in the thermal barrier.

large reduction in the plug density that both reduces the power consumed in the plugs (hence higher Q) and opens up options for less demanding magnet and neutral beam technology. It now appears that end plugs adequate to maintain ignition conditions in the solenoid can be obtained with 400 keV beams and no more than 12 T in conductors (in contrast with 1.2 MeV and 17 T in our earliest designs).

To maintain a thermal barrier in steady state, one other element must be added to the system. As noted, the desired density drop that creates the thermal barrier occurs in the absence of collisions. The drop in density occurs for "passing" particles flowing from the solenoid to the end plugs and back. Collisions among these passing particles--ions and electrons--cause some to become mirror-trapped in the depressed field region. In time, because of the collisions, the trapped particle density would grow until the total pressure is equal to that in the solenoid. To prevent this, it is necessary to pump out trapped ions as they accumulate. One method, illustrated in Fig. 12, utilizes charge exchange on a neutral beam aimed nearly tangential to the axis.[11] Then, if the beam orientation and energy are chosen to correspond to passing ions, a charge exchange event between a trapped ion and a beam neutral swaps a trapped ion for a passing one. Because an energetic neutral is lost, this barrier pumping process consumes power, at a rate proportional to the rate of accumulating trapped ions by collisions. Nonetheless, one finds that the overall power balance is considerably improved. Whereas the original

tandem reactor design yielded Q = 5 at 1000 MWe, it now appears that a 500 MWe reactor, such as that sketched in Fig. 10, could attain Q ~ 10 with still higher Q-values at higher power levels.

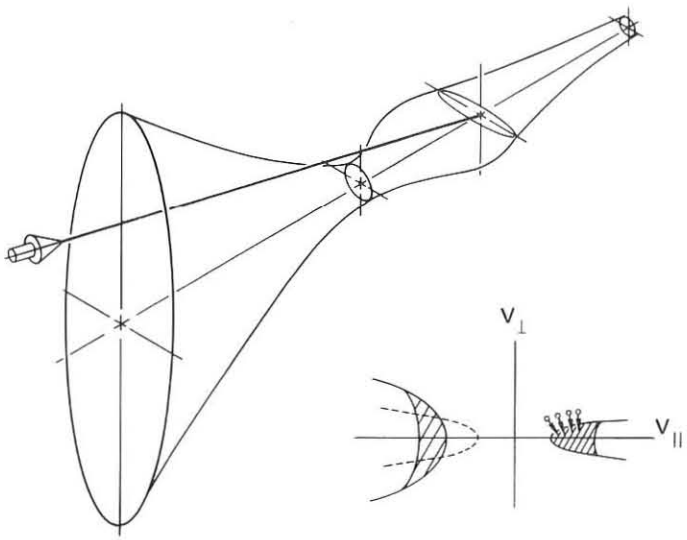

Fig. 12. Sketch of one means of pumping trapped ions out of the thermal barrier (see text).

REFERENCES

1. F. H. Coensgen, et al., Plasma Physics and Controlled Nuclear Fusion Research, Proceedings 6th Int. Conference, Berchtesgaden 2, 135 (1976).
2. G. I. Dimov, V. V. Zakaidakov, and M. E. Kishinevskii, Fizika Plasmy 2 597 (1976); T. K. Fowler and B. G. Logan, Comments on Plasma Physics and Controlled Fusion 2, 167 (1977).
3. R. K. Linford, et al., Plasma Physics and Controlled Nuclear Fusion Research, Proceedings 7th Int. Conference, Innsbruck, 2, 447 (1978).
4. H. H. Fleischman, et al., Plasma Physics and Controlled Nuclear Fusion Research, Proceedings 7th Int. Conference, Innsbruck, 2, 497 (1978).
5. T. C. Simonen, et al., Plasma Physics and Controlled Nuclear Fusion Research, Proceedings 7th Int. Conference, Innsbruck, 2, 389 (1978).
6. H. Alfvén, et al., J. Nucl. Energy, Part C, Plasma Phys. 1, 116 (1960).
7. G. I. Dimov, et al., Plasma Physics and Controlled Nuclear Fusion Research, Proceedings 6th Int. Conference, Berchtesgaden 3, 177 (1976).
8. S. Miyoshi, et al., Plasma Physics and Controlled Nuclear Fusion Research, Proceedings 7th Int. Conference, Innsbruck 2, 437 (1978).
9. Initial TMX results will be presented by the TMX group at the 21st Div. of Plasma Physics, APS meeting (1979), Session 5Q.
10. D. E. Baldwin and B. G. Logan, "An Improved Tandem Mirror Fusion Reactor," Lawrence Livermore Laboratory, Report UCRL-82715 (May 1979).
11. L. L. LoDestro, D. E. Baldwin, T. A. Cutler, B. G. Logan, and T. D. Rognlien, Charge Exchange for Pump-Out of a Barrier Region in a Tandem Mirror, to be presented at the 21st Div. of Plasma Physics, APS Meeting (1979); also Lawrence Livermore Laboratory Report UCRL-83114 (1979).

US TOKAMAK RESEARCH*

H. P. Furth

Plasma Physics Laboratory, Princeton University,
Princeton, New Jersey 08544, USA

ABSTRACT

Current experiments on ISX-B, Alcator C, PDX, and PLT respectively address the four areas of principal concern in the development of a tokamak reactor: optimization of MHD-stability at high β-values; achievement of high $n\tau_E$; preservation of plasma purity; and development of effective techniques for achieving high plasma temperatures. The neutral-beam-heated ISX-B is the first tokamak device to have reached a β^*-level of approximately 3%, thus exploring — or even challenging — the theoretical MHD beta limit. Pellet fueling has also been demonstrated successfully. Alcator C, in its initial half-field operation, has obtained τ_E values exceeding 20 msec and has found a modified empirical scaling pattern. The Poloidal Divertor Experiment (PDX) has entered initial "round-plasma" operation at currents up to 500 kA. Low-power ion-cyclotron heating on PLT has given bulk-ion-temperature rises up to 600 eV and energetic efficiencies exceeding those of neutral-beam heating. Interactive energization of beam-injected ions has also been demonstrated. Some further information on the phenomena accompanying unidirectional tangential neutral-beam injection has been obtained. The Doublet III results are reported at this conference in a separate paper [1].

I. THE ISX-B DEVICE

A schematic of the ISX-B device at the Oak Ridge National Laboratory (ORNL) is shown in Fig. 1. A more detailed discussion of recent experimental results is being presented at this conference in Ref. 2. The nominal machine parameters are $R = 93$ cm, $a_{Lim} = 27$ cm, $b_{Lim} = 50$ cm, $B_T \leq 18$ kG, $I_p \leq 100$ kA. Thus far, operation has concentrated on roundish plasmas ($b/a \sim 1.1$) at limiter q-values in the range 2.8 - 3.2. Neutral-beam heating is applied through coinjection at 40 keV, and has risen in the course of the past year to about 1 MW of hydrogen (two beamlines). The ohmic-heating power drops from about 200 kW before injection to as little as 60 kW during injection. The discharge duration is of order 200 msec, with beam heating applied for 100 msec.

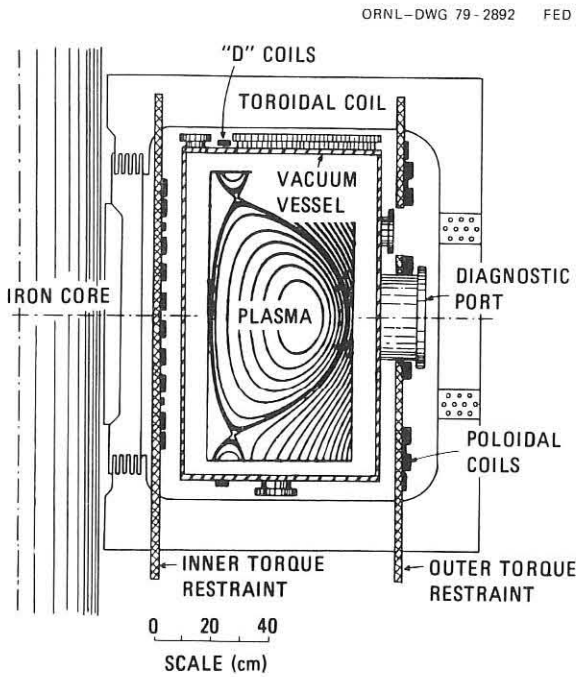

Figure 1. Schematic of the ISX-B device at ORNL.

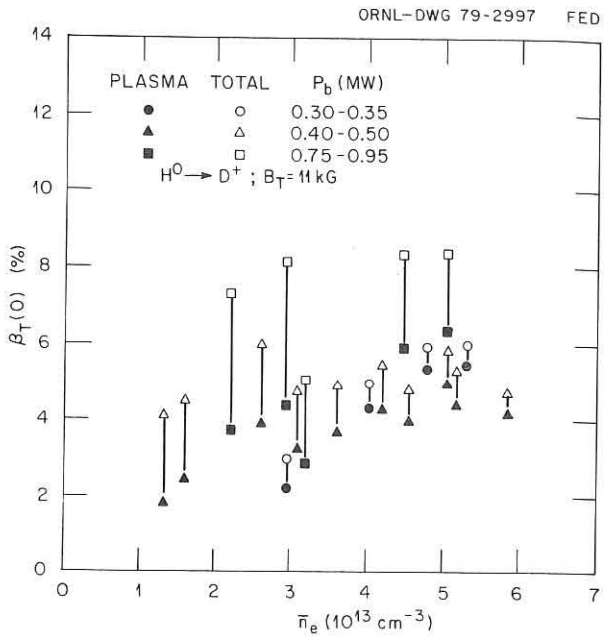

Figure 2. Central β-values obtained by neutral-beam heating in ISX-B. The contributions due to the plasma pressure and the beam-ion pressure are distinguished.

The central β-values achieved at various beam-power levels and plasma densities are shown in Fig. 2. In the lower-density cases, an appreciable fraction of the central β-value is seen to be contributed by the energetic injected ions, rather than by the bulk plasma. At higher plasma densities and for space-averaged β-values, the pressure contribution of the energetic particles is minor.

The dependence of the quantity $\beta^* = 8\pi(\langle p^2 \rangle)^{1/2}/B_T^2$ on beam power and density is shown in Fig. 3. There is no evidence of saturation at the highest power levels used thus far. Correspondingly, no deterioration of τ_E has been observed at the highest β-values. The pattern of MHD activity undergoes some rather marked changes during neutral-beam heating, but these phenomena could well be caused by the injection process itself, rather than by the β-level. In particular, since injection is unidirectional, one would expect plasma rotation (cf. Section IV) to shift the MHD mode frequencies, and quite probably to drive new kinds of MHD modes. As one contemplates the possibilities, it becomes clear that the onset of the true ballooning mode β-limit may be rather difficult to identify uniquely, unless some variation can be introduced in the plasma heating method.

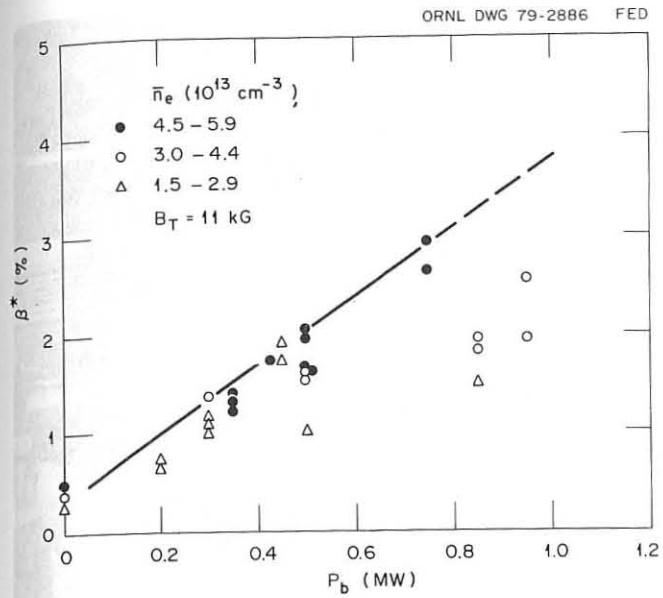

Figure 3. Average beta, $\beta^* = 8\pi(\langle p^2 \rangle)^{1/2}/B_T^2$, in ISX-B versus beam power.

To demonstrate experimentally that the β-value can rise above the theoretical limit is considerably more straightforward. On the basis of the ideal-MHD analysis of Ref. 3, the β-values of Fig. 3 are already somewhat excessive; in the case of a round plasma with an aspect ratio of 4.5 the critical β^* should be around 2%. In the near future, when the injection power is raised above 1.5 MW, a decisive demonstration of the discrepancy — if it is real — will be forthcoming.

In the event that the experimental tokamak β-limit in ISX-B is found to exceed the predictions of the ideal MHD theory, some interesting questions will arise: Are finite-gyroradius effects significant? Do the beam-ions play a helpful role (possibly by helping to shape the poloidal field)? Is a finite level of ballooning-mode activity compatible with adequate energy confinement? Perhaps the most interesting question of all is whether an upward revision of the theoretical β-limit would apply across the board, as a multiplicative factor, or would simply tend to bring the critical betas of round plasmas closer to those of specially shaped plasmas. This question will be addressed in ISX-B — and later in PDX — when their capabilities for noncircular plasma shaping are utilized.

A second new ISX-B result of major reactor significance has been the demonstration of plasma fueling by pellet injection (cf. Fig. 4). Hydrogen pellets of millimeter diameter, with velocities in the 10^5 cm/sec range have been injected successfully. In ohmic-heated plasmas [$T_e(0) \lesssim 0.7$ keV] the pellets traverse most of the plasma and even reemerge. In neutral-beam heated plasmas, the penetration is much shallower. In these experiments, the plasma density has been multiplied severalfold (up to $\Delta n/n \sim 4$) without disturbing the discharge appreciably or causing a substantial instantaneous loss of plasma energy. Many interesting details of the pellet ablation process are being obtained by means of holographic interferometry and shadowgraphy.

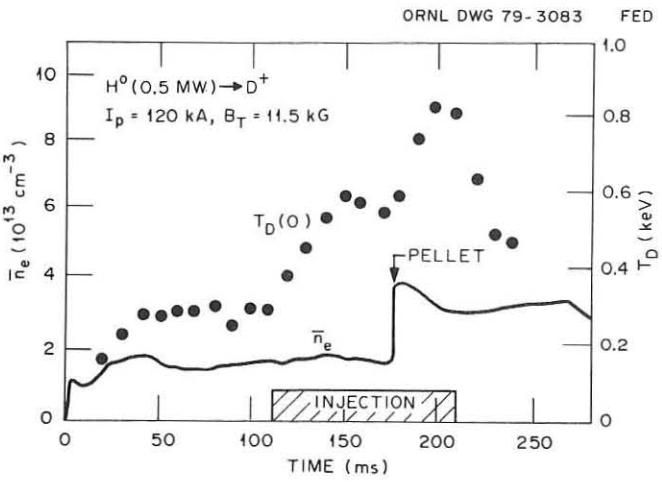

Figure 4. Hydrogen pellet injection into a neutral-beam-heated ISX-B plasma.

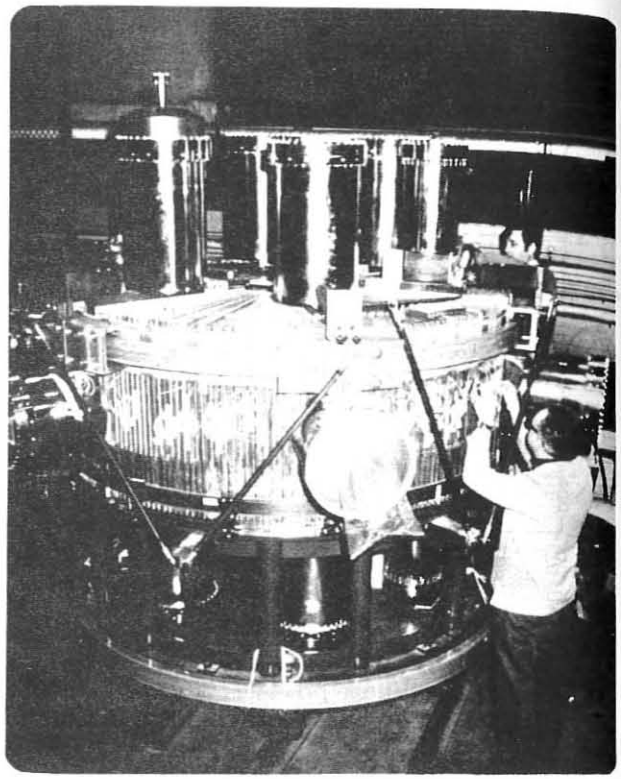

Figure 5. The Alcator C device during assembly.

II. ALCATOR C

The remarkable accomplishments of the Alcator A device [4] at the Massachusetts Institute of Technology (MIT) have now begun to be extended by the Alcator C (Fig. 5), a larger device of the same type ($R = 64$ cm, $a = 17$ cm) with a capability for $B_T = 120$ kG and $I_p = 1.0$ MA. Thus far, experimental operation has been limited by the power supply to $B_T \leq 60$ kG and $I_p \leq 500$ kA, but extension of operations to approximately 100 kG is expected to take place during the next few months.

The initial experimental results of Alcator C will be reported in Ref. 5. A preliminary view of the plasma behavior is given in Fig. 6 for a set of discharges at the 400-kA level. The confinement time of about 20 msec at $\bar{n}_e = 2.2 \cdot 10^{14} cm^{-3}$ represents a simple scale up, according to the a^2-law, relative to Alcator A. The electron and ion temperatures are somewhat higher than in Alcator A. A surprising feature of the new results is that τ_E does not appear to rise with increasing density.

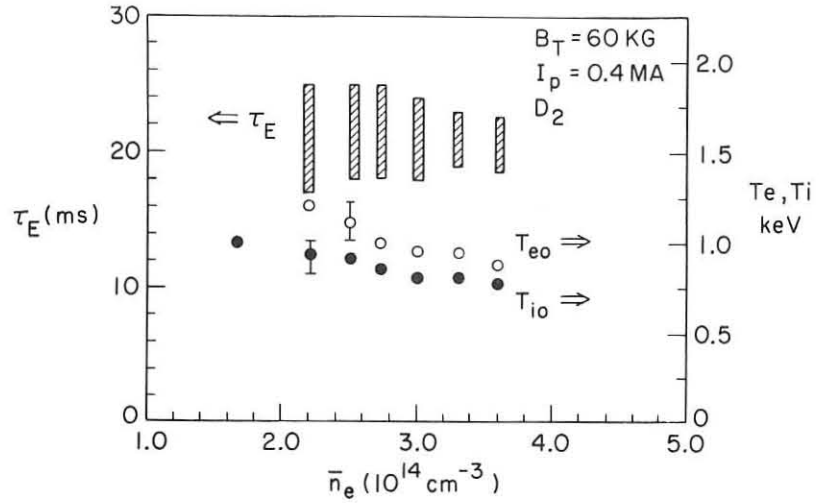

Figure 6. Temperature and energy confinement for half-field operation in Alcator C.

While a saturation of τ_E with rising density has been observed in many previous tokamak experiments, notably in ISX, and has been interpreted in terms of neoclassical ion heat transport, the present Alcator numbers would seem to stretch this hypothesis. The Alcator group regards the saturation phenomenon as perhaps arising from heavy-ion radiation or from a lack of optimization of the discharge conditions. Extensive new experimental information from Alcator C will soon be forthcoming, with the introduction of bolometric scans and higher-current operation. Meanwhile, the reformulation of tokamak transport theory would clearly be premature.

III. THE PDX DEVICE

The Poloidal Divertor Experiment [6] at Princeton (Fig. 7) has been operated initially as a tokamak with ordinary limiters — made of titanium, like the rest of the plasma environment in PDX. The PDX device has been tested up to its full ratings (B_T = 25 kG, I = 500 kA). Typical operating parameters have been: R = 142 cm, a = 40 cm, B_T = 20 kG, I = 360 kA. At $\bar{n}_e = 2 \cdot 10^{13}$ cm^{-3}, PDX has obtained $T_e(0)$ = 1.4 keV, $T_i(0)$ = 0.6 keV, and $\tau_E \sim 30$ msec (cf. Fig. 8).

The effective resistivity Z_η is seen to be quite close to unity. Spectroscopic and x-ray data are in fairly good agreement with the resistivity results. The main contributors to the Z-enhancement appear to be oxygen and titanium. Bolometric measurements show that, for low-density regimes ($\bar{n}_e \sim 2 \cdot 10^{13}$ cm^{-3}), about half the input power of 450 kW is radiated by impurities; the most important radiator is titanium.

Operation with the full PDX divertor system is scheduled to begin during the next month. Neutral-beam heating at 6 MW (a joint project of PPPL and ORNL) will begin in early 1980, and will put the efficacy of the poloidal divertor concept to its critical test.

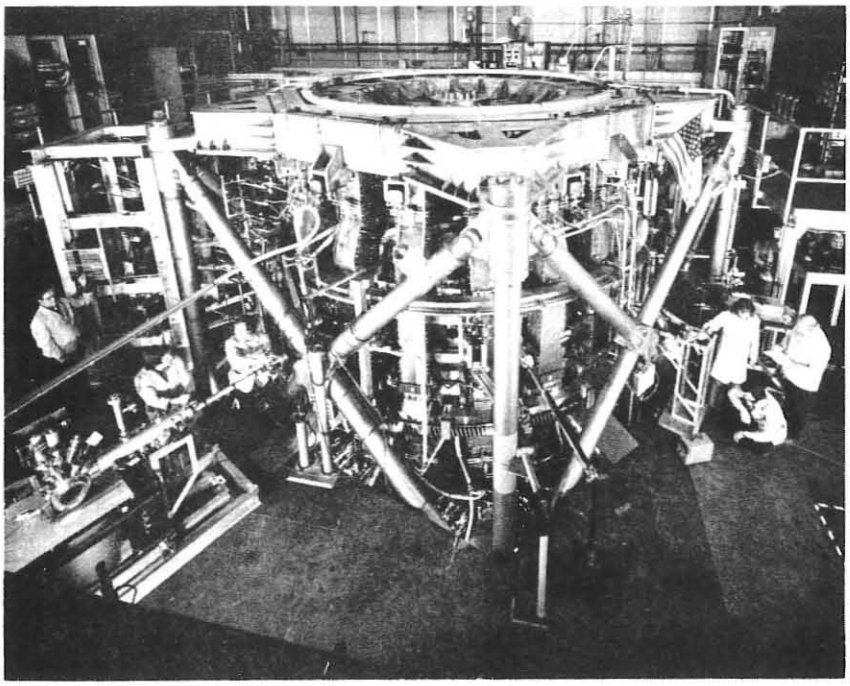

Figure 7. The PDX device in experimental operation. (PPL 794163)

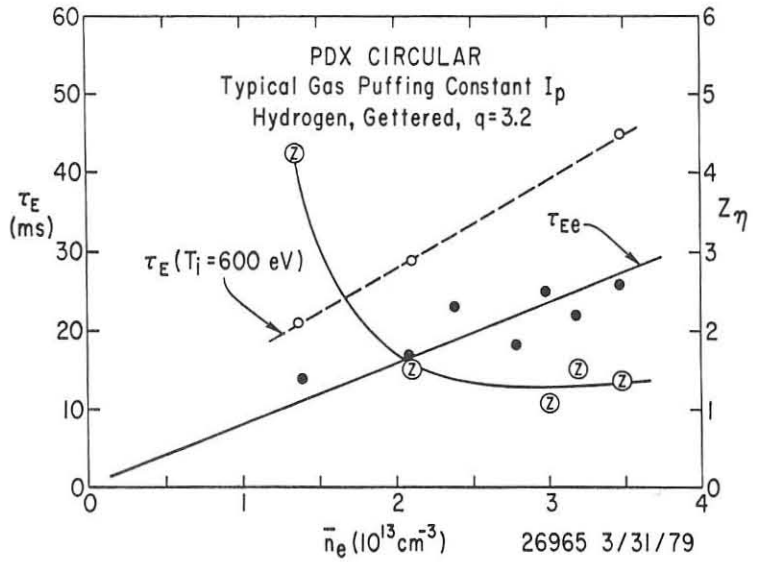

Figure 8. Energy confinement and effective Z in PDX, for a divertorless ohmic-heating operation.

IV. PLT HEATING EXPERIMENTS

A number of PLT technical papers are being reported at this conference [7-10]. The present review addresses itself to some recent results on ICRF and neutral-beam heating that have practical implications for next-generation tokamak heating.

Initial ICRF experiments on PLT [9,11] have used a single half-turn antenna to couple up to 350 kW of 25-MHz power into plasma waves. The most interesting results have been obtained by utilizing minority-ion damping, with the applied frequency adjusted to the fundamental cyclotron frequencies of small admixtures of H^+ or $^3He^{++}$ ions in deuterium bulk plasmas.

In the hydrogen minority experiments, the admixtures were typically 5-10% and the deuterium plasma parameters were B_T = 17 kG, I_p = 300 kA, $T_e(0)$ = 1.4 keV, $T_i(0)$ = 0.6 keV (before heating), τ_{Ee} ~ 20 msec, τ_{Ei} ~ 60 msec and Z_{eff} = 2 - 3; the density was adjusted to reach $\bar{n}_e \sim 2 \cdot 10^{13}$ cm^{-3} at the end of the rf pulse. As illustrated in Fig. 9, the bulk ion temperature rises appreciably during the heating process, as determined from the usual charge-exchange, spectroscopic, and neutron diagnostics.

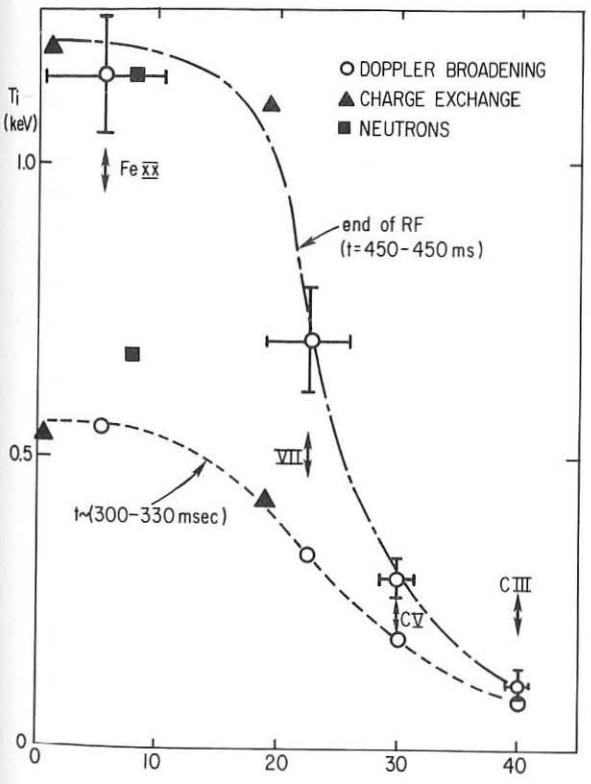

Figure 9. Radial ion temperature profile evolution in PLT for an ICRF heating pulse of 350 kW power and 100 msec duration. (PPL 796013)

In this process the hydrogen minority ions are typically raised to energies of order 10 keV, and have been measured up to 80 keV. The poor orbital confinement of such energetic protons at the relatively low plasma currents that have been used thus far presumably gives rise to wall bombardment and may contribute to the marked density rise (typically from $\bar{n}_e \sim 1 \cdot 10^{13}$ cm^{-3} to $2 \cdot 10^{13}$ cm^{-3}) during the rf heating; alternatively, the typically observed transition of the discharge into a strong sawtooth regime during the rf pulse may be responsible for the density rise.

A promising feature of the ICRF experiments is their energetic efficiency (cf. Fig. 10). Plotting ΔT_i against $P/\bar{n}_e$, for the hydrogen minority heating case, one finds a straight line with a slope very similar to that obtained previously for neutral-beam heating on PLT. The favorable impression is strengthened by experiments using a $^3He^{++}$ minority of 5-10%, together with a resonant field of 25 kG and currents up to 500 kA (cf. Fig. 10). The heating efficiency is then found to be improved by a factor of two.

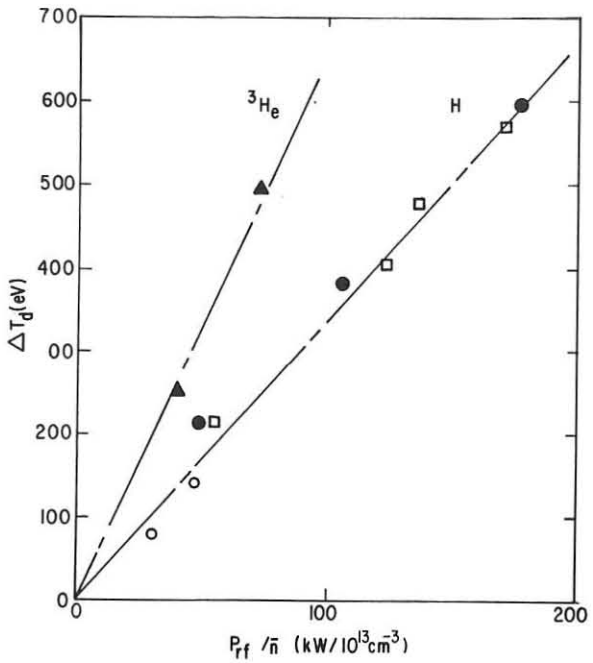

Figure 10. Empirical scaling of the deuterium ion temperature increase in PLT versus ICRF power, normalized by density. Minority heating through H^+ and $^3He^+$ ions has been studied. (PPL 796021)

Recently, two coupled half-turn coils have been put into operation on PLT, an arrangement that offers some control over the parallel wavelengths of the excited plasma modes and may permit the heating power to be deposited more centrally. This modification would be desirable, since the ion temperature profile for single-coil heating is rather broad (Fig. 9) and may be responsible for the observed enhancement of impurity influx during rf-heating — somewhat comparable to that associated with neutral-beam counter-injection. The use of two coupled coils will also allow the input power to be raised; 25-MHz-power levels in the 1-MW range are expected to be reached during the coming months.

The PLT device contains two additional coupling loops, which will begin to be used, this fall, with 43-MHz rf power, thus allowing the study of fundamental hydrogen minority heating in a 30-kG field, or second-harmonic heating at correspondingly lower fields. The ultimate PLT capability is for 4-coil, 43-MHz (or 55-MHz) heating in the multimegawatt range.

Minority heating by ICRF waves can be viewed as a kind of "internal" beam heating, which bears a fairly close resemblance to beam-injection heating. The initial PLT results are helping to establish the ICRF approach as a realistic alternate contender for the achievement of ignition in large next-generation tokamak devices, but the relative attractiveness of ICRF heating equipment will depend on practical details that are still far from clear. Some issues of special importance will be the relative ability of ICRF power to achieve good penetration in large, dense plasmas, and the feasibility of ICRF coupling structures that are suited to the reactor environment. In the latter context, the demonstration of efficient higher-harmonic (i.e., higher-frequency) heating will be particularly important.

A number of experiments have been carried out on PLT to study the phenomena associated with simultaneous ICRF and neutral-beam heating [8] at comparable input powers (approximately 250 kW each). Generally speaking, the ion temperature increments due to these two types of input power are linearly additive, but regimes that are associated with substantial impurity evolution give rise to unfavorable nonlinear effects. An interactive phenomenon that may have useful applications is the secondary energization of

neutral-beam-injected minority ions by the ICRF waves. In the illustrative case of Fig. 11, the normal injected-ion spread of 1.3 keV above the 25 keV injection energy is raised to 4.3 keV by the rf pulse. This phenomenon is of potential interest for "ion-energy clamping" in a TCT reactor, but energy diffusion, rather than net energy input, may turn out to be the principal feature of the rf-beam interaction.

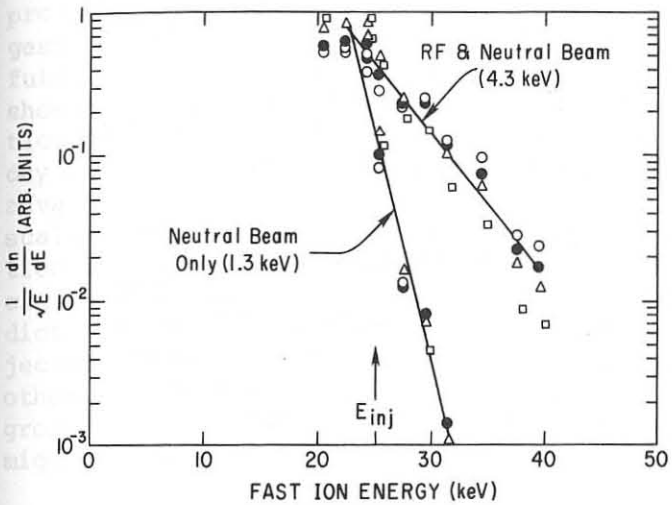

Figure 11. Interactive effect of simultaneous ICRF and neutral beam power in PLT: The beam ions are "heated" above the injection energy. (PPL 793766)

High-powered neutral-beam heating on PLT, first reported in Ref. 12 for the 2.1-MW level, was extended to 2.4 MW in Ref. 13, with resultant ion temperatures ranging up to 6.5 keV. During the past half-year, the power of the injection system has been raised to 3.0 MW. Recent high-temperature heating experiments on PLT have been handicapped, however, by the imposition of an upper limit of 25 kG on the toroidal field. This limit — which was imposed as a cautionary measure following minor TF coil damage — is about to be restored to the 30-kG level of the previous experiments.

While the confinement results obtained in the high-temperature experiments of Refs. 12 and 13 were generally very encouraging, the central mysteries of tokamak transport remain unresolved. The apparent ion heat conductivity is compatible with neoclassical theory, but since the ion heat conduction channel is a relatively minor feature of the energy balance, one cannot exclude an anomalous enhancement up to a factor of approximately 5 in the highest-temperature cases. The effect of trapped-particle modes in PLT is clearly less severe than had been anticipated on the basis of some simplified quasi-linear transport models, but the onset of important anomalous-diffusion losses at collisionalities somewhat below those of the PLT regime cannot be ruled out — and is even rather probable. Fortunately the degree of collisionlessness required in a conventional tokamak ignition reactor need not go beyond that already achieved in PLT, but "hot-ion ignition" schemes, for example, will enter an entirely new regime.

As regards the electron thermal conductivity, further studies on PLT have confirmed the original impression [12] that confinement in the central high-temperature plasma region actually improves during neutral-beam driven electron-temperature excursions. From these observations, one could draw the simpleminded conclusion that τ_{Ee} scales up proportionately with T_e, but a number of other interpretations are equally reasonable. For example,

τ_{Ee} may be affected favorably by the beam-driven increase in T_i/T_e, or by some secondary effect associated with the presence of the beam-injected ion population, so that the rise in T_e is not a cause of the rise in τ_{Ee}, but only an accompanying phenomenon.

While a great deal of effort has been devoted in recent years to the study of plasma energy and particle transport in the tokamak, the investigation of ion momentum transport (i.e., viscosity) has been undertaken only recently [14]. That these three forms of plasma transport are all related and provide essential clues to one central physical transport phenomenon, seems rather likely. The expectation that something important may be learned from rotating-plasma studies is being heightened by the recent PLT data, which continue to confound attempts at simple explanations.

The toroidal velocity profile shown in Fig. 12 was obtained by means of 1.5 MW of tangential deuterium coinjection into a hydrogen plasma of $T_e(0) \sim 2$ keV, with $n_e(0)$ rising from 3 to $5 \cdot 10^{13}$ cm^{-3} during injection. The characteristic viscous-damping times calculated for this profile were of order 10-20 msec — roughly comparable to the electron and ion energy confinement times, but very short compared with classical expectations (2.5 sec), and somewhat short compared with the conceivable damping due to charge-exchange (40-300 msec).

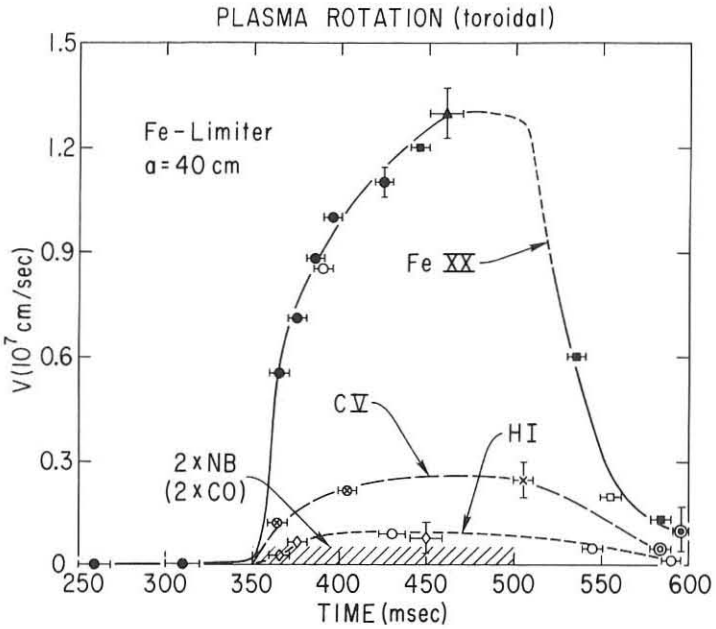

Figure 12. Toroidal velocity profile in PLT during unbalanced tangential injection of 1.5 MW from two coinjectors. (PPL 786284)

The neutral-damping hypothesis could be laid to rest entirely by measuring the dependence of the rotation velocity on plasma density. Recently, the authors of Ref. 14 have carried out this experiment, and find that the rotation velocity shows a moderate inverse dependence on density, with the viscous-damping time increasing only mildly at the higher densities (up to $\bar{n}_e = 5 \cdot 10^{13}$ cm^{-3}) where charge-exchange becomes negligible. At this point, we are left without any known mechanisms that could explain the main damping effect.

Another source of information about the plasma rotation phenomenon is the variation of the relative mass of injected and plasma ions. For example, one might expect a D-beam injected into an H-plasma to give substantially higher rotational velocities than the converse arrangement. Surprisingly, this mass effect has turned out to be quite weak; the literal interpretation would be that the hydrogen plasma has higher viscosity.

Aside from challenging our intuitions about tokamak transport, the unidirectional neutral-beam injection experiments have important practical consequences for next-generation tokamak facilities. It is well known by now that counterinjected neutral beams give rise to far more impurity evolution (at a given power) than coinjected beams. This effect is not surprising, since counterinjected ions are more likely to strike the walls and cause sputtering. In addition, recent PLT experiments with argon admixtures have provided some indication that counterinjection may actually promote the ingestion of edge impurities into the plasma. A critical question for the future is whether unbalanced coinjection into next-generation tokamak plasmas should be utilized to minimize the impurity problem, or must be avoided meticulously in order to prevent rotation-driven instabilities. In present-day tokamak devices, such as ISX-B and PLT, unbalanced coinjection is clearly advantageous, but in the absence of knowledge concerning the nature and scaling of the tokamak plasma viscosity, one worries that long-pulse injection into large, hot tokamak plasmas may result in dangerous rotation velocities. On the basis of the classical transport theory, the velocities predicted for TFTR could clearly become enormous, even when the unbalanced injection is of the near-perpendicular, rather than tangential kind. On the other hand, if the rotation damping time continues to be of the order of the gross energy confinement time, as in PLT, then even tangential coinjection might well present an attractive risk.

ACKNOWLEDGMENTS

I should like to thank the ISX-B, Alcator C, PDX, and PLT groups for their generous contributions of recent experimental data to this review.

This work supported by US Department of Energy Contract No. EY-76-C-02-3073.

REFERENCES

[1] OHKAWA, T., this conference, paper B 1.5.
[2] SWAIN, D. W., et al., this conference, paper B 2.2.
[3] TODD, A. M. M., et al., Nuc. Fus. 19 (1979) 743.
[4] GONDHALEKAR, A., et al., in Plasma Physics and Controlled Nuclear Fusion Research (Proc. 7th Int. Conf., Innsbruck, 1978) I (IAEA, Vienna, 1979) 199.
[5] Alcator Group, 21st Annual Meeting of the American Physical Society, Division of Plasma Physics (Boston, Massachusetts, 1979) paper E8.
[6] MEADE, D. M., this conference, paper D 2.5.
[7] COLESTOCK, P. L., et al., this conference, paper B 2.3.
[8] MEDLEY, S. S., et al., this conference, paper P 2.6.
[9] HWANG, D., et al., this conference, paper B 2.7.
[10] MC CRACKEN, G. M., et al., this conference, paper D 2.2.
[11] HOSEA, J., et al., Workshop on Physics of Plasmas Close to Thermonuclear Conditions (Varenna, Italy, 1979).
[12] EUBANK, H., et al., in Plasma Physics and Controlled Nuclear Fusion Research (Proc. 7th Int. Conf., Innsbruck, 1978) I (IAEA, Vienna, 1979) 167.
[13] EUBANK, H., et al., Phys. Rev. Lett. 43 (1979) 270.
[14] SUCKEWER, S., et al., Phys. Rev. Lett. 43 (1979) 207.

SHAPING AND CHARACTERISTICS OF DOUBLET PLASMAS IN DOUBLET III

T. Ohkawa

General Atomic Company
P.O. Box 81608
San Diego, California 92138

ABSTRACT

The shaping and plasma characteristics of doublet plasmas in Doublet III with high-Z limiters are described. Typical steady-state parameters at B_T = 24 kG are I_p = 1.5 MA, V_{loop} = 1.6 V, $T_e(0)$ = 1.0 keV, $\bar{n}_e = 4 \times 10^{13}$ cm^{-3}, Z_{eff} = 2, $q(0) \sim 1$ and $\tau_E^e(0)$ = 20 msec. Electron energy confinement and maximum plasma density are in agreement with standard circular tokamak empirical scaling laws. Chromium and molybdenum appear to be the dominant high-Z plasma contaminants, with relative concentrations of $\sim 10^{-4}$. The central power balance does not appear to be dominated by high-Z impurity radiation.

KEY WORDS

plasma shaping, doublet cross-section, electron confinement, maximum plasma density, high-Z impurities, plasma characteristics

1. INTRODUCTION

Physics experiments in Doublet III (Fig. 1) began in September 1978. In the ensuing period described in this paper (through July 1979), the primary emphasis has been on shaping the plasma to obtain a steady-state doublet discharge and on making preliminary measurements of the plasma characteristics.

2. PLASMA CHARACTERISTICS

Doublet discharges with plasma currents of 1.5 MA are now routinely obtained at B_T = 24 kG. A peak current of 2.2 MA has been achieved at B_T = 24 kG with rising plasma current. Waveforms for a representative 1.5 MA doublet discharge are shown in Fig. 2. Typical parameters for the flattop phase are V_{loop} = 1.6 V, $T_e^{laser}(0)$ = 1.0 keV, $\bar{n}_e = 4 \times 10^{13}$ cm^{-3}, $q(0) \sim 1$, $Z_{eff} \sim 2$ and $\tau_E^e(0) \cong 20$ msec. These results are obtained with a gas injection rate of 50 Torr-ℓ/sec.

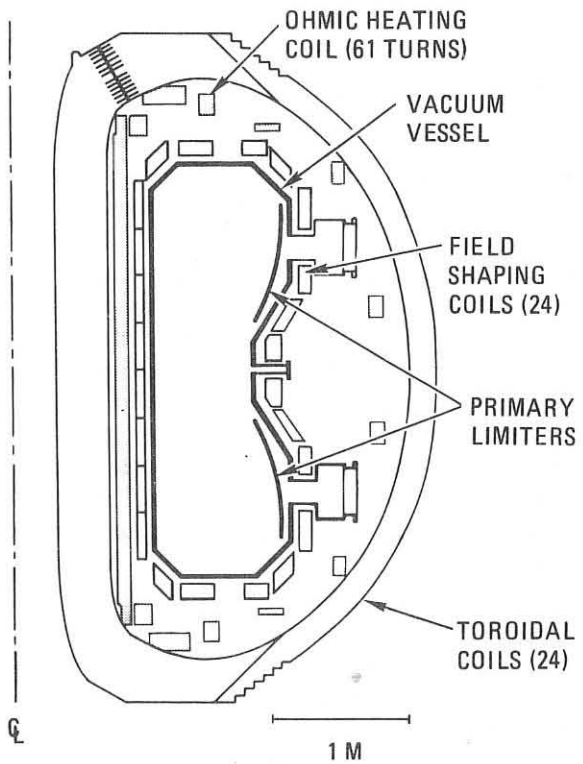

Fig. 1. Cross-section of Doublet III. Machine parameters are R = 1.43 m, a = 0.45 m and B_T^{max} = 26 kG. The primary limiters are tantalum-tungsten alloy. A molybdenum secondary limiter (not shown) also encircles the poloidal circumference of the vessel at three toroidal azimuths.

Experiments to determine the maximum permissible injection rate and plasma density are in progress.

Magnetic measurements indicate that the flattop discharge configuration is a doublet with approximately 90 ± 10% of the poloidal flux inside the separatrix (Fig. 3). The poloidal magnetic field and flux values measured outside the vacuum vessel are essentially time-independent, indicating a constant plasma shape. Second-harmonic cyclotron radiometer measurements confirm that the electron temperature profile is stationary and centrally peaked (Fig. 4). If Z_{eff} is uniform throughout the plasma, the temperature profile shown in Fig. 4 implies $q(0) \cong 0.9$. However, the absence of observable sawtooth oscillations at the plasma center suggests that q(0) is still greater than unity.

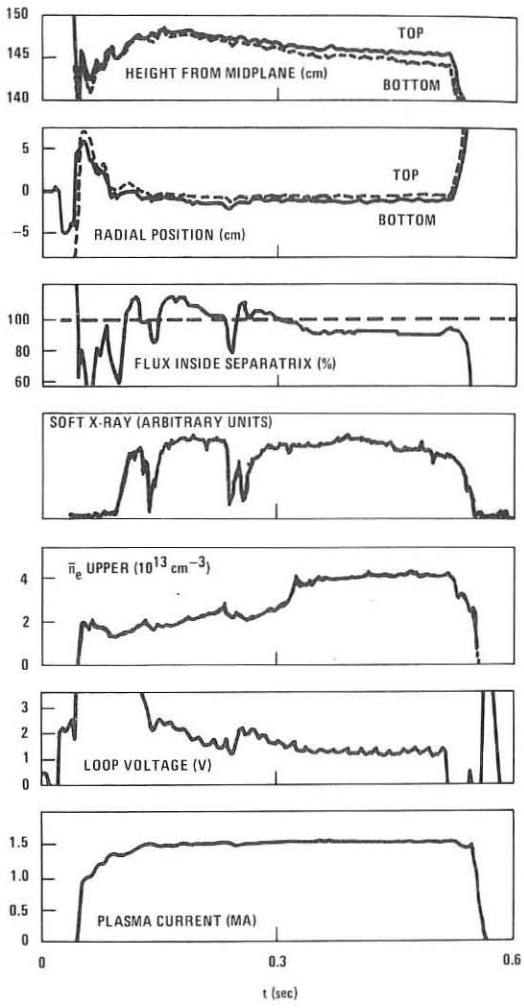

Fig. 2. Typical doublet discharge waveforms

3. PLASMA SHAPING AND MHD ACTIVITY

The plasma shape is controlled by 24 poloidal field-shaping coils (F-coils) that surround the vacuum vessel. Control of the magnetic flux linking these coils allows the cross-section and position of the discharge to be varied. The F-coils are arranged in several parallel-connected groups (Fig. 5), each with a power supply in series. The voltages produced by these supplies determine the coil fluxes, and hence the plasma shape. The parallel connection of the F-coils provides passive stability against axisymmetric motion of the plasma, especially for vertical displacements.

Figure 6, the one-line circuit equivalent of Fig. 5, illustrates more directly how the shaping supplies control the F-coil fluxes. Two principal shaping functions are required to obtain a doublet discharge. The first, the usual vertical field to maintain radial equilibrium, is provided by a combination of a 16 mH inductor L_s in series with the inner F-coils and the V (vertical) power supply in series with the outer F-coils. The second, the flux required to form the doublet waist, is provided by the D (doublet) supply, assisted by a capacitor discharge circuit during the initial plasma current rise. Fine tuning of the plasma shape is provided by "tweaker" supplies T3 and T4 that control the flux at the top and bottom of the plasma. Finally, resistance compensation supplies R1 and R2 minimize differences in the shaping flux on the inner F-coils produced by the F-coil resistance. The construction and specifications of the supplies are summarized in Table I.

TABLE I

DOUBLET III PLASMA SHAPING POWER SUPPLIES

SUPPLY	VOLTAGE (V)	CURRENT (kA)	TYPE	STEP RESPONSE TIME (ms)
D	± 600	14	60 Hz, 12 pulse	8
V	± 600	21	60 Hz, 12 pulse	8
T3, T4	± 400	3	SCR CHOPPER	0.2
R1, R2	0-150	3	60 Hz, 6 pulse	16

In discussing doublet plasmas, the quantity

$$P_s \equiv (\psi_{max} - \psi_{sep})/(\psi_{max} - \psi_{lim})$$

is a useful measure of the shape of the plasma. Here ψ_{max}, ψ_{sep} and ψ_{lim} are respectively the flux values at the elliptic axis, separatrix and limiter. Doublet has $0 < P_s \leq 100\%$. For $P_s > 100\%$, the discharge separates into two current channels, referred to as droplets. For high values of P_s (> 180%), the droplets are nearly circular and evolve independently. Such discharges provide a convenient means of obtaining a circular plasma for comparison purposes.

The time dependences of P_s and other plasma parameters shown in Fig. 2 are typical. The discharge begins with $P_s \sim 30\%$, but evolves rapidly to higher values, with P_s = 80-100%. During the initial phase, the plasma undergoes a series of n = 0, m = 2 oscillations. Two distinct types of oscillations are observed: 1) small amplitude ($\delta P_s \sim 5\%$) sinusoidal fluctuations at ∿ 100 Hz and 2) sudden (∿ 1 ms), larger amplitude (∿ 30-50%) drops in P_s followed by a slower recovery. The first type of oscillation is benign, but the large amplitude fluctuations are troublesome, and in extreme cases, result in termination of the discharge.

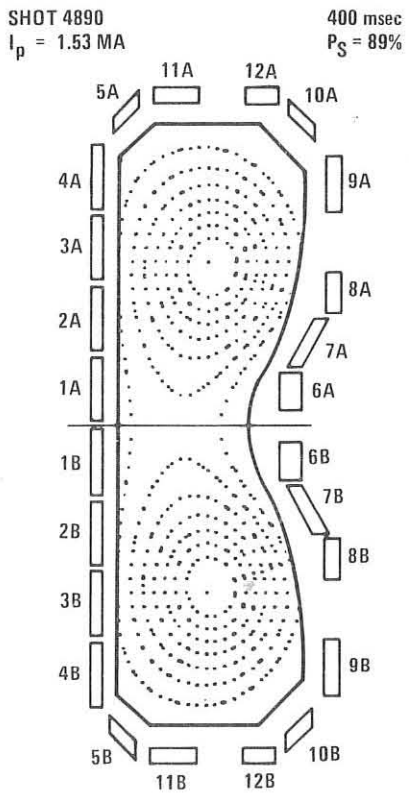

Fig. 3. Magnetic configuration for Fig. 2 at t = 400 msec

The large amplitude fluctuations are accompanied by a rapid cooling of the plasma, as indicated by sudden drops in the central radiometer and soft x-ray signals, and an increase in low-Z impurity line radiation. Framing camera motion pictures of the discharge show increased interaction of the plasma with the limiters. The cyclotron radiometer indicates a sudden broadening of the current profile (Fig. 4, $t \cong 200$ msec), followed by a slower recovery to a centrally peaked profile in about one energy confinement time, which is similar to the time in which recovery to the initial shape occurs.

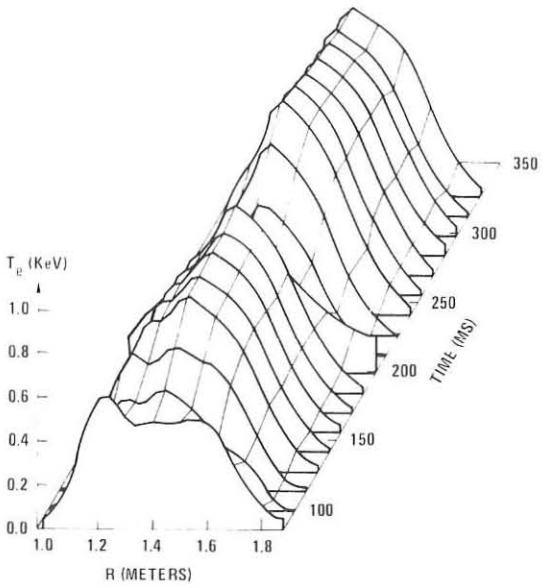

Fig. 4. Electron temperature profile evolution

Presumably, the large amplitude shape fluctuations are a consequence of the broadening of the current profile. The mechanism responsible for this broadening has not yet been identified, but internal MHD activity is probably involved. An enhanced level of odd n-number Mirnov activity is observed during the initial phase of the discharge, but so far none of the modes typically observed in circular tokamaks (e.g., n = 1, m = 2 or 3) have been identified. The fact that the Mirnov signals are incoherent and the lack of any obvious dependence of the shape oscillations on B_T or I_p suggests that high-m modes near the separatrix may be responsible.

4. CONFINEMENT, DENSITY SCALING AND IMPURITIES

The maximum plasma density achieved in these preliminary experiments is in good agreement with the B_T/R scaling observed in other clean, high-density experiments[1-6] (Fig. 7). The maximum line-average density obtained to date is $\bar{n}_e = 5 \times 10^{13}$ cm^{-3}. The central electron confinement increases with plasma density (Fig. 8). The average slope of the data at

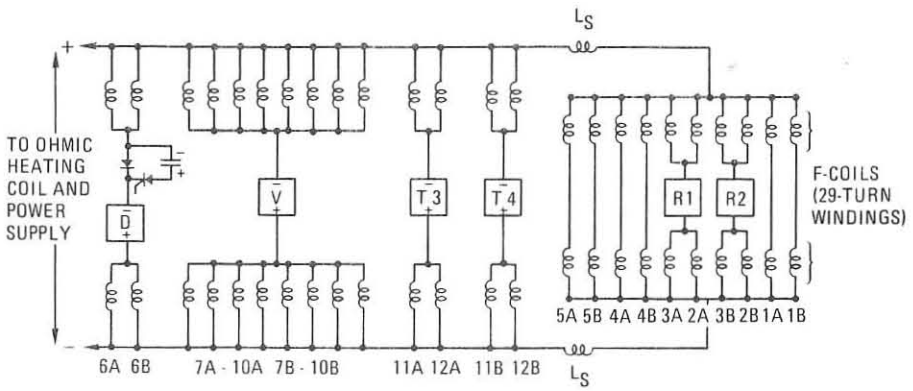

Fig. 5. Poloidal circuit for doublet shaping

high density is similar to that observed for the global electron confinement in PLT with titanium gettering[1]. The best confinement obtained so far is $\tau_E^e(0) = 28$ msec at $\bar{n}_e = 3.9 \times 10^{13}$ cm^{-3}.

Preliminary estimates of the global electron confinement based on the radiometer profile data indicate that the global confinement is about 80 ± 10% of the central confinement.

Although the ion temperature has not been measured, transport code simulations using neoclassical ion conductivity indicate that the ion and electron temperatures should be nearly equal at the higher densities. Thus, for $T_e = T_i$, the total central confinement time presumably is 40-50 msec for $\bar{n}_e = 4.5 \times 10^{13}$ cm^{-3}.

Impurity measurements are still in a relatively preliminary state. Auger analysis of samples exposed to the discharge cleaning plasma and residual gas analysis of the impurities evolved during plasma discharges suggest that carbon is the dominant low-Z contaminant. Chromium and molybdenum lines are prominant in the soft x-ray spectrum (Fig. 10). The concentration inferred from the soft x-ray intensity is about 3×10^9 cm^{-3}. Tantalum (the primary limiter material) is not observed in the soft x-ray region, indicating that the concentration is less than 10^9 cm^{-3}.

Auger analysis shows that molybdenum is the dominant heavy metal transported during plasma operation (∿ 5% monolayer/40 discharges), with tantalum nearly an order of magnitude less. This seems to corroborate the soft x-ray data that molybdenum (from the secondary limiters) and chromium (from the wall) are the dominant high-Z impurities. For coronal equilibrium, the measured impurity concentrations would imply P_{rad}/P_{OH} ∿ 10% in the center of the plasma. This estimate seems to be supported by the relatively good electron confinement,

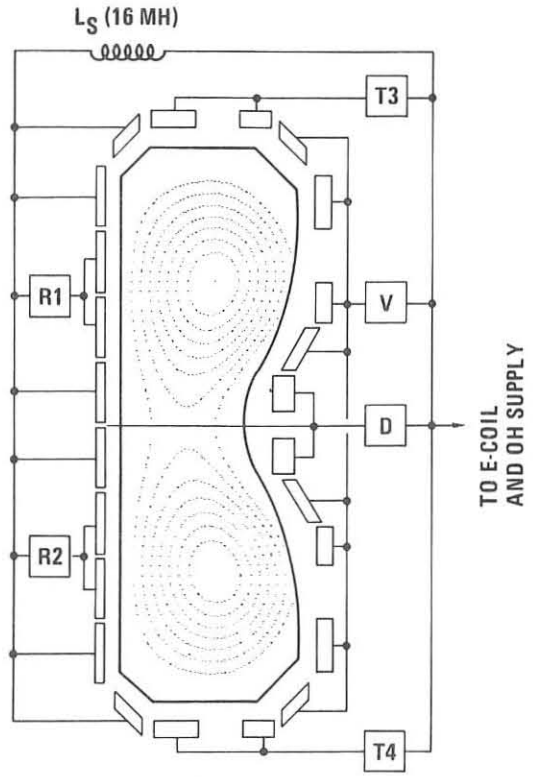

Fig. 6. One-line doublet shaping schematic

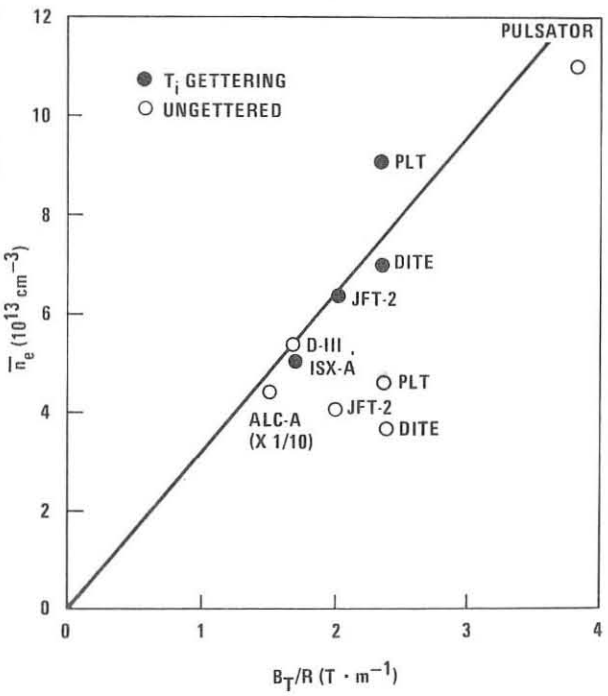

Fig. 7. Comparison of maximum density achieved in Doublet III with other experiments

which is similar to that obtained in machines known to be free from significant high-Z radiation. Forthcoming bolometric and vacuum ultraviolet spectroscopic measurements of the plasma radiation are expected to clarify the impurity question.

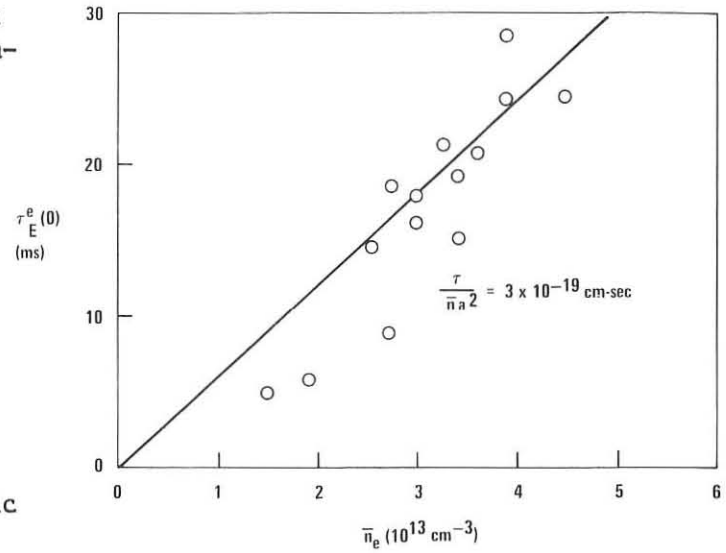

Fig. 8. Dependence of doublet central electron confinement on plasma density

5. SUMMARY

Steady-state doublet plasmas with low loop voltages and low levels of internal MHD activity have been produced. The magnetic configuration during the flattop phase is essentially constant, with about 90% of the poloidal flux inside the separatrix. Radiometer measurements show that the electron temperature profile is stationary and centrally peaked. The electron confinement and maximum plasma density achieved to date are in good agreement with "standard" scaling laws. Indirect evidence suggests that the power balance in the central portion of the plasma is not dominated by high-Z impurity line radiation.

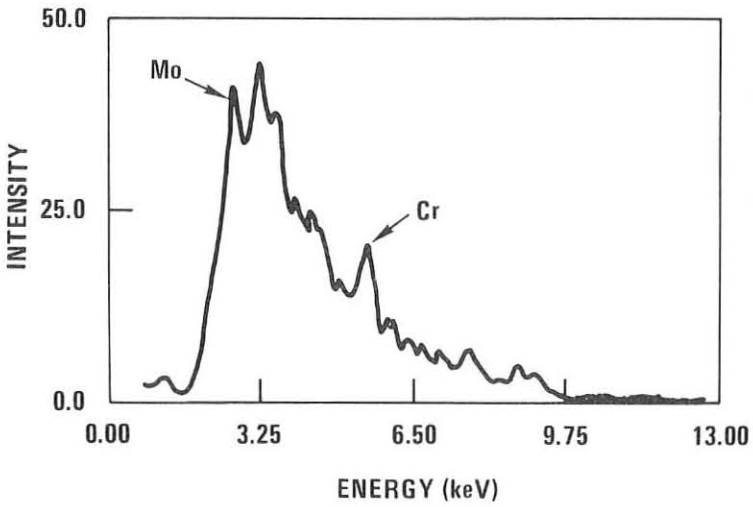

Fig. 9. Typical soft x-ray spectrum

6. ACKNOWLEDGMENTS

The studies reported here were supported by the United States Department of Energy under Contract DE-AT03-76ET51011, and were carried out by members of the Doublet III physics, plasma diagnostics and operations groups: S. Adcock, C. Armentrout, D. Baker, J. Baur, F. Blau, N. Brooks, R. Callis, R. Chase, J. DeBoo, J. deGrassie, S. Ejima, E. Fairbanks, R. Fisher, W. Guss, C. Hsieh, G. Jackson, G. Jahns, J. Lohr, M. Mahdavi, F. Marcus, N. Ozaki*, F. Parlange†, P. Petersen, S. Seki**, R. Seraydarian, L. Srnka††, R. Stambaugh, T. Tamano, T. Taylor and J. Wesley

The Auger surface analysis measurements were done by R. Clausing, L. Emerson and L. Heatherly from Oak Ridge National Laboratory, using a portable surface analysis system supplied by Oak Ridge National Laboratory.

This manuscript was prepared with the assistance of J. Wesley.

7. REFERENCES

[1]K. Bol, et al., in Plasma Physics and Controlled Nuclear Fusion Research (Proc. 7th Intl. Conf., Innsbruck, 1978), IAEA-CN-37-A1, Vienna (1979).

[2]M. Murakami, et al., Phys. Rev. Lett. 42, 655 (1979).

[3]S. Konoshima, et al., Journal Nuclear Materials 76-77, 581 (1978).

[4]S. J. Fielding, et al., Nuclear Fusion 17, 1382 (1977).

[5]E. Apgar, et al., in Plasma Physics and Controlled Nuclear Fusion Research (Proc. 6th Intl. Conf., Berchtesgaden, 1976), IAEA-CN-35-A5, Vienna (1977).

[6]W. Engelhardt, et al., in Plasma Physics and Controlled Nuclear Fusion Research (Proc. 7th Intl. Conf., Innsbruck, 1978), IAEA-CN-37-A5, Vienna (1979).

*Energy Research Laboratory, Hitachi Ltd., Hitachi, Japan.
†On leave from Association Euratom CEA GRENOBLE, France.
**Japan Atomic Energy Research Institute, Tokai Research Establishment, Japan.
††Present address: Exxon Production Research Company, Houston, TX 77001.

A REVIEW OF FUSION-FISSION (HYBRID) REACTOR STUDIES

G. Casini

Joint Research Centre - Ispra Establishment
21020 Ispra (Varese) - Italy

Summary

A survey of the work being pursued worldwide on fusion-fission (hybrid) reactor systems is presented. The following areas have been reviewed:

- plasma modes of operation
- blanket concepts and fuel cycles
- reactor conceptual designs
- safety and environmental problems
- system studies and economic prospectives

Attention has been restricted to systems using magnetically confined plasma, namely to mirror and Tokamak-type concepts.
The aim is to provide sufficient information, even if not exhaustive, on hybrid reactor concepts in order to help understand what may be expected from their possible development and the ways in which hybrids could affect the future energy scenarios.

Introduction

The first studies on fusion-fission (hybrid) concepts data back to the fifties. The primary motivation for these studies was of a military nature, the main reason being the production of plutonium for nuclear weapons. They were supported by the US Atomic Energy Commission and remained classified from their beginning in 1951 until 1958, when it became clear that other ways of producing weapons materials through isotopic separation and small fission reactors were simpler. The interest in the hybrid reactor has been renewed in the 1970's because of the consistent progress achievements in the way toward the controlled thermonuclear fusion.
The emphasis early in that period was focused on fusion drivers that are inherently low in fusion energy gain, Q, such as the classical mirrors. The potential application for a fission blanket was the energy amplification and then economical power generation.
More recently, the interest has been shifted towards the exploitation of the fusion neutrons to produce fuel to be used in fission reactor plants. This approach has extended the range of investigation including from one side also systems as Tokamak's, suited for higher Q-values and, from the other side, fuel cycles adapted for the best utilisation in thermal converters.
In general, we may observe that in a fission reactor, a large amount of energy ($\sim$ 200MeV) is produced per fission event, but a severe economy of neutrons is required to keep the reactor critical; whereas in a fusion reactor, a small amount of energy ($\sim$ 20MeV) is released per fusion event, but the neutrons are not needed to keep the plasma running, and may be used for other purposes. The fusion-fission concept profits of the complementarity of the processes. The flexibility offered by the hybrid for a variety of alternative fuel cycles has pushed recently the public authorities to focus the attention on solutions which are attractive from non-proliferation point of view.

The more extensive studies on fusion-fission (hybrid) systems are being carried-out in USA and USSR. In USA (1) the DOE (Department of Energy) programme has placed emphasis on the development of hybrid reactors, "which are optimized for proliferation resistance". The EPRI (Electric Power Research Institute) programme is directed to identify "the route to commercial operation" of the hybrid reactor.
A joint effort with the USSR is also in progress. In the USSR (2), the studies on fusion appear to be mainly oriented toward the development of hybrid systems. In Europe, the activity in this area is limited to orientative evaluations in France (CEA) (3) and Israel (4) and to a review work at JRC-Ispra (5).
In the following, different aspects of the recent D-T hybrid systems will be reviewed; plasma requirements in Tokamak and Mirror systems, blanket performances, problems related to the fuel cycle, safety and environmental considerations. The main features of a few reference designs of hybrid reactors will also be reported, as well as results of system analyses and economic prospective studies.

1. Plasma parameters

In a hybrid reactor the plasma is operated as an energy amplifier, and there are two burn modes which have been proposed (6). In the first one (7), named TCA (Two Component Amplifier), the temperature of a tritium bulk plasma is maintained against transport and radiation losses by means of injected energetic deuterons, which undergo fusion reactions with the relatively cold tritons. The large beam-plasma fusion reactivity allows a TCA to attain a fusion energy gain, Q, (defined as the fusion power produced divided by the power injected into the plasma), approximately equal to 1 at values of $n_e\tau_E$ many times lower than that required for a $Q = 1$ thermonuclear reactor, where all reacting ions are thermalized. For given values of electron temperature T_e and injection energy W_0, one can maximize the fusion power density P_F, and then the neutron production rate, by optimizing the ratio of the fast-ion bulk-plasma pressure (Γ). Optimal values of Γ and the corresponding Q and P_f are shown in Fig. 1.1 for $W_0 = 200$ keV as well as the maximum P_f for a thermonuclear reactor of the same pressure (7). At $Q = 1$ in a TCA, P_f is a factor of four larger than the maximum P_f attainable in a thermal plasma at any temperature, for the same total plasma pressure. For Q-values larger than attainable in "pure" TCA operation, $n_e\tau_E$ must be increased so that the injected beam power can be reduced while the proportion of the fusion power output coming from thermal plasma reactions increases. At the same time, P_f decreases because of the reduction in beam-plasma reactions. The trade-off between Q and P_f for a given plasma pressure is shown in Fig. 1.2 ($W_0 = 200$ keV). For each $n_e\tau_E$ the D-T composition of the background plasma is adjusted for maximum Q.
In Fig. 1.3 Q is presented as a function of $n_e\tau_E$, considering the α-particle heating and without it (8). It appears that in the TCA regime ($n_e\tau_E \cong 3 \times 10^{13}$ cm^{-3}s), the contribution of α's is so small that the presence of processes leading to possible drifts of the α-particles from the plasma to the first wall should not have practical effect on Q.
In the second mode of operation, named MFA (Maxwellian Fusion Amplifier), the plasma, still subignited, is composed of a 50-50 DT fuel mixture and the ions are raised to a temperature ($\sim$ 10 keV) where the fusions among thermal ions produce power which substantially exceeds the input power. Typical values of Q are in this case larger than 5.
Both TCA and MFA modes are inherently thermally stable (6) and the injected power can be used for additional control of the power output. Importantly, any form of power

injection, neutral beams or RF-heating, is acceptable in the MFA mode since the power amplification comes primarily from thermal fusion reactions. The TCA mode, on the contrary, based on fast fusions between high energy particles and a thermal background target plasma, works best with neutral beam injection.
Typical values of plasma parameters for hybrid reactor applications of Tokamak's in the USA and USSR are given in Table 1.1. The first two cases correspond to Demonstration Tokamak Reactor Studies (9, 10). The third case corresponds to a Russian commercial power Tokamak reactor (2). These values are compared to those of TFTR. In the existing machines $n_e\tau_E$ values of up to 10^{13} $cm^{-3}s$ and averaged temperatures of up to 5 keV have been obtained. This means that, from heating and energy confinement points of view, we are near to satisfying the design requirements of a hybrid reactor. The major problems remain those of the neutral injectors, duty factor and plasma impurity control.
In order to realize economical operation conditions for a hybrid power reactor, a operation with burn-times of at least 100s will be required. This will imply the solution of a number of problems, such as:

- impurity control of the plasma
- pumping of the injected particles after their deceleration in the plasma
- steady state operation of the neutral injectors

The use of a divertor seems, according to the analyses performed up to now (2, 8, 9, 10) inevitable. However, all the matter deserves more investigation.
In Table 1.2 the key physics parameters are compared for the present Mirror Experiment at Livermore, 2 XII B, for the next machine, MTFR, scheduled to be operative in 1981 and for a commercial hybrid reactor jointly proposed by LLL and General Atomics (MHR) (11, 12). The major differences between the MTFR plasma and that required for the hybrid reactor are the physical size and the duty factor. Apart from the development required for the beam injectors (which is similar to what is needed for Tokamak's), it appears that $n_E\tau$ for a commercial facility is about a factor 10 larger than in MFTR. However, MFTR is considered to be a sufficiently versatile experiment to establish scaling laws that will permit to extrapolate to the larger plasmas with a high degree of confidence.
Recently LLL has started the investigation on hybrid reactors based on the tandem-mirror type of confinement (13). A Tandem Mirror Experiment (TMX) is now in operation at Livermore and first results on plasma confinement are encouraging (15). For the hybrid power reactor studies a two-component mode of operation has been assumed to minimize plasma confinement and technology requirements (14). Typical plasma parameters for a Tandem Mirror Hybrid Reactor (TMHR) are given in Table 1.3.

2. Blanket design and fuel cycle

Fig. 2.1 shows a schematic view of the neutron economy in a hybrid blanket. The capacity of the blanket in breeding fissile fuel is indicated by the parameter F, the net number of atoms of fissile fuel produced in the blanket by each fusion neutron. Multiplication of the energy released by fusion is mainly realized through fission events within the blanket; the pertinent figure of merit is M, the energy deposited in the blanket for each neutron referred to the neutron fusion energy. As in pure fusion systems, the tritium breeding is characterized by T, the number of tritium atoms generated within the blanket per fusion neutron. Experience (16) shows that a 14 MeV neutron emitted at the centre of a large block of natural uranium produces about 1.2 fast fissions on U-238, a total energy release of 300 MeV, and 4.1 breeding reactions. Th-232 has a lower efficiency: the values of

energy multiplication M and fuel breeding F calculated for a large block of uranium (12) are respectively 80% and 40% lower than the corresponding values of natural uranium.

Blanket design problems

Many alternative blanket designs have been proposed in order to fulfill the requirements at Fig. 2.1. A first choice is between the case where a moderator is associated to the fission fuel (thermal blanket) and the case without moderator (fast blanket). This choice depends basically on the aim assigned to the hybrid reactor. The primary purpose of the fast blankets is that of fissile fuel production. Most of the conceptual designs presented in the last years refer to gas (usually helium)-cooled fast fission blankets using a high density fuel. Examples are the Livermore Mirror Hybrid Reactors, the Westinghouse design for a Tokamak Demonstration Hybrid Reactor and the Russian concepts of hybrid reactor blankets, already mentioned.
Recently reactor studies involving thermal blankets have been started, the most intensive one being that of the Ben Gurion University (Israel) in collaboration with Princeton (17, 18). In this study, light water moderated blankets are considered, the main purpose of the hybrid reactor (LWHR) being that of generating power. The blanket of LWHR consists of light water moderated and cooled. The pressure tubes housing several standard U_3Si fuel rods clad with Zircalloy.
A second choice is between uranium and thorium as fissile fuel. A comparative analysis of these two options is given in the next sub-chapter.

In the following, we will indicate some typical design problems of the hybrid blankets and the proposed solutions to them. One of the most severe problems is the steep power density gradient across the blanket. In the fast blankets peak-to-average power density ratios varying from about two up to ten are found. The effect is particularly important for solid fuel blankets in which the fuel rods are arranged perpendicularly to the first wall; this fact leads to very large temperature gradients along the fuel itself. In the thermal blankets, the possibility to have a relatively flat power density distribution looks easier. This has been shown for the Israelian LWHR-blanket by taking an arrangement with the lithium positioned ahead and below the fuel lattice and including a graphite reflector (19).
A second source of difficulties for the hybrid blanket design is the change of energy multiplication (and power density) during the reactor life. This is a consequence of the fissile fuel build-up, typically up to few percent. An illustration of this point for the case of the MHR blanket (11) is shown in Fig. 2.2. Methods to maintain a constant energy multiplication during the burn-up cycle have been recently proposed for the case of the LWHR-blanket (inherent control, lithium control, spectral shift control) (19).
From thermomechanical and radiation damage points of view, the limiting factors are those related to the fissile breeding zone. Assuming values of the maximum power density in this zone comparable to those of fission reactors, the corresponding wall-loading remains in general at values around 1 - 2 MW/cm^2. These values are considered as the lower boundary for applications to pure fusion power reactors; commercial materials (such as steel) can be envisaged to satisfy both stress and radiation damage requirements.
The geometry of the fusion driver does not lend itself to simple blanket design solutions. Furthermore, the presence of several large components such as cryopumps, injectors, magnets, etc. gives rise to several contrasting geometrical requirements. Routine and

maintenance operations to be performed on blanket units become very complex and remote handling is required. Modular blanket solutions are then mandatory. An account of some of the solutions proposed for mirrors and tokamak systems is given in chapter 4.
The condition $T > 1$ implies that the tritium breeding zone will be the thicker the lower its coverage (extension around the plasma); but the space between the plasma and the magnet, where the blanket has to be located, is strictly limited. Increasing attention to this problem has been given in the last period, in parallel with the development of more refined engineering design studies.
In Fig. 2.3 (3) the energy released in a uranium blanket of hybrid and the associated LWR-system is shown in function of the blanket coverage factor ($\bar{\omega}$). Typical values of $\bar{\omega}$ for tokamak systems with neutral injection are 0.7—0.8. These results show the importance the geometrical effects can play for the final assessment of the hybrid capability
An idea of the performances that may be expected from a hybrid blanket is given in Table 2.3, which reports the parameters computed for the Livermore Mirror Hybrid Reactor (see Fig. 3.1).

Uranium versus thorium cycle

Uranium has better energy multiplication properties: a factor $M = 10$ and larger can be reached by uranium blankets. It has higher density, which means that a greater uranium than thorium mass can be irradiated in the same volume. The production of plutonium in uranium blankets may vary between 0.5 and 1 kg/y per MW of thermal power to the blanket, or from about 3 to 6 kg/y per MW of plasma power.
For thorium it can be said that F is about 60% compared to the uranium value, and M is about three times smaller. Hence, the thorium cycle provides less energy to the blanket ($M = 3$) and less fissile fuel. On the other hand, U-233 is a better quality fuel because it offers a better efficiency than plutonium, both in LWR and in HTGR (20). If C is the conversion ratio of the burner reactor, the production rate of uranium and plutonium should be multiplied by the efficiency factor $1/(1-C)$ for a proper comparison. An important parameter for this is the "support ratio" defined as the number of fission power reactors which can be supplied in fuel by an hybrid reactor of the same thermal power. In Fig. 2.4 the support ratio for various cycles as a function of the conversion ratio of the fission reactor is plotted (21).
From the point of view of resources availability and of the material performances, it seems that there are no essential differences in favour of one or the other cycle. Undesirable radioactive contaminants are created in both cases. U-233 is contamined with U-232. In the decay chain of U-232 high energy gamma-rays are emitted, whose presence complicates the refabrication of the fuel element. This should be done by remote handling technique. The amount of U-232 present in the fissile fuel increases linearly with irradiation time (22) and reaches the value of 4000 ppm after 400 days. For comparison, in the U-233 produced in HTGRs the amount of U-232 is lower by an order of magnitude; but probably it is already large enough to require remote handling refabrication.
Pu-239 is contamined by Pu-238, which is a strong α-emitter, inducing (α, n) reactions on light elements such as oxygen. The oxide of this fuel will therefore give rise to some neutron shielding requirements. Pu-236 decays in 2.8 y to U-232. But the presence of this isotope is low for plutonium fuel.

The chemical separation of the fissile fuel from the irradiated breeder material produces long-life radioactive wastes in both cases. The toxicity of the actinides produced in the thorium cycle and their RBH (relative biological hazard) is significantly higher.
The comparison of the fuel bred in a hybrid blanket with that produced in a fission reactor shows important differences in quality and quantity. The fuel from the hybrid has higher fissile content: 95% of the plutonium bred from uranium is fissile. The U-233 content in the uranium bred from thorium is around 99%. In fission reactors the (n, γ) reactions on fissile isotopes produce non-fissile isotopes; these amount to 25 - 30%. This purity is advantageous from the point of view of burner efficiency, but undesirable for non-proliferation concerns.
Non-proliferating quality of fissile fuels has received increasing attention in recent times. U-233 may be easily denaturated by diluting into U-238. In this way the fuel produced would not be suitable for weapon construction. Denaturation of plutonium is certainly more difficult. Non-proliferation concerns have resulted in consistent international efforts under the International Fuel Cycle Evaluation (INFCE activity. Recent studies (23, 24) indicate the technical feasibility of a no-reprocessing strategy. Fuel based on HTGR or LWR technology, containing only thorium, would be irradiated in the blanket of the hybrid reactor. When a sufficient concentration of U-233 is reached, around 3- 4%, the fuel could be used in HTGRs or in LWRs. Multiple breeder-burner cycles could be operated. This "Refresh Cycle" system concept offers attractive features and is certainly proliferation-resistant. The use of the fissile fuel would be, of course, less efficient and the cost of energy would increase. Furthermore, doubts have been raised on the capability to meet, for the fuel produced in the hybrid, the stringent design qualifications of the fission reactor.
A new interesting symbiotic system with very simple fuel reprocessing has been proposed by the Kurchatov Institute (25). In the blanket of the fusion reactor, U-233 is produced from thorium circulating in the form of ThF_4. The molten salt fission reactor burns the U-233 and produces, for the fusion reactor, tritium from lithium circulating through its core in the form of LiF.
Recently LLL has taken also in consideration the proposal of a Berillium-Molten Salt Blanket (Be/MS) for hybrid reactors (21). In the LLL approach the hybrid blanket includes lithium in the salt and then tritium production. Perceived advantages of Be+MS blankets are:

- safety . loss of coolant accident (LOCA) problems virtually eliminated by virtue of suppressed fission and the continuous on-line removal of fission products as well as the fissile and fusile materials produced,
  . no plutonium produced;
- high-support ratio (see Fig. 2.4);
- on-line refueling and reprocessing should result in higher capacity factors and continuous sale of ^{233}U. Both should improve hybrid economics;
- low-pressure coolant should simplify mechanical design.

From the molten salt technology point of view, while much of the fission reactor experience (aircraft nuclear propulsion, Molten Salt Reactor Experiment) is applicable, there are important differences in the fusion-blanket environment. Low-blanket fission rate should reduce the fission product corrosion problem encountered (but apparently solved) in the MSRE. On the other hand, high neutron fluxes in structural components (first wall, etc.), magnetic fields and much larger tritium production rates will be more demanding of materials. Magnetic fields will induce electric current in flowing molten-salt which could enhance corrosion.

In the last period the need of exploiting as much as possible the experience of fission reactors for the selection of the fuel of the hybrid blanket has been emphasized (26). The comparison between possible fuel forms is analyzed on the basis of operational reliability, fuel fabrication development, fuel lifetime and module design considerations (including safety). As an example, in the Westinghouse DHTR study, results globally favour the use of ThO_2 fuel pellets in Zircalloy cladding even if this fuel is second to thorium metal fuel in terms of U-233 production.
In Table 2.2 are shown comparative recent results of blanket characteristics involving uranium and thorium in various forms (27). This work was performed by General Atomic for the TMHR scoping studies. The metal-clad thorium blanket has been assumed as reference fuel for further conceptual design work. Also the LWHRs have been found to possess an assemblage of attractive features from the fuel cycle point of view. These advantages features include the following (18):

- elimination of enrichment requirement. The fuel feed can be natural uranium, depleted uranium, or "spent fuel" from LWRs;
- no separation of plutonium is required;
- the fuel cycle technology is similar to that of the LWR;
- with co-processing to extract fission products only (i.e. no separation of ^{239}Pu from ^{238}U), the entire uranium resources (or thorium resources) can be burned.

3. Reactor conceptual designs

In the last years more emphasis has been given to the engineering and overall design aspects of the hybrid systems. In the following we will outline the main features of three of these reactor designs, namely:

- the Mirror and Tandem Mirror Hybrid Reactors, set up by Livermore and General Atomic;
- the Tokamak Demonstration Hybrid Reactor (DTHR) under study at Westinghouse;
- the USSR-Tokamak Prototype Hybrid Reactor (RTTH).

MHR (Mirror Hybrid Reactor)

It is the project for which the most complete conceptual design analysis has been carried out (years 1974 - 78). The main reactor design choices are:

- minimum-B mirror confinement;
- Yin-Yang coil design, NbTi superconductor;
- positive ion injectors with direct recovery;
- fast spectrum blanket neutronics;
- single-stage plasma direct converter;
- cryocondensation vacuum pumping;
- blanket
  - U_3Si fuel (depleted uranium)
  - LiH tritium breeder (natural lithium)
  - Inconel 718 structural material;
- helium primary heat transfer loop;
- prestressed concrete reactor vessel;
- steam thermal conversion system.

The characteristics of the reactor are listed in Table 3.1. A view of the reactor and of a blanket module is shown in Figs. 3.1 and 3.2.

TMHR (Tandem Mirror Hybrid Reactor)

Conceptual design studies on a Tandem Mirror Hybrid Reactor (TMHR) are being carried out jointly by Lawrence Livermore Laboratory, General Electric Co., Bechtel Corp. and General Atomic Co. In Table 1.3 is given a set of parameters for a not yet optimized tandem power reactor (500 MWe). As a tentative point design, a central cell length of 50 m was chosen together with a maximum magnetic field of 12 T and neutral beam injection of 200 keV. The predicted Q and wall loading are 1.1 and 2.2 MW/m^2, respectively. An artist view of the reactor is presented in Fig. 3.3.
The cylindrical geometry of the tandem mirror plasma and solenoid coils lead naturally to an axisymmetric cylindrical blanket module configuration, shown in Fig. 3.4.
The long cylinder is cut into modules and the string of modules is clamped into a longitudinal frame incorporated into the prestressed concrete reactor vault. The clamping force is applied by inflatable all-metal cushions between the cylindrical modules, which also make the major on-line vacuum seal using double knife seals. When pressure in the system is released, modules can be quickly changed. No welding or cutting is required to remove or replace the module. The central breeding zone is replaceable cartridge that slips into the reusable shield. The spent cartridge is quickly replaced with a fresh one and the reactor put back on line.
Concerning the blanket, two solutions involving either molten salts or solid fuel and gas cooling are being investigated.
For the gas-cooled blanket case, metal clad thorium is considered as reference fuel.
Concerning the fuel arrangement in the cylindrical blanket module, both plates and axial-rods solutions are being assessed. A layout of the blanket arrangement and a sketch of a blanket module for the case of the molten salt solution are presented in Figs. 3.5 and 3.6.

DTHR (Demonstration Tokamak Hybrid Reactor)

Westinghouse is performing a conceptual design study of a near-term Demonstration Tokamak Hybrid Reactor. A similar investigation has been performed in the last few years by Battelle Northwest Laboratory (9) in conjunction with the University of Wisconsin. The BNWL-UW design adopted as a fusion driver system that of the Engineering Test Reactor (TETR) previously studied at the University of Wisconsin (29).
Typical reactor parameters of the Westinghouse-TDHR are given in Table 3.2. The main features of the reactor are shown in Figs. 3.7 and 3.8. The characteristics of the fusion driver are in many respects similar to those identified by Westinghouse in previous TNS (The Next Step) scoping studies. As mentioned in chapter 2, the fuel selected as reference for TDHR is thorium oxide in Zircalloy cladding, as developed for light water reactors (Shipping port programme).

RTTH, Tokamak Hybrid Reactor for Fissile Fuel and Electric Energy Production (30)

The RTTH is a preliminary design of a hybrid power reactor intended for plutonium production and electricity generation. From the point of view of the fusion driver, it is a Tokamak reactor, operated according to a two-component mode, with neutral injection and a double null axisymmetric divertor. The plasma parameters are within the range given in Table 1.1. $Li_2Al_2O_4$ is used as tritium breeding material. The fertile fuel is metallic uranium, water as moderator and titanium hydride as shielding for the magnet. The main parameters of the reactor are given in Table 3.3.

4. Safety and environmental problems

There are four major potential hazards in hybrid systems:

a) tritium
b) activation products (first wall, structural, corrosion)
c) actinide elements
d) fission products.

The relative amounts and importance of these hazards will depend on how the system is optimized, in particular concerning the choice of blanket anf fuel cycle materials. Due to the fact that up to now there are only few conceptual designs on hybrid reactors, the safety analyses are at a preliminary stage. In the following we will examine some questions according to the following sequence:

- inventory of radioactive materials
- event trees for typical significant accident sequences
- potential for blanket criticality
- heat decay removal safety problems
- problems related to the safety of the electromagnetic system.

Actinides and fission products

As compared to fission reactors, hybrid-produced plutonium contains less Pu-238, which is the main responsible of α-activity during fuel fabrication. On the contrary, the Pu-236 concentration in hybrid systems is three orders of magnitude larger than in fission reactor-produced plutonium. By-product actinides (essentially Np-237) are also produced by a factor of three to four as compared to similar waste generated in a fast breeder for equivalent masses of plutonium. On the other hand, no americium and curium are produced in hybrids.
The U-233 produced in a hybrid thorium blanket contains substantially higher concentrations of U-232 as compared to HTGRs. There is indeed a production of actinide by-products, namely Th-230 and Pa-231.
Concerning fission products, results obtained from a comparison between the Livermore MHR and a LWR of the same power (1 GWth), after the same operation period (3 years) have shown that the hazard presented by the two systems looks comparable (31).
In conclusion, the picture concerning by-product isotopes and fission products in hybrid blankets appears to be comparable to that of fission systems.

Tritium

In a hybrid reactor the expected values for tritium release under normal operation, as a result of small off-normal events or during a catastrophic accident, are similar to those of pure fusion power stations. Two questions, however, are specifically related to hybrid systems:

- what is the probability of a catastrophic accident which should lead to a dispersion of all the tritium in the plant to the atmosphere, as compared to the case of a pure fusion system;
- how does the potential hazard from tritium compare to that from fission fuel.

The first point is related to the event trees of the accidents. As to the second point, no direct comparisons between tritium and fission products in a hybrid reactor are available. However, in the previous paragraph it has been mentioned that fission products in hybrids have a potential hazard similar to that in fission reactors. Then we can use results (32) which compare the critical dose versus area in case of a major accident due to tritium (10 kg) in a fusion reactor to the case of fission reactors (LWR, release of a substantial fraction of fission products and 0.5% of actinides). From these results it appears that the tritium hazard is lower by two orders of magnitude; this means that in case of hybrids, the radiological effects due to a major accident are dominated by the presence of the fission fuel.

Accident analyses

In order to evaluate the potential for the major hazards previously mentioned, some work has been performed to identify possible mechanisms for breeching containment on hybrid systems (31). Again, such a type of work is largely connected with the specific case investigated, so that it is not easy to draw general conclusions. The work reported in (31) was mainly based on the reference mirror hybrid design (MHR).
Event trees related to loss-of-coolant and steam-ingress accidents have been considered. First, the problem of the state of the fissile/fertile fuel elements has been examined for a helium-cooled reactor. Dominant in the consideration of such an accident is the question of whether the fuel elements can melt, since this could lead to a condition in which bulk fuel motion could occur. As indicated by the event trees, this fuel motion might lead to criticality of the core. The results indicate that reactor shut-down must occur within a comparable time scale if cladding failure is to be avoided. The avoidance of clad failure assumes that decay-heat removal is available.
The consequences of a rupture between the helium primary coolant loop and a steam generator have also been considered. The analysis shows that significant pressure and temperature effects can occur in the blanket, during approximately 10 s, and that while the course of the steam-ingress accident can be quite sensitive to the size of the rupture, the characteristic time for pressurization is much less so. It is concluded that significant effects could be encountered within the blanket before any appreciable change has occurred in the steam generator due to the large thermal mass of steam.
These related events have demonstrated that significant damage to the blanket, the fuel elements, and to the structural components of the reactor can occur in 1 to 10s. These times are comparable to the time required for plasma shut-down, hence it may become difficult to halt reactor operation before significant damage has occurred to reactor components.

Assuming that reactor shut-down has occurred, the problem of decay heat removal was also considered in ref. (31). The sources of decay heat are the induced activity of the first wall ("after heat") and the fission products. Since the power densities in the fissile fuel are comparable to those in LWRs, about 300 - 600 W/cm^3, decay heat removal must be provided. For the helium-cooled blanket, loss of forced circulation heating causes the fuel to melt in the range of 100 - 200 s, due to decay heat.
As a result of these studies, it appears that highly reliable and even redundant decay heat removal must be provided. Loss of ability to remove decay heat results in the melting of fuel, with ultimate release of fission products and actinides to the containment structure.
In addition, the question of criticality must be dealt with. Although fusion-fission hybrid blankets are designed to be far subcritical throughout blanket life, multiplication can change as a result of material composition changes or geometrical reconfiguration. Three changes which might occur due to an accident, were examined in detail:

a) the ingress of steam into a fast spectrum blanket;
b) complete melt-down of the blanket material;
c) steam ingress with resulting blanket expansion.

The general trend of all blanket reconfigurations yielded significant increases in neutron multiplication. However, low blanket residence times and, therefore, low fissile inventories prevented criticality, even for the most reactive geometries attainable.

Concerning the safety aspects of the magnetic field system (toroidal magnets and poloidal field coils), no major differences seem to appear as compared to pure fusion reactors. However, the problem arises of the consequences of magnetically driven missiles from blanket, plasma wall and outer containment integrity points of view. Such consequences could be more severe in the case of hybrids as compared to pure fusion systems, due to the presence of fission products and toxic fissile fuel isotopes in the reactor core. With respect to magnetically driven missiles, preliminary results (31) indicate that relatively small velocities are reached with low efficiency. However, the entire subject deserves much more investigation.

5. System studies and economic perspectives

Since the beginning of the investigation on fusion-fission hybrids, a number of studies have been devoted to the assessment of the interest of this concept in the future energy scenarios. These studies are almost all related to the USA situation, both as concerns the energy demand as well as the economic boundary conditions.
In the following we will summarize some of the results of recent studies performed at LLL (33) and at ANL (34); similar studies have been made at BNWL (35), Rand Corporation (36) and Princeton (28).

LLL-Studies

A schematic view of the system investigated is given in Fig. 3.9. As converters both LWR and HTGR reactors have been considered; two cycles have been compared, namely uranium/plutonium and thorium/U-233. The basic data for the two hybrid reactors are those of previous LLL-investigations (Table 5.1). Two modes of operation for the hybrid reactor have been considered:

- in the first mode (on-line) the thermal power produced by the hybrid is converted to electricity for sale;
- in the second mode (fuel factory) the hybrid would not produce electric power, but would rather obtain its input power needs from the output of its converter reactors, and reject its thermal power.

The results can be summarized as follows:

- the better multiplication properties of U-238 allows a greater relaxation of the plasma requirements: the transition from a consumer to a producer of electric power for a hybrid with U-238 as breeding material occurs at $Q \cong 0.6$. If thorium is used as breeding material, this transition occurs at a Q-value about twice as high;
- the use of the thorium/uranium cycle allows to feed a greater number of converter reactors; the dependence of the support ratio on Q is shown in Fig. 3.10. for the two cycles;
- the Th/U cycle will admit higher hybrid reactor capital costs compared to the U/Pu cycle (Fig. 3.11).

Hybrids and Fast Breeder Reactors

A comparison between the number of thermal converters which could be fuelled by hybrids and fast breeder reactors has been recently made at ANL (29) and the results discussed by Bethe (37). The features of the hybrids considered in the analysis correspond to a thermal power of 3000 MW and to two blanket solutions involving either U+Th or Th, as indicated in Table 5.2. The results are shown in Table 5.3.
As expected, the fast breeder can supply only few converter reactors, then it is important that the breeder itself produces electrical power as well as fissionable material. This implies that the reactor would normally be operated by the utility, just like another power station. On the contrary, in case of hybrids, one can imagine a separation of fuel and electricity production, even if this would imply an increase of the fuel production cost, as shown before. Such a separation could be desirable, at least in the coming years, until the moment where the steady-state operation and the full reliability of the fusion plants will be assured. On these bases, Bethe has emphasized the interest of leaving the operation of the fusion fuel factories to the government, which could deliver to the utilities the nuclear fuel to be used in standard fusion power plants. The direct gouvernamental control of the fuel production could facilitate the problems of non-proliferation because the reprocessing of the spent fuel would be made at the same place where the fuel is produced. In this case, the Th-cycle looks more attractive for the reasons already outlined previously in this paper.

Conclusions

Significant study efforts on fusion-fission hybrids have been conducted during the past years with increasing attention to the engineering aspects of design and performance characteristics. In the area of the fusion drivers (here limited to magnetically confined, D-T systems), both Tokamaks and Mirror machines have been considered and the trade-off between the plasma parameters and the economical impact has been analyzed.
The encouraging results on the plasma machines now in operation have extended the attention, for the Tokamak Demonstration Power Reactor Design studies, towards higher Q-values and to the Tandem Mirror Reactor applications.
The trend of considering hybrids as fuel factories for fission thermal reactors has been confirmed. The possible future development of the hybrid reactor seems to be in an energetic economy largely supported by fission reactors. The number of fission reactors which can be fuelled by the fusion breeder is proportional to their fuel conversion factor. This has

oriented the recent analyses towards the coupling of the hybrid systems with advanced converters (such as HTGR) and, for the case of LWR, to the use of thorium fuel elements. This last tendency has been also supported by the requirements related to the prolification resistant fuel cycles, which have received particular attention in the last few years, in the framework of the International Nuclear Fuel Cycle Evaluation work.

The possibility for the hybrids to use depleted uranium or spent fuel from fission plants has been also recognized.

New blanket designs involve solutions with low power gradients, both in space and during irradiation, geometrically simple and based on fuel forms already proved in fission reactors.

The severe penality on the economics connected with the reduction of the blanket coverage due to the reactor geometrical complexity has been put in evidence.

Molten salt blanket systems, which look very favourable from the point of view of the number of the supported thermal reactors, are under investigation.

The feasibility of "refresh fuel" cycles, where the fuel is produced in the hybrid and burnt in the thermal converter without reprocessing, has been proved; however, the enormous difficulties connected with the design specifications and operation procedures have been recognized.

Safety and environmental studies on hybrids are still at a very early stage; it can be expected that the problems related to the fission fuel will be predominant (after-heat, actinides). This area deserves much more investigation.

References

1) W.C. WOLKENHAUER "Hybrid Reactor Designs in the United States", Trans. Third Meeting "The Technology of Controlled Nuclear Fusion", Santa Fé, p. 23, May 1978
2) I.N. GOLOVIN et al., "The Nuclear-Fuel Problem and Hybrid Reactors", The Kurchatov Institute of Atomic Energy, Moscow 1977
3) D. JAGER, J.B. THOMAS, "Eléments d'évaluation d'un système hybride fusion-fusion", private communication, September 1979
4) E. GREENSPAN et al. "Source-Driven Breeding Thermal Power Reactors. Part I - Using D-T Fusion Neutron Sources." in Proc. Int. Workshop-Thinkshop on Emerging Concepts in Advanced Nuclear Systems (Graz, Austria, 1978).
5) G. CASINI, C. PONTI, "Survey on the Fusion-Fission (Hybrid) Reactors", Technical note No. 1.03.06.78.41, JRC Ispra, August 1978
6) R.W. CONN, "Plasma Parametric Studies and Potential Applications of Driven Fusion Reactors" UWFDM-260, Sept. 1978
7) D.L. JASSBY, "Optimization of Fusion Power Density in the Two-Energy-Component Tokamak Reactor", MATT-1072, October 1974
8) W.I. PISTUNOVICH, "Plasma Physics Basis for the Tokamak Hybrid Reactor with Injection", CONF-760733, p. 57 (1976)
9) R.W. CONN et al., "TDHR - A Tokamak Demonstration Hybrid Reactor", Trans. Am' Nucl. Soc., 27, 26 (1977).
10) C. THOMAS, VARLJEN, "New initiatives in Tokamak hybrid Studies", Second DMFE Fusion-Fission Energy Systems Review Meeting, Washington, D.C., Nov. 2, 1977
11) J.D. LEE, "Mirror Fusion-Fission hybrids", UCRL-80720, March 1978
12) D.J. BENDER et al., " A Reference Mirror Hybrid Fusion-Fission Reactor Design", UCRL-79093, June 1977

13) G.A. CARLSON, "Tandem Mirror Reactors", Fourth International Conference on Driven Magnetic Fusion Reactors, Erice, Italy, Sept. 18-26, 1978

14) R.W. MOIR and J.D. LEE, "Mirror Hybrid Reactors", Fourth International Conference on Driven Magnetic Fusion Reactors, Erice, Italy, Sep. 18-26, 1978

15) Private communication (August 1979)

16) R.C. HAIGHT, J.D.LEE, J.A. MANISCALCO, "Reaction Rates in a Uranium Pile Surrounding a 14 MeV Neutron Source: Calculations of the Weale Experiment", Nucl.Sci.Eng., 61, 53(1976)

17) E. GREENSPAN et al., "Natural Uranium-Fueled Light-Water-Moderated Breeding Hybrid Power Reactors", Princeton Plasma Physics Lab. Report PPPL-1444 (1978)

18) E. GREENSPAN, A. SCHNEIDER, A. MISOLOVIN, "The Physics and Applications of Subcritical Light Water U-Pu Lattices", in Proc. Third Topical Meeting on Advances in Reactor Physics (Gatlinburg, TN, 1978)

19) E. GREENSPAN et al., "Constant-Power Hybrid Reactor Blankets and Lithium Control", Trans. A.N.S., Nov. 1978

20) K.R.C. SCHULTZ, "A Review of Hybrid Reactor Fuel Cycle Considerations", Trans. Am. Nucl. Soc., 27, 344 (1977)

21) J.D. LEE, "The Beryllium/Molten Salt Blanket - A New Blanket Concept", Third US/USSR Symp. on Fusion-Fission - Princeton, New Jersey, January 22-26, 1979

22) B.R. LEONARD Jr., U.P. JENQUIN, "The Quality Fissile Fuel Bred in a Fusion Reactor Blanket", CONF-760935-P2

23) K.R. SCHULZ et al., "Preliminary Evaluation of the ^{233}U Refresh Cycle Hybrid Power System Concept", GA-A14940, April 1978

24) R.P. ROSE et al., "Fuel Production Characteristics of Fusion Hybrid Reactors", The Seventh International Conference on Plasma Physics and Controlled Nuclear Fusion Research, Innsbruck, Austria, August 23-30, 1978

25) V.L. BLINKIN, V.M. NOVIKOV, "Optimized Symbiotic Molten-Salt Fusion/Fission Reactor System", IAE-2819, Moscow 1977

26) U. FARINELLI et al., "Round Table Discussion on Hybrid Reactors", Erice, Fourth International Conference on Driven Magnetic Fusion Reactors", Sept. 18-26, 1978

27) K.R. SCHULTZ, E.T. CHUNG, private communication (August 1979)

28) F.H. TENNEY et al., "A Systems Study of Tokamak Fusion-Fission Reactors", PPPL-1450, November 1978

29) G.L. KULCINSKI et al., "TOKAMAK Engineering Test Reactor", UWFDM-191, June 1977

30) E.P. VELIKHOV et al., "Thermonuclear Tokamak Hybrid Reactor (RTTH) for Fissile Fuel and Electrical Energy Production" (in Russian), Second IAEA - Technical Committee Meeting and Workshop on Fusion Reactor Design, Madison, October 1977

31) W.E. KASTENBERG, D. OKRENT et al., "Some Safety Studies for Conceptual Fusion-Fission Hybrid Reactors", UCLA-report (EPRI-contract RD-236-2), 1977

32) W. HAFELE et al., "Fusion and Fast Breeder Reactors", IIASA report, 1977

33) D.J. BENDER, "Performance Parameters for Fusion-Fission Power Systems", UCRL-80589 Rev. 1, may 1978

34) R. AVERY et al., "Fusion-Fission Hybrid Study", Argonne National Laboratory, July 1978

35) R.L. ENGEL, D.E. DEONIGI, "Evaluations of Fusion-Fission (Hybrid) Concepts: Market Penetration Analysis for Fusion-Fission Hybrids", EPRI ER-469, Jan. 1976

36) B. AUGENSTEIN, "Fusion-Fission Hybrid Breeders - Economic Performance Issues, Role of Advanced Converters, Interdependence between Fission and Fusion Programmes", Rand. Corp. Report P-6047, December 1977

37) H.A. BETHE, "The Fusion Hybrid", Physics Today, May 1979

Acknowledgements

The author likes to thank J.B. Thomas (Saclay), R. Moir (Livermore), K.R. Schulz and E.T. Cheng (General Atomic), for supplying information prior to publication and C. Ponti who has participated in the survey work.

TABLE 1.1.

TOKAMAK PLASMA PARAMETERS

	TFTR	TDHR BNWL-UW	DTHR WESTINGHOUSE	USSR HYBRID REACTOR
A [M]	0.85	0.6	1.2	1.2 - 1.4
R [M]	2.48	3.2	5.2	4.8 - 6.6
$\bar{N} \times 10^{13}$ [CM^{-3}]	4.8	7.7	15	6
T_E [KEV]	6	11.3	13	10 - 15
$N_E\tau_E \times 10^{13}$ [$CM^{-3}S$]	1.0	0.8	7.5	4 - 6
BEAM ENERGY [KEV]	120	150	200	200
Q	1.0	1.8	6.3	2.0
BURN TIME [S]	1.4	60	70-85	100

TABLE 1.2.

MIRROR PLASMA PARAMETERS

	2XII-B	MFTF	COMM. HYBRID
PLASMA LENGTH (M)	1.6	3.4	13
CONDUCTOR FIELD (T)	---	7	8
β	0.4 0.7	0.5	0.7
INJECTION ENERGY (KEV)	20.0 (40.0)	80.0 (20.0)	125.0
$N\tau$ (S/CM^3)	7×10^{10}	10^{12}	10^{13}
L/A_I	35.0	100 - 300	250.0
R_P/A_I	3.0	10 - 50	50.0

TABLE 1.3.

TANDEM MIRROR HYBRID REACTOR

EXAMPLE PARAMETER VALUES

SOLENOID LENGTH, L_C	50 M
SOLENOID RADIUS, R_C	0.37 M
SOLENOID ELECTRON DENSITY, N_C	1.7×10^{20} M^{-3}
SOLENOID DEUTERIUM DENSITY, N_D	6.3×10^{19} M^{-3}
SOLENOID TRITIUM DENSITY, N_T	1.1×10^{20} M^{-3}
ELECTRON TEMPERATURE, T_E	6.0 KEV
INJECTION ENERGIES, E_{INJ}	200 KEV
SOLENOID FIELD, B_C	1.8 T (β_c = 0.8)
PLUG FIELD, B_{OP}	7.0 T (R_p = 2, β_p = 0.7)
PLUG DENSITY, N_P	4.6×10^{20} M^{-3}
PLUG RADIUS, R_P	0.16 M (R_P/e_I = 12)
FUSION POWER	410 MW
NEUTRON WALL LOADING, (AT 1-M RADIUS)	1 MW/M^2

TABLE 2.1.

MHR-BLANKET PARAMETERS

PLUTONIUM PRODUCTION (KG/MW_T Y)	0.53	
FISSION ZONE	U_3Si	
TRITIUM BREEDING ZONE	LiH	
COOLANT	He	
CLADDING	INCONEL	
MAXIMUM CLADDING TEMP.	700°C	
MAX. POWER DENSITY [W/cm^3]	(A) 240	(B) 500
M, ENERGY MULTIPLICATION	(A) 8.8	(B) 18.4
F, FUEL BREEDING RATIO	(A) 1.85	(B) 1.75
PLUTONIUM BUILD-UP [AT %]	(A) 0	(B) 2.3
TRITIUM BREEDING, T	(A) 1.05	(B) 1.42
BLANKET COVERAGE	0.85	

(A) = INITIAL VALUE , (B) = FINAL VALUE

TABLE 2.2.

GA STUDIES

GAS-COOLED BLANKET PARAMETERS FOR THE TMHR

BLANKET	URANIUM METAL	URANIUM/THORIUM METAL	THORIUM METAL	BERYLLIUM/ThO_2 GRAPHITE
BREEDING RATIO*, F Pu	1.8	0.81	---	-----
(ATOMS/FUSION NEUTRON) ^{233}U	---	0.78	0.74	0.49
(WITH T/N = 1.1)				
ENERGY MULTIPLICATION*, M	10	5.6	2.6	1.6
FUEL PRODUCTION * Pu	0.97	0.78	---	-----
(KG/MW_T-YR) ^{233}U	---	0.75	1.54	1.65
ADIABATIC TIME TO MELTING	1 M	1 M	1.5 H	26 H
APPROXIMATE FUEL LIFETIME (MW·YR/M^2)	6	9	9	2
FUEL COST* * - ($/GM) (AT 15 MILLS/KWH ELECTRICITY)	93	77	84	98

* BEGINNING OF BLANKET LIFE VALUES

** ADJUSTED FOR RELATIVE VALUE OF PLUTONIUM VERSUS ^{233}U

TABLE 3.1.

MHR REACTOR CHARACTERISTICS

FUSION POWER	400 MW
THERMAL POWER (AVG)	3600 MW
INJECTED NEUTRAL POWER	625 MW
NET ELECTRIC OUTPUT POWER	525 MW
FISSILE PRODUCTION RATE	2700 KG/Y
PLASMA	
. INJECTION ENERGY D°	125 KEV
. T°	187 KEV
. β	0.7
. CENTRAL ION DENSITY	9×10^{13} cm^{-3}
. Q	0.63
. $n\tau_E$	2×10^{13} SEC/cm^3
. FIRST WALL 14 MEV NEUTRON CURRENT	2 MW/m^2
MAGNET (YIN-YANG TYPE)	
. OUTSIDE DIAMETER	22 M
. DISTANCE BETWEEN MIRROR POINTS	13 M
. MAXIMUM FIELD AT THE CONDUCTOR	8 TESLA
. MAXIMUM CURRENT DENSITY	10^3 A/cm^2
BLANKET	
. TRITIUM BREEDER	LITHIUM HYDRIDE
. FERTILE FUEL, CLADDING	U_3Si, INCONEL - 718
. FUEL DIAMETER	0.7 CM
. TOTAL FUEL EXPOSURE	5 MW - Y/M^2
. PLUTONIUM ENRICHMENT (END OF LIFE)	2.3%
. PEAK FUEL POWER DENSITY (BEGINNING AND END OF LIFE)	240-500 W/cm^3
. MAXIMUM CLAD TEMPERATURE	700°C
. COOLANT	HELIUM
. COOLANT PRESSURE	60 ATM
. INLET-OUTLET TEMPERATURE	280-530°C

TABLE 3.2.

PRELIMINARY DTHR DESIGN FEATURES

PLASMA MAJOR RADIUS	5.2 M
PLASMA MINOR RADIUS	1.2 M
PLASMA ELONGATION	1.6
TOROIDAL FIELD ON AXIS	5.5 T
PLASMA CURRENT	5.1 MA
FIRST WALL NEUTRON LOAD	2.0 MW M^{-2}
FUSION POWER	950 MWT
NEUTRAL BEAM ENERGY, POWER	200 KEV, 150 MW
PLASMA PULSE DURATION, PERIOD	70 S, 85 S
DUTY FACTOR x PLANT AVAILABILITY (ANNUAL)	0.20
VACUUM VESSEL	WATER-COOLED 316 SS
BLANKET FUEL FORM	THORIUM OXIDE OR METAL
BLANKET COOLANT	LOW TEMPERATURE WATER
FUEL ASSEMBLIES	LWBR TECHNOLOGY
PLASMA EXHAUST	BUNDLE DIVERTOR
DIVERTOR PARTICLE COLLECTION	ZrAl AND CRYOPANELS
TF, PF AND DIVERTOR COIL CONDUCTORS	SUPERCONDUCTING Nb_3Sn
COIL CONDUCTOR COOLING	FORCED FLOW LIQUID HELIUM
TF COIL NUMBER	16
PEAK FIELD AT TF WINDINGS	12 T
SF WINDING LOCATION	EXTERNAL TO TF ARRAY
FUEL	ThO_2
U^{233} PRODUCTION RATE (KG/Y)	200
AV. U^{233} CONCENTRATION (1 YEAR)	0.25%

TABLE 3.3.

RUSSIAN HYBRID POWER REACTOR PARAMETERS

THERMAL POWER	6,900 MW
ELECTRICAL POWER	2,500 MW
AUXILIARY POWER	570 MW
URANIUM INVENTORY	1,110 TONS
BLANKET ENERGY AMPLIFICATION	10
PLUTONIUM PRODUCTION	4,200 KG/Y
PLUTONIUM CONCENTRATION (END OF LIFE)	1.5%
TRITIUM CONSUMPTION	37.2 KG/Y
TRITIUM BREEDING	1.04
PLASMA WALL LOADING	0.6 MW/M^2
POWER DENSITY IN THE FUEL (AVERAGE-MAXIMUM)	98-203 W/CM^3

TABLE 4.1.

REACTOR SYSTEM CHARACTERISTICS

LLL-STUDIES

	U/Pu	TH/U-233
HYBRID		
M	10	5
η_H	0.5	0.5
η_{TB}	0.35	0.35
CONVERTER		
C_R	0.67	0.85
η_{TC}	0.35	0.35

TABLE 4.2.

OUTPUT OF HYBRIDS

ANL/BETHE STUDIES

BLANKET	U + TH	TH
PRODUCED U-233 (KG/YR)	1200	1600
PRODUCED Pu-239 (KG/YR)	500	0
FUSION POWER , MW (TH)	510	1150
NET ELECTRIC POWER, MW, Q=1	220	-750
NET ELECTRIC POWER, MW, Q=2	600	120

THE QUANTITIES SWHON ARE FOR A 3000 MW(THERMAL) "STANDARD" FUSION-FISSION REACTOR.

TABLE 4.3.

NUMBER OF "SATELLITES"

ANL/BETHE STUDIES

CONVERTER	LWR	ADVANCED
HYBRID WITH TH	5	16
HYBRID WITH U + TH	4	11
FAST BREEDER	0.7	2.7

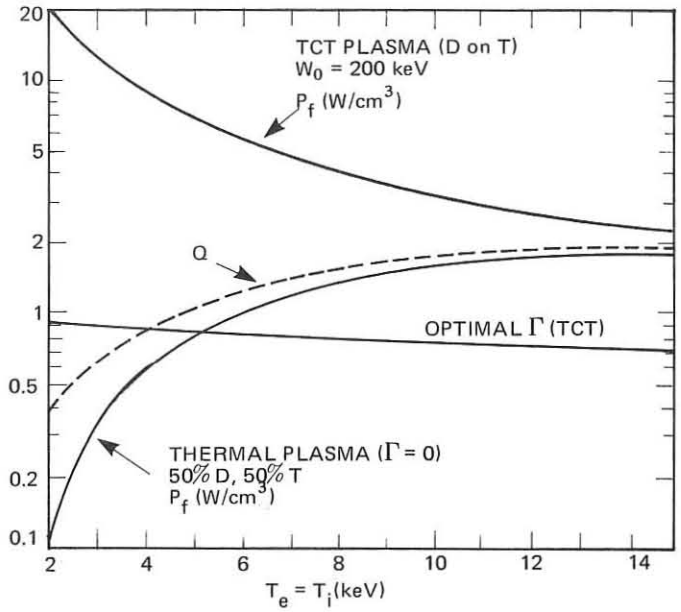

Fig. 1.1. - Comparison of fusion power density P_f for a TCT plasma with optimal Γ and a thermal plasma with $\Gamma = 0$.

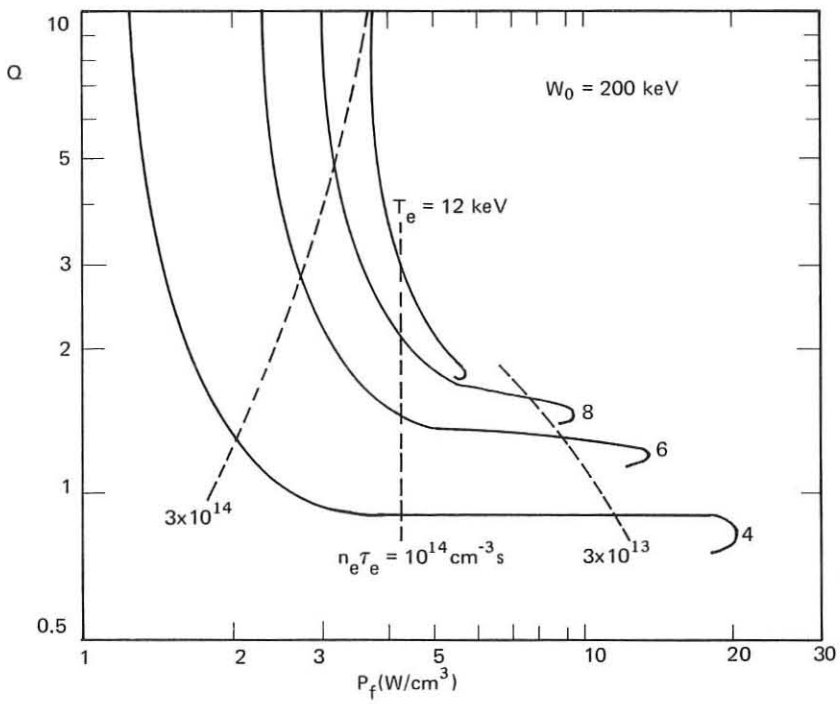

Fig. 1.2. - Plasma amplification versus fusion power density. For each $n_e\tau_E$, the D-T composition is adjusted for maximum Q.

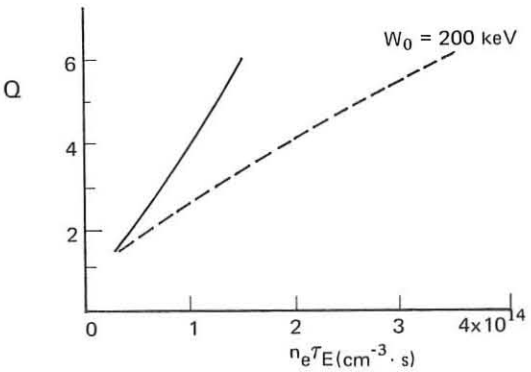

Fig. 1.3. - Q as a function of $n_e\tau_E$ considering the α - particle heating (solid curve) and without it considering the α - particles (dotted curve).

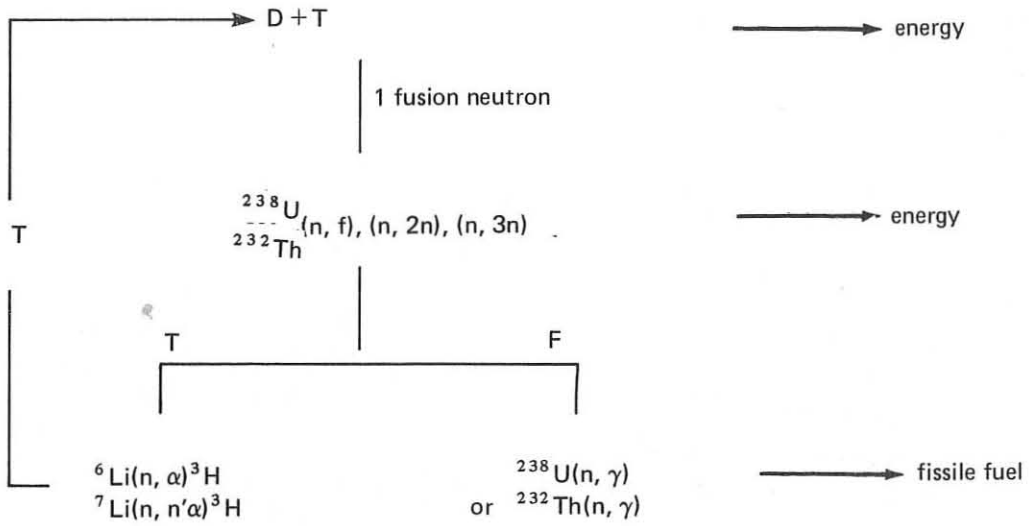

Fig. 2.1. - Schematic diagram of the neutron economy in the blanket of fusion-fission systems. T and F are defined in the text.

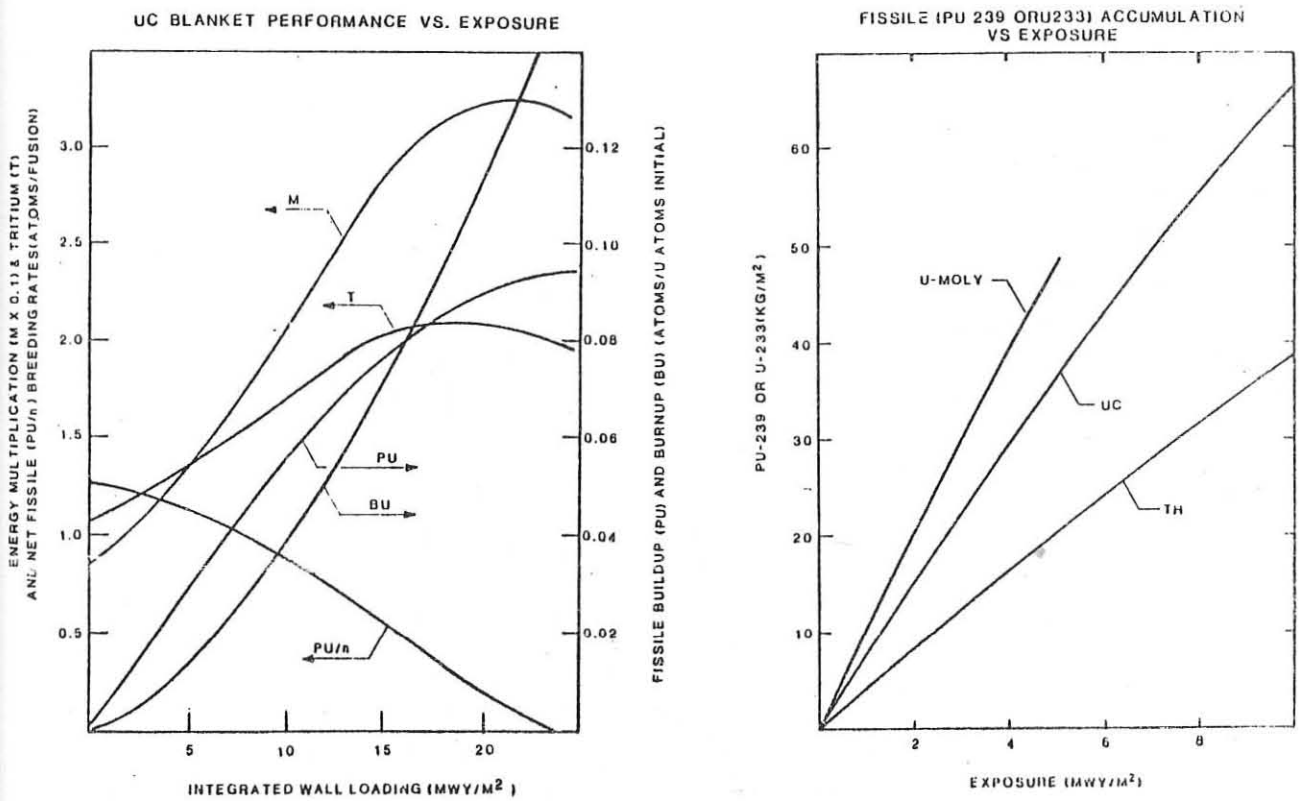

Fig. 2.2. - Blanket characteristics for various fuels

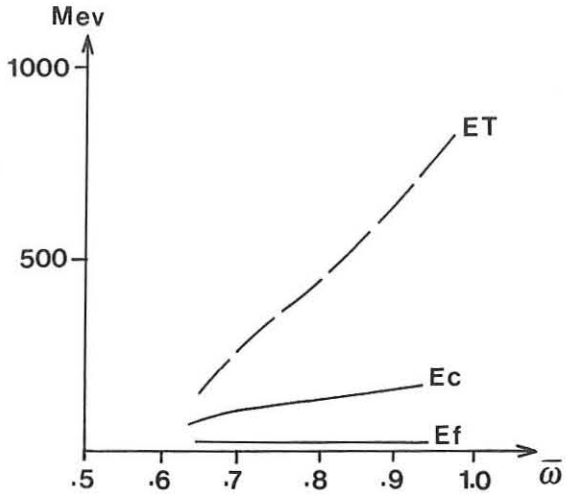

Ef : Fusion energy
Ec : Energy in the blanket
ET : Total energy of the system
$\bar{\omega}$: Blanket coverage

Fig. 2.3. - Energy versus blanket coverage

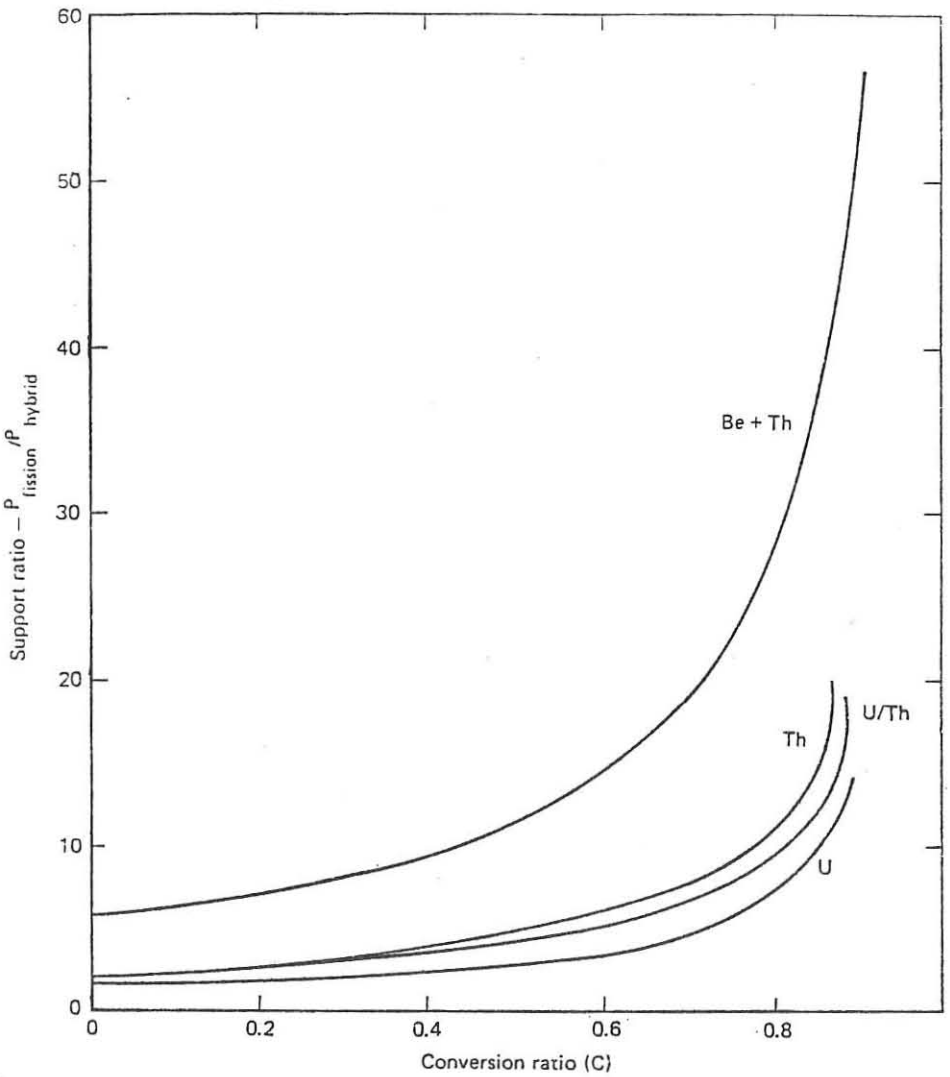

Fig. 2.4. - Support ratio versus conversion ratio for various blanket types

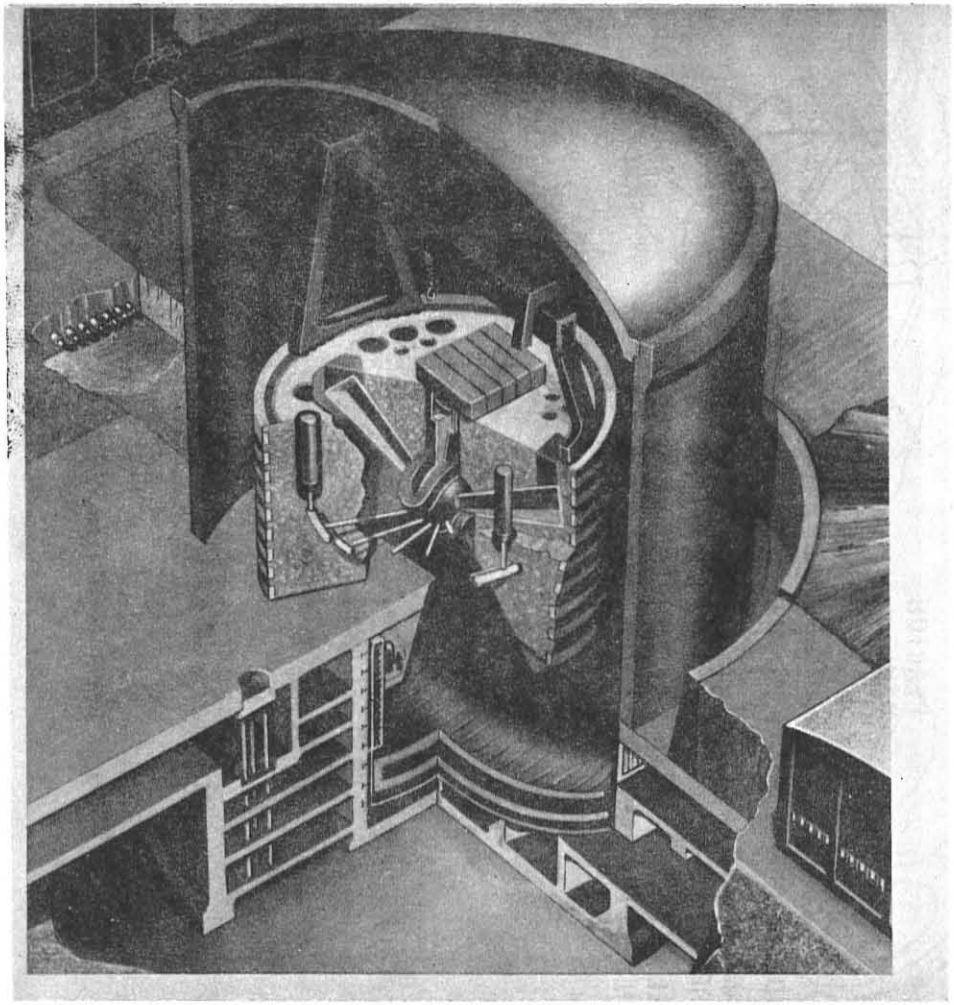

Fig. 3.1. - Fusion-fission mirror hybrid reactor

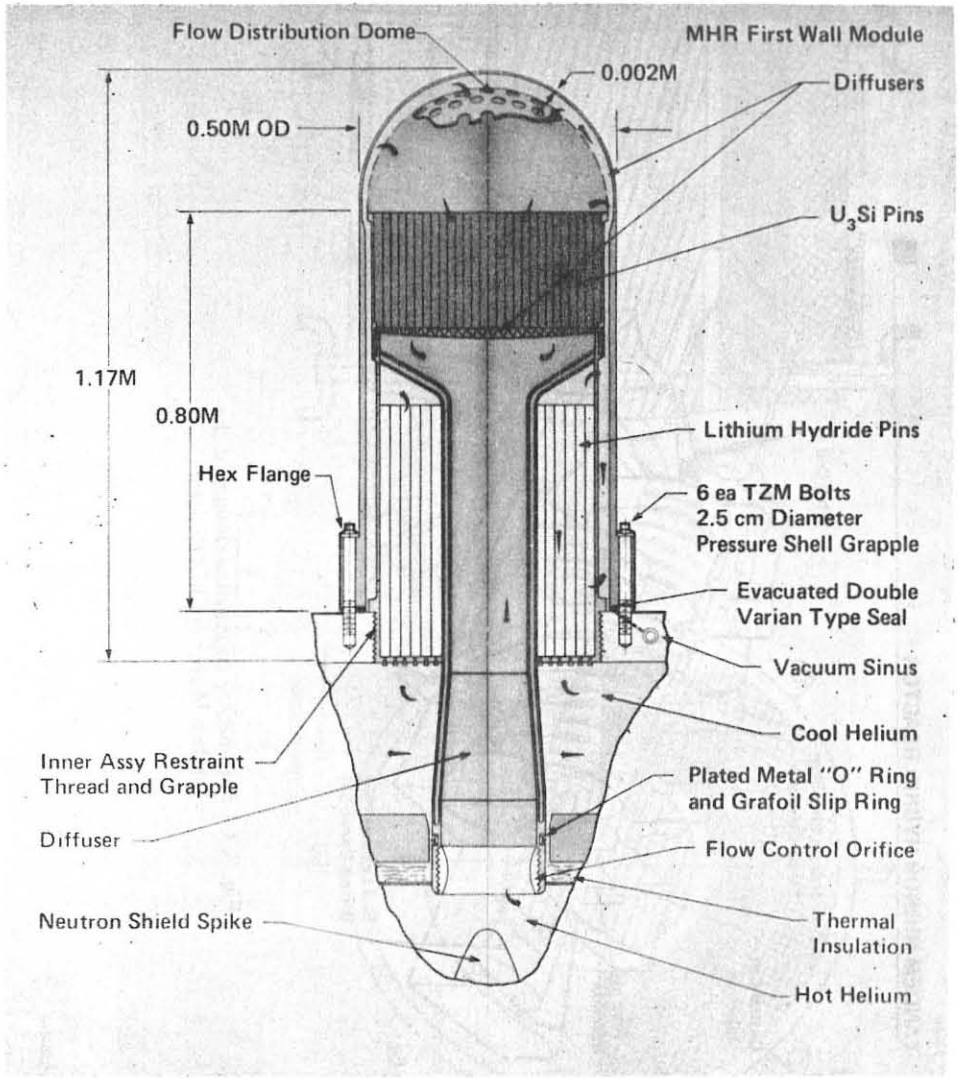

Fig. 3.2. - Fusion-fission mirror hybrid blanket module

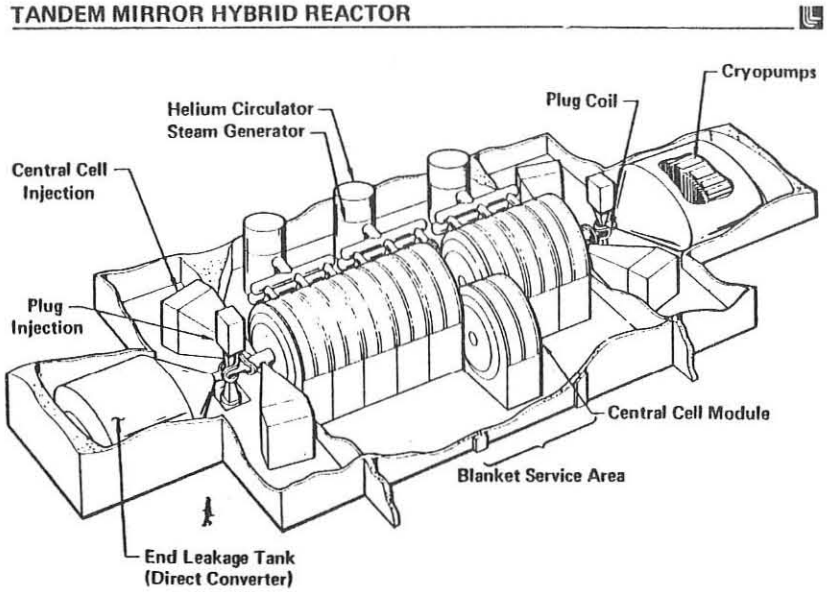

Fig. 3.3. - Preliminary conceptual design of the Tandem Mirror Hybrid Reactor

- RAPID ACCESS AND CHANGE-OUT.
- MODULE TRUCK AND ROLLER PATH FEASIBLE WITH PRESENT TECHNOLOGY.
- ACCESS TO REFUELING FLOOR ALLOWABLE WHEN REACTOR VAULT IS CLOSED.

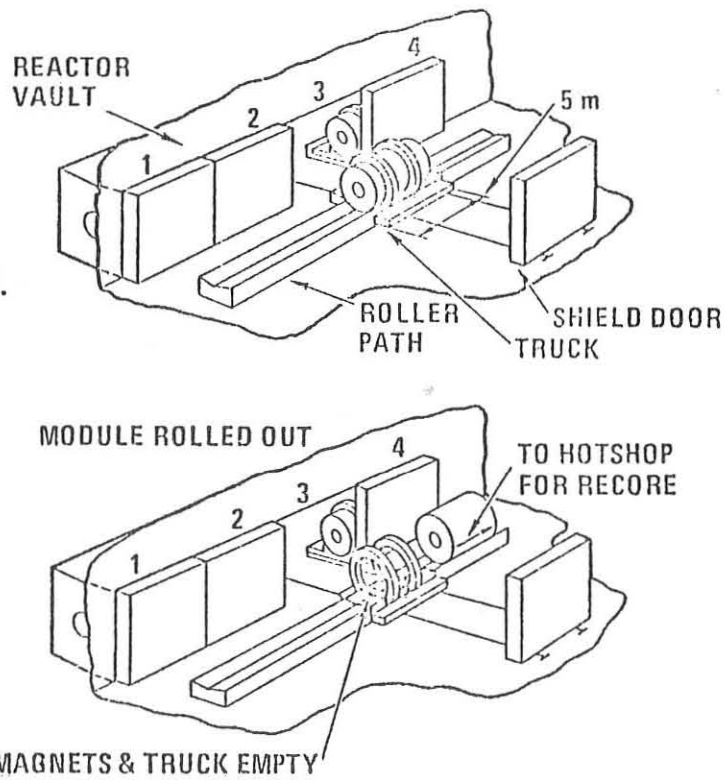

Fig. 3.4. - TMHR lateral access maintenance

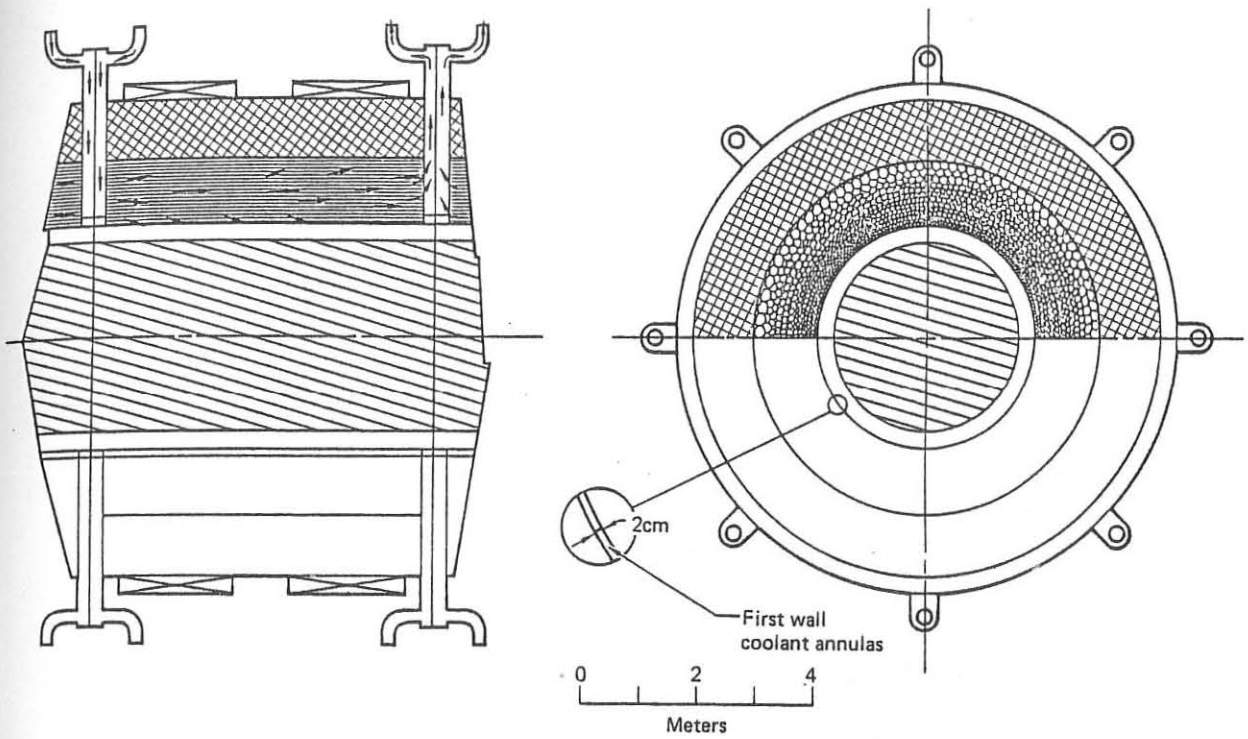

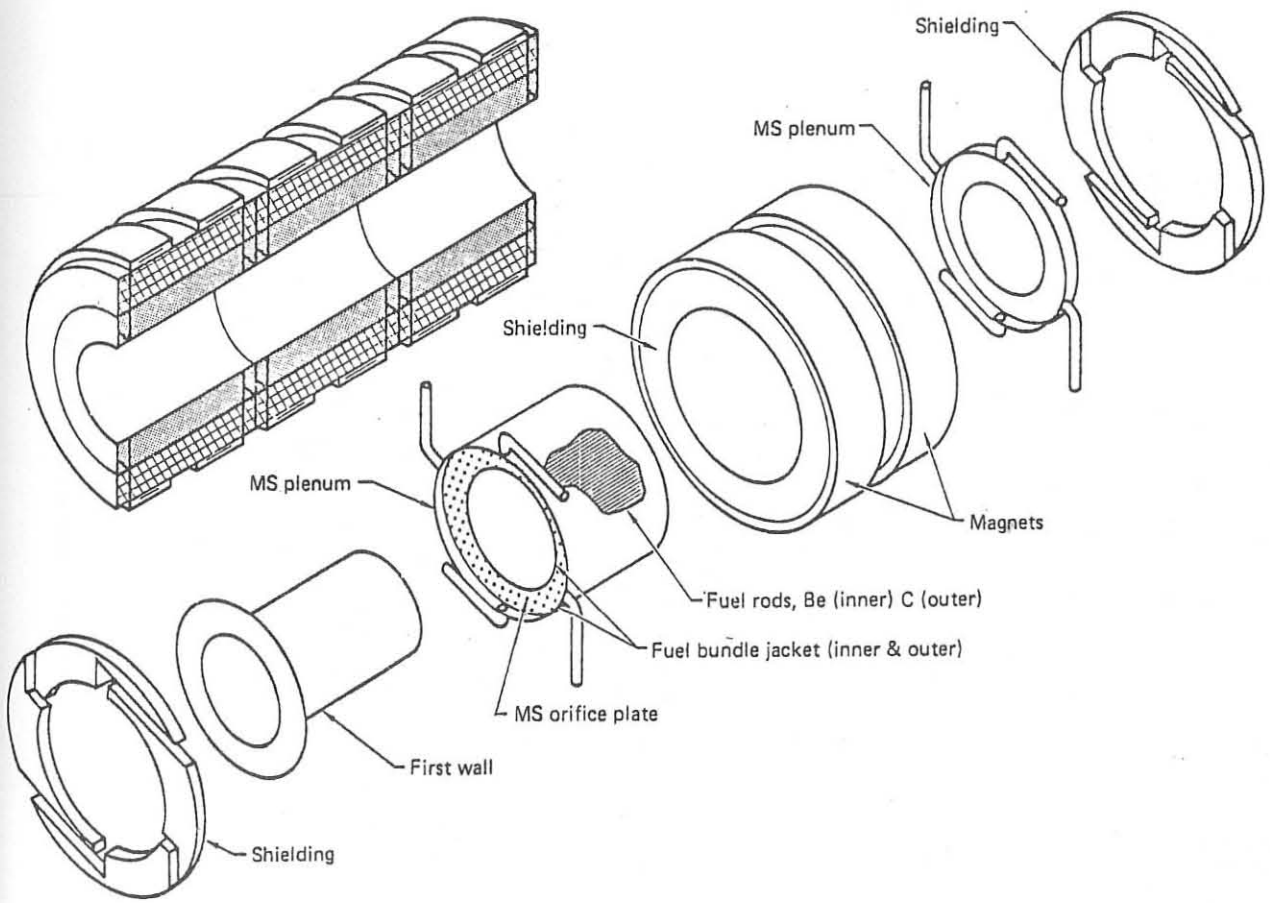

Fig. 3.5.-3.6. - Be/Molten Salt (MS) Blanket Concept

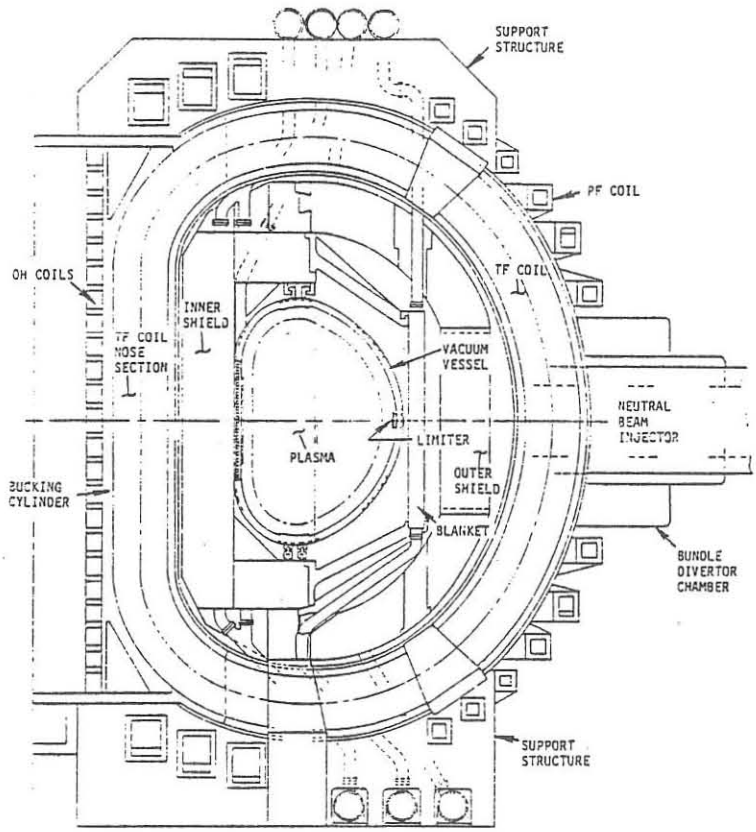

Fig. 3.7. - DTHR cross section

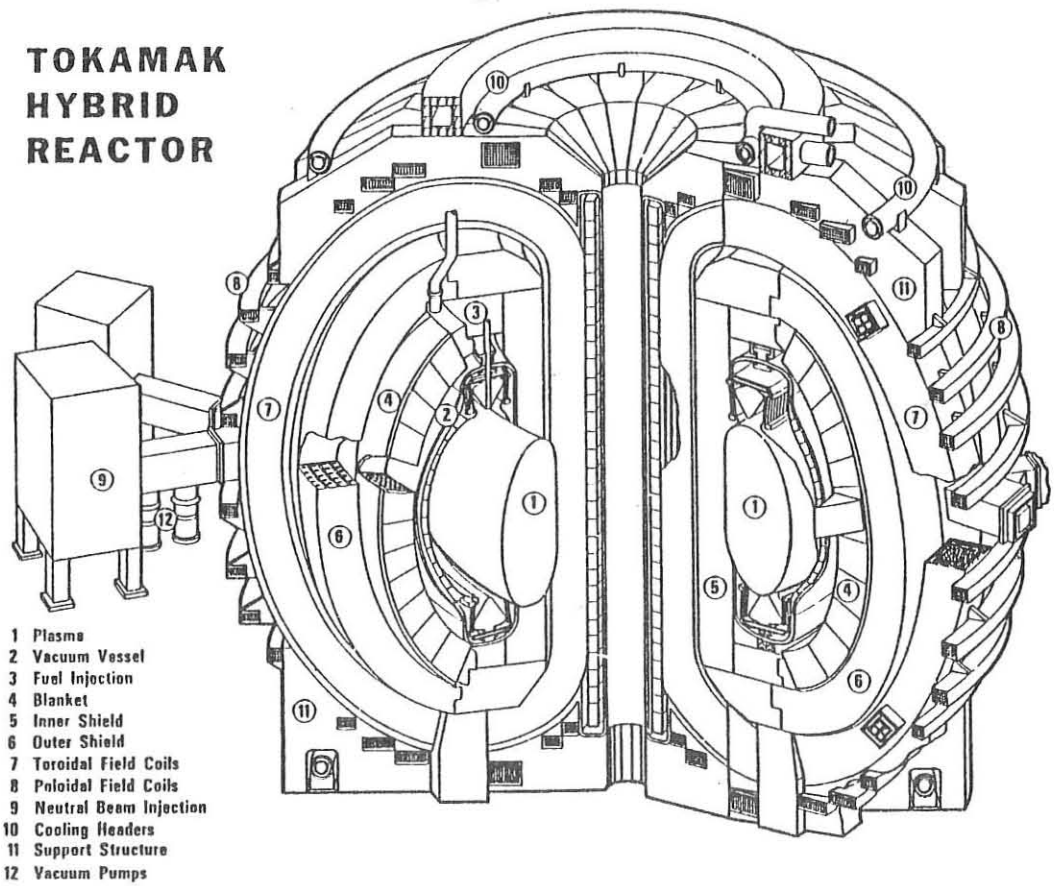

Fig. 3.8. - Tokamak hybrid reactor major components

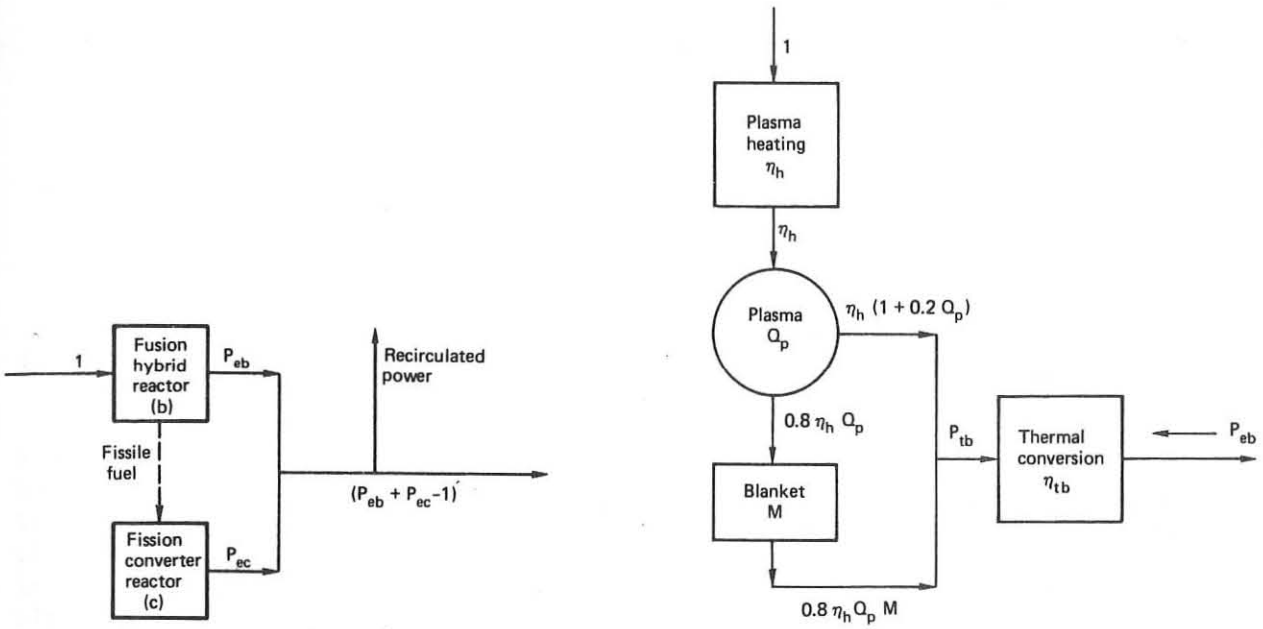

Fig. 3.9. - System electrical power flow and hybrid reactor power flow

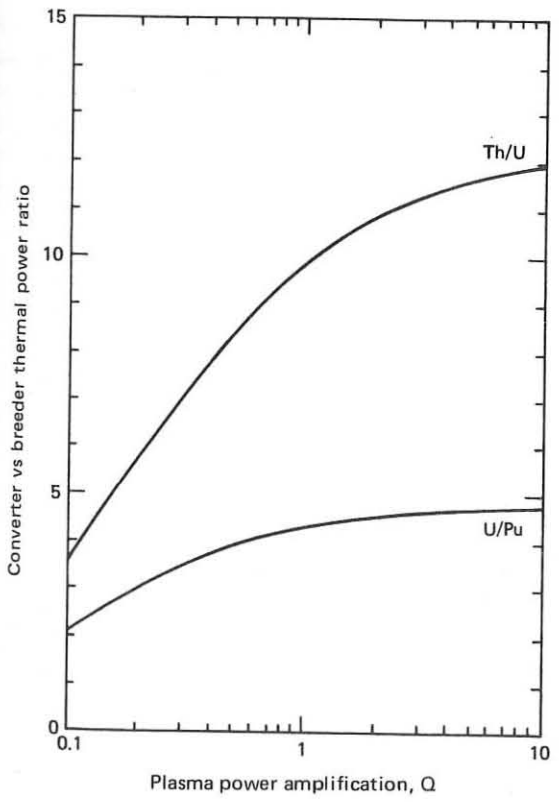

Fig. 3.10. - Support ratio as a function of plasma performance

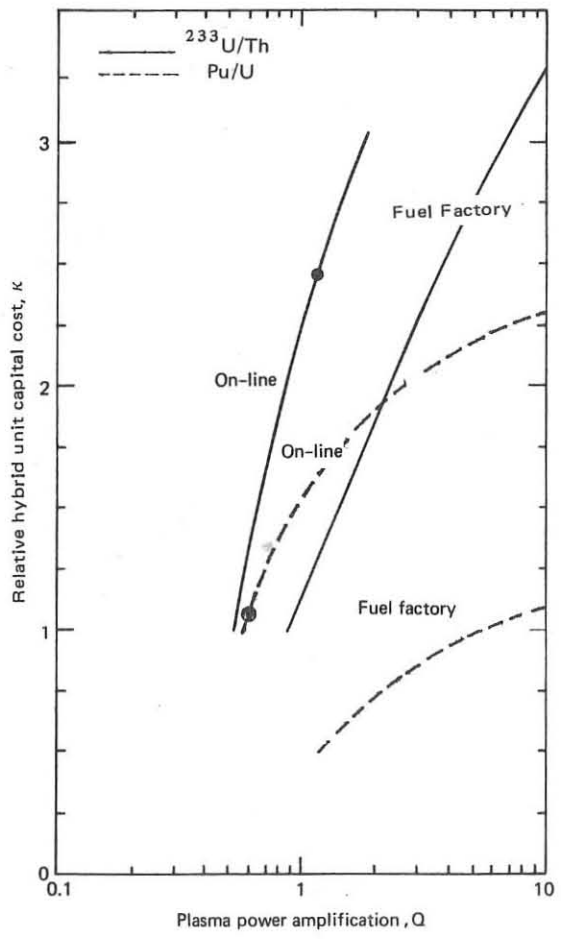

Fig. 3.11. - Hybrid unit capital cost for the Pu/U and Th/U cycle

ICRF HEATING IN TFR AT THE ION-ION HYBRID RESONANCE

TFR GROUP*

ASSOCIATION EURATOM-CEA SUR LA FUSION
Département de Physique du Plasma et de la Fusion Contrôlée
Centre d'Etudes Nucléaires
Boîte Postale n° 6. 92260 FONTENAY-AUX-ROSES (FRANCE)

1. INTRODUCTION

First experimental results on plasma heating in Tokomaks in the ICRF were obtained in ST /1/, TM1-RF /2/ and TO1 /3/. Although definite heating effects were reported, these results also suggested the method might lead to serious perturbation of the plasma confinement : a large increase of the electron density, loop voltage and impurity content, leading eventually to disruptive instability, limited in those experiments the energy coupled to the plasma to a few hundred Joules.

That those deleterious effects are not an intrinsic drawback of the heating method, but should be attributed to the modest confinement characteristics of those early Tokomaks was demonstrated in subsequent experiments, first in ATC /4/ where 1 KJ additional energy was coupled to the plasma, more recently in TFR /5/, PLT /6/ and DIVA /7/ where the results showed it was possible by this method to couple a power comparable to the ohmic power in long pulses without significant alteration of the confinement : in TFR, up to 200 kW RF power could be transfered to a Deuterium plasma for 20 ms leading to a ΔT_i of at least 150 eV at an average density of $3.10^{13} cm^{-3}$.

An important technical progress was also made in TFR /8/ by demonstrating that the RF power could be coupled to the plasma using entirely metallic launching loops, this technique avoiding the cumbersome use of insulating materials used in earlier designs of the antennae. As will be shown here, further progress in this direction seems still possible.

From the more basic point of view of understanding the heating mechanisms, an important step was done after it was realized that the physics of wave damping in Deuterium at $\omega \simeq 2\omega_{CD}$ was in fact determined by the presence in the plasma of a small percentage of protons /9/ /10/. An effort of theoretical analysis was initiated by this observation /11/ /12/ /13/, leading now to a coherent picture of the heating mechanism :

If the H^+ density in a D^+ plasma is larger than a critical value given by

$$n_H = n_D \frac{k_{//}^2 V_{th}(H)}{\omega} \left| \frac{4}{3} + \frac{k_{//}^2 c^2}{\omega^2 pD} \right| \qquad (1)$$

where $k_{//}$ is the wave number along the magnetic field of the fast wave generated by the antenna, the fast wave is locally converted into a slow mode whose energy, in turn, is efficiently transfered to the three kinds of particles : protons (cyclotron heating), deuterons (harmonic cyclotron heating) and electrons (Landau damping). Since the position of the conversion layer, determined by

---

* Paper presented by J. ADAM

$$\frac{k_{//}^2 \; c^2}{\omega^2} = 1 - \sum_i \frac{\omega_{pi}^2}{\omega^2 - \omega_{ci}^2(R)} \qquad (2)$$

depends on the H^+ density, wave conversion, and hence plasma heating, can occur rather far from the cyclotron layer, or even, at sufficiently high n_H/n_D, with the cyclotron layer outside the plasma.

For values of n_H/n_D lower than the limit given by (1), wave conversion becomes inoperant. However, efficient ion heating remains present, the natural shielding of the wave field polarized in the ion direction, which would prevent heating in a pure hydrogen plasma, being now partly compensated by the presence of deuterons. In this case, heating is expected to occur in the immediate vicinity of the cyclotron layer. An example of such a situation is shown in Fig. 1, where the relative amount of power distributed among the three species has been computed on the basis of a numerical model developed by J. Jacquinot /11/.

In both cases, a large fraction of the total wave power is transfered to the protons, so that this minority species is expected to reach very high energies. Including quasi linear diffusion coefficients in the Fokker-Planck equation, T. Stix has shown this should lead to a tail in the proton velocity distribution function and computed the expected distorsion of the energy spectrum as a function of the coupled RF power /14/.

As shown in this paper, the main lines of this general picture of the ion heating in a basically deuterium plasma near $\omega = 2\omega_{CD}$ are in good agreement with the latest experimental results in TFR.

Coupling RF power up to 250 kW to the plasma in a range of high density conditions ($0{,}5 < n_{eo} < 1.4\ 10^{14}\ cm^{-3}$) results in significant ion heating. For n_H/n_D lower than 5 %, this occurs with the $\omega = \omega_{CH}$ layer near the plasma center, resulting in D temperature increase up to 200 eV and a tail in the proton velocity distribution. At higher n_H/n_D, comparable heating effects occur at $\omega < (\omega_{CH})_0$. This however requires the computed position of the conversion layer to be near the plasma center, clearly demonstrating the essential role played in those conditions by the wave conversion mechanism for determining the position of the heating region.

2. RF EQUIPMENT

The general RF equipment is shown schematically in Fig. 2. The amplifier, capable of delivering 500 kW on a dummy load, is connected to the launching structure through a system of two tuning stubs.

A transmission line of adjustable length supplies the two half coils in phase or 180° out of phase, allowing thus $m = \pm 1$ or $m = 0$ waves to be generated in the plasma.

The design of the two semi circular coils (Fig. 3a) used in most experiments described here, is basically similar to the one used previously /8/, with some technical improvement : the Faraday screen is now made of two series of inconel blades arranged in such a way as to prevent particles following the magnetic field lines from penetrating inside the inner part of the antenna. The central and return conductors are both silver-plated and each half coil is mechanically assembled in a rigid way by strong connexions with the vertical ports. As previously, no insulating material was used between the central conductor and the screen.

Before each series of experiments, the two half coils were thoroughly outgassed by RF pulses repeated every 2 or 4 seconds, at 0.3 to 1 kW average continuous RF power, either in vacuum or in the presence of the discharge cleaning plasma.

In vacuum, the loading resistance defined as $\mathscr{R} = 2P\ Z^2{}_0/V_M{}^2$ where P is the transmitted power, V_M the peak RF voltage on the line supplying the coils and $Z_0 = 50\ \Omega$, is about 1 Ω.

Most experiments were done with $\omega \sim \omega_{CH}$ inside the plasma. In these conditions, as noticed earlier /9/, the damping length is shorter than the plasma circumference, no resonant modes are detected, and values of $\mathscr{R}$ almost constant in time are obtained, usually between 5 and 10 Ω. Accordingly, power in the 200 kW range could be transfered at RF voltages between 10 and 14 kV, values which are well supported by the equipment.

A new design of antenna schematically presented in Fig. 3b has been tested very recently. Here the part of the electrostatic screen facing the plasma has been removed while the lateral sections are mechanically reinforced. Such a design is basically similar to the one used in T4 /15/ with the difference that our slotted "side limiters" are transparent to the waves leading to an improved loading resistance. It was successfully used up to RF voltages of 15 kV allowing power coupling up to 250 kW, as with the previous design. Another new feature of this antenna is the addition of a distributed metallic capacitor between the central conductor and the return current which brings the electrical length of the antenna close to the optimum $\lambda/4$ condition.

3. EXPERIMENTAL RESULTS AT LOW PROTON LEVEL

Here we describe the observations made in two series of experimental conditions chosen as standards of operation : "high density" characterized by a central line density around $3.10^{15}\ cm^{-2}$, and "low density" at $n_e l \simeq 1.2\ 10^{15}\ cm^{-2}$. In both conditions, the proton density n_H was much lower than the deuterons n_D (< 5 %) as evaluated from mass spectrometric analysis of the neutral gas immediately after the RF pulse and from the data of the mass/energy CX analyser during the shot.

3.1 - High density conditions

Table I summarizes the general characteristics of the plasma at the time of the RF pulse

TABLE I

Toroidal field	41 - 42 kG
Plasma current	200 kA
Loop voltage	1.6 V
Peak density	$1.2 - 1.4\ 10^{14}\ cm^{-3}$
n_H/n_D	$\leqslant$ 5 %
Z_{eff}	$\sim$ 1.8(N_i and 0 as the main impurities)
$(T_e)_0$	1100 eV
$(T_i)_0$	650 - 700 eV
RF frequency	60 or 61 MHz
RF pulse duration	30 to 50 ms
RF power	up to 250 kW

In these conditions, the radial position of the cyclotron layer

was usually a few centimeters outside the plasma center while, due to the low proton level, the ion-ion hybrid layer was very near the plasma center.

The RF pulse had no noticeable effect on the central plasma density and the loop voltage was increased -if any- by not more than 10 %. An important increase of the soft X-ray was observed which can be attributed to an increase of metallic impurity density, essentially N_i and C_r (Fig. 4 shows the increase in the radiances of OVI and N_iXVIII consequent to the HF pulse). However, the absolute densities of metallic impurities remained small ($n_{Ni}(o) \lesssim 10^{11}$ cm^{-3}), and Z_{eff} lower than 2.5. Moreover, the radial profiles of the impurity emission before and during the HF pulse remained essentially unchanged, indicating that the electron temperature profile does not change considerably.

Definite and coherent results on the ion temperature increase during the RF pulse were obtained from measurements of the neutron rate and energy analysis of CX neutrals.

Fig. 5 compares for instance the evolution of the neutron rate during a 230 kW, 30 ms RF pulse to the signal in the same conditions without RF, showing a gradual increase during the pulse followed by an exponential-like decay after RF is turned off. Taking into account an initial T_D value of 700 eV as derived for these conditions from CX measurements, the corresponding increase in T_D is 150 eV.

Fig. 6 is a plot of the D temperature increase derived from such neutron rate measurements for different RF power levels, indicating a linear dependence characterized by

$$\frac{\Delta T_{DO}}{P_{pl}} = 0.7 \text{ eV/kW} \qquad \text{or} \qquad \Delta T_{DO} \simeq 5 \frac{P_{pl}(\text{kW})}{\langle n \rangle (10^{13} \text{ cm}^{-3})} \qquad (3)$$

Here P_{pl} is the amount of power coupled to the plasma, corresponding to about 85 % of the total RF delivered by the generator.

Neutron flux measurements near the antenna and on the opposite side of the machine indicate a perfect symetry of the emission.

The energy distribution of deuterons obtained from charge exchange measurements up to 8.5 keV shows no tail in the D^+ energy spectrum : this result gives confidence in the temperature increase deduced from the neutron flux measurements. For RF power between 150 and 200 kW, the increase in T_D derived from the slope of the energy distribution reaches 150 to 200 eV. T_D increases gradually during the pulse while radial scanning of the CX analysis indicates a smooth increase of the temperature profile as indicated in Fig. 7.

In contrast with the case of deuterium, the proton energy spectrum clearly reveals in these conditions a non maxwellian distribution characterized by the existence of a tail corresponding to an apparent temperature around 2 keV and an average energy of the protons around 1 keV (Fig. 8).

Preliminary data on ion temperature were also obtained from Doppler broadening of C^{VI} and O^{VII} lines by fast scanning of the UV spectrum using a vibrating mirror. Although definite indications of temperature increase exist ($\Delta T_i \sim 50$ eV), these measurements are until now limited to the external layers of the plasma.

A time evolution of the electron temperature profile has been obtained by electron cyclotron emission measurements, showing a moderate increase (~ 50 eV) in the central region and a tendency to decrease in the outer regions (r > 12 cm). An increase in T_e in the plasma core is confirmed by soft X ray analysis. However, the ΔT_e derived by this method are generally higher (by a factor of about 2), than the values derived from ω_{ce} measurements. The reasons for such a discrepancy are presently conjectural only.

The results described above were obtained both with the m = 0 and m = ± 1 arrangements of the two semi circular antennae, without any significant difference in the heating efficiency.

The total power radiated by the plasma, followed by bolometric measurements using a pyroelectric detector indicates an important increase during the RF pulse, usually around 100 kW (from 350 to 450 kW) during a 200 kW RF pulse. Part of this is due to an increase of H/D recycling evidenced by spectroscopic measurements.

3.2 - Low density conditions

A series of experiments at lower density was done with the m = 0 arrangement of the antenna, in the general conditions given in Table II.

TABLE II

Toroidal field	41 - 42 kG
Plasma current	150 kA
Loop voltage	~ 2. V
Peak density	5 10^{13} cm^{-3}
n_H/n_D	< 5 %
Z_{eff}	~ 3.5
$(T_e)_0$	1200 eV
$(T_i)_0$	450 eV
RF frequency	60 - 61 MHz
RF pulse duration	30 to 60 ms
RF power	up to 200 kW

In these conditions, D^+ temperature derived from CX measurements increases from (450 - 500 eV) to (600 - 650 eV) during a 200 kW RF pulse. An impressive increase in the neutron rate is observed during these runs : as shown in Fig. 9 the neutron signal during the RF pulse reaches a value about 10 times the level without RF. However, since the initial ion temperature derived from CX measurements is lower in these conditions than in the high density situation, this large increase of the neutron rate corresponds to a ΔT_D of 175 eV only (from 450 to 625 eV) in good agreement with the temperature increase measured by charge exchange. Accordingly, in these conditions, the D^+ heating efficiency can be evaluated as

$$\frac{\Delta T_{DO}}{P_{pl}} \simeq 1 \text{ eV/kW} \qquad \text{or} \qquad \Delta T_{DO} \simeq 2.5 \frac{P_{pl}(kW)}{\langle n_e \rangle (10^{13}\ cm^{-3})}$$

The efficiency is lower by a factor of 2 than the one obtained in the high density conditions. This however can be explained by a lower value of the energy containment time (τ_E ~ 8 - 10 ms instead of 20 ms in the high density conditions). Such a reduced value of the energy containment time also explains the general shape of the neutron pulse characterized by steeper rise and decay times than observed in the high density runs.

As observed in the high density conditions, T_e derived from ω_{ce} emission shows an increase near the axis ($\Delta T_e \simeq 80$ eV). However, for $r > 8$ cm, an appreciable cooling is observed ($\Delta T_e \simeq -150$ eV) which may be connected with an impurity influx.

A few experiments were also run in these low density conditions with the m = 1 arrangement of the launching loop. A smaller heating efficiency was observed in those conditions. However this might be due to worse plasma conditions ($Z_{eff} \sim 6$) in this run or to the change in the coupling mode. Very energetic ions (up to 35 keV) were observed at the plasma boundary in this case.

4. EFFECT OF THE H/D RATIO

As summarized above, the basic ideas on wave damping in a plasma containing two ion species predict that the radial position of the ion-ion hybrid layer, dependent on the n_H/n_D and ω/ω_{ci} ratios by eq. (2), determines the plasma radius where heating occurs, and hence the heating efficiency.

A series of experiments, made at different magnetic field levels and different proton concentrations entirely confirms the validity of this picture, both in the high and low density conditions.

Fig. 10 shows the time evolution of the neutron rate in 3 experimental conditions at similar RF power levels, in low density conditions. A large increase of the signal is observed when the conversion layer is in the vicinity of the plasma axis : this is observed at low n_H/n_D (3 %) with the cyclotron layer near the axis ($B_\phi = 41$ kG, Fig. 10a) or at high n_H/n_D (15 %) when $\omega = \omega_{CH}$ near the outer border of the plasma. ($B_\phi = 45$ kG, Fig. 10c). On the contrary a much smaller effect on ion heating is noticed when the conversion layer is far from the center, even with the cyclotron layer near the axis ($n_H/n_D \sim 15$ %, $B_\phi = 41$ kG, Fig. 10b).

Similarly, Fig. 11 shows the results of a series of low density experiments where the n_H/n_D ratio was varied between 5 and 45 % at fixed B_ϕ value of 46 kG, such that the $\omega = \omega_{CH}$ layer was located at R = 112 cm, 14 cm from the plasma axis. (The major radius is $R_0 = 98$ cm, and the limiter radius is a = 18 cm).

The same figure (11a) presents an approximate sketch of the different profiles of the wave conversion layer computed from (2) for the n_H/n_D ratios measured in the experiments (assuming for $K_{//}$ an arbitrary value of 5 m^{-1}). Comparing 11a and 11b clearly reveals that, with the cyclotron layer 14 cm away from the plasma axis, the dominant parameter for maximum heating is the position of the conversion layer.

The same evidence that heating occurs in the vicinity of the conversion layer was obtained in high density experiments. As seen in Fig. 12, which summarizes the heating effects derived from neutron rate measurements in a plasma with $n_{eo} = 1.3\ 10^{14}$ cm^{-3}, an efficient heating of the plasma can be achieved at low n_H/n_D with the cyclotron layer near the plasma axis ($B_\phi = 42$ kG, $\omega = \omega_{CH}$ at R = 104 cm) or at high n_H/n_D with the $\omega = \omega_{CH}$ layer far outside the plasma ($B_\phi = 48$ kG, $\omega = \omega_{CH}$ at R = 118 cm).

ΔT_e measurements by ω_{ce} emission in a series of experiments made at different n_H/n_D ratios lead to the same conclusion : as shown in Fig. 13 maximum heating occurs for a proton level such that the conversion layer is in the vicinity of the axis.

Bolometric measurements of the total radiated power made at different n_H/n_D ratios indicate that working at intermediate values of the n_H/n_D ratio might be of advantage : as shown in Fig. 14 the radiated power is significantly larger at very high or very low proton concentrations. For low proton concentrations the apparent proton "temperature" ($\sim$ 1500 - 1800 eV) is much larger than at intermediate n_H/n_D concentrations (T_p = 900 eV). If these ions are not well confined (for example if these ions are close to the loss cone) sputtering can be increased substantially.

5. LOCAL POWER DEPOSITION

More detailed measurements on the ion and electron temperature profiles would be required for evaluating with some accuracy the global efficiency of the method of plasma heating described here.

However, a simple evaluation of the local RF power required for justifying the heating results has been done in the following way : the proton, deuteron and electron populations on the axis, assumed maxwellian are described by three local energy conservation equations on the basis of collisionnal energy transfer. The energy containment times of each species are derived from the measurements of the ohmically heated plasma just before RF and are assumed to follow a $\tau \propto n_e$ scaling during the pulse. The central n_e value and the ratio n_H/n_D in the code are fitted to the experimental one while the RF power deposited on each species are free parameters which must be adjusted to get the best fit with the experimental results. This code does not include impurities.

For high density conditions at low proton level a fair simulation of the ion heating effects can be obtained only by assuming the additional power is initially transfered to the protons, the temperatures of D, H, and e adjusting then themselves by collisionnal equipartition. The result of such a simulation is shown in Fig. 15 for a plasma with n_H/n_D = 0.02, ion and electron temperatures of 650 and 1100 eV and a RF pulse of 30 ms at a level of 0.6 W/cm^3. The time evolution computed for the neutron rate shows particularly good agreement with the experimental signal of Fig. 5, observed during a 30 ms, 230 kW RF pulse.

The assumption of a maxwellian distribution for proton energy is however not backed up by experiment and a more satisfactory approach seems possible on the basis of the quasi linear theory outlined by T. Stix.

The proton distribution function computed from this theory, assuming RF power of 0.5 and 0.7 W/cm^{-3}, $n_e = 1.4\ 10^{14}$ cm^{-3}, n_H/n_D = 0.04 and T_e = 1100 eV, is shown in Fig. 8 and seen to agree with the experimental points derived from proton CX measurements in a series of experiments where P = 220 kW, n_H, n_D and T_e corresponding to the values assumed in the calculation.

Similarly, computing on the basis of Stix's theory the local power required for fitting the proton energy spectra measured along different chords in a low density discharge leads to an evaluation of the power deposition profile. As shown in Fig. 16, the result depends on the assumption on the nature of the impurities responsible for the Z_{eff} observed in these experiments. Here again however, a central additional power around 0.6 W/cm^{-3} seems adequate for explaining the experimental observations, while integration over the plasma volume leads to total powers comparable to the actual RF power in the experiment.

6. CONCLUSION

RF in the proton cyclotron range of frequency has been coupled to a basically D plasma at power level up to 250 kW, using a couple of all-metal antennae.

In the high density regime ($n_{eo} \sim 1.3\ 10^{14}\ cm^{-3}$), the ion temperature is seen to increase by at least 150 eV, as measured by neutron rate and charge exchange neutrals energy spectrum.

At lower density ($n_{eo} \sim 5\ 10^{13}\ cm^{-3}$) increase in the ion temperature is not proportionally larger but this could be attributed to a lower energy containment time in these conditions.

Increasing the n_H/n_D ratio up to 80 % shows that ion heating can be achieved with the same efficiency as for low proton level provided the magnetic field and hence the radial position of the $\omega = \omega_{CH}$ layer are increased for a fixed frequency. This is in agreement with the presently accepted picture of the wave damping mechanism underlining the dominant role played by the wave conversion layer in the heating scheme.

On the other hand, several important questions require deeper investigation :

- The experiments described here did not allow unambiguous informations on the effect of RF on the electron temperature. Such data are however required, in particular for obtaining a correct evaluation of the global heating efficiency.

- Increasing the RF power to higher levels will require a better understanding of the factors controlling the radiation resistance of the launching loops. Understanding how this resistance varies with the number of antennae and to what extend it depends on the distance between the plasma edge and the RF conductor will be of particular importance for future developments of this heating method.

REFERENCES

1. J. ADAM et al. 5th Conf. Pl. Phys. and Nucl. Fusion Res. (Tokyo 1974) II, 65, (1975).

2. V.L. VDOVIN, V.D. RUSANOV, N.V. SHAPOTKOVSKI, ibid. I, 217, (1975).

3. N.V. IVANOV, I.A. KOVAN, V.S. SVISHCHEV, JETP Lett. 20, 39, (1974).

4. H. TAKAHASHI et al. Phys. Rev. Lett. 39, 31 (1977).

5. TFR GROUP, Heating in Toroidal Plasmas, Grenoble 1978, EUR-CEA Report FC 970 (1978).

6. J. HOSEA et al., Bull. Am. Phys. Soc. 23 (1978) 836, PPL Report 1554.

7. H. KIMURA et al. Nucl. Fusion, to be published.

8. TFR GROUP, to be published in Nucl. Fusion (1979), EUR-CEA Rep. FC 988 (1979).

9. TFR GROUP, 3rd Int. Meeting on Heating of toroidal plasma (Grenoble) I, 87 (1976). 6th Conf. Pl. Phys. and Nucl. Fusion Res. (Berchtesgaden 1976) III, 39 (1977).

10. V.L. VDOVIN, N.V. SHAPOTKOVSKI, V.D. RUSANOV, 3rd Int. Meeting on Heating of Tor. Plasma (Grenoble) II, 349 (1976).

11. J. JACQUINOT, Varenna-Grenoble Inter. Symp. (Grenoble 1978) I, 127 (1978). 3rd Topical Conf. on RF plasma heating (Pasadena) D4-1 (1978).

12. F. PERKINS, Nucl. Fusion 17, 1197 (1977).

13. H. TAKAHASHI, PPPL Rep. 1374 (1977).

14. T. STIX, Nucl. Fusion 15, 737 (1975).

15. V.V. BUZANKIN et al., 6th Conf. on Pl. Phys. and Nucl. Fus. Res. (Berchtesgaden 1976) III, 61 (1977).

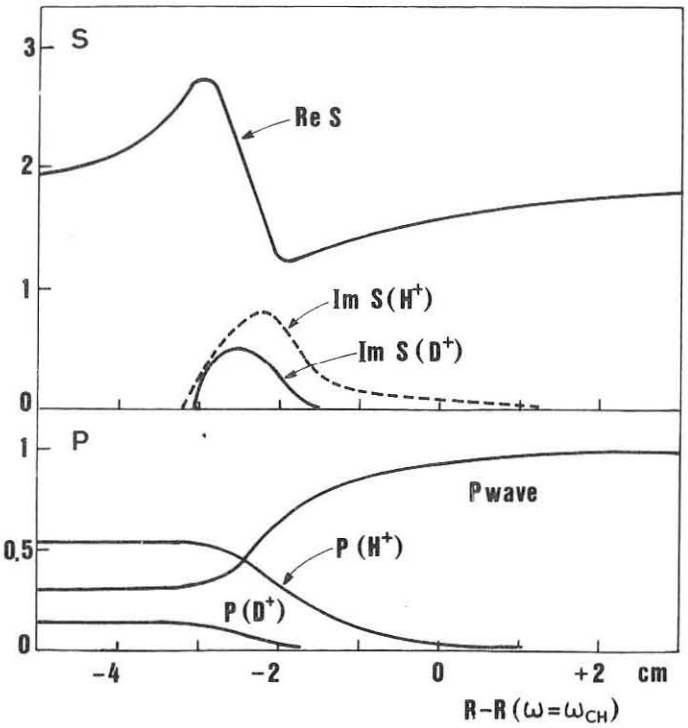

Fig. 1 - Real and imaginary parts of $S = k_x\ c/\omega_{pD}$ and power deposition profile along the wave path in a low proton case ($T_{eo} = 900$ eV, $T_{Do} = 850$ eV, $T_{Ho} = 1190$ eV, $n_{eo} = 1.4\ 10^{14}$ cm^{-3}, $n_H/n_D = 0.03$). In this case, no appreciable power is transfered to the electrons.

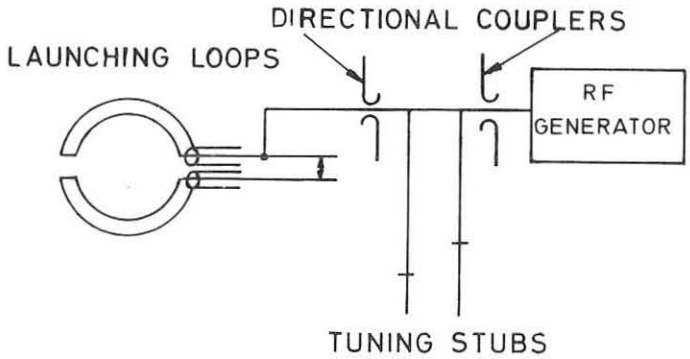

Fig. 2 - Schematic of the RF equipment.

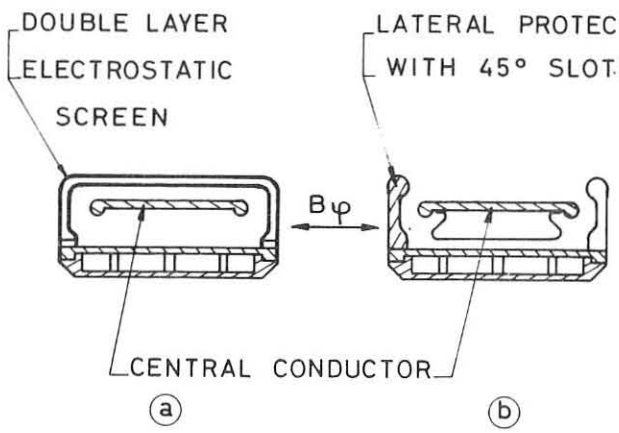

Fig. 3 - Cross sections of the two types of antenna used in TFR.

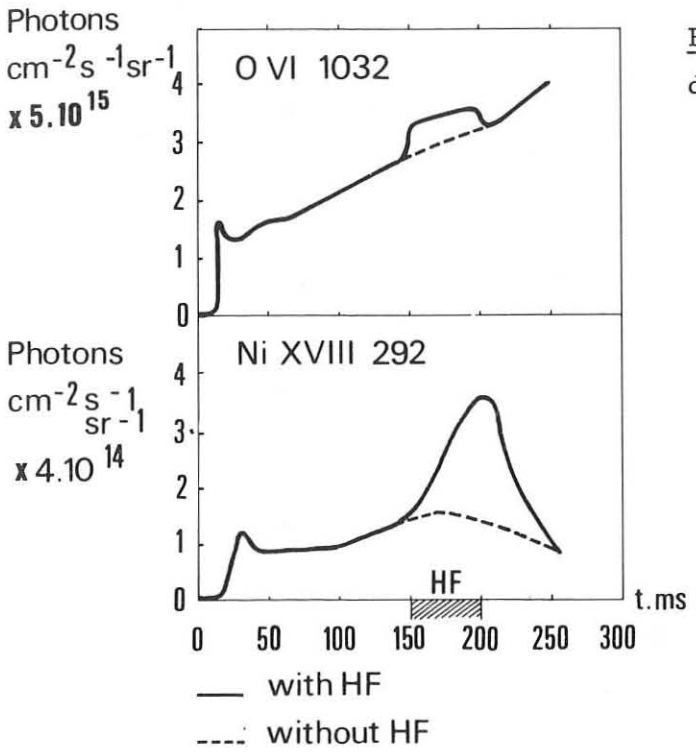

Fig. 4 - O^{VI} and N_i^{XVIII} radiance during a RF pulse.

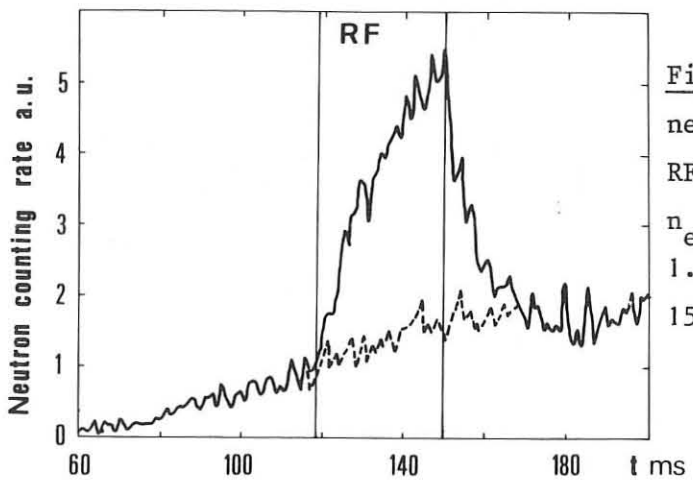

Fig. 5 - Time evolution of the neutron rate with and without RF (230 kW, 30 ms). n_{eo} increases from 1.1 to 1.3 10^{14} cm^{-3} between 120 and 150 ms.

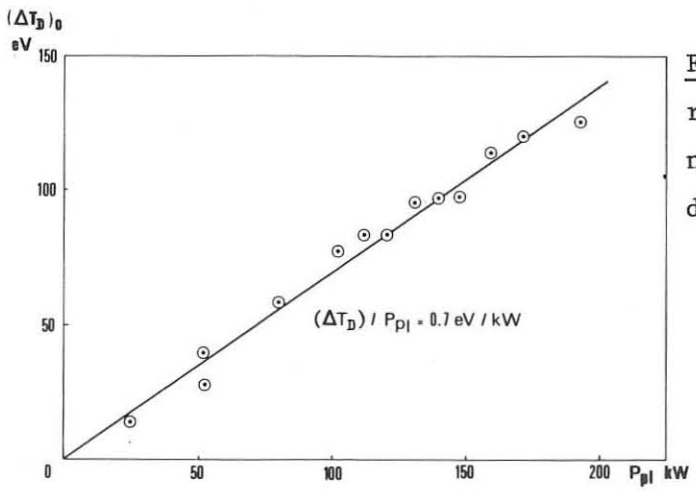

Fig. 6 - Peak deuterium temperature increase derived from neutron rate vs. total RF power delivered to the plasma.

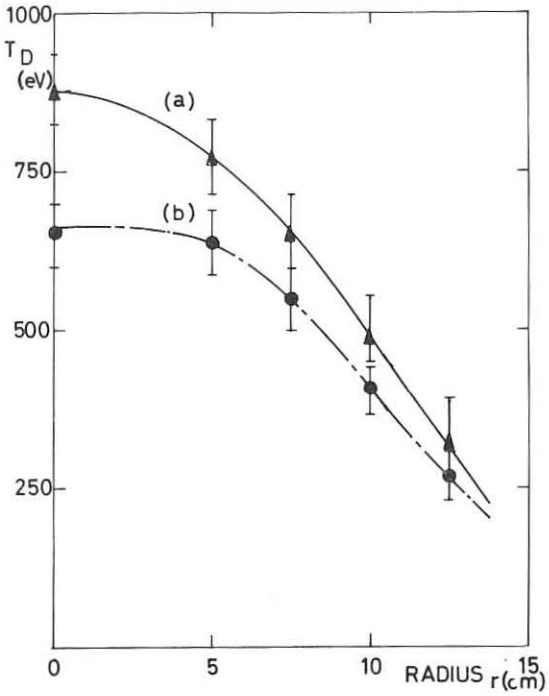

Fig. 7 - Radial profile of T_D with (a) and without (b) RF, computed from radial scanning of CX neutrals signal.
$n_{eo} = 1.2\ 10^{14}\ cm^{-3}$
$P_{RF} = 225$ kW

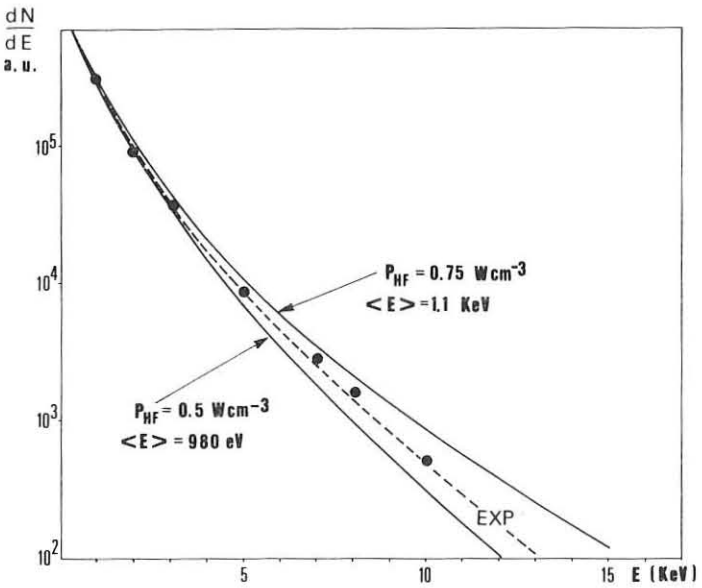

Fig. 8 - Proton energy distribution derived from CX neutrals analysis ($n_{eo} = 1.4\ 10^{14} cm^{-3}$, $T_e = 1$ keV, $T_d = 750$ eV, $P_{RF} = 220$ kW, $n_H/n_D = 0.04$) compared to the distributions computed from Stix's theory assuming RF powers of 0.5 or 0.75 cm^{-3}.

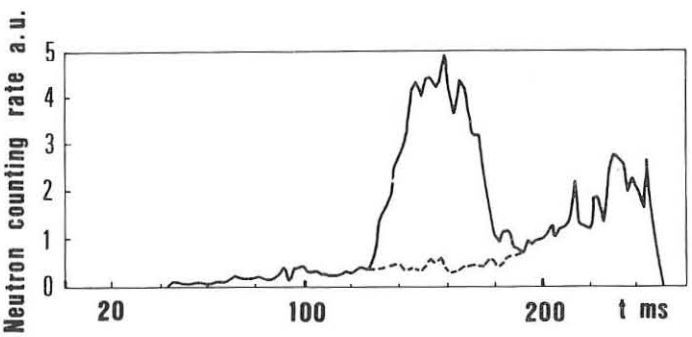

Fig. 9 - Increase of the neutron flux in the "low density" conditions ($n_{eo} = 5.10^{13}\ cm^{-3}$, $P_{RF} = 215$ kW).

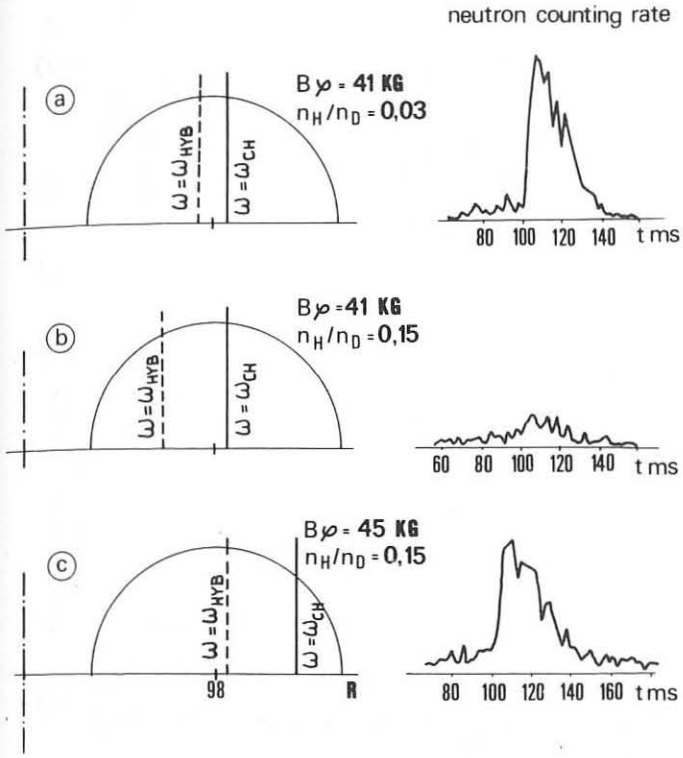

Fig. 10 - Effect of n_H/n_D on the neutron rate at different values of the magnetic field in "low density" plasmas.

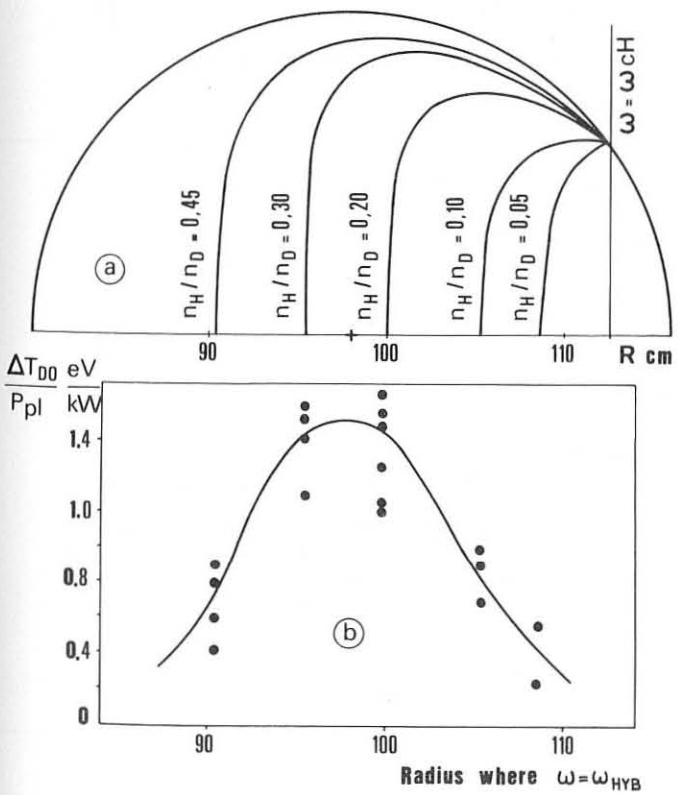

Fig. 11 - Profiles of the wave conversion layer (a) and Deuterium heating (b) for different n_H/n_D ratios with B_ϕ = 46 kG.

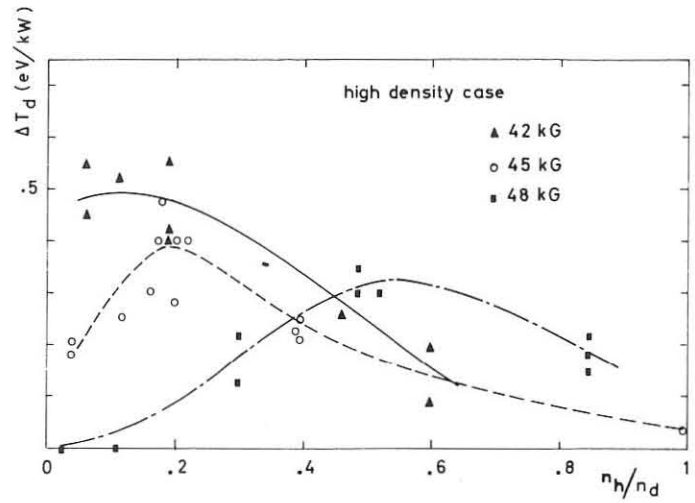

Fig. 12 - Deuterium heating vs n_H/n_D for 3 values of the magnetic field in the "high density" conditions.

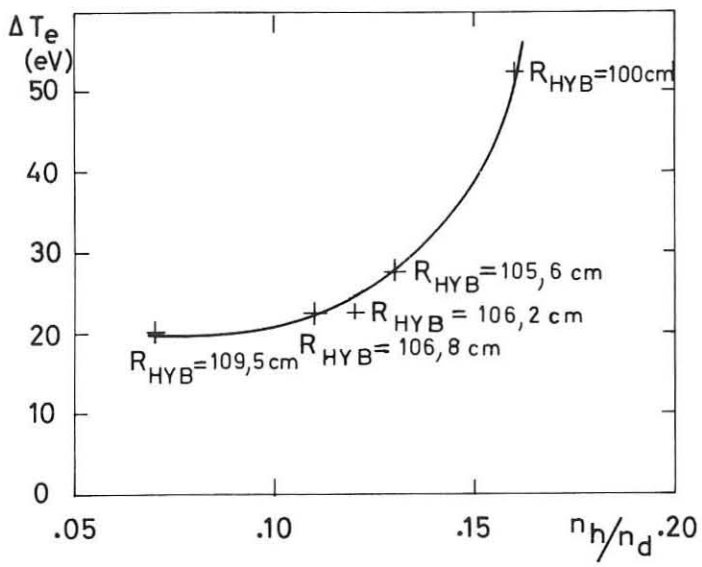

Fig. 13 - Central electron temperature increase measured by ω_{ce} emission for different n_H/n_D.
The position of the hybrid layer is indicated for each experimental point.
The cyclotron layer is at R = 112 cm.

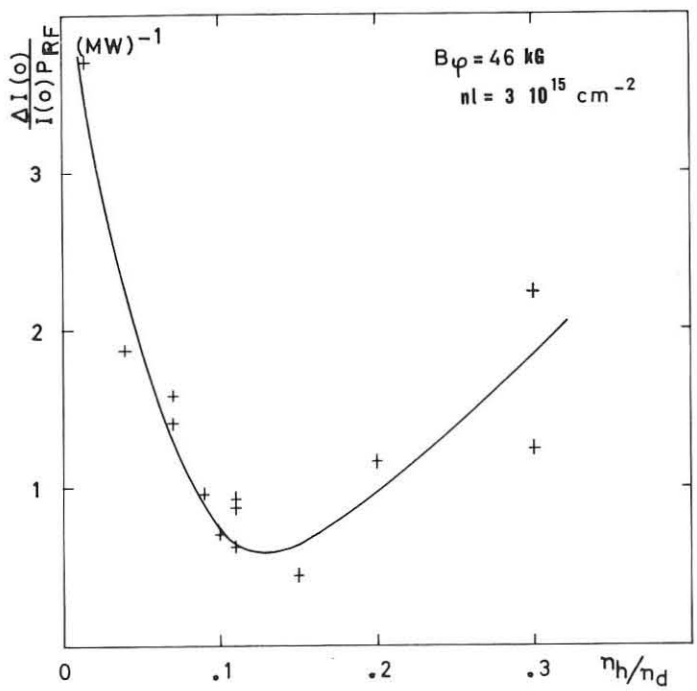

Fig. 14 - Relative increase of the radiated power during the RF pulse, as measured by bolometry.

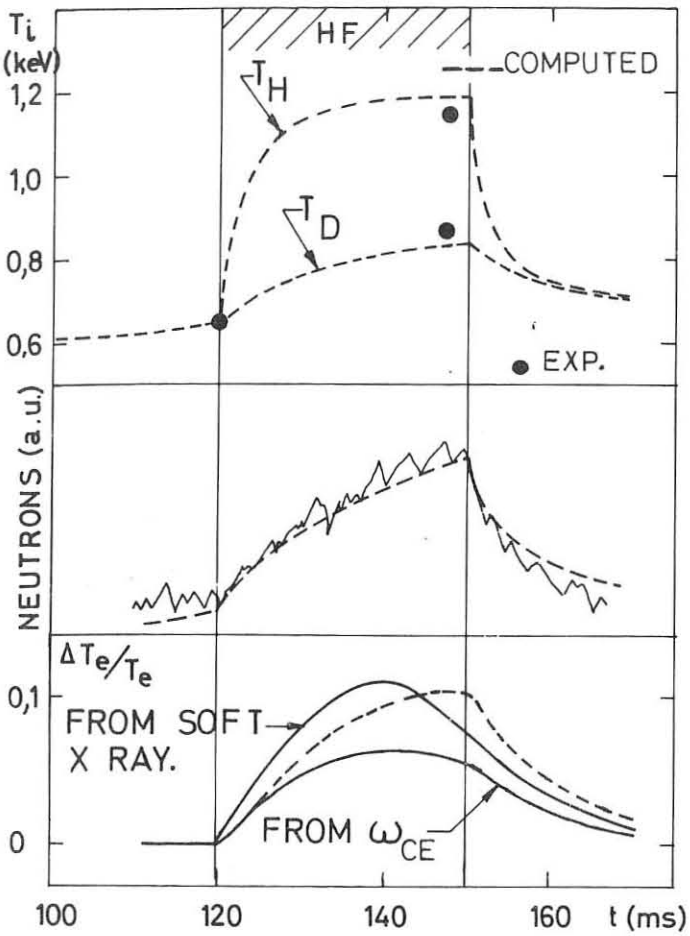

Fig. 15 - T_H, T_D, T_e and neutron flux computed from a local code assuming 0.6 W/cm^{-3} are coupled to the protons, compared to experimental data. (n_{eo} = 1.3 10^{14} cm^{-3}, n_H/n_D = 0.02).

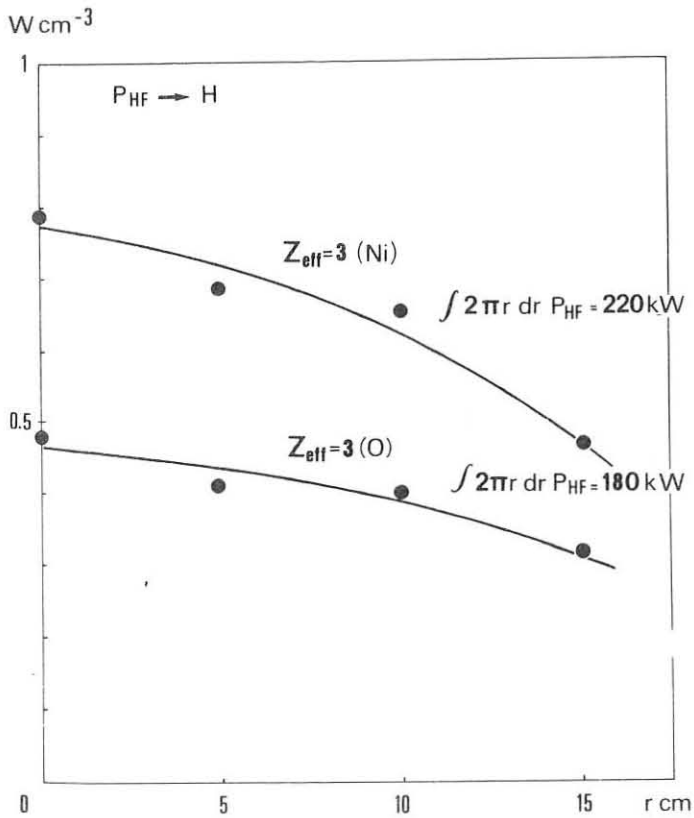

Fig. 16 - Power deposition profiles required by Stix's theory for fitting the proton energy spectra along different chords. The two profiles are computed assuming Z_{eff} = 3 with N_i or O as the impurity.

REVIEW OF DITE WORK

by

J.W.M. Paul

Culham Laboratory, Abingdon, Oxon, OX14 3DB, UK
(Euratom/UKAEA Fusion Association)

ABSTRACT: The behaviour of the DITE tokamak, including both 1 MW injection and the bundle divertor, is reviewed with particular emphasis on MHD activity.

1. INTRODUCTION

Aims: This paper attempts to place the seven contributed papers and some more recent work on DITE into a more general context. The aims of the DITE programme are largely the same as previously, but can now be grouped as activities;

(a) Leading up to and supportative of JET, from plasma physics to diagnostics.

(b) Testing the longer term attractiveness of the bundle divertor for exhaust and control of impurities in the next generation of machines (e.g. TIGER/INTOR).

Both of these activities involve understanding (i) the origin, role and control of impurities and MHD activity and (ii) the physical processes involved in a tokamak dominated by injection heating.

Physics Progress: Five main points can be listed;

1) The injection of 1 MW of neutral beam power to the plasma has tripled the ion temperature to 1 keV and indicated, but not proved, the presence of the beam driven current. The injection work has also revealed some problems of interpretation.

2) Low q discharges are run routinely with $q = 2.2$ for 0.1 s without deterioration of containment.

3) The combination and comparison of diversion and gettering shows that diversion further reduces both low and high Z impurities in a gettered torus.

4) Injection into a diverted discharge has doubled the ion temperature in some preliminary experiments.

5) In all the above work MHD activity plays an important role particularly with clean plasmas. The activity is variable and its origin is not understood but it seems to point to the need for a better understanding of the initial phase of the discharge.

Technological Progress: The last E.P.S. review of DITE work concluded that pure plasmas with auxiliary heating were required. We demonstrated the effectiveness of gettering and the bundle divertor to achieve the former and neutral injection for the latter. Since then we have, and are continuing, to upgrade both injection and divertor systems. The first main technological achievement has been upgrading the injection system to 1 MW to the plasma (Paper AP3), with average reliability of 85% and 100% for single days. Next year this system will be replicated to provide 2 MW. The second achievement is the design of a new bundle divertor (Mk II) for operation at full field (2.8 T) on DITE and this design has greater potential for reactors. The Mk II divertor is under construction and will be installed next year. In the meantime the Mk I has been upgraded to 1.5 T but is operational at 1.0 T at present.

Like most other major tokamaks, there have been technical problems with our machine, in particular with the toroidal and divertor field systems and with the long commissioning of the injection system. While these have severely reduced experimental time, the problems have largely been overcome. However, viewing the whole fusion community, the implimentation of technology needs to be improved so that more machines operate on design performance, on time and most of the time. Such an improvement in reliability would also improve the credibility of the advance to a reactor.

Diagnostic Progress: Apart from improving more standard diagnostics, we have developed a technique for measuring, for the first time, the four Stokes parameters which define properly the polarisation of the electron cyclotron emission (Paper EP13). Studies of the latter, pioneered at Culham Laboratory with the NPL, have now become an extremely convenient method of measuring $T_e(r)$ (Paper EP12).

Although the measurements usually agree with other data, the physical processes and the errors need to be better understood or

documented. This new technique should help. The problems appear to lie in the variability of the polarisation, similarity of spectra from radial, vertical and tangential directions, calibrations and the fact that it appears to work even when the plasma should be optically thin.

DITE Experiment: The layout of DITE is shown in Fig. 1, and the parameters are listed below:

Tokamak:

$r_L = 0.26$ m ; $R = 1.17$ m

$I_g \lesssim 280$ kA ; $B_T \lesssim 2.7$ T

Limiters:

Mo limiters, recently changed to Ti and/or C.

Injection:

$P_{inj} \lesssim 1.1$ MW; $V \lesssim 28$ kV $t \lesssim 50$ ms

Divertor:

$I_g \lesssim 75$ (100) kA, $B_T \lesssim 1.0$ (1.5) T

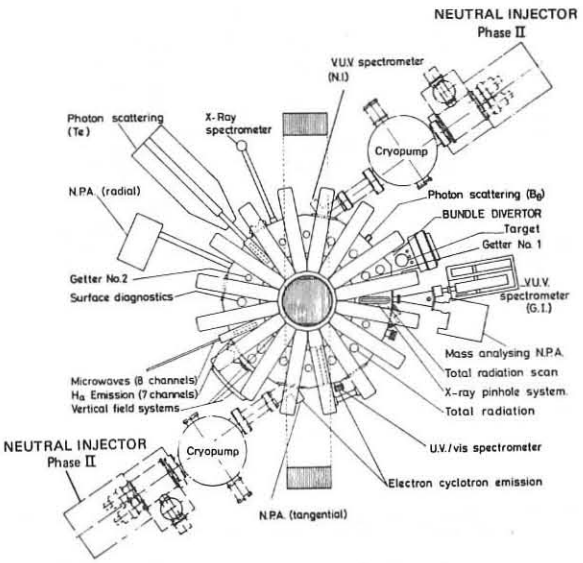

Fig. 1. Schematic layout of DITE.

2. TOKAMAK

2.1 Introduction

For the discussion which follows, two simple diagrams should be useful. The first (Fig. 2) is a schematic $T_e(r)$ which illustrates three regions of the plasma, namely the central core, the intermediate and the boundary layer. These are separated by the 'natural' boundaries of the q = 1 and q = 2 surfaces respectively. The MHD activity at each of these surfaces can permeate the adjacent regions and dominate plasma behaviour. The structure provides the matching of the hot plasma to the cold wall. The second (Fig. 3) is the Hugill operating diagram which illustrates how tokamaks are boxed in by MHD activity leading to disruption.

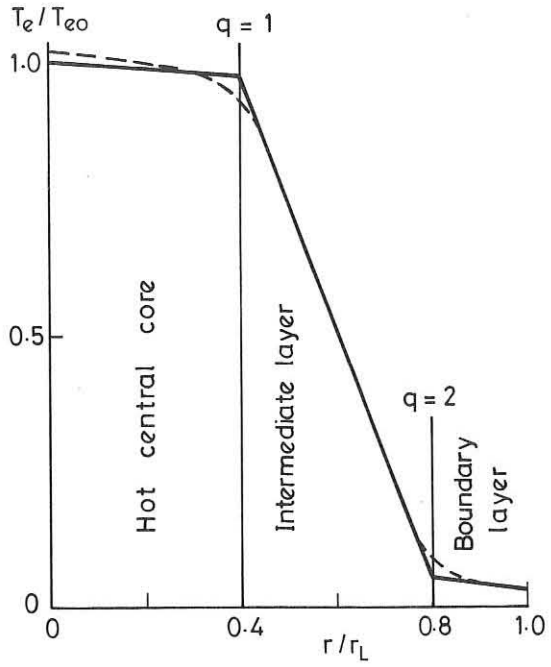

Fig. 2. Schematic plasma structure.

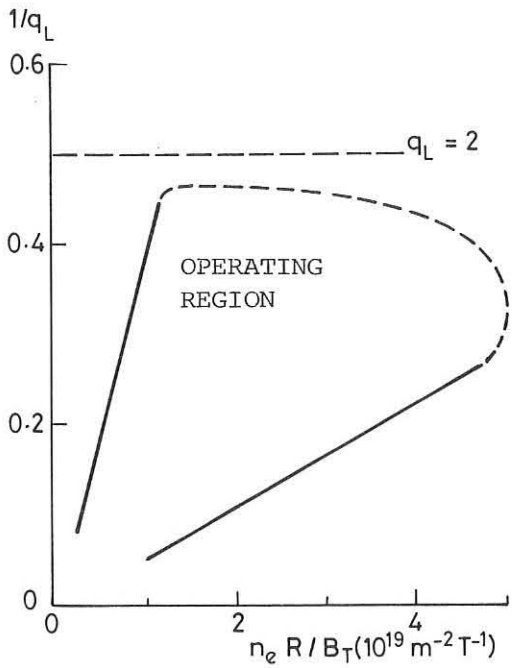

Fig. 3. Schematic operating region.

2.2 Plasma Structure

Boundary Layer: Through this layer, plasma is fuelled with hydrogen, from the walls and the gas feed, and with impurities from the walls. Low Z impurities arise mainly from desorption, while high Z impurities arise from arcs (not necessarily unipolar) and/or sputtering. The emission from hydrogen (H_α) and lowly ionised impurities (eg O II), which tends to be largely from this region, is often asymmetric in major and minor azimuth. The level of m = 2 MHD activity, originating at the q = 2 surface, appears to have an important influence on fuelling (c.f. § 2.3).

Langmuir probe measurements show (a) the ratio of average edge density at the limiter to $\bar{n}_e$ is about 0.1, but is lower with gettered walls or with the divertor on, (b) an edge T_e which falls with increasing n_e and this is probably related to the reduced arcing/sputtering at high n_e and (c) fluctuations which vary from 8% to 100%. As yet, these fluctuations have not been correlated with other parameters such as MHD activity around the q = 2 surface or the influx of impurities.

This region of the plasma is of particular interest because it forms the scrape-off layer for the bundle divertor.

Intermediate Layer: This layer matches the hot core to the cold boundary by providing the main containment. Within the layer the electron thermal conductivity (anomalous) increases with radius. The ion thermal conductivity is normally between 1 and 10 times neoclassical (typically 5 on DITE).

Under certain conditions MHD activity, namely the m = 2 mode at q = 2 and the sawtooth at q = 1, can influence the matching process.

Hot Central Core: With Mo limiters the core is radiation cooled with a peak radiation profile, $P_{rad}(r)$. This results in a tendency for $T_e(r)$ to be hollow.

With Ti or C limiters $P_{rad}(r)$ is lower and almost flat, while T_e is higher. The sawteeth at q = 1 are now more important in both the energy and particle transport. For low q ~ 2.2, this central core can extend to half the radius.

2.3 Operating Diagram (Fig. 4)

High Density Limit: With gettered walls, direct local fuelling by externally controlled gas feed is dominant although fast neutrals are still recycled by the walls. In this situation the H_α emission would need to be resolved in three dimensions to represent the fuelling and neutral density. The evolution of impurities is reduced along with the recycling, but it is believed that even in a 'pure' plasma the density is still limited by impurity cooling of the edge. When the divertor can be operated at higher density, with more effective screening (now only 50% for oxygen), it should extend the density limit appreciably. This limit has already been extended by the application of neutral injection heating.

At the last E.P.S. Conference we reported pauses in a rising density associated with changing profiles which had some associated MHD activity. Now we have clear evidence that the effectiveness of gas feed for increasing the density is impaired, when the m = 2 activity is high (wall $\Delta B_p/B_p \sim 1\%$). The two pulses in Fig. 5 have identical gas feed rates but show markedly different density behaviour because of the difference in MHD activity. This suggests that the initial stage predetermined this MHD level and therefore the subsequent behaviour.

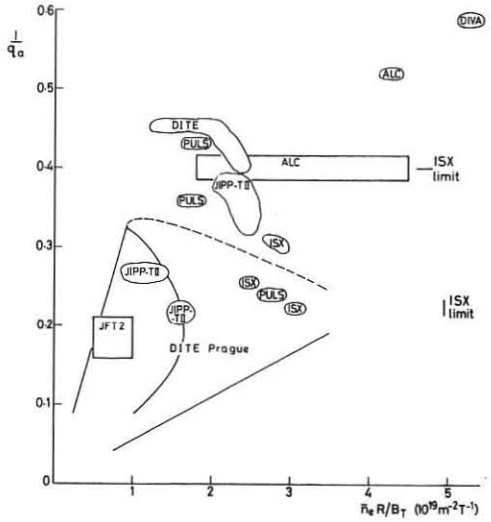

Fig. 4. Hugill diagram.

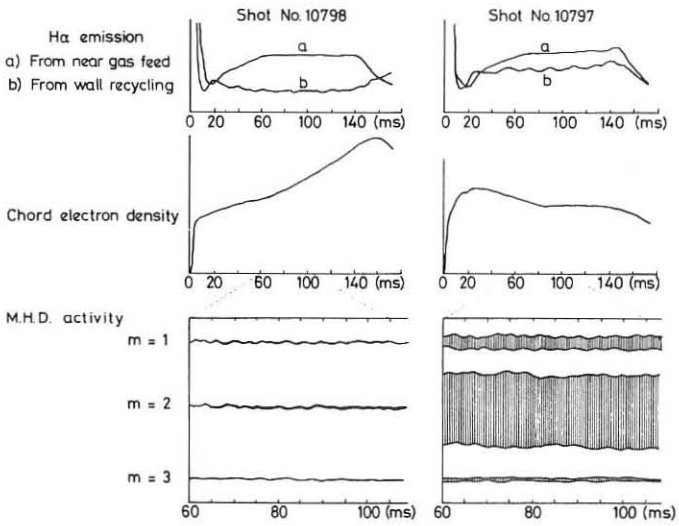

Fig. 5. Gas feed and M.H.D. activity.

Low q Operation: This offers a larger central core and higher β_T. In particular on DITE it should allow operation of the Mk IB divertor at higher currents and densities for neutral injection experiments. Discharges with q = 2.2 have been maintained for 100 ms without any disruptions (Paper EP11). This is easier to achieve with Ti limiters and gettering ($Z_e \sim 1$) and when m = 2 activity is low. Typical profiles for a discharge with q = 2.2 are shown in Fig. 6. There is no appreciable deterioration in the energy containment time with this reduced q.

There is a pause in the rising density (Fig. 7), corresponding with enhanced m = 2 activity, as the current passes through $q_L = 3$. With a more steady but lower density the current passes through q = 3 with a burst of MHD activity (Fig. 8) but without a density pause. The density was raised later, with q = 2.2, by increasing the gas feed.

An attempt to break the q = 2 barrier on DITE (no copper shell) normally resulted in disruption at q = 2 but on the one occasion when q ~ 1.6 was achieved, it resulted in a violent terminal disruption with internal damage to the machine.

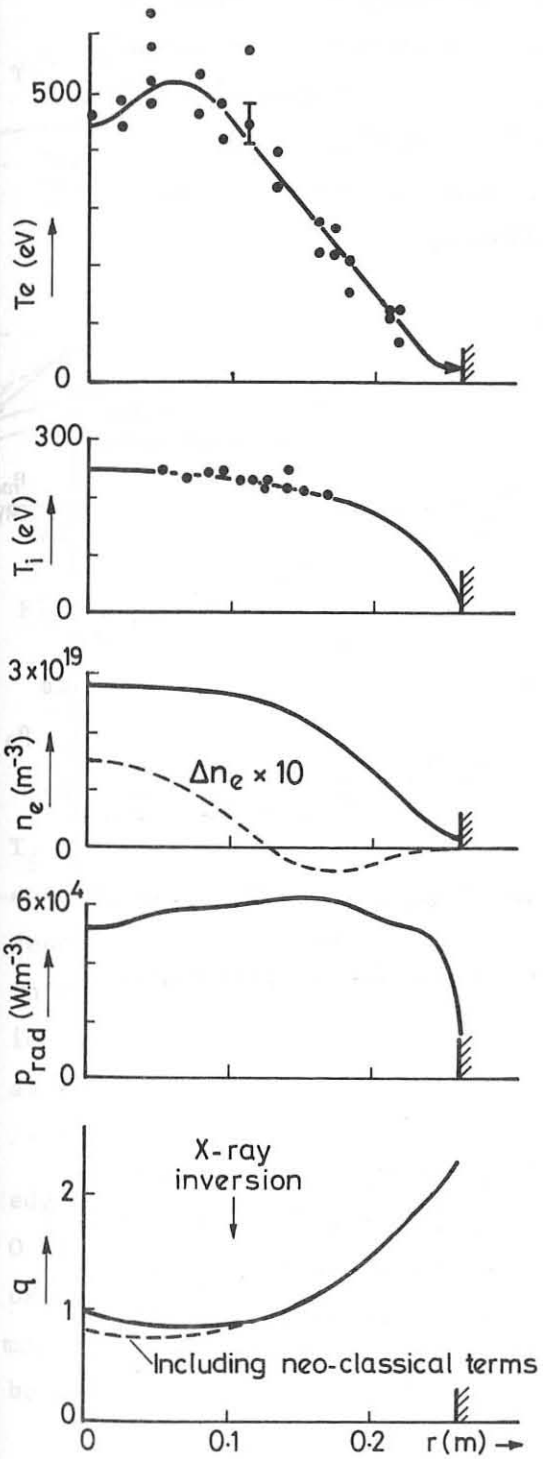

Fig. 6. Radial profiles at low q.

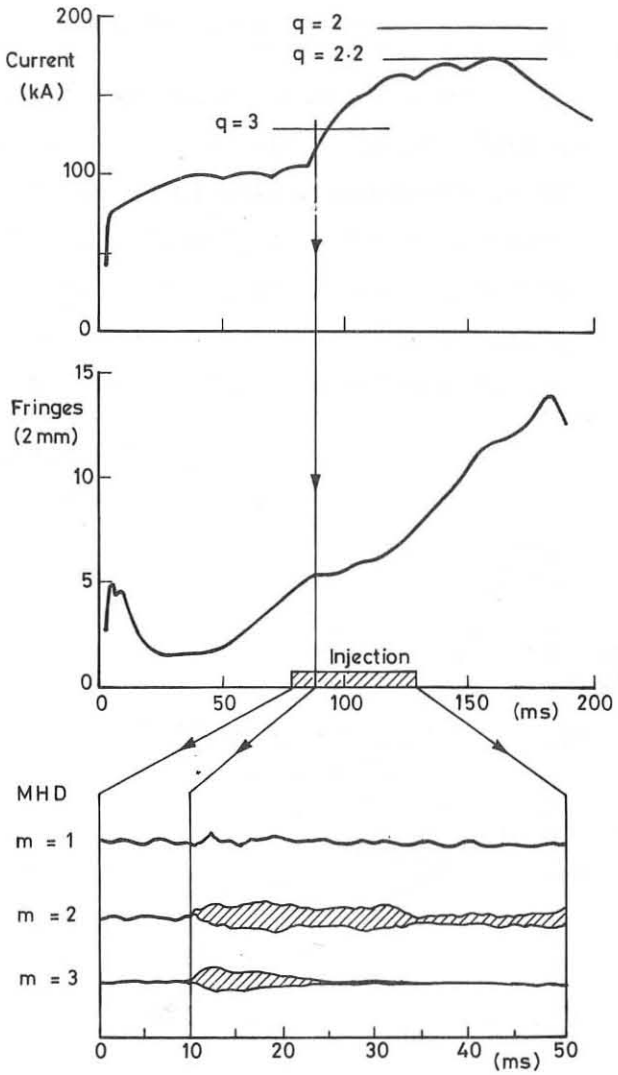

Fig. 7. Low q oscillograms (n_e pause).

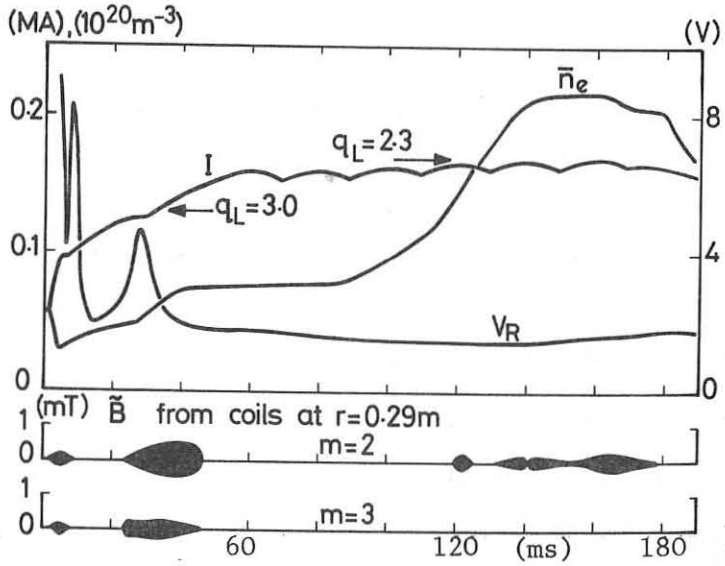

Fig. 8. Low q oscillograms.

3. PLASMA DECAY EXPERIMENT

In a gettered torus, switching off the gas feed gives rise to a rapid decay of density to a low plateau. The decay time, which is about 20 ms for a wide range of densities can be related to a particle containment time of about 15 ms, taking account of particle reflections. However, the density profiles change appreciably during the decay (Fig. 9) and analysis, assuming no recycling but correcting for the neoclassical pinch, gives a diffusion coefficient

$$D \sim \frac{0.5 \times 10^{19}}{n_e} \text{ m}^2 \text{ s}^{-1}$$

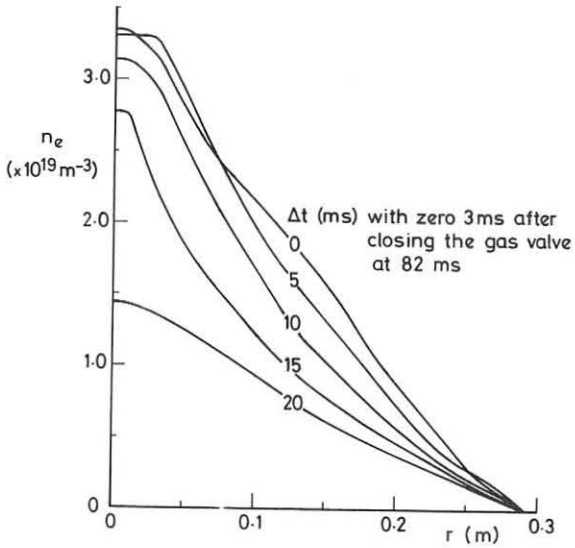

Fig. 9. Density decay profiles.

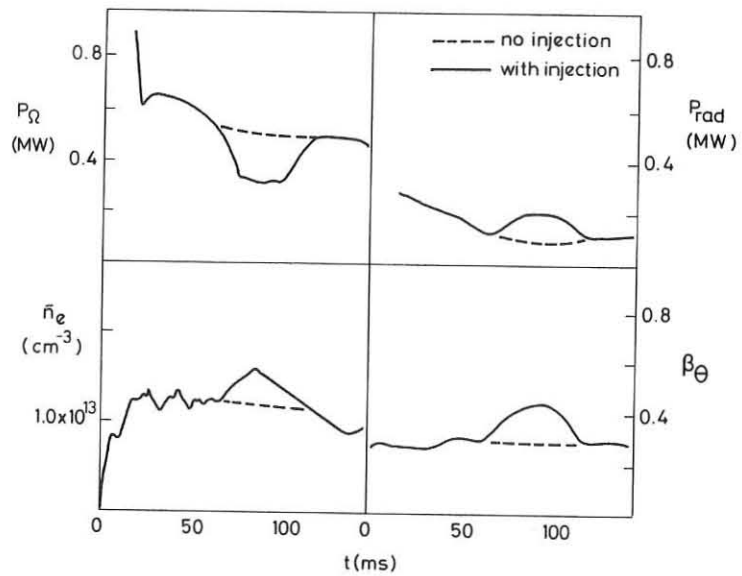

Fig. 10. Injection oscillograms.

4. INJECTION

4.1 Objective

The main objective of the DITE injection programme has been to achieve high ion temperatures rather than high β. At Culham Laboratory the latter is one of the main aims of the Tosca programme. The maximum ion temperature achieved is 1 keV, about three times the initial value. However, without optimisation values of $\hat{\beta}_T$ = 1.5% have been achieved (Paper EP9).

4.2 Mo Limiters

With Mo limiters injection usually induces MHD activity resulting in soft disruptions. There is a large increase in the radiated

power (Fig. 10) and no change in the electron temperature. In Fig. 11 a plot of ΔT_i against P_{inj}/n_e shows saturation at an ion temperature around 0.8 keV.

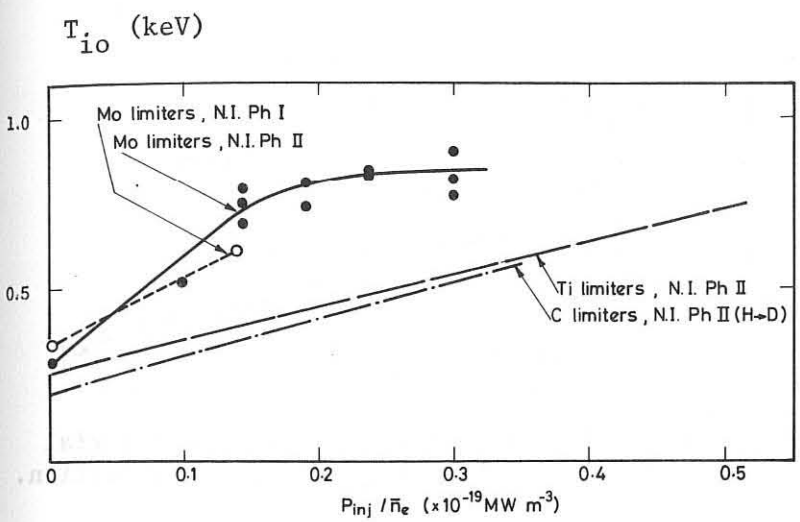

Fig. 11. Injection heating vs power.

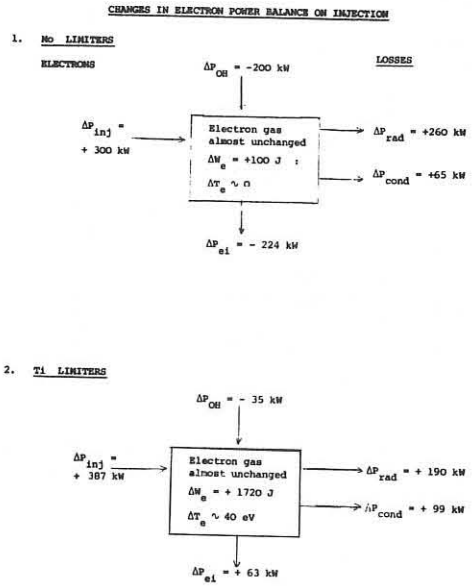

Fig. 12. Changes in electron power balance.

Power balances for the electrons and the ions show that with $T_i > T_e$ the electrons are acting as a thermostat. The temperature setting of the thermostat is presumably determined by the temperature dependence of the radiated power from a dominant impurity. The change in the electron power balance on injection is shown in Fig. 12. The ion power balance results in an ion thermal conductivity, $K_i = (5 \pm 2)K_{NC}$, as shown in Fig. 13.

The central O VII emission increases on injection more than the edge O II emission although $\Delta T_e \sim 0$. The corresponding increase in O II may be localised elsewhere but has not been found. Alternatively oxygen might be injected with the beam but its absence on a test rig makes this unlikely. Finally the beam charge-exchange on oxygen might be directly exciting the O VII emission.

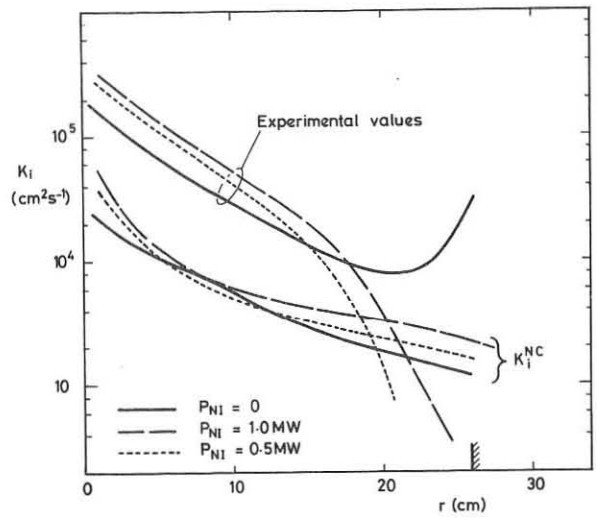

Fig. 13. Experimental and theoretical ion thermal conductivities.

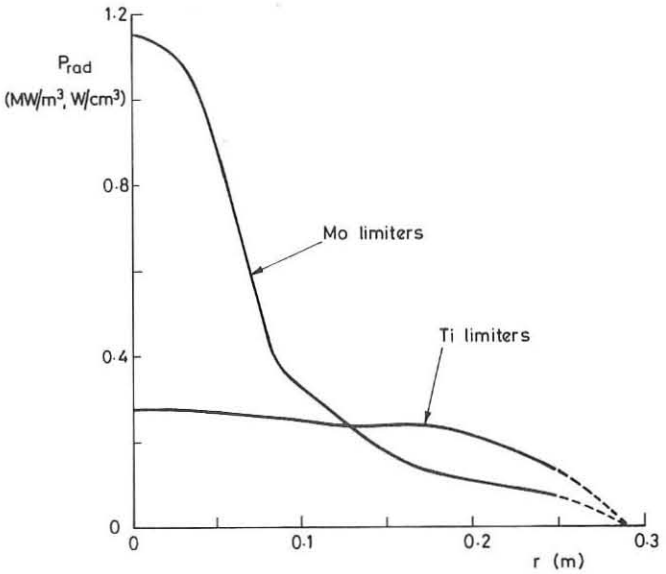

Fig. 14. Effect of limiter material on $P_{rad}(r)$ during injection.

4.3 Ti and C Limiters

These more recent conditions have lower MHD activity and injection no longer induces disruptions. The total radiation and its increase on injection are lower (Fig. 14) and under some conditions T_e increases appreciably. As $T_e > T_i$ the electrons can no longer act as a thermostat. Now injection induces large density and X-ray sawteeth around q = 1 (Fig. 15). The period does not fit a simple 'overheating' model and at present we have no satisfactory model.

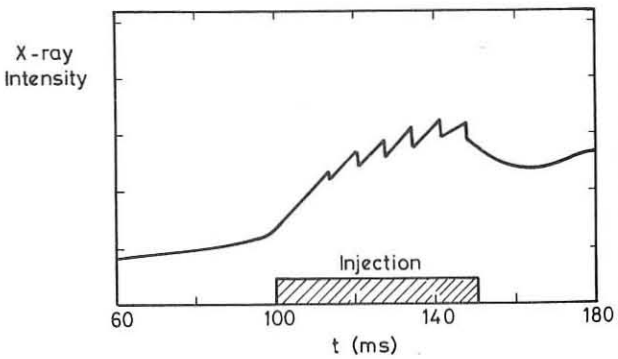

Fig. 15. Beam induced sawteeth.

The plot of ΔT_i vs P_{inj}/n_e is now linear but lower (Fig. 11). Power balances for these discharges are not complete but there are indications that charge-exchange losses may be important. There are difficulties in obtaining representative experimental measurements of the neutral density. This is now appreciably localised at the gas feed and differently averaged by the circulating beam and the plasma ions.

4.4 Beam Refuelling?

For the conditions of these experiments most of the injected beam is trapped by charge-exchange. The resulting hot thermal neutrals can be expected to move away several cm from their point of origin before ionisation or further charge-exchange. In some discharges the density rises smoothly without any sawteeth and the profile of density increase follows closely the deposition profile (Fig. 16). In the presence of sawteeth, (Fig. 17), they are equivalent to an outward flux of particles of magnitude roughly equal to that of the beam input. These equivalences may be fortuitous and are difficult to check without reliable 3-D measurements of the ionisation rate from H_α emission particularly in the localised region of beam deposition.

If the measured increase in density of injection resulted from ionisation of neutrals, then the required neutral density would give adequate charge-exchange losses in some discharges to explain the low ion temperatures.

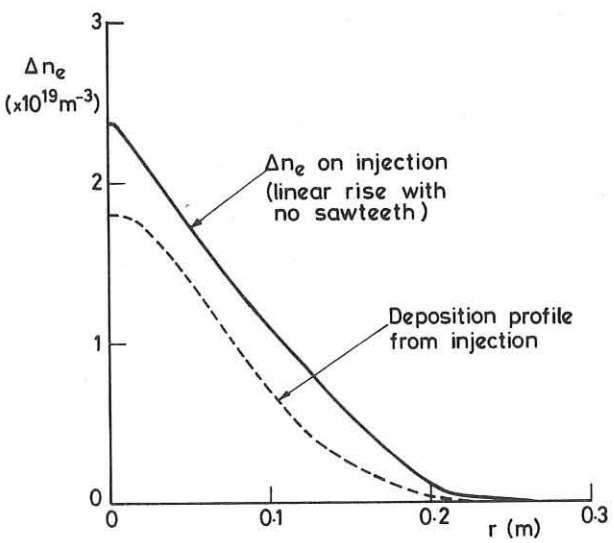

Fig. 16. Density rise on injection.

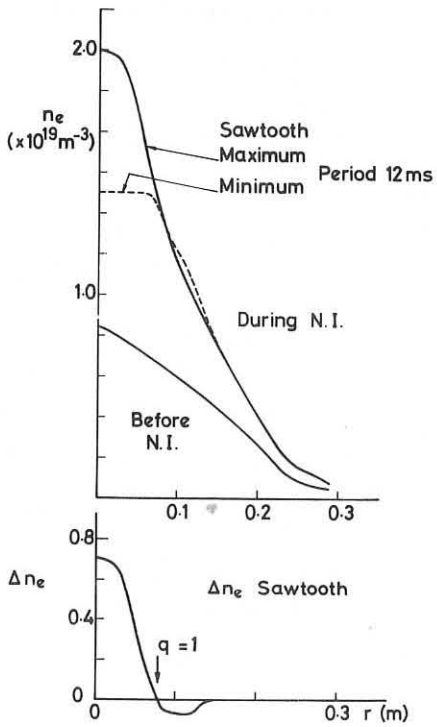

Fig. 17. Density sawteeth on injection.

4.5 Beam Induced Current?

With limiters of Mo there is no change in the electron temperature but a dramatic drop in the loop voltage. The drop in Ohmic power input in Fig. 10 is entirely due to a decrease in the voltage by about one third. This drop is comparable with that to be expected from the beam driven (Ohkawa) current. However, there should be an additional component caused by the plasma rotation which rough estimates suggest should be comparable.

With limiters of titanium the voltage often drops with an overswing as shown in Fig. 18. Such behaviour is predicted as magnetic field transfers from the Ohmic to the beam driven current but the time scales appear shorter than predicted. However, in these experiments the electron temperature did change and a detailed analysis is required to demonstrate whether this could account for the voltage behaviour.

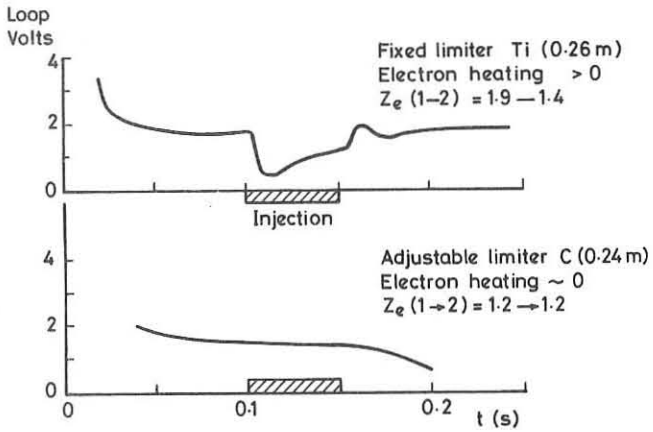

Fig. 18. Change in loop volts on injection.

With limiters of carbon the Z_{eff} is lower and there is negligible change in the loop volts on injection. The beam driven current should decrease with Z_{eff} but a more quantitative treatment is required.

These results are tantalizing in that they indicate the presence of a beam driven current, which cannot yet be demonstrated conclusively.

4.6 Conclusions on Injection

In DITE, with limiters of Mo the injection heating is limited by radiative power losses, while with limiters of Ti or C it may be limited by charge-exchange losses. The various injection experiments on DITE have been compared using a rough consumer figure of merit

$$M = \Delta(n_i T_i)/P_{inj} \sim \Delta(n_e T_i)/P_{inj}$$

where the numerator represents the desired product and the denominator the cost. For interest we extend this data (Table I) to include other experiments and added a volume correction ($M' = MV$).

TABLE I

CRUDE FIGURES OF MERIT FOR INJECTION

Machine	Ref	R (m)	a (m)	B_T (T)	I_g (kA)	Limiter	Gas	$\bar{n}_e$ (2) (10^{19} m^{-3})	Z_{eff}	P_{inj} (kW)	V_b (kV)	T_{eo} (1 → 2) (eV)	T_{io} (1 → 2) (eV)	$\Delta(\bar{n}_e T_i)/P_{inj}$	$\Delta(\bar{n}_e T_i)\ v/P_{inj}$ (ms)
DITE	B	1.17	0.27	2.0	150	Mo	H	1.4	3.7	200	28	450	340 → 610	1.9	5.1
DITE	P	1.17	0.27	2.7	190	Mo	H	2.5	7.6	200	30	1000	540 → 640	1.3	3.5
DITE	P	1.17	0.27	2.0	150	Mo	H	2.1	6.8	200	30	845	440 → 660	2.3	6.1
DITE	OX	1.17	0.26	2.0	150	Mo	H	1.6	5	800	24	650	300 → 850	1.1	2.7
DITE	OX	1.17	0.26	2.0	145	Ti	D	2.2	4	750	24	930 → 970	200 → 560	1.4	3.5
ORMAK	B	0.8	0.23	2.5	175	W	H	2.8	7.9	360	30	1530 → 760	650 → 1830	9.1	12.1
TFR	B	0.98	0.20	6.0	360	Mo	H	5.6	2.8	400	39	1800	1200 → 1600	7.7	9.4
T11	B	0.70	0.18	1.0	110	Mo	D	2.0	-	280	20	650	300 → 500	1.4	0.96
T11	I	0.70	0.18	1.0	100	Mo	D	1.4	-	140	21	400 → 530	150 → 400	2.5	1.76
ISX-B	OR	0.92	0.27	1.2	115	St	H	2.0	-	300	40	800	350 → 700	2.3	4.8
ISX-B	OR	0.92	0.27	1.2	115	St	D	7.0	1.2	500	40	600 → 900	400 → 800	8.0	16.9
PLT	I	1.32	0.40	4.0	~400	C	H	2.0	2.5	2100	40	~ 3000	1000 → 6000	4.8	7.7

B = Berchtesgaden, P = Prague, I = Innsbruck, OR = Oak Ridge, OX = Oxford

There is no reason to expect M or M′ to be constant in Table I but a systematic explanation of the large variation (~ 10) might be useful. There has been a systematic study of Ohmically heated tokamaks resulting in the creation of data banks and empirical scaling laws. Injection heated tokamaks are more complicated both experimentally and theoretically and in that codes and data need to be interleaved. The common statement, that injection heating is well understood, is probably true but needs careful checking because small factors on large machines cost large amounts of money.

The figure of merit takes no account of the scaling of transport processes (eg $M' \propto a^2$) but most experiments have similar dimensions (except PLT), similar currents (except PLT and TFR) and similar densities (except TFR and the high performance ISX-B). There is a tendency for high values of a, I and n_e to give good performance. However, ORMAK has a surprisingly high figure of merit, although the electrons are cooled. The magnitude of ΔT_e and Δn_e in injection experiments, is not always well understood.

The many factors involved in injection experiments can be classified:

(1) target plasma; its basic parameters (r, I, n_e, T_e, T_i, T_e/T_i, n_n) and its impurity level (Z_{eff}, P_{rad}, n_i/n_e),

(2) the beam, (E_b, species, impurity content, direction),

(3) beam induced, (a) impurities, (b) radiated power, (c) fuelling or in some cases apparent defuelling, (d) toroidal current, (e) rotation, (f) MHD activity.

Three problems areas deserve mentioning, (i) the accuracy of the measured/calculated neutral density and refuelling, (ii) the presence or otherwise of the beam driven and rotational currents and (iii) the accuracy of the ratio K_i/K_{NC}, which varies by up to a factor of ten, when it is derived from subtracting large quantities.

5. BUNDLE DIVERTOR

5.1 General

We have only recently returned to a major programme on the bundle divertor. There are many modes of operation involving gettering, injection, mid-pulse switching and varying ratio I_{DIV}/I_{TOR}. The initial dirty discharges provided a dramatic illustration of the effect of the divertor on the plasma wall interactions in that repeated major disruptions were reduced to minor ones or removed altogether.

5.2 Gettering

The results reported at Prague and some preliminary experiments with gettering at that time, have been repeated. The comparison of gettered and ungettered cases, is shown in Fig. 19 (Paper EP8). These discharges have typically $I_g \sim 50$ kA, $T_{eo} \sim 300$ eV, $n_e \sim 10^{19}$ m^{-3}, $q_{sep} \sim 2.5$. The density drop on diversion is less with gettering because more of the fuelling is directly from the gas feed (hydrogen screening efficiency low ~ 0.2) rather than the walls. This refuelling data fits the DITE global recycling model. The screening efficiency for oxygen is the same in both cases (0.5) showing

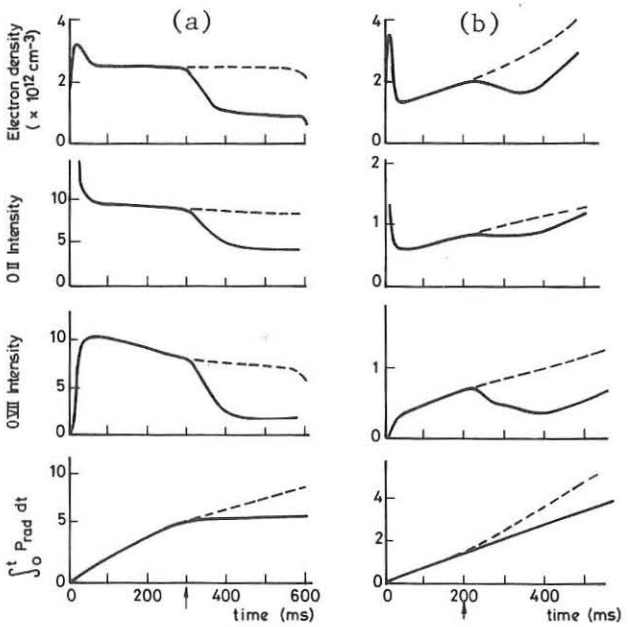

Fig. 19. Diversion without (a) and with (b) gettered walls.

that the divertor further reduces the low Z impurities in a gettered torus. The X-ray anomaly factor for the gettered discharge decreases on diversion by a factor of 4 to a value near unity (Table II) illustrating the further reduction of high Z impurities by the divertor.

Table II: X-Ray Anomaly Factors

Divertor	Ungettered	Gettered
Off	400	4.2
On	80	1.0

Higher densities ($\sim 2 \times 10^{19}$ m^{-3}) and currents ($\sim$ 75 kA) have been achieved with the divertor on but not yet reproducibly. Operation at higher density is important for obtaining better screening of low Z impurities. According to the standard model of the density limit, this should enable even higher densites to be achieved.

5.3 Instability

With increasing current or decreasing I_D/I_T, an instability sets in with a sharp threshold. The instability is observable on the loop volts, MHD coils, H_α and emission from outer (eg O II) but not inner (eg OVII) impurity states. There is still screening and power exhaust to the target. The phenomena appears to be associated with the presence of the q = 2 surface near the divertor separatrix, but this cannot be confirmed until more detailed measurements are made. The behaviour is variable but in one clear case the MHD m = 2 signal grows without rotation, presumably fixed by the divertor asymmetry, and drives a density sawtooth with reversal around the expected position of q = 2. A simultaneous break in the m = 2 growth and the sawtooth is accompanied by m = 1 activity, increased spectroscopic emission and increased voltage. The plasma appears to spill out like a minor disruption. The energy confinement time is appreciably reduced.

6. DIVERTOR WITH INJECTION

6.1 Heating

After preliminary experiments in 1977, we returned to this subject recently by injecting 200 - 450 kW at 16 keV into a discharge with a lower ratio $I_D/I_T = 1.5$ to obtain higher current I_g = 60 kA. The beam transmission was about 20% and large charge-exchange and orbit losses can be expected. The ion temperature was observed to double to 200 eV,

demonstrating power transfer to the plasma. For the electrons $\Delta T_e \sim 0$ with $T_e \sim 400$ eV. Deposition and power balances have not yet been performed but there was no deleterious effect of diversion.

6.2 Diversion

The increase in the central radiated power on injection is decreased by the divertor as shown in Fig. 20. The behaviour of the impurity emission on injection (Fig. 21), which was reported in § 4.2, precludes the measurement of screening efficiency with injection.

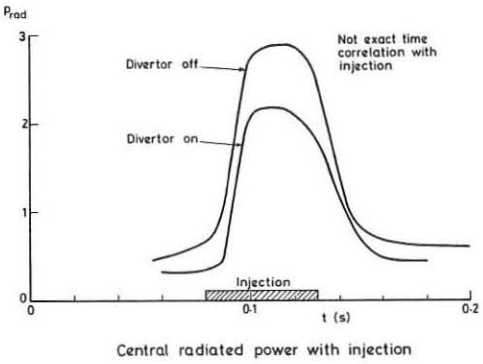

Central radiated power with injection

Fig. 20. Central radiated power on injection with and without diversion.

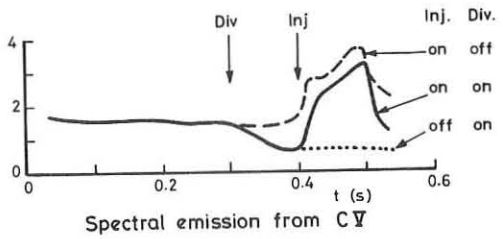

Spectral emission from C V

Fig. 21. Spectral emission from C V with and without diversion.

7. CONCLUSIONS

We report two new results (i) the combination of diversion and injection and (ii) the importance and variability of MHD activity. These promise a fruitful period of research.

8. ACKNOWLEDGEMENTS

The author wishes to acknowledge but not 'incriminate' his colleagues on DITE, particularly Drs J. Hugill, R.D. Gill, A.J. Wootton, S.J. Fielding, R.S. Hemsworth, W.H.M. Clark, D.J. Campbell, P.E. Stott (now on JET) and G. Proudfoot.

TOKAMAK STUDIES IN THE USSR

V.S. Strelkov

I.V. Kurchatov Institute of Atomic Energy, Moscow, USSR

The tokamak program has been successfully developing in the Soviet Union for almost 25 years - the first tokamak TMP started to work on February 1955 in the Kurchatov Institute. This program is now aimed at the construction of T-15 tokamak, which is intended to be the last step before a physical thermonuclear reactor, as regards its parameters and experimental tasks. The next step of studies will be performed in an international tokamak - Intor. It is assumed that T-15 maximum ion and electron temperatures will be 5-7 KeV, with plasma density reaching 10^{14} cm^{-3}, and the energy confinement time about 0.3 s. To achieve such parameters, two methods of supplementary heating are applied together with an increase of the tokamak size. Fast neutrals injection and VHF-heating on the electron cyclotron frequency are used as the ways of heating. The use of superconductors in the toroidal magnetic field coils makes it possible to increase the tokamak size without any significant increase of the power supply.

Since T-15 tokamak has no divertor, the impurity problem, i.e. the ways to decrease impurity density due to effective cleaning of the walls or appropriate choice of the wall material and limiters are regarded to be of the greatest importance both in modern and future experiments.

The main parameters of the Soviet tokamaks and the main directions of the studies are given in Table 1. The studies are obviously aimed at ohmic heating in circular and finger-ring geometry, VHF and HF heating of plasma, injection heating, cleaning

of the discharge chamber walls, quantitive impurity content and their dynamics during the discharge, divertor geometry and adiabatic heating.

T-10 tokamak. This tokamak has operated with a movable carbon limiter during last months, a stainless steel limiter having been used before this. Absolute amounts of iron, carbon and oxygen are given in Fig. 1 in the regimes with stainless and carbon limiters, and also the quantity of iron atoms deposited on the vacuum chamber walls during the discharge. These data were obtained from spectral measurements and Auger-analysis. Obviously the variation of the limiter material causes the change in the impurities. Iron is replaced by light impurities, namely, carbon and oxygen.

The use of hollow discharge cleaning of the chamber walls makes it possible to decrease the amount of light impurities both in stainless limiter regimes and in carbon limiter ones.

Good discharge reproducibility and low q values were obtained in the regimes with light impurities dominant.

Low q discharge oscillograms are given in Fig. 2, with the value q being equal to 1.6 at the limiter radius. Low q regimes are characterized by flat current profiles. The radius, where the phase of sawtooth oscillations of the soft X-ray radiation changes sign, is equal to 10-11 cm in $q = 2.1$ discharges, and 14-15 cm in $q = 1.6$ discharges. Low q regimes in the T-10 are characterized by a distinctive peculiarity which is the absence of the energy confinement time decrease observed in other tokamaks in $q < 2$ regimes.

Radiation losses study shows that in the T-10 from 60 to 80% of the input energy of the discharge fall to radiation. Radiation

losses are dominant in the central region of the plasma column and in periphery energy balance in iron impurity regimes. In carbon limiter regimes they are essential only in the periphery (Fig. 3). Iron density increase is observed during the plasma discharge, simultaneously light impurity density reaches its saturation. A slight increase of the power losses can be explained by this phenomenon in the central regions, together with their constancy in the periphery during long plasma discharges (τ_{pulse} = 1.4 S) (Fig. 4).

The discharge impurity dynamics is also studied in Ar injection experiments. The study of the time variation of Ar^{+16} line radiation shows that the confinement time of Ar is 40-60 ms in the plasma column. The study of the variation in time of Ar^{+16} recombination jump along different chords makes it possible to measure Ar^{+17} diffusion velocity in the center, because Ar^{+17} appears only in the central region of plasma. Comparison of time shifts of Ar^{+17} radiation over 15 cm and 25 cm chords shows that Ar^{+17} outward diffusion velocity is $4-5\cdot10^{2}$ cm/s (Fig. 5).

Electron cyclotron heating experiments were performed in the T-10 at 1.5 T magnetic field. The generator wavelength is 3.5 mm, and plasma heating is on the second harmonic of the electron cyclotron frequency.

VHF - power contributed to the plasma is 100-200 kW, and the ohmic heating power is 700-750 kW. The heating effect was observed by the soft X-ray signal intensity, the plasma diamagnetic effect, the loop voltage drop and the increase of heavy impurities high ionization states. The X-ray radiation spectrum is given in Fig. 6, obtained before and after VHF-heating; the time

variation of electron temperature is calculated using this spectrum for the central region of the plasma column. The variation of the diamagnetic effect derivative is given in Fig. 7 during heating pulse. Line radiation from high ionization states of chromium are given in Fig. 8. Lithium- and helium-like lines of chromium ions appear in the moment of VHF-heating.

It follows from Figs. 6 and 7 that the central regions of plasma cool with a characteristic time 40-50 ms when VHF-pulse is off, although the energy confinement time is 20-25 ms for the whole plasma column in this regime. The following observation points to good plasma thermal insulation of the region subjected to a VHF-pulse. The switch-on of VHF-power causes the decrease of ohmic heating power (because of the loop voltage drop), namely, 60-70 kW (Fig. 7). VHF power contributes 70-100 kW in this case, so that the total input power about 750 kW increases very insignificantly; plasma temperature however, increases from 0.9 to 1.1 keV in the central region.

Numerical simulations of plasma heating processes are given for a hybrid model, including the descriptions of convective processes appearing in the central regions of the plasma column, of relaxation oscillations mode with m = 1, n = 1 together with traditional equations of diffusion of current and temperature. The suggested model makes it possible to describe for the first time all experimental parameters of the relaxation oscillations, namely, their period, location, electron temperature oscillations amplitude, etc. Methodical calculations, using this model showed that the oscillations period τ_r is inversely proportional to the value of the electron thermal conductivity, $\tau_r \sim \chi_e^{-1}$, in a wide region of variation of all parameters. Comparing this result

with the known dependence also experimentally obtained in the T-10, $\tau_r \sim n_e$ (Fig. 9), we obtain a well-known equation $\chi_e \sim n_e^{-1}$. Thus numerical calculation makes it possible to determine the value of electron thermal conductivity in the region occupied with relaxation MHD oscillations. The value of electron thermal conductivity obtained is close to the neo-classical value at high plasma density, and at low density exceeds the latter value by several times, being equal to

$$\chi_e = 1{,}3 \cdot 10^{17} n_e^{-1} \text{ см}^2/\text{с}.$$

The results of numerical calculations of the electron temperature variation are given in Fig. 10 for the central region of plasma during the VHF-pulse, with current density and temperature profiles at different moments of time.

T-11 tokamak. The studies at this tokamak are aimed at injection heating of plasma with $Z_{eff} \simeq 1$ and low q values ($q < 2.5$). Hollow discharge cleaning of the chamber walls makes it possible to obtain plasma with $Z_{eff} \simeq 1$ in the T-11, where radiation losses do not exceed 15% of the ohmic power. Macroscopically stable discharges are obtained up to $q(a_L) = 1.2\text{-}1.4$. In this case, however, the energy confinement time is equal to 2 ms, which is 2-3 times smaller than in discharges with $q(a_L) > 2$.

Two injectors were used in the last T-11 experiments, with a total output power 600-650 kW. Ohmic heating power decreased to 22% of the total input power at the end of the injection pulse. The dose of radiation and charge-exchange losses increases from 10 to 40% (Fig. 11) during the process of injection. Moreover, the bolometer located within the injection port (P_1) gives a larger increase of radiation losses than the distant bolometer (P_2).

β_p value calculated using diamagnetic measurements equals 1.35, and the value

$$\beta_B = \frac{4\pi\left(\langle p_\parallel\rangle + \langle p_\perp\rangle\right)}{B_p^2}$$ reaches 2.1

as calculated from the equilibrium conditions. The value $\langle\beta_T\rangle_B = \beta_B\left(\frac{a}{R}\frac{1}{q}\right)^2$ is 2.5% in this case.

T- tokamak. The study of the influence of plasma currents on the superconducting magnetic system is the first task of this tokamak. The first tests of the superconducting winding demonstrated it working at 2.4 T magnetic field on the system's axis. The tokamak started to operate this year, with a maximum plasma current of 70 kA, toroidal magnetic field 1.5 T.

T-12 tokamak is a finger-ring tokamak with divertor magnetic geometry consisting of two poloidal divertors. Energising the divertor changes the discharge parameters; current amplitude increases and power flux to the limiter and chamber walls decreases. The last experiments were performed with the plasma displaced vertically relative to the equatorial plain. A two-separatrix, drop-like geometry appears in this case, when the inner diverted surface lies inside the outer one. The ratio of the plasma fluxes entering the divertors depends on the vertical displacement of plasma column. The shell provides the vertical stability of the T-12 plasma column. When the height of the plasma column decreases plasma becomes unstable in the vertical direction. Symmetric geometry appears to be more stable at small heights than the drop-like one. This vertical instability of a plasma column with small dimensions is an obstacle to achieving a T-12 regime with an expanding magnetic limiter.

The T-8 tokamak is a non-circular one, where feedbacks are

used to stabilize plasma in the vertical direction and over the major radius. The main task is to study the influence of the plasma column shape on the discharge parameters. The variation of electron temperature versus plasma column elongation is given in Fig. 12 for plasma center. Plasma energy and energy confinement time vary as the electron temperature, and the confinement time reaches 0.6 ms at $2\text{-}4 \cdot 10^{13}$ cm^{-3} plasma density.

TO-1 tokamak. A programme of screw instability studies was completed on this tokamak. A model where the simplest tearing-mode theory is supplemented by the consideration of plasma rotation in the plane of the minor radius of the torus, and the so-called inertial instability are in agreement with the obtained experimental results.

The switch-on of the feedback system leads to the suppression of m = 2 instability, a 1.5 times increase of the electron temperature and the increase of the energy confinement time from 0.5 ms to 1.1 ms. The following conclusions can be made based on the experiments; screw perturbations develop during the process of the plasma discharge and have the nature of tearing modes. These perturbations rotate along the minor radius of the torus at about 20 KHZ characteristic frequencies. These perturbations have stationary or pulsing amplitude showing their non-linear development. The non-linearity of the screw perturbations must be necessarily considered in analysing their suppression by a system of feedbacks.

FT-1 device. Low hybrid ion heating experiments were performed here. The variation of the electron temperature profile and density 2.5 ms after the HF pulse start is given in Fig. 13. The increase of the electron energy was 35% due to heating. The maximum increase of temperature is 100 eV at ζ = 4 cm. However,

no T_e increase is observed in the periphery at r > 8 cm. Obviously this fact points out the cooling of periphery by impurities appearing during HF-power pulse. Central ion temperature increased from 70 to 100 eV.

More than 50% of the input HF power was absorbed by the plasma during the low hybrid heating, and 30-50% of this power went to heating electrons. The portion of energy accepted by ions is 20-30%, moreover, the main part of this energy goes to the formation of fast ions.

Tuman-2A and Tuman-3 devices are intended for the adiabatic compression of plasma by toroidal magnetic fields. Experiments to study the mechanism of the improved plasma thermal insulation previously observed are performed in Tuman-2A during compression.

Tuman-3 device started to work late in 1978; after commissioning studies of the plasma column equilibrium were performed.

TO-2, a tokamak with two toroidal divertors, is now ready for operation.

Concluding this survey of Soviet tokamak studies, the following must be noted.

A stable regime with good reproducibility is obtained in the T-10 with dominant light impurities and $q(a_L) = 1.6$.

The first electron cyclotron heating experiments confirm the conclusions of earlier studies concerning high efficiency of this method.

High β plasma was obtained in the T-11 experiments, moreover, plasma stability was not disturbed there.

Radiation losses are dominant in the energy balance in the major part of experiments; impurities obviously contribute

greatly to the process of current profile formation, which, in its turn, determines the stability of the plasma column. The development of inner instability, which opposes compression, depends on radiation cooling which determines the plasma current profile.

Thermal conductivity factors appear to be connected with the parameters of relaxation oscillations. The mathematical model developed makes it possible to obtain the values of thermal conductivity factors from the experimental data.

The nature of the screw instability is studied and methods developed for its suppression by feedback.

Adiabatic compression causes not only plasma heating but also improves its thermal insulation.

The improvement of thermal insulation is observed in non-circular tokamaks when greater elongations of plasma columns are used.

Finally I wished to thank my Soviet and foreign colleagues who have worked or are working now on Soviet tokamaks, for presented data and assistance in the completion of this paper.

Table 1

Tokamak	R	A_{lh} (m)	A_l (m)	B (T)	B_{max}^{exp} (T)	I_{max}^{exp} (kA)	Main directions of studies
T-15	2,4	0,75	0,7	3,5	0	0	The acquition and studies of plasma with parameters close to the thermonuclear ones
T-10	1,5	0,39	0,29-0,36	5	4,5	650	Joule heating. Electron cyclotron heating. Impurities.
T-11	0,7	0.235	0,14-0,22	1,5	1,2	170	Injection heating. Walls cleaning.
T-12	0,36	0,08	0,075	1.0	0,8	50	Non-circular cross-section. Divertor studies.
T-8	0,28	0,048	0,04	1,0	0,9	24	Non-circular cross-section. The studies of influence of cross-section elongation on the parameters of plasma.
T-7	1,22	0,35	0,31	3	2,4	70	The first tokamak with superconducting toroidal coils.
TO-1	0,60	0,18	0,125	1,5	0,8	35	Screw instabilities suppression.
FT-1	0,62	0,2	0,15	1,2	1,0	35	Low hybrid frequency heating.
Tuman-2A	0,4	0,08	0,8	2,2	2,0	12	Adiabatic heating studies.
Tuman-3	0,55	0,23	0,15	3,0	1,0	90	Adiabatic heating studies.
TM-3	0,4	0,1	0,08	6,0	4,0	75	Ohmic and UHF - heating studies.
TM-4	0,55	0,1	0,085	4,0	0	0	Ohmic and UHF - heating studies.
TO-2	0,6	0,18	-	1,8	0	0	Toroidal divertor studies.

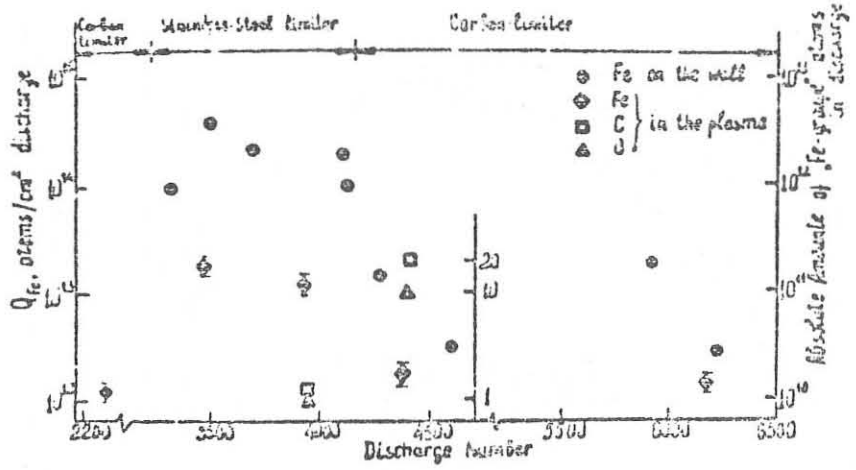

Fig.1. T-10 impurity content variation.

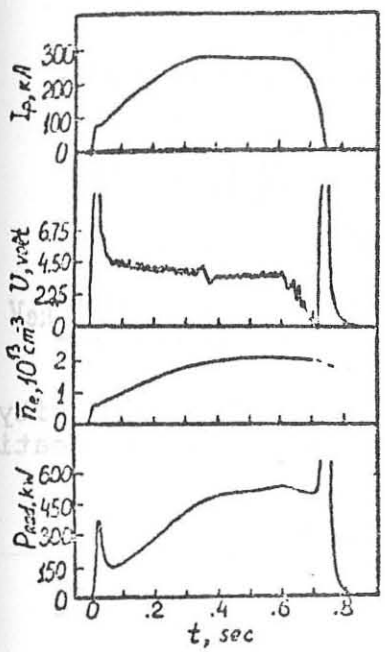

T-10 B_T=1.5 T , q(a.)=1.6

Fig.2. Regime with $q(a_L)=1,6$.

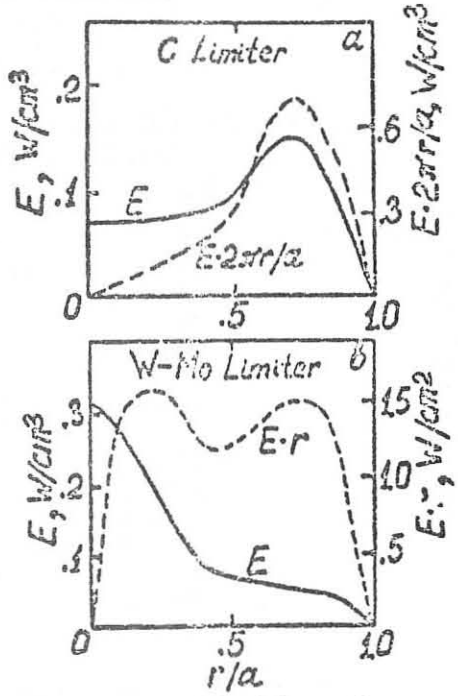

Fig.3. Radiation losses profile on T-10.

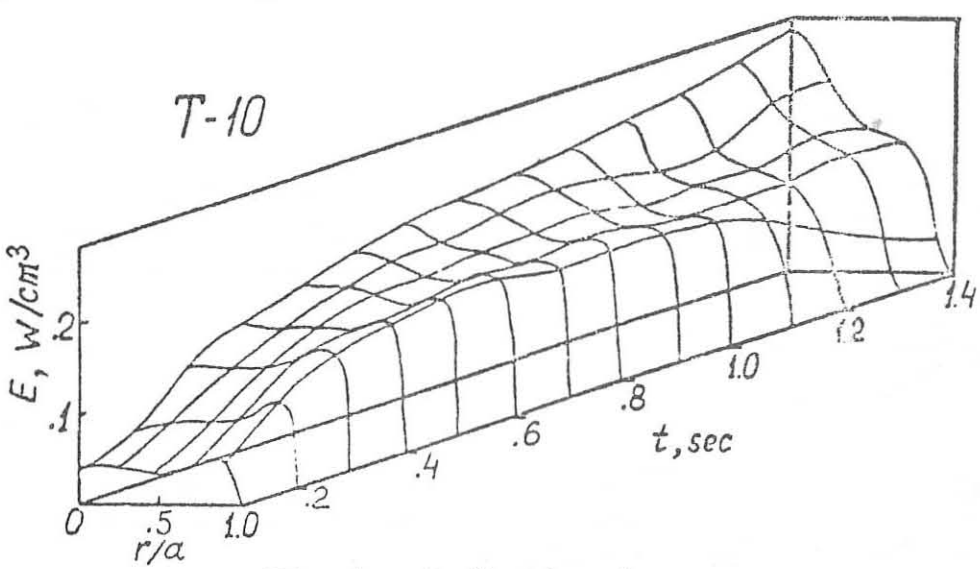

Fig.4. Radiation losses - time variation

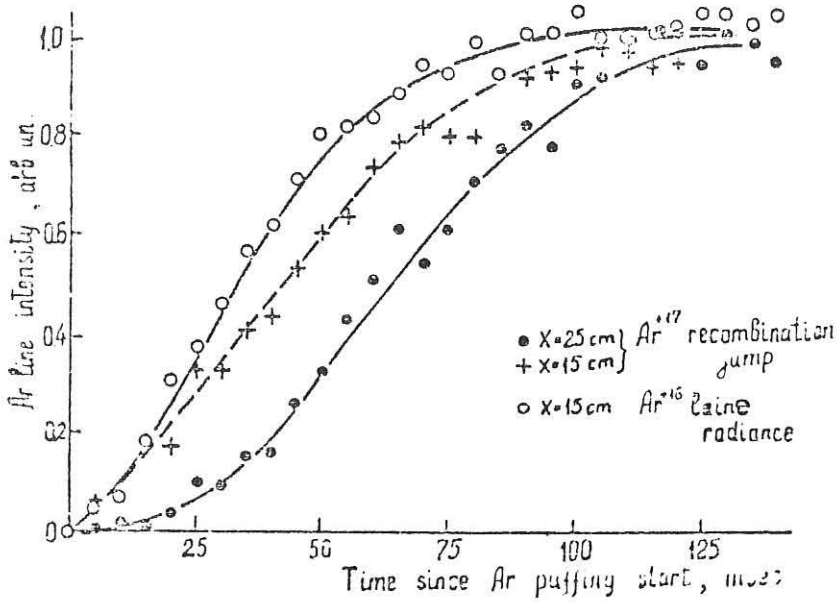

Fig.5. Ar line radiance variation.

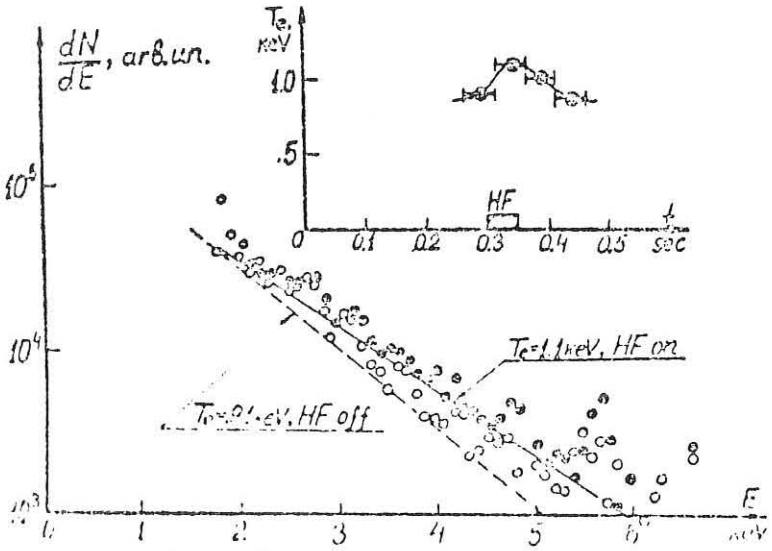

Fig.6. X-ray spectrum.

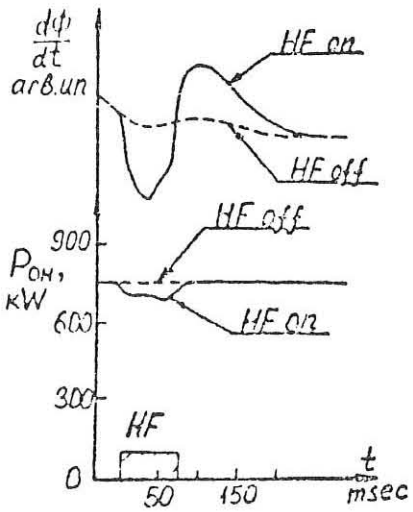

Fig.7 Derivative of the diamagnetic signal $d\phi/dt$ and the ohmic power P_{OH} in regimes with and without r.f. heating.

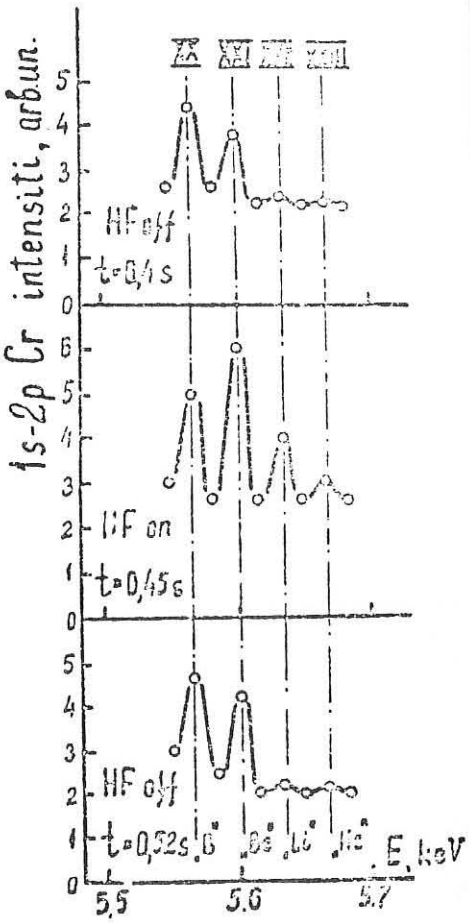

Fig.8. Cr line intensity variation during HF heating.

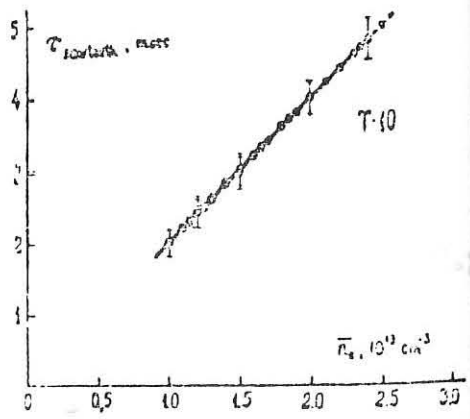

Fig.9. Sawtooth oscillation period versus average electron density.

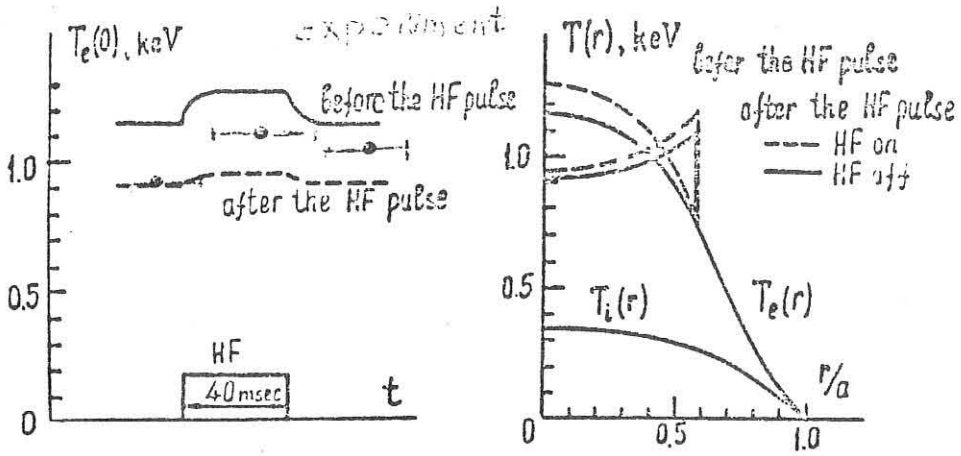

Fig.10. HF heating computer simulation.

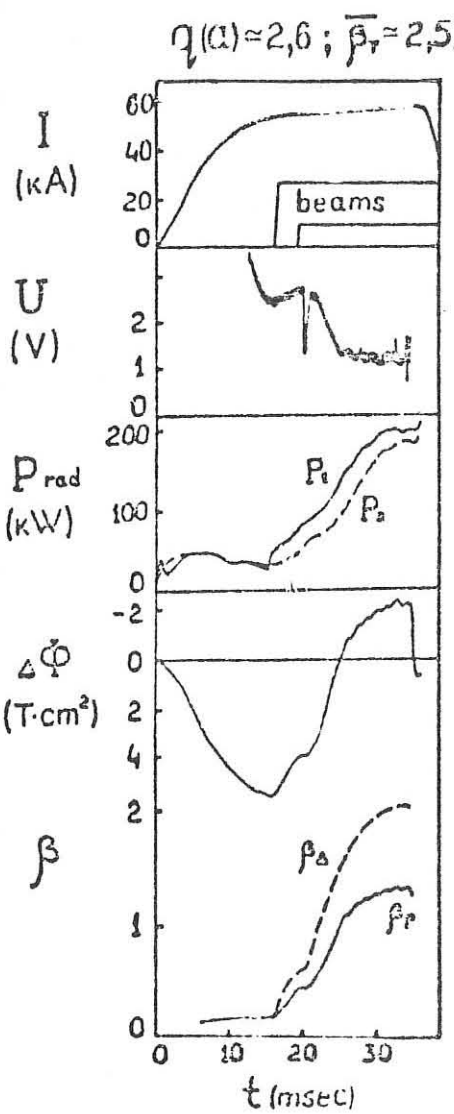

Fig.11. Two beam heating on T-11.

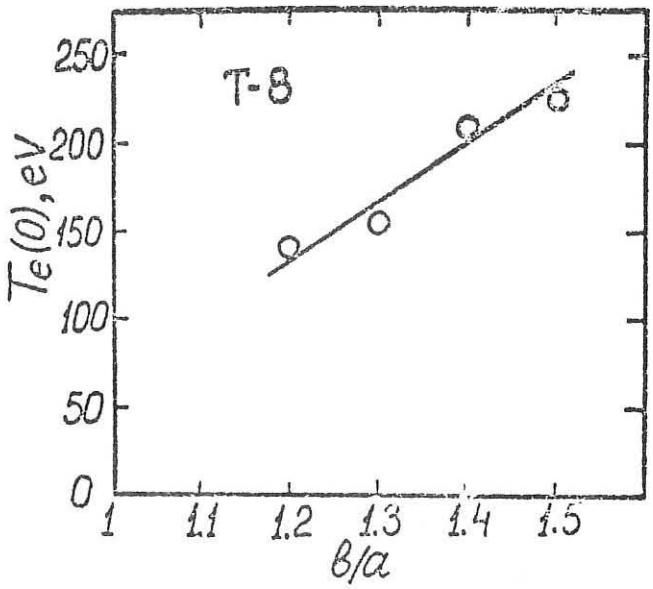

Fig.12. Central electron temperature $T_e(0)$ as the function of plasma elongation b/a.

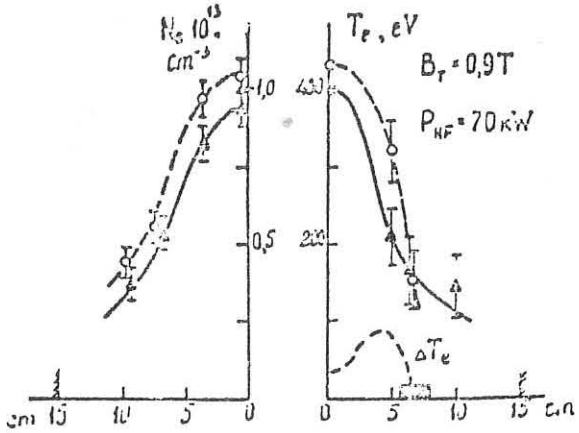

Fig.13. Electron heating during HF heating.

THE PHYSICS OF JET

R J Bickerton

JET Joint Undertaking, Culham, Oxfordshire, England

INTRODUCTION

The Joint European Torus (JET) is a large tokamak at present under construction on the Culham (UK) site. JET is an international enterprise with participation by the nine countries of the Common Market plus Sweden and Switzerland. It is therefore a political as well as a technical experiment. The basic parameters, the technical design and some prototype work were established in the period 1973-78 by the Joint Design Team headed by Dr P-H Rebut[1]. The site was decided in October 1977 and the construction phase began in mid-1978 under the leadership of Dr H-O Wüster. Operation of the machine with plasma is scheduled to begin in 1983.

The objectives of JET are to study

(i) the scaling of plasma containment as parameters approach the reactor range;

(ii) the plasma-wall interaction in these conditions

(iii) plasma heating;

(iv) α-partical production, confinement and effects on plasma stability.

Objective (iv) has the consequence that the machine is designed for tritium operation and is scaled so that it can, to the best of our limited knowledge, reach conditions where the α-particle heating in the central core of the plasma plays a significant role in the local energy balance. Tritium operation implies considerable technical complications in the provision of neutron shielding and of arrangements for remote maintenance of the machine.

APPARATUS

The principal parameters of JET are listed in Table 1 together with those of two other large machines at present under construction, JT-60 (Japan) and TFTR (USA). Also shown are the present guiding parameters for INTOR, a high duty cycle tritium burner now being discussed by an international working party under IAEA auspices in Vienna. Note the designed-in extension

capability of JET represented by the bracketted figures. The plasma and toroidal field coil cross-sections for the four devices are shown on the same scale in Figure 1. Both JET and INTOR use D-shaped plasmas of similar cross-sectional dimensions. Space for a shielding and breeding blanket is provided between the plasma and the coils in the INTOR design. An artist's view of JET is shown in Figure 2. Notable are the double-walled D-shaped vacuum vessel, the closely coupled toroidal and poloidal coils together with the 8-legged iron transformer core.

ADDITIONAL HEATING

Large volume tokamaks need powerful heating in addition to the inescapable ohmic dissipation if they are to reach near-reactor parameters. This is the result of the relatively low current density and the rapid ($T^{3/2}$) increase in plasma conductivity as the electron temperature rises. Adiabatic compression and neutral injection heating are two well-proven methods. Both have been shown to work in an entirely intelligible way at the megawatt level.[2,3] Adiabatic compression is a one-shot heating method. The only practicable version for JET is that in which the major radius of the plasma is reduced by increasing the vertical field. This necessitates a plasma filling only a fraction of the cross-section of the vacuum vessel. JET has been designed to be capable of using adiabatic heating with a compression ratio of up to 1.4 and a compression time approximately 50 ms. The mean minor radius of the plasma is then limited to about 1 metre and the plasma current correspondingly to approximately 1 MA. The power into the plasma during compression is of the order of 20 MW. This mode of operation is only better than using the full aperture and no compression if the plasma losses increase rapidly with temperature, as in the trapped-ion scaling or if the impurity problem is very severe [4]. Since the failure of the trapped ion mode to limit the temperature in PLT [3] the mood is now more optimistic and the main emphasis is on full aperture operation.

Thus the additional heating method that will be used initially is that of neutral injection. The parameters of the planned system are shown in Table 2. The very large 80 kV, 120 A, 5 second pulse hydrogen ion source units required are under development at Culham and Fontenay. Later it is envisaged that these same units will be further developed towards 160 kV, 60A deuterium operation for eventual injection into deuterium-tritium plasmas. The overall efficiency defined as the ratio of neutral power injected into the torus at full energy to the extracted power is only 13%. Initially 8 sources will be installed to give 10 MW at full energy into the machine. Later it is planned to increase the heating power to a total of 25 MW. The additional 15 MW is part of an "extended performance"

proposal not yet approved or funded. The extra power might be provided by RF methods if an experimental demonstration at approximately 1 MW level is given in time on an existing tokamak. Thus the realistic choice is between ion cyclotron resonance and lower hybrid frequencies or of just more neutral injection.

PLASMA EQUILIBRIUM

A key feature of JET is the non-circular (D-shaped) plasma cross-section. This is believed to be favourable for containment and we represent this feature by using $\bar{a} = \sqrt{ab}$ for the mean plasma radius when predicting the containment time. The D-shape is also favourable for MHD stability; we represent this by assuming the effective inverse aspect ratio to be $\bar{a}/R$ and that the critical average β value for stability is proportional to this number.

The experimental evidence for these favourable features is not extensive, but both JET and INTOR rely on their exploitation to achieve near-ignition and ignition conditions respectively. The shape of the JET plasma is to be controlled by the predetermined ratios between the currents in the various poloidal coils while the position of the discharge centre is to be maintained by horizontal and vertical feed-back controlled fields.

PERFORMANCE ESTIMATES

As we move towards ignition a simple performance indicator is the ratio f between the α-power into the plasma and the power lost from the plasma. Ignition is clearly achieved when $f = 1$. Because the product $(\bar{\sigma v})$ for D-T reactions varies like T_i^2 in the temperature range of interest, (7 - 20 keV) then f is determined by the product $(\bar{n}\tau_\varepsilon \bar{T}_i)$, i.e.,

$$f = \frac{(\bar{n}\ \tau_\varepsilon\ T_i)}{\gamma . 2.5\ .10^{21}} \qquad (m^{-3}, sec, keV) \qquad ..(1)$$

where γ is a profile factor which is unity for a uniform density and parabolic temperature dependence. γ decreases as profiles steepen. For a given f the corresponding $\bar{\beta}$ value is,

$$\bar{\beta} = \frac{2\bar{n}\bar{T}_i}{B_\phi^{\ 2}/8\pi} = \frac{8.5\times10^{-2}\gamma f}{\tau_\varepsilon . (B_\phi^{\ 2}/8\pi)} \qquad ..(2)$$

while the power into the plasma required to maintain a given f value is

$$P = \frac{V.3\bar{n}\bar{T}}{\tau_\varepsilon^{\ 2}} = \frac{V.f\ 1.3\times10^6}{\tau_\varepsilon^{\ 2}} \quad \text{Watts} \qquad ..(3)$$

where V is the plasma volume.

Because of the contribution from alpha particles as ignition is approached the input power P_{IN} required to reach ignition in a time comparable with the energy containment time is about half the above figure. For JET the results for B = 3.4T (extended performance) are,

$$\bar{\beta} = \frac{18.\gamma f}{\tau_\varepsilon} \quad \% \qquad ..(4)$$

$$P_{IN} = \frac{96\gamma f}{\tau_\varepsilon^2} \quad \text{Megawatts} \qquad ..(5)$$

From these results we see the critical importance of the energy containment time in determining what performance can be achieved with given values of critical β and of input power.

EVIDENCE ON τ_ε

There is much experimental data on τ_ε in ohmically heated tokamaks and some recent data for experiments in which the additional heating (neutral injection) substantially exceeded the ohmic input. Only in the latter case can the heating and confinement be decoupled to enable an in-principle determination of the variation of containment time with plasma temperature. However the available data is still too limited to come to a clear conclusion on this point, but preliminary indications from PLT are optimistic [3].

For the present the simplest, although not the most accurate, law for all the data is,

$$\tau_\varepsilon = 0.5 \times 10^{-20} \bar{n}a^2 \quad (m^{-3}, m, sec) \qquad ..(6)$$

Figure 3 shows sample data and the line representing (6). Note that this law covers discharges with varying fractions of radiated power and charge exchange losses. It has no theoretical basis. Indeed it does not satisfy the criteria established by Connor and Taylor [5] for scalings based solely on the equations of plasma physics. The near-ignition regime in JET is expected to have $\bar{n}a^2 \sim 2.5 \times 10^{20} m^{-1}$ i.e. $\sim$ 25 times the highest experimental data point on figure 3. A variety of more complex scaling laws [6,7] have been proposed to give more accurate representations of the existing data. Applied to the JET case they lead to a range of predictions for τ_ε in extended performance of 0.6 - 6 seconds. This uncertainty means that JET might ignite easily ($\tau_\varepsilon >$ 2 seconds) or fail to reach near-ignition ($\tau_\varepsilon <$ 1 second).

If we adopt the ALCATOR/INTOR scaling of equation (6) then it is readily shown that for a given input power and negligible alpha-power (small f) the mean temperature is independent of the density and for JET is

$$\bar{T} \text{ (keV)} = \frac{P_{IN}(MW)}{6} \qquad ..(7)$$

while $$\bar{\beta} = \frac{P_{IN}(MW)n_{20}}{8} \quad \% \qquad ..(8)$$

for $B_\phi = 3.4T$,

and $$\bar{\beta} = \frac{P_{IN}(MW)\bar{n}_{20}}{5} \quad \% \qquad ..(9)$$

for $B_\phi = 2.7T$.

PERFORMANCE WITH OHMIC HEATING ONLY

The modus operandi of the machine will be to establish a hot plasma with ohmic heating before switching on the additional heating. We might expect the q profile as a function of poloidal flux to be determined by this phase since the classical skin penetration time is about one minute for a 1 metre radius plasma with $\bar{T}_e \sim 1$ keV. The q-profile established, the subsequent evolution is supposed then to follow the flux-conserving path as the plasma pressure is increased by additional heating. There is little or no experimental support for this supposition; internal rearrangements of poloidal flux may well take place through MHD instabilities of the tearing-mode type. Thus the evolution of the discharge remains uncertain but one certainty is that the ohmic phase must establish a plasma of adequate density for neutral injection, remembering that the injection energy will be chosen primarily to give good penetration at the higher densities near ignition.

It is well known that there is a density limit for ohmic discharges above which the discharge disrupts. This "Murakami limit" has been shown [8] to be fairly well described by the empirical formula,

$$\bar{n}_c = 2 \times 10^{19} \frac{B_\phi}{R} \quad (T,m) \qquad ..(9)$$

Higher figures can be obtained in exceptionally clean and high q ($\sim$5) discharges but equation (9) gives a good working figure for $q \sim 3$ discharges. From (9) the figures for JET are,

$\bar{n}_c = 1.8 \times 10^{19} m^{-3}$ for standard performance

$\bar{n}_c = 2.3 \times 10^{19} m^{-3}$ for extended performance

For perpendicular neutral injection into JET at 80 keV/nucleon $\sim$ 32% of the beam passes right across the plasma for $\bar{n} = 2 \times 10^{19} m^{-3}$. But the injection geometry in JET is such that the beam although near perpendicular when it enters the plasma is quasi-tangential to the inside plasma boundary. Consequently most of the beam that is not absorbed on the first pass has a second passage through the plasma. Thus the effective fraction of the beam that is not absorbed is probably $\sim$ 10%.

Note that because of the "Murakami limit" the product $\bar{n}a^2$ is $\sim 5 \times 10^{19} m^{-1}$ so that the extrapolation on the τ_ε vs $\bar{n}a^2$ diagram (Figure 3) is only a factor 5 over present experiments. Thus we may be reasonably confident that the containment time during the ohmic heating phase will be $\sim$250 ms.

Balancing the ohmic heating against the losses then gives for JET,

$$\bar{T}_e = 0.67 \text{ keV for } I_p = 5 \text{ MA (extended performance)}$$

$$\bar{T}_e = 0.45 \text{ keV for } I_p = 3 \text{ MA (standard performance)}$$

where the corresponding ohmic input powers are 4 and 2.7 megawatts respectively. These figures are consistent with the results of time-dependent 1-D codes where central temperatures of 1.2 keV are obtained with $I_p = 4$ MA in pure plasma with the primary loss determined by the ALCATOR/INTOR scaling.

PERFORMANCE WITH ADDITIONAL HEATING

A basic assumption is that with an increased power input to the discharge the density can be increased several-fold above the "Murakami limit" to the point where the critical β is the determining factor. Only if this assumption is correct can the $\sim$1 - 2 second containment time needed be obtained according to the ALCATOR/INTOR scaling. The experimental evidence for this is weak; in both DITE and ORMAK, discharges with neutral injection could be run at higher densities (factor 1.5) than those without. Since there is no clear theory to account for the "Murakami limit" there is equally no clear theoretical basis for the assumption that increased power density will permit $\bar{n}_c$ to be raised. However such theories as there are [9,10] suggest that qualitatively $\bar{n}_c$ does depend on the power density.

Consider now two cases - standard performance with an injected power of 10 MW at full energy, $B_\phi = 2.7$ T, and extended performance, 25 MW full energy and $B_\phi = 3.4$ T. From the global model given above we find,

	$\bar{T}_i$(keV)	$\bar{\beta}$(%)	$\bar{n}_{20}$	τ(secs)	γf
Standard	1.7	2.8	0.9	1.0	0.10
Extended	4.2	4.3	0.9	1.0	0.24

In fact the total injection power including all species is 18 and 45 MW respectively; we have used the perhaps pessimistic assumption that only the full energy power is effective.

STABILITY LIMITS TO $\bar{\beta}$

There will be some value $\bar{\beta}_c$ above which the plasma is hydromagnetically unstable to the point where the containment is seriously reduced. To

date this limit has not been seen in any experiment and $\bar{\beta}$ values have essentially been limited by the available additional heating power. Values of $\bar{\beta} \sim 2\%$ have been seen on the circular cross-section plasmas in the TOSCA[11] and ISXB[12] tokamaks. These values are somewhat higher than the theoretical threshold values for high mode number ballooning modes. Similar calculations applied to JET show $\bar{\beta}_c \sim 7\%$, the higher figure coming from the shaped cross-section and tight aspect ratio. The value of $\bar{\beta}_c$ depends crucially on obtaining an optimum equilibrium profile, one with flat pressure and current density profiles over most of the volume. In present tokamaks these profiles are uncontrolled and result from a complex interplay between wall and plasma processes. We can hope that the discharge will be driven towards optimum profiles by the self limiting action of marginal stability or we may be forced to expensive additional measures to control positively these processes, (e.g. electron cyclotron heating, multi-energy neutral beams, multi-frequency RF heating etc).

If we combine the ALCATOR/INTOR scaling with the notion that the discharge will be limited at some $\bar{\beta}_c$, then we find a maximum value for f,

$$f_{MAX} = \frac{6 \times 10^{-4} \beta_c^{\,2} B_\phi^{\,4}}{\gamma \bar{T}} \qquad (\%, \text{ Tesla, keV})$$

for JET dimensions. The highest value of f is obtained for the lowest value of $\bar{T}$ for which the calculation is valid, namely 7 keV. Then for $\bar{\beta}_c = 7\%$ we find,

$$f_{MAX} = \frac{0.54}{\gamma} \quad \text{for} \quad 3.4 \text{ Tesla}$$

corresponding to $\bar{n} = 1.4 \times 10^{20} m^{-3}$, $\tau_\varepsilon = 1.8$ seconds and $f_{MAX} = \frac{0.25}{\gamma}$ for $B_\phi = 2.8$ Tesla, corresponding to $\bar{n} = 0.9 \times 10^{20} m^{-3}$, $\tau_\varepsilon = 1.1$ seconds.

1-D STEADY STATE CALCULATIONS

So far we have considered global calculations in which profiles are assumed and are not determined self-consistently. The next step in complication is to use a code to solve the radial energy balance in steady state. Cordey et al[13] have performed such calculations for JET balancing alpha-particle heating against neo-classical ion conduction and electron thermal conduction corresponding to the thermal diffusivity

$$\chi_e = \frac{5 \times 10^{19}}{n_e} \qquad m^2 sec^{-1}$$

(This gives the ALCATOR/INTOR containment result (equation 6) for parabolic density and temperature profiles). The resulting ignition curve is shown in Figure 4. Comparing this with the global condition (1) and

substituting from (6) leads to the very favourable value of $\gamma \sim 0.25$. This is the consequence of a steeper temperature profile in the 1-D calculation which both improves the ratio of alpha-power to losses and reduces the losses.

Changing the containment law to either of the versions proposed as a result of the PLT experiment gives still more favourable ignition curves (Figure 4). Since in all cases the loss through the electron channel is dominant the results are insensitive to modest (factor 5) increases in the ion thermal conductivity.

1-D TIME DEPENDENT CALCULATIONS

1-D time dependent calculations are run in cylindrical geometry with 'toroidal' transport coefficients and an effective radius $\bar{a} = \sqrt{ab}$ to account for the D-shape. Some JET runs have been made using the codes BALDOR(Düchs, IPP), MAKOKOT (Mercier, Fontenay), HERMES (Hughes, Culham) and ICARUS (Watkins JET). In addition many of the calculations made by these and other code groups around the world for INTOR can be simply scaled to JET.

The standard transport assumptions are now.

$$\chi_e = \frac{5 \times 10^{19}}{n_e} \qquad m^2 s^{-1}$$

$$\chi_i = 3 \times \text{Neoclassical (Hazeltine-Hinton)}$$

$$D = \tfrac{1}{4} \chi_e = \text{particle diffusion coefficient.}$$

The recycling coefficient for particles at the wall is normally taken to be unity, so that average density increases only occur by beam fuelling action. Because of the surface nature of the recycling the density profile in steady state is extremely flat.

All the codes show that in the absence of impurities ignition can readily be achieved on JET with the extended performance injection power level of 25 MW at full energy (160 keV deuterium) and the corresponding total power of 45 MW all species. Figure 5 shows a typical trajectory (from HERMES) in $\bar{n}a$ vs. $\bar{\beta}$ space. Again these results are more optimistic than the global calculations and correspond to low values of γ.

To include impurity effects in a self-consistent way we have to deal with three areas of ignorance. These are,

(i) the surface physics phenomena leading to impurity injection.

(ii) the subsequent radial motion of impurities inside the plasma

(iii) the relationship between local impurity concentration and radiated power.

All four European codes use the coronal equilibrium relationship for (iii). With MAKOKOT they then simply determine the fractional contamination of the plasma with a given impurity that stops ignition. For JET this is 5×10^{-4} of iron. The other three codes determine the impurity concentration by combining a sputtering model at the wall and a diffusion model in the plasma. The most apparently pessimistic assumptions are used by the JET group. They assume sputtering of iron by both ions and neutrals at the wall and solely Pfirsch and Schlüter diffusion without temperature screening inside the plasma. They find that the inclusion of this impurity model stops ignition [14]. Some of their results are shown in the $\hat{n}\,\tau_\varepsilon$ vs $\hat{T}_i$ plane in Figure 6. Similar results have been obtained by Düchs with a more optimistic model in which sputtering of carbon and iron by neutrals only is used together with the sum of Pfirsch and Schlüter (including temperature screening) and anomalous diffusion for the motion inside the plasma.

The sensitivity of these results to the models is not yet clear but taken together they do emphasize that JET is very unlikely to reach ignition if any remotely realistic account is taken of impurities.

However it should be noted that, even with the pessimistic (?) JET model, conditions are reached in the core of the plasma where the alpha-power is about 70% of the total power into that volume ('core' = half the plasma radius). This means that although ignition is not achieved nevertheless the objective (iv) of the JET list is reached.

CONCLUSIONS

1. The physics of JET will in broad terms have the same elements as the physics of any other tokamak. Thus although we have discussed JET in simplistic terms the standard complicating features such as internal and major disruptions, discharge cleaning requirements, runaways, etc., will occur and require to be lived or dealt with.

2. In the light of the best present knowledge JET will have the clear capability in extended performance of investigating near-ignition plasmas. But 'best present knowledge' is poor and includes an order of magnitude uncertainty in the key parameter, the energy containment time.

3. The expected temperatures may be summarised as follows

Ohmic heating $\bar{T}_e \sim \bar{T}_i \sim 0.5$ keV $\tau_\varepsilon \sim 250$ ms

Standard performance $\bar{T}_e \sim \bar{T}_i \sim$ 1-3 keV $\tau_\varepsilon \sim$ 1 second

Extended performance $\bar{T}_e \sim \bar{T}_i \sim$ 6 keV $\tau_\varepsilon \sim$ 1 second

4. To achieve near reactor conditions in JET will require
   (i) an increase in the critical density over the "Murakami limit" by a factor of 4 to 5.
   (ii) the full exploitation of the shaped cross-section and the establishment of optimum pressure and current profiles to permit high critical $\bar{\beta}$ values.
   (iii) the reduction of middle and high Z impurities to very low fractional levels ($< 5 \times 10^{-4}$).
   (iv) the operation of effective heating methods which can deposit 10-20 MW of power into the core of the plasma.

ACKNOWLEDGEMENTS

I acknowledge useful discussions with and information received from Drs A Gibson, M Watkins, J G Cordey, M H Hughes, D E T F Ashby, D Düchs, C Mercier and J Hugill.

REFERENCES

1. P Noll, Proceedings of 7th European Conference on Controlled Fusion and Plasma Physics, (Lausanne). Vol II, 91, (1975)

2. K Bol et al. Proceedings of 5th International Conference on Plasma Physics and Controlled Nuclear Fusion (Tokyo), Vol. I, 83, (1974)

3. H Eubank et al. Proceedings of 7th International Conference on Plasma Physics and Controlled Nuclear Fusion (Innsbruck), Vol. I, 167, (1978).

4. B J Green, P Noll and J Sheffield, Plasma Physics 17, 1101, (1975).

5. J W Connor and J B Taylor, Nuclear Fusion, 17, 1047 (1977).

6. J Hugill and J Sheffield, Nuclear Fusion, 18, 15, (1978).

7. W Pfeiffer and R E Waltz, Nuclear Fusion, 19, 51 (1979).

8. M Murakami, J D Callen and L A Berry, Nuclear Fusion, 16, 347 (1976).

9. A Gibson, Nuclear Fusion, 16, 546 (1976).

10. P H Rebut and B J Green, Proceedings of 6th International Conference on Plasma Physics and Controlled Nuclear Fusion (Berchtesgaden), Vol. II, 3, (1976).

11. K McGuire, D C Robinson and A J Wootton, Proceedings of 7th International Conference on Plasma Physics and Controlled Nuclear Fusion, (Innsbruck) Vol. I, 335 (1978).

12. D W Swain et al. 9th European Conference on Controlled Fusion and Plasma Physics, (Oxford) Vol. 1, 44 (1979).

13. I Robertson, J G Cordey and J J Field, Proceedings of Varenna Conference Workshop, August 1979.

14. M L Watkins and A Gibson, 9th European Conference on Controlled Fusion and Plasma Physics, (Oxford), Vol. I, 164 (1979).

RJB/JC

TABLE 1

	JET	JT60	TFTR	INTOR
R_o(m)	3.0	3.0	2.65	4.5
a(m)	1.25	0.95	0.85	1.2
b(m)	2.10	0.95	0.85	1.9
$\bar{a}$(m)	1.6	0.95	0.85	1.5
B_ϕ(T)	2.7(3.4)	4.5	5.2	5.0
I_p(MA)	3.8(4.8)	2.7	2.5	4.0
$q(\bar{a})$	3.0(3.0)	2.5	2.8	3.1
FLAT-TOP TIME FOR B_ϕ SECONDS	20(15)	5.0	1.6	∞ Super-conducting coils
VOLT-SECONDS AVAILABLE	25(34)	25.0	14.0	?
PLASMA VOLUME(m^3)	150.0	53.0	38.0	200

Footnotes

(I) Bracketted figures correspond to extended performance

(II) a = half-height of plasma, parallel to major axis

(III) b = half-width of plasma in the equatorial plane

(IV) $\bar{a} = \sqrt{ab}$ = mean plasma radius

(V) $q(\bar{a}) = \frac{5\bar{a}^2 B_\phi}{R_o I_p}$ = "cylindrical" q

TABLE 2

NEUTRAL INJECTION HEATING

	JET
BEAM ENERGY (keV)	80(160)
BEAM TYPE	$H_2(D_2)$
BEAM POWER (MW)	
(i) FULL ENERGY	10(25)
(ii) TOTAL	18(45)
NO. OF INJECTOR BOXES	2(4)
NO. OF SOURCES PER BOX	4
ANGLE OF INJECTION	TANGENTIAL AT R_o -a $\sim 70^o$ AT R_o +a
SOURCE SPECIFICATION	120A x 80kV 5 SECONDS (60A x 160kV, 5 SECONDS)
ESTIMATED OVERALL EFFICIENCY	13%

Bracketted figures correspond to extended performance, or to later developments

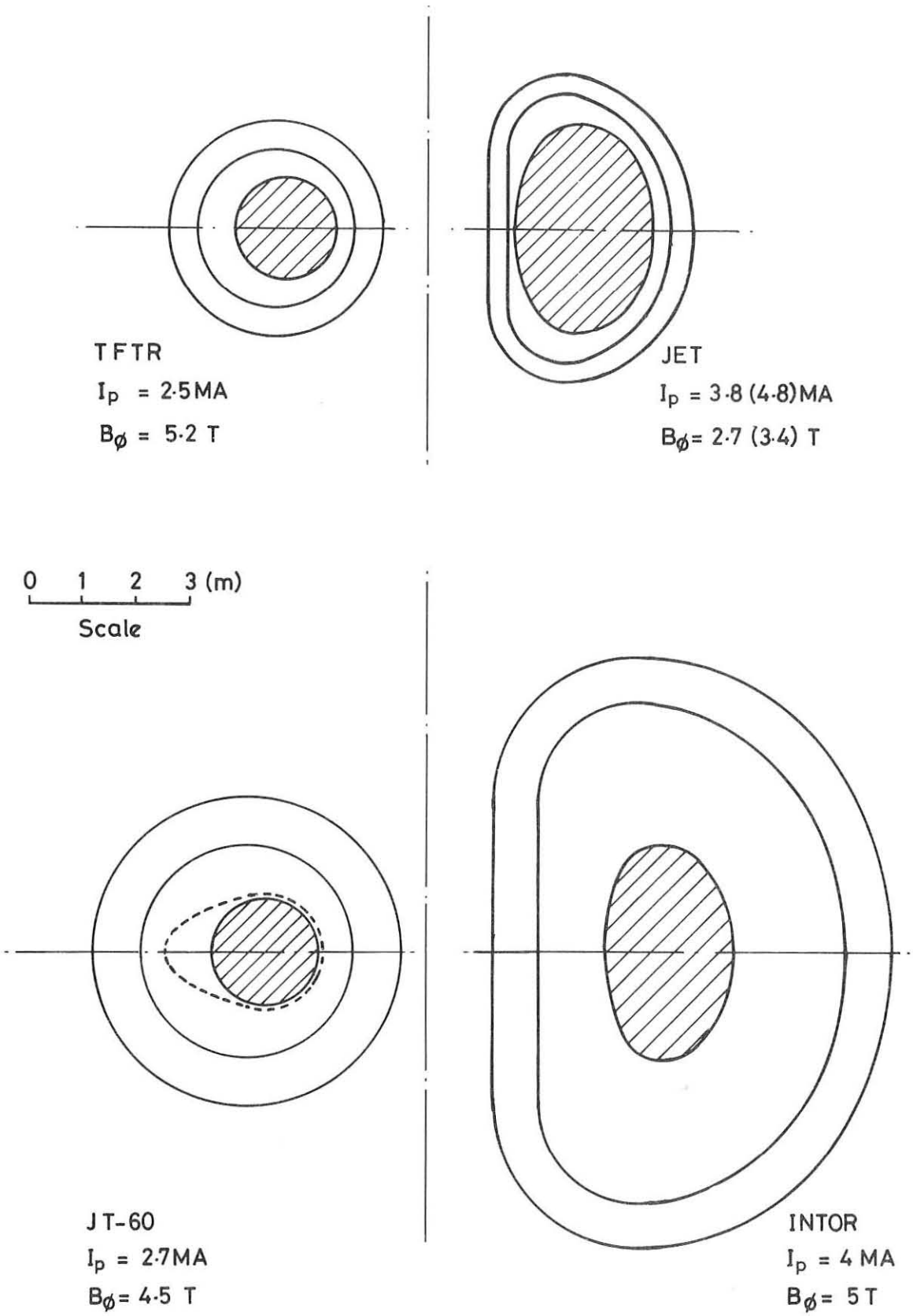

Figure 1. Plasma and toroidal field coil cross-section.

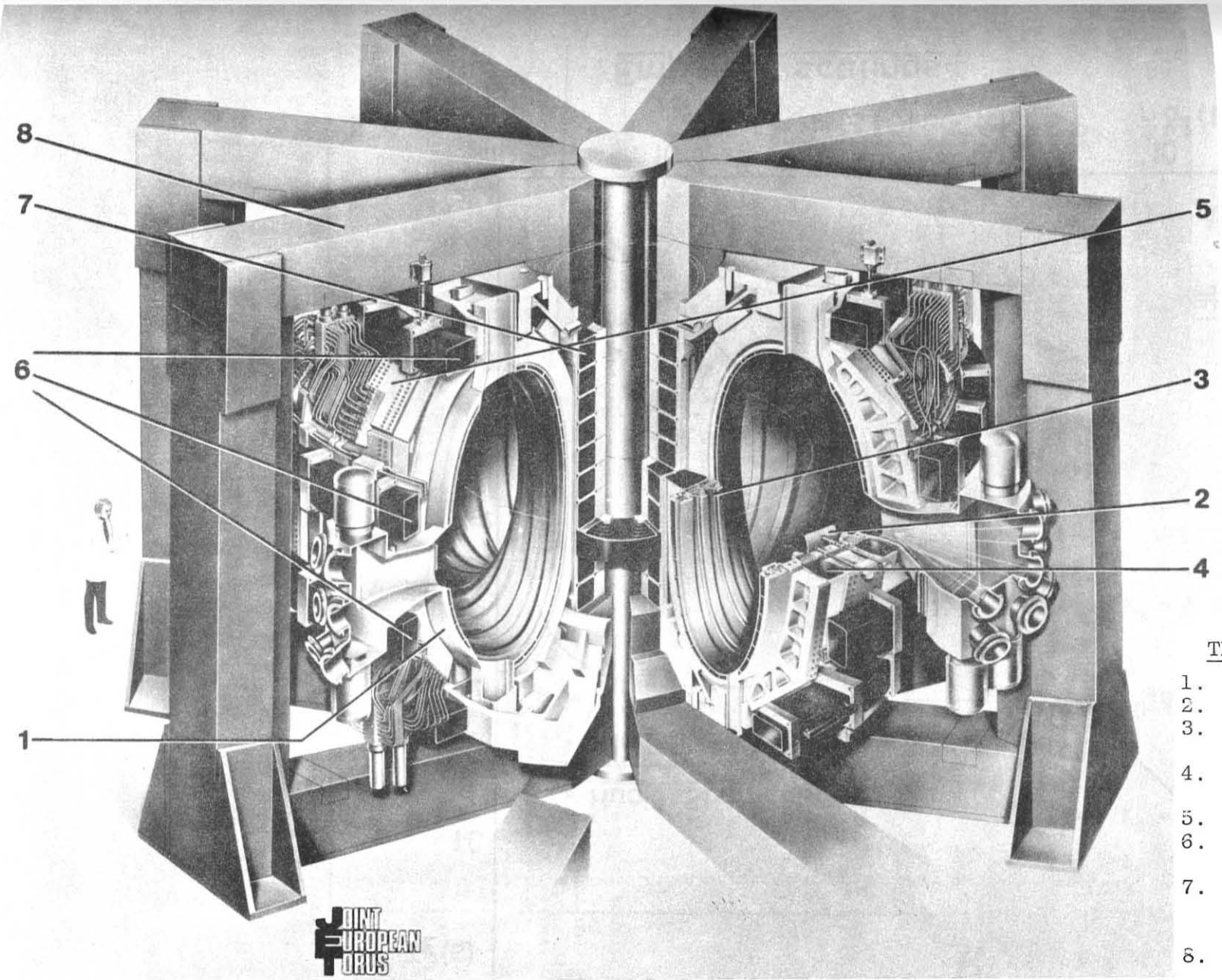

THE JET APPARATUS

1. Vacuum vessel
2. Limiter plates
3. Poloidal protective shields
4. Toroidal field magnet
5. Mechanical shell
6. Poloidal field coils
7. Poloidal field coils - primary windings
8. Iron transformer core

FIG. 2

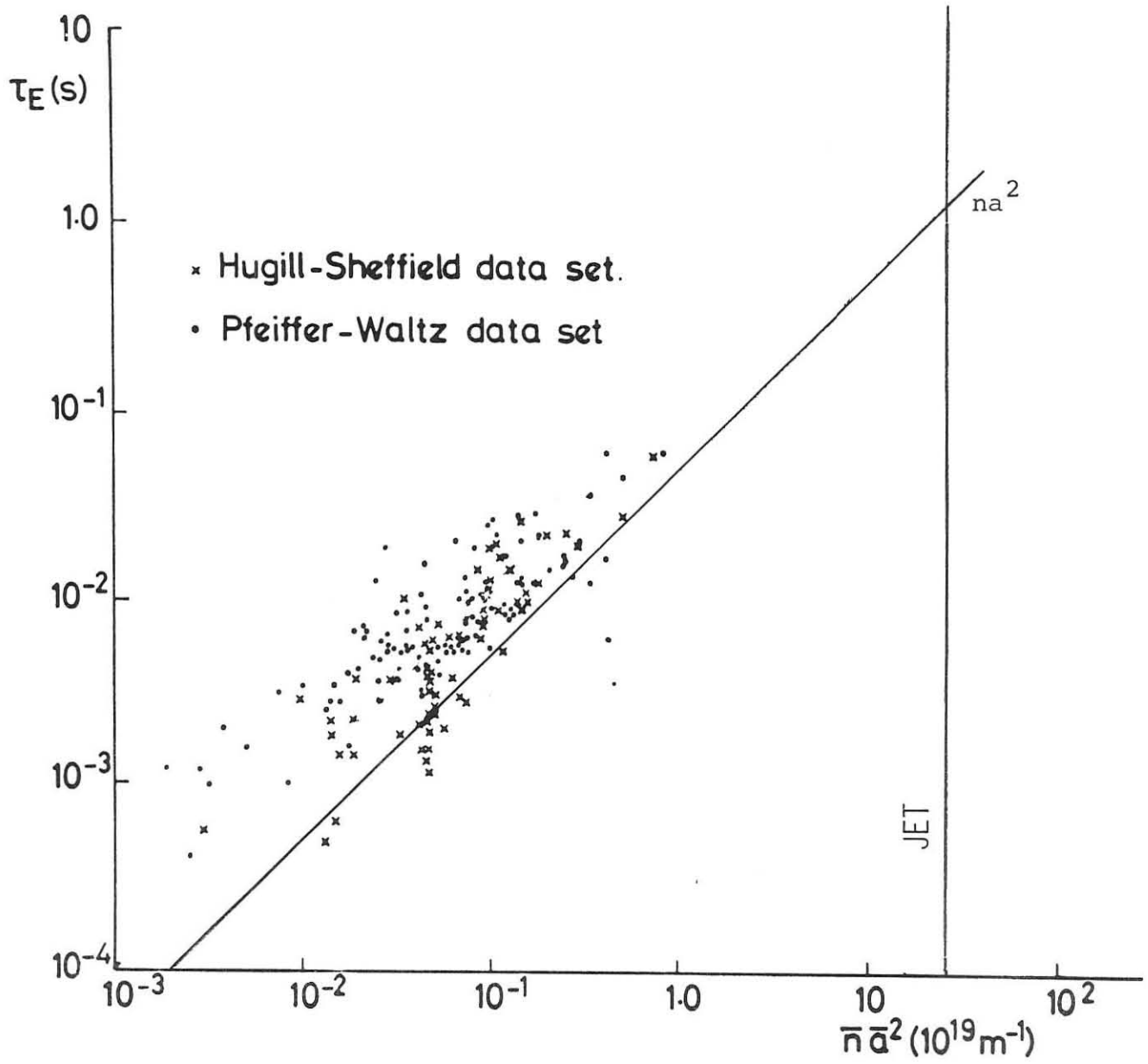

FIGURE 3 Empirical scalings

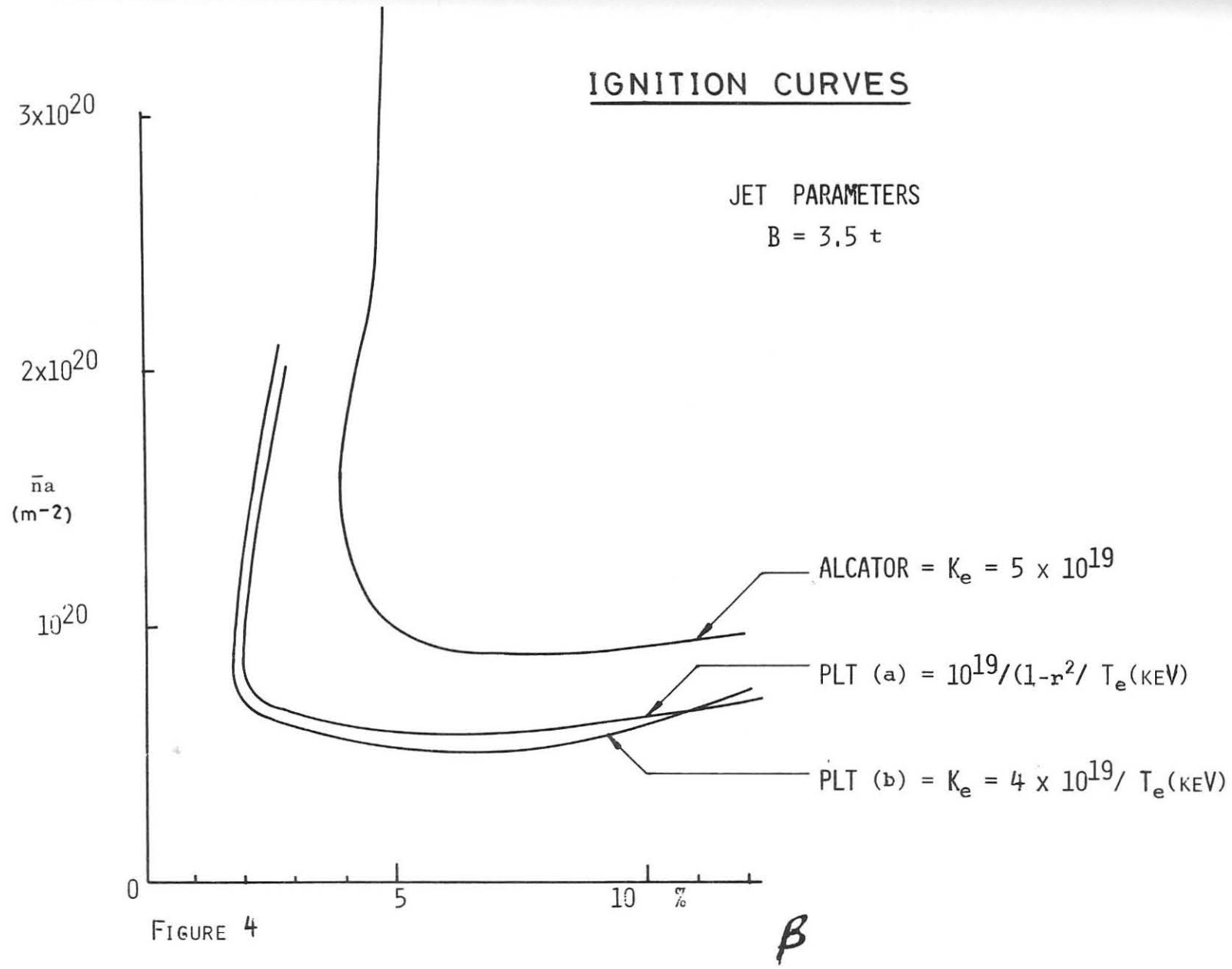
IGNITION CURVES
JET PARAMETERS
B = 3.5 t
3x10^20
2x10^20
10^20
0
n̄a
(m-2)
5
10
%
β
ALCATOR = K_e = 5 x 10^19
PLT (a) = 10^19/(1-r^2/ T_e(KEV)
PLT (b) = K_e = 4 x 10^19/ T_e(KEV)

FIGURE 4

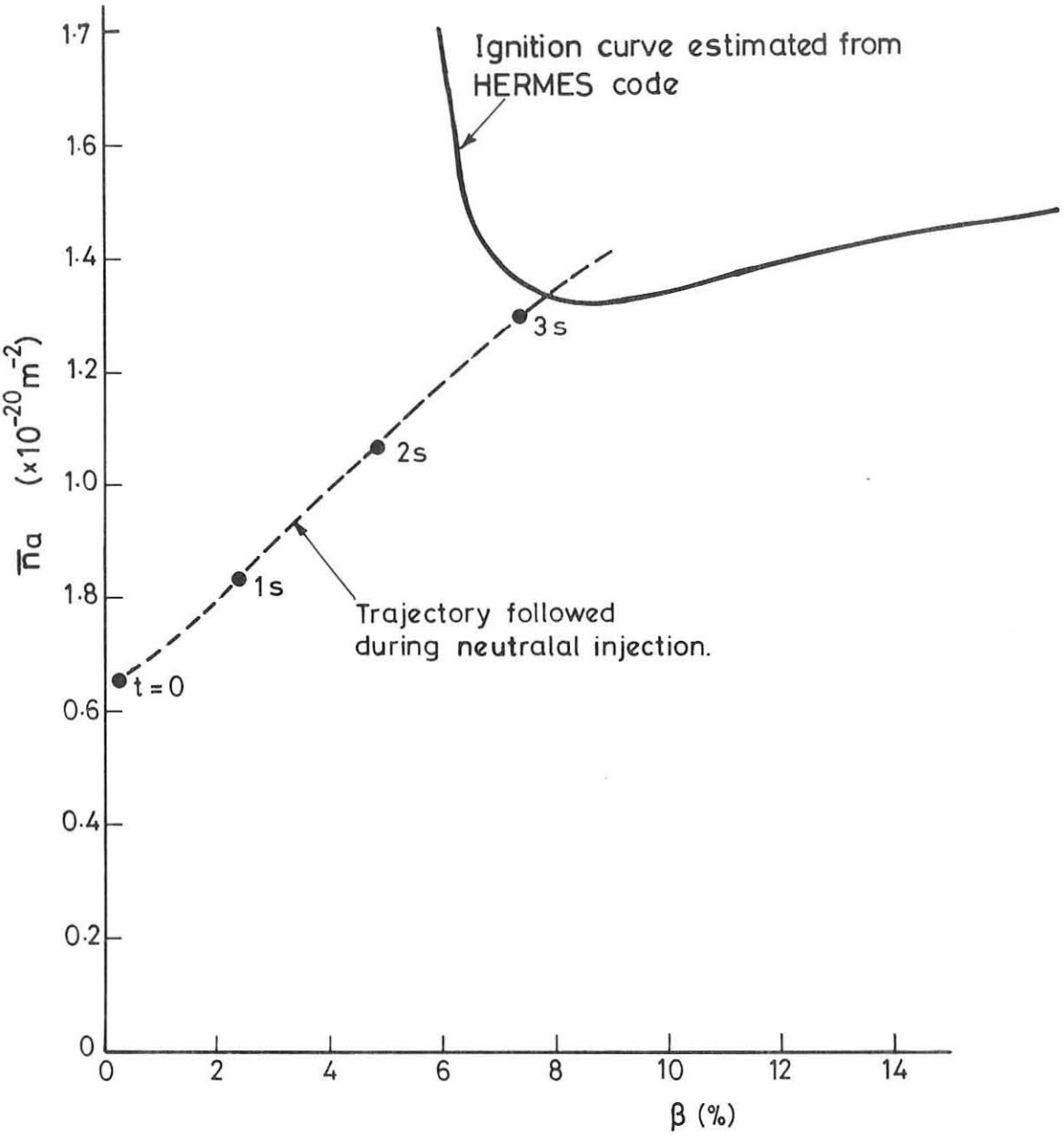

Fig. 5 JET Injection into ohmic steady state - no impurities
E_B = 120 keV , P = 45 MW
(M.H. Hughes, Culham)

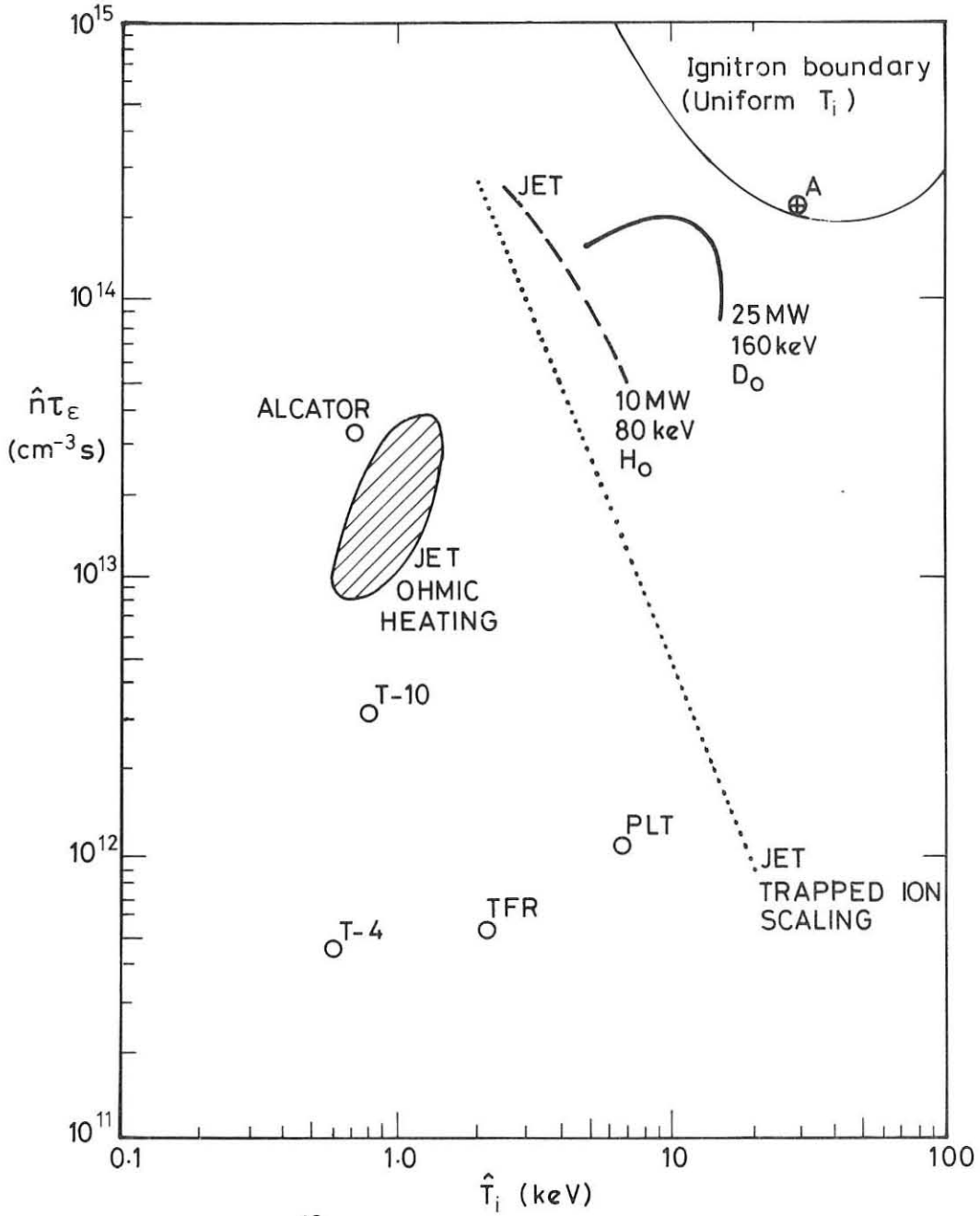

——— $X_e = \frac{510^{19}}{n}\ m^2s^{-1}$, $D = \frac{X_e}{4}$, X_i = neo-classical , plus radiation from sputtered iron (25MW D_o at 160 keV)

– – – – As above , (10MW H_o at 80keV)

Point A Transport as above, no impurity radiation (25MW D_o at 160 keV)

Figure 6. JET performance predictions.

INVESTIGATION OF LASER FUSION PHYSICAL PROCESSES

V.B. Rozanov
P.N. Lebedev Physical Institute, USSR Acad. Sci., Moscow, USSR

1. A lot of problems are interrelated in laser fusion: the problems of powerful lasers and optical systems; the study of physical processes in targets; target preparation and optimization; the development of physical-mathematical models for irradiation, compression and target burning and the calculation codes; various reactor problems, e.g. energetic, economic and systemization problems, and the problems of materials technology.

2. In the present paper we report mainly the results obtained from physical investigation of targets, irradiated by laser pulse at moderate fluxes, when the "compressed" shell (abalative mode) regime is realized. The processes considered are as follows:

   - laser radiation absorption with regard to refraction and reflection;
   - generation of fast electrons in the corona, which cause preliminary heating of the thermonuclear fuel;
   - thermal radiation of the corona;
   - heat-conductivity and evaporation of the shell;
   - acceleration and the motion of the shell towards the center, characterized by hydrodynamic efficiency;
   - hydrodynamic instabilities at compression;
   - magnetic field generation;
   - transformation of shell kinetic energy into the thermal DT plasma energy;
   - thermonuclear reaction initiation and the development of the combustion wave.

   Here arises the problem of distinguishing the role and estimating quantitative characteristics of these processes in modern small-scale experiments, as far as possible, and to determine the ten-

dency and predict the changes in the processes under the increase of the laser pulse.

3. Mathematical codes "Luch" and "Rapid", based on classical ideas of the laser target corona, describe the laser radiation absorption processes, the electron heat-conductivity, hydrodynamic motion. The comparison is presented of the experimental (obtained at Nd-Laser "Kalmar") and theoretical data in particular the dependence of the absorbed energy fraction on the target size and the ablator material, the shell velocity and collapse time, the measurements and simulations of various gasdynamic profiles (e.g. the profile containing a shock wave reflected from the centre of the target and passing the "corona"). These results may serve as evidence of a satisfactory description of the "compressed" shell regime. Analytical models are developed, which enable one to easily describe the shell evaporation and motion, and the gas compression. These results in total give a possibility to obtain similarity relations which may help to predict analogous parameters for the next generation laser "Dolphin".

4. Calculations of X-ray radiation, based on "RIM" code, and the measurements make it possible to find out its influence on the energy balance and hydrodynamic parameters of the "corona" and the compressed core of the target. For "compressed" shell the influence of radiative transfer is not strong. Non-equilibrium ionization, which affects the most hard part of the spectrum, is of importance. The quantity of fast electrons is proportional to the energy fraction, absorbed by resonance mechanism and does not exceed 1%. Taking into account the fact that the shell optical thickness grows ($E^{1/3}$) with the increase in laser energy, one may expect the fast electrons' heating not to be considerable. Profile "steepening" at moderate fluxes is of no significance.

5. Stationary corona model allows one to develop an approximate theory of gas compression by thin target which describes well the average temperature, density and compression values. For studying more sophisticated problems such as gasdynamic distributions, the effect of the state equation, the effects of the velocity multiplication at shell collisions we have used one-dimensional gasdynamic programmes.
6. We have studied the conditions in the target core dependent on the energy absorbed, the gas pressure, the radius and thickness of the target wall, the symmetry of preparation and irradiation of the target (for "Kalmar" experiments). At high compression of deuterium the temperature lies within the range where the neutron yield sharply depends on the temperature (0.2-0.6 keV). The experiments are in conformity with the theory and calculation.
7. Under target compression the magnetic fields are generated. Magnetic field generation is connected with the development of hydrodynamic instability, which results in crossed gradients of the density and temperature. Magnetic field generation is performed in the hydrodynamic instability region in the external and internal side of shell. Various dissipation processes are responsible for the maximal magnetic field amplitude. Near the collapse the field inside the target exceeds 20 MGs (under conditions at "Kalmar"). The magnetic field could serve as the means of observation and diagnostics of the instability. This field may influence different processes in laser targets, specifically on the transport of fast electrons from the "corona", and the heat-conductivity from internal "hot" regions.
8. The problem of thermonuclear reaction initiation in laser targets is studied. The initial plasma state is presented conveniently by a point on the plane (ρ, T). Numerical simulations make it possible to predict the development of thermonuclear reactions at

arbitrary initial state with account of temperature, density and velocity variations at compression. However, it is convenient to study generally the development of thermonuclear reaction by using so-called dynamic coefficients, which are analogous to self-similar constants in the problem of thermonuclear wave. One of such coefficients describes the variations of plasma energy, the other- the optical thickness. Under arbitrary non-self-similar initial conditions time variations of the dynamic coefficients present a certain trajectory corresponding to the development or decay of thermo - nuclear reaction.

9. The analysis of the dependence of various processes on the laser pulse energy within the frames of the "compressed" shell regime suggests that the following may take place in case of 200-300 kJ energy:

- absorbed energy will constitute 50-80% (in comparison with 30-40% at "Kalmar" for 100-200 J energy);
- heating by fast electrons will be insignificant;
- evaporable part of the shell will be 50%, and hydrodynamic efficiency at aspect ratio 100 will be 10-15% (at present the values 3-5% have been achieved). This corresponds to the increase of shell velocity up to 300 km/sec (at present velocities of 70-100 km/sec have been measured);
- volume compression of 3.10^4 needed for obtaining the DT plasma density of 300-400 g/cm^3 (which ensures efficient combustion) exceeds more that by one order of magnitude the measured compression. Nowadays there are no available experimental data on the influence of instability processes at 3.10^4 compression; the problem is being studied theoretically;
- experiments and numerical calculation indicate a possibility of the shell kinetic energy to be sufficiently well transformed into thermal energy of thermonuclear fuel, and it will constitute 10% of the laser pulse energy. Under these conditions a sufficient thermonuclear target burning can be realized.

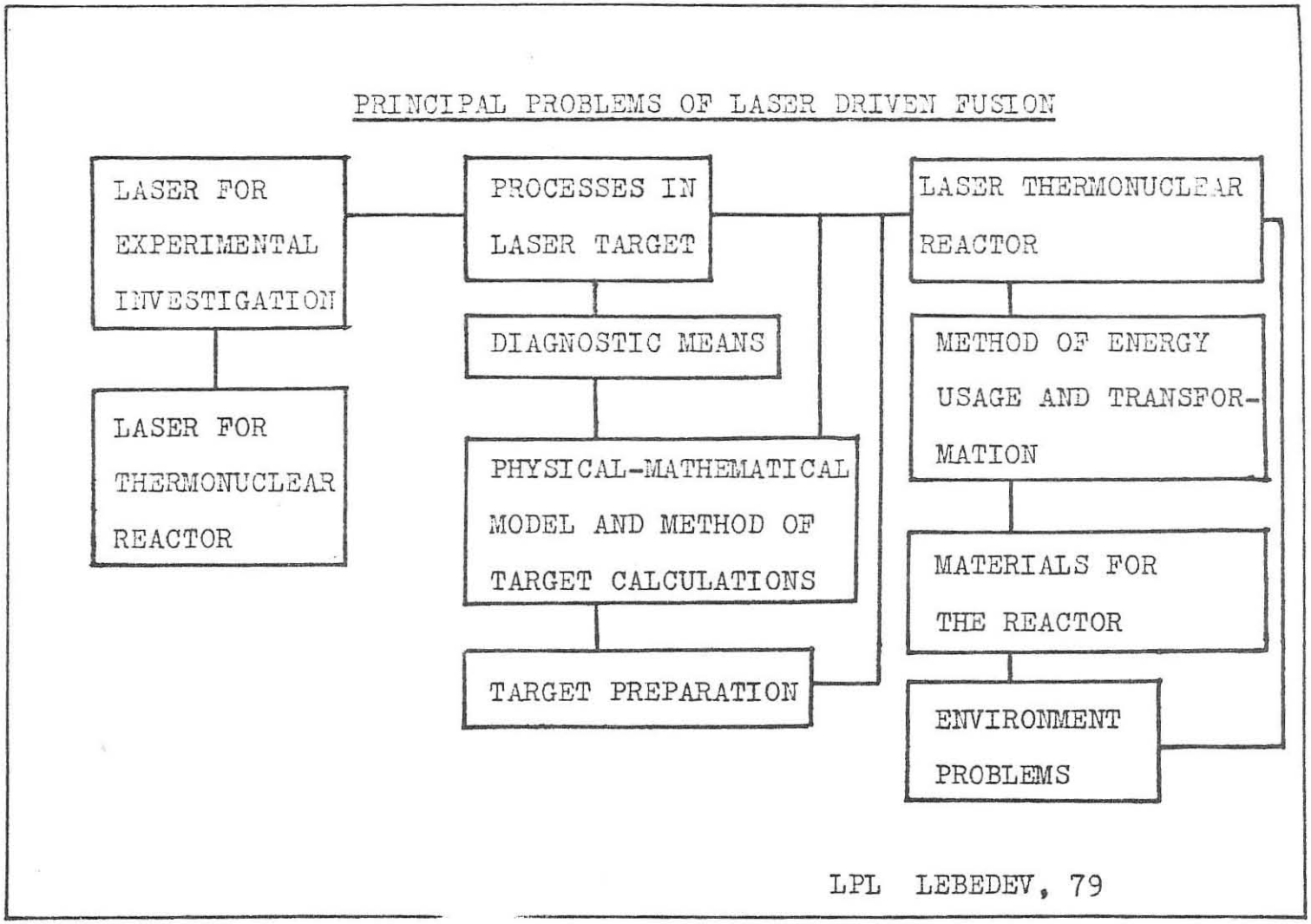
PRINCIPAL PROBLEMS OF LASER DRIVEN FUSION
LASER FOR EXPERIMENTAL INVESTIGATION
LASER FOR THERMONUCLEAR REACTOR
PROCESSES IN LASER TARGET
DIAGNOSTIC MEANS
PHYSICAL-MATHEMATICAL MODEL AND METHOD OF TARGET CALCULATIONS
TARGET PREPARATION
LASER THERMONUCLEAR REACTOR
METHOD OF ENERGY USAGE AND TRANSFOR-MATION
MATERIALS FOR THE REACTOR
ENVIRONMENT PROBLEMS
LPL LEBEDEV, 79

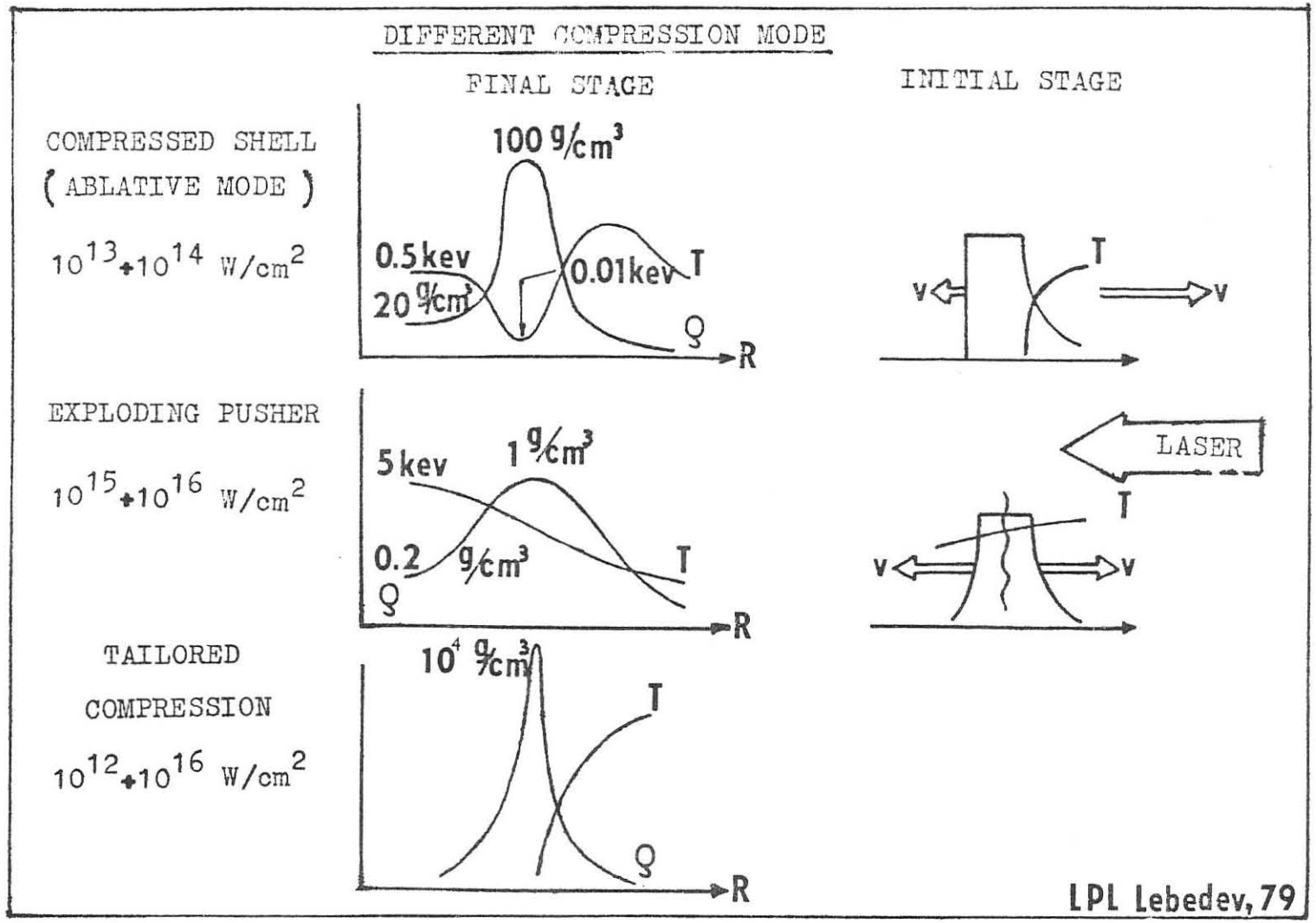
DIFFERENT COMPRESSION MODE
FINAL STAGE
INITIAL STAGE
COMPRESSED SHELL
(ABLATIVE MODE)
10^{13}÷10^{14} W/cm^2
100 g/cm^3
0.5kev
20 g/cm^3
0.01kev
T
ϱ
R
v
T
v
EXPLODING PUSHER
10^{15}÷10^{16} W/cm^2
5kev
1 g/cm^3
0.2 g/cm^3
T
ϱ
R
LASER
T
v
v
TAILORED
COMPRESSION
10^{12}÷10^{16} W/cm^2
10^4 g/cm^3
T
ϱ
R
LPL Lebedev, 79

ABSORPTION OF LASER RADIATION (CODE RAPID)

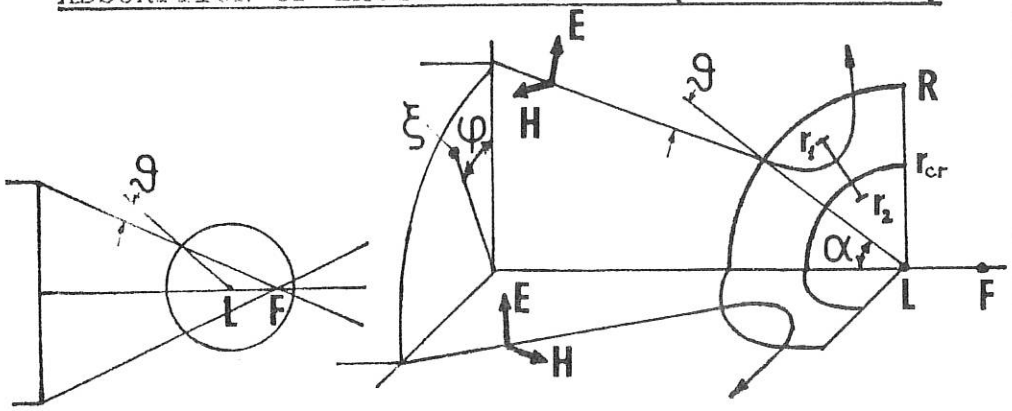

RAY TRACE AND REGION OF WAVEOPTICS PROBLEM

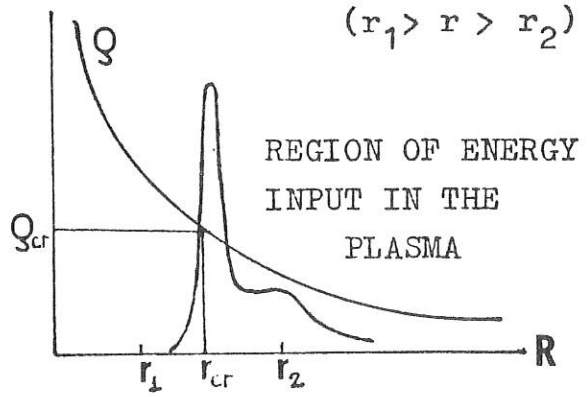

ENERGY ABSORPTION FOR TARGET R=50-100 μm

λ μm	τ ns	Mode	E_{abs}/E_{las}	Resonant absorption
1.06	2.0	compressed shell	30%	1%
1.06	0.1	exploding pusher	25%	50-70%
10.6	2.0	exploding pusher	20%	80-90%

LPL Lebedev, 79

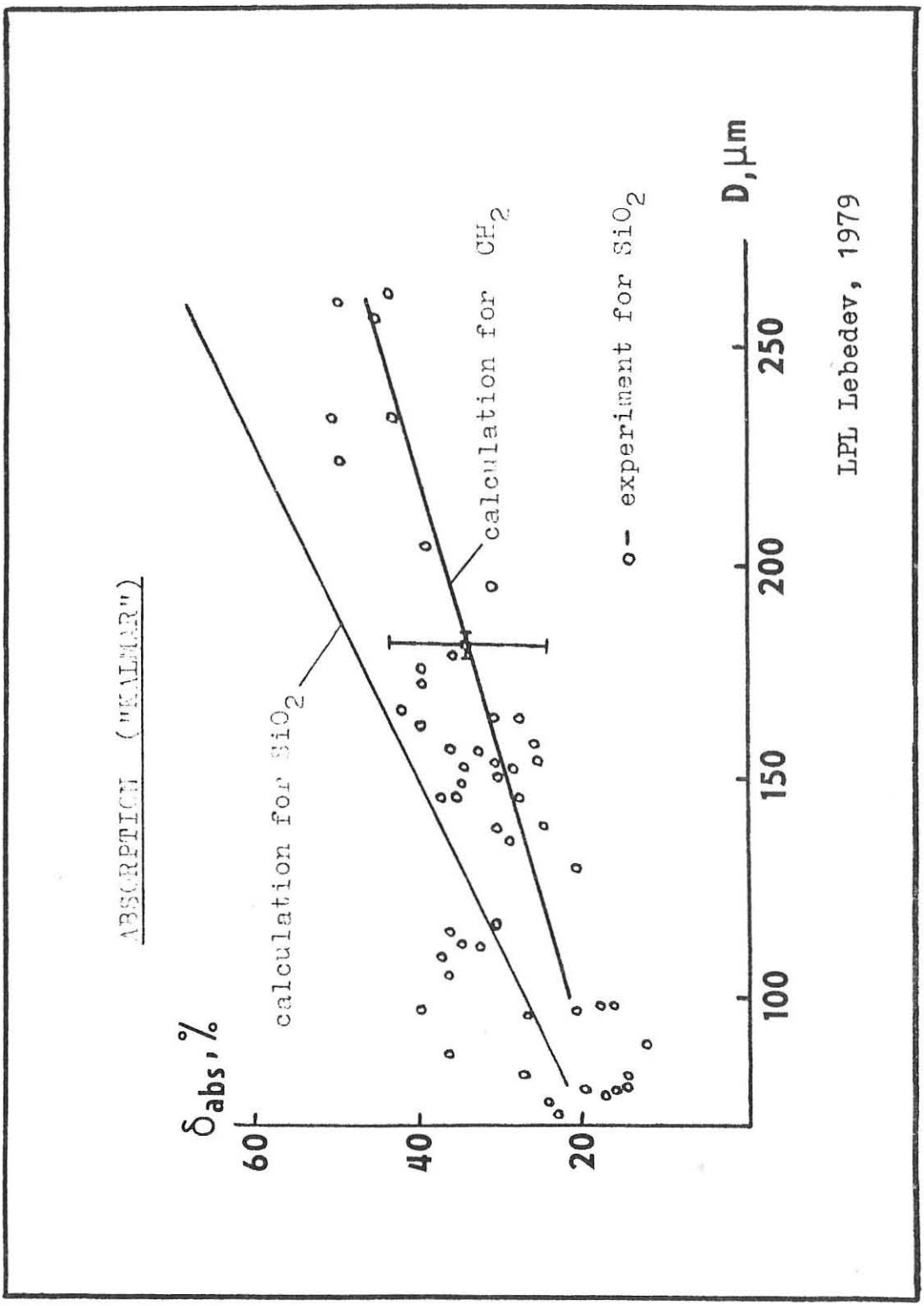
ABSORPTION ("PLATEAU")
δ_{abs}, %
60
40
20
100
150
200
250
D, μm
calculation for SiO_2
calculation for CH_2
o – experiment for SiO_2
LPL Lebedev, 1979

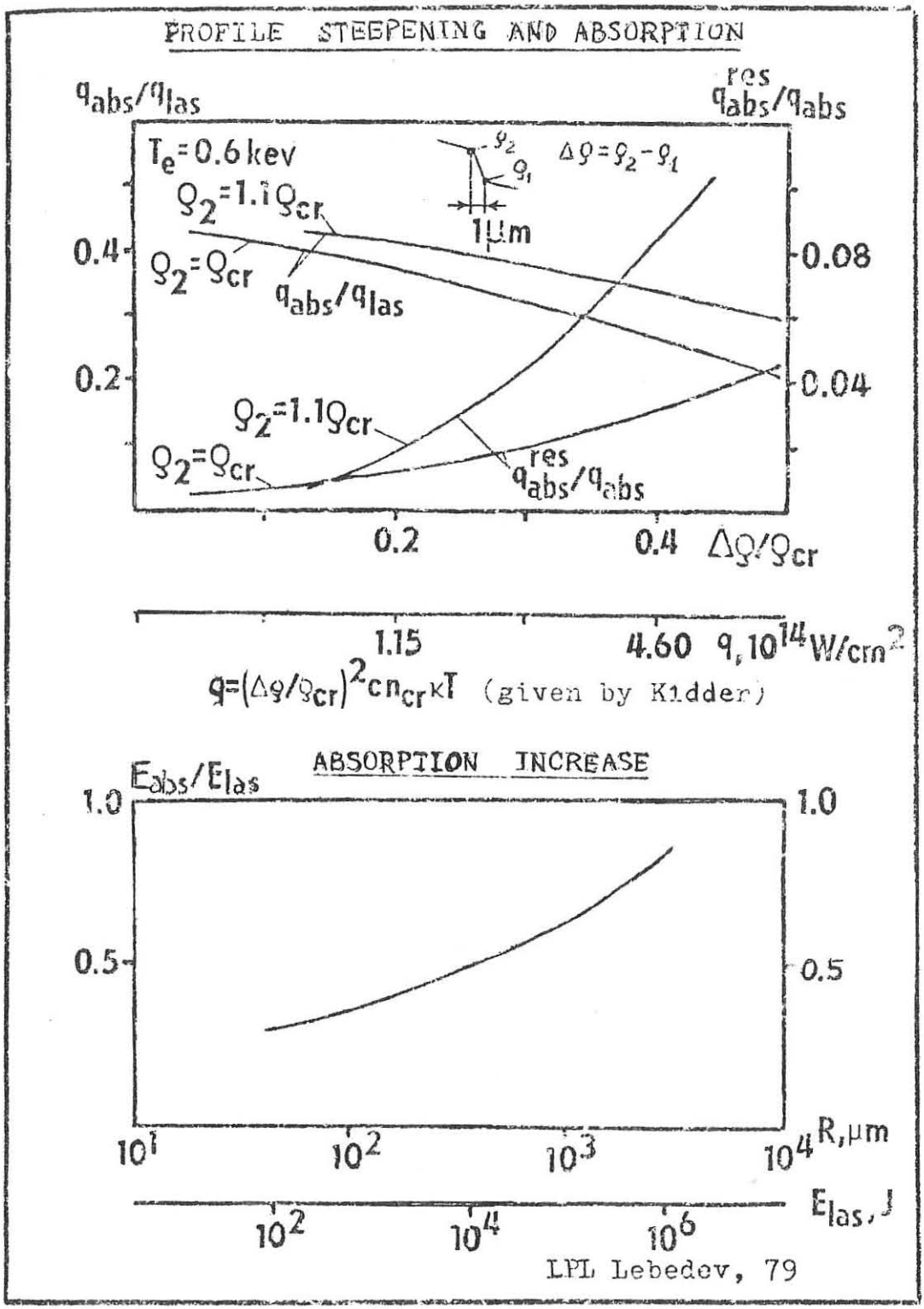
PROFILE STEEPENING AND ABSORPTION
q_{abs}/q_{las}
q^{res}_{abs}/q_{abs}
$T_e = 0.6$ kev
$\varrho_2 = 1.1\varrho_{cr}$
$\varrho_2 = \varrho_{cr}$
$\Delta\varrho = \varrho_2 - \varrho_1$
1 μm
0.4
0.2
0.08
0.04
q_{abs}/q_{las}
q^{res}_{abs}/q_{abs}
0.2
0.4 $\Delta\varrho/\varrho_{cr}$
1.15
4.60 $q, 10^{14}$ W/cm^2
$q=(\Delta\varrho/\varrho_{cr})^2 c n_{cr} \kappa T$ (given by Kidder)
ABSORPTION INCREASE
E_{abs}/E_{las}
1.0
0.5
10^1
10^2
10^3
10^4 R, μm
10^2
10^4
10^6 E_{las}, J
LPL Lebedev, 79

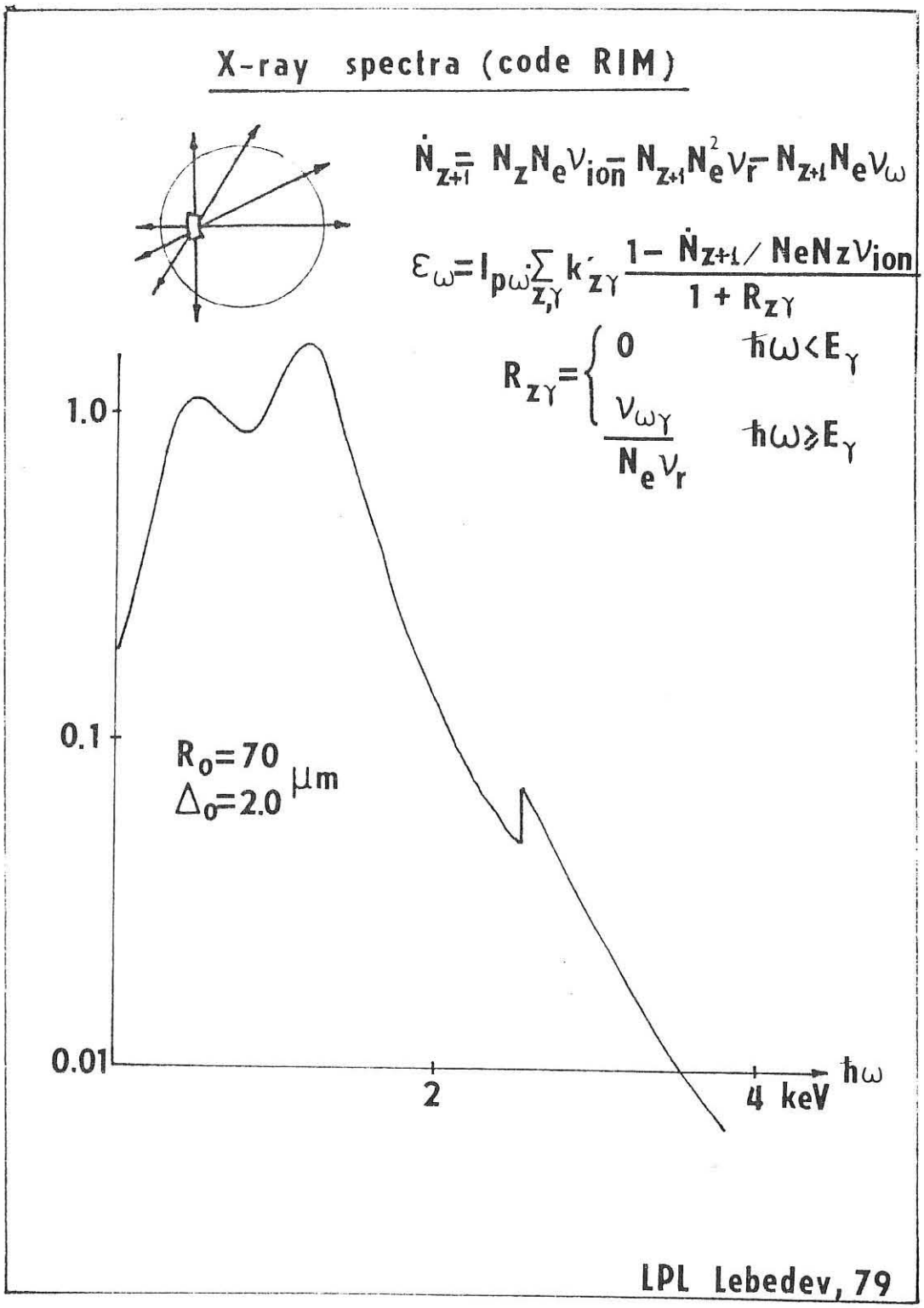
X-ray spectra (code RIM)
$\dot{N}_{z+1} = N_z N_e \nu_{ion} - N_{z+1} N_e^2 \nu_r - N_{z+1} N_e \nu_\omega$
$\varepsilon_\omega = I_{p\omega} \sum_{z,\gamma} k'_{z\gamma} \frac{1 - \dot{N}_{z+1} / N_e N_z \nu_{ion}}{1 + R_{z\gamma}}$
$R_{z\gamma} = \begin{cases} 0 & \hbar\omega < E_\gamma \\ \frac{\nu_{\omega\gamma}}{N_e \nu_r} & \hbar\omega \geq E_\gamma \end{cases}$
1.0
0.1
0.01
$R_0 = 70$ μm
$\Delta_0 = 2.0$ μm
2
4 keV
$\hbar\omega$
LPL Lebedev, 79

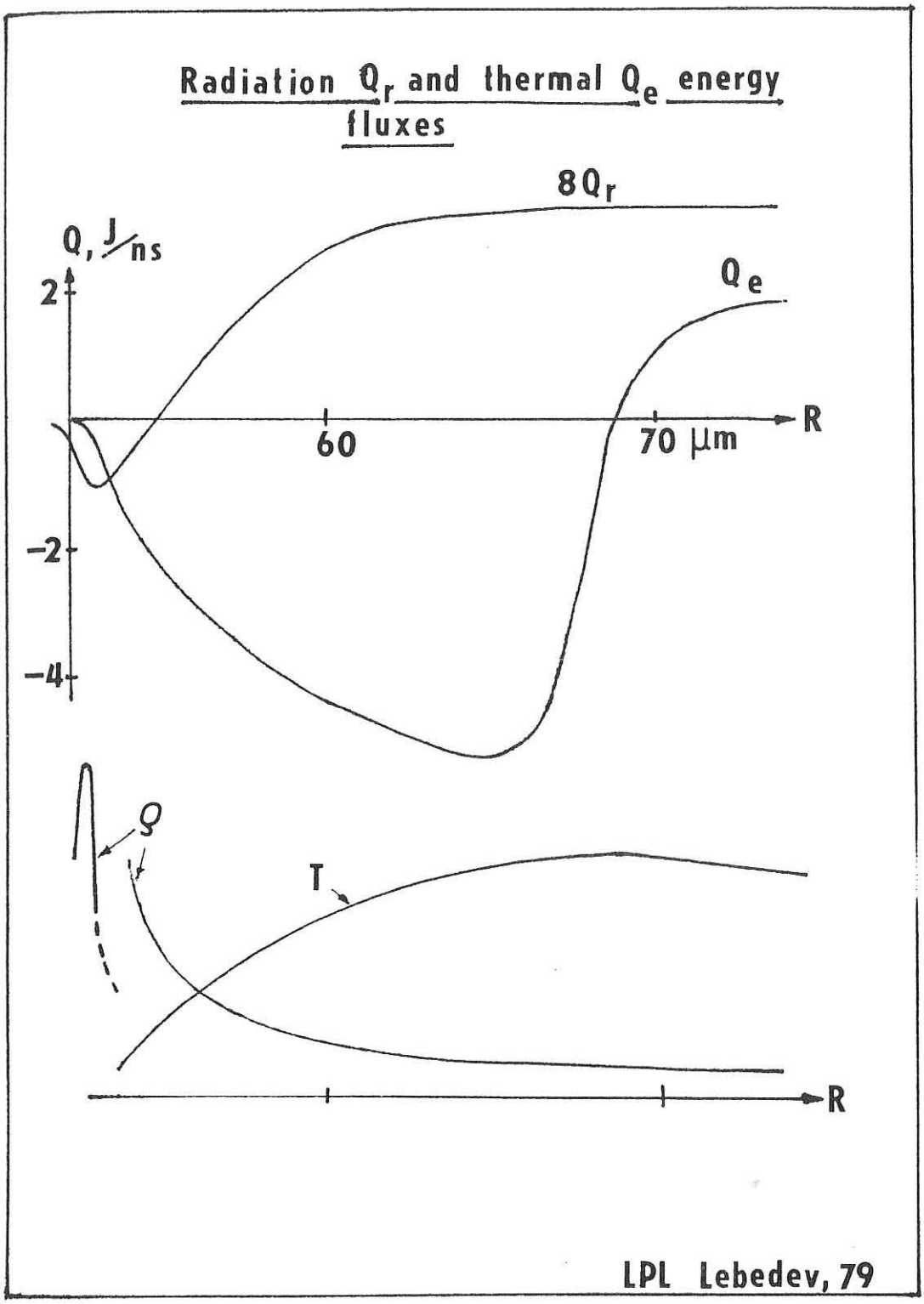
Radiation Q_r and thermal Q_e energy fluxes
$8Q_r$
Q, J/ns
Q_e
2
-2
-4
60
70 μm
R
ϱ
T
R
LPL Lebedev, 79

THIN SHELL COMPRESSION WITH STEADY-STATE CORONA (CODE "CORONA")

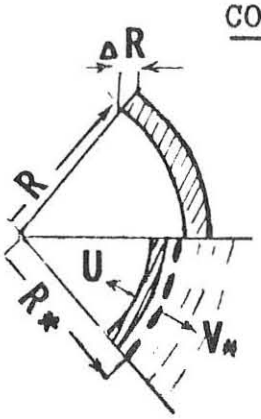

$$\begin{cases} (M_0 - M_{evp})\dfrac{dU}{dt} = -4\pi R^2 p \\ p = 2.28\,\varrho_* V_*^2 - \mathcal{P} \\ \dfrac{dM_{evp}}{dt} = 4\pi R_*^2 V_* \\ \dfrac{dR}{dt} = U \\ \dfrac{dR_{sw}}{dt} = \dfrac{4}{3}U, \quad A = \dfrac{R}{\Delta R} \end{cases}$$

CONDITIONS FOR THEORY APPLICABILITY

1. 1. $\Delta R \ll R$
   2. $U < V_*$; $\left(\dfrac{dU}{dt}, \dfrac{dV}{dt}\right) \ll (V_* \nabla)\, V_*$
   3. $U \gg D$, WHERE D IS THE RATE OF EVAPORATION WAVE FRONT
   4. SUPERTHERMAL ELECTRONS, DENSITY STEPPING, RADIATION, AND MAGNETIC FIELD GENERATION ARE NOT TAKEN INTO ACCOUNT.
   5. δ -SHAPED ENERGY INPUT.

LPL Lebedev, 79

CODE "CORONA" (CONTINUED)

$$\gamma_0 = \frac{\varkappa_0 Q}{\varrho_{cr}^{7/4} R^{11/4}} \left(\frac{M_i}{1+Z}\right)^{21/8}; \quad Q = Q_0 - \frac{\varepsilon_{ion}}{4\pi} \frac{dM_{evp}}{dt}$$

$$R_* = \begin{cases} (1. + 0.010095\,\gamma_0^{4/3})\,R & \gamma_0 < 10 \\ 1.2175\,R & \gamma_0 \geqslant 10 \end{cases}$$

$$V_* = \begin{cases} \frac{1}{3^{1/3}} \left(\frac{R}{R_*}\right)^{2/3} \left(\frac{Q}{\varrho_{cr} R^2}\right)^{1/3} & \gamma_0 < 10 \\ f(\gamma_0) \left(\frac{Q}{\varrho_{cr} R^2}\right)^{1/3} & \gamma_0 \geqslant 10 \end{cases}$$

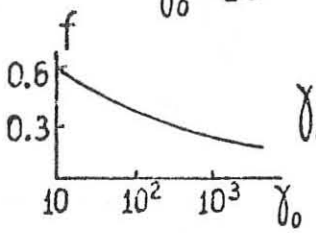

$$\varrho_* = \begin{cases} \varrho_{cr} & \gamma_0 < 10 \\ \frac{1}{1.815} \frac{\varkappa_0}{R} \left(\frac{M_i}{1+Z}\right)^{7/2} V_*^4 & \gamma_0 \geqslant 10 \end{cases}$$

$$\mathcal{P} = p_{g1} \left(\frac{R_1}{R}\right)^5 (1 + \mu(t))$$

$$\mu(t) = \frac{(M_0 - M_{evp})\,3}{\varrho_{s2}\,4\pi R^3}; \quad \varrho_{s2} = 4\varrho_{s0}$$

$$p_{g1} = \frac{2}{3} \varrho_{g1} U_1^2$$

$\varrho_{g1}, p_{g1}, U_1, R_1$ - GAS PARAMETERS AT THE MOMENT OF SHOCK WAVE ARRIVAL TO THE CENTRE

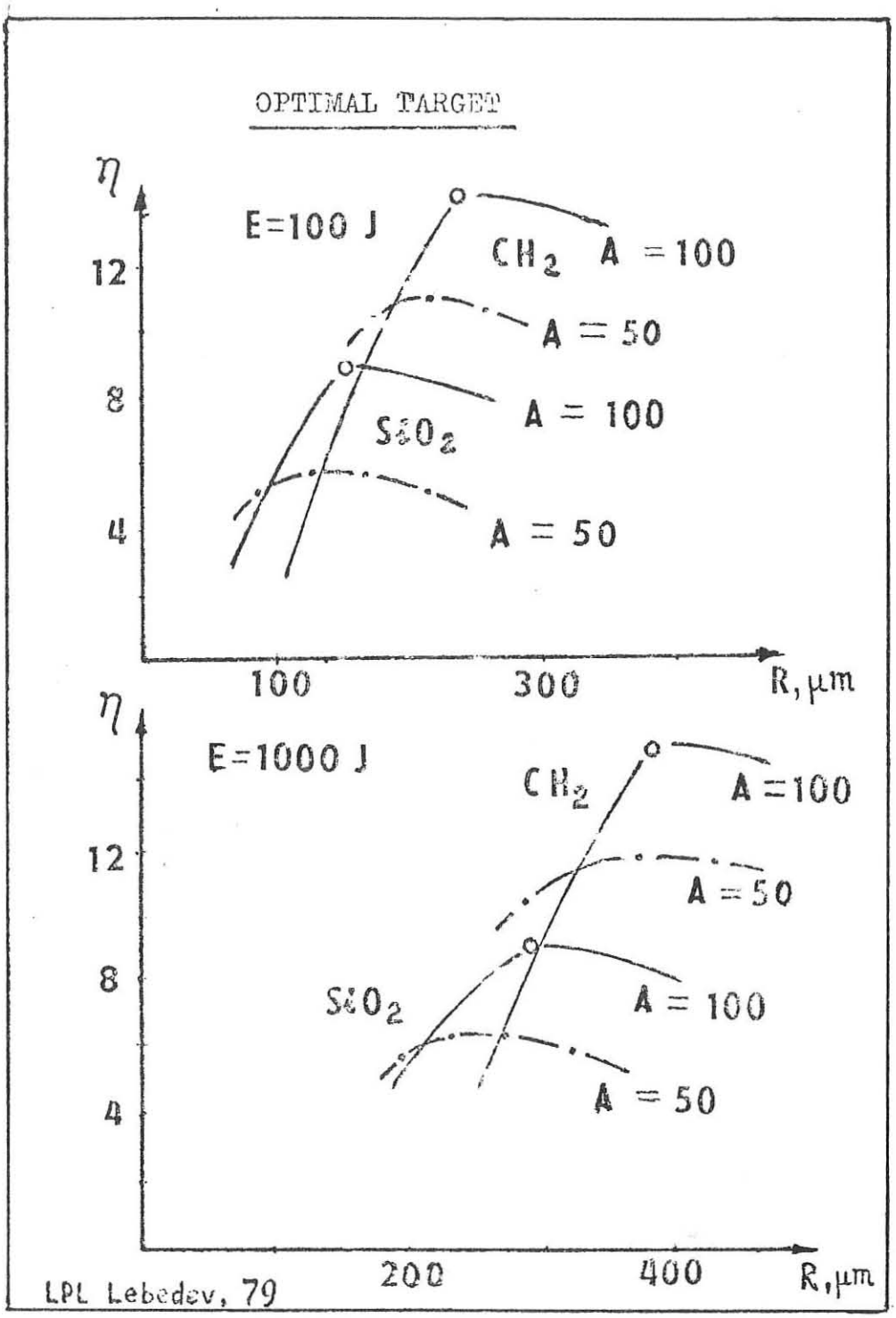
OPTIMAL TARGET
η
E=100 J
CH2
A = 100
A = 50
SiO2
A = 100
A = 50
12
8
4
100
300
R, μm
η
E=1000 J
CH2
A=100
A = 50
SiO2
A = 100
A = 50
12
8
4
200
400
R, μm
LPL Lebedev, 79

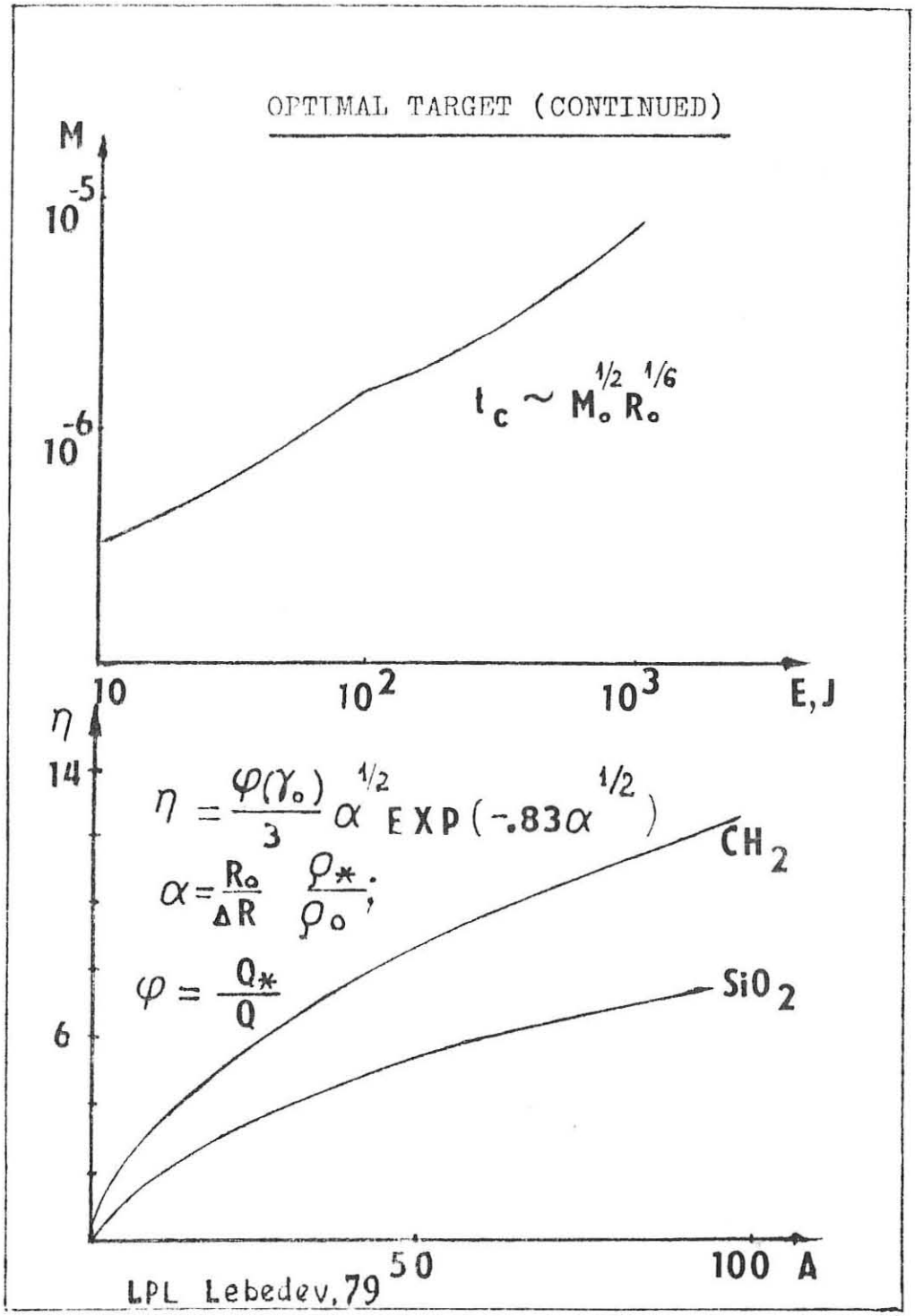
OPTIMAL TARGET (CONTINUED)
M
10^{-5}
10^{-6}
$t_c \sim M_o^{1/2} R_o^{1/6}$
10
10^2
10^3
E, J
η
14
6
$\eta = \frac{\varphi(\gamma_o)}{3} \alpha^{1/2} EXP(-.83\alpha^{1/2})$
$\alpha = \frac{R_o}{\Delta R} \frac{\rho_*}{\rho_o}$;
$\varphi = \frac{Q_*}{Q}$
CH_2
SiO_2
50
100 A
LPL Lebedev, 79

Compression time (KALMAR)

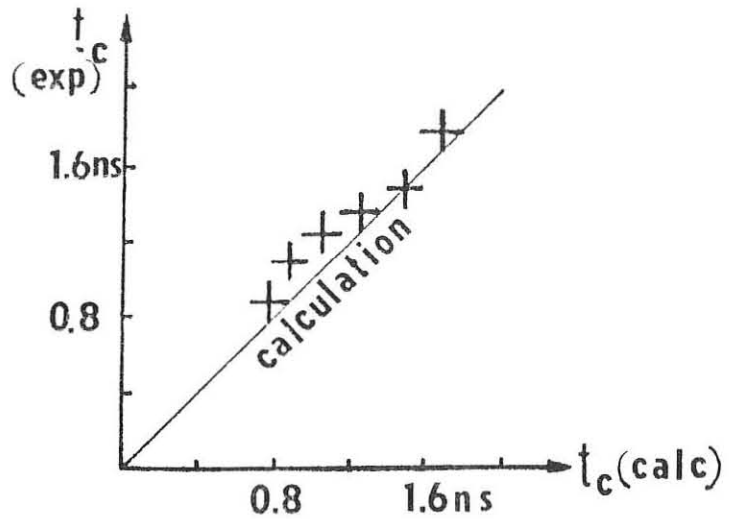

$$t_c = \beta \frac{R_0^{7/6} (\Delta_0 \cdot \varrho_0)^{1/2}}{\varrho_{cr}^{1/6} \dot{E}_{abs}^{1/3}}$$

Experiment

$2R_0$ μm	Δ_0 μm	E_{abs}, J	t_c, ns
125	2.1	9±1.5	1.8±0.2
100	1.2	13±2.5	1.25±0.1
75	0.9	10±2	0.9±0.1

LPL Lebedev, 79

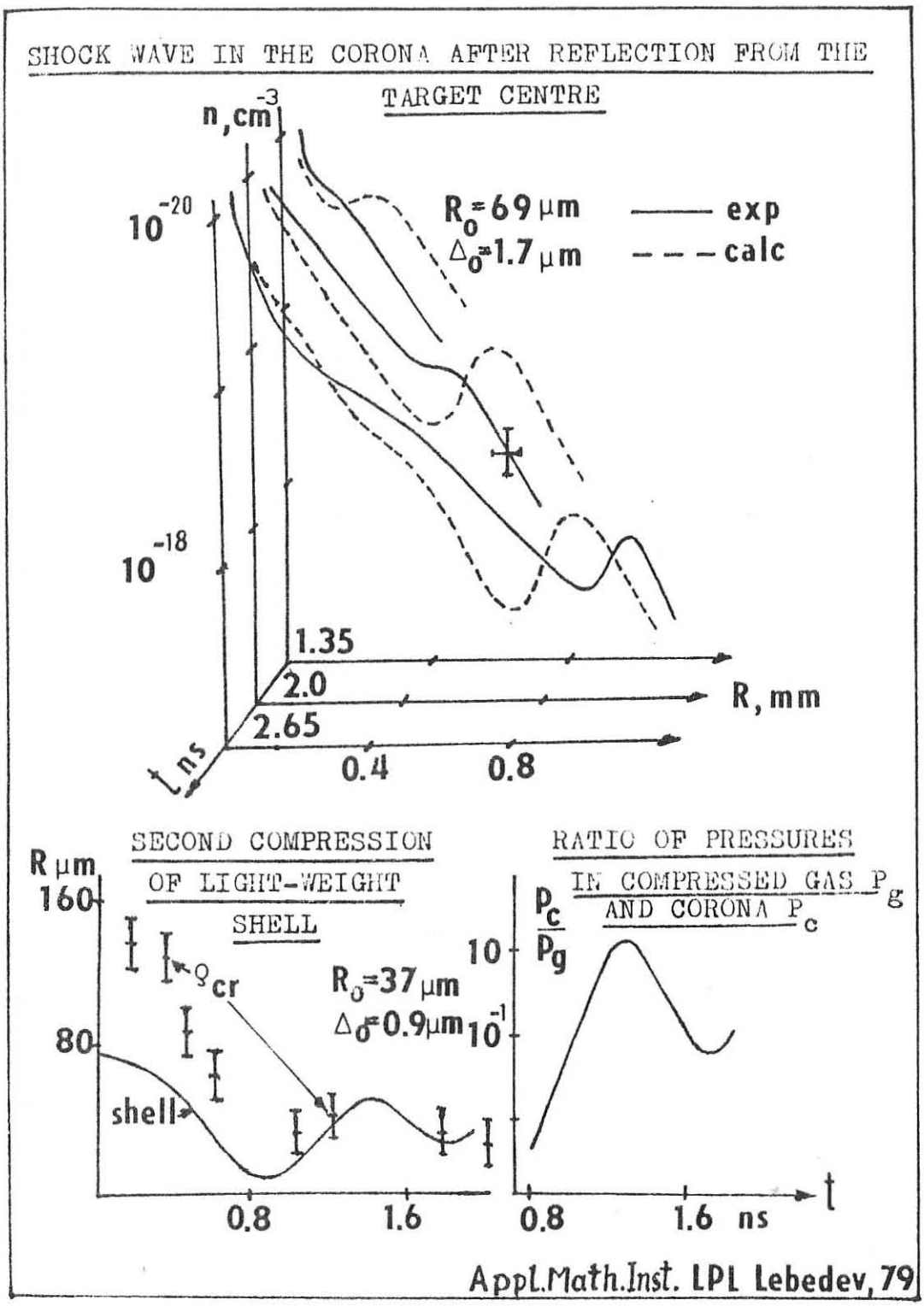
SHOCK WAVE IN THE CORONA AFTER REFLECTION FROM THE TARGET CENTRE
n, cm^-3
10^-20
10^-18
R0=69 μm
Δ0=1.7 μm
exp
calc
1.35
2.0
2.65
R, mm
t, ns
0.4
0.8
SECOND COMPRESSION OF LIGHT-WEIGHT SHELL
R μm
160
80
ρcr
R0=37 μm
Δ0=0.9μm
shell
0.8
1.6
RATIO OF PRESSURES IN COMPRESSED GAS Pg AND CORONA Pc
Pc/Pg
10
10^-1
0.8
1.6 ns
t
Appl.Math.Inst. LPI Lebedev, 79

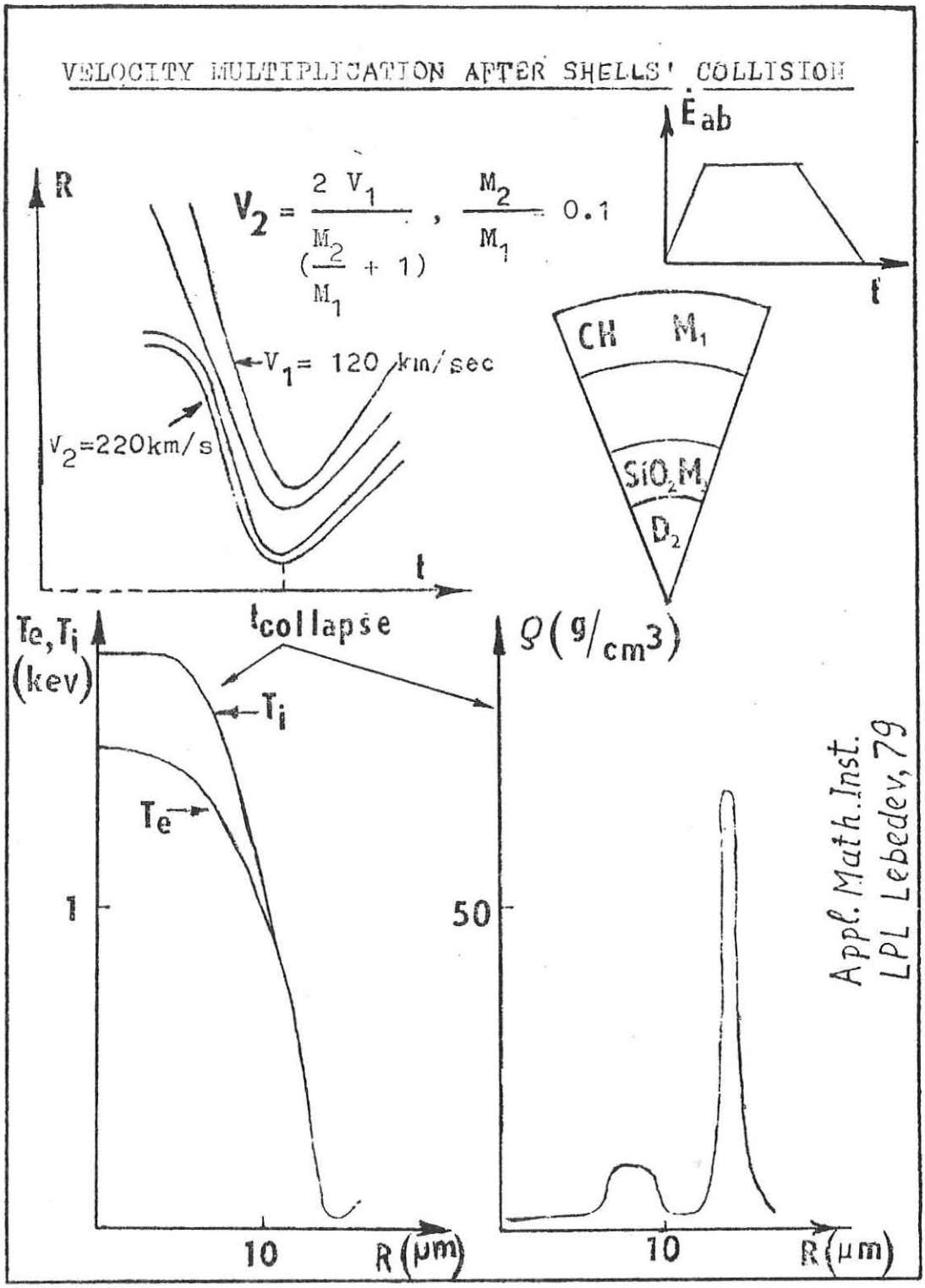
VELOCITY MULTIPLICATION AFTER SHELLS' COLLISION
$\dot{E}_{ab}$
t
R
$V_2 = \frac{2V_1}{(\frac{M_2}{M_1} + 1)}$, $\frac{M_2}{M_1} = 0.1$
V_1= 120 km/sec
V_2=220km/s
t
CH M_1
SiO_2 M_2
D_2
$t_{collapse}$
T_e, T_i (kev)
T_i
T_e
1
10
R (μm)
ϱ (g/cm^3)
50
10
R (μm)
Appl. Math. Inst.
LPL Lebedev, 79

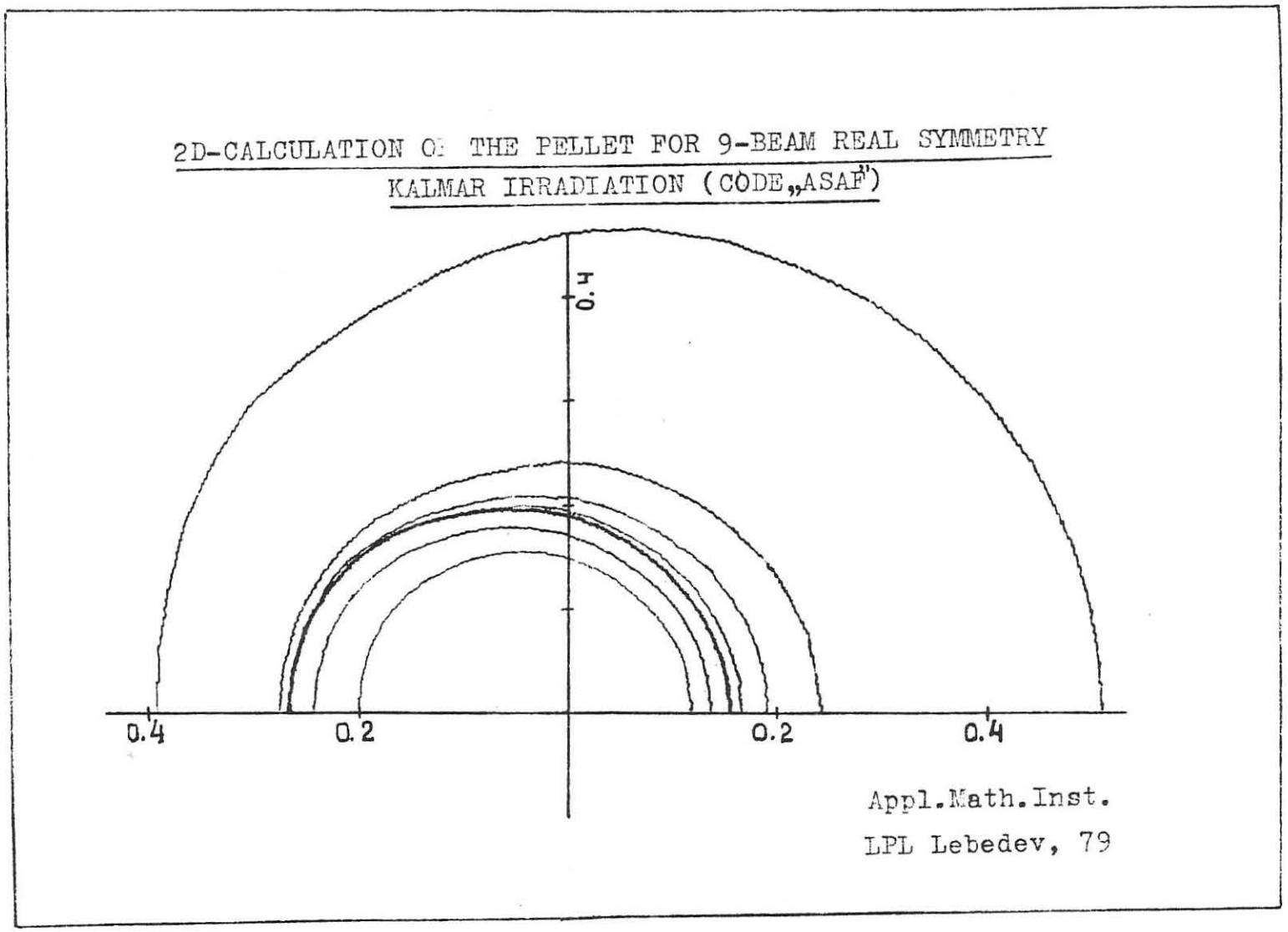
2D-CALCULATION OF THE PELLET FOR 9-BEAM REAL SYMMETRY
KALMAR IRRADIATION (CODE „ASAF")
0.0
0.4
0.2
0.2
0.4
Appl.Math.Inst.
LPL Lebedev, 79

2D-CALCULATION OF THE PELLET (CODE „ASAF")

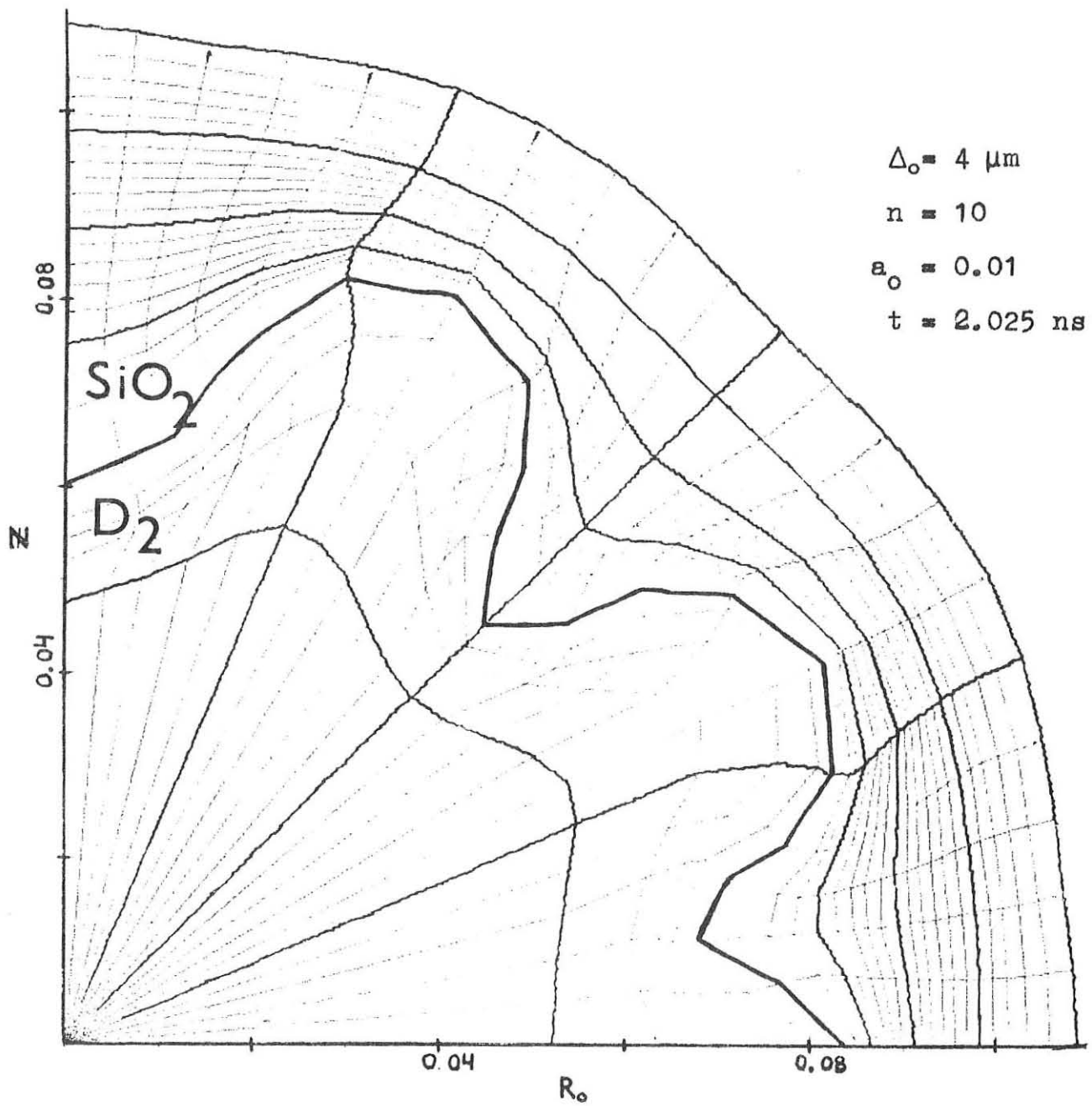

Appl.Math.Inst., LPL Lebedev, 79

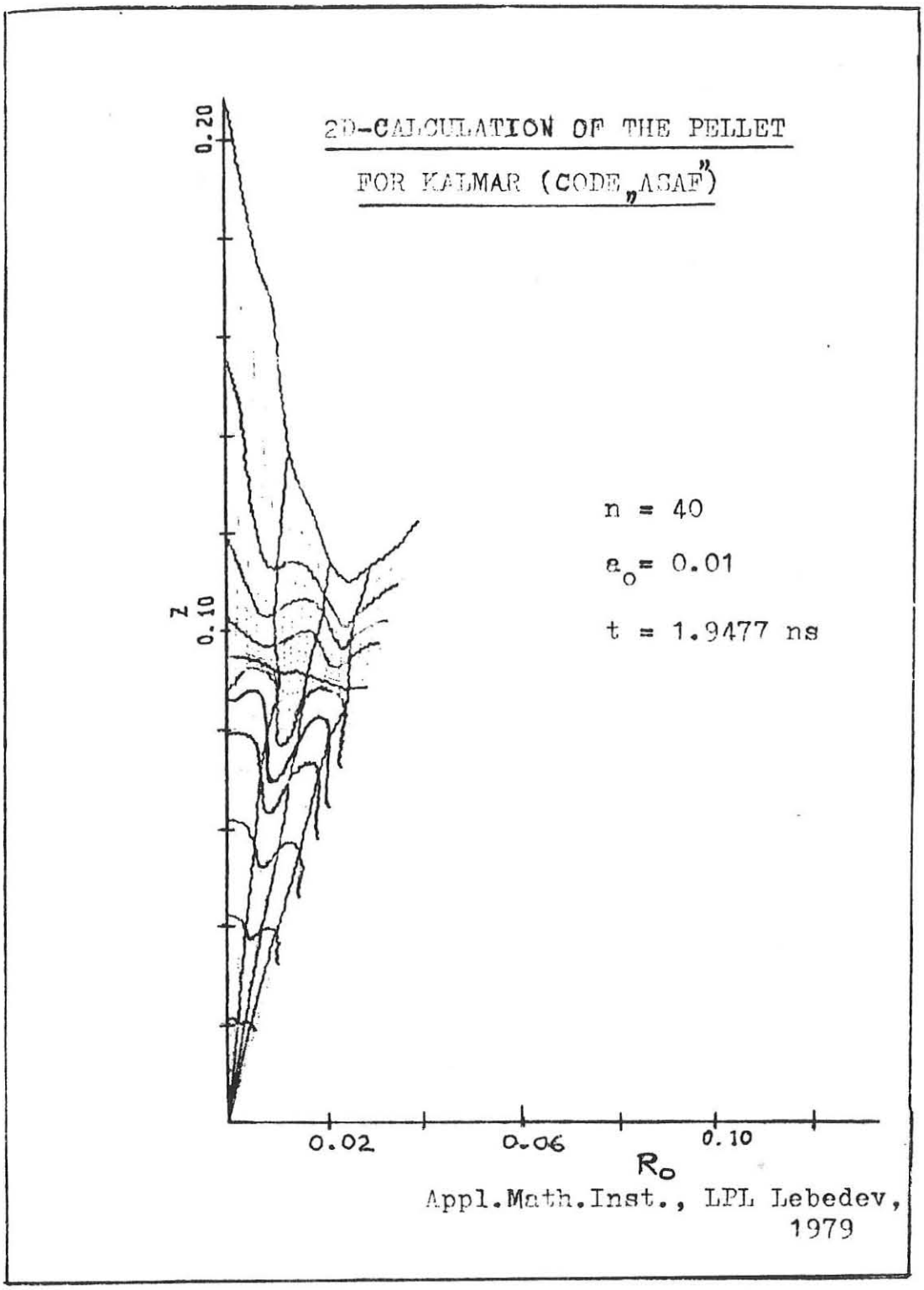
2D-CALCULATION OF THE PELLET
FOR KALMAR (CODE „ASAF")
n = 40
ε_0 = 0.01
t = 1.9477 ns
Z
0.20
0.10
0.02
0.06
0.10
R_0
Appl.Math.Inst., LPL Lebedev, 1979

OUTLINE OF EQUAL DENSITY LINES (2D CODE „ASAF")

TARGET FOR "KALMAR"

Δ_o = 4 μm

t = 1.9687 ns

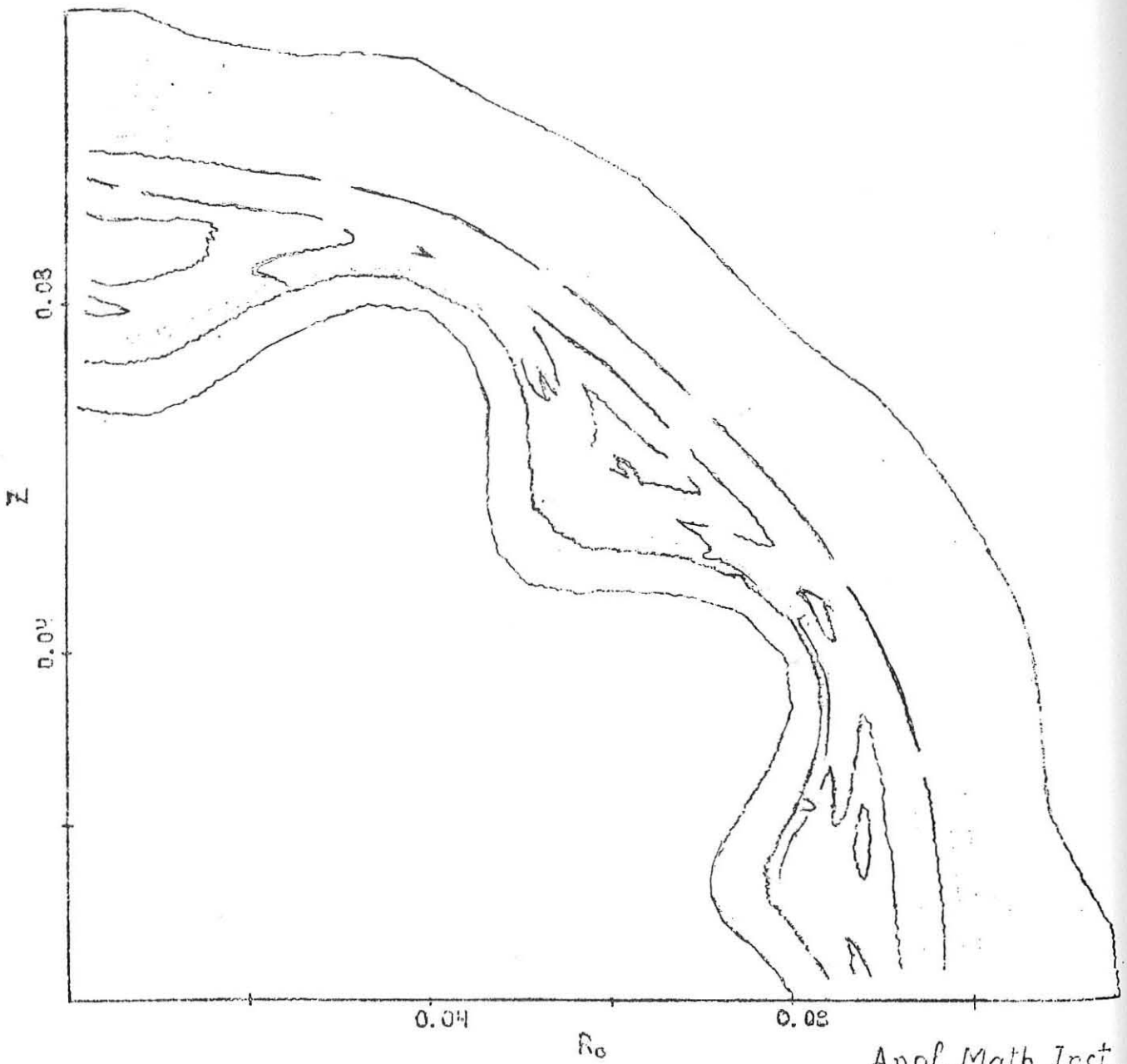

Appl. Math Inst.
LPL Lebedev, 79

CONTOUR OF EQUAL PRESSURE (2D CODE „ASAF")

TARGET FOR "KALMAR"

Δ_o= 4 μm

t = 1.9687 ns

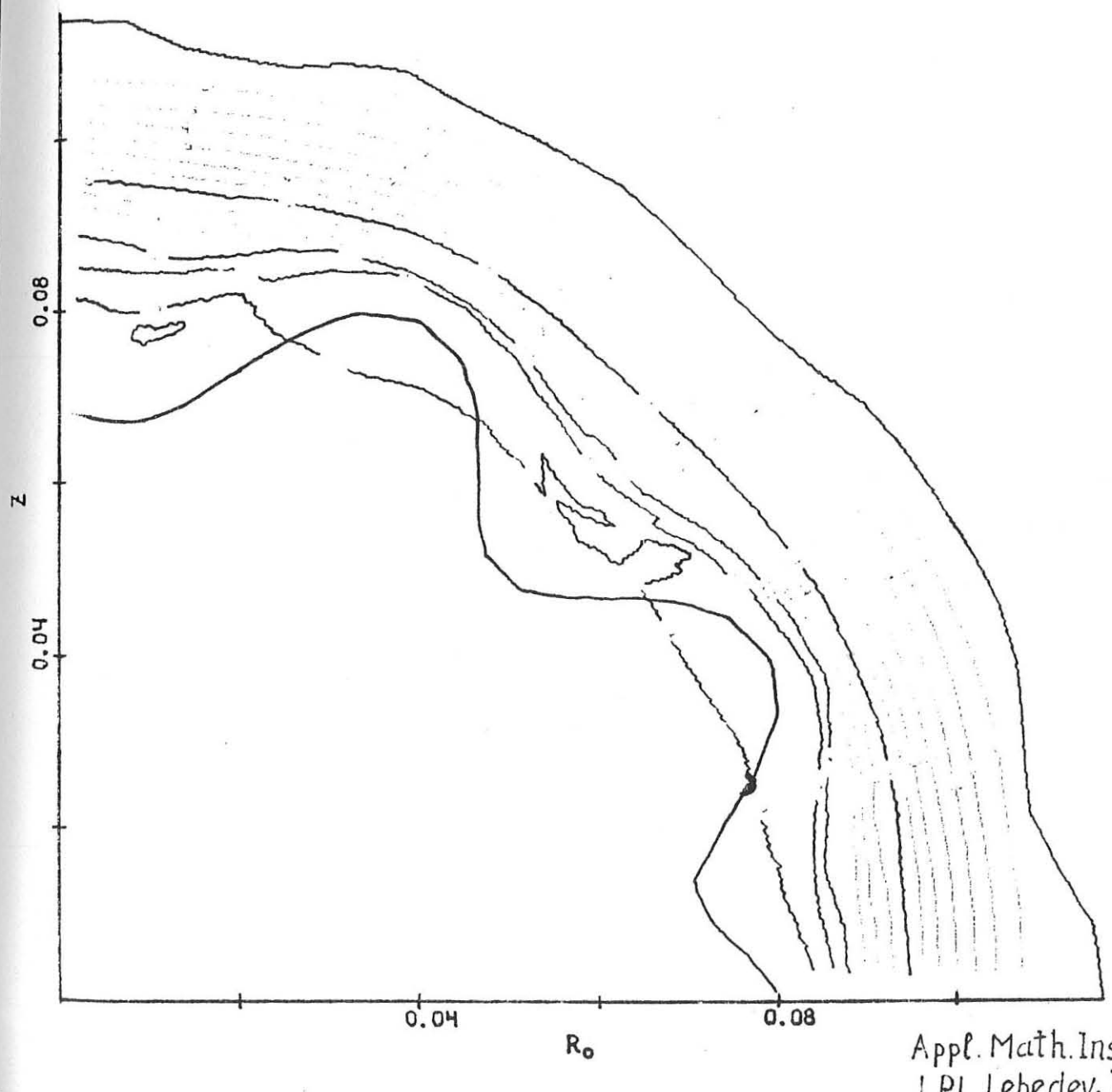

Appl. Math. Inst.
LPL Lebedev, 79

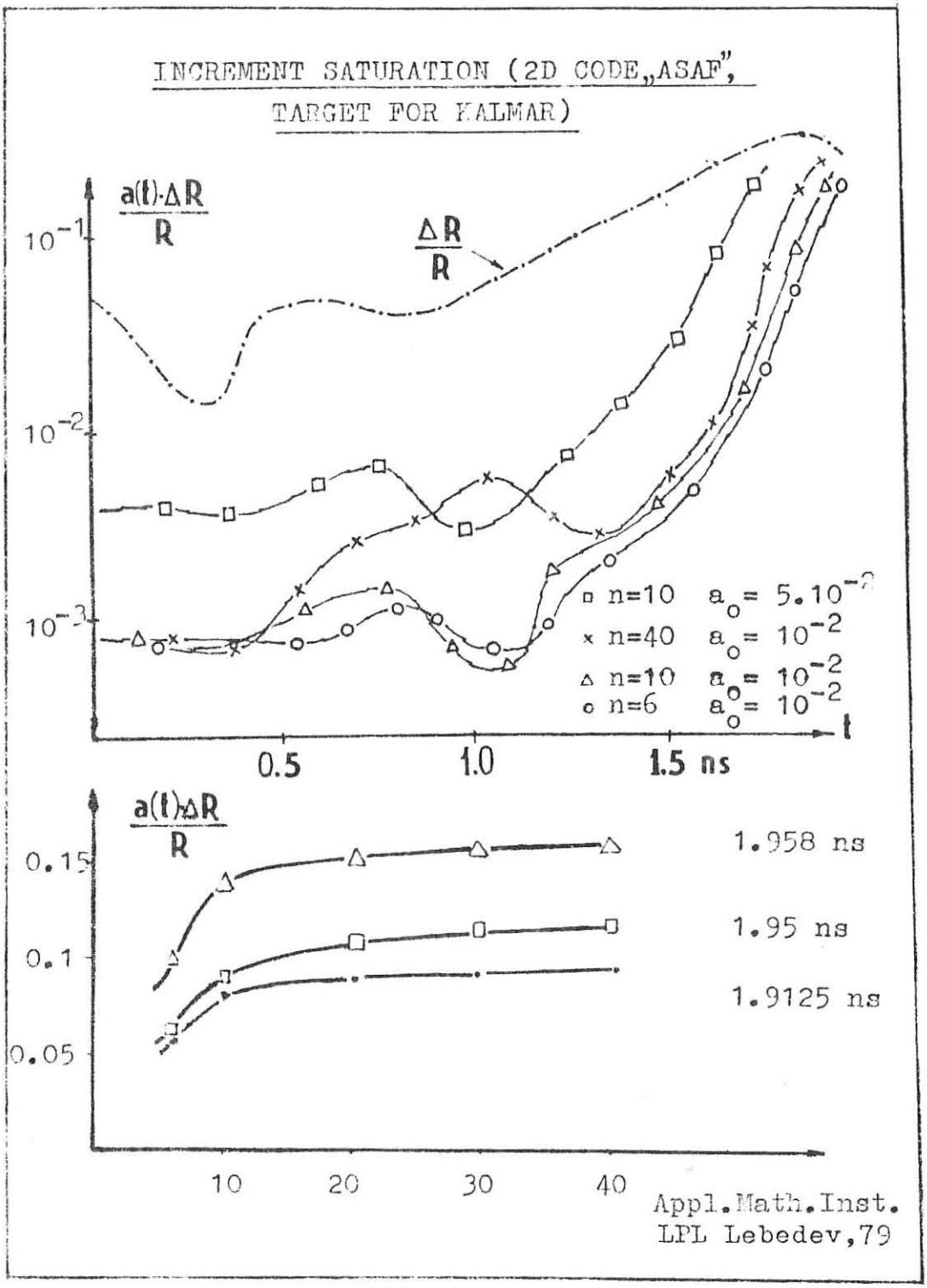
INCREMENT SATURATION (2D CODE „ASAF",
TARGET FOR KALMAR)
a(t)·ΔR / R
ΔR / R
10^-1
10^-2
10^-3
n=10 a_o = 5.10^-2
n=40 a_o = 10^-2
n=10 a_o = 10^-2
n=6 a_o = 10^-2
t
0.5
1.0
1.5 ns
a(t)·ΔR / R
0.15
0.1
0.05
1.958 ns
1.95 ns
1.9125 ns
10
20
30
40
Appl.Math.Inst.
LPL Lebedev,79

Luch–Kalmar

	E_{ab} (J)	P_{D_2} atm	V_s km/sec		η %	E_{br}(J)		$\varrho_{D_2}^{max}$ g/cm^3		$T_{D_2}^{max}$ keV	$P_{D_2}^{max}$ atm		N	
			Luch	Kalm.		Luch	Kalm.	Luch	Kalm.		Luch	Kalm.	Luch	Kalm.
1	20	27	61	60–70	2.8	0.2–0.6	0.5–1	7.4	5–10	0.22	2.10^9	$(2-5)\times 10^9$	2.10^4	10^4–10^6
2	40	27	81		3.6			7.1		0.47	3.10^9		3.10^5	
3	20	5	67		2.6			12.3		0.6	7.10^9		1.4×10^5	
4	40	5	83		3.4			23.2		0.78	14.10^9		10^6	

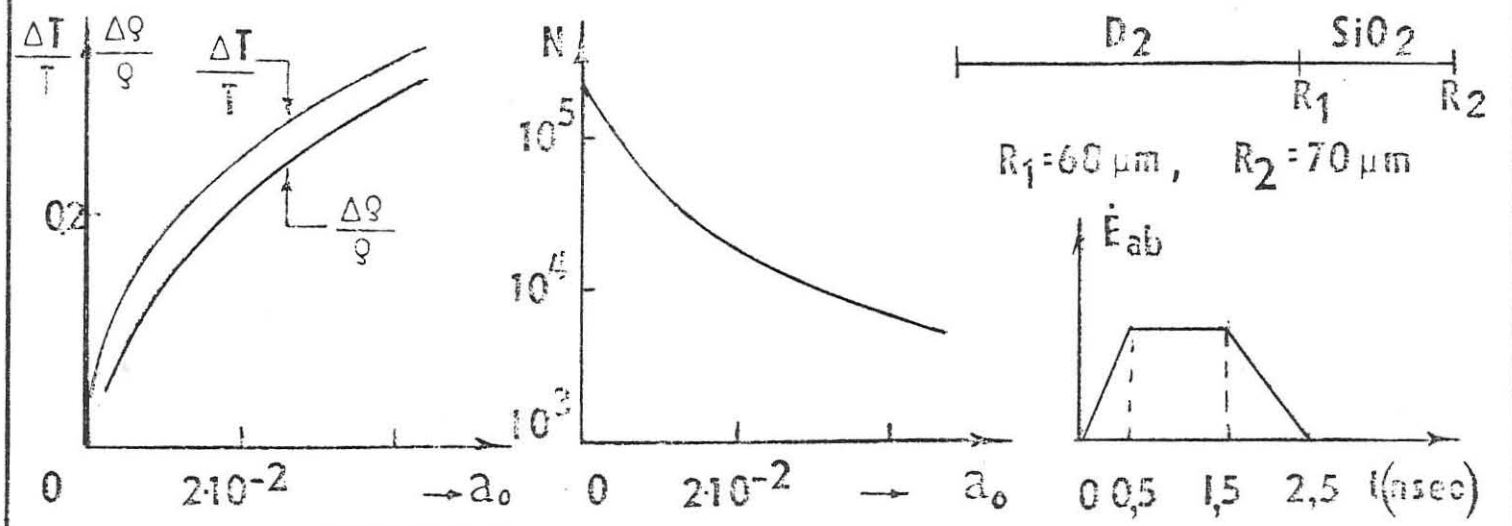

MAGNETIC FIELD GENERATION

TWO-DIMENSIONAL LAGRANGIAN CODE „ASAF"

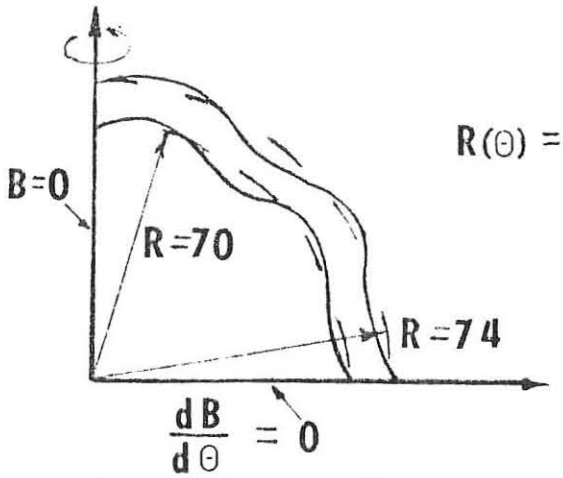

$$R(\Theta) = R\left(1 + \frac{\Delta}{R}\sin K\Theta\right)$$

$$\frac{dB}{dt} = \nabla\times V\times B - \frac{c^2}{4\pi}\nabla\times\frac{1}{\sigma}\nabla\times B + \frac{c}{e}\nabla T\times\nabla\ln\varrho$$

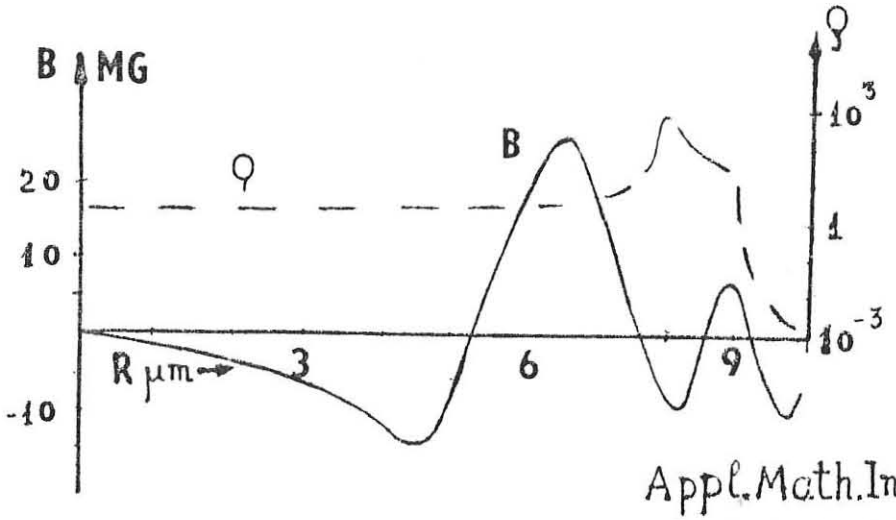

Appl. Math. Inst
LPL Lebedev, 79

LPL Lebedev, 79
Appl. Math. Inst.

DEVELOPMENT OF GAS-DYNAMIC PERTURBATIONS AND MAGNETIC FIELDS (CODE „LMGD")

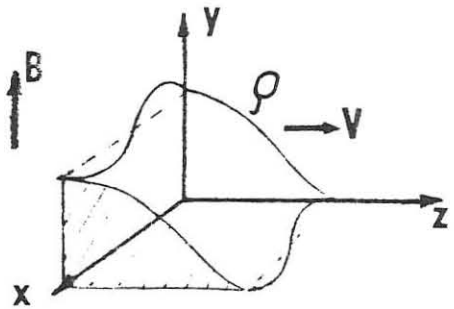

BACKGROUND SOLUTION
V, T_0, ρ_0

LINEAR APPROXIMATION

1. DYNAMICS EQUATIONS

2. HEAT CONDUCTIVITY EQUATION WITH ALLOWANCE FOR THE CROSSED THERMAL FLOW

$$3.\ \frac{dB}{dt} = -\frac{\partial VB}{\partial z} + \frac{c^2}{4\pi}\left(\frac{\partial}{\partial z}\frac{1}{\sigma}\frac{\partial B}{\partial z} + \frac{1}{\sigma}\frac{\partial^2 B}{\partial x^2}\right) - \beta\frac{\partial}{\partial z}\left(\frac{\tau_e}{m_e}\frac{\partial T_0}{\partial z}B\right) + \frac{c}{e\rho_0}\left(\frac{\partial T_0}{\partial z}\frac{\partial \rho_1}{\partial x} - \frac{\partial \rho_0}{\partial z}\frac{\partial T_1}{\partial x}\right)$$

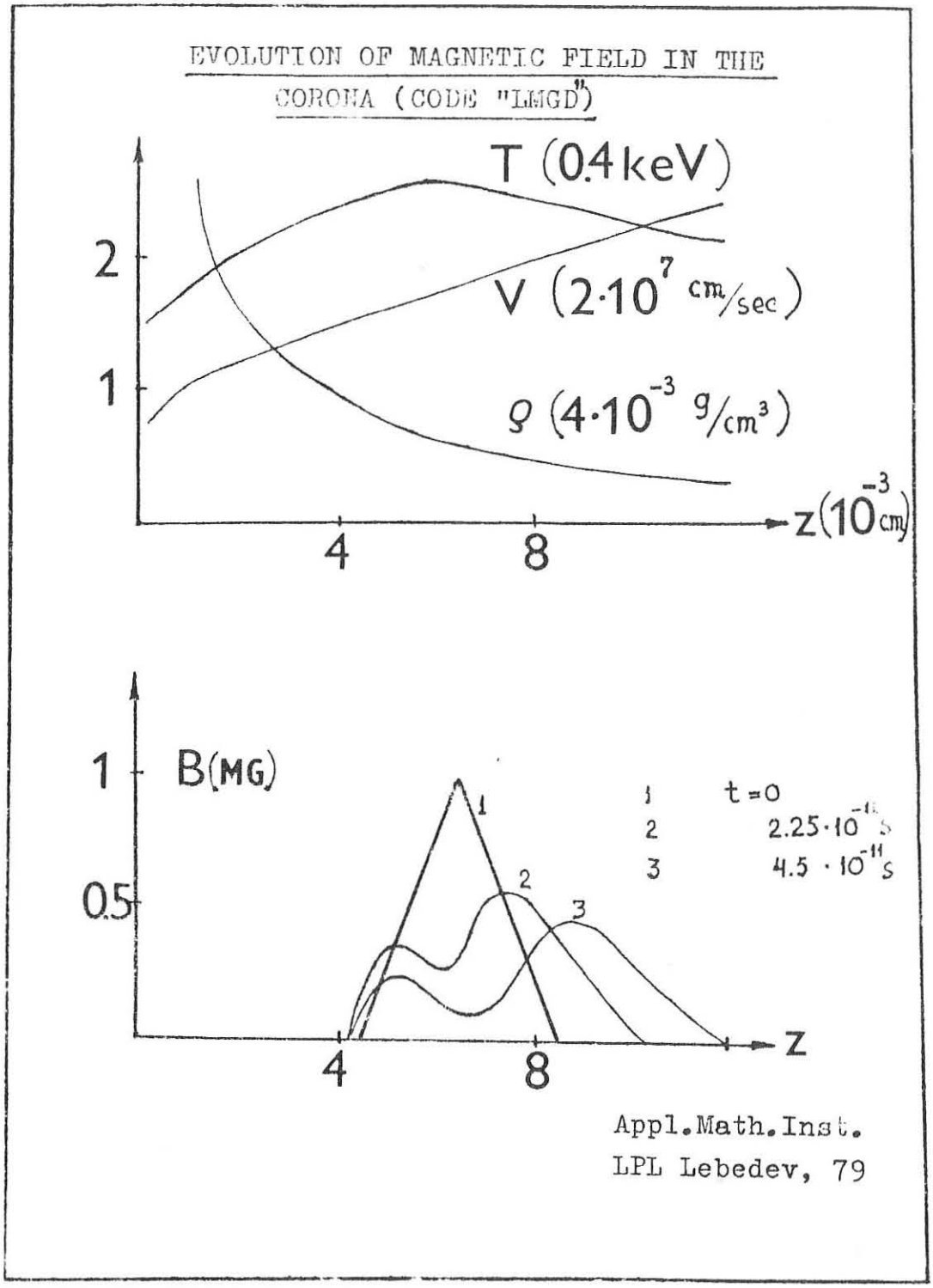
EVOLUTION OF MAGNETIC FIELD IN THE CORONA (CODE "LMGD")
T (0.4 keV)
V (2·10^7 cm/sec)
ϱ (4·10^-3 g/cm^3)
2
1
4
8
z(10^-3 cm)
B(MG)
1
0.5
1 t=0
2 2.25·10^-11 s
3 4.5 · 10^-11 s
z
Appl.Math.Inst.
LPL Lebedev, 79

INITIATION OF THERMONUCLEAR BURN WAVE IN THE LASER TARGET

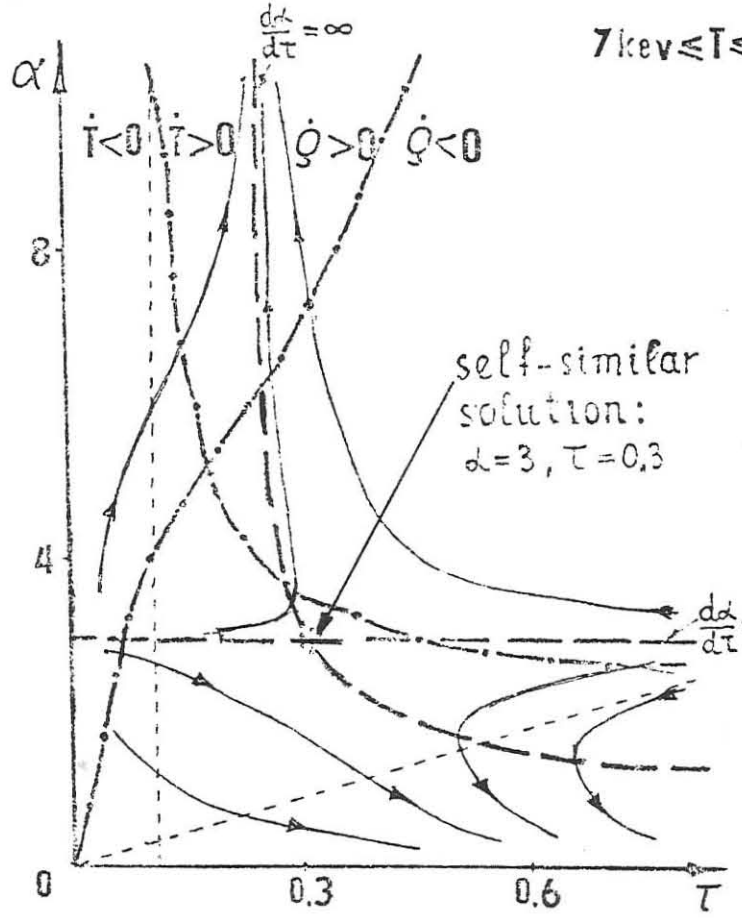

$7\,\text{kev}\le T\le 20\,\text{kev}\ ;\quad \langle\sigma V\rangle_{DT}=BT^{M}\ ;\quad M=2\ ;$

$$\begin{cases}\dfrac{\dot T}{T}=\dfrac{\dot R}{R}\left(E_{\alpha n}\alpha-3(\gamma-1)\right)\\ \dfrac{\dot\varrho}{\varrho}=\dfrac{\dot R}{R}\left((1-E_{\alpha n})\alpha-3\right)\\ \dot R=\beta\sqrt{T\varrho}\end{cases},\qquad E_{\alpha n}=\begin{cases}2\tau\ ;\ \tau\le\frac14\\ 1-\frac{1}{8\tau}\ ;\ \tau\ge\frac14\end{cases}$$

$$\alpha=\frac{\frac{dE_{TN}}{dt}\cdot\frac{R}{R}}{E_T}\ ;\quad \tau=\frac{R}{\lambda_\alpha}$$

$\tau\le\frac14$

$$\begin{cases}\dot\alpha=\dfrac{\dot R}{R}\alpha\left(\left(\frac12+2(M-2)\tau\right)\alpha-2\left(M-\frac32\right)-\frac12\right)\\ \dot\tau=\dfrac{\dot R}{R}\tau\left((1-5\tau)\alpha+1\right)\end{cases}$$

$\tau\ge\frac14$

$$\begin{cases}\dot\alpha=\dfrac{\dot R}{R}\alpha\left(\left(M-\frac32\right)\alpha-\left(M-2\right)\dfrac{\alpha}{8\tau}-\left(2M-\frac52\right)\right)\\ \dot\tau=\dfrac{\dot R}{R}\left(\dfrac{5\alpha}{16}-\dfrac32\alpha\tau+\tau\right)\end{cases}$$

LPL Lebedev, 79

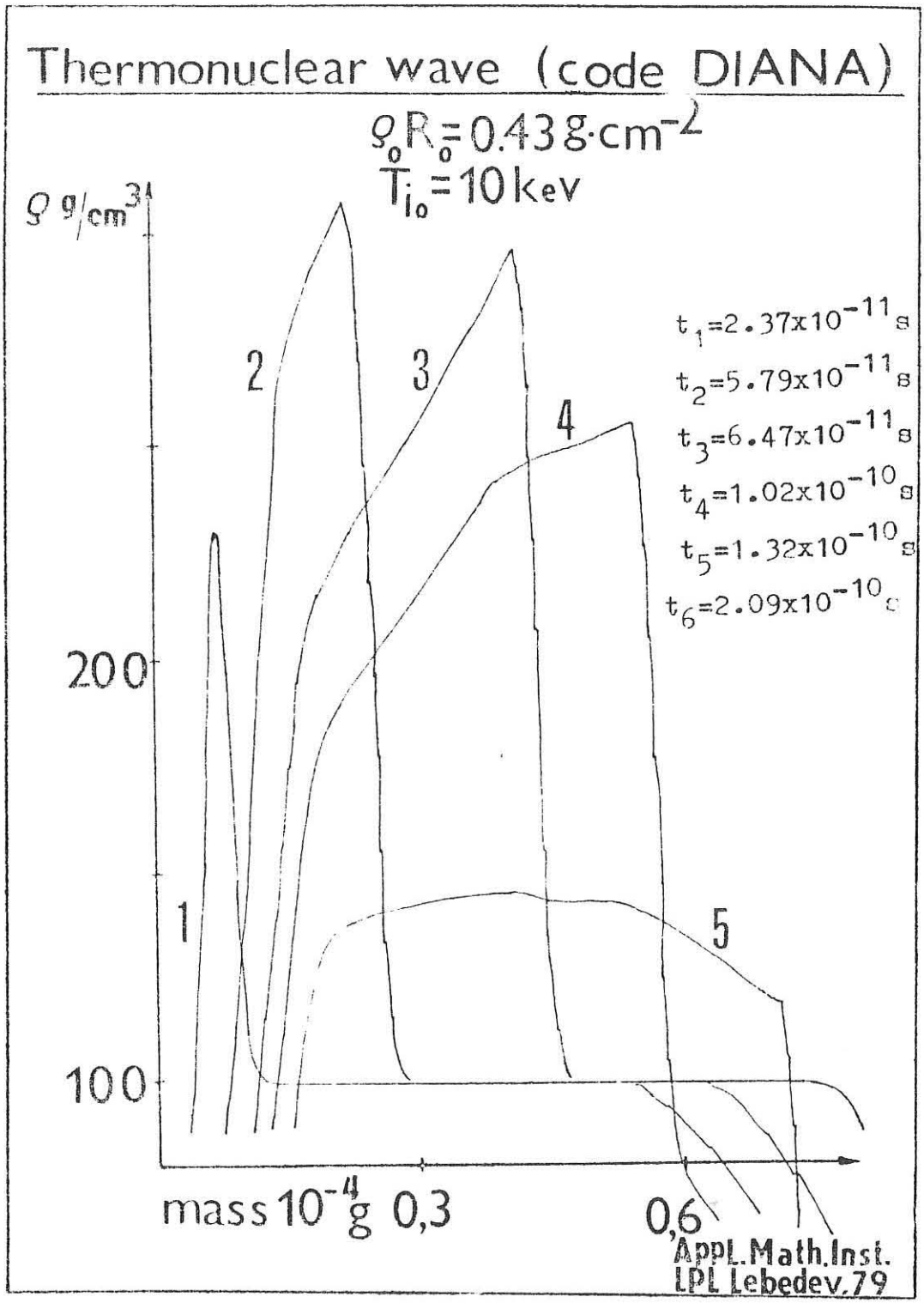
Thermonuclear wave (code DIANA)
$\varrho_0 R_0 = 0.43\ g\cdot cm^{-2}$
$T_{i_0} = 10\ keV$
ϱ g/cm^3
$t_1 = 2.37 \times 10^{-11}$ s
$t_2 = 5.79 \times 10^{-11}$ s
$t_3 = 6.47 \times 10^{-11}$ s
$t_4 = 1.02 \times 10^{-10}$ s
$t_5 = 1.32 \times 10^{-10}$ s
$t_6 = 2.09 \times 10^{-10}$ s
200
100
1
2
3
4
5
mass 10^{-4} g 0,3
0,6
Appl. Math. Inst.
LPI Lebedev, 79

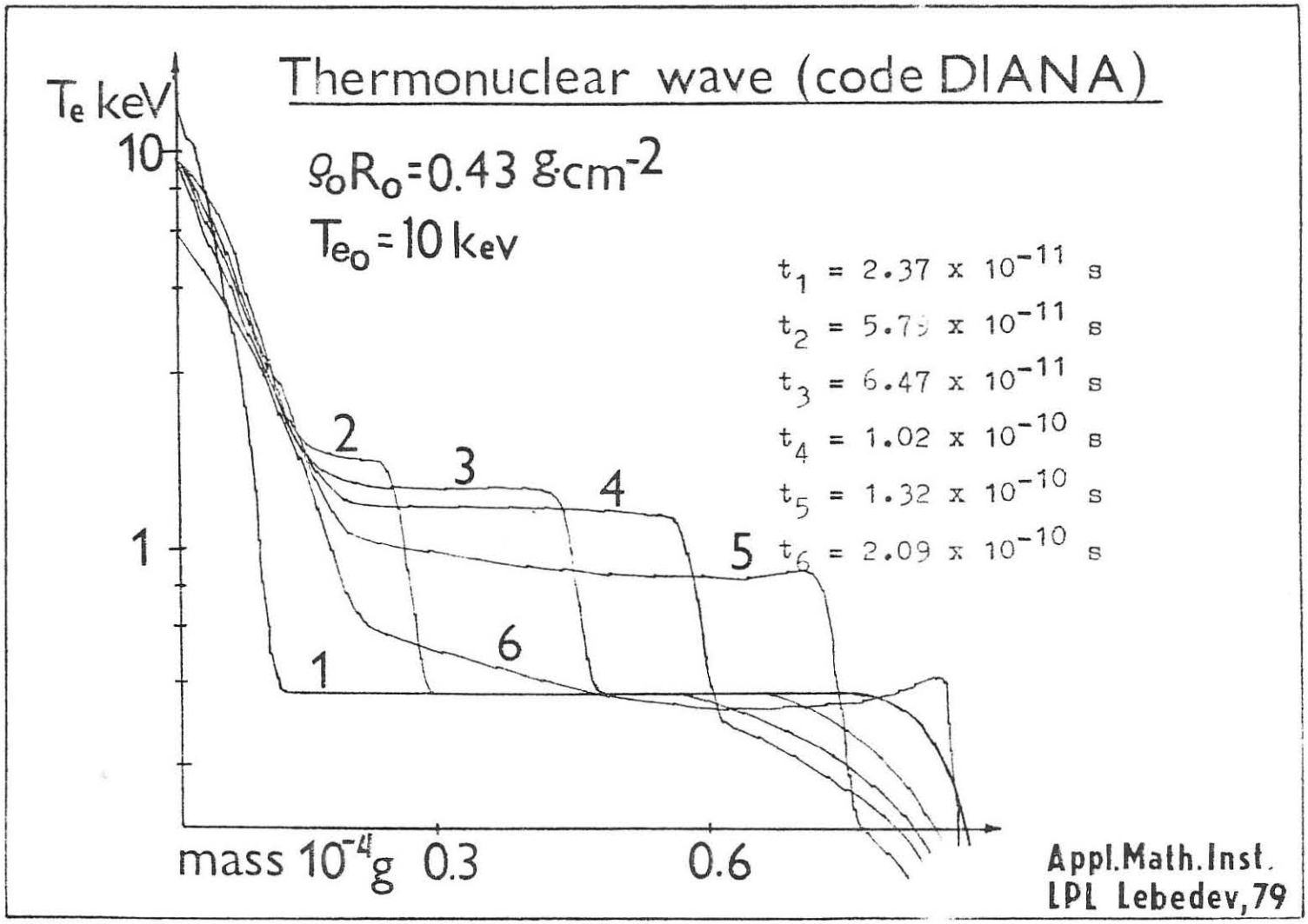
Thermonuclear wave (code DIANA)
T_e keV
10
1
$\varrho_o R_o = 0.43$ g cm^{-2}
$T_{eo} = 10$ kev
$t_1 = 2.37 \times 10^{-11}$ s
$t_2 = 5.79 \times 10^{-11}$ s
$t_3 = 6.47 \times 10^{-11}$ s
$t_4 = 1.02 \times 10^{-10}$ s
$t_5 = 1.32 \times 10^{-10}$ s
$t_6 = 2.09 \times 10^{-10}$ s
1
2
3
4
5
6
mass 10^{-4} g
0.3
0.6
Appl.Math.Inst.
LPL Lebedev,79

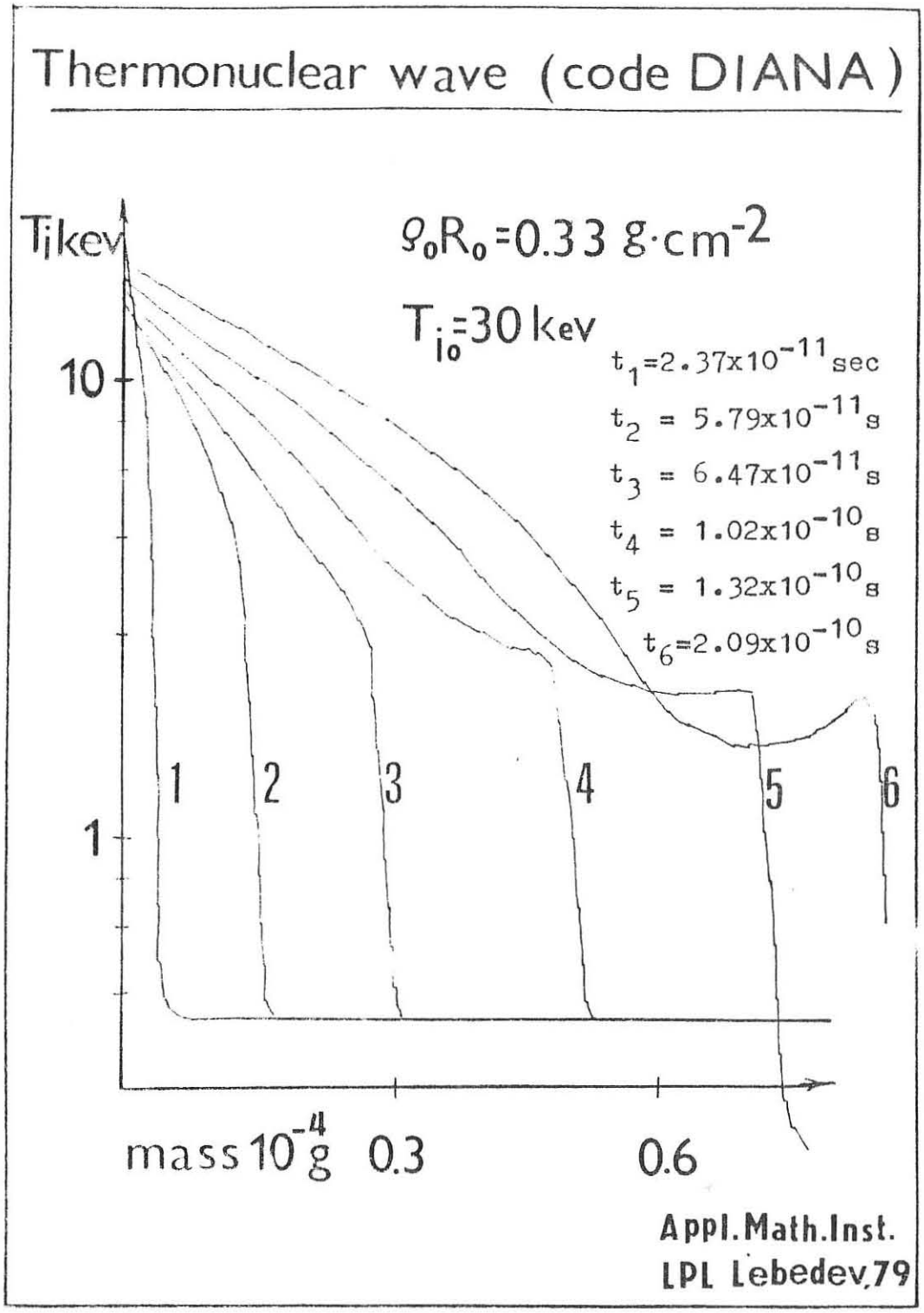
Thermonuclear wave (code DIANA)
Tikev
$\rho_0 R_0 = 0.33$ g·cm^{-2}
$T_{i0} = 30$ kev
$t_1 = 2.37 \times 10^{-11}$ sec
$t_2 = 5.79 \times 10^{-11}$ s
$t_3 = 6.47 \times 10^{-11}$ s
$t_4 = 1.02 \times 10^{-10}$ s
$t_5 = 1.32 \times 10^{-10}$ s
$t_6 = 2.09 \times 10^{-10}$ s
10
1
1
2
3
4
5
6
mass 10^{-4} g
0.3
0.6
Appl.Math.Inst.
LPL Lebedev,79

9th EUROPEAN CONFERENCE ON CONTROLLED FUSION AND PLASMA PHYSICS
OXFORD - September 17-21,1979

PROGRESS ON LASER FUSION RESEARCH IN EUROPE

R. DAUTRAY and JP. WATTEAU

Centre d'Etudes de Limeil
BP n° 27 - 94190 Villeneuve St Georges, France

Abstract

Recent results on laser fusion research obtained in the main laboratories of Western Europe are presented. Emphasis is placed on interaction at various wavelengths and laser intensities, on transport inhibition of absorbed laser energy inside the target and on implosion experiments in both exploding pusher and ablation modes.

I - INTRODUCTION

The main laboratories of Western Europe engaged in research on laser-matter interaction are listed in figure 1. Four of them are members of the Euratom Association. Several like Bruxelles and Göteborg,are restricting their work to theory at present. It is also interesting to note that at Rutherford and Ecole Polytechnique laser facilities are used respectively by several English and French university groups.

The main lasers and their characteristics are indicated in figure 2. Most of them are neodymium glass lasers (wavelength 1,06µm) with energy range from 10 J to 1 kJ and maximum power from 250 GW to 2 TW for 100 ps pulses. CO_2 gas lasers (wavelength 10.6µm) are used at Frascati and Ecole Polytechnique. Garching developed successfully an iodine gas laser which delivers 1.3 TW on target with a pulse duration of 300ps /1/.

Though these lasers are less powerful than those recently built in the United States of America /2a/ and in the Soviet Union /2b/, the European laboratories have nevertheless obtained with them significant results which contribute to better understanding the complex field of laser-matter interaction. These results on interaction, transport and glass microballoon implosion are successively examined below.

II - INTERACTION

Interaction experiments are done mostly with a single laser beam focused on a plane target at various incidence angles. Emphasis will be put on recent results related to absorption rates, harmonic emissions, stimulated Brillouin backscattering, density profile and megagauss field generation.

Absorption rates have been studied at Ecole Polytechnique with respect to wavelength and pulse duration. Figure 3 gives the absorption rates of a polystyrene massive plane target irradiated through a f/1.3 aperture lens at normal incidence, using neodymium glass laser light and its second harmonic with 100ps pulses and 1ns pulses. Absorption rates increase with longer pulses and shorter wavelengths. At low fluxes these results can be interpreted with the assumption that absorption is due to inverse Bremsstrahlung.

$3/2\ \omega_o$ and $2\ \omega_o$ harmonic emissions of the laser pulsation ω_o have been detected and their spectrum has been resolved either in time or in space. Blue and red shifts are observed and may be attributed to a Doppler effect produced by target blow off towards the laser and the excitation of ion acoustic waves, respectively [3,4]. At Limeil, for example, the spectrum of the $2\omega_o$ light emitted by a solid deuterium plane target irradiated at normal incidence with a 80ps, S polarized Nd glass laser pulse, shows a few angströms shift which moves from the blue to the red side as the laser flux is increased, the onset of ion acoustic waves at 2.10^{15} W.cm^{-2} producing a shift which exceeds the Doppler shift.

A careful study of backscattered light has been done at Garching [5,30] (figure 4). The iodine 0.5 TW - 280 ps Asterix III laser is focused on a polished massive steel plane target at an incidence angle of 45° in order to separate specular and backscattered light. Approximately 60% of incident light is reflected, 40% as specular light and 20% as backscattered light into the focusing lens solid angle. Figure 4 gives specular and backscatter reflexion coefficient R versus incident flux Φ_{inc} for out of focus (400µm diam.) and in focus (60µm diam.) conditions : $R_{specular}$ is quite constant while $R_{backscatter}$ shows the transition from small signal threshold to saturation, which characterizes stimulated Brillouin backscattering.

../..

At the Rutherford laboratory radiation pressure steepening of the density profile has been clearly observed from 0.266μm wavelength interferograms of 45μm diam. glass microballoons irradiated by a Nd glass laser beam at an intensity of 10^{16} W.cm^{-2} and with a pulse duration of 50ps /3,6/.The microballoon corona is probed to 2 times the critical density and the density gradient length is of the order of the incident 1.06μm wavelength (figure 5). Megagauss magnetic fields generated by cross density and temperature gradients have also been measured from the Faraday rotation at 0.633μm - Raman shifted second harmonic Nd laser beam - or at the 0.266μm fourth harmonic in the UV region /7/.

III - TRANSPORT

Several experiments have been done to estimate the transport inhibition of absorbed laser energy and the preheating due to supra-thermal electrons. At Limeil and Rutherford the depth along which the absorbed energy diffuses inside the target or burn depth, has been deduced using plane or microballoon glass targets coated with aluminium /8,9/. X-ray Si lines emitted by glass through aluminium and Al lines are observed (figure 6) and for a given laser flux, Si lines disappears when the aluminium coating thickness is larger than the burn depth. With a 100ps Nd glass laser pulse and fluxes of the order of 10^{15}W.cm^{-2}, burn depths of 1000 Å to 1500 Å have been measured in both laboratories. At Rutherford the energy penetration is increased by a factor of 2 to 3 when the target is irradiated with the second harmonic (0.53μm) of the laser light /9/. At Limeil line intensity variations with aluminium thickness have been compared to numerical results given by a code in which the coronal assumption is used : a good fit is obtained if the classical electron thermal conductivity is reduced by a flux limited factor F of 2.10^{-2} (figure 6).

Garching has also evaluated energy penetration in the following way /10/. Low Z plastic foils of increasing thicknesses were irradiated with the 100 J - 300 ps iodine laser at fluxes of 10^{14}- 10^{15}W.cm^{-2}. The transmission T of the laser light through the foil and the hydro-dynamical efficiency η,i.e.the ratio of the energy (thermal and kinetic)

../..

of the accelerated foil measured by a calorimeter placed behind the foil to absorbed laser energy, are plotted versus foil, thickness d_F in figure 7. Ablation depth d_a corresponding to almost null transmission is 1600 Å at 2.10^{14} W.cm^{-2} and 4500 Å at 3.10^{15}W.cm^{-2}; similar results have been found by Ecole Polytechnique with larger burn depths at 0.53µm/11/. A simple rocket model explains satisfactorily T and η variations with respect to thickness. When attempts are made to fit these experimental measurements with numerical results given by a one dimension hydrodynamical code, it is again necessary to introduce a flux limited factor f of 5.10^{-3} as in the work done at Limeil on aluminium coated targets. All these experiments indicate that the transport of absorbed laser energy inside the target is strongly inhibited.

Ecole Polytechnique has deduced from X-ray continuum the temperature T_h of suprathermal electrons produced by plastic or aluminium targets at 1.06 and 0.53µm laser wavelength λ, for 100ps pulses and intensities Φ varying from 2.10^{13} to 2.10^{15} W.cm^{-2}. T_h scales like $\Phi^{0.4}$ but taking as reference the variations of T_h at 1.06µm, its value at 0.53µm is smaller than the one computed from the usual scaling law $[\Phi \lambda^2]^{0.4}$.

Using a few µm layered targets (for example Al - SiO_2 - KCl - mylar - CaF_2) the Rutherford laboratory has determined the suprathermal electron energy spectrum and the resulting preheat as a function of depth and laser intensity at 1.06µm, covering the range 5.10^{14} - 5.10^{15} W.cm^{-2} /3/. Suprathermal electrons excite fluorescent potassium and calcium K_α lines which are compared with those given by various models of electron energy distribution. The dependence variation on intensity of the deduced suprathermal electron temperature agrees well with X-ray continuum measurements, and preheat is of the order of 10% of the 20 J incident laser energy delivered in 100ps.

IV - IMPLOSION EXPERIMENTS

In Western Europe implosion experiments are being conducted at Rutherford and Limeil with neodymium glass lasers of 2 and 8 beams, respectively, and more recently at Aldermaston. Most experiments done with 100µm diameter bare glass microballoons filled with gas at a few tens bars and imploded by 100ps laser pulses at 10^{15} W.cm^{-2} are relevant to the exploding pusher mode which allows to reach keV

../..

temperatures and the density of solid. More recently in order to observe the ablation mode, and obtain higher final core densities, implosions of low Z material coated microballoons by nanosecond pulses have been undertaken. In both types of experiments special emphasis has been put on measuring the core features by the development of several diagnostic techniques such as X-ray imaging and spectroscopy, and particularly X-ray shadowgraphy for high core densities. For the exploding pusher mode, experimental results fit more or less with numerical simulations and analytical models which makes believe that this mode of implosion is partially understood. The experiments have also given some insight into symmetry and stability matters which are crucial to satisfy inertial confinement fusion requirements.

IV.1 - Exploding pusher mode

As other laboratories doing implosion experiments Limeil and Rutherford have extensively studied the exploding pusher mode in which laser energy is absorbed almost instantaneously and causes the glass shell explosion with the inner part imploding the gas contained in the shell. The main contributions of these laboratories to understand such a mode of operation deal with implosion symmetry, hydrodynamics, core features, and prepulse effects.

The influence of the beam number on implosion symmetry has been observed at Limeil using the 8 beams of the OCTAL laser which are focused on the target along the four diagonals of a concentric cube /12/. When the microballoon is imploded by 2 opposed beams only, 2 ω_0 and X-ray pinhole images show that the absorbed energy remains in the vicinity of the two interaction zones with the consequence of an irregular core structure. With 8 beams, on the contrary, pinhole images are symmetrical, the core being well contrasted. This result underlines that energy transport by thermal conduction or suprathermal electrons cannot compensate entirely laser beam dissymetries which have to be minimized to produce spherical implosions.

../..

Let us now give examples of measurements which were done to follow the implosion hydrodynamics and to determine core features.

Using an X-ray streak camera, Limeil measured the time delay between corona and core emissions for different microballoon diameters (60 - 120μm), DT gas filling pressures (10 - 30 atmospheres) and laser energies. The variation of the time delay (50 - 200ps) versus useful specific absorbed energy (0.03 - 0.15 $J.ng^{-1}$) (i.e. the part of the absorbed energy which contributes to the DT gas compression) is in fairly good agreement with the implosion time computed from a Livermore analytical model /14/ . Similarly at Rutherford, in order to follow the implosion hydrodynamics, it has been observed on neon filled glass microballoons the time delay between the Na Lyα and Ne Lyβ line emission originating from the glass plasma and the compressed neon gas, respectively, and it was found a dependence of the time delay on the microballoon size /15/.

Core features have been diagnosed with several means. From X-ray pinhole images Limeil has measured a DT gas volume compression of about 70 which corresponds to a density of 0.5 $g.cm^{-3}$ for a 80μm diam. glass microballoon filled with 30 bar of DT gas and incident laser energy of 35 J delivered in 50ps; maximum neutron yield of 10^7 has been observed /13/. At the Rutherford laboratory neon core density of 4 ± 2 $g.cm^{-3}$ has been measured from pulsed X-ray shadowgraphy : the 65μm diameter, 87 Bar neon filled microballoon irradiated at 5.10^{14} $W.cm^{-2}$ with 100ps, 1.06μm pulse was probed with 100ps duration, 1.8 keV X-rays emitted by a laser produced plama /16/ . This laboratory has also largely developed X-ray spectroscopy to diagnose the core viz.the space resolved spectrum along a microballoon diameter to distinguish the corona and core X-ray emissions which gives the core size, the electron temperature deduced from the slope of recombination continuum,the ionization state determined from the ratio of optically thin emission lines, the density ρ and density-length product ρr of the imploded glass and of the compressed gas from the line broadening of helium-like and hydrogen-like emission lines of silicon and neon, respectively/15/.

../..

In the latter measurement, experimental line profiles are compared with profiles calculated for various values of the electron density n_e and of the product $n_1 \ell$ (n_1 ground state density, ℓ line of sight depth), and then ρ and ρr are deduced from the unique values of n_e and $n_1 \ell$ that fit all the different He-like and H-like line data /3/. For example, electron density of $10^{23} cm^{-3}$ has been found from the Stark broadening of a He-like argon line emitted by an imploded argon filled microballoon, as argon is a more suitable tracer than neon for the diagnosis of very dense cores /15/.

Analytical models have been developed by STORM /14/, ROSEN and NUCKOLLS /17/, AHLBON and KEY /18/, in order to find scaling laws giving final density ρ and electron and ion temperatures of the compressed core with respect to the experimental parameters such as : aspect ratio $\frac{R}{\Delta R}$ (R radius, Δ R thickness) of glass shell, fill gas density ρ_o, energy density $\frac{E}{M_p}$ (E absorbed laser energy, M_p pusher mass). The scaling laws vary widely from one model to another as can be seen, for instance, in figure 8 relative to the final density ρ_F versus the initial fill gas density ρ_o for $\frac{R}{\Delta R} = 50$; the experimental data of different laboratories are widely scattered and do not cover a sufficiently large parameter range to validate any one of these models.

The effect of a prepulse on the implosion of 80µm diameter, 30 bar DT filled glass microballoons by a main 600 GW - 50 ps laser pulse at 1.06µm has been studied at Limeil /13/. When the prepulse power is increased from 10^{-6} to 10^{-4} times the main pulse power, the 0.2 $J.ng^{-1}$ absorbed specific energy is reduced by a factor of 2, the 3.10^6 neutron yield by a factor of 100 and the X-ray core emission is less intense. The smooth density gradients set by the early expansion of the glass shell due to the prepulse, seem to be at the origin of the lower absorbed energy and core performances.

../..

IV.2 - Ablative mode

Because it appeared difficult to reach densities much larger than solid density with the exploding pusher mode in which short duration (100ps) laser pulses irradiate bare microballoons at high intensity (10^{15} W.cm^{-2}), experiments have been done more recently with plastic coated microballoons which are progressively ablated by 10^{14}W.cm^{-2} nanosecond pulses in attempt to obtain high final densities. In this second mode the fill gas is not preheated by a strong shock and consequently higher core densities are obtained but also lower temperatures and neutron yield. It is not possible any longer to deduce core data from the observations of X-ray and neutron emissions and one has to develop new diagnostic techniques such as X-ray shadowgraphy.

At Limeil, a delayed ninth beam of the OCTAL laser is focused on a plane brass target, the X-ray emission of which probes the microballoon imploded by the other eight beams /19/. The experimental set up is shown in figure 9. The 30µm diameter, 50 ps duration, 1.3 keV X-ray copper line source and the imploded microballoon are imaged by a 2 pinhole X-ray camera in such a way that the source alone, the microballoon alone and both source and microballoon emissions are recorded on the same film, the Al foil filter improving the source signal - microballoon noise ratio. The X-ray transmission $\left(\frac{E}{E_o}\right)_c$ of the target along its diameter is given in figure 10 for bare and plastic coated 80µm diameter microballoons and for specific absorbed energy of the order of 0.2 J.ng^{-1} delivered in 50ps. Low transmissions are observed with low intensities and thick microballoons, bare or coated with plastic; the shell thickness is larger than the energy penetration depth and part of it remains at low temperature (less than a few 100 eV) and is opaque to the 1.3 keV X-ray radiation. On the contrary in the exploding pusher mode, thin glass shells irradiated at high intensities reach 1 keV temperature all over their thickness and their transmission is close to 1. Therefore, this diagnostic technique which will be used with nanosecond laser pulses gives information on the implosion mode behaviour.

../..

X-ray shadowgraphy has also been developed at Rutherford in a similar manner /3, 16/. The microballoon and the backlighting laser plasma source are mounted on the same stand. A streak camera resolves in time along a microballoon diameter both the microballoon self emission and the X-ray source radiation transmitted through the microballoon. The latter is delayed with respect to the imploding laser pulse in a variable way.

Experiments have been done at 1.06μm with 1.6ns laser pulses and low intensities of 3.10^{13}W.cm^{-2} on 240μm diam., 1.4μm thick glass microballoons coated with 1 to 6μm of polymer. The ratio of hot electron preheating range to shell thickness is of the order of 0.1 to 0.5. With X-ray backlighting delayed by 1.8ns relative to microballoon irradiation the peak compression appears on the streak film as an absorbing zone with 100μm minimum width corresponding to a glass core density of 10g.cm^{-3} and the outer boundary radius r of the central opacity region plotted vs. time (figure 11:dots) fits well with numerical simulation results (curve). Moreover, the careful examination of streak microdensitograms suggests the development of Rayleigh-Taylor instabilities in the imploding shell; one observes :

- very intense shell X-ray emission probably due to the mixing of cold glass with the hot ablation polymer plasma;
- the diffuse boundary of the central absorption zone;
- the backlighting X-ray opacities lower by a factor of 4 than the one calculated.

These facts are consistent with initial 0.3μm ripples in the polymer coating and the computation of Rayleigh-Taylor instability growth exponent γt (γ growth rate) reaching 10 before a 20% radius compression of the shell (figure 11). The Rutherford laboratory had made similar observations for an exploding pusher type implosion with outside aluminium coated glass microballoons imploded with 100ps laser pulses, where aluminium was detected in the core itself from space resolved X-ray spectroscopy /3/.

../..

V - THEORY AND NUMERICAL SIMULATION

The experiments which have been described are supported by extended work on theory and numerical simulation in order to gain better knowledge of the significant phenomena, and to prepare these experiments and interpret their results. Analytical work deals, in particular, with the following topics :

- Resonance absorption. The time and space electric field variations in the resonance peak have been calculated at the University of Berne /20/ and the electron energy distribution as altered by this peak (with the creation of a high energy tail) has been deduced. Work has also been done on magnetic field generation and on effects due to a rippled critical surface /3, 21/.
- Electron thermal flux limitations. At Limeil, to model fluid behaviour when high gradients exist, a system giving the fourteen moments of a kinetic equation has been set which describes both adiabatic collisionless and collisional flows /13/. Flux inhibition due to the ion acoustic instability /13/ or to a turbulence induced chaotic magnetic field /23/ has been evaluated, and at Université Libre de Bruxelles /24/, anomalous transport coefficients in a weakly turbulent plasma have been calculated.
- Plasma radiation, the observation of which is a powerful diagnostic tool. One uses non LTE plasma ionisation models line broadening and radiation transport /3,13/.
- Hydrodynamical expansion of the laser produced plasma. The influence of radiation pressure on plasma flow was investigated at Garching; there are domains of subsonic and supersonic flows/25/. At the University of Madrid it was studied the transition from isentropic to isothermal expansions created by long-low intensity and short-intense laser pulses, respectively /26/. Similarity solutions of the expansion flow have been found /22,23/, in particular approximate solutions for a two component plasma at Chalmers University of Technology in Göteborg/27/.

../..

- Analytical models of the laser implosion. The exploding pusher model [14,17,18] or the model developed at Frascati [28] are useful to optimize target and laser parameters in order to obtain high fuel core densities and temperatures. The scaling laws which are deduced from them serve as guides to target design and laser development.
- Fluid dynamic stability. At Limeil small perturbation growth has been described by an analytical model including viscosity and self-generated magnetic fields [29].

Owing to the complexity of the phenomena, plasma numerical simulation and hydrodynamical codes are developed extensively and supplement the above theoretical investigations. The interaction of laser electromagnetic field with plasma is simulated by $1\frac{1}{2}$ dimension (i.e. one spatial and two velocity and field components) or $2\frac{1}{2}$ dimension (two spatial and three velocity and field) particle-in-cell codes which are used for various studies such as incident laser light harmonic generation, long pulse Brillouin scattering, density profile steepening by ponderomotive force, fast electron generation and radiation induced magnetic field [3, 23]. One dimension and two dimension hydrodynamical codes, with always greater sophistication, have been worked out to understand laser light absorption, energy transport and implosion mechanisms. Recent work is relative to laser light ray tracing in the expanding corona, non LTE ionisation models, flux limited thermal conduction [31], Monte Carlo or multigroup diffusion simulations of fast electron penetration and preheat [32], magnetic field generation and consequent thermal conduction inhibition [3], radiation transport, hydrodynamic stability of the ablation layer and of converging shock fronts [33].

VI - CONCLUSION

The experimental investigations with refined diagnostic techniques as well as the theoretical and numerical studies which have been reported supplement research conducted in other laboratories and give some insight into the complex field of laser-matter interaction. They show greater absorption at shorter wavelengths, transport inhibition, preheat by suprathermal electrons, and exploding pusher and ablation mode behaviours The laboratories of Europe continue their work which will be conducted in the future with larger facilities now under construction (figure 2).

REFERENCES

/1/ G.BREDERLOW, R.BRODMANN, K.EIDMANN, M.NIPPUS, R.PETSCH, S.WITKOWSKI, R.VOLK, K.J. WITTE : Performance of the Asterix III high power iodine laser - Garching- (CLEA Conf. Washington, 1979, June).

/2a/ J.EMMETT : US research on initial confinement (9th Europ. Conf. on Control. fusion and plasma physics, Oxford, September 17-21, 1979 - D1.5).

/2b/ V.B. ROSANOV : Laser fusion research in the Soviet Union (Oxford, September 17-21, 1979 - D1.1).

/3/ Annual Report to the Laser Facility Committee 1979 (Rutherford Laboratory)

/4/ J.L.BOCHER, JC.COUTURAUD, M.DECROISETTE, G.GOUEDARD, M.LOUIS-JACQUET, J.MARTINEAU, B.MEYER, C.PATOU, M.RABEAU, A.SALERES, G.THIELL : Light plasma interaction studies (12th Eur.Conf. on Laser Interaction with Matter and Laser Thermonuclear Fusion, December 11-15, 1978 Moscow).

/5/ K.EIDMANN, G.BREDERLOW, R.BRODMANN, R.PETSCH, R.SIGEL, G.TSAKIRIS, R.VOLK, S.WITKOWSKI : Stimulated Brillouin backscattering losses in weakly inhomogeneous laser produced plasmas (Garching)(to be published).

/6/ A.RAVEN, B.AHLBORN, Rutherford
O.WILLI, Oxford
Structures in the electron density profiles of laser produced plasmas at high irradiances (Conf.Gordon, Tilton, August 1979).

/7/ A.RAVEN, O.WILLI and P.T.RUMSBY : Megagauss Magnetic Field Profiles in Laser-Produced Plasmas (Vol.41 N 8, Physical Review Letters 8-21,79)

/8/ G.THIELL, B.MEYER, M.LOUIS-JACQUET, JC.COUTURAUD : Spectrometrie X dans les plasmas créés par laser : Application à l'étude des phénomènes de transport de l'énergie (14e Conf. Intern. sur les phénomènes d'Ionisation dans les gaz, Grenoble, July 9-13, 1979) (to be published in the "Journal de Physique".

/9/ JD.KILKENNY, DJ.BOND, DR.GRAY, JD.HARES, RG.EVANS, M.KEY, W.TONER and JG.LUNNEY : Energy transport from 1.06µm and 0.53µm laser plasmas interactions at 10^{15} W cm^{-2} (Oxford, September 17-21, 1979 - E1.3)

/10/ G.BREDERLOW, R.BRODMANN, K.EIDMANN, P.MULSER, R.PETSCH, R.SIGEL, G.SPINDLER, G.TSAKIRIS, R.VOLK and S.WITKOWSKI : Acceleration of thin foil targets under intense laser irradiation (Oxford, September 17-21, 1979 - E1.4).

/11/ F.AMIRANOFF, R.FABBRO, E.FABRE, C.GARBAN, J.VIRMONT and M.WEINFELD (Lab. Ecole Polytechnique) - Vol. 43 N 7, Physical Review Letters 8-13, 1979.

/12/ D.BILLON, JC.COUTURAUD, M.DECROISETTE, PA.HOLSTEIN, J.LAUNSPACH, M.LOUIS-JACQUET, C.PATOU, JL.ROCCHICCIOLI, A.SALERES, D.SCHIRMANN : Eight beams implosion experiments at Limeil (12th Conf. on Laser Interaction with Matter and Laser Thermonuclear Fusion, December 11-15, 1978 Moscow).

/13/ A.BEKIARIAN, A.BERNARD, E.BURESI, R.DAUTRAY, M.DECROISETTE, F.DELOBEAU, P.GUILLANEUX, JM.REISSE, B.SITT, JM.VEDEL and JP.WATTEAU : Laser-matter interaction and implosion studies at Limeil Research Center (Oxford, September 17-21, 1979 - E1.6).

/14/ E.K. STORM, HG AHLSTROM, MJ. BOYLE, DE CAMPBELL, LW COLEMAN, SS.GLAROS, HN KORNBLUM, RA LERCHE, DR MACQUIGG, DW PHILLION, F.RAINER, R.RIENECKER, V.C. RUPERT, V.W.SLIVINSKY, DR SPECK, CD SWIFT and KG TIRSELL : Laser fusion experiments at 4 TW (Livermore) - Vol. 40 N 24, Physical Review Letters,June 12, 1978.

/15/ JG.LUNNEY, MH.KEY, J.KILKENNY and RW.LEE : X-ray spectrometry of laser compressed microballoons (Rutherford) - Oxford, September 17-21, 1979 - DP25.

/16/ CLS. LEWIS, L.COOKE, JG.LUNNEY, A.MOORE, JM.WARD, RG.EVANS, MH.KEY and TA HALL : Studies of laser driven implosions by time-resolved shadowgraphy (Rutherford) - Oxford, September 17-21, 1979 - E1.5.

/17/ MD. ROSEN and JH. NUCKOLLS : Exploding pusher performance - A theoretical model (Phys.Fluids 22(7) July 1979).

/18/ B.AHLBORN and MH. KEY : Scaling laws for exploding pusher targets Rutherford (Internal Report RL 79-033).

/19/ J.LAUNSPACH : Eight beams exploding pusher type implosion experiments in Limeil (Laser Matter Interaction Gordon Conference, Tilton,August 13-18, 1979).

/20 JE.BALMER, P.LADRACH, AP.SCHWARZENBACH, TP.DONALDSON and HP.WEBER : Interaction of short 1.06µm laser pulses with low-z plasma (University of Berne) - Oxford, September 17-21, 1979 - DP 23).

/21 P.MORA and R.PELLAT : Kinetic theory of magnetic field generation in the resonant absorption of light (Le Journal de Physique - Lettres Tome 40, June 15,1979 p.245).

/22 P.MORA, R.PELLAT : Self similar expansion of the plasma into vacuum (to be published in the Physics of Fluids).

/23 Rapport d'activité 1978 du Groupement de Recherches Coordonnées (GRECO) Interaction Laser Matière - Ecole Polytechnique.

/24 R. BALESCU and I.PAIVA-VERETENNICOFF : Anomalous transport coefficients in a turbulent plasma (J.Plasma Physics (1978) vol.20, part 2 pp.231-263)

/25 P.MULSER, G.SPINDLER : Radiation pressure dominated plasma flow (Max-Planck Gesellschaft - Garching) (Internal Report PLF 12, December 1978).

/26 A.BARRERO and JR. SANMARTIN : Transition from isentropic to isothermal expansion in laser-produced plasmas (University of Madrid) - Oxford, September 17-21, 1979 - DP 26.

/27/ D.ANDERSON, J. FAULKNER and H.WILHELMSSON, University of Göteborg K.NISHIKAWA and T.TANGE, University of Hiroshima : Study of Similarity Flows of Two Component Laser Produced Plasmas (Physica Scripta Vol. 18, 141-145, 1978).

/28/ A.CARUSO : Model experiments for laser driven hydrodynamics (CNEN Frascati) (11th Eur.Conf. on Laser Inter.with Matter, Oxford, September 19-23, 1977).

/29/ B.SITT : Analytical and numerical studies of the linear stability of inertial confinement fusion target implosion (Bulletin of APS 24(4)721(1979)).

/30/ PLF Jahresbericht 1978 (Max-Planck-Gesellschaft - Garching)

/31/ R.BENATTAR, C.POPOVICS, R.SIGEL and J.VIRMONT : Transport inhibition implied by density profile flattening in the corona of laser-heated microspheres (Ecole Polytechnique) - Physical Review Letters Vol. 42, N 12, March 19,1979.

/32/ J.P. NICOLLE : Etude du ralentissement d'électrons suprathermiques dans un plasma créé par laser (Rapport CEA - R 4898)

/33/ N.WILKE, B.SITT : Stability of a spherical shock wave in the implosion of an ICF target (APS 1979 Topical Conference on Shock Waves and Condensed Matter, Pullman (Washington) June 11-13,1979).

LASER FUSION RESEARCH LABORATORIES IN WESTERN EUROPE

COUNTRY	LABORATORIES	TOWN	OBSERVATION
BELGIUM	* Université Libre de Bruxelles	Brussels	theory
ENGLAND	Rutherford Laboratory	Chilton	university groups implosion
	Atomic Weapons Research Establishment	Aldermaston	implosion
FEDERAL REPUBLIC OF GERMANY	* Projektgruppe für Laserforschung, Max-Planck-Gesellschaft	Garching	
FRANCE	GRECO Interaction Laser-Matière - Ecole Polytechnique	Palaiseau	12 CNRS and university groups
	Centre d'Etudes de Limeil, Commissariat à l'Energie Atomique	Limeil	implosion
ITALY	* Comitato Nazionale per l'Energia Nucleare	Frascati	
SPAIN	Universidad Politécnica de Madrid	Madrid	
SWEDEN	* Institute for Electromagnetic Field Theory, Chalmers University of Technology	Göteborg	theory
SWITZERLAND	Institute of Applied Physics, University of Berne	Berne	

* Euratom

Figure 1

MAIN LASER FACILITIES IN WESTERN EUROPE

COUNTRY	LABORATORY	AMPLIFYING MEDIUM	ENERGY J	POWER (100 ps) TW	PULSE DURATION ns	NUMBER OF BEAMS	OBSERVATIONS
ENGLAND	Aldermaston	Nd	1 000	2	1	2	
	Rutherford	Nd	200 (2 000)	0.7 (6)	1.7 (1)	2 (6)	Implosion experiments
FEDERAL REPUBLIC OF GERMANY	Garching	I	300	1	0.3	1	
FRANCE	Ecole Polytechnique	Nd	120	0.25	2.5	1	at 0.53 μm : 6J - 60GW - 2ns
		CO_2	12		1	1	
	Limeil	Nd	800	1.3	1	8	Implosion experiments
			20	0.3	0.06	1	
ITALY	Frascati	Nd	10 (500)		2	1 (2)	
		CO_2	50 (2 000)		1	1 (2)	1981

( ) : under construction or in project.

Figure 2

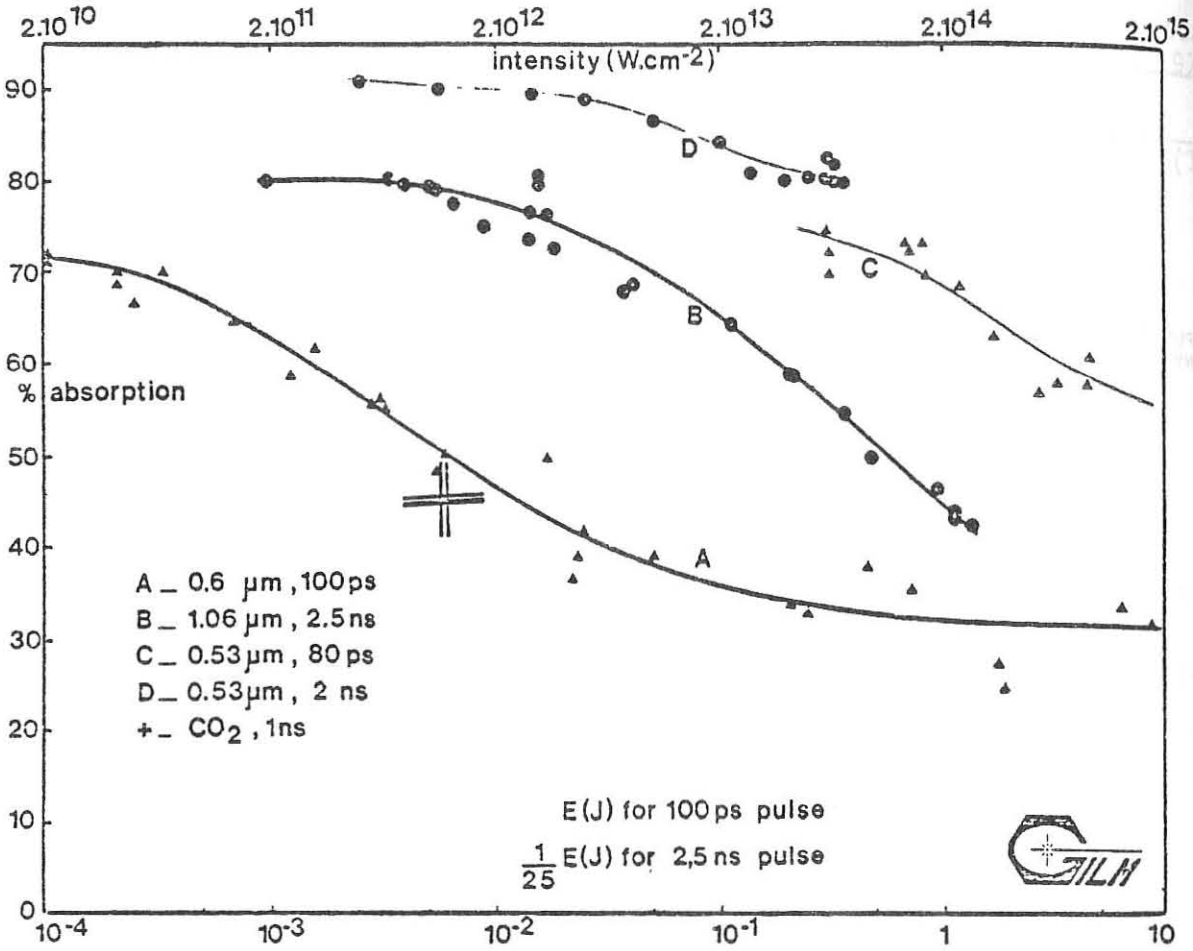

Figure 3

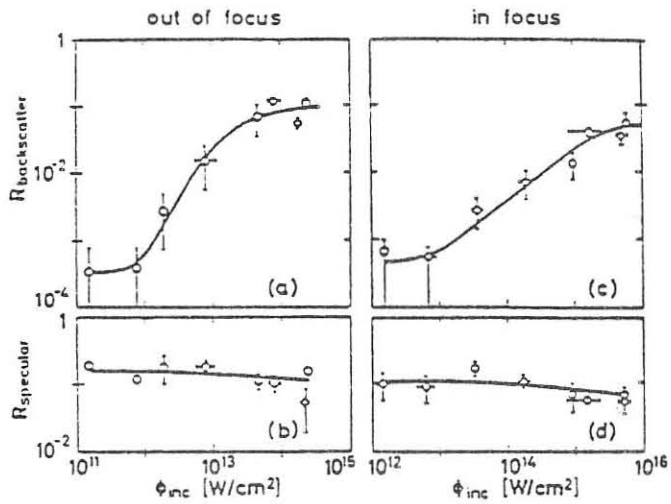

Figure 4 : SPECULAR AND BACKSCATTER REFLEXION COEFFICIENT R VERSUS INCIDENT FLUX ϕ_{inc}

Figure 5 : RADIATION PRESSURE STEEPENED DENSITY PROFILE AT 1.06µm WAVELENGTH.

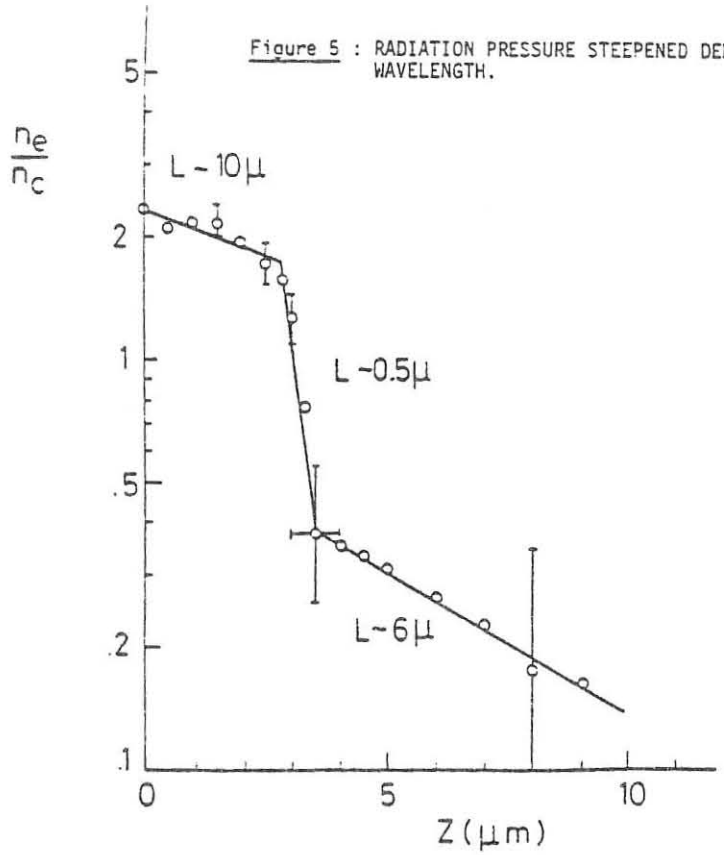

EXPERIMENTAL AND CALCULATED (a.u) X RAY LINE ENERGIES

EMITTED BY A PLANE TARGET COATED WITH ALUMINIUM

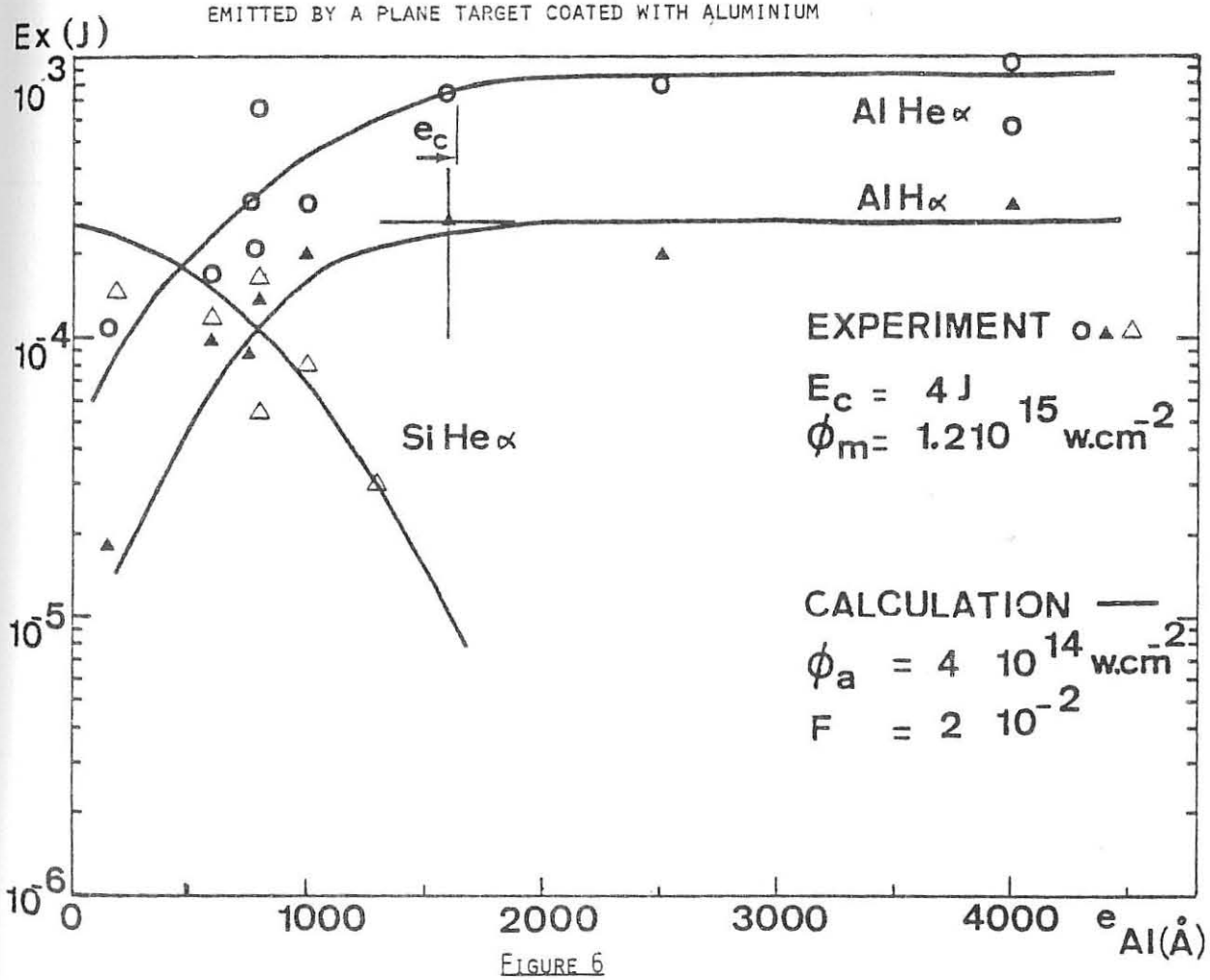

FIGURE 6

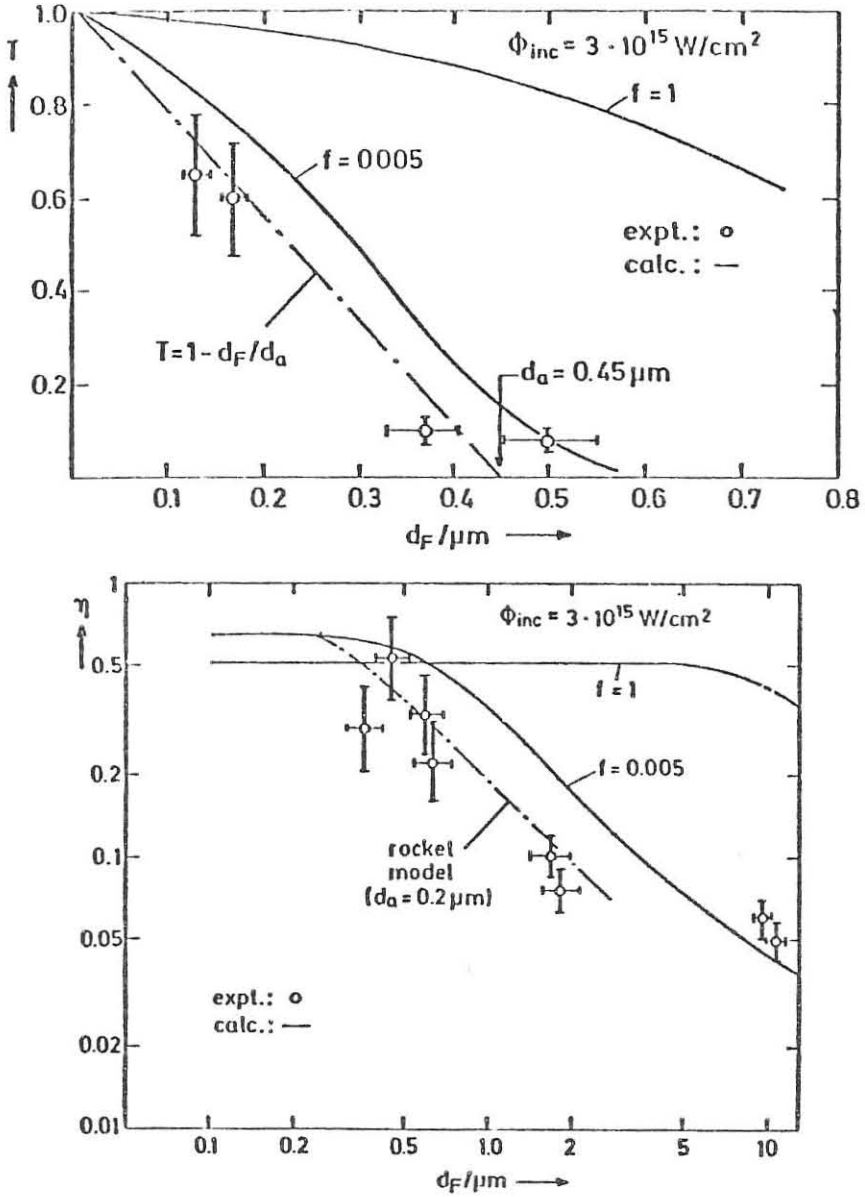

Figure 7 : LASER LIGHT TRANSMISSION T AND HYDRODYNAMIC EFFICIENCY η VERSUS FOIL THICKNESS d_F

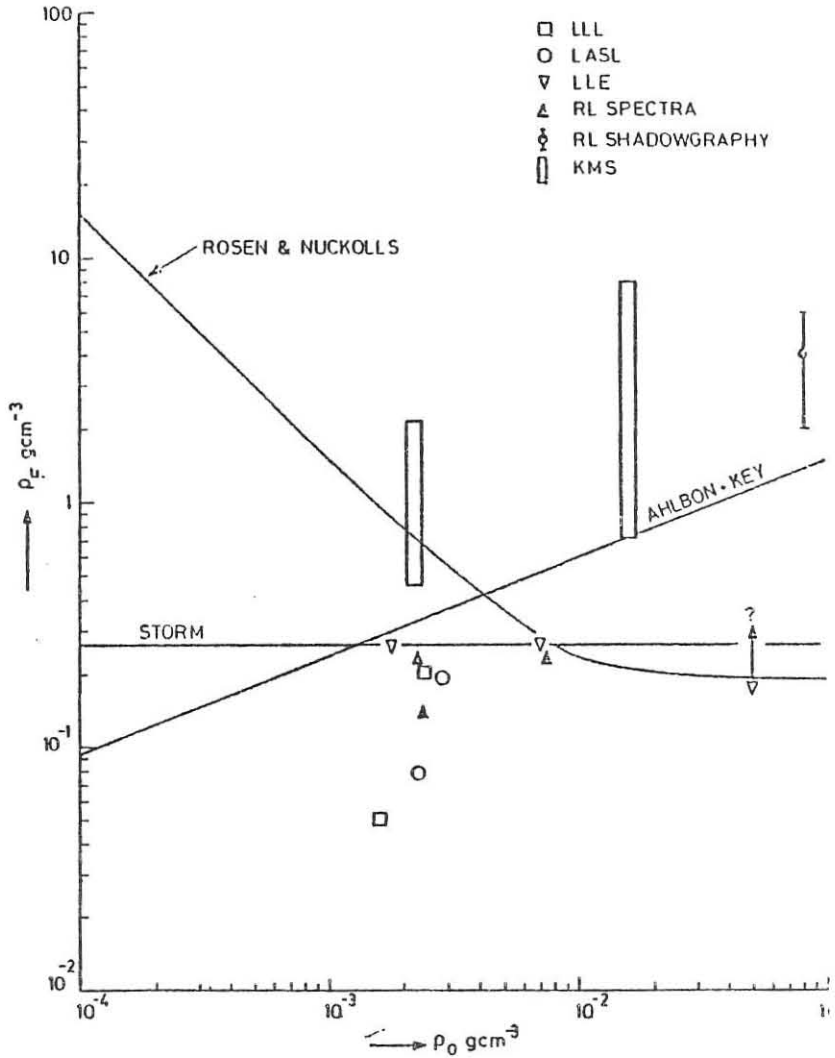

Figure 8. Comparison of the maximum density ρ_F calculated with the models of Rosen Nuckolls (RN), Storm (S) and our model (AK) with experiments (référence 18).

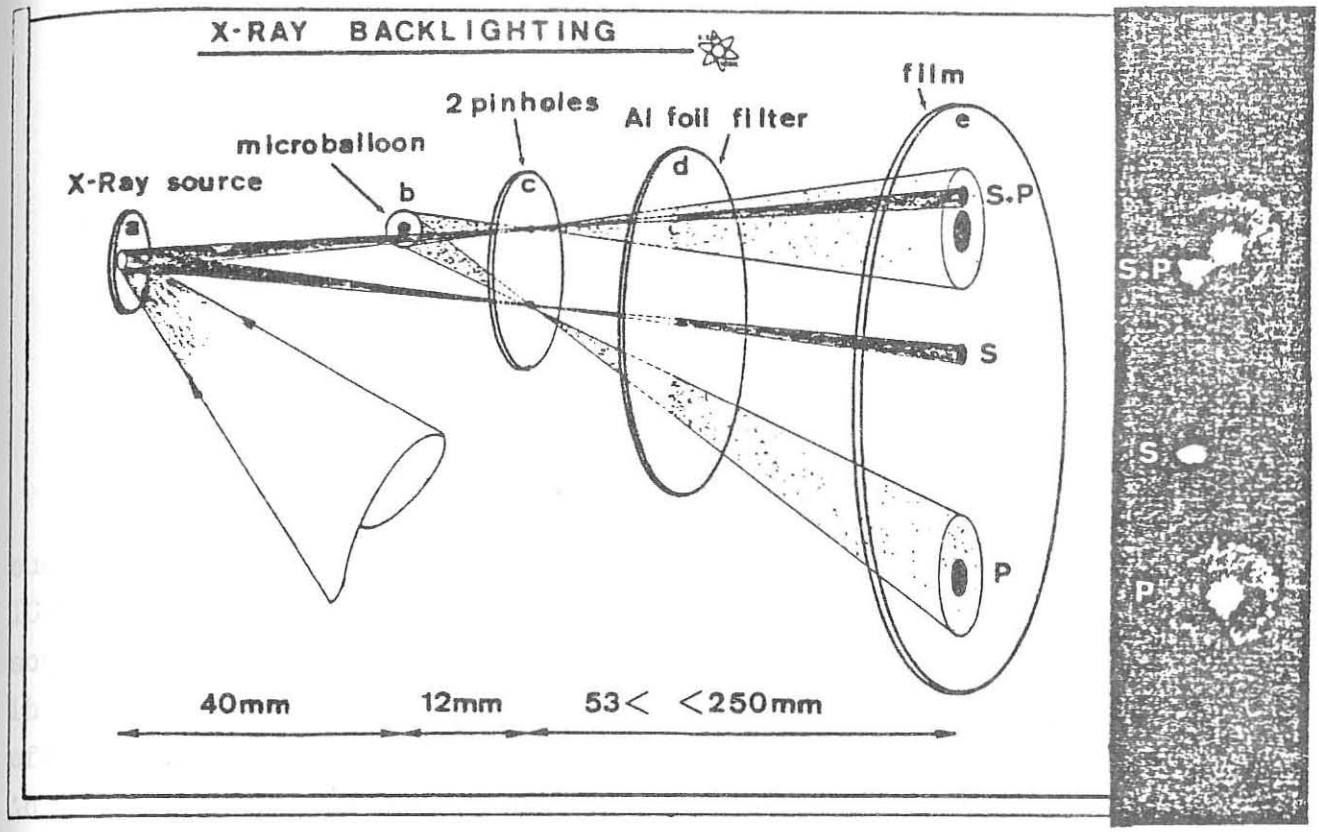

Figure 9

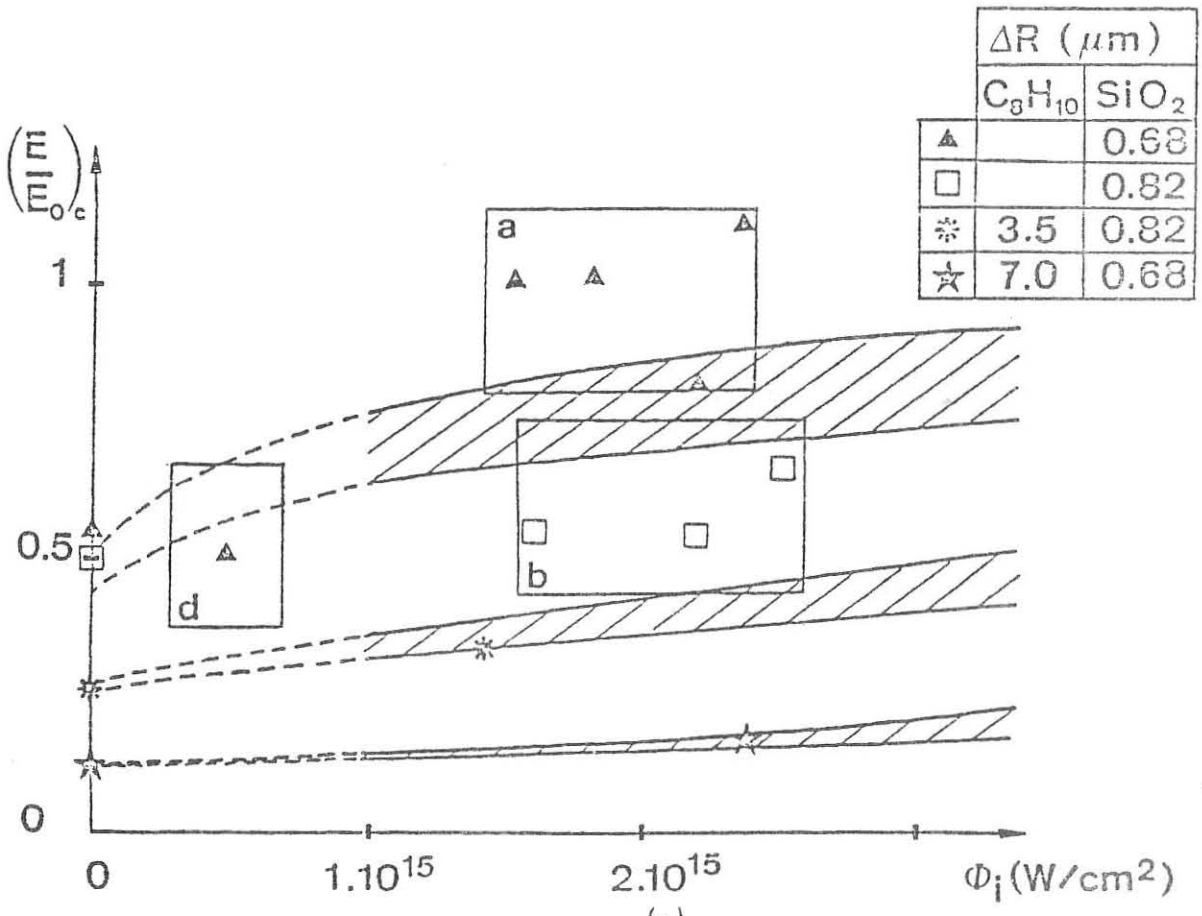

MICROBALLOON X-RAY TRANSMISSION $\left(\frac{E}{E_0}\right)_c$ VERSUS INCIDENT INTENSITY Φ_i

Figure n° 10

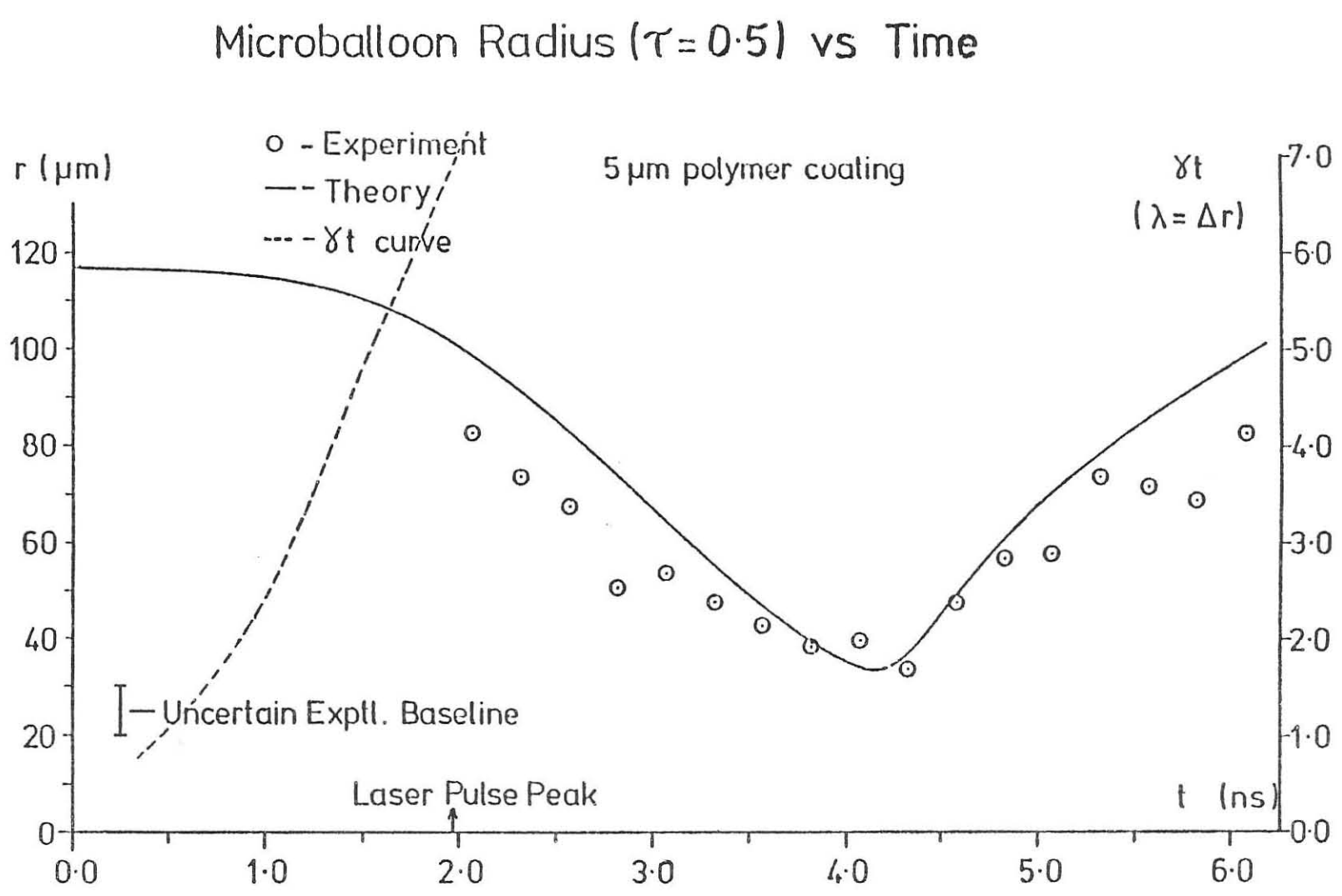
Microballoon Radius (τ = 0·5) vs Time
r (μm)
o - Experiment
— - Theory
--- - γt curve
5 μm polymer coating
γt
(λ = Δr)
120
100
80
60
40
20
0
7·0
6·0
5·0
4·0
3·0
2·0
1·0
0·0
Uncertain Exptl. Baseline
Laser Pulse Peak
t (ns)
0·0
1·0
2·0
3·0
4·0
5·0
6·0

Figure 11

Progress in the production and energy flux concentration of the REB accelerator for ICF

V.P. Smirnov

I.V. Kurchatov Institute of Atomic Energy, USSR

1. Introduction

The energy flux concentration on the surface of a thermonuclear target is the main problem at the present stage of the ICF investigations with high power pulse generators as an energy source. The efforts are aimed mainly at achieving high efficiency in the transmission and at investigating the mechanisms of an efficient energy deposition on the outer surface of the pellet. An analysis of the transmission requirements has shown that it is necessary to provide energy flux transportation from the generator output to the pellet surface for a distance of a few meters and to reach a 10 TWt/cm^2 energy flux density [1]. At present several schemes of the transportation have been proposed. The first scheme is based on to the use of a selfmagnetic insulation vacuum transmission line (MITL), connecting the generator output directly with the pellet surface. A selffocused electron beam is formed in the diode gap between the external pellet shell and negative line electrode. The results obtained recently at the Kurchatov Institute on the reliability of this scheme are described in sec II.

The REB energy can be also transported along the plasma channel between the pellet and accelerator output [2] . The electron beam is confined in the channel by the magnetic field generated by an external source. The application of the plasma channel allows us, in principle, to avoid microexplosion distruction of MITL in the vicinity of the pellet. However, in large scale experiments with a few tens of channels, an increase of the energy flux density on the pellet surface is rather small, 3÷4 [3] . The works on the application of high current light ion beams generated in a REB accelerator have recently found

increasing development [2-4] It is also possible to use an ion beam for the energy concentration on the pellet [4] The propagation of ion beams along the plasma channels provides a means for increasing the peak power due to spatial bunching when the diode voltage grows during a pulse.

The present paper outlines the recent results on the energy flux concentration, obtained at the Rudakov's division of the Kurchatov Institute.

2. Magnetic insulation vacuum transmission lines (MITL)

It is wellknown that in a self magnetic field, an equilibrium state exists in an electron layer arising around the negative electrode due to the influence of a very high electric field. To provide such an equilibrium the line current must exceed certain critical value, calculated from the Brillouin model for a minimum line energy per unit length (I min). This fact is confirmed by a number of experiments [5] . Some experiments [6] show that the critical insulation current may exceed I min and approximate the paropotential current $I_p = 8{,}5 \frac{R}{d} \gamma \ln(\gamma + \sqrt{\gamma^2 - 1})$, which corresponds a situation when the interelectrode gap is entirely filled by the electron layer ($\gamma = 1 + \frac{eV}{mc^2}$, $2\pi R$ - the perimeter of the line crosssection). In practice, however, these currents differ from one another by no more than 1.5 times. The majority of experiments show that the electron layer is sufficiently stable in a uniform line and the electron leakage in small when the line current exceeds the critical value.

Usually for $\geqslant 1 MV$, $\sim 50 ns$ experiments the pulse propagation time along MITL is comparable with the pulse front or even with the pulse duration time. The wave regime of the self-magnetic insulation arising in this case was investigated in Refs. [5, 7] , and it was shown that the wave current behind the front was close to the minimum one. The wave dissipation was caused by the front leakage current. The transmission efficiency is about 70 - 90 per cent for practically important cases, $\gamma \sim 5$, $\ell \sim 5 \div 7 m$ The theoretically calculated value is in good agreement with experiment [7] . (Fig. 1).

Thus, the problem of efficient propagation can be solved by using a uniform MITL. A demand for an energy flux concentrated on ~1 cm pellets leads to the use of a converging line on the top of MITL. From technological considerations the converging line length should be small and the wave effects are not essential. Therefore, the converging line can be regarded as the MITL load resistance.

The load resistance at the uniform line top gives rize to a reflected wave. A.V. Gordeev and V.V. Zajivihin developed a Brillouin flow model with incident and reflected waves. They have showed that there is no reflection when the load resistance is larger than the MITL impedance. The energy output decreases in comparison with that of the conventional line. The intensity and velocity of the reflected wave can be calculated from the following expressions [8] ,

$$\frac{u}{c} = \frac{\gamma_1 - \gamma_2}{\alpha_2 - \alpha_1}, \quad i_1\left(1 + \frac{u}{c} th\psi_1\right) - i_2\left(1 + \frac{u}{c} th\psi_2\right) = 0$$

where indices 1 and 2 denote the incident and reflected waves, respectively. The above expressions should be supplemented with the equations,

$$\gamma_k - 1 = i_k th\psi_k - \psi_k sh\psi_k - ch\psi_k + 1$$
$$\alpha_k = i_k - \psi_k ch\psi_k - sh\psi_k$$
$$\gamma_k^e = ch\psi_k$$

(i_k — the line currents, γ_k^e — the potential of electron layer boundary).

At present the investigation of the converging line is being made both theoretically and experimentally at the Kurchatov Institute of Atomic Energy. The main problems are equilibrium and stability of the electron layers, plasma formation on the electrode line surfaces, the effect of ion leakage on electron layers equilibria and dissipation along the line, plasma motion across the interelectrode gap. The most important problem is the matching of MITL with a high aspect ratio diode, this is probably responsible for the main contribution to the energy losses. The first experiments with the converging lines have shown that energy transmission along a biconical line at relatively small angles on the line top can be descrioed by the

Brullouin flow model where the line current is larger than the minimum current. This is also true for a nonuniform line where the interelectrode gap in the end part of the line remains constant. This line geometry seems to be more reliable because a $\sim 10^{-2}$cm gap needed for high power experiments can be rapidly filled with plasma.

Unfortunately, no theory of converging nonuniform lines has been developed so far. Therefore, the optimistic result of the model experiment with a voltage not larger than 400 KV should be confirmed by higher power level experiments.

A plasma sheath appears on the positive line electrode surface during the formation of the self-magnetic insulation regime and diode impedance. This occurs after the electron leakage energy deposition has reached 100-200 j/g . The MHD calculation shows that the electron layer equilibrium still exists if the line current is increased. The current is increased to compensate for the growth of an electric force due to the electric field redistribution across the gap. A.V. Gordeev showed that the minimum current increased by 1/3 when $\gamma \gg 1$ and the ion leakage slightly exceeded the value calculated from the Child-Langmuir law [8] . Fig. 2 demonstrates the calculated dependences of the minimum current on γ . For comparison one may see the experimental points obtained in the model experiments. The scheme of the experiments is given in Fig. 3. A part of the external cylindrical electrode was replaced by a dielectric tube of the same diameter. The flashover created a plasma sheath and caused an ion leakage. Theory and experiment are sufficiently well consistent when the plasma sheath motion can be neglected. It should be pointed out that there are no instabilities leading to considerable losses at $\ell = 20d$ (d- the interelectrode gap).

The expansion of the electrode surface plasma layer can be suppressed. The one-dimensional MHD calculations taking into account Joule and ion heating, electron and radiation thermal conductivity demonstrate the possibility of suppressing the plasma expansion. These calculations were made by V.V. Gorev, S.B. Popov and Yu. P. Popov. Fig. 4 shows the position of a

cathode plasma front expanding towards the anode at different instants of time. The voltage and current pulses used in the calculation code have a trapezoidal form with the footstep pulse duration of 90 ns and 30 ns rise and decay times. Future experiments should check the validity of the one-dimensional calculations of plasma confinement near the electrodes.

The impedance of the output line diode will be larger than a line one, its value can be decreased due to the appearance of plasma as has been suggested in the previous papers [9] . The direct measurements made using the 5 frame laser interferometry in the strip line model experiment (see Figs. 5, 6) have shown that the diode is filled with cathode and anode plasma of the density of $10^{16} cm^{-3}$ and the velocity of $3 \cdot 10^{6}$ cm/s. The plasma layers have a sharp gradient of 10^{18} cm^{-4}. An analysis of a diode impedance behavior has shown that there is a lower density plasma of 10^{14} cm^{-3} located just ahead of the gradient.

This plasma can reduce the diode impedance by a factor of 100.

The recent experiments carried out with the beam current of 200 KA showed that more than 70 per cent of the energy could be deposited into a 1-2 mm focal spot. Future experiments are aimed at line and diode matching, the improvement of focusing.

3. Acceleration of a cylindrical shell by the magnetic field pressure.

The previous experiments with REB foil heating have demonstrated a feasibility of obtaining a velocity of $2 \cdot 10^7$ cm/s, needed for initiating a reaction [10] . However, only ~10% of the energy is converted into the kinetics shell energy in the ablation regime. . It is possible to increase the energy transfer coefficient if the shell is accelerated by a magnetic field pressure. The Liner acceleration investigations have a long history. As a rule the energy sources with an operation time τ greater than 10^{-6}s were used in these experiments [11, 12, 13]. The scaling laws show that the required energy W is proportional to τ^3 Therefore a decrease in τ when using REB generators ($\tau \leq 10^{-7}$s) will cause a considerable energy reduction.

In November 1978 S.G. Alichanov, V.P. Smirnov and I.R. Yampolsky under the guidance of Rudakov who initiated this work prospects of applying REB generator to liner acceleration. The same investigation were conducted in the USA on the Proto II and Pithon accelerators [14] . As the 0-dimension calculation have shown to transfer 40-50% of the generator energy the shell a time-dependent part of the system inductance ~~e~~- the generator output -- MITL - liner -- should be approximately equal to the initial inductance. On the other hand the transmission line voltage must reach a value $V \sim \frac{4I}{\tau} \sim 1MV$ for a cylindrical 1 cm high shell with a radiu of 1 cm and a pulse duration of 10^{-7} s, which are of practical interest. Thus, the energy transmission problem can be solved only with MITL.

The energy transmission is made easier when a line load impedance is the inductive type. In this case the electron leakage must be smaller especially near the shell at the pulse front. Therefore the influence of a line nonuniformity will be weaker. It will allow decrease in the MITL inductance when using a 3-dimensional scheme for the energy flux concentration (see Fig.7).

The application of a liner accelerated by the REB generator as an energy source is associated with such problems as uniformity, stability and heating, which should be solved. It is possible to reduce the required generator energy if a magnetic field is produced in the plasma and thus to diminish plasma thermal conductivity: $W \sim k^{-1}$ (k-the reduction coefficient of thermal conductivity). In this case the shell velocity is

$$V \simeq \frac{2 \cdot 10^7}{k^{1/2}} \text{ cm/s.}$$

4. The Angara-5 accelerator.

The problems of the Angara-5 accelerator constructing are being studied at the Kurchatov Institute. Angara-5 has 5 beam energy, 2 MV diode voltage, 40 MA beam current 90 ns half-width pulse duration.

The full-scale Angara-5 accelerator will consist of 48 units located on two floors (see Fig. 8).

At present the main scheme of the Angara-5 energy transmission and concentration is based on MITL connected electrically with the pellet through the diode gap. Nevertheless Dr. E.Z. Tarumov and his co-workers continue to study the electron beam trapping into a cusp and the production of the electron cloud to heat the pellet [15] . Dr. S.L. Nedoseev group started the investigation of the combined transportation scheme [16] , in which a particle beam propagates along the magnetic field into a reverse diode [17] . In the diode, its energy is transfered into electric pulse which energy is transmitted along the system of the converging MITL onto the pellet. The first experiments revealed a sufficiently good efficiency of 30-40 per cent.

An experimental Angara-5 module has been made by the Efremov Institute. Now the module assembly is about to be completed at the Kurchatov EInstitute. The general unit lay-out is shown in Fg. 9 . The main calculated unit parameters are as following:

Marx generator energy storage	- 305 kJ
Marx capacitance	- 85,7 nF
Marx voltage	- 2,67 MV
Blumlein capacitance	- 76,5 nF
Transmission waterline length	- 5 m
Number of Blumlein switches	- 10
Diode volgate	- 2 MV
Diode current	- 0.8 MA
Pulse duration	- 90 ns
Pulse energy	- 102 kJ.

Fig. 10 demonstrates the view of the module. The individual parts of module are being tested now.

References

1. L.I. Rudakov. Fizika Plazmy 4, 72 (1978).
2. G. Yonas 3rd International Topical Conf. on High Power Electron and Ion Beam Research and Technology 3-6 July 1979, Novosibirsk, USSR.
3. G. Freeman. Ibid.
4. D. Mosher. Ibid.
   G. Kuswa. Ibid.
5. E.I. Baranchikov, A.V. Gordeev, V.D. Korolev, V.P. Smirnov ZhETF 75, 2103 (1978)
6. A Toepfer Journ. of Appl. Phys. 45. 4390 (1978)
8. L.E. Aranchuk et al see ref 2
9. V.I. Liksonov, Yi. L. Sidorov, V.P. Smirnov Pis'ma v ZhETF 19 516-520 (1974)
10. S.L. Bogolyubskiy et al. Pis'ma v ZhETF 24, 206 (1976)
11. G. Linchart Nucle Fus. 13,321, (1973)
12. S.G. Alichanov 6th Conf. of IAEA on Plasma Physics and Controlled Thermonuclear Fusion, E-19-2. Berchtesgarden. 1976.
13. V. Baker et al. Journ. Appl. Phys. 45, 4694 (1978)
14. Bull. Amer. Phys. Soc. 23, 822, 847 (1978).
15. Yi. I. Archangelskiy et al. 7th Conf. of IAEA on Plasma Physics and Controlled Thermonuclear Fusion. Insbruck 1978.
16. Yi. I. Archangelskiy et al. see ref. 2
17. I. Smith 1st Intern. Topical Conf on High Power Electron and Ion Beam Research and Technology 3-6 November, Albu.

Figure Captions

Fig. 1. Theoretical dependences of a nonlinear wave velocity $\frac{u}{c}$ (1), a front leakage current ζ_{yr} (2) and a transportation efficiency for different values of $\ell/c\tau$ parameter against γ ; Δ , $\blacktriangle$ - experimental points, O, $\bullet$ -- calculated value of velocity and leakage [5] , $\square$ - velocity value from [7] . (ℓ - a line length τ - a pulse duration, c - the light velocity).

Fig. 2. Line voltage - current curves 1-1 and 2-2 theoretical curves without and with ion leakage, O, $\square$ - experimental points without and with ion leakage; a, b -- traces of the line voltage and current of 5,4 cm OD and 2.2 cm ID line.

Fig. 3 Scheme of the experimental determination of an ion leakage influence on selfmagnetic insulation regime 1 -- inner negative electrode, 2 - a Faraday cup, 3 - a dielectric part of outer electrode, 4 - a Faraday cup for ion leakage measurement, 5 - outer positive electrode, 6 - an anode, 7 - X-ray diode.

Fig. 4. Time-dependent cathode plasma layer boundary position for various current of coaxial line (0.8 cm OD, 0.4 cm ID).

Fig. 5. Experimental scheme of a plasma motion measurement in the triplate line (3 cm electrode width 0.2 cm interelectrode gap, 0.5 cm cathode-anode gap) 1 - a negative line electrode, 2 - an anode, 3 - an anode current resistor 4 - a X-ray diode.

Fig. 6. a: traces of the voltage, line (I_1) and anode (I_d) currents and light intensity pulses; b: interferogram 1-5 frames correspond the light pulses; 6- reference frame.

Fig. 7 . Lowinductance scheme of liner feed using strip line.

Fig. 8 . General view of the fullscale Angara-5 accelerator.

Fig 9 . The lay-out of experimental unit of Angara-5.

Fig.10 . The view of experimental unit of Angara-5.

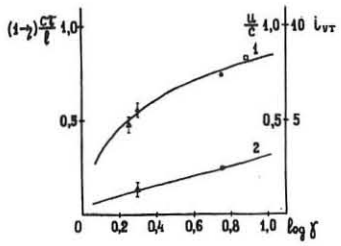

Fig. 1.

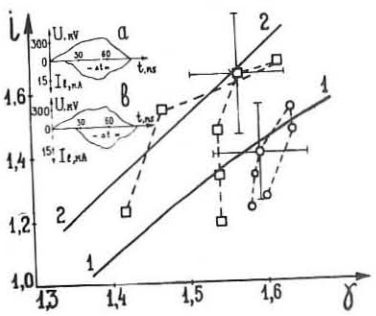

Fig. 2.

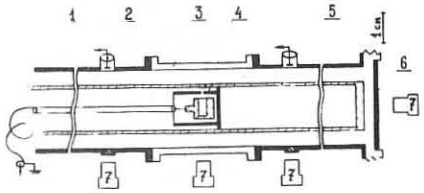

Fig. 3.

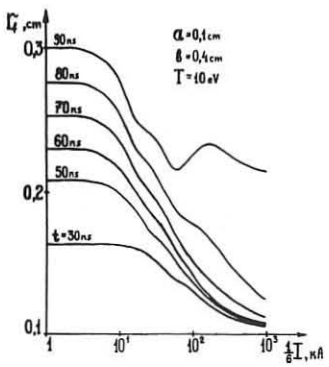

Fig. 4.

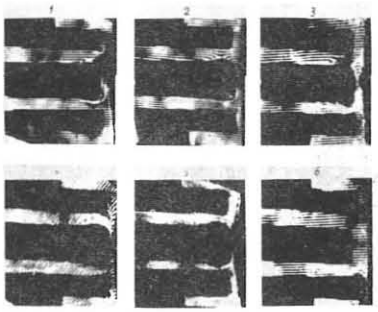

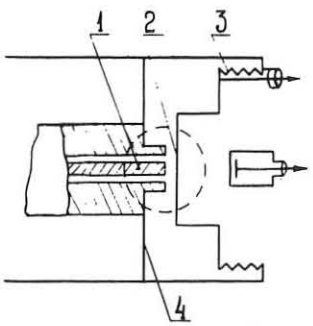

Fig. 5.

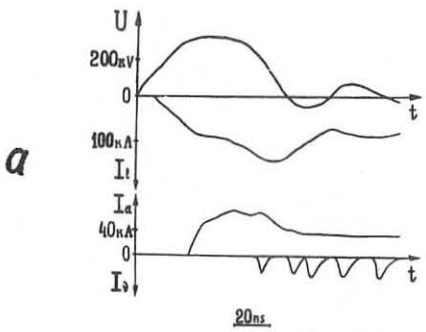

Fig. 6.

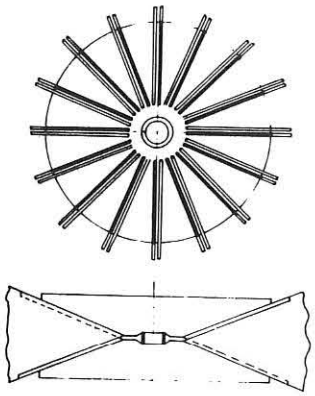

Fig. 7.

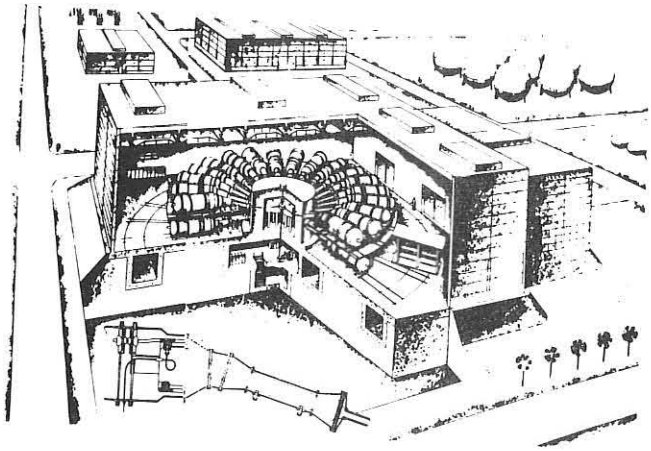

Fig. 8.

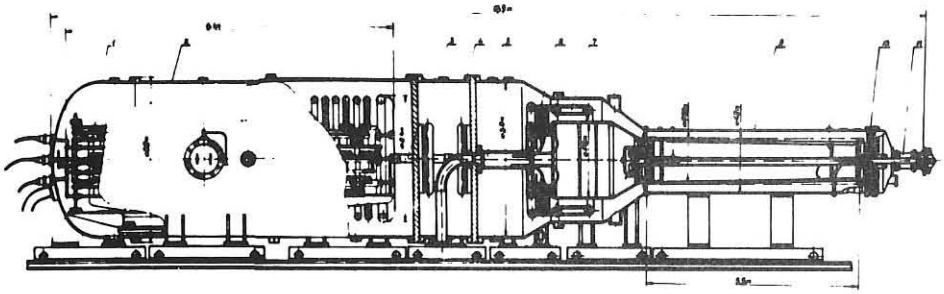

Fig. 9.

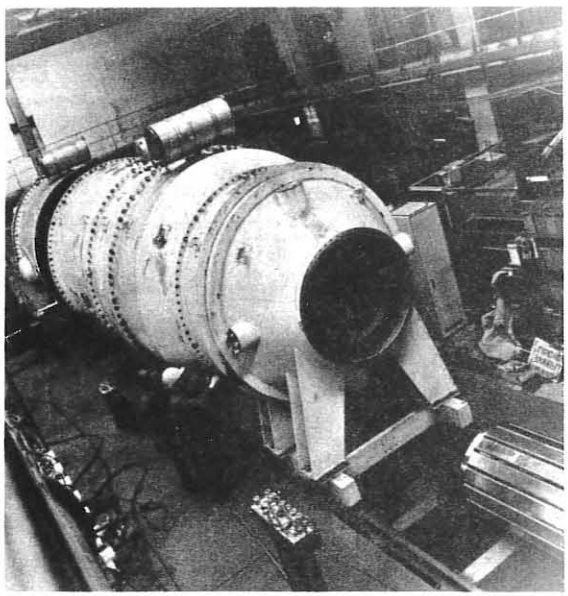

Fig. 10.

CONTROLLED FUSION RESEARCH IN CHINA

LI Zhengwu

Southwestern Institute of Physics
Leshan, Sichuan, People's Republic of China

CONTENTS: Fusion reactor studies; toroidal magnetic confinement; mirror magnetic confinement; fast pulsed discharges; plasma focus experiments; laser fusion research.

1. Fusion Reactor Studies

Utilization of fusion energy is the long range aim of controlled fusion research. Our objective at present is to understand the physics sufficiently and to develop the technology needed to design and construct a power-producing reactor in the not too distant future.

Conceptual design studies of both pure fusion and fusion-fission hybrid systems and for a number of blanket compositions and energy retrieval schemes have been made. These studies point to the great importance of further research into energy conversion and reactor materials, especially structural materials for which the order of importance is roughly in proportion to the proximity of the material to the plasma boundary, before decision can be made concerning the choice of type of reactors.

2. Toroidal Magnetic Confinement

A tokamak, CT-6, has been in operation since 1974 at the Institute of Physics, Beijing (Peking).

Its main characteristics are:

Major radius	45 cm
Radius of limiter (molybdenum)	9 cm
Radius of liner bellows	10-13 cm
Inner radius of stabilizing conductors	19 cm
Toroidal field (capacitor banks)	20 kG
Magnetic flux for ohmic heating (iron core)	0.28 V-sec

Investigations on the evolution of discharge and the effect of different limiters and other impurity sources are being made, along with many modifications of the apparatus.

Toroidal magnetic confinement research at the Southwestern Institute of Physics consists of a series of experiments: a medium-sized tokamak, HL-1, under construction, two small devices of the bench-test style, a non-circular cross-section tokamak of the Doublet type and a screw pinch set-up operable for high beta tokamak study. Besides extensive theoretical and computational work on equilibrium, stability and transports in tokamak plasmas, some theoretical study on toroidally linked mirror systems and planar and three-dimensional stellarators have been made.

Main design parameters of HL-1 (Toroidal Plasma Current Machine No.1) are as follows:

Major radius	102 cm
Radius of limiters	20 cm
Toroidal field	50 kG
Plasma current	400 kA
Stray field in the plasma region with compensation	< 25 G
Plasma density	10^{14} cm^{-3}
Ion temperature	800 eV

The apparatus is of conventional design, with an iron core of 70 tons and a very heavy copper shell of thickness 5 cm. The inner vacuum liner of high-nickel non-magnetic alloy bellows has been welded and the quarter sections of the outer copper shell fabricated and tested. The sixteen wedge-shaped coils for the toroidal field are in assembly. Part of the power supplies with a total rating of about 200 MW has been installed in the experimental building. HL-1 is scheduled to go to operation by the end of next year.

The aim of HL-1 is for us to have a first-hand experience in the design, construction and experimentation in this approach of magnetic fusion and to train the scientific and engineering personnel. For experiments in physics and on supplementary heating and for the preparation of diagnostics and data acquisition we have up-to-dated our objectives as:

(1) the study of the build-up phase of tokamak discharge. For the pulse range appropriate to an apparatus like HL-1, it is expected that the detailed behavior at the build-up stage will

have far-reaching effects on the whole of the later development of the discharge; particularly,

(2) the manipulation of this stage in conjunction with the procedure of heating and the gas supply and recovery which are closely related to refuelling to improve the performance of the apparatus;

(3) the study of plasma-wall interactions and the control of impurity;

(4) the scaling of confinement properties and plasma parameters as affected by the heating procedure.

After a first period of experiment we plan to concentrate on supplementary heating to further improve the plasma parameters attained.

Cognizant of the complexity of toroidal magnetic confinement, we have constructed several smaller toroidal devices recently after the design of the larger one, HL-1, was completed. Two of them, the Mini-Torus and the Pre-test Torus have been useful for preparatory tests of various kinds. And the other two, the Non-circular Tokamak and the Screw Pinch, are for follow-up studies. The characteristics of the first three are shown in the following:

	Mini-Torus	Pre-test Torus	Non-circular
Major radius (cm)	20	26	48
Minor radius (cm)	4.5	>5	10 x 25
Toroidal field (kG)	12	20	10-15
Plasma current (kA)	15	12	180 (designed value)

3. Mirror Magnetic Confinement

Magnetic mirror confinement research is being conducted at the Southwestern Institute of Physics and much earlier at the Institute of Atomic Energy, Peking, a smaller set-up of magnetic mirrors with slow magnetic compression and plasma gun injection recorded an ion temperature of about 300 eV in the density range of several times 10^{13} cm^{-3} by microwave and optical diagnostics and magnetic probes.

A mirror device with superconducting coils and vacuum ionization of 100-keV neutral beam is recently in operation at the Southwestern Institute. The main characteristics of this apparatus are as follows:

Radius of vacuum vessel	10 cm
Spacing between mirrors	48 cm
Central magnetic field	15 - 25 kG
Axial mirror ratio	1.75
Background pressure	1 x 10^{-9} torr

For the present, the main emphasis of work on this approach is put on fusion technology and at the same time maintaining our attention to the mirror concept because of its intrinsic merits. The neutral beam injector now in use has a D.C. 1 A ion source working with H_2. A 20 kV, 3 A ion source of the multi-aperture type has been tested and a 20 - 50 A version under development.

4. Fast Pulsed Discharges

Since late fifties several groups have worked on Z- and θ-pinches.

A high beta belt-pinchtype torus, GBH-1, is under construction at the Institute of Physics. The elongated plasma will be heated by fast magnetic compression. A separate set of toroidal field coils is used in addition to the plasma current-induced coil so that the safety factor q can be changed in a wide range from $q > 1$ to $q < 1$. A capacitor bank of total energy 2.7 MJ is to power this apparatus with an Al_2O_3 vacuum chamber of outer diameter 130 cm, inner diameter 50 cm and height 100 cm.

At the Southwestern Institute two linear θ pinches and a toroidal screw pinch are in operation. The linear θ pinches, with 60 kJ and 150 kJ of main capacitor banks respectively, have produced neutron yields in deuterium up to 10^6 neutrons per pulse, attaining an ion temperature of 1 keV. Spiralling structures of the plasma with and without stellarator type field have been studied. In general, magnetic probes, ruby laser 90° scattering, He-Ne laser and microwave interferometry, optical spectroscopy and particle detectors are used for diagnostics.

The screw pinch has the following characteristics:

Major radius of discharge tube	29 cm
Minor radius of discharge tube	6 cm
Total energy of capacitor bank	80 kJ
Maximum toroidal field	13 kG
Plasma current	30 kA

Plasma lifetime	3-4 sec
Plasma density	$0.5 - 1 \times 10^{16}$ cm^{-3}

Detailed field and plasma mapping has been made with multi-probes. The plasma temperature is found to be a few tens of eV. Modifications to increase the energy and the plasma current of the Screw Pinch and for reverse field operation are underway.

5. Plasma Focus Experiments

Plasma foci have been studied by several groups.

The 40 kJ plasma focus setup at the Institute of Atomic Energy used a Mather gun with coaxial electrodes of diameters 52 and 90 mm respectively. Experiments were done by x-ray pictures and neutron energy spectrum analysis. A maximum yield of 4×10^9 neutrons per pulse was obtained, the yield being roughly proportional to I^4 where I was the discharge current at the instant of focus formation. The neutron energy was found to be anisotropic, indicating a partial beam-target mechanism. Studies on the effect of nitrogen content in the feed gas gave interesting results which seemed to be relevant to plasma-wall recycling.

6. Laser Fusion Research

Experimental and theoretical research of laser fusion is being conducted at the Shanghai Institute of Optics and Fine Mechanics.

Shortly after the operation of the first high power ruby laser in 1963, suggestion was put forward to obtain neutrons by heating deuterium-contained materials with high power lasers. Research along this line and further developments lead to plasma heating and compression with neodymium glass lasers. A neutron yield of more than 2×10^4 per pulse was obtained in 1973 with a single beam laser of output 10^{10} W. Although the neutrons were not of thermonuclear origin, they indicated that laser light can be used to generate high temperature plasma with high density. A six-beam neodymium glass laser system was constructed in 1976, with an output of $2\text{-}3 \times 10^{11}$ W in nanosecond pulse. Experiments were done on multi-beam laser irradiation of solid $(CD_2)_n$ pellets and glass shell targets with the above apparatus and plasma compression observed when glass shells were used. Computer simulation of laser implosion with a one dimensional hydrodynamic code performed under the assumption that the heat conduction coefficient was about one hundredth of that of the classical value was found to be in agreement with the experimental results. The six-beam laser system is at present operated with sub-nanosecond pulses. Experiments have been done with 2 or 4 beams and an output of 10^{11} W in 100 psec for each beam on thin glass shells filled with deuterium or neon.

U.S. RESEARCH IN INERTIAL CONFINEMENT

John L. Emmett
University of California, Lawrence Livermore Laboratory
P.O. Box 5508, Livermore, California USA 94550

ABSTRACT

Early in the next century diminishing reserves of fossil and fissile fuels will force us to place increasing reliance in inexhaustible sources of energy. There are three such inexhaustible sources: fission breeder reactors, solar energy, and fusion energy. Although the scientific feasibility of fusion will not be demonstrated until the mid-1980's, the potential rewards of fusion are great--not only in terms of direct power production, but also in producing other fuels such as fissile fuels or hydrogen.

During the last year, the U.S. inertial fusion program has seen a number of significant accomplishments. Two large lasers, Shiva (LLL), at 1.06 μm, and Helios (LASL) at 10.6 μm, operate with energies of up to 15 kJ and 30 TW. At Sandia, the Proto-II electron beam produces 50 to 100 kJ and 4 to 8 TW. Encouraging progress has been made in electron beam and light ion technology, including magnetic insulation and light ion focusing. Two promising approaches have been identified for advanced drivers: the RF Linac for the heavy ion accelerator, and the KrF-pumped, backward-wave Raman compressor as a uv laser source with a projected efficiency of up to 4%.

Additionally, advances have been made in understanding pellet fusion and laser-plasma interaction. Fusion burn has been achieved with 0.53 μm, 1.06 μm and 10.6 μm drivers. In exploding pusher experiments, neutron yields have been obtained as follows: Shiva (LLL) at 1.06 μm, 2.7×10^{10}; Helios (LASL) at 10.6 μm, 1×10^{8}; and Zeta (University of Rochester) at 1.06 μm, 3×10^{8}. At LLL, a DT gain of 10^{-2}, $n\tau$ of 2×10^{12} cm^{-3}/sec and DT ion temperature of 10 keV have been obtained. In ablative implosion experiments, DT densities in excess of 50X liquid density have been obtained, using the Shiva laser.

The good agreement observed between Zohar/Lasnex codes and experimental results shows that the basic laser-plasma interaction phenomena at short pulse lengths ($\lesssim$ 200 ps) are well understood. Significant progress has been made in experiments quantifying such processes as absorption, hot electron generation and stimulated scattering at the high intensity, long pulse length regimes. Finally, multi-layered complex targets with surface qualities exceeding reactor design requirements have been produced, and concepts for minimizing first wall materials problems in reactors have been refined.

These results, and in particular the attainment of $\geq$ 50X liquid DT density on Shiva, gives us confidence that scientific breakeven will be demonstrated by the mid-1980's with the Nova laser facility. This is particularly important in light of the recent progress made in magnetic fusion, as we believe it imperative for the U.S. to have as many choices as possible in deciding upon future engineering test facility devices and engineering prototype reactor schemes.

In addition to the work in progess at the three major DOE facilities (LLL, LASL and SLA), the present and future efforts at other DOE sponsored laboratories will be discussed. These include KMSF, the University of Rochester, and the U.S. Naval Research Laboratory.

TWO MAJOR APPROACHES TO FUSION (D-T)

Magnetic confinement

Temperature $\approx$ 10^8 °C (10 keV)

$\eta\tau \approx 10^{15} \frac{\text{Atoms}}{\text{cm}^3}$ ·seconds

$\tau \approx$ 10 seconds (magnetic "bottle")

$\eta \approx 10^{14} \frac{\text{Atoms}}{\text{cm}^3}$ (10^{-5} times the density of air)

Inertial confinement

Temperature $\approx$ 10^8 °C (10 keV)

$\eta\tau \approx 10^{15} \frac{\text{Atoms}}{\text{cm}^3}$ · seconds

$\tau \approx 3 \times 10^{-11}$ seconds (microexplosion)

$\eta \approx 3 \times 10^{25} \frac{\text{Atoms}}{\text{cm}^3}$ (12 times the density of lead! ~ 1000 times the density of liquid DT!)

95-01-1078-3725

9/79

ENERGY DENSITIES

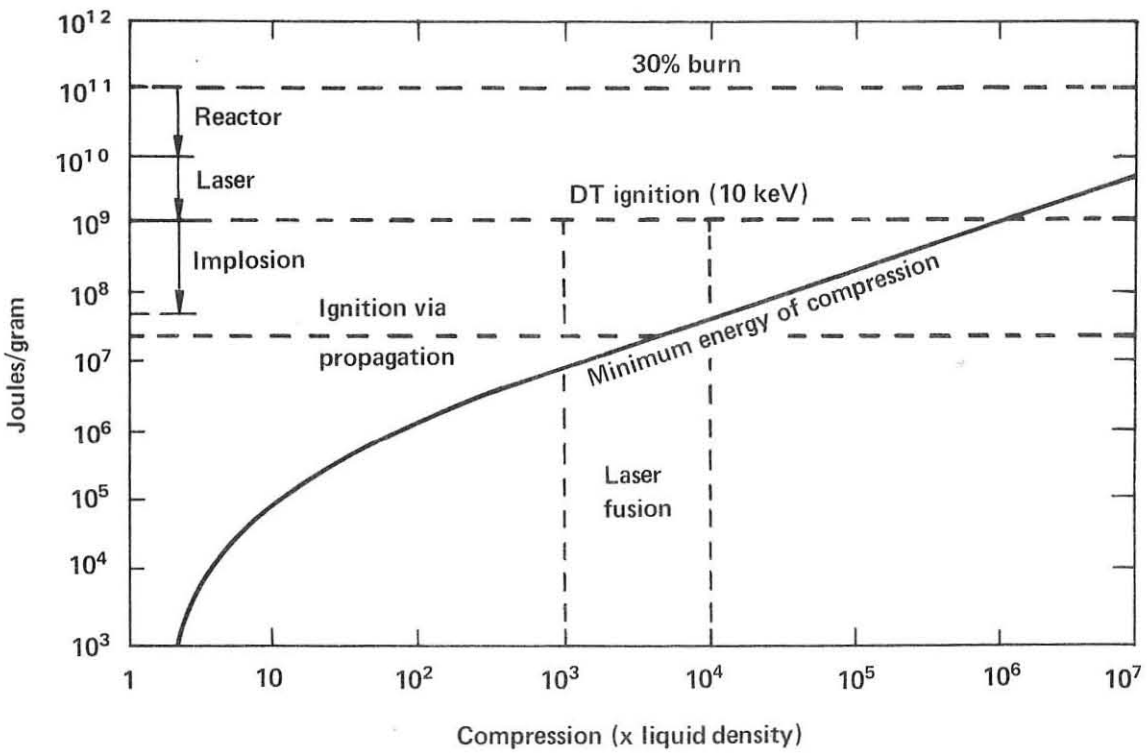

POTENTIAL ICF DRIVERS

• Lasers	Various wavelengths
• Heavy ions	20 GeV, 10 kA $^{238}U^{+}$
• Light ions	10 MeV, 20 MA $^{2}H^{+}$
• Electrons	2 MeV, 100 MA
• Hypervelocity pellets	0.5 gm, 3–4 $\times$ 10^{7} cm/sec

95-01-1078-3724 9/79

TARGET GAIN VERSUS DRIVING ENERGY

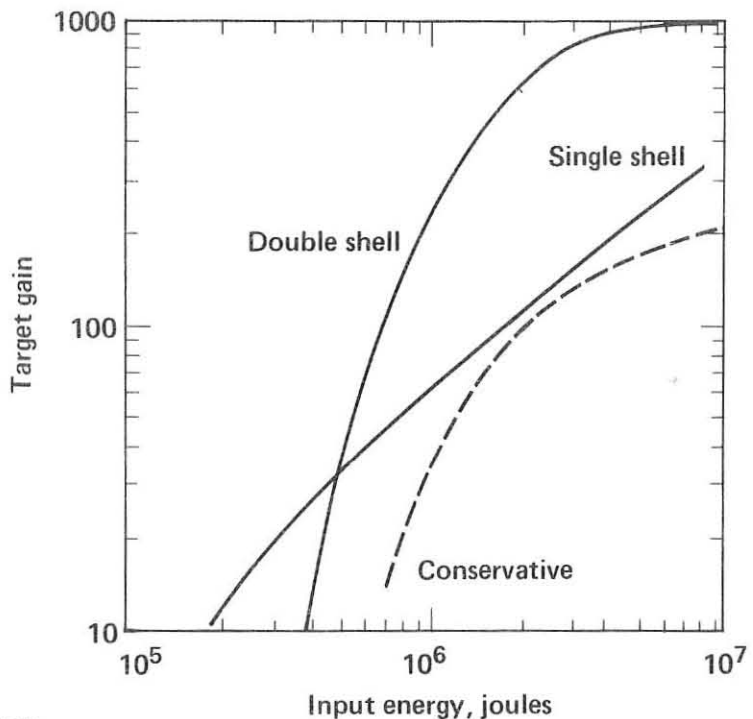

50-60-0979-2892

PELLET GAIN AND DRIVER EFFICIENCY REQUIREMENTS

^{238}U – Pu hybrid	$\eta_D Q = 1 - 3$
^{233}U – Th hybrid	$\eta_D Q = 3 - 6$
Pure fusion (25% recirculating power)	$\eta_D Q = 10$
Pure fusion (14% recirculating power)	$\eta_D Q = 18$

Pellet gains (Q) of 100 – 1000 appear achievable

95-01-1078-3728

LASER FUSION FACILITIES

	Operating on target		Under construction		Design work funded	
1.06 μm						
NRL	Pharos	0.5 kJ 1.0 TW	Pharos II	1.0 kJ 2.0 TW		
Univ. of Rochester	Zeta	1.2 kJ 3-4 TW	Omega	4.8 kJ 12-16 TW		
KMSF	Chroma I	1 kJ 2 TW				
LLL	Shiva	10 kJ 26 TW	Nova I	100 kJ 150 TW	Nova II	300 kJ 300 TW
10.6 μm						
LASL	Helios	5-10 kJ 10-20 TW	Antares	100 kJ 100-200 TW		

Energy quoted reflects maximum performance at long pulses
Power quoted reflects maximum performance at short pulses

95-01-0979-2896

ION BEAM FUSION FACILITIES

Location	Operating on Target	Under Construction	Design Work Funded
Sandia	PROTO I – 12 kJ 0.5 TW	PROTO II – 160 kJ 4.8 TW	PBFA II – 2-4 MJ 60-100 TW
		PBFA I – 1 MJ 30 TW	
L B L		Ion sources and low-β section	ADF* – induction linac 0.5 kJ
Argonne		Ion sources and low-β section	ADF* – RF linac 1 kJ

*Not on target

95-01-0979-2895

ADVANCED LASERS FOR FUSION REACTORS

Type	Medium/pump	Wavelength	Efficiency (%)			
Solid state*	Nd:glass/flashlamp	1.06 μm	1–2	3	X	
Hybrid	Tm^{+3}:glass/XeF*	0.46 μm	0.7–1	2	X	
Gas	Photolytic Group VI					
	Sulfur/Kr_2^*	0.78 μm	0.4–1	1.5	X	
	Selenium/Xe_2^*	0.49 μm	0.8–1.6	2.5	X	
Gas	Iodine/surface discharge	1.3 μm	0.5–1	1.5	X	
Gas	CO_2/electrons	10.6 μm	3–5	10		Possible candidates
Gas	HF/electrons-chemistry	2.7 μm	3–5	7		
Gas	KrF stacker/compressor	0.24–0.27 μm	4–5	7		
Gas/solid	Advanced concepts	$\lesssim$ 1 μm	$\gtrsim$ 10			

* Maximum repetition rate ~5 Hz
☐ Percentage with possible breakthroughs

AL8-0-4
9/79

04-90-0878-2863

LASER AND LIGHT ION DRIVER ISSUES

- Lasers – KrF appears attractive as a reactor driver

  Short $\lambda \Rightarrow$ low target physics risk

  High repetition rate

  Acceptable efficiency

  However, developing a laser with higher efficiency and lower projected cost is very desirable

- Light ions are potentially very attractive because of low cost and high efficiency – however,

  Much physics and technology remains to be demonstrated

  Attractive reactor concepts are yet to be developed

50-60-0979-2891

INTEGRATED IMPLOSION EXPERIMENTS – STATUS

Experimental Facility	Density Achieved (times liquid DT density)	Concurrent Diagnostics
University of Rochester	7 – 20	Argon line – Stark broadening
KMSF	7 – 35	X-ray pinhole picture α-particle spectrum
LASL	1 – 8	X-ray pinhole pictures Argon line – Stark broadening Neutron interval time
	8 – 30	X-ray pinhole pictures
LLL	0.5 – 2	Radiochemistry Argon line imaging α-particle imaging
	4 – 15	Radiochemistry Argon line imaging
	30 – 160	Radiochemistry Neutron interval time

95-01-0979-2897

HIGH-DENSITY COMPRESSION MEASUREMENT USING STARK PROFILE OF ARGON LYMAN–β X-RAY LINE

UR LLE

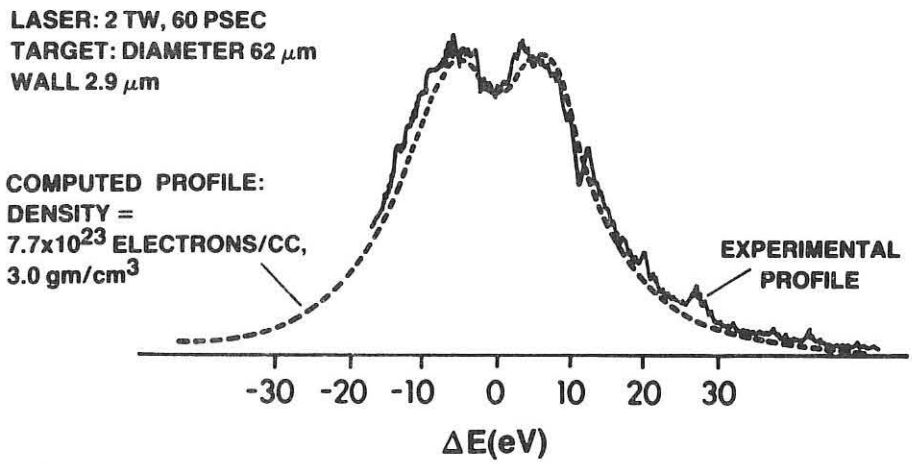

E612

HIGHER DENSITIES ARE ACHIEVED WITH CRYOGENIC FUEL

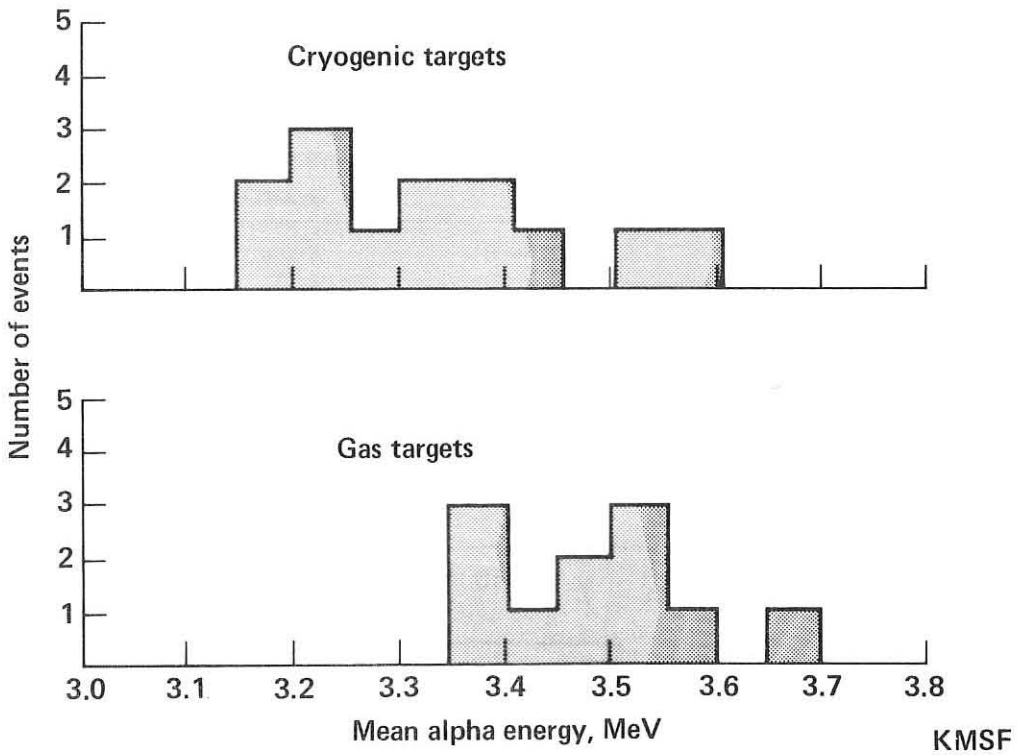

KMSF

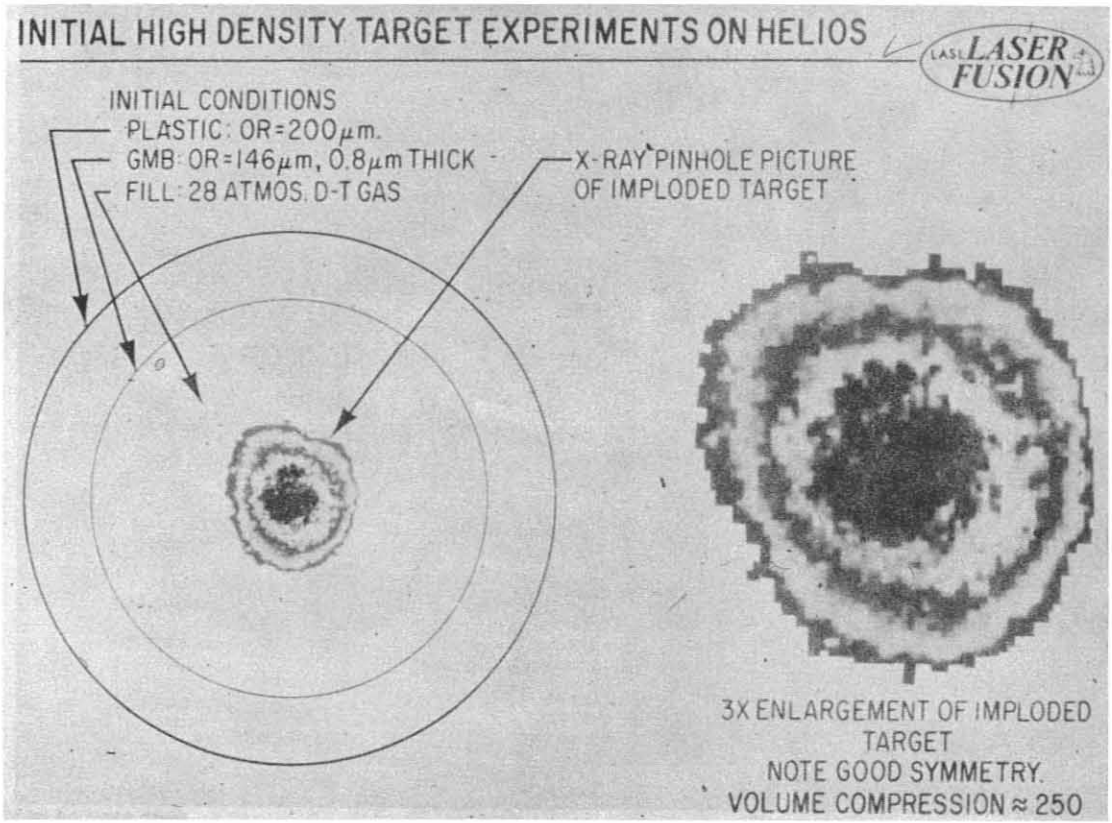
INITIAL HIGH DENSITY TARGET EXPERIMENTS ON HELIOS
LASL LASER FUSION
INITIAL CONDITIONS
PLASTIC: OR=200μm.
GMB: OR=146μm, 0.8μm THICK
FILL: 28 ATMOS. D-T GAS
X-RAY PINHOLE PICTURE OF IMPLODED TARGET
3X ENLARGEMENT OF IMPLODED TARGET
NOTE GOOD SYMMETRY.
VOLUME COMPRESSION ≈ 250

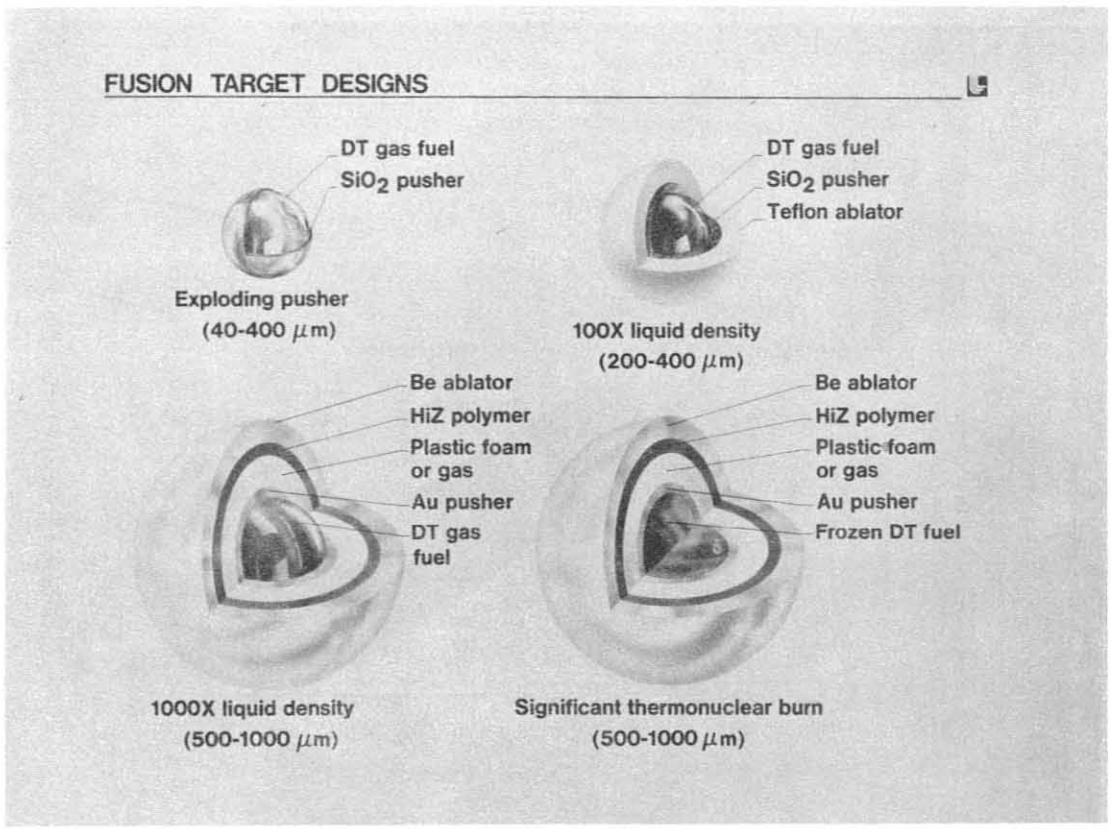
FUSION TARGET DESIGNS
DT gas fuel
SiO2 pusher
Exploding pusher
(40-400 μm)
DT gas fuel
SiO2 pusher
Teflon ablator
100X liquid density
(200-400 μm)
Be ablator
HiZ polymer
Plastic foam or gas
Au pusher
DT gas fuel
1000X liquid density
(500-1000 μm)
Be ablator
HiZ polymer
Plastic foam or gas
Au pusher
Frozen DT fuel
Significant thermonuclear burn
(500-1000 μm)

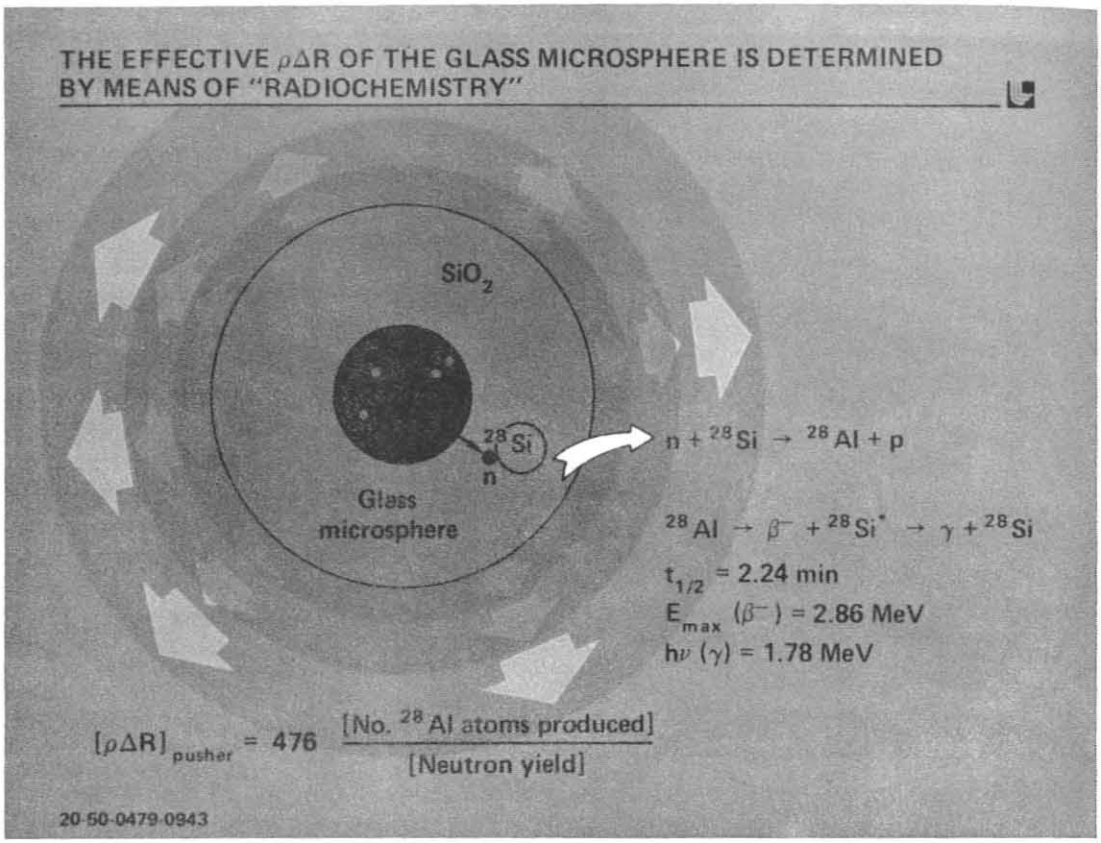
THE EFFECTIVE ρΔR OF THE GLASS MICROSPHERE IS DETERMINED BY MEANS OF "RADIOCHEMISTRY"
SiO2
28Si
n
Glass microsphere
n + 28Si → 28Al + p
28Al → β− + 28Si* → γ + 28Si
t1/2 = 2.24 min
Emax (β−) = 2.86 MeV
hν (γ) = 1.78 MeV
[ρΔR]pusher = 476 [No. 28Al atoms produced] / [Neutron yield]
20-50-0479-0943

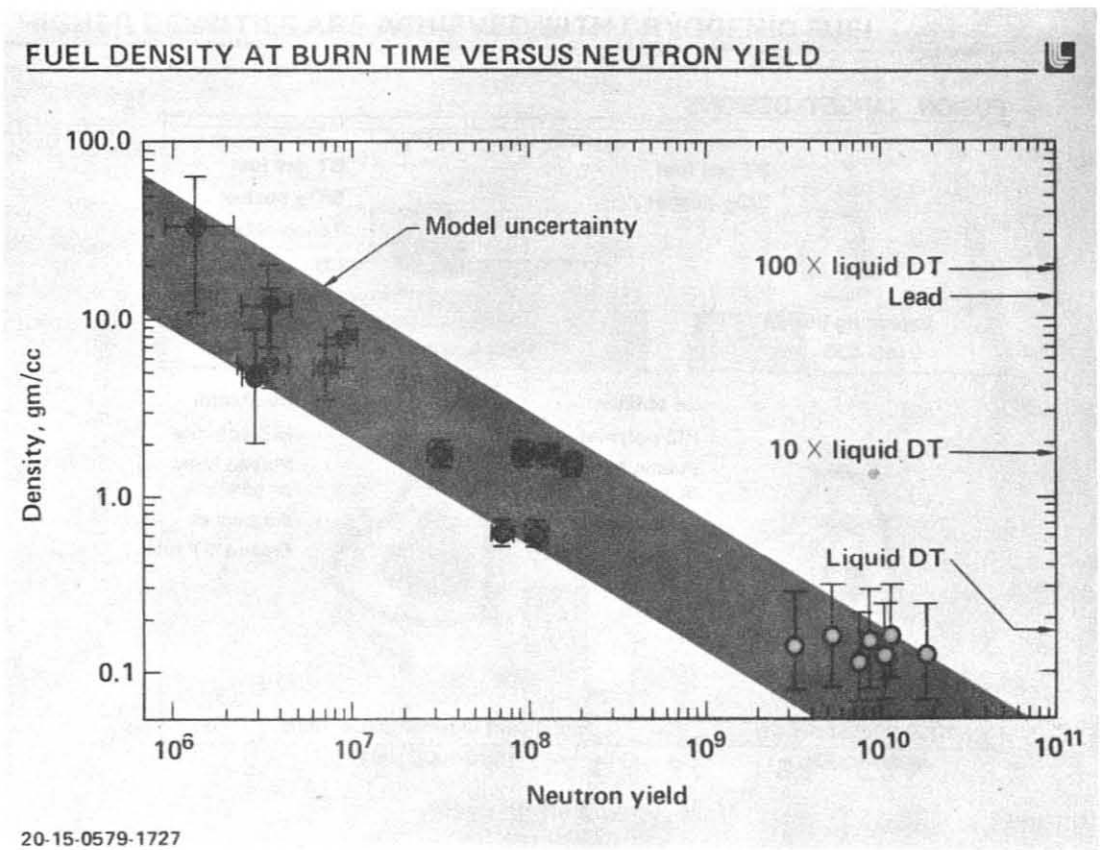
FUEL DENSITY AT BURN TIME VERSUS NEUTRON YIELD
100.0
10.0
1.0
0.1
Density, gm/cc
Model uncertainty
100 × liquid DT
Lead
10 × liquid DT
Liquid DT
10^6
10^7
10^8
10^9
10^10
10^11
Neutron yield
20-15-0579-1727

SHORT λ AND SPREAD SPECTRUM PROMISE IMPROVED COUPLING

$\nu_{ei} \propto \lambda_o^{-\alpha}$	Inverse bremsstrahlung in greater.
$\alpha \approx 4$	Instability thresholds are higher.
	Fewer suprathermals are generated.
	Electron transport is improved.
$\theta_h \propto \lambda_o^{0.8}$	Characteristic suprathermal temperature is less.
$Q \propto \lambda_o^{2.2}$	Brillouin scatter and filamentation is reduced.
$Q \propto \frac{1}{N}$	Where N is the number of frequencies spaced greater than the Brillouin line width.

All of these coupling issues need experimental quantification

50-60-0979-2889

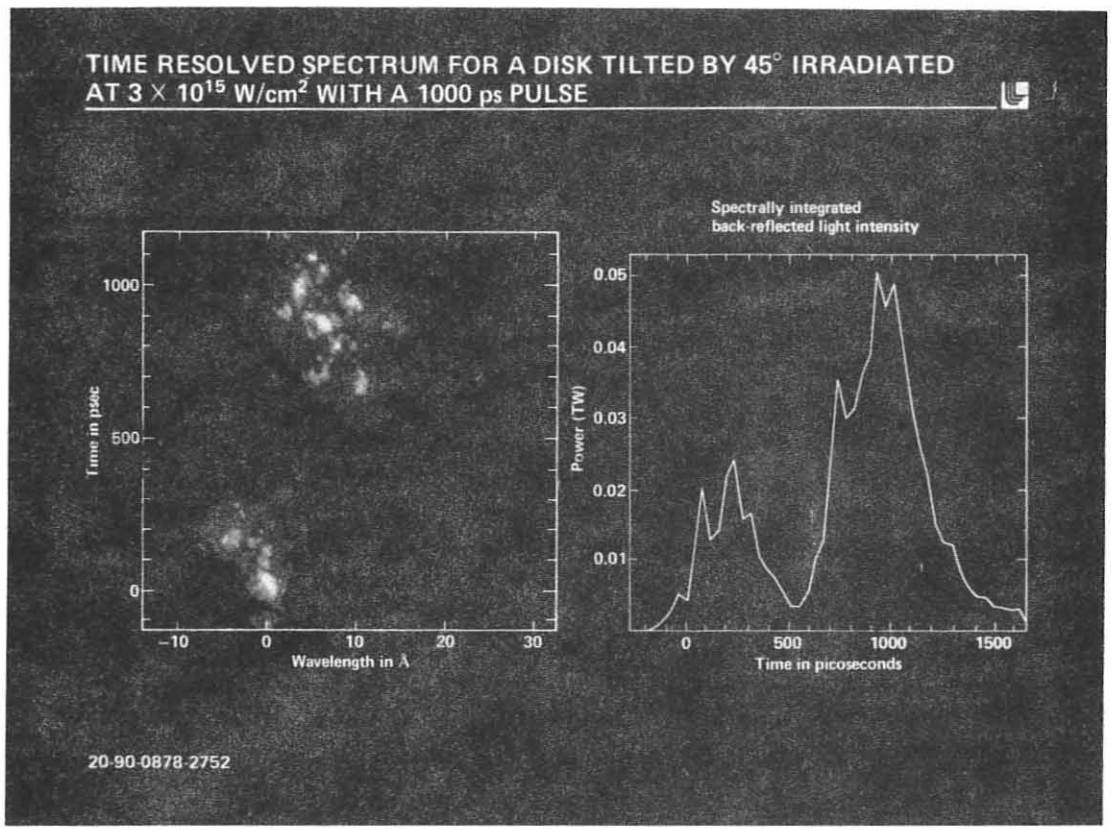

HYLIFE CONVERTER CONCEPT

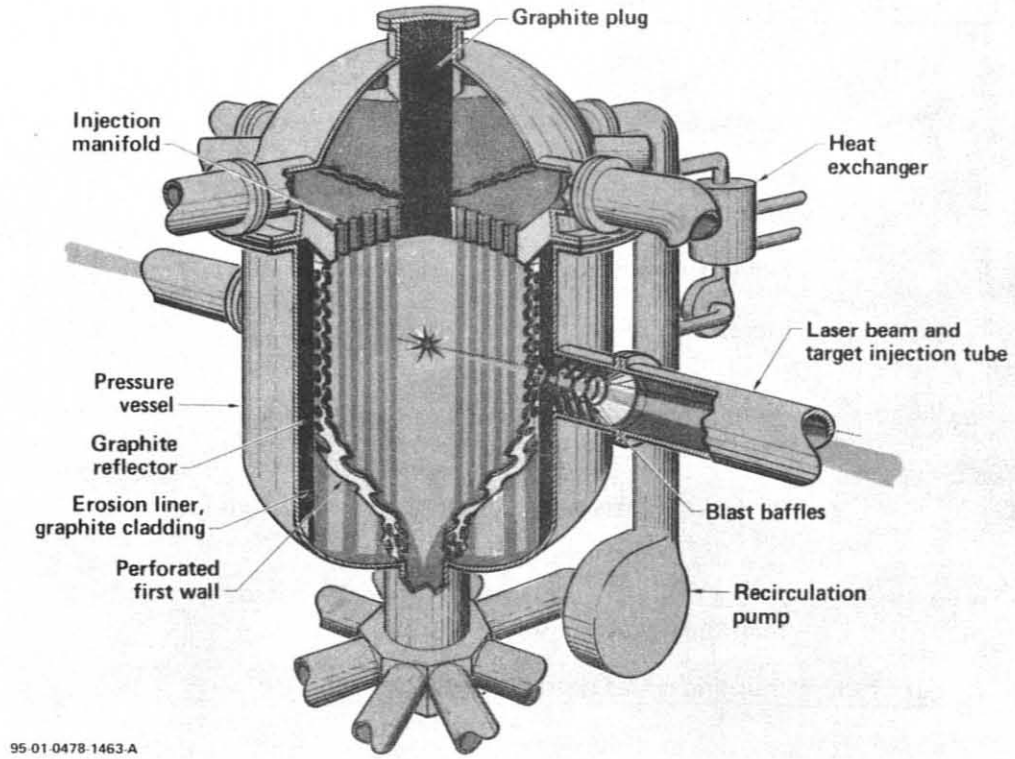

ICF SUMMARY

- Record-breaking thermonuclear conditions have been achieved
- Initial high density implosions (10-100X) complete
- Very high density implosions (100-1000X) underway
- Very high gain targets designed – relaxing driver efficiency and target cost constraints
- Techniques have been conceived for low cost, high volume reactor pellet fabrication
- A low cost, simple, long lifetime reactor concept has been developed
- Laser and heavy ion reactor drivers appear feasible. Light ions show much promise.. The multiplicity of options greatly enhances probability of success

50-90-1177-2683 9/79

THEORETICAL STUDY OF TOROIDAL SYSTEMS

V.D.Shafranov
I.V.Kurchatov Institute of Atomic Energy, Moscow, USSR

At the present time the choice of the direction in theoretical research is governed not only by the plasma physics itself but also by the engineering and technological problems of future fusion reactors, which have become quite tangible and burning due to the progress in tokamak experiment. These include, for example, removal of spent fuel from a reactor, or maintaining the steady-state or quasi-continuous operating conditions in a reactor. We shall concern here with some problems of this kind.

1. EQUILIBRIUM

a) Problem of the β -limit.

The economy of a magnetic thermonuclear reactor depends on the achievable ratio of the plasma to the magnetic pressure $\beta = 8\pi p / B^2$. The calculations carried out at the Oak-Ridge /1/ and other laboratories have shown that for a reasonable value of the safety factor $q \sim 1\text{-}3$, one could get equilibria for $\beta \sim 20\%$. One should however keep in mind that these equilibria generally speaking are non-stationary. If the duration of a pulse exceeds the skin-time, an equilibrium corresponding to the following stationary equilibrium equation /2,3/ should be established:

$$\frac{\partial^2 \Psi}{\partial z^2} - \frac{1}{z}\frac{\partial \Psi}{\partial z} + \frac{\partial^2 \Psi}{\partial z^2} = -4\pi^2 p'(\Psi)\left[z^2 - \frac{\langle B_\tau^2 \rangle}{\langle B^2 \rangle \langle 1/z^2 \rangle}\right] - \frac{\langle B_\tau^2 \rangle}{\langle B^2 \rangle}\sigma_\parallel \mathcal{E}_0$$

Here $p(\Psi)$ is the pressure of the plasma, $\sigma_\parallel$ - its conductivity, $\mathcal{E}_0$ - the loop voltage, B_τ -the toroidal field, angle brackets denote averaging over the magnetic layer. For the collisionless regime the term corresponding to the bootstrap current should be added in the right-hand side.

Because of large gradients corresponding to high β the relaxation to the steady state may occur during a small part of the skin time. The problem has been investigated numerically both in two - and onedimensional models. In the latter case a simple moment method using the Klark-Sigmar model of circular magnetic surface cross-sections was applied /4/. In the moment method the form of the magnetic surfaces is prescribed by a few parameters-displacement, ellip-

ticity, triangularity, etc. A twodimensional equilibrium equation is then reduced to a set of ordinary moment equations:

$$p' + \langle B_p^2 \rangle_f' + \frac{FF'}{2\pi^2} \langle \frac{1}{r^2} \rangle_f = 0 ,$$

where $\langle G \rangle_f = \oint G f \, dl_p / B_p \Big/ \oint f \, dl_p / B_p$,

f is one of the solution of the uniform equation

$$div (\nabla f / r^2) = 0$$

Fig.1. shows the evolution of the plasma equilibria in a tokamak for the uniform both conductivity and initial q profile after an instant increase of p' at t=0. One can see some steepening of q, an increase in displacement Δ , field and current distribution asymmetry during a short stretch of time. In a small period of skin time the poloidal magnetic field tends to zero on the inner edge of the plasma torus. This must lead to the opening of the magnetic surfaces and scraping off the plasma surface layer. The evolution of the equilibria after the zero poloidal field point has been formed requires further studies.

b) Nonadiabatic mixing of plasma columns.

Creation of the zero poloidal field point may take place inside the plasma when it exhibits squeezing over the entire length of the torus. In an a diabatic approximation corresponding to a slow (compared to the poloidal alfven time) change of the boundary conditions, this problem has been investigated in a series of papers by Grad et al /5,6/. With a rapid variation in the external conditions this process may be accompanied with a change in entropy and a heat release. Possibility of a rapid release of the energy contained in the magnetic field was considered in a number of papers /7-11/ in connection with solar chromosphere flares and some phenomena in the terrestrial magnetosphere. It is caused by reconnection of the magnetic field lines near zero point in the plasma of high conductivity. The reconnection phenomena according to Kadomtsev is responsible for disruptions in tokamak. It openes a possibility of plasma heating in a tokamak as well. One of these has been considered in Refs./12,13/. It is connected with excitation of low frequency oscillations expi (mQ-ns) resonant with respect an inner magnetic surface. According to the authors, periodic creation and disappear ance of the island structure leads to dissipation of the energy of oscillations.

Papers /14,15/give an account of the idea of heating due to a change in the topology of an equilibrium configuration without applying the H.F. power. Here an energy of the parallel current interaction is used (Fig.2). Sketch of the method is shown in Fig.3. Two plasma columns separated by a horisontal conducting sheet (a) or placed at different radii are weakly stable relative to the radial displacement. Violation of the equilibria condition forces plasma columns into the common chamber where they are rapidly brought together and then mix both due to the appearence of a neutral current layer and magnetic field line reconnection (Fig.4). The plasma moves free along the magnetic field lines. As a result the time of mixing is square root of the poloidal magnetic Reynold number Re_m less than skin time. The corresponding power is Re_m times larger than the Ohmic one. The energy is released directly in the neutral current layer. The heat is further transferred along the magnetic surfaces bounding the separatrix. The periphery nature of such heating seems to be the disadvantage of the method. Experimental studies could show both the efficiency of the process and the physics of the reconnection phenomena under the tokamak conditions.

c) Divertor problem.

The problem of heat removal from the plasma whose temperature is five orders of magnitude higher than that of the surrounding walls under reactor conditions is one of the main problems for a tokamak-reactor. A few different divertor systems have been proposed to defend the chamber walls from the hot plasma and prevent the particles from the walls to enter the plasma. In the toroidal divertor suggested by L.Spitzer the local reversing of the total magnetic field allows divertion of a tubular layer of magnetic flux from the plasma. The encouraging experiments with a bundle-divertor on the DITE /16/ have shown that it is sufficient that the magnetic field can be reversed not over the whole azimuthal direction but only at a single point. In this case in contrast to the strong topological limitations a "handle" of a magnetic tube is appear on the toroidal magnetic surfaces. Mathematically, the system of nested magnetic surfaces is violated in this case. Fortunately to confine plasma no perfect magnetic surfaces are necessary due to finite size of the charged particle orbits. The bundle-divertor has again confirmed the wise proverb: the proof of the pudding is eating. It is rather compact, does not require a large aspect ratio, produce rather weak

magnetic field nonuniformity in the plasma. It's disadvantage-large mechanical stretches because of necessity to reverse the total magnetic field.

A poloidal divertor involves the reversal only of a poloidal component of the field. In this case the magnetic field lines are rather slowly deflected to the divertor volume by a comparatively low transverse (poloidal) field during a few walus along the torus. The great disadvantage of the poloidal divertor is that it is positioned inside the toroidal coils. This requires large volume of the coils and leads to technological and constructive problems.

B.B.Kadomtsev has recently suggested a kind of poloidal bundl-divertor named by him as a branch-divertor. A tube of the magnetic field lines is deflected from a hot plasma and then introduced to it by means of a rather low local transverse field (for example, using two current-carrying frames positioned along a force line, Fig.5). In this case the "handle" is seen in the cross-section of the torus. To take it outside the toroidal coils it is suggested that two magnetic tubes started almost at the same place are closed externally using a section of a nonuniform solenoid (Fig.6). The ends of such a divertor looks like branches of a tree. The expanding part of the tube contains an ion recycling amplifier having a large surface electron emitter in contact with the plasma. This provides besides of ion recicling a strong influx of cold electrons to the plasma, i.e. an electron shower cooling the plasma boundary with the destructed magnetic surfaces. It also allows the plasma heat to be released not with ion thermal (sound) ambipolar velocity, which is insufficient for the heat removal, but with an electron velocity, v_{Te}.

d) Quasi-continuous reactor.

An important characteristic of a pulsed reactor is the duty factor, i.e. the ratio of the working pulse time to the total time of cycle. There are suggestions to improve this factor. In a continuous tokamak suggested by S.Yoshikawa and supported by equilibria calculations in Ref./17/ a plasma column is formed in chamber 1, Fig.7. By altering the currents in the shaping coils the plasma column is moved into the burning chamber 2 and then in pumping chamber 3. Simultaneously, a new discharge is ignited in chamber 1, and so on. A similar idea of using two plasma columns merging into one is described in Ref. /15/.

Paper /18/ has studied a possibility to realize a two-stroke tokamak-reactor, in which the plasma column is exhausted automatically by raising certain critical plasma pressure from the internal chamber into the external one. Conducting walls of the slit connecting the chambers prevents exhaust untill plasma pressure exceeds some critical value. The critical pressure has been recently calculated by Degtjarev et al. using flux-conserving equilibria problem.

The equilibria under and over critical plasma pressure are shown in Fig.8.

2. STABILITY

Following instabilities of the tokamak plasma attract most attention:

a) local balooning high number, m,n>>1 modes,
b) nonlocal internal modes, m,n~1,
c) internal kink, m=1,
d) tearing modes,
e) free boundary kink modes,
f) disruptive instability.

a) Balooning modes. In the recent two years the theory of the local MHD instability in a plasma of large shear $s = rq'/q \neq 0$ has been developed most actively. An analysis of the numerical calculations made at Princeton /20/ and analitical treatment of small-scale (m,n >>1) modes /20-23/ clarified the situation with local modes in toroidal geometry.

In contrast to a cylinder the perturbations of the form expi (mQ-ns) are not independent eigenmodes in a torus. Coupling parameter is $\alpha = -2p'Rq^2/B_T^2 \approx \frac{a}{R}\beta_p$ where β_p is the poloidal beta. For $\beta_p \sim R/a$ perturbations with different m,n, but close ratio of m/n are coupled into a single balooning mode (Fig.9). Refined solution of the problem of local balooning modes is based on Connor, Hastic, Taylor (CHT) transformation /24/. Basically it implies representation of the Fourier-components a_{mn} of the expansion

$$\xi(a,\theta,\zeta) = \sum_{m,n} a_{mn} \exp i(m\theta - n\zeta)$$

in the form of the integral along magnetic field line $\theta = \theta_1(\eta)$, $\zeta = \zeta_1(\eta)$ on the magnetic surface $\alpha(\vec{r}) = Const$:

$$a_{mn} = \int_{-\infty}^{\infty} \hat{\xi}(a, \theta_1, \zeta_1) \exp[-i(m\theta_1 - n\zeta_1)]\, d\eta .$$

The image $\hat{\xi}(a,\eta)$ is appear to satisfy the same equation as $\xi(a,\theta,\zeta)$ Due to such representation, a smooth image $\hat{\xi}$ corresponds to a rather complicated original local perturbation ξ elongated along field line. If a nonperiodic function t is introduced as integral of the "local shear" S along field line

$$B\nabla t = S \quad ; \qquad S = \frac{[B\nabla a]}{|\nabla a|^2}\,\eta\,t\,\frac{[B\nabla a]}{|\nabla a|^2} ,$$

and functiones F,G, connected with normal K_n and geodesical $K_\perp$ curvature

$$\frac{2K_n}{|\nabla a|} = \frac{\nabla a\,\nabla(2p+|B|^2)}{|\nabla a|^2\,|B|^2} = F, \quad \frac{2K_\perp|\nabla a|}{|B|} = \frac{[B\nabla a]\nabla|B|^2}{|B|^4} = G ,$$

then asymptotically ($m,n\to\infty$) equations for the CHT-image take the form

$$\rho\omega^2(\vec{B}\,\hat{\vec{\xi}}) = -\vec{B}\nabla Q ,$$

$$\rho\omega^2 H\hat{\xi} = -\vec{B}\nabla(H\vec{B}\nabla\hat{\xi}) - p'(F+tG)\hat{\xi} - FQ ,$$

where $H = 1 + |\nabla a|^4 t^2/|B|^2$, $Q = -\gamma p|B|^2[(F+tG)\hat{\xi} - B\nabla\frac{\vec{B}\hat{\vec{\xi}}}{|B|^2}]/(\gamma p+|B|^2)$

$$Q = -\gamma p|B|^2\left[(F+tG)\hat{\xi} - B\nabla\frac{\vec{B}\hat{\vec{\xi}}}{|B|^2}\right]/(\gamma p+|B|^2) .$$

For margin stability, $\omega^2=0$, this system is reduced to a single equation with condition of regularity of $\hat{\xi}$ at $\eta\to\pm\infty$, p' being eigenvalue /24,25/

$$\vec{B}\nabla(H\vec{B}\nabla\hat{\xi}) + p'(F+tG)\hat{\xi} = 0 .$$

At the $m,n >> 1$ the most restricting β -value perturbations were shown to be those with $m,n\to\infty$. Thus solving of the last equation have turned in one of necessary verification of plasma stability.

Fig.10 presents a schematic diagram of the stability in the plane s, α. In the range of a small shear and large pressure gradients the stability criterion of the balooning modes transfers to the Mercier criterion. The branch M is rather sensitive to the magnetic well contained in K_n, and consequently, to the shape of the cross-section of the plasma torus. As the pressure increases the magnetic well grows more rapidly than does the field line curvature-variant responsible for the balooning mode, and the plasma selfstabilization effect /26/ manifests itself. Recent calculations /27/ have shown that as s increases the instability region of p' may become narrower (dashed line). At moderate p' as the shear increases the stability first deteriorate. This fact is reflected explicitly in an analytical necessary

stability condition derived in Ref. /27/

$$\frac{1}{2}S^2 + \frac{2\varepsilon p'}{B^2}\left\{1 - q^2\left[1 - \frac{7R}{4\varepsilon}\left(1 - \frac{5}{7}S^2\right)\exp\left(-\frac{1}{|S|}\right)\right]\right\} - \frac{3Sq^4R^2}{\varepsilon^2}\left(\frac{p'^2}{B^2}\right)^2 > 0 .$$

Term with exponent exp $(-1/|S|)$ describes this destabilization effect.

At present the consequence of the balooning instability is not clearly understood. We know how should optimum profiles of current and pressure look like. A flat current profile in the region of steep plasma pressure gradient, and small pressure gradient in the region of current drop provide sufficiently high critical $\beta^* = 2\sqrt{\langle p^2\rangle}/\langle B^2\rangle$ (Fig.11).

Fig.12 illustrates an example of equilibrium stable with respect to the local modes at $\beta \sim 10\%$ with q changing from 1,1 to 2.2. Plasma is, however, unstable in a narrow region of the outside part of torus for a more peacked current, $1{,}1 < q < 4$. It is seen that if the balooning mode causes undesirable effects such as an appreciably enhanced transport then the careful control of the current density and plasma pressure should be done.

b) Lower inner modes. According to the available calculations these modes impose a weaker restriction on β than the local ones However, there is evidence that these modes may lead to a limitation on pressure even at $\beta_p \sim 1$ if the shear is small and the q-values are near to the resonant values.

c) Inner mode, m=1. The existing theory of the development of this mode explains well the structure of sawtooth oscillations of the electron temperature at the plasma centre. It remained, however, to clarify the radius of the resonance surface, $q = 1$, at which an internal disruption occurs. V Parail and G. Pereversev have recently noticed that following the disruption, the central zone of the plasma cools as a result of mixing the outer and inner plasma regions in accordance with the mechanism suggested by Kadomtsev. This leads to a hollow current density and nonmonotone profile $q(r)$ with two resonant surfaces (Fig.13). Assuming that a disruption starts developing at a time moment when the second extreme of the magnetic flux $\psi^* = \int_0^{r_2}(B_\vartheta - \frac{r}{R}B_z)\,dr$ comes to zero so that conditions for the reconnection of the axial and outer surfaces are fulfilled, and using the electron thermal conductivity coefficient, which is usually applied for simulating macroscopic transfer phenomena, these authors reached a good agreement between the values of the calculated period of relaxation oscillations (tooth widths) and experiment.

d) Helical tearing modes. At the stage of current growth in a tokamak its radial profile is unstable with respect to kink modes with m=16 - 3. According to the calculations /30,31/ at this stage periodic rearrangement of magnetic surface configuration due to reconnection (Fig.14) takes place causing rapid growth of the current into the plasma column. Thus, these modes prepare a stable current distribution in a heated plasma.

e) Free boundary plasma kink modes. These modes turned out to be stabilized at the current profile, which has established at the initial stage. Their stabilization is made easier due to the formation of a low density plasma mantle around a hot plasma column.

f) Disruptive instability. This catastrophical phenomena may be most likely attributed to nonlinear $m/n = 1/2$ and $3/2$ mode interactions and under favourable conditions for their development, giving rise to the explosive instability. Callen's paper at the Innsbruck Conf., 1978 describes this well /31/.

3. TRANSPORT

Transport in a plasma has remained to be the most intriguing problem for physicists. It contains the most amount of uncertainties. Nevertheless, the application of various semiempirical formulas for transport coefficients allows the simulation of a tokamak discharge. The initial stage, relaxation oscillations due to the kink instability, neutral beam and HF plasma heating etc. are simulated sufficiently well. It should be pointed out that as regards the feasibility of a reactor, in principle, the existing level of plasma confinement is quite satisfactory. The development of theory is necessary for more profound understanding of physics and more acurate estimates of the design and operating conditions of a reactor. The PLT experiments have confirmed that neoclassical coefficients associated with the ionic plasma component are close to those observed experimentally both in the range of intermediate and rare collisions. As to electron transport, it remains to be anomalous. Electrons differ from ions by a smaller size of the cyclotron orbits. This fact suggests that the cause of the anomality should lie in disturbing the structure of nested magnetic surfaces and appearance of "braiding" or"trembling" magnetic force lines. A stochastic motion of the field line and the attached electrons leads to an electron thermal conductivity coefficient proportional to square of the transverse oscilla-

tion amplitude of the force lines /32-34/ , $\chi_e = \chi_{ue} \frac{\langle (\Delta B)^2 \rangle}{|B|^2}$. It is shown in /34/ that this formula is valid both in collisional and strongly turbulent cases.

Statical and flunctuating inhomogeneities of the toroidal magnetic field /35/ have essentially an appreciable effect the transport. In the latter case, according to the calculations made recently by Morozov and Pogutse the thermal conductivity coefficient depends on the number of coils on the field correlation length ΔN as, $\chi \sim (\Delta N \ln N/\Delta N)^{3/4}$.

4. STELLARATORS

It is usually assumed that the equilibrium β in a stellarator may be close to unity for the given rotational transform per unit length if the aspect ratio tends to infinity. This is however not the case. A linear stellarator ($R/a \longrightarrow \infty$) has not magnetic well. The presence of a magnetic "hill" leads to an instability of plasma as a whole (mode m=1, n=0) as in the case of simple mirror traps. In contrast to the open traps, the instability appears in stellarators only above certain critical pressure, $\beta > \beta_{cr}$, due to the presence of the rotational transform. **In a toroidal stellarator the presence of the hill increases** the displacement of the magnetic surfaces. These results obtained by Green et al /36/ in 1966 has been recently confirmed by the calculations made at the Kurchatov Institute. If there is no magnetic well the critical β_{cr} determined by stability is also small. In an circular magnetic axis stellarator, the demand for the magnetic well is inconsistent with that for an appreciably large rotational transform since the well is dependent on the curvature and requires a small aspect ratio while a large rotational transform may be obtained only at a large aspect ratio. Both these conditions are, however, consistent in a spatial axis stellarator with the D-shaped magnetic surface cross section Refs./37-38/ . Therefore, these systems deserve proper attention.

REFERENCES

1. R.A.Dory, Y.-K.M.Peng. Nucl.Fusion, 17 (1977) 21.
2. J.B.Taylor. Culham Lab.Rep. PPN 10/75 (1975).
3. G.V.Pereversev, V.D.Shafranov, L.E.Zakharov. In "Theoretical and Computational Plasma Physics", IAEA, Vienna, 1978, p.469.
4. Л.Е.Захаров, В.Д.Шафранов. Препринт ИАЭ-3075, Москва 1978.

5. H.Grad,P.N.Hu,D.C.Stevens.Proc.Nat.Acad.Sci.USA 72(1975) 3789.
6. H.Grad, P.N.Hu,D.C.Stevens,E.Turkel.Proc.6-th Int.Conf.,Berchtesgaden,1976,Vol.2, IAEA, Vienna (1977)355.
7. J.W.Dungey. Phil.Mag.44(1953) 725.
8. E.N.Parker. Astrophys.J.Suppl.8 (1963) 177.
9. M.E.Petchek. 1964 NASA SP-50,p.425. US Govt Printing Office.
10. С.И.Сыроватский, ЖЭТФ 50/1966/ 1133.
11. А.А.Галеев, Л.М.Зеленый. Письма в ЖЭТФ, 25/1977/407.
12. T.H.Jensen,W.B.Thompson,J.Plasma Phys. 19(1978) 227.
13. M.Bonnedal,E.Canobbio.Proc. 8-th Int.Conf., Innsbruck,1978,Vol.2, p.535, IAEA,Vienna (1979).
14. V.D.Shafranov,Nucl.Fusion, 19(1979)187.
15. N.Ohyabu, C.L.Hsieh,T.H.Jensen,J.Plasma Phys.21 (1979)253.
16. S.J.Fielding et al.,Proc. 7-th Europ.Conf.,Prague,1977, 1(1977) 36
17. Y.-K.M.Peng. Oak-Ridge Nat.Lab.Rep.,ORNL/TM-6319, 1978.
18. П.Н.Вабищевич, Л.М.Дегтярёв и др. Препринт ИПМ №119/1978/ Москва.
19. A.M.M.Todd,M.S.Chance,J.M.Green,R.C.Grimm,J.L.Jhenson,J.Manickam. Phys.Rev.Lett., 38 (1977) 826.
20. D.Dobrott et al., Phys.Rev.Lett., 39 (1977) 943.
21. M.S.Chance et al., Proc. 7-th Int.Conf.Insbrick, 1978. Vol.1, p.677, IAEA,Vienna (1979).
22. C.Mercier, ibid, p.701.
23. L.E.Zakharov,ibid, p.689.
24. J.W.Connor, R.L.Hastie,J.B.Taylor.Proc.Roy.Soc. A 365 (1979) 1.
25. D.Correa-Restrepo.Z.fur Naturforsch., 33a (1978) 789.
26. А.Б.Михайловский, В.Д.Шафранов, ЖЭТФ 66 /1974/ 190.
27. H.R.Strauss et al., Plasma Phys.Lab.Rep. PPPL-1535 (1979).
28. О.П.Погуце, К.И.Юрченко. Письма в ЖЭТФ 28/1978/ №6.
29. L.E.Zakharov. Nucl.Fusion 18 (1978) 339.
30. Yu.N.Dnestrovskij,S.E.Lysenko,G.V.Pereversev,K.N.Tarasyan.Proc. 7-th Int.Conf.,Innsbruck. 1978. Vol. IAEA, Vienna (1979) 443.
31. J.L.Callen, B.V.Waddel et al., ibid, p.415.
32. A.B.Rechester, M.N.Rosenblut. Phys.Rev.Lett. 40 (1978) 38.
33. B.B.Kadomtsev, O.P.Pogutse. 7-th Int.Conf. Innsbruck,1978, vol.1,p.649,IAEA,Vienna,1979.
34. A.A.Galeev, L.M.Zeleny.Pis'ma Zh.Exp.Theor.Phys. 29 (1979) 669.
35. А.В.Гуревич, Я.С.Димант,Ю.Н.Днестровский, К.А.Разумова. Письма ЖЭТФ. 26/1977/733.
36. J.M.Greene,J.L.Jhonson and K.E.Weimer.Plasma Physics 8(1966) 145.
37. V.D.Shafranov,E.I.Yurchenko.Nucl.Fusion 8(1968) 329.
38. В.М.Глаголев, А.Е.Ленева. Препринт ИАЭ-3052, Москва 1978.

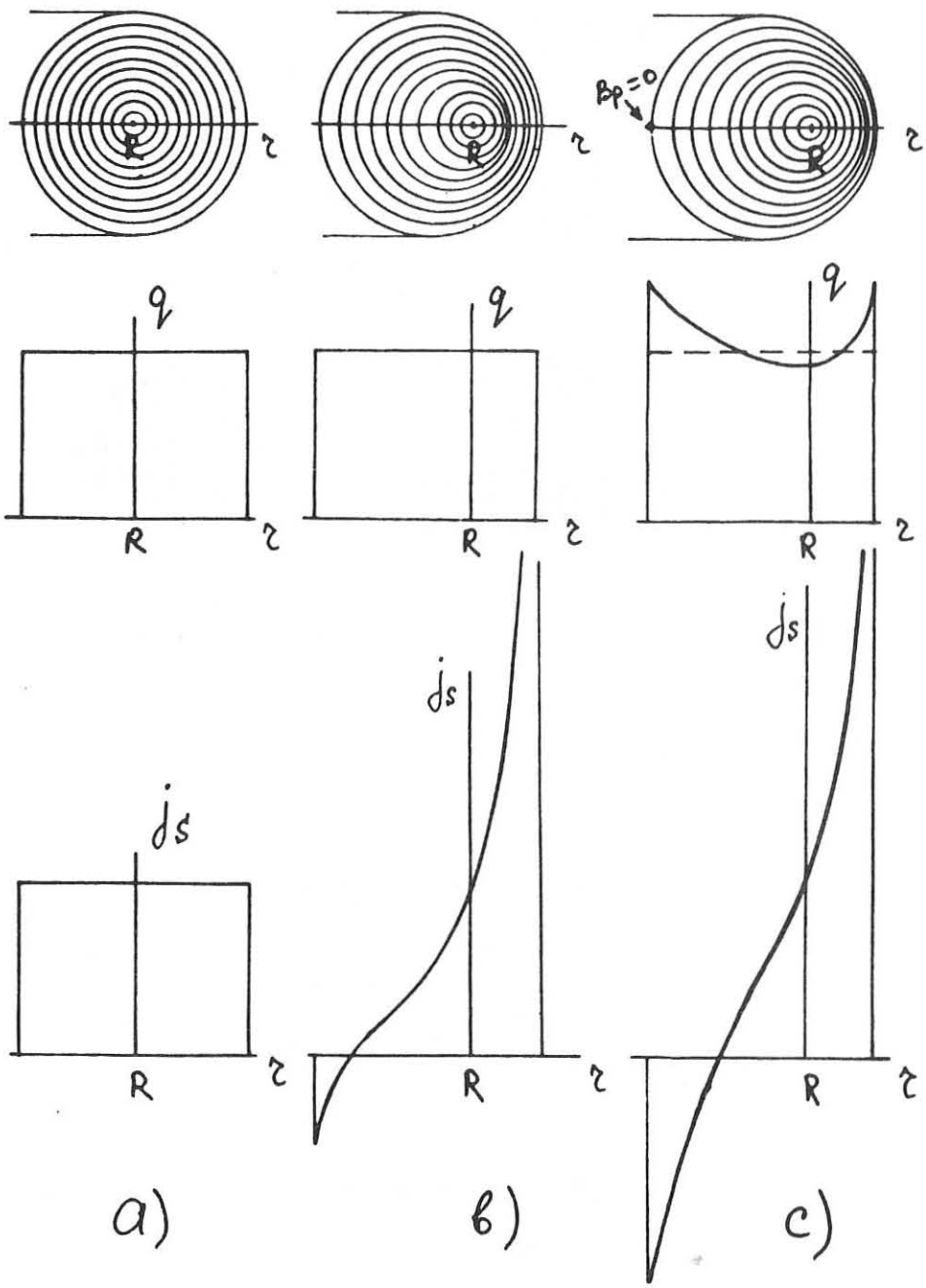

Fig. 1 Relaxation of FCT equilibris

a) t o; β_p = o

b) t = +0; β_p = 1.5 R/a; q(,t)/ t = 0

c) t = 0.4τ_{sk}; τ_{sn} = $\frac{1}{4}\sigma a^2$;

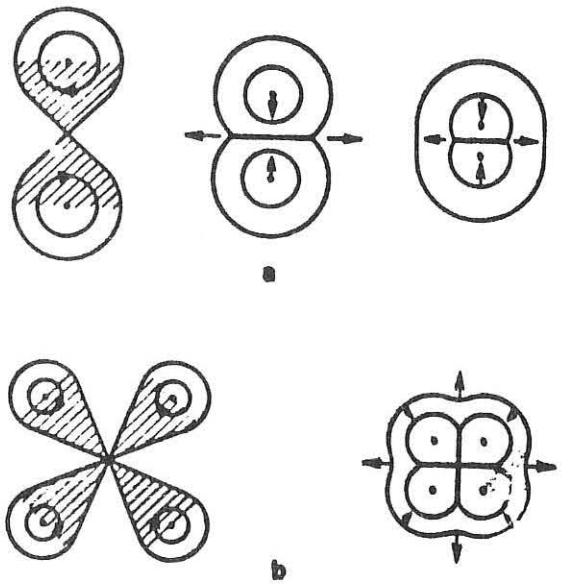

Fig. 2 Mixing process of a) two and b) four columns into one.

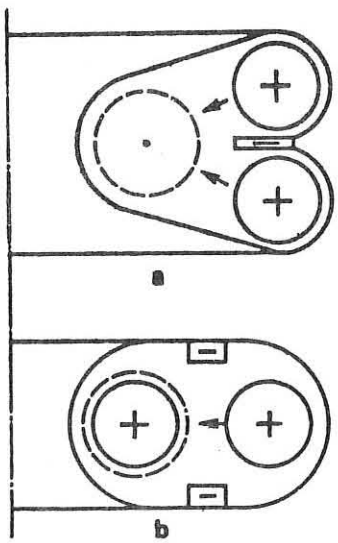

Fig. 3 Scheme of pushing of columns to be mixed.

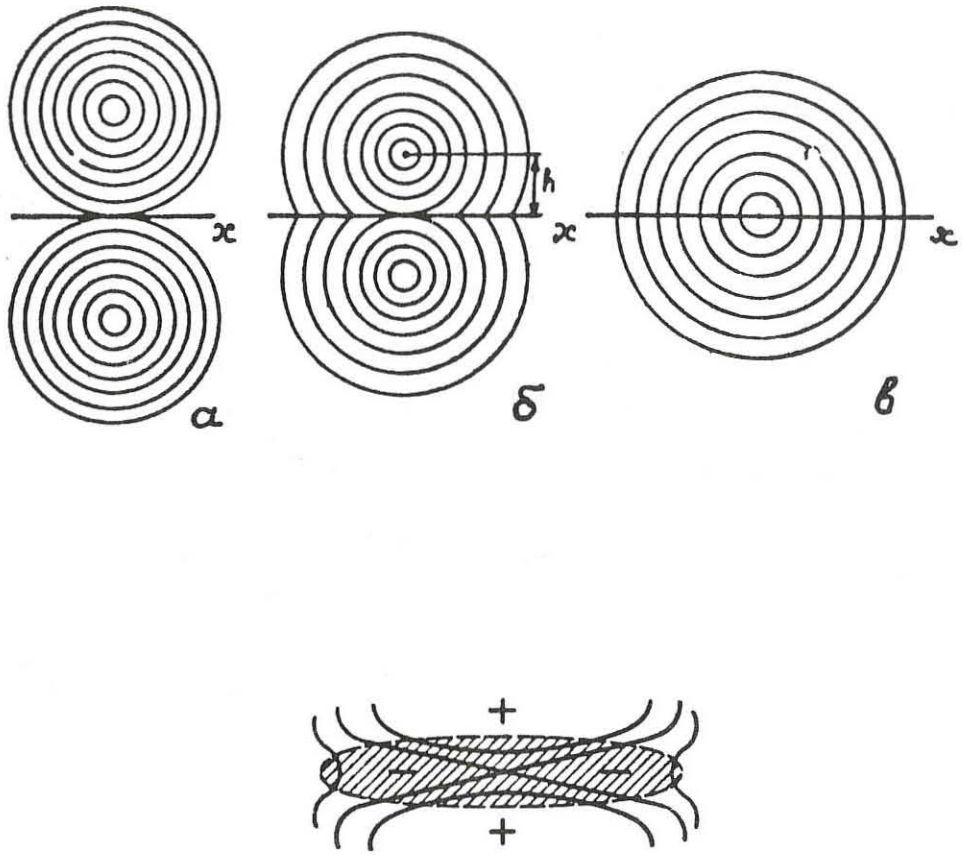

Fig. 4 Field line reconnection during mixing and the structure of the current layer.

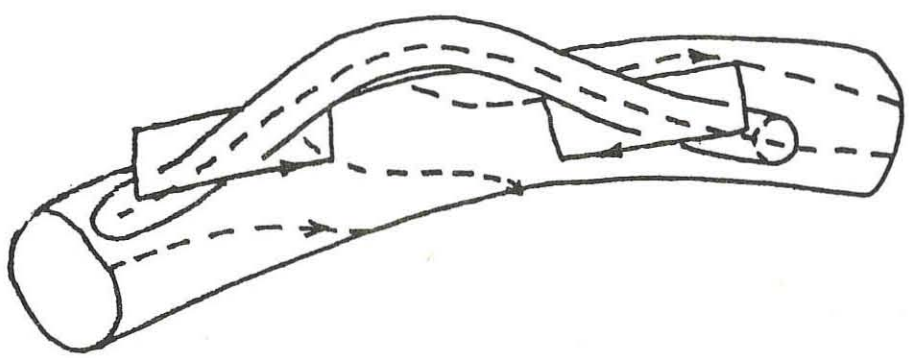

Fig. 5 Divertion of a magnetic tube.

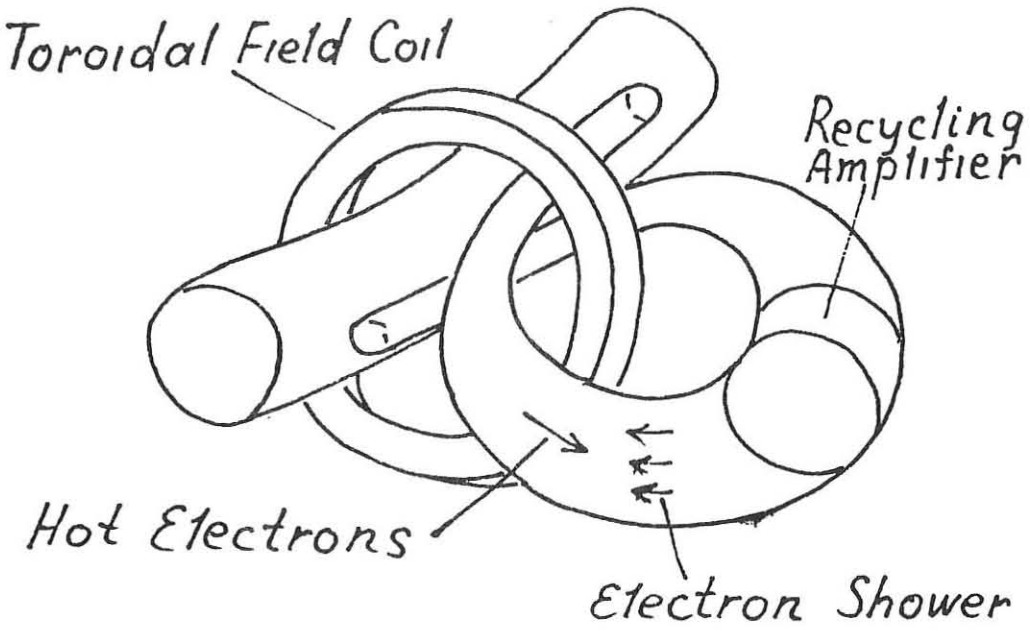

Fig. 6 Branch divertor.

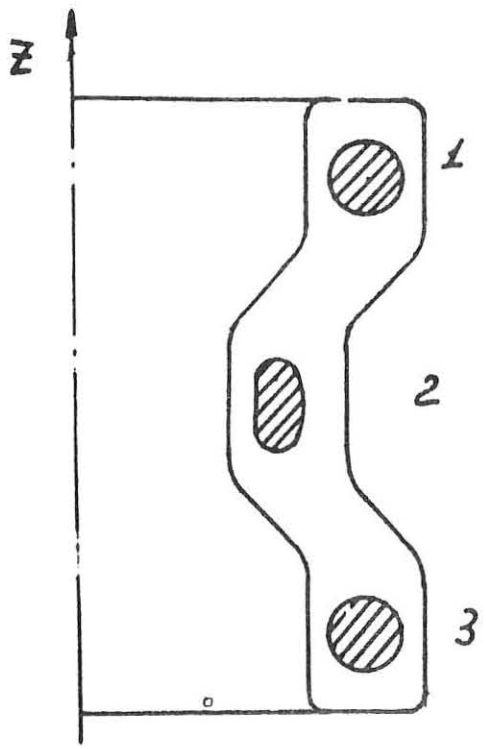

Fig. 7 Continuous tokamak.

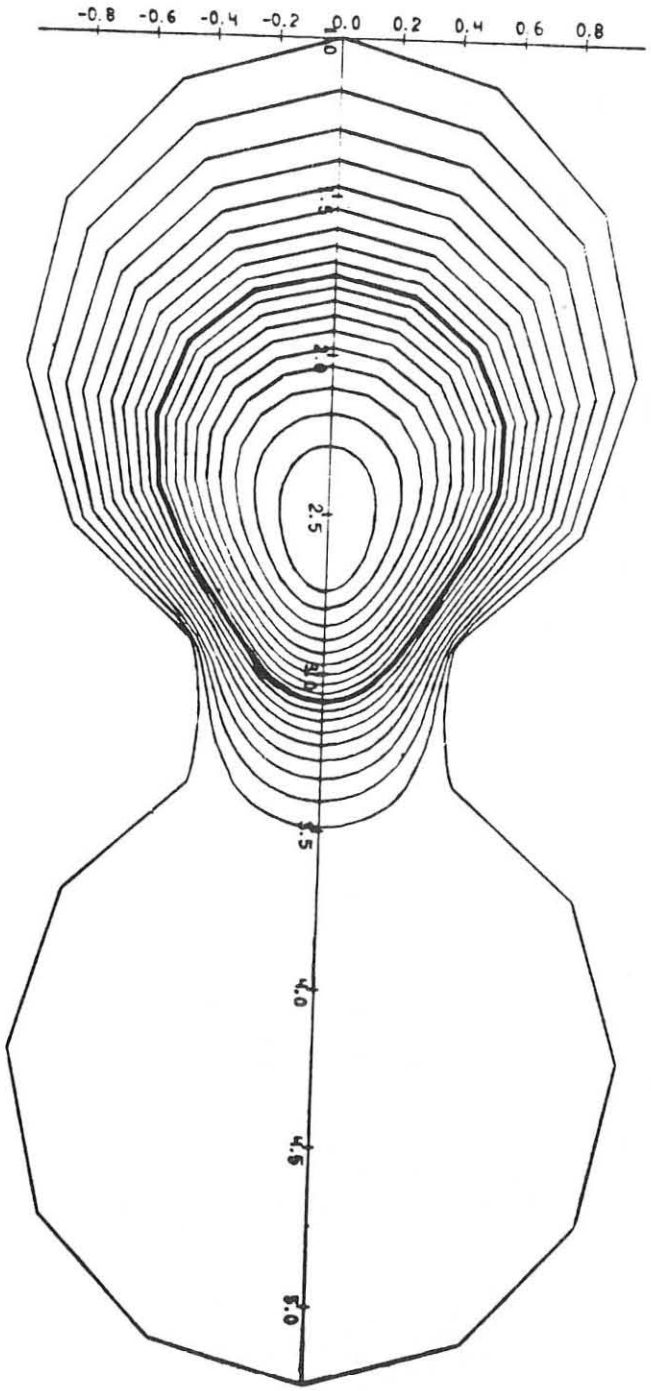

Fig. 8a

Fig. 8 The equilibria in a two stroke tokamak; a,c) plasma pressure is near crictical one, b) plasma pressures exceed the critical one.

$q(\psi) = 1.5$; a) $p'(\psi) = 1.5$; $\beta^* = 4.7\%$; b) $p'(\psi) = 3$;

c) $p'(\psi) = 1.5$; $\beta^* = 8.1\%$

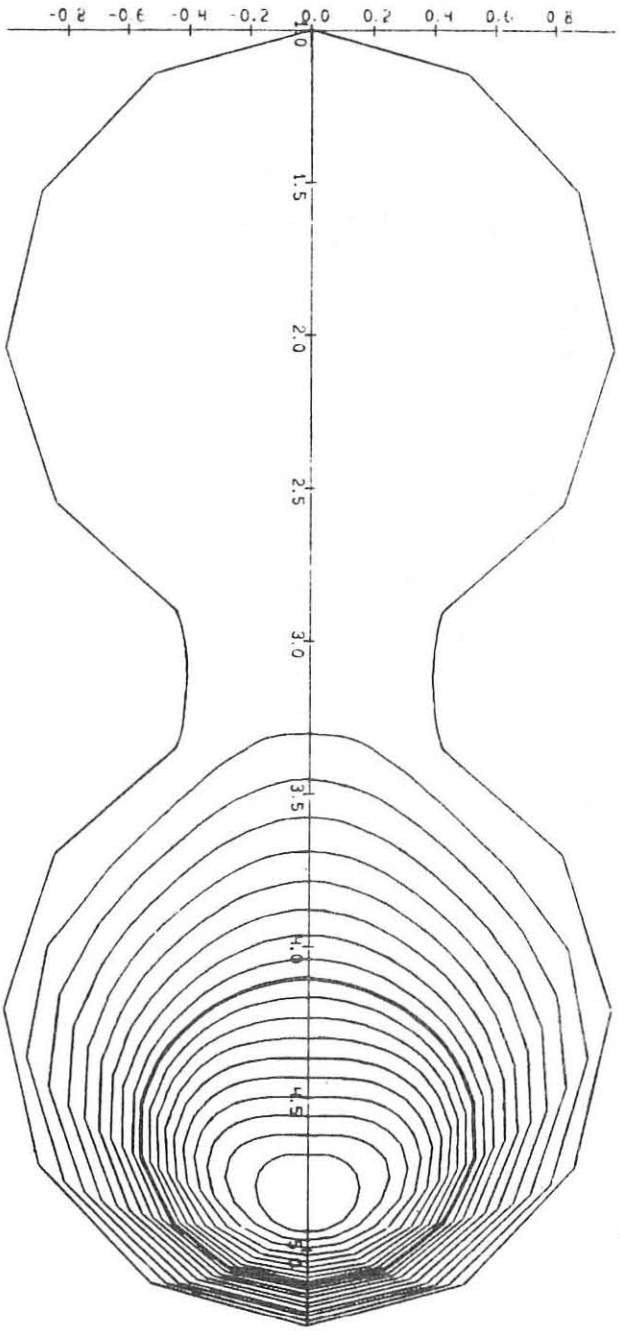

Fig. 8b

Fig. 8 The equilibria in a two stroke tokamak; a,c) plasma pressure is near crictical one, b) plasma pressures exceed the critical one.

$q(\psi) = 1.5$; a) $p'(\psi) = 1.5$; $\beta^* = 4.7\%$; b) $p'(\psi) = 3$,

c) $p'(\psi) = 1.5$; $\beta^* = 8.1\%$

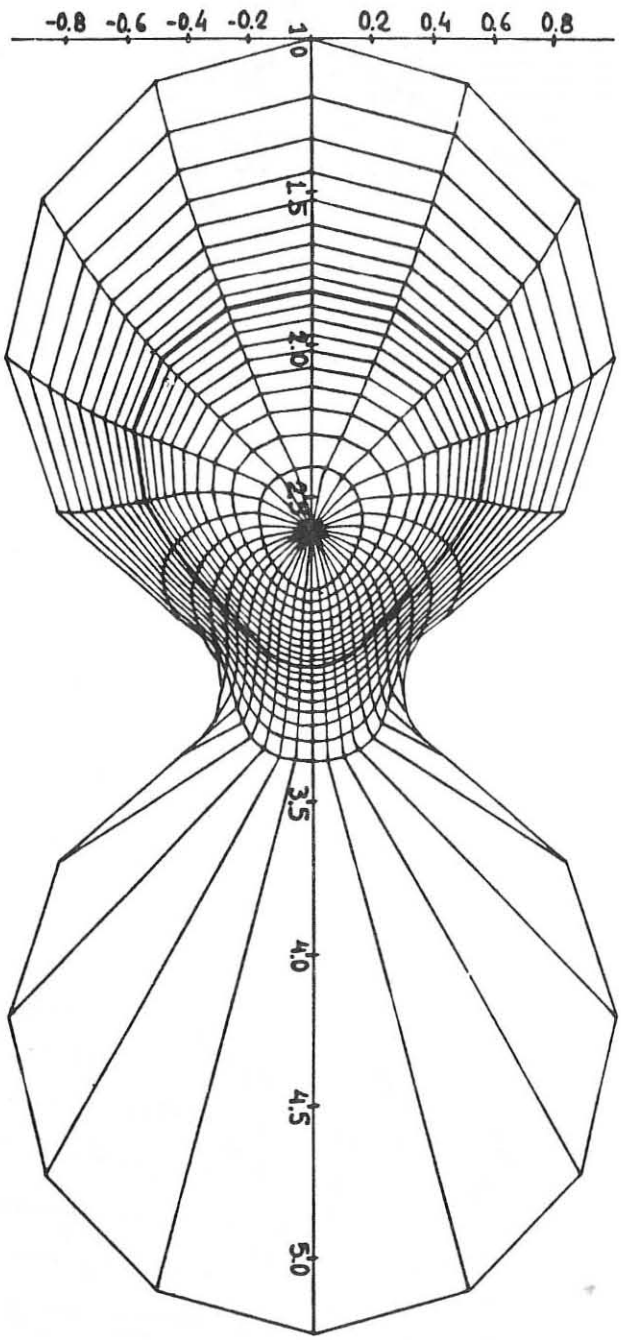

Fig. 8c

Fig. 8 The equilibria in a two stroke tokamak; a,c) plasma pressure is near crictical one, b) plasma pressures exceed the critical one.

$q(\psi) = 1.5$; a) $p'(\psi) = 1.5$; $\beta^* = 4.7\%$; b) $p'(\psi) = 3$,
c) $p'(\psi) = 1.5$; $\beta^* = 8.1\%$

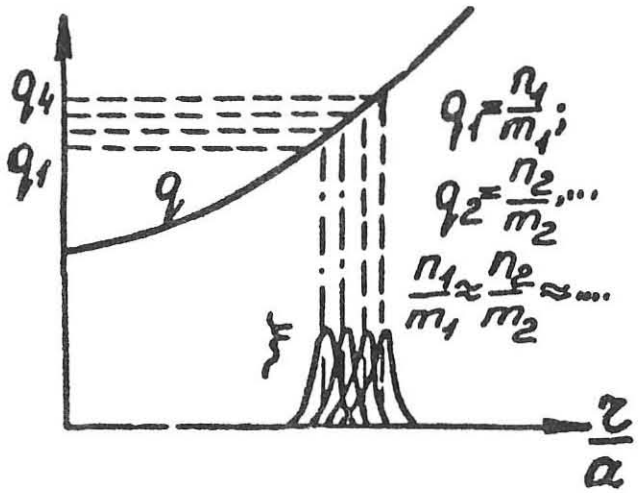

Fig. 9 Ballooning mode structure

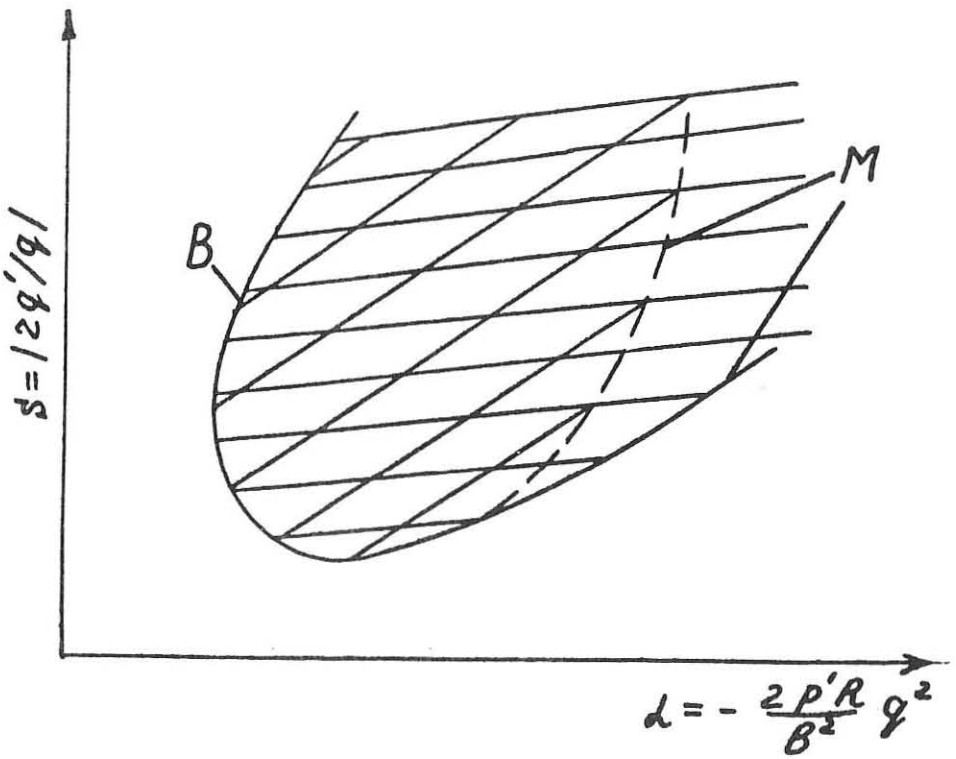

Fig. 10 Schematic diagram of ballooning mode stability

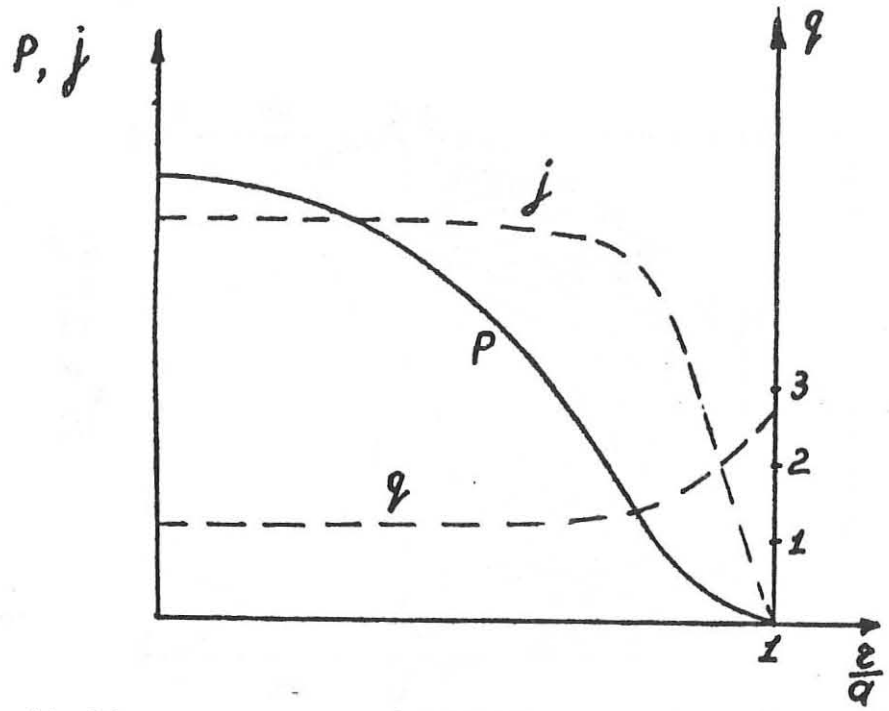

Fig. 11 Plasma pressure and current distribution favourable for stability

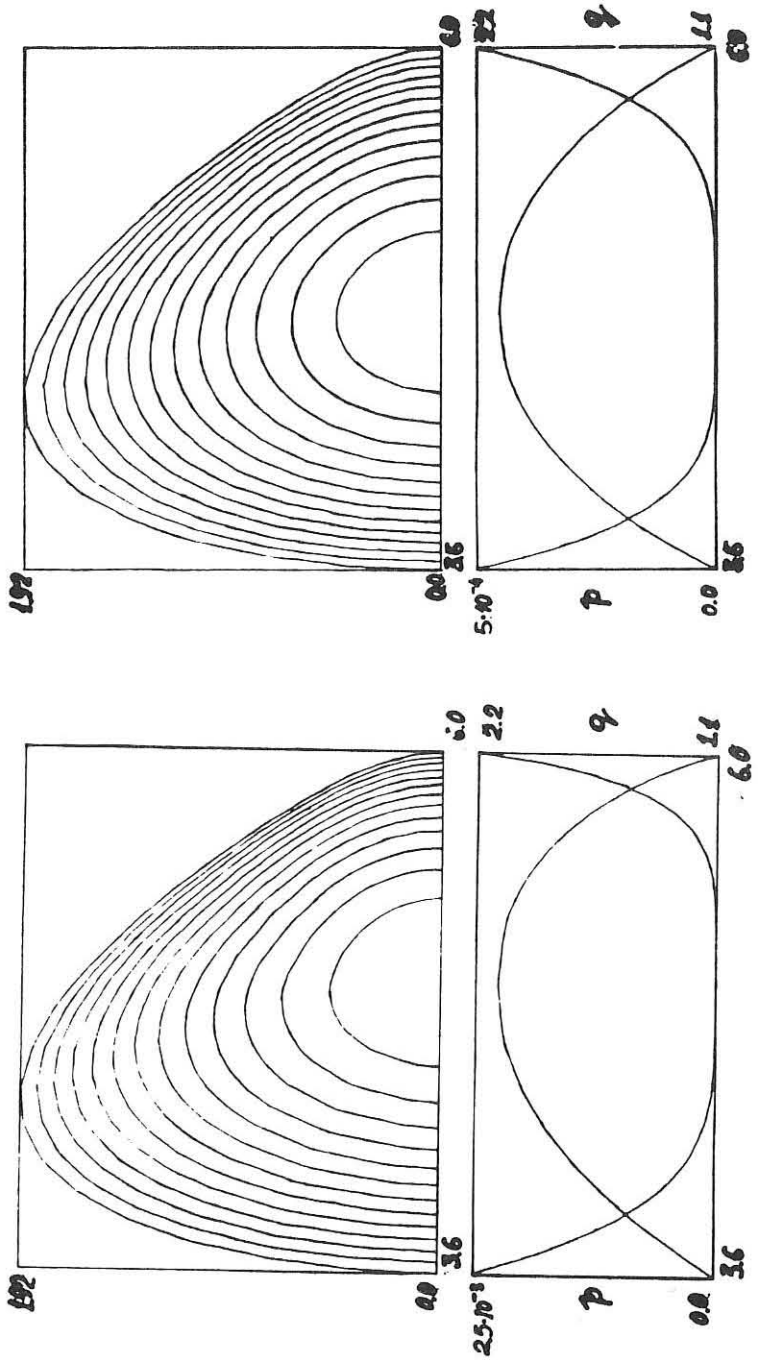

Fig. 12 Ballooning stable equilibria

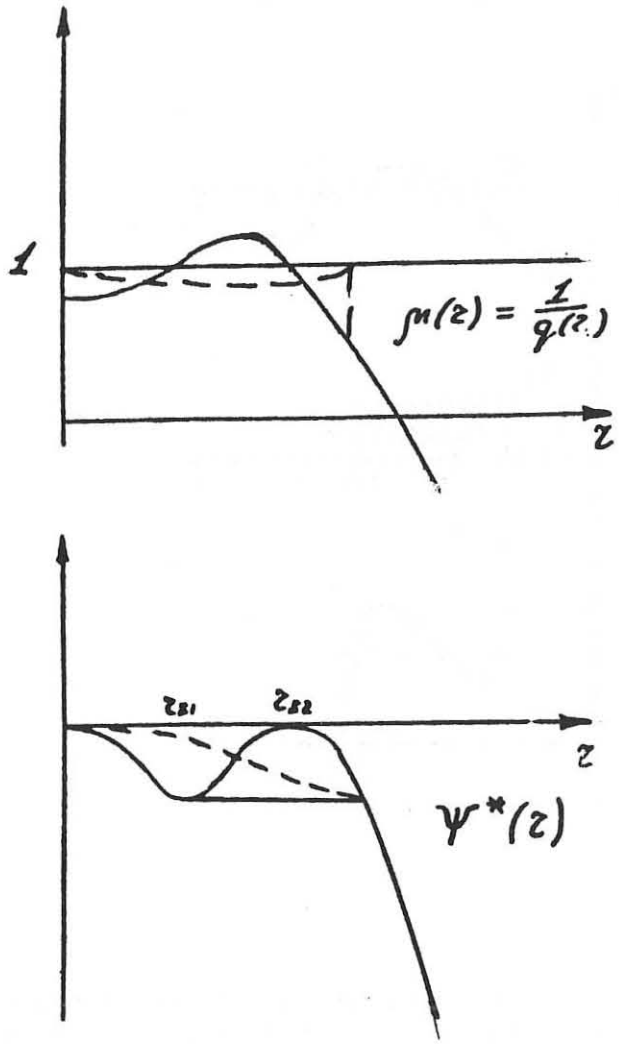

Fig. 13 f_m and ψ^* versus z.
Solid line - before internal disruption dashed
Dashed line - after internal disruption

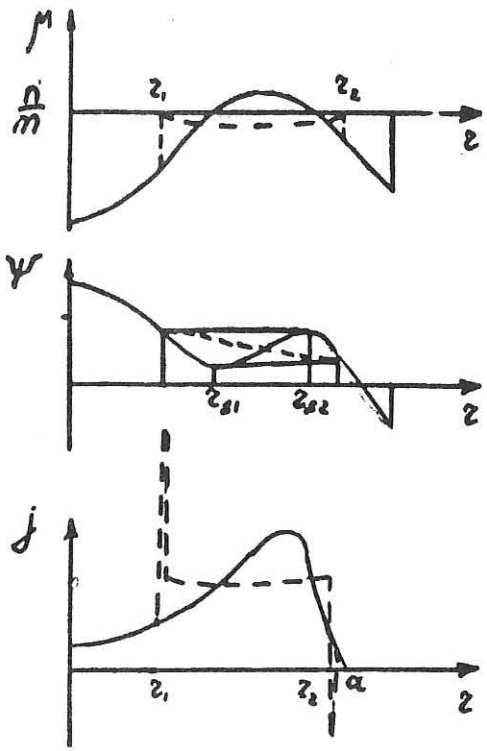

Fig. 14 μ, ψ^*, j versus z on the initial stage of the current growth Solid line - before, and dashed line - after the rearrangement of the magnetic surfaces.

in 9th Europ.Conf.on Controlled Fusion and Plasma Physics, Invited Papers: UKAEA Culham Lab., Abingdon, Oxon, 1979, p. 525

REVIEW OF FUSION REACTOR PROBLEMS

G. Grieger

Max-Planck-Institut für Plasmaphysik
EURATOM-Association, D-8046 Garching

In reviewing fusion reactor problems this paper will deal only with systems based on toroidal magnetic confinement - essentially tokamaks. In addition, it will concentrate on DEMO or even pre-DEMO devices, i.e. on physics and technology problems rather than on questions of fusion reactor economy or on the competition of fusion power with other power sources. Use will be made, however, of the results of the INTOR Workshop presently running at the IAEA Headquarters in Vienna [1].

The paper will compare the knowledge required for the successful construction and operation of a fusion reactor with the state of the art, and will analyse the major remaining problems for their degree of influence on reactor performance and for the chances of their solution.

In tackling this the field has to be narrowed down even further. From a reactor point of view there would be a strong desire for a continuously burning, steady power source because a considerable number of the existing problems would be eased if pulsed operation could be avoided. This is particularly true for the cycling stresses to which all the reactor materials are exposed by pulsed loads. And, indeed, there are proposals for steady operation by using the bootstrap current, or wave or particle driven currents for systems with internal confinement, or by using the inherent properties of external confinement systems, like stellarators. With the present experience, however, there seems to be no chance to aim at steady tokamak operation already with the DEMO generation, and there is even some doubt whether it can be achieved at all. For this paper, therefore, a pulsed plasma operation with the following phases will be considered: (i) start-up, (ii) burn, (iii) shut-down, (iv)dwell time, with the conditions for the dwell time to be as short and for the burn to be as long as possible, and to produce a high enough fusion power at sufficient power density.

The integral reactor system can be broken up into a number of subsystems which, with their functions and properties, are setting boundary conditions to the reactor core, the plasma, and vice versa. These subsystems have to

- absorb the thermal part of the fusion power in the first wall;
- absorb the neutron energy in the blanket;
- breed the fuel in the blanket;
- shield the external components from neutron and γ-radiation;
- generate the magnetic fields;
- take up all forces in a space-saving structure;
- allow for remote handling of all components;
- generate the required vacuum;
- refuel and remove the ashes;
- guarantee that all safety and environmental conditions are observed.

All these subsystems interact with each other; the properties of most of them are determined by the mechanical, electrical, and

radiation damage and activation properties of the materials they are made from, and quite a number of the fusion reactor problems have their origin in the limitation of parameters introduced by the subsystems.

It is most appropriate to start the review with the burn phase and to argue later on how to achieve it. The considerations will also be restricted to deuterium-tritium plasmas. This is quite obvious because the D-T reaction is the most powerful one already at not too high plasma temperatures. But its selection immediately introduces a set of complications: (i) tritium has to be bred in a breeding blanket and (ii) most of the fusion power comes with high energy neutrons which, due to their high energy, may lead to intense He generation in materials, to swelling, and to activation. Both these complications could be avoided in principle. The D-D reaction would not require fuel breeding and most of the neutrons would have somewhat lower energy, and the p-"B reaction, for instance, would not produce any neutrons at all. But unfortunately both of these reactions have comparatively low cross-sections. On the other hand, there is also some advantage coming along with the high-energy D-T neutrons: Their penetration depth allows to clearly separate the energy conversion region, the blanket, from the energy production region, the plasma, and therefore allows a rather free choice of the first wall temperature.

In selecting the plasma operating conditions one often looks for the ignition condition, where the α-power starts to balance the plasma losses, and for a thermally stable working point. But it might be more appropriate to optimize for the highest fusion power density at a given ß because probably ß will be the most stringent limitation for magnetic confinement. Fig. 1 shows the fusion power density vs. temperature, each curve normalized for thermal plasmas of constant pressure [2]. It is well known that there is an optimum at kT ≈ 13 keV.

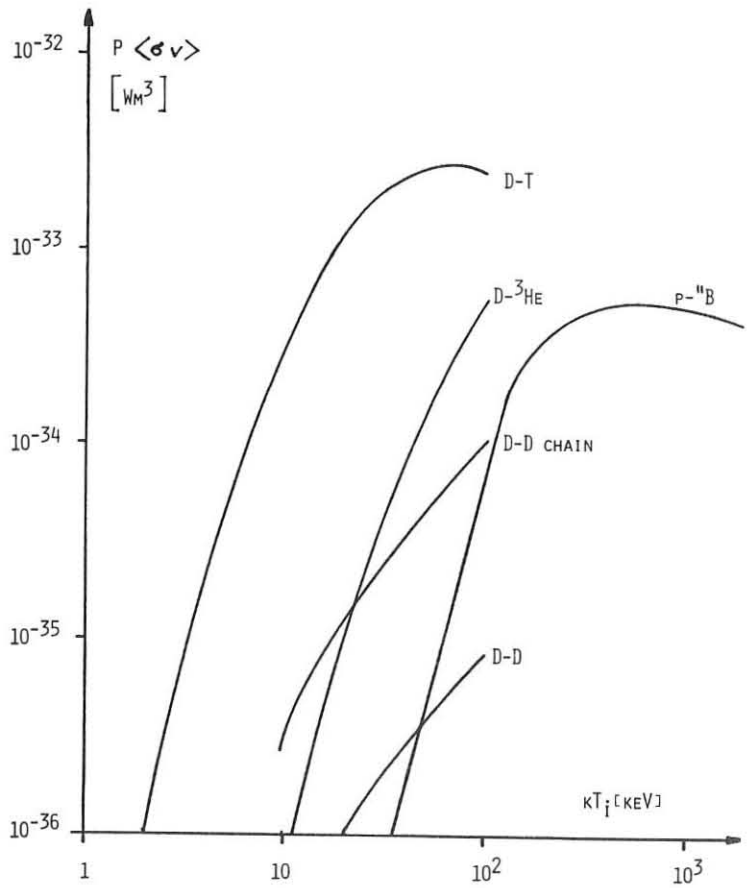

Fig. 1: Normalized power density produced by fusion reactions. Power density = $P\langle\sigma v\rangle \cdot N_1 \cdot N_2$, the alphas containing 1/5.

This result is obtained under the only assumption that the ions are Maxwellian in their distribution; and it is only the absolute value of the power density which goes up or down if the electron mean energy differs from the ion temperature or if the pressures of the alphas or the impurities are using up part of the achievable ß.

In this context it is worth discussing the hot ion mode of operation [3] which has been suggested for next step reactor concepts. In principle, it has some very attractive properties:

Since only the ions are needed for the generation of fusion power, it is more economic to aim at heating only them to the required high temperatures, particularly since the energy from the plasma is observed to be lost mainly through the electron channel, whereas the ion heat conduction seems to be close to neoclassical and hence much smaller. But the hot ion mode can only be obtained with a not too high collisionality, i.e. with not too high density, compensated by a high ion temperature. Typical values are $kT_i = 40$ keV and $kT_e \approx 5$ keV (in order to get sufficient heat flux from the alphas into the ions). But this kind of operation simultaneously means that β is used only to a reduced extent. Therefore, the hot ion mode offers advantages if the leading plasma problems were with confinement. If they are with power density or β, which are the more likely cases, one would prefer operation with thermal plasmas at $kT \approx 13$ keV.

Apart from the magnitude of B, the maximum achievable power density in tokamak reactors is then given by the maximum achievable β. According to theory, the limitation is manifold. But if one follows its recommendations [4] and tries to lower q to the lowest value tolerated by the disruption limit, arranges for suitable profiles of current and pressure distribution, assumes an elongated cross-section, installs some passive and some active feed-back loops against the most critical modes, one can hope to achieve volume average betas of 6 % or perhaps a little bit higher. This takes into account that the aspect ratio for reactors can hardly be below 4 since extra space is required within the main field coil system for blanket and shield.

The plasma pressure and hence the fusion power density is then fully determined by the magnetic field technology. Here the state of the art is a 10 T technology using NbTi as superconducting material. This technology seems to be sufficiently developed but means that 10 T must not be exceeded at any point at the superconducting cable. With the magnet aspect ratio this condition restricts the strength of the magnetic field on the magnetic axis to about 5 T, and thus yields a maximum plasma energy density

$$\langle E \rangle \leq 300 \frac{kJ}{m^3}$$

possible to be confined, or with $kT_e = kT_i = 13$ keV a maximum particle density of

$$\langle n_e \rangle \leq 1.5 \cdot 10^{20}\ m^{-3}$$

which in turn limits the total power density to

$$P \leq 3\ MW/m^3.$$

This is about 30 times the power density in the combustion chamber of a coal fired plant.

One is now starting to develop the 12 T technology by going to Nb_3Sn as superconducting material or by alloying NbTi with Ta in order to increase its performance. 12 T, i.e. about 6 T on the magnetic axis, then seems to be the limit of the magnetic field compatible with the strength of the structural material. It would allow raising the total power density to

$$P \leq 4\ MW/m^3$$

which, from a reactor point of view, is still rather low compared to the complicated and volumenous technology needed but, from the properties of the materials to be used in the first wall and blanket region, it is already very difficult to deal with.

In evaluating the above numbers no account was made yet for the contribution of helium to the pressure balance. If its density were about 10 % of the D-T density, it easily could use up what could be gained by the transition to the 12 T technology, particularly since the mean α energy is higher than the temperature of the reacting plasma. On the other hand, one might be forced to allow an accumulation of the ashes to such concentrations in order to be able to remove them with acceptable pumping speeds of about 10^6 l/s. 1 GW_{th} corresponds to the generation of $3.6 \cdot 10^{20}$ α-particles per second and no matter how the ash removal is done in the first place, via a divertor or not, stationary conditions will then require such helium concentrations at least in the outer plasma regions.

With respect to the power balance one also has to recognize that the above quoted figures on power density include what is occurring with the neutrons. For directly balancing the plasma losses, however, only the α-power is available which amounts to about 0.6 MW/m^3. This would be sufficient if only the unavoidable losses, like heat conduction, bremsstrahlung, etc., were to be considered. In this respect it is conventional to assume the ALCATOR scaling [5] as a lower bound for the energy confinement time

$$\tau_E \approx 5 \cdot 10^{-21} \langle n \rangle a^2$$

particularly since there are some indications from PLT and ohmically heated stellarators that τ_E might show some increase with temperature. On the other hand, one cannot neglect that there are also some experiments showing a reduction of τ_E once a certain energy density is surpassed so that some uncertainty remains. Unfortunately, there is also no generally accepted theory describing the present experimental results and yielding sufficiently safe theoretical grounds. At least in part this is due to the difficulty to reliably relate micro-instabilities and transport.

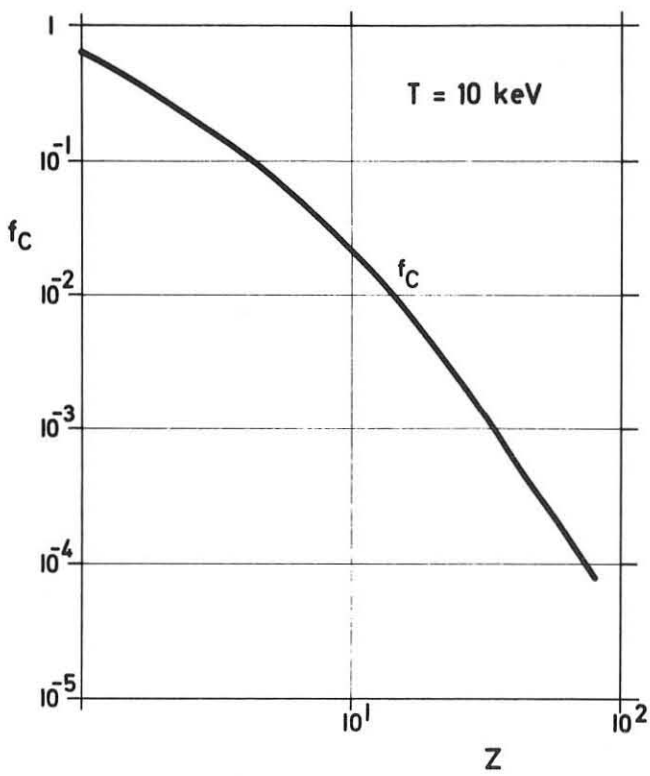

Fig. 2: f_C: impurity concentration leading to doubling of the losses via its radiation.

In any case, there is not much room left for additional power losses from the plasma, and this sets a rather stringent limit to the tolerable impurity concentration. In Fig. 2 the relative impurity concentration, f_C, leading to just a doubling of the total plasma losses by impurity radiation is given for the different elements [6]. The plasma temperature assumed there is 10 keV. Since the doubling of the power losses is probably already unacceptably high, the tolerable fractions of impurities are coming out extremely low, indeed.

The primary source of impurities is the wall surrounding the plasma

and, apart from its excessive heating, the main effect of their generation is sputtering. Fig. 3 shows that the sputtering coefficients become rather large if the energies of impinging particles exceed 10 - 100 eV, depending on wall material [7].

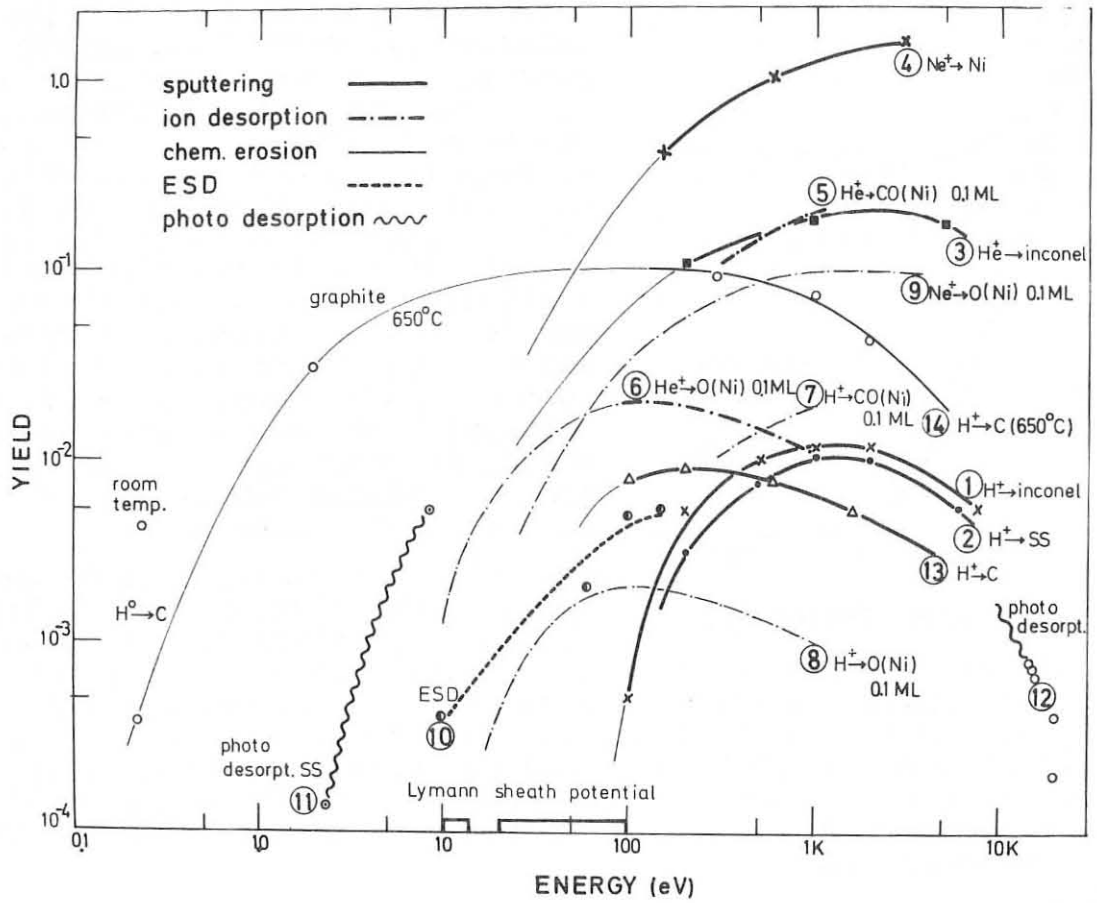

Fig. 3: Sputtering yields vs. energy of impinging particles for various wall materials.

A better way of looking at this problem is to compare sputtering and radiation properties for the various elements. In Fig. 4 the ratio between "tolerable" concentration and sputtering coefficient defines a figure of merit which is given as a function of the plasma edge temperature for various potential wall materials [8]. This figure explains the proposals for low-Z coatings if the plasma edge temperatures would turn out to be high. The technology for the application of coatings exists in principle, only their properties in the fusion environment require further studies. Fig. 4 also explains the preference for high-Z wall materials if the plasma edge temperature could be kept sufficiently low.

But even if one optimizes the plasma wall conditions for impurity generation, there remains considerable uncertainty on impurity transport, and it is surprising to see how little is known in this respect. Theory predicts accumulation of the impurities towards the plasma centre under many (but not all) circumstances. Present experiments, however, if they are not too collisional, seem to indicate that there is also an anomalous outward particle motion compensating the theoretically predicted inward motion, and often it is found that the relative concentration is rather independent of the radius. It would be very important if such a finding could be substantiated by more conclusive experimental results because then measures taken at the plasma edge would be sufficient to determine the impurity contribution all over the plasma.

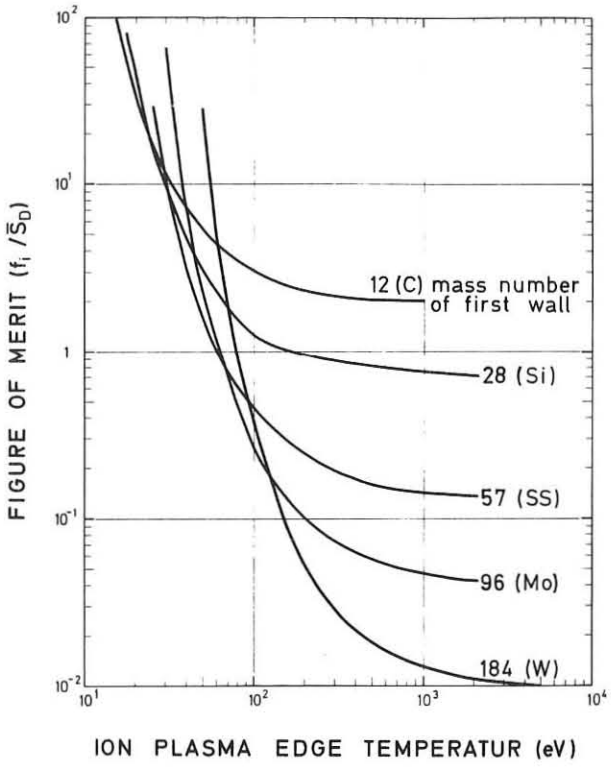

Fig. 4: Figure of merit for different wall materials.

With the present knowledge, however, forecasts about the impurity behaviour in dense high energy plasmas are connected with large uncertainties, perhaps the largest and most influential ones we have to face at present. Experimental evidence coming from the JET generation , when it is in operation, will be extremely important and, hopefully, relax the situation. But at present, there is a growing tendency to go the safest way and to take all measures to reduce the impurities already at their generation. Two main options are open, the cold plasma mantle and the inclusion of a divertor.

The cold plasma mantle would be the optimum solution. With a low enough temperature of the plasma edge it would put the sputtering rate to almost zero. But the condition for its stable existence is a complicated balance between heat flow, edge impurity concentration, edge radiation, etc. which is difficult to treat theoretically and to arrange experimentally. Experimental evidence is very poor here and before JET comes into operation, there are also no major programmes which would yield the required information soon.

All the present emphasis is therefore put on divertors. Under optimal circumstances they should carry most of the particles leaving the plasma along a scrape-off layer towards outside divertor chambers, and,by the same layer,they should shield the plasma from the rest of the wall generated impurities. By the same action,also the exhaust problem should be greatly facilitated. Experimental evidence on divertor physics was gained already early from the model-C-stellarator, then mainly came from DITE and DIVA and will come soon from ASDEX and PDX. But none of their systems is particularly attractive from a reactor point of view. A poloidal divertor whose coils are interlinked with the toroidal field coils is not compatible with the requirements for easy assembly and remote maintenance and repair. Breaking up the coils into modules would probably lead to excessive forces and large stray fields. Poloidal divertors with coils outside the toroidal field coils avoid these problems but lead to rather weak configurations, sensitive to stray fields, wide divertor throats and not so favourable back-flow conditions and are not attractive from this point of view.

In this respect, bundle divertors look better, but they have to divert a large fraction of the toroidal flux over a short distance, and this requires the divertor coils to be close to the plasma, introduces large forces and moments and, in addition, leads to an unacceptably high ripple field for the undiverted region.

Therefore, here is an area where creativity is urgently requested. A divertor is needed, which diverts a layer of a reasonable cross-section of about 1 m^2 through the space between the main field

coils into an outside chamber, has favourite streaming and power deposition properties, is not conflicting with segmentation and modularization requirements and is not introducing too large ripple fields.

Under reactor conditions the magnetic field ripple [9] seems to have a rather deleterious effect on plasma energy confinement. Reactor designers have to aim at simplicity in order to solve their problems on "easy" assembly and credible solutions for remote maintenance and repair. Therefore, they tend to reduce the number of coils generating the main magnetic field to the largest possible extent. But this simultaneously increases the ripple of the magnetic field such that it starts to govern the energy confinement by the heat conduction of the ripple trapped ions. Fig. 5 shows the results of a calculation done for INTOR [1], i.e. for a case where the coil bore is large enough to provide the space required for blanket and shield around the plasma. The number of coils is 12, leading to a field ripple of 4 % ptp at the plasma edge and of 0.4 % ptp at the plasma centre. The extra heat losses by ripple trapped ions then exceed the neoclassical ion heat losses by about two orders of magnitude or, what is more important, the empirical electron heat diffusivity by about one order of magnitude. Therefore, care has to be taken and perhaps even correction coils have to be applied to keep the ripple at a tolerable level which seems to be somewhat less than 1 % at the plasma edge and about 0.1 % at the plasma centre. But also deeper

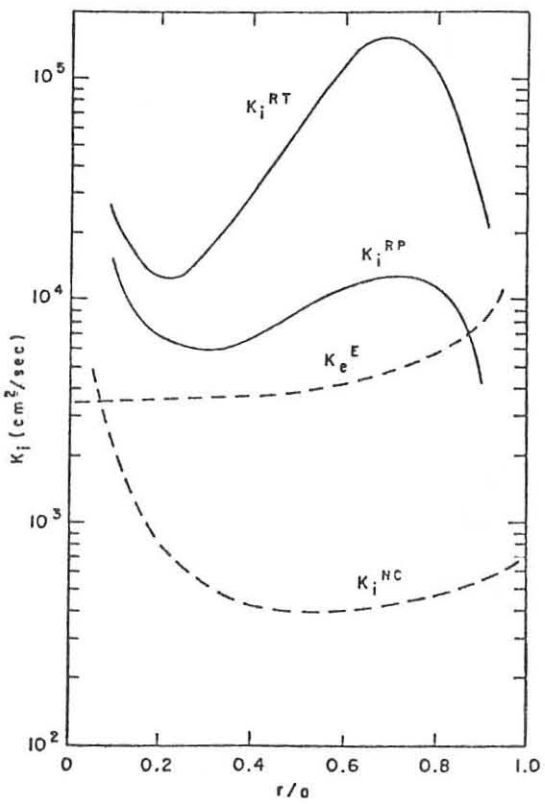

Fig. 5: Field ripple contributions K_i^{RT} and K_i^{RP} to ion thermal diffusivity in the 12-coil 6 m bore ignited INTOR plasma, compared with the neoclassical K_i^{NC} and empirical electron thermal diffusivity K_e^E.

theoretical treatment of this effect is required. Because it might well be that proper inclusion of all effects, particularly those arising from the electric field, might lead to a drastic change and might make the situation much easier.

On the other hand, if the ripple effect would be that influential and if a fast change of the ripple by external means would be feasible, it would provide an interesting tool for burn control by affecting the plasma energy loss rate. Other proposals are by some major radius compression and decompression [10] which requires some extra space for the plasma to move but offers the possibility of getting some percent of the

fusion power by direct conversion as electric power. The easiest and even automatic burn control would be by the ß-limit itself if approaching this limit would not lead to a sudden loss of plasma confinement but rather to a steep but reversible increase of the loss rate by the excitation of turbulence. There is a hope for this process to be feasible but certainly, since experimental evidence is missing, one should not rely on it alone but should prepare at least one of the above mentioned alternatives for back-up.

After having dealt with the burning phase one has now to discuss how to establish these plasmas.

There is general consensus that one should start with ohmic heating and, again in connection with INTOR, the scenario of Fig. 6 was discussed [11]. There an ionization and current initiation phase is followed by current and temperature built-up. From present day experiments it follows that a loop voltage of about 300 V might be required to overcome the radiation barrier. But for reactor conditions, this loop voltage is difficult to establish and might rather be limited to about 50 V or so by the superconducting ohmic heating transformer technology. In this respect, there would be no problem with stellarators because they provide confinement already with zero OH current and can be started with low loop voltages, indeed. But for tokamaks, other means are needed and RF heating is proposed to supply the missing power which is estimated to about 30 MW for 10 - 100 ms.

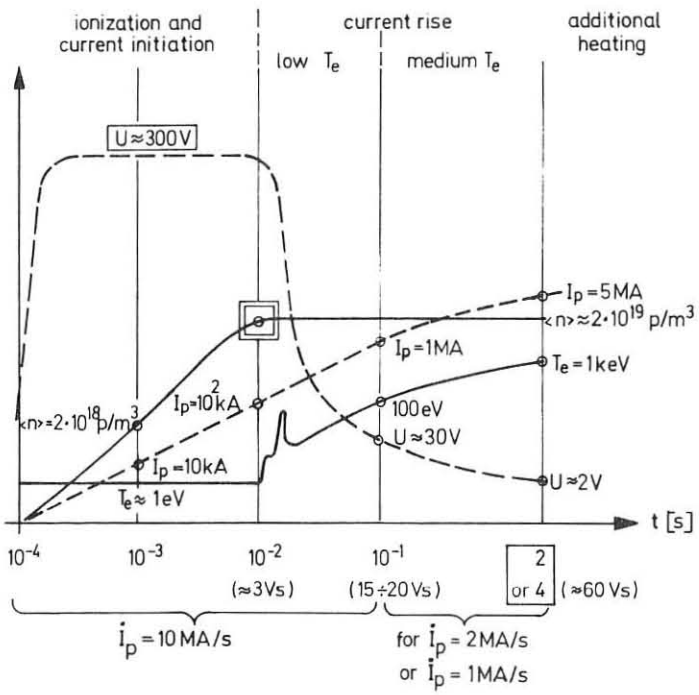

Fig. 6: Plasma start-up.

A suitably adjustable RF-heating, if made available during the full start-up phase of about 5 seconds, should offer the additional chance of tailoring the plasma temperature profile and the current profile in turn. When discussing the achievable ß during the burn phase, the tacid assumption was made that the plasma current profile can be adjusted to the optimum, indeed. There is doubt, however, whether this is feasible because external power sources aiming at influencing the plasma temperature distribution have to compete with the deposition profile of the intense α-power which might lead to a conflict. The temperature profile might then be better adjusted by proper arrangement of the local heat conduction properties. But this is also a difficult and delicate task.

For INTOR it is therefore proposed to circumvent all these difficulties by limiting the burn time to 100-200 seconds which is short compared to the skin time, and to adjust the required temperature profile already during the heating phase before the α-power occurs and then to rely on flux conservation. The gradual extension of the burn pulse can then be tackled later when sufficient experience is accumulated.

With this initial ohmic and RF heating the plasma current should be built up to the required values but the plasma temperature will only grow to about 1 keV and the density has to be kept below the Murakami limit [12]

$$n_{crit} < 1.5 \cdot 10^{20} \frac{B}{q \cdot R \cdot Z_{eff}}$$

in order to avoid disruptions.

Further heating is then required to reach the ignition temperature and, simultaneously, to increase the density. Usually, neutral injection is foreseen for this purpose. But if it is provided via positive ions, the injection energy is limited to 160 keV or so for deuterium. This might be alright with the lower, initial density, but once it gets higher the power deposition is shifted more and more towards the plasma edge and higher injection energies should be needed to avoid part of the power to be wasted or to bombard the wall to an unnecessary extent. But higher energies require the transition to negative ion acceleration for which no significant development programme is running at present.

If the heating is done via neutral injection, care has also to be taken to arrive at a proper fuel mix between deuterium and tritium. If only pure deuterium is injected in order to avoid unnecessary tritium problems with the injector, one has probably to start from a pure tritium plasma for achieving a 50/50 mix at ignition. Refuelling will then be done by the injection of pellets of proper composition. This is only a condition to the mass separation and fuel production system. Also the acceleration of pellets to velocities of a few km/s seem to provide no extraordinary problems since they seem to show a rather high mechanical stability.

Another and, as it seems, more appropriate heating would be by RF. It should not only give an easier approach to the desired power deposition profile at higher densities, but should also have the potential of reducing some of the other draw-backs of neutral injection. There the beam lines represent rather large penetrations reaching from the plasma through the blanket straight to the outside beam sources, and a large flux of neutrons is leaving the machine along these paths. These neutrons lead to activation of the outside equipment, make its handling difficult, and require large and

massive shields around it. An RF transmitter, on the other hand, can be put far away from the reactor into the accessible region and the cable or wave guide be carried more easily through the blanket in such a fashion that excessive shielding could be avoided.

Certainly, RF heating technology is not developed to the same extent as neutral injection. But if minority heating at the ion cyclotron frequency would be employed, one could work under conditions which at least in part are resembling the positive aspects of neutral injection because also here some ions will be accelerated to rather high energies and then transmit their energy to the bulk of the plasma by Coulomb collisions; but with RF, the acceleration takes place already inside the plasma by electric fields excited from the outside so that the penetration of high energy neutral particles is replaced by the penetration of waves which should offer a much higher flexibility.

The shut-down phase should not present additional problems except it occurred in an uncontrolled manner as a disruption. It seems to be unacceptable for a device of reactor dimensions to be exposed to disruptions. The mechanical strength to safely withstand them repeatedly would probably require unacceptably large amounts of structural material. On the other hand, for a tokamak there is no recipe at present for reliably preventing them without drastically reducing the performance of the device. This is another item requiring intensive research.

To convert the energy of the fusion neutrons into useful heat and to breed tritium are the primary tasks of the blanket. For this purpose, it has to completely surround the plasma and needs a thickness of about 2 m if the shield is included. Both together also have to reduce the neutron flux by about six orders of magnitude before it reaches the magnet because higher fluxes would lead to a degradation of the insulating material, to an increase of the resistance of the stabilizing material, to a degradation of advanced superconductors, and to excessive heat deposition.

Tritium breeding will be done from lithium via the two reactions

$$^{6}\mathrm{Li} + n \rightarrow {}^{4}\mathrm{He} + T + 4.8\ \mathrm{MeV}$$
$$^{7}\mathrm{Li} + n \rightarrow {}^{4}\mathrm{He} + T + n - 2.47\ \mathrm{MeV}$$

Natural lithium contains ^{6}Li and ^{7}Li in a ratio of 7.3/92.7. A large variety of possibilities, like pure lithium metal, its alloys or compounds in form of liquids, ceramic powders or molten salts are in discussion for their use as breeders, and an intense R and D programme on their properties under reactor conditions is required before a final choice can be made. Last year there occurred some doubt on the world-wide used cross-section for the ^{7}Li-reaction and that it might be smaller by 20 % or so [13]. If this were true, it would certainly affect the breeding ratio, and to keep it larger than one would require not to dilute the blanket zone with excessive structural material or penetrations. In the extreme case, it even might exclude the use of natural liquid lithium metal as breeding material and require the transition to enriched ^{6}Li and the use of neutron multipliers, like Be or Pb. The production of ^{6}Li then needed should be possible at rather low cost of about 10^{3} $ per kg [14]. The simultaneous use of liquid lithium as coolant would then be excluded, but this has a low probability anyway because of the MHD losses if it is pumped through the magnetic field. The preferred coolant candidate is helium where experience exists from the high temperature fission

reactor. But also water is considered. Its use might be burdened, however, by the corrosion products coming from the cooling ducts and their activation.

For fuel recycling, the basic technologies seem to be at hand but they have to be optimized for fast throughput, effective cleaning and isotope separation and low inventory in turn. Recovery of the bred tritium from the blanket requires preparatory work which largely depends on the breeding material chosen. Particular problems occur with the permeability of tritium through most of the interesting materials at their envisaged working temperatures.

Also internationally accepted safety standards for fusion have to be developed including new rules for tritium transport. With tritium inventories of the order of kg it seems to be unacceptable to live with the present containers which allow a transport of only 20 g tritium and with an accountability of 0.01 g tritium in view of a breed and burn of 0.1 to 1 kg per day. These are tasks which should urgently be tackled by the responsible organizations.

Another burden for the designer of the first wall, blanket and shield is to provide their required electrical properties. Conditions of easy assembly have led to the request to have all the poloidal coils outside the main field coils and to not have them embedded in the blanket region. From the plasma point of view this seems just possible but requires that the first wall region of the blanket should have a time constant of at least one ms to avoid fast plasma motions, whereas the time constant of the full blanket should not exceed about 30 ms to allow the poloidal fields to penetrate fast enough. Also the loop resistance should be high enough to avoid interference with ohmic heating. In view of the massive and partly metallic blocks the blanket is composed of, it might become difficult to satisfy all the requirements without allowing for at least some deviations from axisymmetry.

The final topic is on materials. Their technology is probably the most problematic one. Some comments have been made already on the first wall, blanket and breeding, and magnet materials. What remains are the structural materials. There a material is needed which in the fusion environment under rather elevated temperatures shows high strain-stress properties, low fatigue under cycling loads, sufficient ductility, low radiation damage, low activation coupled with its fast decay and vanishing tritium permeation. In addition, it should be easy to manufacture, to machine, and to weld, and should be easily available. But even if there were enough money and manpower behind, it would take more than a decade to develop a new material with all the related technologies of manufacturing and handling it industrially in big quantities and to measure all its properties. Therefore, for the DEMO generation, there seems to be very little chance other than selecting from materials already developed for fission purposes and to measure for the most interesting candidates their properties for the fusion neutron spectrum and the envisaged temperatures under pulsed load conditions. Already this is an enormous task, and fission results are only of limited use since fusion neutrons generally lead to a higher number of (n,α) reactions per dpa , and also the pulsed conditions have little counterpart in fission.

But for the DEMO it might be allowed to choose the projected lifetime shorter and the operating temperatures somewhat lower than necessary for a commercial fusion reactor. Under these conditions, some of the stainless steels are expected to have sufficient properties for DEMO application if this can be substantiated by further

mesurements. Even their high activation levels could be reduced if the typical Ni-constituent could be replaced by Mn. Also such materials exist, but if manufactured under industrial conditions, they still contain enough Ni as impurity so that their activation properties are only gradually reduced. This is an example of the general experience that activation properties are strongly determined by impurities in the metals which are difficult to avoid on an industrial scale.

On the other hand, materials with low activation and fast decay properties might be an essential element in DEMO design. Because even if full remote maintenance and repair is foreseen, also this equipment might fail. There is also a limit to redundancy by additional complications and cost implied. Therefore, it might be essential to maintain some access by man which is still the most reliable way if unexpected difficulties occur, but this requires a fast enough decay of the activation. Aluminium and some of its alloys seem to have such properties but they can be used only at rather low temperatures. Nevertheless, they should be applied whenever the local temperature allows it.

Since some time there is also a growing interest in ferritic steels. Their manufacturing and handling experience is ample, although irradiation data are available only for low helium content, they seem to promise a lifetime against radiation damage about 2 to 3 times longer than for stainless steels. Their use was somewhat neglected up to now for their ferromagnetic properties, but for operating magnetic fields of 5 T or so their magnetization should be highly saturated. Nevertheless, the rather complicated distribution of the structural material and the need for penetrations raises the question whether the influence of these magnetized regions on the magnetic field structure can be tolerated. This is a very important question, because if ferritic steels would have the needed properties indeed and if their presence could be tolerated from a plasma confinement point of view, the problems with the structural material for a fusion reactor would become much easier than they seem to be at present.

In reviewing the fusion reactor problems a number of points were identified where experimentally proven solutions to them are not yet at hand. On the plasma side the most essential ones were impurities, start-up, profile shaping and disruptions, and on the technology side materials under high energy neutron irradiation and cycling load conditions and the complicated geometry, particularly with divertors, leading to conflicts with easy solutions for remote maintenance and repair. But if the fusion programme will be broadened to include all the problem areas with sufficient emphasis, it is fair to say that,with some confidence in progress, ignition devices are in practical reach today; and as the situation stands the first ones will be of the tokamak type. But one has to recognize that some of the essential problems are connected with the tokamak principle as such and one has to keep its mind open for modified or alternative systems which could avoid these tokamak specific problems. Certainly, these systems then might show other difficulties, but what finally counts is the average over all positive and negative aspects. May be that the optimum is already found and that it is the tokamak in its present form indeed but it might be more likely that there are still considerable improvements necessary and possible.

REFERENCES

[1] INTOR-Report to be published by IAEA Vienna

[2] G.Grieger, D.Palumbo; Development of Pure Fusion. Proc.2nd UNESCO Int. Forum of Fundamental World Energy Problems, 2nd Edition, IAEA Vienna (1979)

[3] Cordey J.G., Hass F.A., 6th Int.Conf.on Plasma Physics and Controlled Fusion Reserach II, 423 IAEA Vienna(1977)

Cordey J.G.; Hot Ion Toroidal Reactors and Exotic Fuel Cycles. Proc. of Course held in Varenna, Italy, Sept. 1977

[4] K.V. Roberts; The theory of a Fusion Reactor. Paper A1.1 of this conference

[5] M.Murakami, H.P.Eubank; Recent Progress in Tokamak Experiments. Physics Today, May 1979, p.25-32

[6] H.Vernickel, J.Bohdansky; A General Formula for Impurity Radiation Loss of Fusion Plasmas in Corona Equilibrium. Nucl.Fusion (Letters) 18, 10 (1978)

[7] P.Staib, G.Staudenmaier; Surface Effects and Impurity Production in Tokamak Machines. J.Nucl.Materials, 76 & 77 (1978), 78-91

[8] J.Bohdansky, J.Roth, H.Vernickel; Low Energy Light Ion Sputtering and Consequences for First Wall Material Selection. 10th Symposium on Fusion Technology, Padua (1978)

[9] Uckan N.A., Tsang K.T., Callen J.D., Oak Ridge National Laboratory; Report ORNL/TM-5438 (1976)

[10] K.Borrass, K.Lackner, E.Minardi; Direct Energy Conversion and Control of Unstable Burn by Cyclic Major Radius Compression and Decompression. Paper DP16 of this conference.

[11] F.Engelmann; private communication

[12] M.Murakami, J.D.Callen, L.A.Berry; Murakami Limit. Nucl.Fusion 16, 2 (1976) Letters, p.347

[13] H.Bachmann, U.Fritscher, F.W.Kappler, D.Rusch, H.Werle, H.W.Wiese; Neutron Spectra and Tritium Production Measurements in a Lithium Sphere to Check Fusion Reactor Blanket Calculations. Nucl.Science and Engineering 67, 74-84 (1978)

[14] T.Ben Rhinehammer and Layton J.Wittenberg; An Evaluation of Fuel Resources and Requirements for the Magnetic Fusion Energy Program. Mound Facility, Monsanto Research Corp. Report MLM-2419 UC-20d and 20e, Ohio (USA)(1978).

HF HEATING OF PLASMA AT $\omega \simeq 2\omega_{LH}$ IN TOKAMAK TM-1-MH

Ďatlov J., Jakubka K., Kopecký V., Körbel Š.,
Magula P., Musil J., Stöckel J., Žáček F.

Institute of Plasma Physics, Czechoslovak Academy of Sciences,
Pod vodárenskou věží 4, 180 69 Prague 8, Czechoslovakia

Preliminary experiments on plasma heating above lower hybrid resonance at frequency $f \simeq 2f_{LH}$ have been carried out in tokamak device TM-1-MH. For toroidal magnetic field 1.3T, the frequency 1.25 GHz and HF power 40 kW the increase of ion temperature of plasma up to $\Delta T_i/T_i^{OH} \simeq 1$ was measured. The ion heating increases with the plasma density and a threshold character on incident HF power is observed. This HF heating is accompanied by changes in loop voltage and electron plasma density.

Recently a considerably progress in the LHR heating of tokamak plasma was achieved [1-4]. In the following results of the heating experiments at $f \simeq 2f_{LH}$ in TM-1-MH device are given.

The parameters of the TM-1-MH device are as follows: R = 0.4 m, limiter a=0.075 m, maximum toroidal magnetic field B_t = 1.5 T, plasma current I_p up to 30 kA, loop voltage U_{loop} = 2-4V. Schematic arrangement of diagnostics and a position of the HF coupling element is shown in Fig. 1. A quasistationary state of the plasma discharge is reached after about 2 ms, while the total discharge length is 8 ms, see Fig. 2a. Working gas is hydrogen at initial filling pressure usually 2×10^{-2}Pa. To control the electron density, the additional pulse hydrogen gas injection by means of the piezo-electric valve is used. The effect of this additional gas injection on plasma parameters is demonstrated in Figs. 2a,b, where time dependences without the injection are given as well (dashed lines). It may be seen that while the plasma current does not change at all and the loop voltage is only slight increasing, the electron density can be increased remarkably. The magnitude of the electron density strongly influences the ion temperature (measured by 5-channel charge-exchange analyzer [6]) of the ohmically heated plasma T_i^{OH}, see Fig. 3. Maximum value of the density on the axis $N_e(0)$, given in Fig. 3, was evaluated under assumption of the parabolic density distribution, from the line averaged density measured by the 4 mm interferometer.

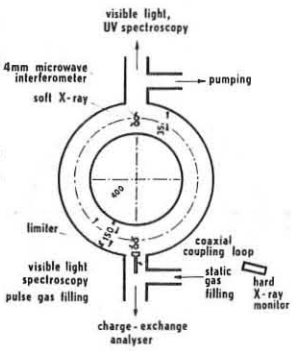

FIG. 1

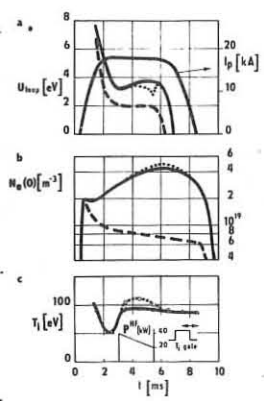

FIG. 2

Heating experiments at $f \simeq 2f_{LH}$ were performed under following conditions: toroidal magnetic field B_t = 1.3 T, plasma current I_p = 17 kA, line-averaged electron density $N_e=(0.5\text{-}2.5)\times10^{19}m^{-3}$, ion temperature of the ohmically heated plasma on the axis $T_e(0)$ = =50-150 eV and electron temperature on the axis $T_e(0)$ = 300-400 eV (estimated from conductivity measurements, UV radiation of impurities and recently from soft X-rays as well).

As a HF oscillator the CW magnetron (f=1.25GHz, P=45kW) was used. It was operated in the pulse regime: maximum output power 50 kW, pulse length 3 ms, output power drops during this pulse to about 50% of maximum value. HF power is fed to the device through the ferrite isolator, calibrated directional couplers and impedance matcher. As a launching element a coaxial coupling loop is used. The HF power is switched on in the third ms after the beginning of the plasma pulse, that is in the moment, when the plasma current and loop voltage achieve the stationary value, see Fig. 2. All changes caused by the HF power are shown in Fig. 2 by dotted lines. For HF power of 40 kW (at the beginning of pulse) the ion temperature measured by charge-exchange increases by 25% (see Fig. 2a). The bulk of ions is not heated, but most probably a few tens percent of the total ion number only. Fig. 2a shows the effect of the HF power on the loop voltage. This voltage decreases by factor 10-20%. It corresponds to the electron temperature increase by 7-15%. The beginning of the loop voltage decrease is retarded by about 0.5-1.0 ms with regard to the beginning of the HF pulse. After HF pulse the voltage returns to the starting value quickly. The presence of HF power results in the moderate increase of the electron density by about 10% (see Fig. 2b).

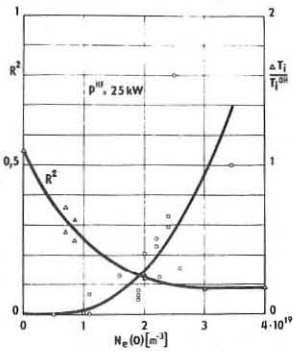

FIG. 4

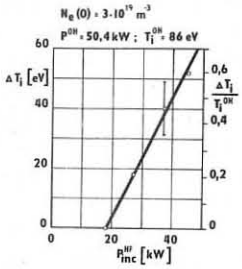

FIG. 5

The relative increase of the ion temperature $\Delta T_i/T_i^{OH}$ is shown in Fig. 4 in dependence on the plasma density for HF power 25 kW. For densities $N_e(0)$ smaller than $1\times10^{19}m^{-3}$ practically no heating is observed. Considerable heating takes place at $N_e(0) = 2\times10^{19}m^{-3}$ when nearly 90% of incident power is delivered to the device (see measured power reflection coefficient R^2).

Very important is also dependence of ion temperature increase on the HF power, see Fig.5. This dependence has a threshold character. Measurable HF heating is observed for powers greater than 20 kW only. The data given in Fig. 5 were obtained from spectra of charge-exchange neutrals displayed in Fig. 6. The spectra were measured in the 1 ms time gate (4-5th ms). The threshold character of HF heating is now under study.

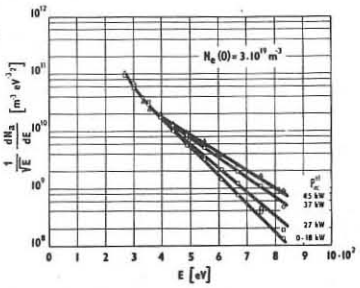

FIG. 6

It is not clear to us, if the ion heating in our experiments with additional gas injection is caused by the plasma density increase or by more efficient coupling due to change in plasma density profile. Our next experiments will be devoted to the detailed study of the influence of form and position of the coupling loops on the heating efficiency.

Authors are gratefull to Dr. Klíma for stimulating discussions .

[1] Briand P. et al.: 7th Conf. on Plasma Physics and Contr. Nucl. Fusion Research, Innsbruck 1978, Vol.I, A-4-1
[2] Fujii T. et al.: 7th Conf. on Plasma Physics and Contr. Nucl. Fusion Research, Innsbruck 1978, Vol.I, A-4-2
[3] Pacher H.D. et al.: 7th Conf. on Plasma Physics and Contr. Nucl. Fusion Research, Innsbruck 1978, Vol.I, A-4-3
[4] Ohkubo K., Matsuura K. and JIPP T-II Group: Res. Rept. IPPJ-366, Nagoya Univ., February 1979
[5] Gladkovskij .P. et al: Fizika plazmy 5 (1979), 512
[6] Afrosimov V.V. et al.: Zh. Tech. Fyz. 45 (1975), 56

AP.5

INTERACTION OF TRAPPED PARTICLES IN A TOKAMAK WITH AMPLITUDE MODULATED RF FIELDS.

E. Lazzaro and S. Nowak

Laboratorio di Fisica del Plasma C. N. R. EURATOM Association

Milan- Italy.

Abstract- Numerical evidence is presented of the onset of stochastic instability of trapped electrons under the action of a coherent low frequency wave.

In high temperature collisionless tokamak regimes, charged particles trapped in the wells of the confining magnetic field may interact with modes in the frequency range ω_0 below or around the bounce frequency $\omega_B = \frac{v_{th}}{qR}\sqrt{\frac{a}{R}}$, where a, R, q are the tori radii and safety factor, and v_{th} the particle thermal speed. The unperturbed particle dynamics is that of a nonlinear oscillator(pendulum). Under the action of a suitable spectrum of waves, with $\omega_0 < \omega_B$, with a component of the electric field along the magnetic confining field, the motion may become stochastically unstable. A reduction of the fraction of trapped particles resulting from this interaction could be important in controlling transport phenomena. As a model problem we consider the effect of waves in the frequency range well below the ion cyclotron frequency, on the dynamics of trapped electrons. The shear Alfvén wave, excited as an evanescent mode at the boundary of a magnetized warm plasma, mode converts[1] to a kinetic quasi-acoustic mode at a point in the plasma where $\omega = k_{\parallel} c_A$ c_A being the local Alfvén speed :the wave has $\frac{\omega_0}{\omega_B} \sim 5.2 \times 10^3 B\,[2R/nT_e a]^{1/2} \lesssim 1$ and a perpendicular wavelength of the order of ion gyroradius, larger than an electron banana width, and a finite component of electric field parallel to the magnetic toroidal field. Alternatively the excitation of Alfvén waves may result[2], in thermonuclear regimes, from α particle saturated instabilities . The onset of stochasticity for a test electron is studied numerically on the basis of the model similar to that proposed in ref. (3), suitable to describe a saturated instability spectrum, using the set of equations of motion

$$\ddot{z} + \frac{\omega_B^2}{K_0}\sin K_0 z = -\frac{eE_{\parallel}}{m}\sum_{-N}^{N} C_n \cos(K_0 z - n\omega_0 t)$$

$$B_1 \ll B_0\,, \quad K_0 \sim \frac{2\pi}{qR}\,, \quad Q = K_0 z \qquad P = \frac{kV_{\parallel}}{\omega_B} \tag{1}$$

associated to the set of variation equations

$$\delta\dot{Q} = \delta P$$

$$\delta\dot{P} = -\left[\cos Q - \varepsilon \sum_{-N}^{N} \sin\left(Q - n\frac{\omega_0}{\omega_B}\tau\right)\right]\delta Q \tag{2}$$

and evaluating the maximal Liapounov characteristic number , defined by[4] $\lambda_{LIM} = \lim_{t\to\infty}\frac{1}{t}\ln\left[\delta Q^2 + \delta P^2\right]^{1/2}$

This is a measure of the local orbital instability, and is related to the rate of mixing in phase space. Plotting λ versus t for various strengths of the perturbation , a monotonic decreasing behaviour indicates an ordered motion with $\lambda_{LIM} = 0$, while a positive fairly well stabilized value of λ indicates an exponential instability of the phase space trajectories. In the figures the two cases are shown associated to a picture of the particle phase space. The adimensional variables used are $\varepsilon = \frac{eE_{\parallel}K_0}{m\omega_B^2} \ll 1$, $\tau = \omega_B t$

The data considered are those of a plasma with $B_0 = 20KG$ $T_e = 1.2^{Kev}$ $a/R = 1/3$ $\omega_B \sim 3\,Mhz$ $\omega_0 \sim 1.5\,Mhz$

As discussed elsewhere[5], detrapping may occur, consequent to a systematic increase of particles energy, at an approximate rate $\frac{1}{N}\frac{dN}{dt} \simeq \varepsilon\frac{\omega_B^2}{k\bar{v}_{th}}\frac{\omega_0^2}{k\bar{v}_{th}}$

The mechanism of the stochastic behaviour described can be traced back to the overlap of nonlinear resonances in phase space. Casting the Hamiltonian of the motion in action angle variables, (expressed in terms of Jacobi functions and elliptic integrals), it is straightforward to obtain the resonance width and overlap criterion.

$$H_0 + \varepsilon H_1 = \int \Omega(J)\,dJ + \varepsilon\sum_{-N}^{N} C_n \sin\left(Q - n\frac{\omega_0}{\omega_B}\tau\right) \tag{3}$$

$$Q = 2\arcsin\left[\sigma\,sn\left(\frac{\varphi}{\Omega}\right)\right]\,, \quad \sigma^2 = \frac{1}{2}\left[1 + H_0\right] \quad \Omega = \frac{\pi}{2K(\sigma)}$$

$$\theta = \frac{N}{S}\omega_0 t - \varphi$$

$$\Omega_R = \frac{N}{S}\omega_0 + O(\varepsilon)$$

$$\frac{d}{dt}(\Omega - \Omega_R) = \varepsilon C_N \Omega^2 \frac{d\Omega}{d\sigma}\frac{\partial^2}{\partial\theta^2}\,cn\left(\frac{\theta}{\Omega}\right) \tag{4}$$

$$\frac{d\theta}{dt} = \Omega - \Omega_R$$

$$(\Delta\Omega)^2 = \varepsilon C_N \Omega \frac{d\Omega}{d\sigma}\sqrt{1-\sigma^2} \qquad \delta\Omega = \omega_0/S \tag{5}$$

Finally the condition for overlap of subharmonic resonances requires $\left(\frac{2\Delta\Omega}{\delta\Omega}\right)^2 = 2\varepsilon C_N \frac{N^2}{\Omega_R}\left.\frac{d\Omega}{d\sigma}\right|_R > 1$ and a rich spectrum of waves.

References

1-A. Hasegawa, L. Chen, The Phys. of Fluids 19 1924 1976

2-D. J. Sigmar Nucl. Fus. 18 1569 1978

3-T. H. Stix Princeton university Report PPPl-1539 April 1979

4-M. Casartelli, E. Diana, L. Galgani, A. Scotti, Phys. Rev. A 13 1921 1976

5-G. Casati, E. Lazzaro, S. Nowak, Report FP 79/12 Laboratorio di Fisica del Plasma CNR Milan- Italy.

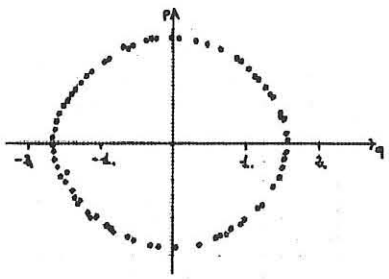

STABLE CASE $\varepsilon = .05$

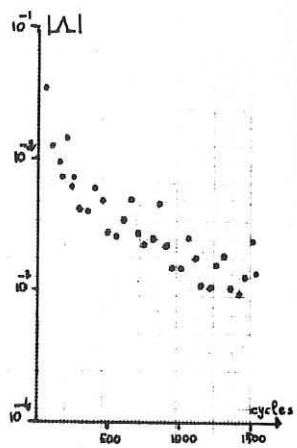

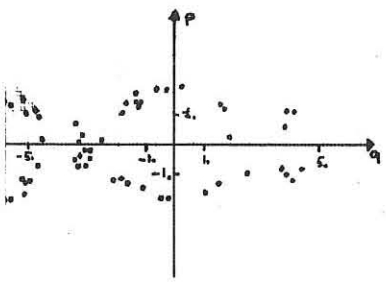

UNSTABLE CASE $\varepsilon = .1$

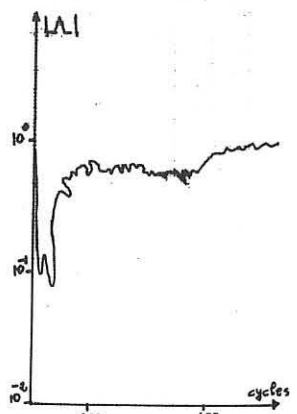

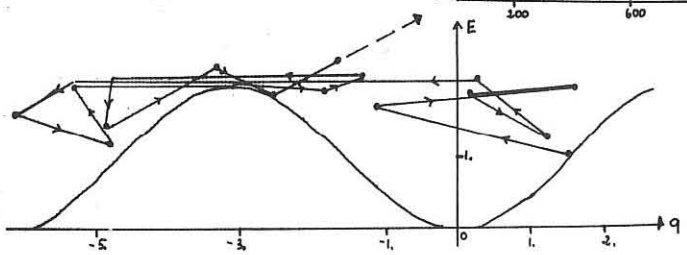

EFFECT OF A MAGNETIC HILL ON PLASMA EQUILIBRIUM IN A STELLARATOR

M.I.Mikhailov, V.D.Shafranov
I.V.Kurchatov Institute of Atomic Energy, Moscow, USSR

It is considered that there is no plasma pressure limit in the stellarators of a large aspect ratio and of a great number of period of helical magnetic field.Meanwhile as early as 1966 Green et al/1/shown that there is a critical plasma pressure β_{cr} in such systems and for $\beta > \beta_{cr}$ the equilibrium of a plasma column became unstable against the shift.This instability was related with the absence of the magnetic well in such systems.

If the potential of the vacuum magnetic field is

$$\mathcal{V} = \varepsilon_2 \frac{R}{m} B_0 I_2\left(\frac{2mr}{R}\right) \sin 2(\omega - m\zeta)$$

then the critical β_{cr} is defined by $\beta_{cr} \approx \frac{1}{2}\varepsilon_2^2$ approximately.Magnetic hill effects also the displacement of the plasma equilibrium configuration due to the curvature of the torus.It is seen (Fig.1) that in $V''_{vac}(\Phi) > 0$ case (no well) the equilibrium β defined from the condition $\Delta(a) = a/2$ (Δ is the plasma column shift) is less than it is in $V''_{vac}(\Phi) = 0$ case.

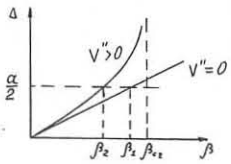

Fig.1.

Some data for working systems are presented in Table I.

Table I.

Installation	$\frac{a}{R}$	m	$t_a(0)$	$t_a(a)$	β_1 %	β_2 %	β_{cr} %
W VII A	0.067	2.5	0.22	0.23	0.36	0.36	7.0
Liven-2	0.115	7	0.22	0.7	5.0	1.4	3.0
Wega	0.18	2.5	0.21	0.3	1.4	1.2	7.7

These results were obtained for a single helical l-harmonic. To consider an influence of the magnetic well one should take a mixture of a different pitches harmonics of a helical magnetic field. To treat this case we shall use the method of variable conversion. We shall use the flux coordinate system with the "strightened" magnetic field lines.

Let r, ω, ζ be a quasicilindrical coordinates the metrics of which is

$$d\ell^2 = dr^2 + r^2 d\omega^2 + (R - r\cos\omega)^2 d\zeta^2$$

and let

$$r = \rho + \delta(\rho, \theta, \zeta)$$
$$\omega = \theta + \lambda(\rho, \theta, \zeta)$$

where ρ, θ, ζ - the flux stright magnetic field lines coordinates and δ, λ - small corrections. We can express the metric tensor g_{ik} as functions of δ and λ and define δ and λ from the equilibrium equation and from the relation between co- and contravariant components of the magnetic field $\vec{B}$:

$$t\frac{\partial \nu}{\partial \theta} + \frac{\partial \nu}{\partial \zeta} = \frac{4\pi^2 \rho'}{\Phi'}\left[\langle\sqrt{g}\rangle_{\theta,\zeta} - \sqrt{g}\right]$$
$$-\nu + \frac{\partial \mathcal{V}}{\partial \rho} = \frac{g_{12}}{\sqrt{g}}\chi' + \frac{g_{13}}{\sqrt{g}}\Phi'$$
$$J + \frac{\partial \mathcal{V}}{\partial \theta} = \frac{g_{22}}{\sqrt{g}}\chi' + \frac{g_{23}}{\sqrt{g}}\Phi'$$
$$-I + \frac{\partial \mathcal{V}}{\partial \zeta} = \frac{g_{23}}{\sqrt{g}}\chi' + \frac{g_{33}}{\sqrt{g}}\Phi'$$

Here χ, Φ - are poloidal and toroidal magnetic fluxes, J, I - are currents, ν and $\mathcal{V}$ are periodic functions of the coordinates θ and ζ characterizing the charge separation current and the potential of the magnetic field respectively.

We shall use the so-called stellarator ordering

$$\frac{r}{R} \sim O(\varepsilon^2), \quad \frac{mr}{R} \sim O(1), \quad \beta = \frac{2\langle p\rangle}{B_0^2} \sim O(\varepsilon^3)$$

For the case of vacuum configuration taking into account condition m >> 1 it is easy to define δ and λ and such characteristics of the configuration as t_a and $V''_{vac}(\Phi)$. For l=2 stellarator, for example,

$$\delta = \varepsilon_2 \frac{R}{m} I_2' \cos 2(\theta - m\zeta), \quad \lambda = -\varepsilon_2 \frac{R^2}{m^2\rho^2} I_2 \sin 2(\theta - m\zeta),$$
$$t_a = \frac{\chi'}{\Phi'} = -\frac{\langle \frac{g_{23}}{\sqrt{g}}\rangle R}{\rho} = 2m\varepsilon_2^2\left[\frac{R^2}{m^2\rho^2}\left(I_2'\right)^2 - \frac{R^3}{m^3\rho^3} I_2 I_2' + \frac{R^2}{m^2\rho^2}\left(1 + \frac{R^2}{m^2\rho^2}\right) I_2^2\right],$$

$$V''_{vac}(\Phi) = \frac{1}{\rho R B_0^2}\left(\langle\sqrt{g}\rangle\left\langle\frac{g_{33}}{\sqrt{g}}\right\rangle\right)'_\rho = \frac{R\varepsilon_2^2}{B_0^2}\left[-\frac{4R^2}{m^2\rho^4} I_2^2 - \frac{4}{\rho^2}\left(I_2'\right)^2 + \left(\frac{16m}{R\rho} + \frac{16R}{m\rho^3}\right) I_2 I_2'\right]$$

Let's consider now the configuration of non-zero plasma pressure. Let ρ_0, θ_0, ζ are the flux coordinates for vacuum and ρ, θ, ζ are those for a plasma configuration. It is possible to prove that the following simple relations take place

$$\rho_0 = \rho + \Delta(\rho)\cos\theta$$
$$\theta_0 = \theta + \lambda_0(\rho)\sin\theta$$

in our ordering. By transforming the metric to new variables we can get g_{ik} as functions of Δ and λ_0 . Exoluding after that λ_0, $\mathcal{V}$, ν from eq.(1) we obtaine the following equation for $\Delta(\rho)$:

$$\left(t^2\rho^3\Delta'\right)' + t\left(t_0'\rho^3\right)'\Delta - p'\rho^2 R\, V''_{vac}(\Phi)\Delta = -\frac{2p'\rho^2 R}{B_0^2}$$

where $t = t_J + t_0$

We have omited here the term corresponding to the vacuum shift of the magnetic surfaces.

This equation is analogous to the equation derived in/1/ but now $V''_{vac}(\Phi)$ has a more general form.

In a case of a single l-harmonic an expression $V''_{vac}(\Phi)$ coincides with that obtained by Green et al /1/ and is positive.

If vacuum magnetic field is discribed by the mixture helical harmonics $\mathcal{V} = \mathcal{V}_2 + \mathcal{V}_3$ where

$$\mathcal{V}_2 = \varepsilon_2 \frac{R}{m} B_0 I_2\left(\frac{2mr}{R}\right)\sin 2(\omega - m\zeta); \quad \mathcal{V}_3 = \varepsilon_3 \frac{R}{m} B_0 I_3\left(\frac{2mr}{R}\right)\sin(3\theta - 2m\zeta)$$

then $V''_{vac}(\Phi)$ near the axis has the form

$$V''_{vac}(\Phi) = \frac{2m^2\varepsilon_2^2}{R B_0^2}\left(1 - \frac{\varepsilon_3}{t_0\varepsilon_2} - \frac{3}{2m^2\varepsilon_2^2}\right)$$

and may become negative.

In this case however additional rather complicated terms enter in the equation for Δ . Nevertheless it is clear that magnetic hill is unfavourable for equilibria. Thus the stellerator magnetic system should possess magnetic well.

The necessity of the magnetic well follows also from the Mercier criterion for the localized mode

$$\frac{1}{4}(t_0)^2 + p' V''_{vac}(\Phi)\frac{R}{\rho} > 0, \quad \beta < \frac{1}{4}\varepsilon_2^2\left(\frac{m\rho}{R}\right)^4$$

For example, for installation Liven-2 this criterion gives $\beta \approx 1\%$ /2/. If the magnetic well presents, the criterion won't give any serious limitation /3/.

CONCLUSION

To obtain large enough β in stellarator with circular magnetic axis one should provide a magnetic well. This implies the presence of the different pitches harmonics of the magnetic field and as a consequence - nonuniformity of $|B|^2$ and presence of the blocked particles which is unfavourable for confinement. To make a system close to that of helical symmetry one can use space axis system which has a well without rough distortion of the symmetry /4/.

REFERENCES

1. J.M.Green, J.L.Johnson, K.E.Weimer Plasma Physics 8, 145 (1966)
2. I.S.Danilkin Physika Plasmy 4, 1033 (1978)
3. V.D.Shafranov, E.I.Yurchenko Nucl.Fusion 8, 329 (1968)
4. V.D.Shafranov, E.I.Yurchenko Nucl.Fusion 9, 285 (1969)

DEPENDENCE OF INTERELECTRODE INSULATING SYSTEM SHAPE ON THE P.F. PARAMETERS AND EXPERIMENTAL VERIFICATION OF 2D SNOW PLOW CODE

J. Nowikowski, Z. Jankowicz, A. Jerzykiewicz, C. Pochrybniak, J. Waliszewski

Institute of Nuclear Research, Świerk, Poland

Abstract: A distinct dependence of neutron yield Y_n and the time of its emission /characterised by half width $\tau/2$ of neutron impuls/ on the shape of interelectrode insulating system has been found. After small modification /change of version A to C - Fig. 1/ an increase about 3 times of $\overline{Y}_n$ and about 1.5 times of $\overline{\tau}/2$ was obtained. The comparison of the measured current and voltage traces to these ones, calculated from the modified 2D snow plow model [1], showed their good agreement.

Investigations on the low energy device: E=11.4 kJ at V_o=33 kV [2] have been undertaken in order to recognize the influence of electrodes [3] and interelectrode insulating system on the P.F. parameters, especially on the neutron yields and its reproducibility; which according to [3] and [4] depend on the material and shape of the mentioned above elements of P.F. device. We hope that in this way the circumstances to optimize low energy devices will be settled, and the trends found here may further the yield and application also of large devices.

Investigations presented in this paper were made with three versions of interelectrode insulating system A, B and C - Fig. 1. The general character of insulators geometry, their material /Al_2O_3/ and length, as well as the length and material of electrodes /Cu/ was kept unchanged.

The average neutron yield $\overline{Y}_n$ calculated in all cases from 40 discharges as minimum at optimum pressure and V_o=33 kV increased from $4.5\cdot10^8$ to $5.9\cdot10^8$ as a result of replacement a radial shape of outer electrode ring /version A/ by a parabolic one /version B/. After modification of version B to C by reduction of insulator diamater to this of inner electrode the $\overline{Y}_n$ has reached $1.2\cdot10^9$.

In the whole range of pressures in use at a practically the same current amplitudes for the definited pressure, different neutron yields for different versions were obtained /Fig.2/.

Instead, the half width of neutron impulses - Fig. 3 - and amplitudes of voltage singularity practically similar for versions A and B, increased for version C. The half width of neutron impulses - Fig. 3 - increased about 1.5 times and the amplitudes of voltage singularity increased about twice and reached the value 70 kV at the maximum neutron yields equal to $2.6\cdot10^9$.

The scalling law versus current at the moment of pinch beginning I_p - Fig. 4 at V_o = 27 ÷ 33 kV and optimal pressures has the form $\overline{Y}_n \sim I_p^{4.5}$.

Remarkable number of asymetrical discharges registrated by a pin-hole camera amounted 56% and 49% for versions A and B, respectively, has been decreased to 27% for C version. Unfortunately, dispersion of neutron yields for all versions A, B and C remained the same and was equal about one order of magnitude.

Using a modified 2D snow plow model [1] some traces of current and voltage for some values of pressure were calculated. On their bases the following characteristics as a function of pressure were made: I_{max}; I_p; I_{pp}; τ_{max}; τ_p; $i\frac{dL}{dt}\Big|_{i=I_{max}}$; ΔI, ΔV - see Fig. 5.

The results of calculations were compared to the measured ones. On Fig. 5 the calculated and measured traces of current and voltage as well as the methode of determination characteristic points of traces are shown.

The comparison showed that the range of pressure 1.5 ÷ 2 Torr in which experimentally maximum neutron yields were obtained, is this one, for which according to calculations practically total energy of a condenser bank is transferred to the circuit at the moment of maximum radial compression. In this range the modified Imshennik's criterion $\alpha_I \geq 2\cdot10^{33}$ for the Mather's type devices [1] is also fulfiled.

In conclusion we may say that a good agreement of calculated and measured results confirmed the correctness of the model assumed to describe the P.F. discharge. Remarkable enhancement of neutron yields as a result of a relatively small change of insulating system suggests the need of investigaticns with use of appropriate diagnostics in order to understand the influence of all being changed here parameters on the neutron production and its mechanism in general.

1. Z. Jankowicz et al., Paper prepared to 9-th Europ. Conf. CFPP, Oxford, 1979.
2. J. Nowikowski, Nukleonika 20 No 12, 1081, 1974.
3. J. Nowikowski, Ph. D. Thesis.
4. A. Bernard, Invited Paper to III High-Beta Conf. Culham 1975.

Fig.1

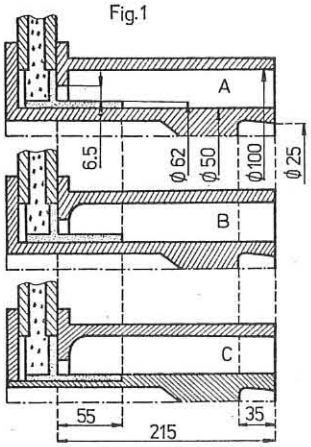

Fig.2

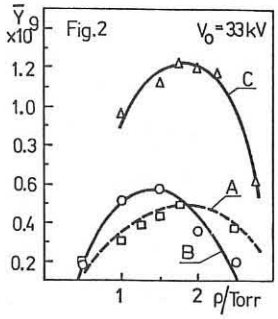

Fig.3

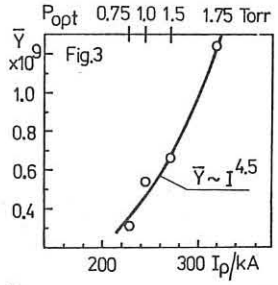

Fig.4

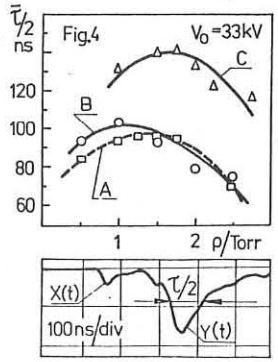

Fig.5

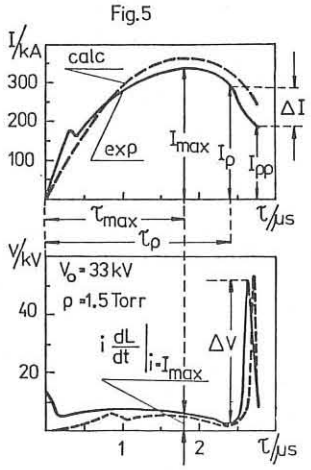

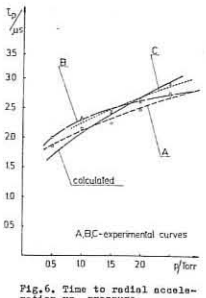

Fig.6. Time to radial acceleration vs. pressure.

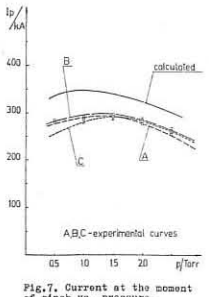

Fig.7. Current at the moment of pinch vs. pressure.

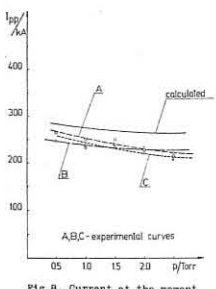

Fig.8. Current at the moment of voltage peak vs. pressure.

ON THE INTERACTION OF SOLID HYDROGEN PELLETS IN CONTACT WITH MAGNETIZED PLASMAS AND THE SELF-CONSISTENT ELECTRIC FIELD AT THE SOLID SURFACE

*S. Mercurio**

Department of Physics, University of Wisconsin, Madison WI 53705 (USA)

1. INTRODUCTION

Recent semiempirical studies by the author[1] on the interaction of solid hydrogen in contact with magnetized plasmas have indicated that the external magnetic field can be *postulated* to be an upper bound to the self-consistent electric field at the solid surface. A simple formula for the ablation rate of the solid was then derived in agreement with all experiments to date. In this paper we first outline the derivation of the above formula and then we exploit it to derive an expression for the velocity of expansion of the cloud which surrounds the evaporating pellet by invoking a mass-energy balance. The formula obtained turns out to be also in agreement with experiments if the above postulate is invoked. Besides we show that the observed deviation of the pellet from the straight path upon injection in a magnetized discharge chamber offers a simple and direct evidence for the above postulate.

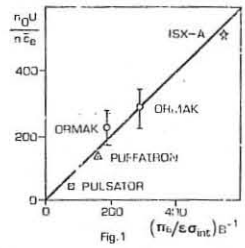

Fig.1

2. FORMULA FOR THE ABLATION RATE

The fact that the solid hydrogen can be regarded as a superdense gas (the binding energy is W_B = .005 eV/atom) implies that

a) The phase transition is just an expansion of a gas, the thermoelastic relaxation time of which is just the thermal conduction relaxation time τ_{TH} which in turn is equal to the electrical conduction relaxation time which is defined as $\tau_D \equiv D_\infty/4\pi J_D(o)$, where D and J_D are the electric displacement field and current respectively.

b) The range in which the energy is deposited is given by $\ell = (n_o\sigma_{int})^{-1}$ where n_o is the solid number density and σ_{int} the Lenard-Darrow interception cross-section.

c) The ratio ℓ/τ_D is the actual ablation front speed U, because τ_D is the exactly the time in which the solid layer of thickness ℓ undergoes the phase transition. We can actually show that U is the speed with which plasma pressure driven oscillations of period $T = \tau_D$ can propagate towards the solid carrying the ablation energy with them.

Since at t = 0 there is no sheath we can identify the initial displacement current with $J_r = en\bar{c}_e/4$, the unshielded random current, so that

$$\tau_D = D_\infty/\pi\, e\, n\, \bar{c}_e$$

where n is theplasma density, $\bar{c}_e$ the average speed of the electrons before the interaction with solid takes place and e the electron charge.

If the magnetic field is sufficiently high that $\omega_c > \omega_p$, τ_{coll}^{-1} then the Hall's electromotive force $E_H \equiv (v/c)B$ dominates over the thermoelectromotive force and we have shown elsewhere[2] that

$$\tau_D = \alpha^\star\, \tilde{t}^\star;\quad \alpha^\star \equiv \frac{\sqrt{\pi}}{4}\beta_e^{\frac{1}{2}} + \beta^\star;\quad \beta_e \equiv \frac{8\pi n k T_e}{B^2};\quad \beta^\star = v/c;\quad \tilde{t}^\star \equiv \frac{\varepsilon B}{\pi e\, n\, \bar{c}_e}$$

where ε is the dielectric constant of the solid, ω_c and ω_p the electron cyclotron and plasma frequencies, τ_{coll} the electron-neutral collision time and v is the electron drift along the surface, as shown in Fig. 2.

Since experiments show that $\alpha^\star = 1$ we have

$$\frac{n_o U}{n\,\bar{c}_e} = \frac{\pi e/\sigma_{int}}{\varepsilon B} \qquad (1)$$

and as shown in Fig. 1 the ablation rates predicted by this formula are in excellent agreement with all experiments to date.[1,2]

3. VELOCITY OF EXPANSION OF THE CLOUD

Since in the presence of a sufficiently high magnetic field the Langmuir sheath becomes a current sheet[2] the energy balance in a volume element of sheath (see (Fig. 2) can be easily studied by invoking the Poynting vector technique. By using one-dimensional model in which B is parallel to the plane solid surface we have that

$$S_p - S_S = S_{sh};\quad S \equiv \frac{E_H B}{4\pi} c$$

$$E_H = vB/c = \omega_c\tau_{coll}\, uB/c$$

where u and v are two mutually perpendicular drifts across B, c the speed of light in vacuum and where S_p and S_S are the magnitudes of the Poynting vector across the plasma edge and the solid surface respectively, while S_{sh} that along the sheath. We notice incidentally that

$$\frac{S_p}{S_S} = \frac{\tau_{coll}^{(P)}}{\tau_{coll}^{(s)}} = \frac{n_{os}}{n_{op}} \sim 10^5; \qquad \tau_{coll} \equiv (n_o\sigma_{coll}u)^{-1}$$

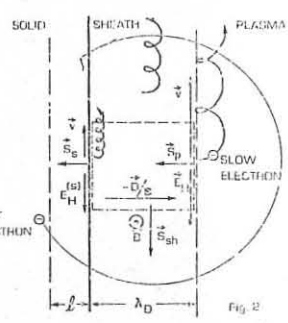

Fig. 2

This implies that $S_p \cong S_{sh}$ which tells us that most energy from the plasma is conveyed along the sheath and eventually reflected. This energy is stored in the sheath and it is available for inelastic processes which inevitably occur in the cloud.

The velocity of expansion of the cloud can be easily obtained from the following flux balance

$$\frac{E_H^{(s)}\, B}{4\pi}\,\frac{c}{\varepsilon} = \frac{1}{2} n_c M_c \overline{v^2}\,\bar{v} + n_o U W_B \qquad (2)$$

where M_c is the atomic mass of the cloud.

By invoking mass conservation, $n_o U = n_c \bar{v}$.(2) reads

$$\frac{E_H^{(s)}\, B}{4\pi}\,\frac{c}{\varepsilon} = \left(\frac{1}{2} M_c \overline{v^2} + W_B\right) n_o U \cong \frac{1}{2} M_c\, n_o U\, \overline{v^2}$$

By introducing (1) into (2) we have

$$\overline{v^2} = \left(\frac{2\pi}{\beta_e}\right) v^{\star 2}\,\alpha^\star \qquad \text{where}$$

$$v^\star \equiv \frac{B}{(4\pi M_c n_o)^{\frac{1}{2}}},\quad \alpha^\star \equiv D/\varepsilon B,\quad E_H^{(s)} = \omega_c\,\tau_{coll}^{(s)}\, D/\varepsilon$$

From Table I we see that on the average $\alpha^\star = .9$ which confirms once confirms once again that the self consistent electric field at the boundary is *close* and less than the external magnetic field.

Since experiments give $n_o U \sim 10^{23}$ cm^{-2} sec^{-1} and

$$\bar{v} = (\overline{v^2})^{\frac{1}{2}} \sim 10^6 \text{ cm/sec, then } n_c \sim 10^{17} \text{ cm}^{-3} \text{ and } \omega_c\,\tau_{coll}^{(P)} \sim 10$$

which turns out not to be in contradiction with the above assumption.

4. DEVIATION OF THE PELLET TRAJECTORY

Solid hydrogen pellets injected in both tokamak and rotating plasmas have been observed to deviate from the straight path.

Rotating plasmas have large external electric field ($E_{ext} \neq 0$) but negligible magnetic field gradient ($\vec{\nabla} B = 0$). On the contrary tokamak plasmas have $E_{ext} = 0$ but $\nabla B = B/R \neq 0$, where R is the radius of curvature of the field lines.

It has been pointed out[2] that pellets in contact with magnetized plasmas are surrounded with a sheath which besides being an electrostatic double layer is also a *current sheet*. The pellet will therefore interact with E_{ext} because of the charge $Q^\star$ on its surface and with ∇B because of its magnetic moment $m^\star$. The observed displacement Δ can therefore be obtained by simply invoking the expression for the displacement in a time t due to a constant acceleration a, namely

$$\Delta = \frac{1}{2} a\, t^2 \qquad a = \frac{1}{M}\left[Q^\star E_{ext} + \nabla(m^\star \cdot B)\right] \qquad (3)$$

where M is the mass of the pellet, as shown in Table II.

For pellets interacting with rotating plasmas[3] (3) reads

$$\Delta = \frac{1}{2}\,\frac{3\varepsilon}{4\pi}\,\frac{B\, E_{ext}}{n_o m_H}\,\frac{\tilde{t}^2}{\tilde{r}} = .456 \times 10^6\,(\tilde{t}^2/\tilde{r}) \text{ cm}$$

For those interacting with tokamak plasmas we have

$$\Delta = \frac{\varepsilon}{2}\,\frac{v^{\star 2}}{R}\, t_{max}^2\, \beta^\star$$

if use is made of $D = \varepsilon B$ and $v = \beta^\star$ where $\beta^\star \leq 1$.

We notice incidentally that $v_c^\star = B/(4\pi n_o M_c)^{\frac{1}{2}} = 1.26\, B$ cm/sec, which appears both in the expression for $(v^2)^{\frac{1}{2}}$ and Δ, is not the Alfvén speed because solid hydrogen is not at all a *good conductor*. (*Gaussian units have been used throughout*).

REFERENCES

1. Mercurio S. (1979), ICPIG, 4-11 July Grenoble, France, Suppl.J.Physique C-7
2. Mercurio S. (1979), CNEN Report 79.36, Ass. EURATOM-CNEN, Frascati, Italy
3. Jørgensen L.W. et al. (1977), Plasma Phys. 19, 1093
4. Foster C.A. et al. (1977), Nuclear Fusion 17, 5, 1067
5. Amende W. et al. (1977), Fueling Workshop, 1-3 November, Princeton (USA)
6. Milora S.L. et al. (1978), ORNL/TM-6496, Oak Ridge Nat.Lab. Oak Ridge (USA)
7. Sillesen A., private communication.

TABLE I - $\alpha^{\star\frac{1}{2}} = .9$

DEVICE	$(v^2)^{\frac{1}{2}}/v^\star$	$(2\pi/\beta_e)^{\frac{1}{2}}$	$\alpha^{\star\frac{1}{2}}$
PUFFATRON [3]	37	41.9	.88
PULSATOR [5]	100	97.4	1.03
ISX-A [6]	115	121.7	.95

TABLE II

DEVICE	$(\Delta)_{theory}$	$(\Delta)_{exp}$	
PUFFATRON [3,7] ($\tilde{t}$=50 μsec; $\tilde{r}$=5.10^{-3}cm)	.23 cm	.2 cm	
ORMAK [4] (t_{max} = 1.1 msec, R = 1 m)	1.8 cm	1.6 cm	$\beta^\star$ = .89

* *Present address: Ass. EURATOM-CNEN sulla Fusione, Centro di Frascati, Frascati, Rome, Italy.*

FIRST RESULTS FROM THE ETA-BETA II RFP EXPERIMENT

Buffa A., Costa S., De Angelis R., Di Marco J.N.*, Giudicotti L., Malesani G., Nalesso G.F., Ortolani S., Scarin P.

Centro di Studio sui Gas Ionizzati
del Consiglio Nazionale delle Ricerche e dell'Università di Padova
(Associazione Euratom-CNR)-Padova (Italy)

ABSTRACT: Diffuse pinches are studied on the new experiment ETA-BETA II. High temperature, reduced fluctuations and improved confinement are observed when a RFP plasma is formed.

ETA-BETA II[1] is a toroidal diffuse pinch experiment designed to investigate the reversed field pinch concept. Both self-reversal and aided reversal of the toroidal magnetic field internal to the stainless steel liner can be studied by controlling the external toroidal field. This experiment is one of the new generation of RFP experiments that includes: ZT-40, HBTX-1A, and TPE-1R[2]. The minor and major diameters are 25 cm and 130 cm. The stainless steel (bellows) is the vacuum wall, its thickness is 0.25 mm, and the resistance in the ϕ and θ directions are 30 mΩ and 0.24 mΩ. Toroidal current (I_ϕ) is driven by a 132 μF, 40 kV capacitor bank, and the toroidal magnetic field (B_ϕ) circuit uses a 96 μF, 40 kV bank. Typical circuit characteristics for the data reported here are: I_ϕ=210 kA at 35 kV, with a rise time to peak current of 90 μs. B_ϕ=0.3 T at 25 kV, with peak B_ϕ occurring in $\sim$150 μs.

Work reported here includes operation of ETA-BETA II in both the stabilized pinch and aided reversal mode. Preionization of the deuterium gas is not used. Filling pressures are 3 to 14 mTorr, although gas breakdown problems preclude operation below 4 mTorr, after the liner becomes conditioned (100 shots). Base pressure is $\sim 4 \times 10^{-8}$ Torr.

STABILIZED PINCH (SP)

The stabilized pinch mode is obtained by crowbarring the B_ϕ circuit and then initiating I_ϕ. Plotted in figure 1 is the time τ_D for I_ϕ to decay to one-third of its peak value vs the filling pressure. Figure 2 displays the temperature measured with Thomson scattering from the axis at the time of peak I_ϕ. Superimposed on figure 1 and 2 are the results of a computer simulation of the circuit-plasma characteristics with specific amounts of oxygen and iron impurities assumed for the plasma. The correlation between the time behaviour of the impurity lines, the measured electron temperatures and the computer simulation leads to the following understanding of the physics of the plasma discharge. The rapid increase in τ_D at 6.5 mTorr could be explained as the burning out of the oxygen impurity, In the plasma model classical resistivity is used and the experimental results for both the temperature and the current decay time versus pressure are quantitatively reproduced. The apparent saturation of τ_D at lower densities can also be explained by the effect of iron impurities although the quantitative role of turbulent diffusion is unknown. It should be noted that, if the line density remains constant, the β_θ is $\geq$0.1 at 5 mTorr and 210 kA. The values of k and k_e, the poloidal flux loss and poloidal field energy loss defined by, $k=\int V_\phi dt/\phi_\theta$ and $k_e=\int V_\phi I_\phi dt/W_\theta$, are 1.1 and 1.5 for a specific 5 mTorr discharge. The magnetic field radial distribution measured by a series of probes inserted into the plasma is used to compute the flux (ϕ_θ) and the energy (W_θ). The bank volt seconds are in this case $\sim$0.2 of which $\sim$0.13 are applied at the liner and $\sim$0.12 correspond to magnetic flux (ϕ_θ) inside the liner.

AIDED REVERSAL

Aided reversal is accomplished by letting the toroidal field circuit complete a half-period oscillation before crowbarring, while I_ϕ is initiated at or near the peak of the toroidal magnetic field. This technique should not be confused with field programming where the reversal is driven on a timescale shorter or comparable with the Alfvén time. In ETA-BETA II the Alfvén time is $\sim$0.5 μs and the timescale for the applied external reversal is $\sim$100 μs (the liner diffusion time constant for B_ϕ is $\sim$60 μs). Nevertheless aided reversal is very useful to reduce the effect of the toroidal flux outside the metal liner being $\lambda=\phi_{ext}/\phi_{int}\simeq 1$.

Aided reversal results in a substantial change in the performance of the electrical characteristics of the experiment. Figures 3a,b show the appropriate waveforms for different values of the filling pressure. At 7 mTorr the I_ϕ decay time is improved by a factor of 1.5, compared to the stabilized pinch (see figure 1). Decreasing the filling density to the range of 5.6 to 6.5 mTorr results in a substantial change in the decay time of I_ϕ. The time to decay to 1/3 of the peak value is 0.8 ms by extrapolating the measured signals, but it can be observed after the peak current a period of slow current decay, which lasts for up to $\simeq$0.7 ms; during this period the e-folding time for the current decay is $\sim$1.5 ms (see figure 3a). Value of $\Theta=B_{\theta W}/<B_\phi>$ during the field reversal phase are comprised between 1.5 and 2 with $|F|=|B_{\phi W}/<B_\phi>|\leq 0.5$. The loop voltage V_ϕ is negative during the slow current decay indicating that poloidal field energy is going from the pinch into the external circuit. The negative V_ϕ can be explained on the basis of the simple circuit shown in figure 4. The voltage drop on the crow-bar can be neglected; then we have $V_\phi=-R_1I_1-L_d\frac{dI_\phi}{dt}-I_\phi\frac{dL_d}{dt}$. During the decay $\frac{dI_\phi}{dt}<0$ and, due to the field penetration in the flux guides and in the shell, $\frac{dL_d}{dt}>0$. Typical values in ETA-BETA II are $R_1I_1\simeq$30 V, $I_\phi\frac{dL_d}{dt}\simeq$5 V and $L_d\left|\frac{dI_\phi}{dt}\right|\simeq$15 V which explain the observed $V_\phi\sim$-20 V. A negative loop voltage is then only observed when $\frac{dI_\phi}{dt}$ is small and even neglecting $\frac{dL_d}{dt}$ it would always appear in the limit $\frac{dI_\phi}{dt}\to 0$ due to the finite resistance of the external primary circuit.

Time resolved spectra of the OIV and OV lines (see figure 5) show that OV is burned through and remains so until the current is terminated, implying that T_e remains high for $\sim$500 μs. The T_e from Thomson scattering is also shown in figure 2 for times corresponding to the peak of I_ϕ, 40-50 eV are measured on axis at the lower pressures. Higher temperatures are measured at later times up to $\sim$100 eV before current termination. Magnetic probes inserted part way into the discharge indicate that the fluctuation level of the toroidal and poloidal magnetic field is changed by the reversed B_ϕ field, which may indicate that the turbulent transport is changed by the established RFP configuration. A clear change in the fluctuation of the $\frac{dI_\phi}{dt}$ signal is observed between the stabilized pinch and the RFP configuration. The corresponding I_ϕ, and $\frac{dI_\phi}{dt}$ signals are shown in figure 6. Possible explanations for the I_ϕ termination are: the β_θ may become too high, since I_ϕ is decaying while the temperature increases, resulting in instability. The field reversal is lost when the termination occurs. Whether the loss of reversed B_ϕ triggers the termination or the opposite is true remains to be resolved.

CONCLUSIONS

ETA-BETA II has been able to overcome the radiation barrier imposed by light elements (oxygen). The values of k and k_e can be low, 1.1 and 1.5 respectively for a stabilized pinch discharge. Good confinement of an RFP plasma can be achieved by aided reversal; long current e-folding times of 1.5 msec, with reversal of the toroidal field lasting for 0.7 ms have been obtained with values of $\beta_\theta\geq$0.1. The level of the fluctuation in the dI_ϕ/dt signal is largely reduced when a high temperature RFP configuration is formed. The increased plasma temperatures ($\sim$100 eV) resulting from ohmic heating, are consistent with an improved confinement time.

Acknowledgements: We gratefully acknowledge the continuous technical collaboration on the experiment of E.Baseggio, G.Bertocchi, I.Dalla Libera, G.Mella, I.Molon, A.Tamiazzo and S.Zago; and C.Cavaggion, N.Guarino and A.Polo for developing and assisting on the data acquisition system.

References: [1] Fellin L., Maschio A., Stella A.: 10th SOFT, Sept. 78, Padova, Italy
[2] Proc. Workshop on the RFP, Sept. 78, Padova UPee 78/08.

FIG. 1

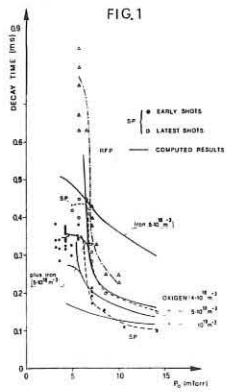

FIG. 2

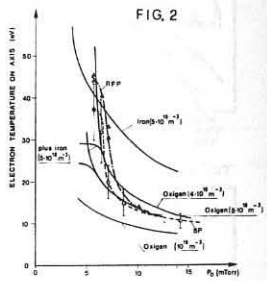

FIG. 3a

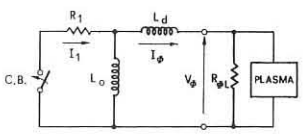

FIG. 4

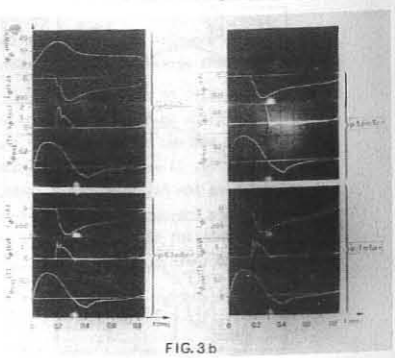

FIG. 3b

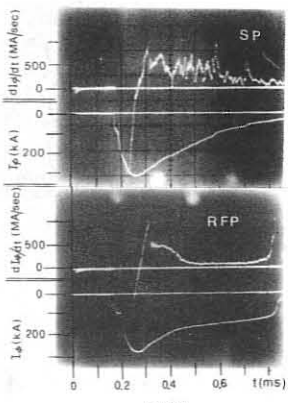

FIG. 6

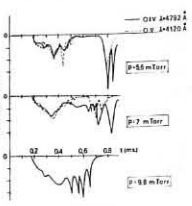

FIG. 5

On leave from Los Alamos Scientific Laboratory, N.M.

MAGNETIC TOPOLOGY NEAR THE q = 1 SURFACE DERIVED FROM THE SOFT X-RAYS MEASUREMENTS IN THE TFR 600 TOKAMAK

TFR GROUP*

ASSOCIATION EURATOM-CEA SUR LA FUSION
Département de Physique du Plasma et de la Fusion Contrôlée
Centre d'Etudes Nucléaires
Boite Postale n° 6. 92260 FONTENAY-AUX-ROSES (FRANCE)

The q = 1 magnetic island structure is investigated by soft X-ray technique and interpreted with a numerical model, in order to give some insight about some open questions [1, 2, 3, 4] : q = 1 surface radius, island existence, island size evolution, ... etc ...

A conventional silicon detectors array [5] with a central spatial resolution of 1 cm and a bandwidth of 50 kHz measures the soft X-ray flux from a 6 cm radius plasma cylinder (The limiter radius is 20 cm).

An observed internal relaxation, is synthetized by the numerical model. At a given time a magnetic surface set is assumed ; the synthetic signal obtained by integrating the X-ray emissivity along each chord, is then fitted to the experimental fluxes, by adjusting several parameters of the numerical model [6].

Magnetic surfaces : they depend on different parameters like the q = 1 surface radius r_0, the q = 1 island width δ_{isl} and the q = 1 surface shift. The island overlaps the q = 1 surface.

X-ray emissivity : the emissivity $\phi(r)$ outside the island is constant on each magnetic surface. It is assumed as $\phi(r) = \phi_0 \exp(-p(r/a)^2)$ [7] where p is the peaking index and (r/a) a normalised radius of the magnetic surface.

The initial value of the peaking index p_0 is experimentally fitted to the data (Fig. 1a) at a time of the regeneration phase t_1 where the island size is supposed to be very small.

Inside the island ϕ can be constant or with a "positive" or a "negative" hump.Such an emissivity is schematically shown on Fig. 2.

System evolution : experimentally the peaking index can vary (from 5 to 20) during the regeneration phase of the sawtooth and then strongly decreases back to its initial value (p_0) at the end of the disruption. So in the model $p(t) \sim (t/\tau_p)^{\alpha}$ during the regeneration phase and $\dot{p}(t) \sim -\frac{k}{\tau_p}$ during the disruption.

k is of the order of 20 to 300 and corresponds to the measured ratio (regeneration time/disruption duration).

α and τ_p the characteristic regeneration time are adjusted empirically (although τ_p is always found very close to the actual one).

Accordingly to the work [8] the island cannot grow indefinitely without leading to a catastrophic event . So it is assumed that the disruption phase happens when the island width δ_{isl} reaches a critical value δ_{crit}.

The evolution of δ_{isl} is given by $\frac{d}{dt}(\delta_{isl}^2) \sim K$ (K resistivity - like dimension). $K \sim (p(t) - p_1)\, \tau_{isl}^{-1}$, τ_{isl} is the island growth time. p_1 is an adjustable value of p below which δ_{isl} decreases. It is further assumed that the island width does not evolve below a minimum size δ_{min}. The cycle starts back as p reaches p_0.

The whole map is then rotated with the m = 1 mode frequency ν which can vary in order to reproduce the mode slowing down eventually observed.

Results : the synthetic signals shown on Fig. 1b can be compared to the experimental ones (Fig. 1a). The parameters ν, a, k, p_0 are directly measured. τ_p, α, τ_{isl}, p_1, r_0, δ_{crit} and δ_{min} must be empirically chosen until a satisfactory agreement is reached. From our tests and except for α ($\sim$ 0.8 in most cases), all these parameters are sensitive and a 20 % variation of one of them can destroy the fit. Fig. 1b results where obtained with the following parameters :

$\nu \sim 6$ kHz , $p_0 = 7.5$, $k = 100$, $a = 20$ cm , $r_0 = 6$ cm ; $\tau_p \sim 2.4$ ms , $\alpha = 1.0$, $\tau_{isl} = 240$ µs , $p_1 = 15$, $\delta_{min} = .1$ cm and $\delta_{crit} = 2.8$ cm.

* Paper presented by D.A. MARTY

Fig. 3 shows δ_{isl} versus time during the last 2 ms of the relaxation. On the same picture is plotted the m = 1 mode frequency ν (from Fig. 1a) which exhibits a strong slowing down as the island grows.

From the fitting of several relaxations the conclusion are the following :

1) The disruption happens when the q = 1 island width is rather small : $(\delta_{crit}/r_0) < 1/2$. Its growth is also rather slow with respect to the disruption duration.

2) The q = 1 surface radius is larger than the radius r_{INV} where the sawtooth signals inversion occurs, typically by a factor of 2 with flat flux profiles ($p_0 \sim 4 - 5$) and 1.5 with peaked profiles ($p_0 \sim 8 - 15$). This implies that the losses due to the internal relaxations might have been underestimated up to now and that the q = 1 surface lies in the gradient region.

3) The frequency doubling (ff on Fig. 1a) which occurs on the signal close to $r = r_{INV}$ cannot be obtained without a "cooling" inside the island.

REFERENCES

[1] B.B. KADOMTSEV, Fiz. Plazmy 1 (1975) 710.

[2] R.B. WHITE and al. Plasma Physics and Controlled Nuclear Fusion Research (Proc. 6th Int. Conf. Berchtesgaden 1976) 1 (IAEA Vienna) 569 (1977).

[3] A.F. DANILOV and al., Plasma Physics and Controlled Nuclear Fusion Research (Proc. 6th Int. Conf. Berchtesgaden 1976) 1 (IAEA Vienna) 591 (1977).

[4] N.R. SAUTHOFF and al., IAEA Workshop on disruption Garching (1979).

[5] D.A. MARTY, P. SMEULDERS, D. LAUNOIS, Association EURATOM-CEA pour la Fusion Contrôlée, Internal Report EUR-CEA-FC-969 (1978).

[6] M.A. DUBOIS, D.A. MARTY, A. POCHELON, Nuclear Fusion Letters, to be published.

[7] EQUIPE TFR, Association EURATOM-CEA pour la Fusion Contrôlée, Annual Report 1978, EUR-CEA-FC-995 (1979) 103.

[8] M.A. DUBOIS, A. SAMAIN, Association EURATOM-CEA pour la Fusion Contrôlée, Internal Report EUR-CEA-FC-965 (1978).

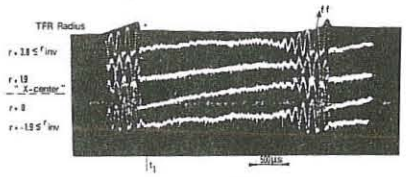

FIG. 1a

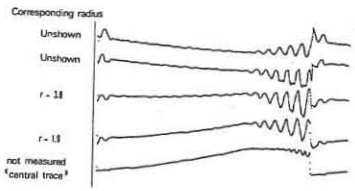

FIG. 1b

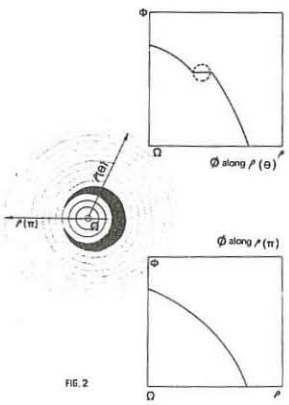

FIG. 2

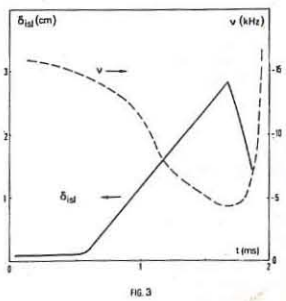

FIG. 3

REDUCTION OF ELECTRON HEAT TRANSPORT ANOMALY IN CLEANER AND DENSER TFR DISCHARGES

TFR GROUP

ASSOCIATION EURATOM-CEA SUR LA FUSION
Département de Physique du Plasma et de la Fusion Contrôlée
Centre d'Etudes Nucléaires
Boite Postale n° 6. 92260 FONTENAY-AUX-ROSES (FRANCE)

The energy balance in TFR 400 discharges [1] was dominated by electronic heat transport and X_e reached 100 times the neoclassical value. It was shown later that, as the density increases, the ion loss term becomes more important and the X_e anomaly is reduced [2] [3].

In this paper we analyze the energy balance of 400 kA discharges in order to evaluate the Xe anomaly factor in TFR 600.

High densities ($\overline{n_e} = 1.1\ 10^{14}\ cm^{-3}$) where obtained after a thorough wall conditioning [3] [4] and a stable radial equilibrium was achieved by superimposing a programed vertical field and a fast feedback loop [5]. Consequently the plasma has a longer duration. The main characteristics of these discharges are given in table 1, together with these of the reference discharge (R.D) in TFR 400 published at Berchtesgaden conference [1]. Both ~ 50 kG discharges have the same density profile, the same mean ion and -roughly- electron temperature.

From the time evolution of I, U, $\overline{n_e}$ (Fig. 1) and $T_e(o)$, $T_i(o)$, $n_e(o)$ (Fig. 2), one can show that although the central electron temperature decreases as the density increases, the total energy contained by electrons remains nearly constant.

The electron heat conduction is calculated during the current plateau at t = 250 ms, when the profiles are measured (Fig. 3, 4, 5).

TABLE 1

a = 20 cm Deuterium

	B_T kG	I kA	U V	$n_e(o)$ 10^{13} cm^{-3}	$\overline{n_e}$	$T_e(o)$	$\overline{T_e}$ keV	$T_i(o)$	$\overline{T_i}$
TFR 600	51	400	1.8	16.1	10.9	1.2	0.677	0.95	0.549
R.D	53.6	292	1.96	7.1	4.6	1.8	0.726	0.95	0.529

	W_e kJ	W_i	T_e ms	q(a)	Z_{eff}	Prad kW	K_e exp $cm^2 s^{-1}$	anomaly factor
TFR 600	13.7	11.1	34.4	2.6	1.53	158	2500	50
R.D	6.14	4.47	18.6	3.75	2.72	361	5000	100

Electron heat conduction

Considering a quasi stationary state plasma, the power lost by heat transport inside a volume bounded by the radius r is defined as [1] :

$$P_e\ cond = P_\Omega - P_{rad} - P_{ei} - \frac{dW_e}{dt} \quad \text{here } \frac{dW_e}{dt} \sim 0$$

P_e cond is the sum of conduction and convection losses.

The flux due to heat transport is $\phi_e\ cond = \frac{P_e\ cond}{4\pi^2 rR}$ and $X_e\ exp = \frac{\phi_e\ cond}{n_e T_e\ \nabla T_e/T_e}$

It is convenient to estimate the heat transport in the region of the maximum gradient, between the q = 1 and q = 2 surfaces, where the relative error on ∇T_e is minimum.

- The ohmic power profile P_Ω is determined with the following assumptions, the same as for the R.D : the electric field is radially constant, the resistivity is neoclassical [6]. The current density is either fixed as $j = j_o(1 - \frac{r^2}{a^2})^{q(a)}$ or computed assuming Z_{eff} = ct .

Using either assumption the q = 1 surface is in the range r_1 = 9/10 cm and q = 2 surface close to r_2 ~ 17 cm.

The soft X ray sawteeth measurements show q(o) < 1 and the inversion radius r_0 ~ 6/7 cm. It is shown in [7] that this is compatible with r_1 = 9/10 cm in the case of a flat T_e profile in this region.

- Radiation losses : $P_{rad} = P_{bol} - P_{ex}$

The bolometric profile, measured by mean of a pyroelectric diode, presents a maximum near the edge of the plasma column (Fig. 4).

The calculated charge exchange losses, P_{ex} ~ 9 % P_Ω is the same as for the R.D but P_{rad} ~ 22 % P_Ω is less than for the R.D where P_{rad} ~ 63 % P_Ω .

Abel inverted line emission radial profiles of some ions are shown in Fig. 5. They have been obtained by scanning in about 1 ms the lower half of the plasma . The central radiated power of 0.3 W cm^{-3} Fig. 4 is compatible with the observed metallic ion densities. (The signal of N_i, C_r, F_e, respectively in the ratio 5, 2, 1, are not much different from the inconel chemical composition of the walls and the limiter). The peripheral peak of Fig. 4 is caused by oxygen and deuterium radiation. So our feeling is the atomic processes play an important role at the plasma boundary.

The overall radiation losses are half of that of R.D. Conductivity calculations and soft X ray measurements yield Z_{eff} ~ 1.5/1.8 Z_{eff} remains almost constant during the current plateau. One has to remark that during all the experience time an important cold gas blanket exists between the plasma and the walls. (n_{D_2} ~ $3 10^{12}$ $D_2 cm^{-3}$).

- P_{ei}, the classical electron-ion energy transfer term is now dominant P_{ei} ~ 50 % P_Ω (R.D ~ 13 %).

- P_e cond, Fig. 6 shows the power lost by heat transport.In the gradient region this term has the same order of magnitude as P_{ei} and the heat transport coefficient is Xe exp ~ 2500/3000 cm^{2}s^{-1}. The heat flux, ϕ_e cond, and ∇T_e are the same as in the reference discharge, but the Xe exp value is reduced by a factor of 2 due to the increase of density by the same factor. Similar absolute value has been found in Alcator for the same density [3].

Compared to the heat flux given by the neoclassical theory (conduction + convection, neglecting the Ware effect) [6], the anomaly electron heat transport becomes ~ 50, instead of 100 in R.D.

Ion heat conduction

In the same way we define : $P_{i\ cond} = P_{ei} - P_{ex} - dW_i/dt$ so in the gradient region K_i ~ 2000/2500 cm^{2}s^{-1} ν_i^N ~ 1 which corresponds to a maximum anomaly factor 1.5/2.

Conclusion

The main effects resulting from an increase of the density are the increase of energy content and of the energy life time. This agrees with the scaling laws of the type $\tau_e = (5/6)\ 10^{-16}\ \overline{n}\ \sqrt{q}\ a^2$
or $\tau_e = (5/6)\ 10^{-16}\ n_e(o)\ T_e(o)^{1/2}\ a^2$ (ms, cm, keV).

In addition the reduction of radiation losses allows to reach a lower value of q(a) and a greater value of $\overline{n_e}$, meanwhile as T_e becomes lower, the energy exchange between electron and ions is improved.

While $\overline{n_e}$ was increased by a factor 2 the experiment Xe was reduced by the same factor.

References

[1] TFR GROUP in Plas. Phys. & Cont. Nucl. Fus. Research (Proc. 6th Int. Cong. Berchtesgaden 1976) Vol. 1, IAEA, Vienna (1977) 35.
[2] TFR GROUP in Plas. Phys. & Cont. Nucl. Fus. Research (Proc. 7th Int. Conf. Innsbruck 1978) Vol. 1, IAEA, Vienna (1979) 135.
[3] Energy Confinement in Alcator, A. Gondhalekar et al. Sub. in Nucl.Fus.
[4] TFR GROUP, J. of Nucl. Mater. Vol. 76 n° 1 & 2, Sept. 78, pp 587-593.
[5] Influence of the iron core on plasma equilibrium and stability in TFR 600, a tokamak without copper shell. J. Blum et al. 10th Symp. on Fusion Technology, Padua 4-9 September 1978.
[6] F.L. Hinton & R.D. Hazeltine in Rev. of Modern Phys. Vol.48 n° 2 part. 1, April 1976, PP 239-308.
[7] q = 1 island cartography derived from the soft X-ray sawteeth activity in the TFR Tokamak, TFR GROUP this Conference.

Figure Caption

Fig. 1 Time evolution of current I, voltage U, mean density $\overline{n_e}$
Fig. 2 Time evolution of $T_e(o)$, $T_i(o)$, $n_e(o)$, $Z_{eff}(o)$, $\overline{Z_{eff}}$
Fig. 3 Electron (T_e), ion (T_i) temperatures and density (n_e) profiles. The peripheral electron temperature is obtained from the radial positions of the emission peaks of the indicated ions. It is supposed that the different emission shells are always at the same electron temperature the comparison with Thomson scattering having been performed in other discharges.
Fig. 4 Density power lost by radiation and neutral particles (Bolometry).
Fig. 5 Line emission radial profiles for the indicated ions (Ly_α is strong since the spectrometer is at the cold gas injection port).
Fig. 6 Profile of power contained inside a volume limited by the radius r Ohmic power : P_Ω, radiated power : P_{rad}, exchange electron to ion : P_{ei}, conduction + convection losses : P_e cond. Xe exp profile.

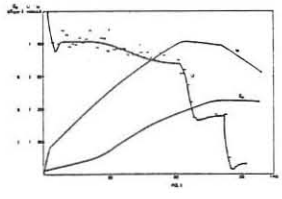

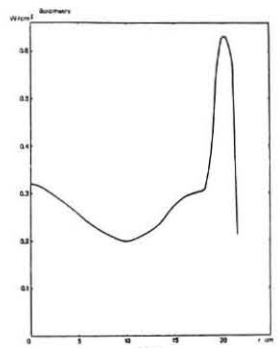

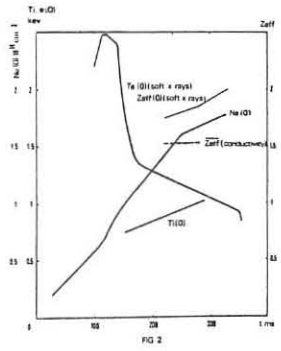

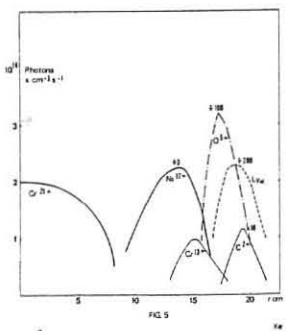

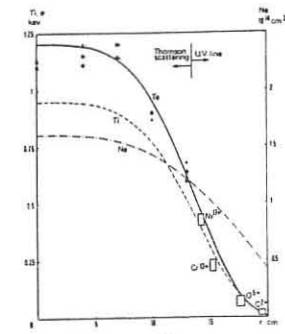

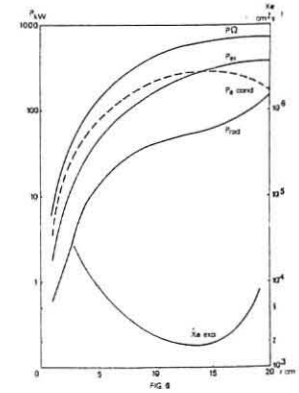

ELECTRON CYCLOTRON PLASMA HEATING IN FT-1 TOKAMAK BY THE WAVE LAUNCHED FROM A STRONGER MAGNETIC FIELD SIDE

D.G.Bulyginsky, V.E.Golant, M.M.Larionov, L.S.Levin, N.V.Shustova

A.F.Ioffe Physical-Technical Institute, Leningrad, USSR

Experiments on electron cyclotron resonance heating (ECRH) using gyrotron generators were carried out at TM-3 /1/ and FT-1 /2/ tokamaks. In both cases the heating wave was launched by a horn antenna from the external side of a toroidal plasma in the zone of lower magnetic field. ECRH efficiency can be improved due to elimination of the evanescence region for an extraordinary wave, if it is launched in a proper direction from the inner side of torus, in the stronger magnetic field zone. The paper describes the preliminary result of the experiment on ECRH using the wave excitation of this type. FT-1 tokamak (R= = 62 cm, a = 15 cm, B 11 kGs, I = 30 kA) is provided by the gyrotron generator (30 GHz, 100 kW, 2 ms). The power is fed by the circular waveguide 32 mm in dia. It is introduced in the discharge chamber and placed in the limiter shadow. The end of the waveguide serves as an antenna. At the inner side of a torus it is oriented along the toroidal magnetic field direction and is cut by a proper way (Fig.1). The wave in a plasma is polarised perpendicularly and is launched at about 40° to the magnetic field. Experimentally, during ECRH pulse the discharge current was kept constant. Changes in a loop voltage U_1 and in a plasma diamagnetism $\Delta\phi$ were observed. Mean electron density $\overline{n}_e$ was registrated also. No increase of a density was observed during ECRH pulse. When the wave was launched by a horn from the lower magnetic field side a decrease of U_1 about 20% and $\Delta\phi$ signal ($\overline{n\Delta T}\sim 1.10^{14}$ eV.cm^{-3}) were observed in a proper magnetic field range B> 8.5 kGs only in a low density discharges, $\overline{n}_e < 3.10^{12}$cm^{-3}. No influence of ECRH on plasma parameters was found, if $\overline{n}_e > 3.10^{12}$cm^{-3}. Heating by the wave launched from the stronger field side was studied only at $\overline{n}_e = 6.10^{12}$cm^{-3}; $T_{e\ max} \approx 300$ eV, $\tau_E \approx 0.6$ ms. An essential drop of U_1 from 2.2 V to 1.5 V, was observed in this case (Fig.2). It indicates the 30% electron heating, in spite of decrease of ohmic heating of

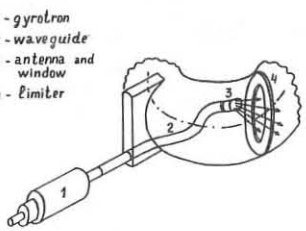

Fig.1

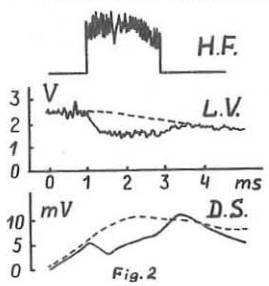

Fig.2

the same order. $\Delta\phi$ signal was observed also(Fig.2). Its value gives $\Delta\overline{nT} = 2.10^{14}$ eV.cm^{-3}. It can be compared with ohmic heating value $\overline{nT} = 6.5 \times 10^{14}$cm^{-3} was found. The rise and decay time of $\Delta\phi$ and U_1 signals are close to τ_E. Data obtained allow us to estimate the efficiency of ECRH in comparison with ohmic heating. Taking into account the rise of $\overline{nT}$, the decrease of ohmic heating and assuming τ_E = const, we obtain: $P_{ECRH} = P_{OHM} \cdot \left(\frac{\Delta\overline{nT}}{\overline{nT}} + \frac{\Delta U_l}{U_l}\right) = 42$ kW. There is a strong dependence of efficiency on the magnetic field. Effects of ECRH exist at B> 8.5 kGs and vanish at B< 8.5 kGs, when the resonance zone removes itself from a plasma volume. The hard X-ray flux was observed and found to be decreasing during ECRH. Thus, run-away electrons are not produced by the microwave pulse.

In conclusion, we point out the main result of this experiment. ECRH by the extraordinary wave launched from the inner side of a torus is effective in a plasma with rather high density, $n_{e\ max} \gtrsim 10^{13}$cm^{-3}, $\omega_{pe} \approx \omega_{ce}$, while the wave launching from the external side produces some heating only in a low density plasma, $n_{e\ max} < 5.10^{12}$ cm^{-3}.

REFERENCES

1. V.V.Alikaev et al. JETP lett., 15, 1, 41, 1972; Fizika plasmy, 2, 3, 390, 1976.
2. V.E.Golant, M.M.Larionov, L.S.Levin et al. Proc. VI ECCFPP, Moscow 1973, v.I, p.587. Proc. III Int.Symp. on Toroidal Plasma Confinement, Garching 1973, E-5.

ON TOROIDAL VACUUM FIELDS AND PARTICLE ORBITS IN MODIFIED STELLARATORS AND TORSATRONS

W VII-A Team[+] and W. Lotz, presented by F. Rau

Max-Planck-Institut für Plasmaphysik, Association EURATOM-IPP
D-8046 Garching, Federal Republic of Germany

Abstract: Guiding center trajectories of high energy deuterons are studied in the "Reduced-Q-Configuration" /1/. If the energy exceeds a value depending critically on the starting point, the particles can get azimuthally untrapped for some time. Then $J_c = \int v_{\parallel} dl_+ + \int v_{\parallel} dl_-$ is found to change appreciably (dl_+, dl_- path elements $\uparrow\uparrow$ and $\uparrow\downarrow$ to B). No particle loss appears to be caused if the energy is not too large.

Introduction: The "Reduced-Q-Configuration" introduced in /1/ is characterized by a small poloidal variation of $q = \int_0^L dl/B$, L = length of a field period. Certain regions show superbananas closed within one field period /1/. The adiabatic invariants $\mu = \frac{W_\perp}{B}$ and $J = \oint v_{\parallel} dl$ are used. This should be applicable up to moderate particle energies.

Large Particle Energies: In this supplement to /1/ we study the influence of large particle energies on guiding center trajectories for the Reduced-Q-Configuration in the absence of collisions and electric fields. Different starting points are considered, mainly in the azimuthal plane $\varphi = \pi/10$, (see /1/, Fig. 5, drawn curve) at R = 182 cm and variable Z. Fig. 1A shows R(φ) of a deuteron with energy W = 82 keV starting at Z = 5 cm. Similar to /1/, Fig. 6, the superbanana is closed within one field period. Increasing W to 167 keV yields a different guiding center trajectory, Fig. 1B: after ≈1.5 superbananas at large excursions the deuteron gets untrapped, passes the second field period and gets trapped for some time within the third field period (not shown in Fig. 1B), etc. The computation ends in the 9th field period. The time evolution of J_c is shown in Fig. 1C for the two cases. The sharp peaks of the upper curve correspond to the azimuthal transits of the 167 keV trajectory; J_c remains nearly constant during the localized parts, at different values however. For W = 82 keV the quantity J_c is found to be constant to within ≈10% (lower curve in Fig. 1C). Increasing Z by 1 cm reduces the critical energy by a factor of ≈2. Reducing Z to 1 cm allows W up to 0.25 MeV for guiding center trajectories still localized within one field period. Deuterons at 0.5 MeV drift out of the confinement region. Therefore, at large energies the single particle trajectory should be analysed also.

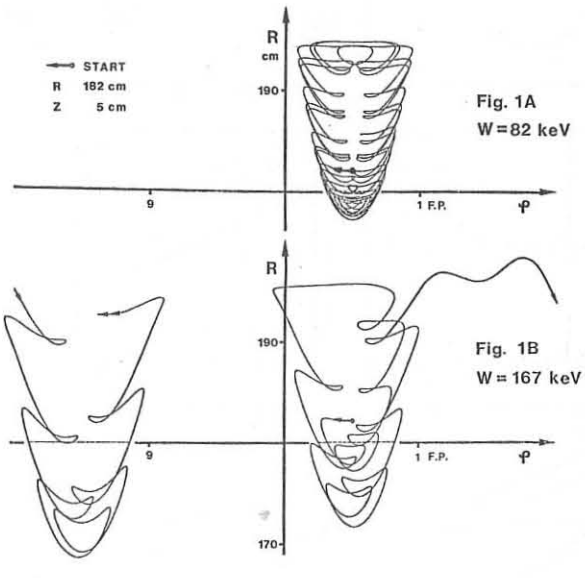

Fig. 1A
W=82 keV

Fig. 1B
W = 167 keV

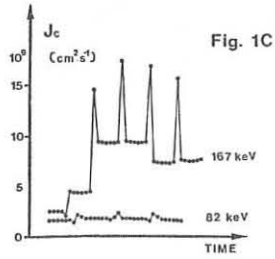

Fig. 1C

Figure Captions

Fig. 1A, 1B : Guiding center trajectories R (φ) for deuterons at energies W = 82 and 167 keV : localized and partially untrapped orbits

Fig. 1C : Time evolution of $J_c = \int v_{\parallel} dl_+ + \int v_{\parallel} dl_-$ for the cases of Fig. 1A, 1B ; arbitrary abscissa

References : /1/ these proceedings, Vol. I, paper BP 22

[+] W VII-A Team : cf these proceedings, Vol. I, paper BP 24

in 9th Europ.Conf.on Controlled Fusion and Plasma Physics, Invited Papers; UKAEA Culham Lab., Abingdon, Oxon, 1979, p. 547

THE ACCESSIBILITY OF THE RESONANT SURFACES AND THE ROLE OF SURFACE WAVES IN RF PLASMA HEATING

Ernesto Canobbio

Department of Physics, University of California
Los Angeles, California 90024, USA*

and

Association EURATOM-CEA, Departement de Physique du Plasma
et de la Fusion Contrôlée
Centre D'Etudes Nucleaires, Grenoble, 38041, FRANCE**

In this Supplement we present a quantitative study of the low-frequency wave characteristics of a finite-β plasma, of which only a crude account was given in the Main Paper (MP). With the assumptions and notations used to derive Eq. (1) in MP, the relevant dispersion relation reads

$$\tfrac{1}{2}\beta(A-1)(1+X_{II}T_e/T_i)X_\perp^2+\{X_{II}-A-\tfrac{1}{2}\beta(2-A)X_{II}^2T_e/T_i\}X_\perp+\{A-2AX_{II}+X_{II}^2-\tfrac{1}{2}\beta X_{II}^3T_e/T_i\}=0 \quad (1')$$

which replaces the incomplete Eq. (1) in MP.

The two solutions $X_\perp=X_\perp(X_{II})$ ($X_{II} \geq 0$) have been computed for various A, β ($\beta \ll 1$), and T_e/T_i values. The results are shown in Figs. (a)-(f) (plane lines) for the following parameters. (a) A=2, $\beta = 2.10^{-2}$, $T_e/T_i=3$. (b) A=1.1, $\beta=2.10^{-2}$, $T_e/T_i=3$. (c) A=1.01, $\beta=10^{-1}$, $T_e/T_i=3$. (d) A=1.01, $\beta=2.10^{-2}$, $T_e/T_i=1;3;10$. (e) A=-1, $\beta=10^{-1}$, $T_e/T_i=3$. (f) A=-1, $\beta=2.10^{-2}$, $T_e/T_i=1;3;10$. One solution appears close to the well known cold-plasma fast wave. The other solution has been discussed so far only in the limit of large $|X_\perp|$: if $|X_\perp|$ is large and $X_{II}=0(A;T_i/T_e)$, Eq. (1') reduces to

$$\tfrac{1}{2}\beta(A-1)(1+X_{II}T_e/T_i)X_\perp \approx A-X_{II}$$

which corrects and generalizes previous results (MP, Ref. 1.). If both $|X_\perp|$ and X_{II} are large, one solution tends to the asymptote $X_\perp=-X_{II}+T_i/T_e$ and the other one to the asymptote $X_\perp=(X_{II}-2T_i/\beta T_e)/(A-1)$. The latter is the branch which gives rise to resonance cones when A > 1 (MP, Ref. 2). The asymptotes are plotted as dashed lines in the figures. For $X_{II} > 0$, there are up to 3 zeros of $X_\perp$ if A > 1, and 2 zeros if A < 0. If A < 0 there is no mode conversion layer (contrary to what is stated in the MP).

I am grateful to Inge Jechart for her assistance with the numerical work.

*Partially supported by USDOE
**Permanent address

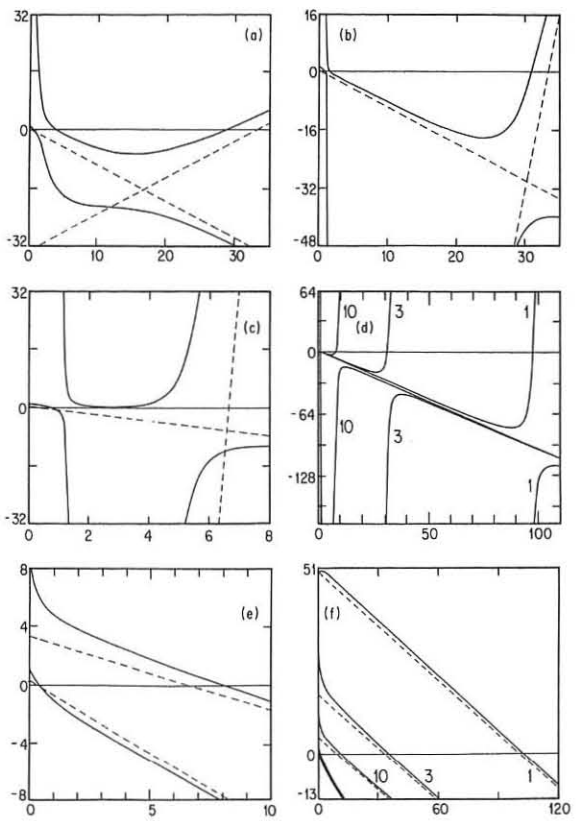

POLARIZATION AND MILLISECOND SPECTRAL MEASUREMENTS OF ELECTRON CYCLOTRON EMISSION FROM DITE TOKAMAK

D.J. Campbell+, W.H.M. Clark, A.E. Costley*, P.J. Fielding, L.C. Robinson+, G.D. Tait** and B Walker*

Culham Laboratory, Abingdon, Oxon, OX14 3DB, UK
(Euratom/UKAEA Fusion Association)

+University of Sydney, Sydney, Australia, *Division of Electrical Science, National Physical Laboratory, Teddington, U.K. **University of Maryland, College Park, Maryland, U.S.A.

a) The measured Stokes parameters in the second section of the paper should be $I_o = 23 \pm 1$, $I_p = 4.5 \pm 1.5$, $M = -4 \pm 1$, $C = 0 \pm 1.5$, $S = -1.0 \pm 1.5$. The units are in units of intensity of an arbitrary value.

b) Due to a sign error in reference (8), the function G(q,θ), for the angular variation of the optical depth $\tau_{o,e}$, is incorrect. The correct form should be:

$$G(q,\theta) = 3q\,n^3 \sin^2\theta \,\frac{[n^4 \sin^2\theta - n^2(1-q)(1+\cos^2\theta) + 2(1-2/3\,q)(1-q-n^2\sin^2\theta)]}{2(1-2q)(3-2q)(1-q-n^2)-qn^2(1+\cos^2\theta)}\,.$$

As a consequence, in contrast to Fig. 3, the correct behaviour of G(q,θ) indicates that the optical depth for the O-mode at oblique angles is an order of magnitude smaller than the e-mode and the finite density theory gives a small correction to the result obtained from the low density theory given in reference (3). A particular result for q = 0.2 is shown in the figure below.

The absence of strong polarisation in the observed emission can thus be explained only by taking account of wall reflections as in reference (1).

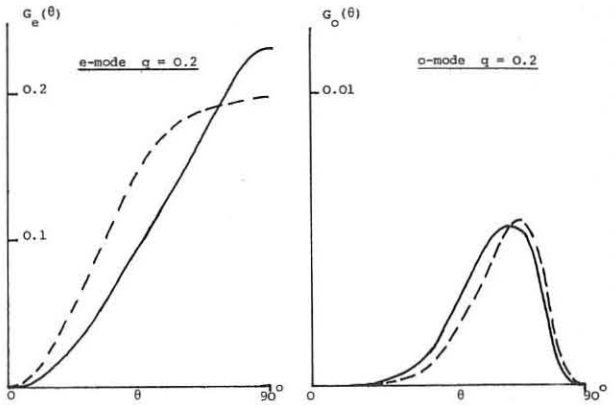

Fig: The function G(q,θ) for q = 0.2. Dashed line is the corresponding variation according to the low density theory of reference (3).

LIST OF PARTICIPANTS

ADAM J.
CEA, Fontenay, France

ALLEN J.E.
Univ. of Oxford, UK

ALLEN T.K.
UKAEA, Culham, UK

ANDERSEN V.
RISO, Roskilde, Denmark

ANDERSON D.
Chalmers Univ. of Tech., Goteborg, Sweden

ANDERSON D.T.
Univ. of Wisconsin, Madison, USA

ASHBY D.E.T.F.
UKAEA, Culham, UK

BAITY F.W.
Oak Ridge Lab, Oak Ridge, USA

BALDWIN A.
IEE, Inspec., Hitchin, UK

BALMER J.E.
Univ. of Berne, Switzerland

BAR-AURAHAM E.
Gov. of Israel Research Dept., Israel

BARTIROMO R.
CNEN, Frascati, Italy

BARTLETT D.V.
IPP Garching, FRG

BEIER R.
Ruhr-Univ., Bochum, FRG

BEIN B.K.
Ruhr-Univ., Bochum, FRG

BERGE G.
Bergen Univ., Norway

BERNARD A.
CEA Limeil, France

BERNARD L.C.
General Atomic Co., San Diego, USA

BERNARD M.G.
CEN, Grenoble, France

BERS A.
MIT, Cambridge, USA

BHATNAGAR V.P.
Ecole Royal Milit., Brussels, Belgium

BICKERTON R.J.
JET, Culham, UK

BILBAO L.
Univ. Buenos Aires, Argentina

BINGHAM R.
CRPP Lausanne, Switzerland

BIRNBOIM A.
NRC, Negev, Israel

BOBIN J.L.
CEA Limeil, France

BODIN H.A.B.
UKAEA, Culham, UK

BOGUSCH E.
Interatom GmbH, FRG

BONNEVIER B.
Royal Inst. Techn., Stockholm, Sweden

BORRASS K.
IPP Garching, FRG

BOSIA G.
Ecole Royale Milit., Brussels, Belgium

BOYD D.
Univ. of Maryland, USA

BRAAMS C.M.
FOM, Rijnhuizen, Netherlands

BRAMBILLA M.
CEN, Grenoble, France

BRIFFOD G.
CEN, Grenoble, France

BROCKEN H.
FOM, Rijnhuizen, Netherlands

BROWNELL J.H.
Univ. California, Los Alamos, USA

BRUZZONE H.
Univ. Buenos Aires, Argentina

BUFFA A.
CSGI Padova, Italy

BYRNE R.N.
Science Applications, La Jolla, USA

CABE J.
CEA Bruyeres le Chatel, France

CALDERON M.
Ecole Royale Milit., Brussels, Belgium

CANO R.
CEA, Fontenay, France

CANOBBIO E.
CEN, Grenoble, France

CAP F.
Univ. of Innsbruck, Austria

CAPES H.
CEA, Fontenay, France

CAROLAN P.G.
UKAEA, Culham, UK

CASINI G.
JRC-Ispra, Varese, Italy

CATTO P.J.
Science Applications Inc., Colorado, USA

CAVALLO A.
CEA, Fontenay, France

CHANG C.T.
RISO, Roskilde, Denmark

CHEETHAM A.D.
CRPP, Lausanne, Switzerland

CHRISTIANSEN J.P.
UKAEA, Culham, UK

CIMA G.
CNEN, Milan, Italy

CLARK W.H.M.
UKAEA, Culham, UK

COLE H.A.
TRW Incorporated, Los Angeles, USA

COLE H.C.
UKAEA, Culham, UK

CONNOR J.W.
UKAEA, Culham, UK

CONSOLI T.
CEN, Grenoble, France

CORDEY J.G.
UKAEA, Culham, UK

CORE W.G.
JET, Culham, UK

COSTLEY A.E.
National Physical Lab., Teddington, UK

COX M.
UKAEA, Culham, UK

CRAWFORD F.W.
Stanford Univ., California, USA

CZEKAJ S.
Inst. of Plasma Physics, Warsaw, Poland

DAGENS L.P.
CEA, Limeil, France

DAVENPORT P.A.
UKAEA, Culham, UK

DAVIDSON R.C.
MIT, Cambridge, USA

DAVIES C.
Imperial College, London, UK

DAYBELGE U.
Ruhr-Univ., Bochum, FRG

DE GOTTAL P.
Univ. of Mons, Belguim

DE HAAN P.H.
FOM, Kruislaan, Amsterdam, Netherlands

DE KLUIVER H.
FOM, Rijnhuizen, Netherlands

DE KOCK L.C.J.M.
FOM, Rijnhuizen, Netherlands

DE MARCO F.
CNEN, Frascati, Italy

DECKER J.
Dept. of Energy, Washington, USA

DEDYUKIN M.T.
IAE Kurchatov, Moscow, USSR

DELLIS A.N.
UKAEA, Culham, UK

DELVAUX J.
CEA, Valduc, France

DERR J.A.
Univ. Wisconsin, Madison, USA

DIPPEL K.H.
KFA, Julich, FRG

DONALDSON T.P.
English Electric Valve Co., Chelmsford, UK

DOUCET H.
Ecole Polytechnique, Palaiseau, France

DRAKE J.F.
Univ. Maryland, USA

DRAKE J.R.
Royal Inst. of Tech., Stockholm, Sweden

DRINAN A.H.
Gulton Industries Inc., California, USA

DRUAUX J.
CEA, Fontenay, France

DUESING G.
JET, Culham, UK

DYMOKE-BRADSHAW A.
Imperial College, London, UK

EDLINGTON T.
UKAEA, Culham, UK

EIDENS J.
KFA, Julich, FRG

EMMETT J.L.
LLL, Livermore, USA

ENGELHARDT W.
IPP Garching, FRG

ENGELMANN F.
FOM Rijnhuizen, Netherlands

ERENTS S.K.
UKAEA, Culham, UK

FAULCONER D.W.
Ecole Royale Milit., Brussels, Belgium

FAULKNER J.E.
IPP Garching, FRG

FIELD J.J.
UKAEA, Culham, UK

FIELDING P.J.
UKAEA, Culham, UK

FIELDING S.J.
UKAEA, Culham, UK

FONTANESI M.
CNEN, Milan, Italy

FORREST M.J.
UKAEA, Culham, UK

FOWLER T.K.
LLL, Livermore, USA

FRANKLIN R.N.
City Univ., London, UK

FUJISAWA N.
JAERI, Ibaraki-ken, Japan

FUKUYAMA A.
Okayama Univ., Japan

FURTH H.P.
PPPL Princeton, USA

FUSSMANN G.
IPP Garching, FRG

GAISFORD P.A.
Univ. London, UK

GALANTI M.
CNEN, Frascati, Italy

GIBSON A.
JET, Culham, UK

GIERKE G. von
IPP Garching, FRG

GILL R.D.
UKAEA, Culham, UK

GLASSER A.H.
PPPL, Princeton, USA

GOEDBLOED J.P.
FOM, Rijnhuizen, Netherlands

GOLANT V.E.
Ioffe Inst., Leningrad, USSR

GOLDENBAUM G.C.
Univ. Maryland, USA

GONZALEZ J.
Chile

GOTO Y.
Tohoku Univ., Sendai, Japan

GREEN B.
JET, Culham, UK

GRESILLON D.
Ecole Polytechnique, Palaiseau, France

GREVE P.
Ruhr-Univ., Bochum, FRG

GRIEGER G.
IPP Garching, FRG

GRUBER O.
IPP Garching, FRG

GU YONG-NIAN
Southwestern Inst. of Physics, P.R. China

GUSTAFSSON H.I.
National Defence Research Inst., Stockholm, Sweden

HAAS F.A.
UKAEA, Culham, UK

HACKER H.
IPP Garching, FRG

HAEGI M.
CNEN, Frascati, Italy

HAINES M.G.
Imperial College, London, UK

HAMBERGER S.M.
Australian National Univ., Canberra

HAMMERLING P.
Science Applications, La Jolla, USA

HARBOUR P.J.
UKAEA, Culham, UK

HARRISON M.F.A.
UKAEA, Culham, UK

HASTIE R.J.
UKAEA, Culham, UK

HELLERMAN M.G. von
Univ. Essen, FRG

HELLSTEN T.A.K.
Royal Inst. Tech., Stockholm, Sweden

HEMSWORTH R.S.
UKAEA, Culham, UK

HENDER T.C.
Univ. London, UK

HENKES P.R.W.
IKUZ, Karlsruhe, FRG

HERRNEGGER F.
IPP Garching, FRG

HERTZBERG A.
Univ. of Washington, USA

HESKETH K.W.
UKAEA, Culham, UK

HICKOK R.L.
Rennselaer Poly. Inst., New York, USA

HINTZ E.
KFA Julich, FRG

HOEKZEMA J.A.
FOM, Rijnhuizen, Netherlands

HOLTER O.
Univ. Oslo, Norway

HOLZHAUER E.
Univ. Stuttgart, FRG

HOPMAN H.J.
FOM, Kruislaan, Netherlands

HUGHES M.
UKAEA, Culham, UK

HUGILL J.
UKAEA, Culham, UK

HWANG D.Q.
PPPL, Princeton, USA

IKEDA N.
Japan

INUTAKE M.
IPP, Nagoya Univ., Japan

ITOH S.
Kyushu Univ., Japan

IVANOV N.V.
IAE Kurchatov, Moscow, USSR

JAEGER E.F.
Oak Ridge Lab., Oak Ridge, USA

JAENICKE R.
IPP Garching, FRG

JANKOWICZ Z.
Inst. Nucl. Res. Otwock-Swierk, Poland

JANSSEN P.A.E.M.
Tech. Univ. Eindhoven, Netherlands

JENSEN P.B.
RISO, Roskilde, Denmark

JENSEN V.O.
RISO, Roskilde, Denmark

JOHNSON P.C.
UKAEA, Culham, UK

JOHNSON R.R.
KMS Fusion Inc., Michigan, USA

JOHNSTON J.W.
Oxford Polytechnic, UK

JONES I.R.
Flinders Univ., Australia

JORGENSEN L.W.
UKAEA, Culham, UK

KARDON B.
Centr. Res. Inst. for Phys., Budapest, Hungary

KARLSON E.T.
Uppsala Univ., Sweden

KAUFMANN M.
IPP Garching, FRG

KEILHACKER M.
IPP Garching, FRG

KELLER R.
Ecole Polytechnique, Lausanne, Switzerland

KERNER W.
IPP Garching, FRG

KILDAL A.
Univ. Of Oslo, Norway

KISTEMAKER J.
FOM, Kruislaan, Netherlands

KITO M.
Electrotechnical Lab., Tanashi, Japan

KLUEBER O.
IPP Garching, FRG

KOCH R.E.J.G.
Ecole Royale Milit., Brussels, Belgium

KOGOSHI S.
Oxford Univ., UK

KOLB A.C.
Maxwell Laboratories Inc., San Diego, USA

KONDOH Y.
Gunma Univ., Japan

KOPECKY V.
Inst. Of Plasma Phys., Prague, Czechoslovakia

KOPPENDORFER W.
IPP Garching, FRG

KREBS K.H.
ZIE, Berlin, GDR

KRUCKEWITT T.W.
Univ. Wisconsin, Madison, USA

KUNZE H.J.
Ruhr-Univ., Bochum, FRG

KUTHY A.
Royal Inst. of Tech., Stockholm, Sweden

LACKNER K.
IPP Garching, FRG

LAEDRACH P.
Univ. Bern, Switzerland

LALLIA P.P.
JET, Culham, UK

LASHMORE-DAVIES C.N.
UKAEA, Culham, UK

LAWSON J.D.
Rutherford Lab., Chilton, UK

LEES D.J.
UKAEA, Culham, UK

LEHNERT B.
Royal Inst. of Tech., Stockholm, Sweden

LEWIS C.L.S.
Queens Univ., Belfast, N. Ireland

LI ZHENG-WU
Southwestern Inst. of Physics, P.R. China

LILLETHUN E.
Univ. of Bergen, Norway

LIPSON J.
Univ. California, Los Alamos, USA

LISAK M.
Chalmers Univ. of Tech., Goteborg, Sweden

LISITANO G.
IPP Garching, FRG

LISTER J.B.
CRPP, Lausanne, Switzerland

LITUNOVSKI V.N.
Efremov Inst., Leningrad, USSR

LOK J.
FOM, Rijnhuizen, Netherlands

LORTZ D.
IPP Garching, FRG

LUNNEY J.G.
Queens Univ., Belfast, N. Ireland

MCGUIRE K.M.
Oxford Univ., UK

MAISONNIER C.
CEC, Brussels, Belgium

MALEIN A.
CEC, Brussels, Belgium

MALESANI G.
CSG, Padova, Italy

MALFLIET W.
Univ. of Antwerp, Belgium

MANERO F.
Junta de Energia Nuclear, Madrid, Spain

MARK E.
Univ. Of Innsbruck, Austria

MARSHALL S.J.
IEE, Inspec., Hitching, UK

MARTY D.
CEA, Fontenay, France

MAYSENHOELDER W.
Univ of Dusseldorf, FRG

MEDLEY S.S.
PPPL, Princeton, USA

MEISEL D.
IPP Garching, FRG

MELIN G.
CEN Grenoble, France

MERCURIO S.
CNEN Frascati, Italy

MILEY G.H.
Fusion Studies Lab., Illinois Univ., USA

MINARDI E.
UKAEA, Culham, UK

MONTANES J.L.
ETSI Aeronauticos, Madrid, Spain

MORGAN P.D.
CRPP Lausanne, Switzerland

MOURIER G.
Thomson/CSF Co., Velizy Villacourlay, France

MUDFORD B.S.
Oxford Univ., UK

MULLER G.
Univ. Stuttgart, FRG

MURMANN H.
IPP Garching, FRG

NAKACH R.
CEN Grenoble, France

NEWTON A.A.
UKAEA, Culham, UK

NICOLAI A.
KFA, Julich, FRG

NICOLLE J.P.
CEA Limeil, France

NISHIKAWA K.
Hiroshima Univ., Japan

NOLL P.
JET, Culham, UK

NUHRENBERG J.
IPP Garching, FRG

OEPTS D.
FOM, Rijnhuizen, Netherlands

OHKAWA T.
General Atomic Co., San Diego, USA

OHKUBO K.
IPP, Nagoya Univ., Japan

OLIVAIN J.
CEA, Fontenay, France

OOMENS A.A.M.
FOM, Rijnhuizen, Netherlands

ORNSTEIN L.TH. M.
FOM, Rijnhuizen, Netherlands

ORTOLANI S.
CSGI, Padova, Italy

PANARELLA E.
National Res. Council, Ottawa, Canada

PAUL J.W.M.
UKAEA, Culham, UK

PEASE R.S.
UKAEA, Culham, UK

PEGORARO F.
Scuola Normale Superiore di Pisa, Italy

PERICART J.C.
Electricite de France

PERSSON P.H.L.
Swedish Fusion Office, Spanga, Sweden

PFIRSCH D.
IPP Garching, FRG

PIEKAAR H.W.
FOM, Rijnhuizen, Netherlands

PLATZ P.
CEA, Fontenay, France

POCS L.
Cent. Res. Inst. for Phys., Budapest, Hungary

POFFE J.P.
JET, Culham, UK

POLMAN R.W.
FOM, Rijnhuizen, Netherlands

POST R.F.
LLL, Livermore, USA

POTS B.F.M.
Tech. Univ. Eindhoven, Netherlands

PROHOROFF S.
Free Univ., Brussels, Belgium

PROUDFOOT G.
UKAEA, Culham, UK

RAEDER J.
IPP Garching, FRG

RAGER J.P.
CNEN, Frascati, Italy

RAMETTE J.
CEA Fontenay, France

RAU F.
IPP Garching, FRG

REBUT P.
JET, Culham, UK

REM J.
FOM, Rijnhuizen, Netherlands

RENNER H.
IPP Garching, FRG

REWOLDT G.
PPPL, Princeton, USA

REYNOLDS J.A.
UKAEA, Culham, UK

RIGHETTI G.B.
CNEN, Frascati, Italy

RINGLER H.
IPP Garching, FRG

RIVIERE A.C.
UKAEA, Culham, UK

ROBERTS J.R.
National Bureau of Standards, Washington, USA

ROBERTS K.V.
UKAEA, Culham, UK

ROBERTS M.
Dept of Energy, Washington, USA

ROBINSON D.C.
UKAEA, Culham, UK

ROBOUCH B.V.
CNEN, Frascati, Italy

ROBSON A.E.
Naval Research Lab., Washington, USA

ROGISTER A.
KFA, Julich, FRG

ROGNLIEN T.
LLL, Livermore, USA

ROLLAND P.
CEN, Grenoble, France

ROSANOV V.B.
Lebedev Inst., Moscow, USSR

RUTGERS W.R.
FOM, Rijnhuizen, Netherlands

SAISON R.
CEC, Brussels, Belgium

SAITO K.
Nihon Univ., Tokyo, Japan

SALOMAA R.R.E.
Nuclear Engineering Lab., Helsinki, Finland

SAND F.
CEC, Brussels, Belgium

SANMARTIN J.R.
ETSI Aeronauticos, Madrid, Spain

SCHEP T.J.
FOM, Rijnhuizen, Netherlands

SCHLUTER A.
IPP Garching, FRG

SCHMIDT G.L.
PPPL, Princeton, USA

SCHMIDT H.
Univ. of Stuttgart, FRG

SCHMIEDBERGER P.
Technical Univ. Of Prague, Czechoslovakia

SCHMITTER K.H.
IPP Garching, FRG

SCHNEIDER W.
IPP Garching, FRG

SCHOPF K.F.
Univ. of Innsbruck, Austria

SCHRITTWIESER R.W.
Univ. of Innsbruck, Austria

SCHUELLER F.C.
JET, Culham, UK

SCHWARZ H.J.
Rens. Poly., New York, USA

SELIN K.
JET, Culham, UK

SHAFRANOV V.D.
IAE, Kurchatov, Moscow, USSR

SHARP L.E.
Australian National Univ., Canberra

SHIMOIDE S.
Okaya Co., Nagoya, Japan

SHOHET J.L.
Univ. Wisconsin, Madison, USA

SHOJI T.
IPP, Nagoya Univ., Japan

SHUKLA P.K.
Ruhr-Univ., Bochum, FRG

SIEGRIST M.R.
CRPP, Lausanne, Switzerland

SIGEL R.
IPP Garching, FRG

SIGMAR D.J.
Oak Ridge Lab., Oak Ridge, USA

SINMAN A.
Ankara Nuclear Res. & Training Centre, Turkey

SINMAN S.
Middle East Tech. Univ., Ankara, Turkey

SMIRNOV V.P.
IAE, Kurchatov, Moscow, USSR

SOLDNER F.
IPP Garching, FRG

SPETH E.
IPP Garching, FRG

SPIES G.O.
IPP Garching, FRG

START D.F.H.
UKAEA, Culham, US

STEINMETZ K.
CNEN, Frascati, Italy

STEPANOV K.
Phys. Tech. Inst., Kharkov, USSR

STERNLIEB A.
Univ. Maryland, USA

STEUER K.H.
IPP Garching, FRG

STEYAERT J.R.L.
Univ. Louvain, Belgium

STOKES P.G.
Univ. Sydney, Australia

STORK D.
UKAEA, Culham, UK

STORM E.K.
LLL, Livermore, USA

STOTT P.E.
JET, Culham, UK

STRELKOV V.S.
IAE, Kurchatov, Moscow, USSR

STRINGER T.E.
JET, Culham, UK

SUNDARAM A.K.
Univ. of Texas, Austin, USA

SUPRUNENKO V.A.
Phys. Tech. Inst., Kharkov, USSR

SWAIN D.W.
Oak Ridge Lab., Oak Ridge, USA

SWEETMAN D.R.
UKAEA, Culham, UK

SYKES A.
UKAEA, Culham, UK

TACHON J.
CEA, Fontenay, France

TAKAYAMA K.
IPP, Nagoya Univ., Japan

TANG W.M.
PPPL, Princeton, USA

TATARONIS J.
Courant Inst. of Math. Sciences, New York, USA

TAYLOR J.B.
UKAEA, Culham, UK

TELESCA G.
Ecole Royale Milit., Brussels, Belgium

TENDLER M.
Uppsala Univ., Sweden

TENNFORS E.H.
Royal Inst. of Tech., Stockholm, Sweden

THOMPSON E.
JET, Culham, UK

TROYON F.
CRPP, Lausanne, Switzerland

TWERSKY D.
IAEA, Vienna, Austria

UCHIDA T.
Univ. Of Tokyo, Japan

UO K.
PPL, Kyoto Univ., Uji, Japan

VACLAVIK J.
CRPP, Lausanne, Switzerland

VAN DER MEER A.F.G.
FOM, Rijnhuizen, Netherlands

VAN VEEN A.
Technical Univ., Delft, Netherlands

VARMA R.K.
Physical Res. Lab., Navrangpura, India

VASELLI M.
LAFAM-CNR, Italy

VERHEEST F.
Rijksuniversiteit Gent, Belgium

VLASENKOV V.
IAEA, Vienna, Austria

VOITENKO D.A.
Sukhumi Inst. of Tech., USSR

VOLLMER O.
IPP Garching, FRG

VORONOV G.S.
Lebedev Inst., Moscow, USSR

VUKOVIC S.
Inst. of Physics, Belgrade, Yugoslavia

WAELBROECK F.
KFA, Julich, FRG

WAIDMANN G.
KFA, Julich, FRG

WATKINS M.L.
JET, Culham, UK

WATTEAU J.P.
CEA, Limeil, FRANCE

WATTS M.R.C.
UKAEA, Culham, UK

WEBER P.G.
Columbia Univ., New York, USA

WEBER W.J.
Univ. of Tromso, Norway

WEINSTEIN B.W.
LLL, Livermore, USA

WESSON J.A.
UKAEA, Culham, UK

WEYNANTS R.R.
Ecole Royale Milit., Brussels, Belgium

WHITE R.
Maxwell Laboratories Inc., San Diego, USA

WILHELMSSON H.
Chalmers Univ. of Tech., Goteborg, Sweden

WILLIAMSON J.H.
Univ. of Reading, UK

WOBIG H.
IPP Garching, FRG

WOLF G.H.
KFA, Julich, FRG

WOODING E.R.
Royal Holloway College, Surrey, UK

WOODS L.C.
Oxford Univ., UK

WOOTTON A.J.
UKAEA, Culham, UK

WUSTER H.O.
JET, Culham, UK

YABE T.
Osaka Univ., Japan

YE YOU-ZHANG
Southerwestern Inst. of Physics, P.R. China

ZWICKER H.
Univ. of Stuttgart, FRG